Interdisciplinary
Applied Mathematics

Daniel D. Joseph
Yuriko Y. Renardy

Fundamentals of Two-Fluid Dynamics

Part II: Lubricated Transport, Drops and Miscible Liquids

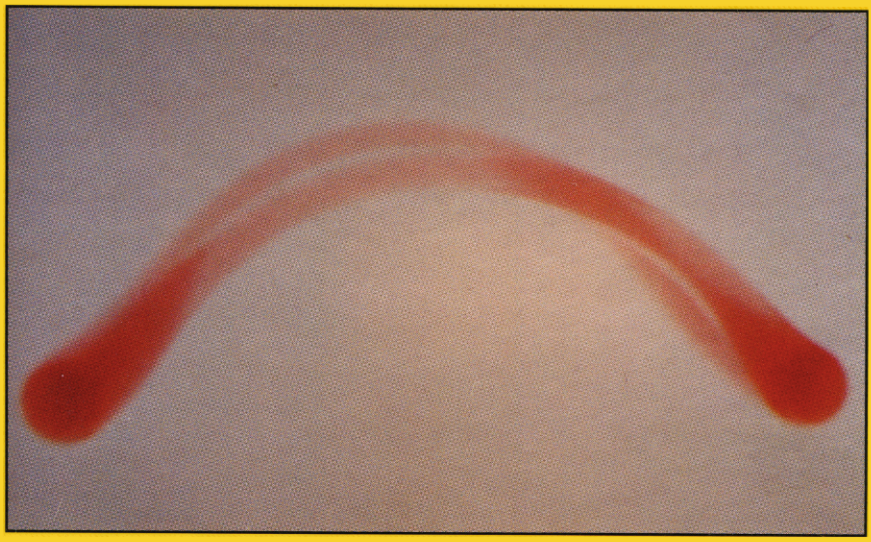

Springer Science+Business Media, LLC

Interdisciplinary Applied Mathematics

Volume 4

Interdisciplinary Applied Mathematics

---

1. *Gutzwiller:* Chaos in Classical and Quantum Mechanics
2. *Wiggins:* Chaotic Transport in Dynamical Systems
3. *Joseph/Renardy:* Fundamentals of Two-Fluid Dynamics:
   Part I: Mathematical Theory and Applications
4. *Joseph/Renardy:* Fundamentals of Two-Fluid Dynamics:
   Part II: Lubricated Transport, Drops and Miscible Liquids

Daniel D. Joseph Yuriko Y. Renardy

Fundamentals of Two-Fluid Dynamics

Part II: Lubricated Transport, Drops and Miscible Liquids

With 306 illustrations, 30 in color

Springer Science+Business Media, LLC

Daniel D. Joseph
Department of Aerospace
Engineering and Mechanics
University of Minnesota
Minneapolis, MN 55455 USA

Yuriko Y. Renardy
Department of Mathematics
Virginia Polytechnic Institute
and State University
Blacksburg, VA 24061 USA

Cover illustration: Vortex ring (Rayleigh-Taylor) instability. (See color plate IX.2.2 (c-d).)

Mathematics Subject Classifications (1991): 76E05, 76E15, 76E30, 35B20

Library of Congress Cataloging-in-Publication Data
Joseph, Daniel D.
Fundamentals of two-fluid dynamics / Daniel D. Joseph, Yuriko Y. Renardy.
p. cm. – (Interdisciplinary applied mathematics : v. 3/4)
Includes bibliographical references and index.
Contents: part 1. Mathematical theory and applications – part 2. Lubricated transport, drops and miscible liquids.
ISBN 978-1-4615-7063-9

(Springer-Verlag New York Berlin Heidelberg : part 2 : alk. paper). –
ISBN 978-1-4615-7063-9
2 : alk. paper).
1. Fluid dynamics. I. Renardy, Yuriko Y. II. Title.
III. Series.
QC151.J67 1992
620.1'064–dc20 92-34044

Printed on acid-free paper.

Production managed by Henry Krell; manufacturing supervised by Vincent Scelta.
Photocomposed copy prepared from the authors' TeX file.

9 8 7 6 5 4 3 2 1

ISBN 978-1-4615-7063-9 ISBN 978-1-4615-7061-5 (eBook)
DOI 10.1007/978-1-4615-7061-5

Preface

Two-fluid dynamics is a challenging subject rich in physics and practical applications. Many of the most interesting problems are tied to the loss of stability which is realized in preferential positioning and shaping of the interface, so that interfacial stability is a major player in this drama. Typically, solutions of equations governing the dynamics of two fluids are not uniquely determined by the boundary data and different configurations of flow are compatible with the same data. This is one reason why stability studies are important; we need to know which of the possible solutions are stable to predict what might be observed. When we started our studies in the early 1980's, it was not at all evident that stability theory could actually work in the hostile environment of pervasive nonuniqueness. We were pleasantly surprised, even astounded, by the extent to which it does work. There are many simple solutions, called basic flows, which are never stable, but we may always compute growth rates and determine the wavelength and frequency of the unstable mode which grows the fastest. This procedure appears to work well even in deeply nonlinear regimes where linear theory is not strictly valid, just as Lord Rayleigh showed long ago in his calculation of the size of drops resulting from capillary-induced pinch-off of an inviscid jet. In two-fluid problems, there are many sources for instability and the active ones may be determined to a degree by analysis of different terms which arise in the energy budget of the most dangerous disturbance.

Though we have presented many results from nonlinear analysis of two-fluid problems, this side of the subject is not yet well-developed. We are also certain that the direct simulations of two-fluid problems which have commenced only in the years just passed have a potentially huge domain for increased understanding.

Applications of two-fluid dynamics range from manufacturing to lubricated transport. Different mechanisms which are unique to the flow of two fluids can be exploited for this purpose. Density-matching can be used to depress the effect of gravity, or of centripetal acceleration in rotating systems, allowing one to manipulate the places occupied and the shapes of

the interfaces between fluids. Viscosity segregation can be used to promote mixing and demixing, to promote say the displacement of one fluid by another as in the problem of oil recovery, or to segregate one molten plastic from another by encapsulation. The lubrication of one fluid by another is a particularly important branch of two-fluid dynamics; if one fluid has a surpassingly large viscosity, it may be lubricated by a less viscous fluid. The most beautiful of the lubricated flows are the rollers discussed in chapter II of the first part, *Mathematical Theory and Applications.* The most useful of the lubricated flows are the water-lubricated pipelines, which are discussed in chapters V through VIII in the second part, *Lubricated Transport, Drops and Miscible Liquids.* It is our hope that this book will lead to deeper understanding of the principles and applications of two-fluid dynamics.

The topics treated in this book are displayed in the table of contents. Four of the six chapters in this part, *Lubricated Transport, Drops and Miscible Liquids*, are about water-lubricated pipelining. We have reported results of systematic studies of ideal flows and linear and nonlinear stability analyses with experimental and field observations. Some techniques of analysis which are applied here are discussed in the first part, *Mathematical Theory and Applications*, and they are also explained again here at the places where they appear. We present all the analysis with enough details to teach students. As always, it is certain that a number of excellent studies of two-fluid dynamics which deserve mention have not been mentioned.

Water-lubrication of viscous materials is a nascent technology with a proven potential for great economy. This feature of the subject is a motivation for our work and we have tried to direct readers, wherever possible, to the remaining problems which impede the technology.

Our research for this project could not have been done without the help of certain persons: Mike Arney, Runyan Bai, Nick Baumann, Gordon Beavers, Kangping Chen, Howard Hu, Paul Mohr, John Nelson, Ky Nguyen, Luigi Preziosi and Michael Renardy. We are especially indebted to Chen, Hu and Preziosi for their excellent analytical and numerical studies of lubricated pipelining and to Bai for the design and execution of very elegant experiments. We thank Michael Renardy for reading through the manuscript.

Our nominee for the "gold core flow" medal is Veet Kruka, a petroleum engineer at Shell Development in Westhollow, Texas. He was the first to make a water-lubricated line work on a commercial scale (see chapter V). We are indebted to him, his co-worker, Greg Geiger, and to Gustavo Nunez and Emilio Guevara of Intevep, PDVSA, for various kinds of help and encouragement.

The last two chapters of the book, IX and X, are completely independent of the others. Chapter IX is a description of the immiscible vortex rings which develop in free fall. In chapter X, we develop a new theory of binary mixtures of incompressible liquids based on the observation that the velocity of a fluid particle in such a mixture cannot be solenoidal when

diffusion is active. It explores the idea that gradients of composition can induce direct stresses which will mimic the effects of a transient interfacial tension when the gradients are large.

The work of Joseph was supported mainly by the Department of Energy, Office of Basic Energy Sciences and also by the fluid mechanics branch of the National Science Foundation, the mathematics division of the Army Research Office, by the Army High Performance Computing Center, and the Minnesota Supercomputer Institute. Joseph's research on water-lubricated pipelining was funded initially under a special small NSF grant for innovative research involving the lubricated transport of coal-oil dispersions. Joseph is grateful to Steve Traugott for this initial grant which was later picked up by Oscar Manley at the DOE.

Renardy's research was funded by the National Science Foundation under Grant No. DMS-8902166. This project was begun during the Winter Quarter of 1989 at the Institute for Mathematics and Its Applications at the University of Minnesota.

Yuriko dedicates this book with love to her father Sadayuki Yamamuro ("Papa, arigato"), and to her mother Akiko ("osewani narimashita"). Dan dedicates this book to Adam, Bai, Chris, Claude, Dave, Geraldo, Harry, Howard, John, Kangping, Luigi, Mike, Paul, Pushpendra and Terrence.

January 1992

Minneapolis, Minnesota
Blacksburg, Virginia

Contents

Contents of *Part II: Lubricated Transport, Drops and Miscible Liquids*

Contents of *Part I: Mathematical Theory and Applications*

Chapter V
Introduction to Lubricated Pipelining

V.1 Nature of the Problem

There is a strong tendency for two immiscible fluids to arrange themselves so that the low-viscosity constituent is in the region of high shear. We can imagine that it may be possible to introduce a beneficial effect in any flow of a very viscous liquid by introducing small amounts of a lubricating fluid. Nature's gift is evidently such that the lubricating fluid will migrate to the right places so as to do the desired job. This gives rise to a kind of gift of nature in which the lubricated flows are stable, and it opens up very interesting possibilities for technological applications in which one fluid is used to lubricate another. The particular case of lubricated pipelining is discussed in chapter I.1 (b) and is the subject of chapters VI - VIII. A good source for the literature prior to 1985 is the review paper of Oliemans and Ooms [1986] and the monograph of Oliemans [1986].

Various arrangements of oil and water occur in experiments. The arrangements which appear in horizontal pipes are:

1) Stratified flow with heavy fluid below
2) Oil bubbles and slugs in water
3) A concentric oil core in an annulus of water (this is called core-annular flow and is possible only when the two fluids have the same density)
4) Various kinds of shear stabilized lubricated wavy flow, called wavy core flows
5) Water in oil (w/o) emulsions.

Some of these arrangements are shown in figure 1.1.

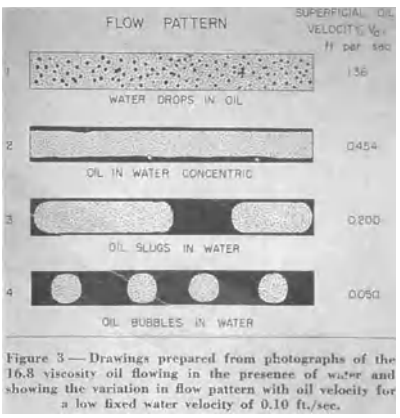

Figure 3 — Drawings prepared from photographs of the 16.8 viscosity oil flowing in the presence of water and showing the variation in flow pattern with oil velocity for a low fixed water velocity of 0.10 ft./sec.

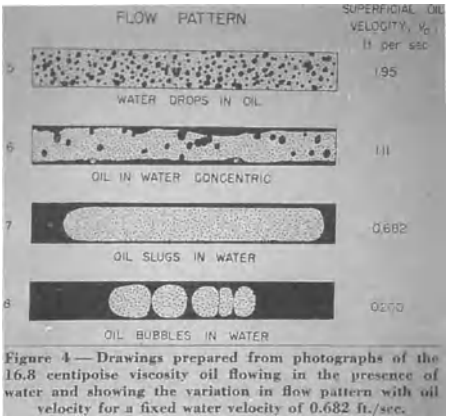

Figure 4 — Drawings prepared from photographs of the 16.8 centipoise viscosity oil flowing in the presence of water and showing the variation in flow pattern with oil velocity for a fixed water velocity of 0.682 ft./sec.

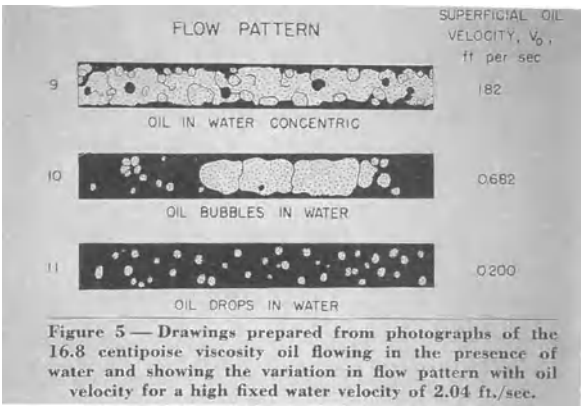

Figure 5 — Drawings prepared from photographs of the 16.8 centipoise viscosity oil flowing in the presence of water and showing the variation in flow pattern with oil velocity for a high fixed water velocity of 2.04 ft./sec.

Fig. 1.1. [Charles, Govier and Hodgson, 1961, Canadian Society for Chemical Engineering] The sketches are taken from Charles, Govier and Hodgson [1961]. The density of the oil has been raised to that of water by adding carbon tetrachloride to the oil. These experiments are discussed further and their results are compared with theory in sections VI.1 (m), VI.2 (g) and in chapter VII.

Similar arrangements of oil and water appear in the vertical flows discussed in chapters VI and VII. The problem for vertical flow, including the effect of gravity, possesses axisymmetry, and the flows are axisymmetric, at least in an average sense. In vertical pipes we can identify robustly stable regimes exhibiting

6) Bamboo waves (see plate V.1.2) and
7) Intermittent corkscrew waves (see plate V.1.3).

All of the arrangements (1) through (7) except (1) and (5) are well-lubricated with drag reductions of the order of the viscosity ratio, with reduction factors of 10^{-4} or more for viscous oils with viscosities greater than 100 poise. The arrangements (1) and (4) give rise to a loss of lubrication; emulsification of water is particularly onerous because the emulsion will not be lubricated and will have a higher viscosity than the oil.

Considerable progress in understanding these complicated two-fluid flows can be made by comparing the results of stability studies of perfect core-annular flows with experiments giving rise to the different arrangements which are observed. These kinds of studies are given in the chapters which follow.

V.2 Chronology of Experiments and Applications

The first mention of lubrication of oil by water in pipes appears to be in the patent application of Isaacs and Speed [1904]. The density of the lubricating fluid here is greater than oil. They note that concentric flow may be established if a rotational motion is imparted to the flowing liquids by means of a rifle on the inside of the pipe. Their invention consists in delivering to the pipe the fluid to be conveyed, together with a fluid of greater density, and in making the fluids advance through the pipe with a helical motion, so that the denser fluid is caused to separate from the lighter and to encase it, thus reducing the frictional resistance to the flow of the lighter fluid.

The foregoing idea may perhaps be usefully reformulated as a competition between centripetal and gravity forces, with film lubrication when centripetal acceleration is dominant, and vertically stratified flow when gravity is dominant (see, for example, Chernikin [1956], and section VI.2 of this book).

When gravity is dominant, stratified flow will result. In this case, only a part of the pipe wall may be lubricated by the water. Looman [1916] patented an invention for a method of conveying oils or similar substances through pipes by passing them over relatively stationary bodies of water lying at the bottom of the pipe. His idea was to have an array of these *water traps* at the bottom of the horizontal pipe. (Obviously there would be no need for a water trap if the two fluids were delivered together in a stratified arrangement.)

Theoretical methods are available for estimating the pressure drop reduction for completely stratified laminar flow. This flow is a lot less efficient than the encapsulated arrangement in transporting the viscous fluid. Yu and Sparrow [1967] and Charles and Redberger [1962] find that the ratio of the depth h of the lubricating layer to pipe radius R for maximum reduction is $h/R = 0.4$. The pressure gradient reduction factor found by Yu and Sparrow is about 1.37 for liquids with a viscosity ratio greater than

1000. Charles and Redberger [1962] find a slightly smaller reduction factor. Other theoretical studies which assume laminar flow and a flat interface are by Gemmell and Epstein [1962] and Ranger and Davis [1979]. The experiments of Charles and Lilleleht [1965] and Kao and Park [1972] indicate that the *perfectly stratified flow* assumed in these theoretical studies is stable at least for some of the operating conditions in their experiments. The discrepancies in the results of the experiments of Russell, Hodgson and Govier [1959] and Charles [1960] on nominally stratified flow of two immiscible liquids in circular pipes may be due to instabilities of *perfectly stratified flow* which have not yet been analyzed. The same cause may be at the root of the difference between the idealized prediction for stratified laminar flow between infinitely wide parallel plates by Russell and Charles [1959] with experimental data for circular pipes.

The water in a stratified oil-water flow will tend to encapsulate the oil. This is a dynamic effect which is independent of the wetting properties between the liquids and the pipe walls. Charles and Lilleleht [1965] observed a curving of the interface in the neighborhood of the duct walls, but concluded that this is not an effect of first importance except in ducts of small horizontal dimensions. Bentwich [1976] has considered some problems of laminar stratified flow with an eccentric interface in the form of a circular arc. This could be called *perfect partially stratified flow* and it would be unstable under certain conditions. It is not clear whether or not the Bentwich model captures some effects of encapsulation.

We shall not consider vertically stratified flows further, but they are important.

We have already noted that if the density difference between water and oil is not too great and if the viscosity difference is great enough, the water will automatically encapsulate the oil all around. The earliest application of this idea to the practice of pipelining that we could find is by Clark [1948] (cited as a private communication by Russell and Charles [1959])

"...who studied the heavy crude oil from the McMurray oil sand of Alberta, and observed a pressure drop reduction when the water was injected into this oil in a 0.375 inch pilot pipeline. The flow was laminar, with Reynolds numbers ranging from 10 to 20, and at temperatures investigated the oil viscosity ranged from 800 to 1000 cp. Injection of 7-13% water reduced the pressure gradient, which is the pressure drop per unit length of the pipe in the direction of flow, by factors from 6 to 12. The relative positions of the oil and water were not known, but it was suggested that the water wetted the inside of the pipe preferentially."

The patent application by Clark and Shapiro [1949] is the first that appears to address the problem of core-annular flows of heavy petroleum. Here gravity effects are reduced by density matching to an acceptably small level and the heavy oil and water can flow in a lubricated manner, without stratification. Clark and Shapiro were engineers for the Socony Vacuum Oil

company. They did extensive tests in a three mile length of six-inch pipe. They

"...found that the flow of viscous petroleums in pipelines can be greatly facilitated by the use of water containing minute proportions of a water soluble anionic surface-active agent and of an alkali-metal phosphate and having its pH adjusted to within the range pH 5.7 to pH 7.9, preferably pH 6.6."

Clark and Shapiro emphasized the method of additives and surface active agents in controlling the emulsification of water into oil. The emulsification is an undesirable condition since the emulsion has a higher viscosity than the oil alone. When water emulsifies into oil, lubrication is lost. Emulsification occurs readily in the so-called *light oils* with viscosities less than 500 cp. Lubricated pipelining is a viable proposition for *heavy oils* which can be defined roughly as oils whose viscosity exceeds 500 cp with a density near to water, say $\rho_{\text{oil}} > 0.9\text{g/cm}^3$.

Various options in the selection of pipelines for transporting 48,000 bbl per day of viscous crude oil from Temblador in the southern part of the state of Monagas, Venezuela, to the Carpite refinery and terminal 92 miles north on the San Juan River are considered by Leach [1957] of the Creole Petroleum Corp., VZ. He rejects water-lubrication and says that:

"Had the water injection line been selected, a considerable saving in initial investment would probably have been realized, and if, upon operating the water injection system, the formation of emulsions proved to be no problem and operating cost proved to be as anticipated, this line would have been the best selection. In view of the large investment involved, however, and the considerable amount of uncertainly that existed concerning the formation of emulsions, dehydration of the crude, and pumping difficulties after a shutdown, it was concluded that the construction of a water injection line could not be justified at this time."

It would be very good for lubricated pipelining if materials for pipes, or pipe linings, could be developed to keep the oil from sticking to the wall. Then one could lubricate with 2 to 5 percent water and dehydration would not be necessary.

Clifton and Handley [1958] addressed this problem of emulsification in another way. They were engineers for Shell Development Co. in Emerville, CA, and they wrote a patent application specifying methods and apparatus to be used in preventing emulsification and improving film lubrication. They say that:

"It is also known that substantial amounts of water may be introduced into a stream of viscous petroleum flowing through a pipe line to reduce the viscosity of the stream and thus facilitate the flow through the pipe line. Instead of adding substantial amounts of water to a viscous petroleum to reduce its viscosity, it is now proposed to add only minor amounts of water, say, about 1%, into a stream of a viscous petroleum so that the water forms

a lubricating film between the flowing petroleum and the inner wall of a pipe line.

"It is therefore an object of this invention to provide a method and means of facilitating the flow of heavy oil through a pipe line by lubricating the pipe line with another liquid of low viscosity, preferably one having a specific gravity (or density) approximately that of the heavy oil.

"It has been found, however, that while water may be employed to reduce the viscosity of a heavy oil, or to lubricate it through a pipe line, water loses its beneficial qualities if the combined water and oil is run through a pump. Upon running a viscous oil and any amount of water through a pump, the water generally becomes thoroughly emulsified in the oil with the formation of a water-in-oil emulsion having a substantially higher viscosity than that of the unemulsified water and oil mixture upstream of the pump. It may be readily seen that it would not be practical to introduce water into a heavy oil being transported by pipe line over a distance sufficiently great to necessitate the use of more than one pump between the shipping and receiving terminals, since additional emulsification of the oil and water would occur at each pump with a concomitant increase in viscosity.

"Therefore, it is also an object of this invention to provide means for introducing a film of water between the inner wall of a pipe line and a stream of viscous oil flowing therethrough, and for subsequently removing substantially all the water from the flowing stream before the stream enters a pump in the pipe line.

"Another object of this invention is to provide means for introducing a thin aqueous film completely around the inner wall of a pipe line.

"A further object of the invention is to provide a method and means for adjusting the specific gravity of a lubricating aqueous film to substantially that of the liquid that it surrounds.

"Another object of the present invention is to provide a method and means for lubricating a stream of heavy oil in a pipe line so that increased flows through the pumps may be realized without any increase in pumping pressures."

An important series of experiments on water-lubricated pipelining were carried out in Alberta, Canada by Russell and Charles [1959], Russell, Hodgson and Govier [1959], Charles [1960] and especially by Charles, Govier and Hodgson [1961]. The latter experiments are described in figure 1.1 and in sections VI.1 - 3.

Glass [1961] of Esso Research and Engineering has described his experiments and results as follows:

"All experimental work was carried out by flowing oil and water through a 4 ft length of 1 cm inside diameter glass tubing. Oil viscosity was varied from 10 to 30,000 centistokes, oil specific gravity from 0.97 to 1.03; volumetric water rate from 10 to 400% on oil; and oil superficial velocities (that is, the mass flux per cross-sectional area) from 0.2 to 4.2 ft/sec.

Visual observations of the flow were made. Pressure gradients were determined by two manometer taps situated 1 ft and 3 ft downstream of the oil injector.

"**Results.** With the more viscous oils, the initial "core" of oil was readily maintained. The less viscous the oil, the more this core would break up into "globs" of oil of various sizes. At low enough viscosity, no distinguishable core-annulus structure was maintained.

"As the percent of water on oil increased, the pressure gradient first dropped, passed through a minimum at 30-40%, and then rose again. Figure 1 shows a typical plot. With 35% water, a pressure gradient of only 5 in H_2O/ft was sufficient to move 200 centistoke oil at a superficial velocity of 4.1 ft/sec. Without water, a gradient of 108 in H_2O would have been needed.

"The initial drop in pressure gradient with increasing water rate is due to the widening of the water annulus. There is more water to intervene between the rapidly moving oil core and the stationary tube wall. Eddying and energy dissipation in the water layer is thus less violent. As the percent water goes up, however, the oil core continues to neck down, and must go faster and faster to maintain the same oil flow rate. The average velocity of the water will also increase, and the pressure gradient goes up despite the slight additional widening of the annulus.

"The pressure gradient at a given percent water for core-annulus flow was found to go up with the 1.8 power of the flow rate. This can be ascribed to the turbulent losses in the water annulus.

"Oil core-water annulus formation was stable for oils heavier than water, as well as for oils lighter than water. Changing oil density in the range 0.97 to 1.03 had no discernible effect on pressure gradient. For oil lighter than water, the oil was carried slightly high in the tube. That is, there was less water above the core than below. For oils heavier than water, the core was carried low in the tube. Oil viscosity had no great effect on pressure gradient, as long as core-annulus flow was maintained. Shearing and the attendent energy dissipation occurred primarily in the water annulus. Increasing oil viscosity, however, did result in a small decrease in pressure drop. As oil viscosity went up, the core consisted of fewer and fewer globs of oil. It thus also contained less and less water trapped between globs. At high enough viscosity, only a single continuous stream of oil was left. With fewer globs and less water trapped in the core, the core is slightly smaller and the annulus slightly wider; this results in a somewhat lower pressure drop. Thus, a 20-fold increase in viscosity (from 50 to 1,000 centistokes) resulted in roughly a 30% decrease in pressure gradient."

Other experiments on water lubrication in horizontal pipes were reported by Stein [1978], Oliemans, Ooms, Wu and Duÿvestin [1985] and by Arney, Bai, Joseph and Liu [1992].

Shell Oil has pioneered the development of commercially viable pipelines. One of their commercial lines is described in figure 2.2. Recently

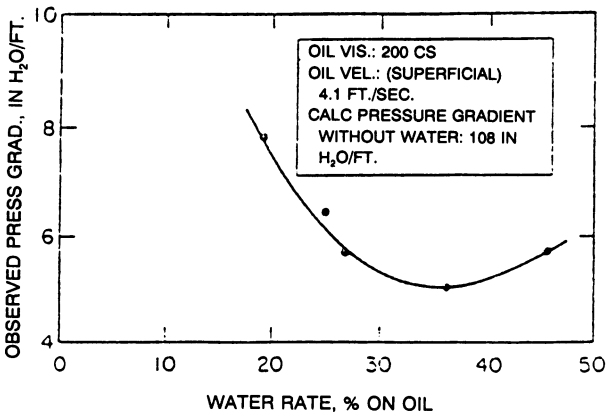

Fig. 2.1. [Glass, 1961, Chem Eng Prog 57, 116[(v2)6,8] Reproduced by permission of the American Institute of Chemical Engineers, ©1961 AICHE] 30-40% water gives lowest pressure gradient.

Maraven of PVSA (Petroleos de Venezuela Sociedad Autonomia) has placed in operation a 60-kilometer line to transport heavy crudes in the lubricated mode. In general such lubricated lines become attractive when the lighter crudes are expensive or locally in short supply. Plate V.2.3 is a photograph of a core-annular flow in a test loop at San Tome, Venezuela.

Water-lubrication in a vertical pipe was studied in the experiments of Bai, Chen and Joseph [1991] which are described in chapter VII.

Finally we draw the reader's attention to some experiments which are indirectly related to water-lubricated pipelining. Shertok [1976] studied flow development in a vertical pipe. Hasson, Man and Nir [1970] studied film rupture in the pipe flow of water inside an annulus of slightly heavier and more viscous organic liquid (see also Hasson and Nir [1970]). Aul and Olbricht [1990] studied the instability of an oil film $O(1\mu m)$ on the wall inside a capillary tube of 54 μm filled with water. Their experiment is related to secondary oil recovery.

Oil-water line moves highly viscous crude

PIPELINING highly viscous crude oil, an economic barrier to development of heavy-oil fields, has been made possible via a new technique, oil-water core flow.

It involves transporting a stream of oil inside a jacket of water. Frictional drag is reduced, since the oil is surrounded by water and does not come into contact with the pipe wall.

Shell Oil Co. is using the technique in a 24-mile, 6-in. line transporting an ...-gravity crude from its Midway-Sunset producing area to its Ten Section dehydration plant. The line has a design capacity of about 27,000 b/d of liquids. The flow is 70% oil and 30% water.

Liquids are injected into the line at the single station with the aid of a specially designed nozzle. Oil flows through the center of the nozzle while water is injected through a jacket surrounding the oil.

The nozzle's design causes the oil and water to enter the pipeline at approximately the same velocities and in the desired configuration. The oil core remains stable as long as the flow rate in the line maintains a minimum velocity of 3 ft/sec.

There are four positive-displacement pumps at the station, one 200-hp unit for water, two 150-hp units for oil and one 150-hp unit for either service. Purchased water along with water used for steam injection are used in the line.

The oil, with a viscosity at 100° F. 50,000 times greater than water, is produced by secondary recovery using steam injection.

It is gathered in a heated pipeline system and stored in a 30,000-bbl tank before shipment.

After injection into the line, the oil core and water jacket are pumped to the dehydration plant. There heavy crude is combined with a lighter crude oil. This mixture goes to a 40,000-bbl separation tank where the water settles out. Remaining water is removed in a dehydration plant, the oil is blended and then goes through an 8-in. line to Bakersfield before going on to Shell's Martinez refinery near Oakland.

The oil-water pipeline has been in operation for about a year. Its startup culminated several years of study at the Shell Pipe Line Corp.'s research and development labratory in Houston. It is expected to make the operation of some submarginal heavy oil fields economic.

Heated pipelines or tank trucks, both expensive, have been used in this service.

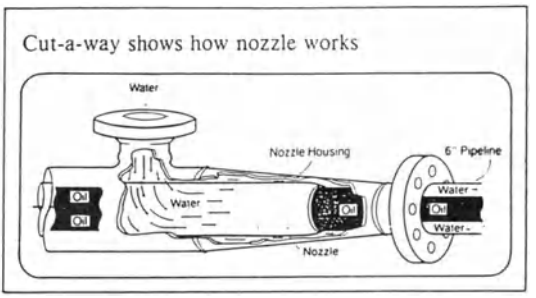

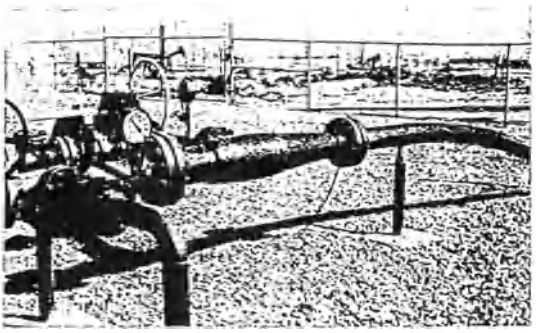

INJECTION NOZZLE, the tapered unit between the two flanges (at center in photo), channels the water and oil into Shell's unusual 6-in. line (right) moving Midway-Sunset field's viscous crude.

Fig. 2.2. [1972, Pennwell Publishing Co.] An editorial from *The Oil and Gas Journal* describing Shell's pipeline.

V.3 Effects of Gravity

Oil, being lighter than water, will rise to the top of a horizontal pipe in which oil and water are flowing. The oil can then ride high in a pipe while maintaining a lubricated situation, with a film of water all around, the film being thinner at the top than at the bottom. Another possible arrangement occurs when the pressure gradients are not too small: the oil is again surrounded by a film of water but seizes parts of the wall on the top where it runs as rivulets in the water. In some cases, there is oil at the top of the pipe, with a film of water below it and the water partly lubricates an oil core.

Ooms, Segal, Van der Wees, Meerhoff and Oliemans [1989] developed a model to explain their experimental observation of a rippled core lubricated by water through a horizontal pipe. They write:

"Special attention was paid to understanding how the buoyancy force on the core, resulting from any density difference between the oil and water, is counterbalanced. This problem was simplified by assuming the oil viscosity to be so high that any flow inside the core may be neglected and hence that there is no variation of the profile of the oil-water interface with time. In the model the core is assumed to be solid and the interface to be a solid/liquid interface.

"By means of the hydrodynamic lubrication theory it has been shown that the ripples on the interface moving with respect to the pipe wall can generate pressure variations in the annular layer. These result in a force acting perpendicularly on the core, which can counterbalance the buoyancy effect.

"To check the validity of the model, oil-water core-annular flow experiments have been carried out in a 5.08 cm and a 20.32 cm pipeline. Pressure drops measured have been compared with those calculated with the aid of the model. The agreement is satisfactory."

The foregoing model is semi-empirical. Data from experiments is required to make the model work. A later revision of this model by Oliemans, Ooms, Wu and Duÿvestin [1985] incorporates some effects of turbulence in the lubricating water:

"**Abstract.** Core flow tests with a 3000 mP as fuel oil in a 5 cm test facility have revealed important information on the amplitudes and lengths of waves at the oil/water interface. The wavelengths vary considerably with water fraction and oil velocity. Moreover, the flow in the water annulus is turbulent. A previously developed theoretical model for steady core-annular flow in pipes has been extended by incorporating the effect of turbulence in the water film surrounding the oil core. The adapted model predicts the pressure-gradient increase with oil velocity correctly, provided that actual wave amplitudes and wavelengths observed during these tests are used as input data. The possible contribution of inertial effects is discussed."

Purely theoretical nonlinear amplitude equations for a plane layer based on lubrication theory have been given by Ooms, Segal, Cheung and Oliemans [1985], and by Frenkel, Babchin, Levich, Shlang and Sivashinsky [1987], Frenkel [1989] and Papageorgiou, Maldarelli and Rumschitzki [1990]. In chapter VIII we shall review these theories and show that they apply only under very restricted conditions which exclude essential effects of inertia.

Since the effect of gravity is such as to destroy axisymmetry in horizontal pipes, the study of horizontal flow with gravity included is difficult. None of the lubrication-based theories and none of the stability studies treat the asymmetric effect of gravity in horizontal pipes. This is a pity since the effect of gravity is possibly more dangerous to lubrication the larger the pipe, but we cannot say anything definite because the analysis has not been done.

Gravity plays an important role for the lubrication of heavy crudes because the oil and water will stratify whenever the flow is stopped. In general, the pressure gradient required for restarting a line which is filled with oil above and water below is much greater than for steady flow. Maximum load designs therefore are associated with startup. These maximum loads can, it turns out, be greatly reduced by the use of additives in the water. It is also probable that large improvements can be achieved by constructing the pipe out of the right material. The general goal would be to coat the inside of pipes with hydrophilic materials. We are unaware of systematic studies along these lines.

V.4 Stability Studies

There have been a number of studies of the flow of two immiscible fluids of different viscosities and equal density through a pipe under a pressure gradient (see chapter I for examples of experimental and analytical studies). This problem has a continuum of solutions corresponding to arbitrarily prescribed interface shapes. The question therefore arises as to which of these solutions are stable and thus observable. Experiments have shown a tendency for the thinner fluid to encapsulate the thicker one. This had previously been "explained" by the viscous dissipation principle (see section I.3 (f)), which postulates that the amount of viscous dissipation is minimized for a given flow rate. For a circular pipe, this predicts a concentric configuration with the more viscous fluid located at the core. Later stability analyses discussed in more detail below show that while this configuration is stable when the more viscous fluid occupies most of the pipe, it is not stable when there is more of the thin fluid. Therefore the dissipation principle does not hold, and the volume ratio is a crucial factor. The additional effects of a density difference and interfacial tension have also been investigated and are discussed below.

Perfect core-annular flow (PCAF) is an exact steady laminar solution of the problem of flow in a pipe of circular cross-section and is the subject of chapters VI - VIII. PCAF is a rectilinear flow with one nonzero component of velocity that varies only with the radial coordinate. The two fluids are arranged centrally, one fluid in the core, the other in the annulus. This solution possesses maximum symmetry. Since the effects of gravity are such as to destroy the axial symmetry in the problem for the horizontal pipes, PCAF cannot be realized unless gravity is nullified by density matching as in the experiments of Charles, Govier and Hodgson [1961]. In vertical pipes of circular cross-section, the inclusion of gravity in the analysis does not break down the axial symmetry present in the problem, and PCAF is possible without matching densities.

PCAF is an idealized model problem for which all the measures of efficiency, pressure drops and holdup ratios can be computed when the volume flow rates of oil and water are given. We are going to study the stability of PCAF in the following chapters and we find that it is stable only for a very small set of conditions which typically do not occur in the applications. The other more robust core flows like wavy-core flow, which are well-lubricated and well-liked in the oil industry, are far from PCAF so that it is not clear at the outset that stability studies will have a practical application. Fortunately it turns out that the study of stability of PCAF is indeed helpful in understanding, predicting, and possibly in controlling the flows far from PCAF which arise in the applications.

Hickox [1971] studied the linear theory of stability of PCAF in a vertical pipe with the long-wave approximation. All the principal physical effects, the viscosity ratio, the density ratio, the ratio of radius of the interface to the pipe radius, surface tension, gravity and a Reynolds number are in his governing equations. However, his analysis is restricted to long waves; up to first order in an expansion in powers of the wave number and only axisymmetric disturbances and disturbances with a first mode in azimuthal periodicity were considered. Hickox further restricted his study to the case in which the viscosity of the core is less than the annulus; for example, water inside oil. He found all such flows are unstable to long waves. He did not consider the case of lubricated pipelining in which the core viscosity is greater. This latter problem was studied by Joseph, Renardy and Renardy [1985], who showed that the lubricated flows could be stable.

Ooms [1971] considered the stability of core-annular flow of two ideal liquids through a pipe. He found that the flow undergoes capillary instabilities and Kelvin-Helmholtz instabilities, due to a velocity difference at the interface. This difference is suppressed by viscosity and is replaced by a discontinuity in the velocity gradient. The flow is unstable to short waves if surface tension is zero in both the viscous and inviscid cases. The instability in the inviscid case is catastrophic, however; the growth rate goes to infinity with the wave number (Hadamard instability). The short-wave instability which arises in the viscous case when surface tension is zero is discussed

in chapter IV and can be called a viscous regularization of the Kelvin-Helmholtz instability (see the review paper by Joseph and Saut [1990] for a discussion). A viscous-inviscid model for core-annular flow has been analyzed by Power and Villegas [1990]. They predict instability to long waves and surface tension stabilizes short waves.

Hickox's study was extended to all wavenumbers by Joseph, Renardy and Renardy [1985]. Preziosi, Chen and Joseph [1989] (see section VI.1) and Hu and Joseph [1989 a] (see section VI.2) extended the analysis, including the effects of surface tension and density, but excluding gravity. They present numerical results for the axisymmetric mode. Surface tension is important: it is not possible to derive a theory without it which could be used in the design and control of lubricated pipeline technologies. A stability study concerning a different parameter range is that of a viscous liquid jet surrounded by a viscous gas in a vertical pipe in the presence of gravity and interfacial tension given by Lin and Ibrahim [1990]. Their results are relevant to the atomization of a liquid jet forced into an ambient gas.

Russo and Steen [1989] consider the stability of an annular liquid film flowing down a rod with a free surface. The cylindrical interface is subject to a capillary and a surface-wave instability. Axisymmetric and nonaxisymmetric disturbances are studied. When the annular layer is thin, they find that the shear can stabilize capillary breakup (this stabilization also occurs in core-annular flow). The physical mechanism responsible for long-wave stabilization is discussed in Dijkstra and Steen [1991]. These works extend the results of Xu and Davis [1985] which demonstrate that capillary breakup can be suppressed by shear.

Deferring to one important application, we say oil and water when we mean more viscous and less viscous liquids. In section VI.2, three arrangements are examined:

(i) oil is in the core and water on the wall,
(ii) water is in the core and oil is outside and
(iii) three layers, oil inside and outside with water in between.

The arrangement in (iii) is a model for lubricated pipelining when the pipe walls are hydrophobic. The arrangement in (ii) was also studied by Hickox [1971] and recent experiments of Aul and Olbricht [1990] are of interest. The arrangement in (i) was also studied by Preziosi, Chen and Joseph [1989]. Neutral curves, growth rates, maximum growth rates and wavenumbers for maximum growth are presented, as well as the various terms which enter into the analysis of the equation for the evolution of the energy of a small disturbance. The energy analysis allows us to identify the three competing mechanisms under way: interfacial tension, interfacial friction and Reynolds stress.

Hu and Joseph [1989b] analyzed the linear stability of core-annular flow in rotating pipes for a particular situation modeling the flow of oil and water. Attention is focused on the effects of rotation and the difference in

density of the two fluids. It is found that for two fluids of equal density, the rotation of the pipe stabilizes the axisymmetric mode and destabilizes the nonaxisymmetric modes. Except for small Reynolds numbers, where the axisymmetric capillary instability is dominant, the first azimuthal mode is the most unstable. When the heavier fluid is outside, centripetal acceleration of the fluid in the rotating pipe is stabilizing; there is a critical rotating speed above which the flow is stabilized against capillary instability for a certain range of small Reynolds numbers. When the lighter fluid is outside, the particular arrangement studied is unstable, although for a thinner annulus or a larger viscosity difference, the adverse density stratification can be stabilized by shear, just as in the case of the thin-layer effect discussed in section IV.6.

Couette flow of two fluids between sliding coaxial cylinders is considered by Preziosi and Rosso [1991]. The effects of surface tension and viscosity difference are included. They study the linear stability of the cylindrical interface numerically, as well as with the long-wave asymptotic method and the energy equation. Long waves may be unstable due to surface tension, and short waves may be unstable due to the viscosity ratio.

It is known that the stability problem for core-annular flow of very viscous crude oil and water is singular: the water annulus appears to be inviscid with boundary layers at the pipe wall and at the interface. Hu, Lundgren and Joseph [1990] treat this singular problem by the method of matched asymptotic expansions (see section VI.3). There are two cases of instability corresponding to different positions of the critical point in the annulus. One case is when the critical point is far away from the interface, the other is when the critical point is close to the interface. In both cases, explicit forms for the neutral curves are obtained. These are in agreement with numerical results obtained with a finite element code. An asymptotic analysis similar to that of Hu, Lundgren and Joseph was carried out by Miesen, Beijnon, Duijvestijn, Oliemans and Verheggen [1991] for a two-dimensional Couette flow with the less viscous fluid bounded by a wall and the other fluid unbounded. For lubricating core-annular flow with a thin annulus, large viscosity ratio, large Reynolds number for the lubricating fluid, and wave speeds close to the speed of the core, their theory predicts there will be waves with wavelengths of about 1-10 times the gap size. They show qualitative agreement with experiments. Boomkamp and Miesen [1991] have examined the nonaxisymmetric disturbances in core-annular flow with the method of matched asymptotic expansions for a small viscosity ratio.

The linear stability of core-annular flow in vertical pipes is analyzed in chapter VII. The flow is studied for two cases: in one case, gravity opposes and in the other aids the applied pressure gradient. The prediction of stability for perfect core-annular flow in a carefully selected window of parameters is verified with experimental results for the case of free fall in which the applied pressure gradient vanishes. The related problem of vertical plane Poiseuille flow in three layers has been studied in Renardy [1987b],

Lister [1987] and Than, Rosso and Joseph [1987]. Lister's work on vertical three-layer flow concerns the case when the walls are an infinite distance apart, with a thin plume of fluid falling down. For the other works, there is an analogy between the plane flow and a cross section of the pipe if the layers next to the walls are thin. For example, the arrangement with a thin layer of the less viscous fluid at the wall can be stable in both flows. The results in Renardy [1987] indicate that an intuitive reasoning may provide a guideline for the location of the fluids when the densities are markedly different: one expects the heavier fluid to be placed at the center for downward flow, and at the wall for upward flow. In fact, it is found that when the fluids have equal viscosity, the flow downward under gravity may be linearly stable only if the central fluid is markedly heavier. This stability occurs for a narrow interval of volume ratios. If this flow is forced upward against gravity, it may be linearly stable only if the heavier fluid is outside. This stability occurs for a restricted range of volume ratios and when the densities are markedly different. In the case of instability, the largest growth rates often occur at order 1 wavenumbers. A study of vertical pipe flow with density stratification has been given by Smith [1989] for axisymmetric long waves. He finds that when the densities are similar, stable flows are usually downward flows when the light fluid is at the center, and are usually upward flows when the heavier fluid is at the center. He explains this behavior in terms of a physical mechanism for the long-wave instability. In Renardy [1987], both the snake mode and the varicose mode are taken into account for the plane flow. It is then found that when the densities are similar, either one or the other mode produces instability, and that stability is only possible when the densities are markedly different, as mentioned above.

In the latter half of chapter VII, we present experimental results [Bai, Chen and Joseph 1991] on a water-lubricated pipelining of oil for modest flow rates. The force of gravity is axial in the apparatus, in the direction of the pressure gradient in up-flow and against the pressure gradient in down-flow. Measurements are compared with theoretical predictions based on the linear theory of stability of laminar core-annular flow. In the analysis of vertical plane Poiseuille flow, Renardy [1987 b] found that a varicose instability occurs in up-flow and a snake instability occurs in down-flow. These are reminiscent of the bamboo waves and corkscrew waves reported here. A summary of the published data of many authors is collapsed on friction factor versus Reynolds number plots.

In chapter VIII, the nonlinear stability of core-annular flow near points of the neutral curves at which perfect core-annular flow loses stability is studied using the Ginzburg-Landau equations [Chen and Joseph 1991a]. The results of the bifurcation theory are consistent with observations of flows that are close to perfect core-annular flows. We also present a review and critique of various weakly nonlinear long wave equations used to describe waves on the interface [Chen and Joseph 1991b]. Viscoelastic effects have been investigated by Chen [1991a, 1992].

V.5 Plan of Chapters VI - VIII, and List of Acronyms

Chapters VI through VIII give an account of the work by D. D. Joseph *et al.* on the subject of water-lubricated pipelining. Our discussions are basically restricted to flows of two liquids (typically water and oil) through pipes of circular cross-section. We are going to present results chronologically, as they appeared. Our material on lubricated pipelining is taken from the following list of eleven papers. The acronym for each of these is followed by the topic or authors.

ABJL ..... Arney, Bai, Joseph and Liu 1992
BCJ ..... Bai, Chen and Joseph 1991
CAF ..... Core-annular flow
CBJ ..... Chen, Bai and Joseph, 1990
CGH ..... Charles, Govier and Hodgson 1961
CJ_1 ..... Chen and Joseph 1991 a
CJ_2 ..... Chen and Joseph 1991 b
HJ_1 ..... Hu and Joseph 1989 a
HJ_2 ..... Hu and Joseph 1989 b
HLJ ..... Hu, Lundgren and Joseph, 1990
JRR ..... Joseph, M. Renardy, and Y. Renardy 1984
PCAF ..... Perfect core-annular flow
PCJ ..... Preziosi, Chen and Joseph 1989

Some of the theoretical papers, JRR, PCJ, HJ_1, HJ_2, and HLJ, are for horizontal flow with gravity neglected. Negligible gravity can be achieved by density-matching as in the experiments of CGH. In the analysis without gravity, we equate the coefficient of gravitational acceleration g to zero and retain the different densities elsewhere. Experiments on lubricated flow in horizontal lines in which densities are not matched (as in ABJL) are certainly influenced by gravity. For horizontal circular pipes, the inclusion of gravity kills the axial symmetry in the problem. The papers of CBJ, BCJ, CJ_1 and CJ_2 are for vertical pipelines in which gravity is included in the analysis; for the vertical circular pipe, gravity does not kill the axial symmetry in the problem and can be incorporated readily in the analysis.

Chapter VI
Lubricated Pipelining: Linear Stability Analysis

[1] For acronyms, see section V.5

VI.1 Neutral Curves, Waves of Fastest Growth, Comparison with Experiments of CGH

VI.1(a) Introduction

This section is based on the paper by Preziosi, Chen and Joseph [1989] (PCJ) and incorporates some results from Joseph, Renardy and Renardy [1983, 1984] (JRR). We present the linear stability of core-annular flow (CAF) with emphasis on the case of viscous fluid in the core. The effects of surface tension and density difference, neglecting gravity, are considered. As in the case of other layered shearing flows, surface tension plays an important role (cf. section IV.5) in the stability theory.

Upper and lower branches of the neutral stability curve are found in a Reynolds number ($\mathbb{R}$) versus wave number (α) plane. A window of parameters is identified in which CAF is stable to small disturbances. When $\mathbb{R}$ is below the lower critical value, CAF is destabilized by surface tension and long waves break up into slugs and bubbles. The size of slugs and bubbles of oil in water, observed by CGH, are given by the wavelength of the fastest growing wave. This instability persists in the long-wave limit and is a capillary instability, modified by shear, which reduces to Rayleigh's instability in the appropriate limit. At higher $\mathbb{R}$, the capillary instability is stabilized by shear. At yet higher $\mathbb{R}$ above the upper critical value, the flow is unstable to generally shorter waves which lead to emulsification, and water droplets in oil. There is an optimum viscosity ratio for stability: greater stability can be obtained by using a heavy liquid as a lubricant when the flow is unstable to capillary modes on the lower branch and by using a light liquid when the flow is unstable to emulsifying disturbances on the upper branch.

Our results appear to be in quantitative agreement with the results of experiments of Charles, Govier and Hodgson [1961] (CGH) on bicomponent flow of water and oil-carbon tetrachloride solutions density-matched with water. Gravity is made negligible by density-matching, so that their experiments and our analysis are compatible. Their results are summarized

in figure V.1.1 and discussed in section VI.1 (m). For now, it will suffice to note that

(a) there is a minimum speed, observed in experiments, but not previously treated by analysis, below which core-annular flow is unstable and gives way to oil slugs in water, and
(b) there is a maximum speed, observed in experiments, but not previously treated by analysis, above which core-annular flow is replaced by emulsions of water in oil.

The conditions in the experiments of CGH are not directly of interest in lubricated pipelining. In pipelines, one usually sees a form of wavy core flow when the oil viscosity is greater than 500 cp. In terms of the parameters used in this chapter the viscosity ratio m in practice is less than 0.002, much smaller than the value of 0.0532 used by CGH. Moreover, in some practical applications the density difference between oil and water causes the oil to ride high in the pipe and at low speeds the oil may rise up and seize the wall, leading to a failure of lubrication (see Oliemans and Ooms [1986] for a photograph and discussion of the effects of gravity). Fortunately, the oil core need not touch the upper wall. A lubricating layer can persist. The exact hydrodynamic mechanism, which maintains the lubrication layer at the top of the pipe, is not understood. Oliemans and Ooms think that a lubrication effect associated with ripples is important. Oliemans [1986] has developed a lubricating film model for core-annular flow which agrees with experiments in some details and disagrees in others. Evidently, the stronger shear in the small gap at the top of the pipe stabilizes the big capillary waves which are evident in the large gap at the bottom of the pipe. M. Renardy and Joseph [1986] have shown that traveling ripples will occur as a bifurcation of core-annular flow so that wavy-core flow which is observed in pipelines may arise as a subcritical bifurcation of core-annular flow.

Experiments were carried out on water-lubricated transport of SAE 30 motor oil and number two fuel oil and on 30% and 40% dispersions of 70 μm coal in these two oils. The oils are usually well-lubricated if the pressure gradient is not too small, even though the oil rides high in the pipe due to gravity. In general, the experiments resulted in lubricated flows even when the oil at the top seized the wall, but these are not concentric core-annular flows. In these cases, there is oil at the top of the pipe, sometimes running as rivulets, and underneath this, there is oil at the core lubricated by water all around. The effects of gravity are not so serious as to impede successful lubrication in our small pipes, but these effects could be more serious in pipes of larger diameter. There are some interesting situations in which the density of the oil and water are nearly the same, so that gravity is not important. This is the case, for example, with heavy oil extracted from the Alberta oil sands and with the dispersions of 40% coal in SAE 30 motor oil used in our experiments. The most serious problem for the technology of water-lubricated pipelining associated with stratification due

to gravity is start-up from rest. The effects of gravity under transient and steady conditions have not yet been treated in a theoretically satisfactory manner.

In this section, we confine our attention to parameter values in the range of the experiments of CGH. The second type of failure of lubricated pipelining, emulsification of water in oil, already occurs in these experiments and is apparently correlated with the higher-Reynolds-number instability identified in our linear theory. A finite-element program was implemented with an adaptive mesh in the boundary layer at the wall (cf. section VI.2 (d)). This calculation agreed with the pseudospectral code used in the present section but it also worked well at the small values of m <0.002 characteristic of field practice. The results of this finite-element calculation were compared with field data provided from experiments in 6 in. diameter pipes. The linear theory predicted wavy-core flow when the oil viscosity was greater than a critical one, with emulsification of water into oil for smaller viscosities. These predictions agree with the field data.

VI.1(b) The Equations and Basic Flow

Two liquids are flowing down a pipe of inner radius R_2. The interface between the two liquids is given by $r = R(\theta, x, t)$ where (r, θ, x) denotes cylindrical coordinates and $\hat{\mathbf{U}} = (\hat{U}, \hat{V}, \hat{W})$ are the corresponding components of velocity. The region $0 \leq r \leq R(\theta, x, t)$ is occupied by the first liquid with viscosity μ_1 and density ρ_1 and the second liquid (μ_2 and ρ_2) is located in $R(\theta, x, t) \leq r \leq R_2$. The pipe axis is at r=0 and the pipe is infinitely long $-\infty \leq x \leq \infty$. The mean value of R^2 over θ, $andx$, is a constant fixed by the prescribed volumes of each of the two liquids, independent of t. We denote the mean of R^2 by $R_1^2 = \bar{R}^2(\theta, x, t)$.

The equations of motion, gravity neglected, are

$$\rho_l \frac{d\hat{\mathbf{U}}}{dt} = -\nabla \hat{P} + \mu_l \nabla^2 \hat{\mathbf{U}}, \qquad \text{div}\hat{\mathbf{U}} = 0 \tag{1b.1}$$

where l=1 when $0 \leq r \leq R$ and l=2 when $R \leq r \leq R_2$,

$$\hat{\mathbf{U}} = \mathbf{0} \text{ on } r = R_2, \tag{1b.2}$$

and $\hat{\mathbf{U}}$ is bounded at $r = 0$. The kinematic free surface condition is

$$\hat{U} = \frac{\partial R}{\partial t} + \hat{W}\frac{\partial R}{\partial x} + \frac{\hat{V}}{R}\frac{\partial R}{\partial \theta}, \qquad \bar{R} = R_1. \tag{1b.3}$$

The jump in the quantity $(\cdot)$ across the interface is denoted $[\![(\cdot)]\!] = (\cdot)_1 - (\cdot)_2$. The jump in $\hat{U}$ over $r = R$ is

$$[\![\hat{U}]\!] = 0. \tag{1b.4}$$

The normal stress condition is

$$-([\![\hat{P}]\!] + 2HT)\mathbf{n} + [\![2\mu \mathbf{D}[\hat{\mathbf{U}}]]\!] \cdot \mathbf{n} = 0, \tag{1b.5}$$

where $\mathbf{D}[\hat{\mathbf{U}}] = \frac{1}{2}(\nabla\hat{\mathbf{U}} + \nabla\hat{\mathbf{U}}^T)$, $2H$ is the sum of the principal curvatures, T is the coefficient of surface tension, $\mathbf{n} = \mathbf{n}_{12}$ is the normal to $r - R = 0$ from liquid 1 to 2 (see chapter I for the derivation of the governing equations).

We shall study the stability of core-annular flow

$$\left.\begin{aligned} \hat{\mathbf{U}} &= (0, 0, W(r)) \\ [\![\hat{P}]\!] &= [\![P]\!] = T/R_1 \end{aligned}\right\} \tag{1b.6}$$

where $\nabla P = -\mathbf{F}, F > 0$ is the magnitude of the constant pressure gradient, and

$$W(r) = \left\{\begin{array}{ll} -\frac{F}{4\mu_1}(r^2 - R_1^2) + \frac{F}{4\mu_2}(R_2^2 - R_1^2), & 0 \le r \le R_1, \\ \frac{F}{4\mu_2}(R_2^2 - r^2), & R_1 \le r \le R_2. \end{array}\right\} \tag{1b.7}$$

To study the stability and bifurcation of core-annular flow, it is necessary to introduce an *extended* core-annular flow, for which in (1b.7) we write $0 \le r \le R(\theta, x, t)$ and $R(\theta, x, t) \le r \le R_2$, respectively (see chapter I.3 (e) for a discussion on extending the definition of the basic flow).

VI.1(c) Perturbation Equations

We now perturb extended core-annular flow

$$\hat{\mathbf{U}} = (u, v, W + w), \ \hat{P} = P + p, \ R = R_1 + \delta(\theta, x, t) \tag{1c.1}$$

and consider the linearized equations for (u, v, w, p, δ).

$$\left.\begin{aligned} \rho_l\left[\frac{\partial u}{\partial t} + W\frac{\partial u}{\partial x}\right] &= -\frac{\partial p}{\partial r} + \mu_l\left[\nabla^2 u - \frac{u}{r^2} - \frac{2}{r^2}\frac{\partial v}{\partial \theta}\right], \\ \rho_l\left[\frac{\partial v}{\partial t} + W\frac{\partial v}{\partial x}\right] &= -\frac{1}{r}\frac{\partial p}{\partial \theta} + \mu_l\left[\nabla^2 v - \frac{v}{r^2} + \frac{2}{r^2}\frac{\partial u}{\partial \theta}\right], \\ \rho_l\left[\frac{\partial w}{\partial t} + W\frac{\partial w}{\partial x} + W' u\right] &= -\frac{\partial p}{\partial x} + \mu_l\nabla^2 w, \ \frac{1}{r}\frac{\partial}{\partial r}(ru) \\ &\quad + \frac{1}{r}\frac{\partial v}{\partial \theta} + \frac{\partial w}{\partial x} = 0, \end{aligned}\right\} \tag{1c.2}$$

where $(\rho_l, \mu_l) = (\rho_1, \mu_1)$ in $r < R_1$ and (ρ_2, μ_2) in $r > R_1$ and $W' = dW/dr$. Moreover,

$$u = v = w = 0 \text{ at } r = R_2, \tag{1c.3}$$

u, v, w are bounded at $r = 0$ and satisfy other conditions to be stated later. At the linearized position of the interface $r = R_1$, we find that

$$u = W\delta_x + \delta_t, \ \bar{\delta} = 0, \tag{1c.4a}$$

where $\bar{\delta}$ is the average value of δ,

$$[\![u]\!] = [\![v]\!] = 0, \tag{1c.4b}$$

$$\left[\!\!\left[\mu\left(\frac{\partial u}{\partial x} + \frac{\partial w}{\partial r}\right)\right]\!\!\right] = 0, \tag{1c.4c}$$

$$\left[\!\!\left[\mu\left(\frac{\partial u}{\partial \theta} + R_1\frac{\partial v}{\partial r} - v\right)\right]\!\!\right] = 0, \tag{1c.4d}$$

$$-[\![p]\!] + 2\left[\!\!\left[\mu\frac{\partial u}{\partial r}\right]\!\!\right] = \frac{T}{R_1^2}(\delta_{\theta\theta} + R_1^2\delta_{xx} + \delta), \tag{1c.4e}$$

and

$$[\![W']\!]\delta + [\![w]\!] = 0. \tag{1c.5}$$

Equation (1c.5) shows that w is not continuous across $r = R_1$, and it is this jump in the shear rate $[\![W']\!]$ that produces instability. We can eliminate $\delta = -[\![w]\!]/[\![W']\!]$ from our problem.

VI.1(d) Dimensionless Equations and Parameters

We shall now make our equations dimensionless. Lengths are scaled with the mean radius R_1, velocity is scaled with the centerline velocity

$$W_0 = F\{R_1^2(\mu_2 - \mu_1) + R_2^2\mu_1\}/4\mu_1\mu_2$$

and time with R_1/W_0. We shall use the same symbols for dimensional and dimensionless variables.

The differential equations satisfied by the dimensionless u, v, w, p are of the same form as (1c.2) with $\rho_l = 1$ and μ_l replaced by $1/\mathbb{R}_l$ where

$$\mathbb{R}_l = \rho_l W_0 R_1/\mu_l, \quad l = 1, 2. \tag{1d.1}$$

A dimensionless function $W(r)$ also appears in these equations and is given by

$$W(r) = \begin{cases} 1 - mr^2/(a^2 + m - 1), & 0 \le r \le 1 \\ (a^2 - r^2)/(a^2 + m - 1), & 1 \le r \le a \end{cases} \tag{1d.2}$$

where $$m = \mu_2/\mu_1 \le 1$$

is the viscosity ratio and $$a = R_2/R_1 \ge 1$$

is the dimensionless ratio of the outer cylinder. The ratio of the volume of the liquid outside to the volume of liquid inside is $a^2 - 1$. The boundary conditions (1c.3) are required to hold at $r = a$. The mean position of the dimensionless interface is at $r = 1$. Equation (1d.2) shows that $W(r)$ is continuous across $r = 1$

$$W(1) = (a^2 - 1)/(a^2 + m - 1), \tag{1d.3}$$

but, because the shear stress is continuous, the derivatives of W are different on sides 1 and 2 of $r = 1$

$$\left.\begin{aligned} W_1'(1) &= -2m/(a^2 + m - 1), \\ W_2'(1) &= -2/(a^2 + m - 1). \end{aligned}\right\} \tag{1d.4}$$

Equations (1c.4a, b) and (1c.5) are unchanged in form. Equations (1c.4$c - e$) take the following form in dimensionless variables

$$\left[\!\left[\frac{\zeta}{\mathbb{R}} \left(\frac{\partial u}{\partial x} + \frac{\partial w}{\partial r} \right) \right]\!\right] = 0, \tag{1d.5}$$

$$\left[\!\left[\frac{\zeta}{\mathbb{R}} \left(\frac{\partial u}{\partial \theta} + \frac{\partial v}{\partial r} - v \right) \right]\!\right] = 0, \tag{1d.6}$$

$$-[\![\zeta p]\!] + 2 \left[\!\left[\frac{\zeta}{\mathbb{R}} \frac{\partial u}{\partial r} \right]\!\right] = S(\delta_{\theta\theta} + \delta_{xx} + \delta), \tag{1d.7}$$

where p_i is scaled by $\rho_i W_0^2$,

$$\zeta_i = \frac{\rho_i}{\rho_1}, \tag{1d.8}$$

is a density ratio and

$$S = \frac{T}{\rho_1 W_0^2 R_1} \tag{1d.9}$$

is the dimensionless surface tension.

The parameter S has been used in previous studies of instability of two fluids, but it is not a good parameter because it depends strongly on the velocity or the rate of shear in the basic flow. It is better to use J defined by

$$S = \frac{J}{\mathbb{R}_1^2}, \quad J = \frac{TR_1}{\rho_1 \nu_1^2}. \tag{1d.10}$$

This is a surface tension parameter introduced by Chandrasekhar [1961] in his study of capillary instability of jets of viscous liquid in air, and R_1 is the dimensional radius of the undisturbed interface. The advantage of using the parameter J instead of S is that it measures surface tension, and involves variables that remain constant in an experiment.

For core-annular flow the parameter

$$J^* = TR_2/\rho_1 \nu_1^2, \quad J^* = aJ, \tag{1d.11}$$

is more convenient to use because it is given when the pipe radius is known, whereas the core radius would have to be known for J.

The problem is characterized by six dimensionless parameters: m, a, ζ_2, J, $\mathbb{R}_1$ and $\mathbb{R}_2$ of which five are independent: $\mathbb{R}_1/\mathbb{R}_2 = m/\zeta_2$ where $m = \mu_2/\mu_1$.

VI.1(e) Normal Modes

We replace $[u_l, v_l, w_l, p_l](r, \theta, x, t)$ and $\delta(\theta, x, t)$ with amplitude functions $[\mathrm{i}u_l, v_l, w_l, p_l](r)$ and an amplitude constant δ times $\exp[in\theta + \mathrm{i}\alpha(x - Ct)]$ in the usual way. The kinematic condition

$$u(1, \theta, x, t) = \delta_t + W(1)\delta_x$$

then reduces to

$$u(1) = \alpha(W(1) - C)\delta, \tag{1e.1}$$

giving δ. In each of the two regions, corresponding to $l = 1 (0 \le r \le 1)$ and $l = 2 (1 \le r \le a)$, we get

$$u' + \frac{u}{r} + \frac{n}{r}v + \alpha w = 0, \tag{1e.2}$$

$$\alpha(W_l - C)u = p' - \frac{\mathrm{i}}{\mathbb{R}_l}\left\{u'' + \frac{u'}{r} - \left(\alpha^2 + \frac{n^2+1}{r^2}\right)u - \frac{2n}{r^2}v\right\}, \tag{1e.3}$$

$$\alpha(W_l - C)v = -\frac{np}{r} - \frac{\mathrm{i}}{\mathbb{R}_l}\left\{v'' + \frac{v'}{r} - \left(\alpha^2 + \frac{n^2+1}{r^2}\right)v - \frac{2n}{r^2}u\right\}, \tag{1e.4}$$

$$\alpha(W_l - C)w + W_l' u = -\alpha p - \frac{\mathrm{i}}{\mathbb{R}_l}\left\{w'' + \frac{w'}{r} - \left(\alpha^2 + \frac{n^2}{r^2}\right)w\right\}. \tag{1e.5}$$

The boundary values of the amplitude functions are such that

$$u(a) = v(a) = w(a) = 0, \quad u(0), v(0), w(0), p(0) \text{ finite.} \tag{1e.6}$$

On the interface $r = 1$, we have

$$[\![u]\!] = [\![v]\!] = 0, \tag{1e.7}$$

$$[\![W']\!]u(1) + \alpha(W(1) - C)[\![w]\!] = 0, \tag{1e.8}$$

$$\left[\!\left[\frac{\zeta}{\mathbb{R}}(w' - \alpha u)\right]\!\right] = 0 \tag{1e.9}$$

$$\left[\!\left[\frac{\zeta}{\mathbb{R}}(v' - v - nu)\right]\!\right] = 0, \tag{1e.10}$$

$$-[\![\zeta p]\!] + 2\mathrm{i}\left[\!\left[\frac{\zeta}{\mathbb{R}}u'\right]\!\right] = \frac{J}{\mathbb{R}_1^2}(1 - \alpha^2 - n^2)\frac{u(1)}{\alpha(W(1) - C)}. \tag{1e.11}$$

We eliminate p from the system (1e.2) to (1e.11). Equations (1e.3) to (1e.4) are reduced to

$$\frac{\mathrm{i}}{\mathbb{R}_l}u'' + \left(\frac{\mathrm{i}}{\mathbb{R}_l}\frac{1}{r} + \frac{W_l'}{\alpha}\right)u' - \left\{\frac{\mathrm{i}}{\mathbb{R}_l}\left(\alpha^2 + \frac{n^2+1}{r^2}\right) - \frac{W_l''}{\alpha} - \alpha(W_l - C)\right\}u$$

$$+\frac{\mathrm{i}}{\alpha\mathbb{R}_l}w''' + \frac{\mathrm{i}}{\alpha\mathbb{R}_l}\frac{1}{r}w'' - \left\{\frac{\mathrm{i}}{\alpha\mathbb{R}_l}\left(\alpha^2 + \frac{n^2+1}{r^2}\right) - (W_l - C)\right\}w'$$

$$-\frac{2\mathrm{i}n}{\mathbb{R}_l}\frac{1}{r^2}v + \left\{\frac{2\mathrm{i}n^2}{\alpha\mathbb{R}_l}\frac{1}{r^3} + W_l'\right\}w = 0 \qquad (1e.12)$$

and

$$\left\{\frac{2\mathrm{i}}{\mathbb{R}_l}\frac{1}{r^2} + \frac{W_l'}{\alpha}\frac{1}{r}\right\}nu + \left\{\frac{\mathrm{i}}{\mathbb{R}_l}\left(\alpha^2 + \frac{n^2+1}{r^2}\right) - \alpha(W_l - C)\right\}v$$

$$-\frac{\mathrm{i}}{\mathbb{R}_l}v'' - \frac{\mathrm{i}}{\mathbb{R}_l}\frac{1}{r}v' + \frac{n\mathrm{i}}{\alpha\mathbb{R}_l}\frac{1}{r}w''$$

$$+\frac{n\mathrm{i}}{\alpha\mathbb{R}_l}\frac{1}{r^2}w' - \frac{n}{r}\left\{\frac{\mathrm{i}}{\alpha\mathbb{R}_l}\left(\alpha^2 + \frac{n^2}{r^2}\right) - (W_l - C)\right\}w = 0. \qquad (1e.13)$$

where $l = 1, 2$ corresponds to regions one and two.

We eliminate $[\![\zeta p]\!]$ from the normal stress condition (1e.11) by equating it to $[\![\zeta p]\!]$ obtained by evaluating (1e.5) at $r = 1$. After some simplifications, using the other interface conditions, we get

$$\frac{J}{\mathbb{R}_1^2}(1 - \alpha^2 - n^2)\frac{[\![w]\!]}{[\![W']\!]} + 2\mathrm{i}\left[\!\left[\frac{\zeta}{\mathbb{R}}u'\right]\!\right] + \frac{\mathrm{i}}{\alpha}\left[\!\left[\frac{\zeta}{\mathbb{R}}\{w'' + w' - (\alpha^2 + n^2)w\}\right]\!\right]$$

$$+(W - C)\left\{[\![w\zeta]\!] - \frac{[\![W'\zeta]\!]}{[\![W']\!]}[\![w]\!]\right\} = 0. \qquad (1e.14)$$

The governing equations are (1e.2), (1e.6) - (1e.10), (1e.12), (1e.13) and (1e.14).

We next discuss the conditions (1e.6) at $r = 0$. The following conditions are inferred from the fact that the velocity at the origin $\mathbf{u}(0, \theta, x, t)$ must not depend on θ; otherwise, the velocity would be multi-valued at the origin. We may decompose $\mathbf{u}$ into an axial part $\mathbf{e}_x w$, and a part that lies in a cross-section, which will be named the "tangential" part, $\mathbf{e}_t u_t = \mathbf{e}_r u + \mathbf{e}_\theta v$. Of course, $w(0, x)\mathrm{e}^{\mathrm{i}n\theta}$ is independent of θ when $n = 0$, or when $n \neq 0$ and $w(0, x) = 0$. The tangential velocity

$$u_t = \cos\theta[\mathrm{i}u(0, x)\mathrm{e}^{\mathrm{i}n\theta}] - \sin\theta[v(0, x)\mathrm{e}^{\mathrm{i}n\theta}]$$

is independent of θ when

$$\frac{\partial u_t}{\partial\theta} = -\{(nu + v)\cos\theta + \mathrm{i}\,\sin\theta(u + nv)\}\mathrm{e}^{\mathrm{i}n\theta} = 0.$$

When $n \neq 1$, u_t cannot be independent of θ unless $u(0, x)$ and $v(0, x)$ are both zero because of the presence of the $\cos\theta$ and $\sin\theta$ terms. Therefore,

u_t is zero. When $n = 1$, it is enough to have $u(0)+v(0) = 0$. The tangential component u_t need not vanish when $n = 1$. Some further conditions at $r = 0$ can be deduced from (1e.2) at $r = 0$, using the results just obtained.

$$\lim_{r\to 0}\left\{\alpha w + u' + \frac{u+nv}{r}\right\} = \alpha w(0) + 2u'(0) + nv'(0) = 0.$$

Summarizing our results,

$$\left.\begin{array}{ll} n=0: & u(0)=v(0)=\alpha w(0)+2u'(0)=0, \\ n=1: & u(0)+v(0)=w(0)=0, \\ n\geq 2: & u(0)=v(0)=w(0)=0. \end{array}\right\} \qquad (1e.15)$$

We define system I for u, v and w to be equations (1e.2), (1e.7) - (1e.10), (1e.12), (1e.13) and (1e.14). We define system II to be the equations for u and v alone which can be derived from system I by using (1e.2) to eliminate w. System II is defined by the condition

$$u(a) = v(a) = u'(a) = 0 \qquad (1e.16a, b, c)$$

and the following equations in the two regions $l = 1$, 2:

$$f_l \stackrel{\text{def}}{=} \mathrm{i}\alpha \mathbb{R}_l (W_l(r) - C)r^2,$$

$$\begin{aligned} r^4 u'''' + 2r^3 u''' - [f_l + 2\alpha^2 r^2 + n^2 + 3]r^2 u'' \\ -[f_l + 2\alpha^2 r^2 - n^2 - 3]ru' + [f_l(\alpha^2 r^2 + 1) \\ +\alpha^4 r^4 + (n^2+2)\alpha^2 r^2 + 3n^2 - 3]u + nr^3 v''' - 2nr^2 v'' \\ -[f_l + \alpha^2 r^2 + n^2 - 3]nrv' + [f_l - \mathrm{i}\alpha \mathbb{R}_l W_l' r^3 \\ +3(\alpha^2 r^2 + n^2 - 1)]nv = 0, \end{aligned} \qquad (1e.17)$$

$$\begin{aligned} nr^3 u''' + 2nr^2 u'' - [f_l + \alpha^2 r^2 + n^2 + 1]nru' \\ -[f_l - \mathrm{i}\alpha \mathbb{R}_l W_l' r^3 + 3\alpha^2 r^2 + n^2 - 1]nu \\ +(\alpha^2 r^2 + n^2)r^2 v'' + (\alpha^2 r^2 - n^2)rv' - [f_l(\alpha^2 r^2 + n^2) + \alpha^4 r^4 \\ +(2n^2+1)\alpha^2 r^2 + n^2(n^2-1)]v = 0. \end{aligned} \qquad (1e.18)$$

At the interface $r = 1$, we have

$$[\![u]\!] = [\![v]\!] = 0, \qquad (1e.19a, b)$$

$$(m-1)W_2'(1)u_2 - (W(1) - C)[\![u']\!] = 0, \qquad (1e.20)$$

$$v_1' - mv_2' + (m-1)v + n(m-1)u = 0, \qquad (1e.21)$$

$$u_1'' + u_1' + (\alpha^2 + n^2 - 1)(1-m)u - mu_2'' - mu_2' = 0, \qquad (1e.22)$$

$$u_1''' + 2u_1'' - (f_1 + 3\alpha^2 + n^2 + 1)u_1' + nv_1'' - nv_1'$$
$$- mu_2''' - 2mu_2'' + [f_1\zeta_2 + m(3\alpha^2 + n^2 + 1)]u_2'$$
$$+ [f_1(\zeta_2 - 1) - i\alpha\mathbb{R}_1 W_2'(1)(\zeta_2 - m) + (m-1)(\alpha^2 + n^2 - 1)]u$$
$$- nmv_2'' + nmv_2' + [f_1(\zeta_2 - 1) + (m-1)(\alpha^2 + n^2 - 1)]nv$$
$$+ \frac{i\alpha J}{\mathbb{R}_1(W(1) - C)}(\alpha^2 + n^2 - 1)u = 0. \qquad (1e.23)$$

Equation (1e.23) may be put into a more convenient form, using (1e.20)

$$u_1''' + 2u_1'' - (3\alpha^2 + n^2 + 1)u_1' + nv_1'' - nv_1'$$
$$- mu_2''' - 2mu_2'' + \{f_1(\zeta_2 - 1) + m(3\alpha^2$$
$$+ n^2 + 1)\}u_2' + \{f_1(\zeta_2 - 1) - i\alpha\mathbb{R}_1(\zeta_2 - 1)W_2'(1) + (m-1)(\alpha^2$$
$$+ n^2 - 1)\}u_2 + \{f_1(\zeta_2 - 1) + (m-1)(\alpha^2 + n^2 - 1)\}nv_2 - nmv_2''$$
$$+ nmv_2' + \frac{i\alpha J(\alpha^2 - n^2 - 1)}{\mathbb{R}_1(W(1) - C)}u_2 = 0. \qquad (1e.24)$$

In the axisymmetric case ($n = 0$), the equations for u and v decouple and the unstable eigenvalues are determined from the equations for $u(r)$. The v-equation gives rise only to stable eigenvalues. Most of the results given below are computed for the case of matched density ($\zeta_2 = 1$) and axisymmetric disturbances ($n = 0$). In this case, u is governed by

$$r^4 u'''' + 2r^3 u''' - [f_l + 2\alpha^2 r^2 + 3]r^2 u''$$
$$- [f_l + 2\alpha^2 r^2 - 3]ru' + [f_l(\alpha^2 r^2 + 1)$$
$$+ \alpha^4 r^4 + 2\alpha^2 r^2 - 3]u = 0, \qquad (1e.25)$$

where $u_1(0)$=0 and $u_1(r)$ has bounded derivatives at $r = 0$,

$$u_2(a) = u_2'(a) = 0, \qquad (1e.26)$$

and, at the interface, $r = 1$

$$u_1 = u_2, \qquad (1e.27a)$$

$$(m-1)W_2'(1)u - (W(1) - C)(u_1' - u_2') = 0,$$
$$u_1'' + u_1' + (\alpha^2 - 1)(1 - m)u - mu_2'' - mu_2' = 0,$$
$$u_1''' + 2u_1'' - (3\alpha^2 + 1)u_1' - mu_2''' - 2mu_2'' + m(3\alpha^2 + 1)u_2'$$
$$+ (m-1)(\alpha^2 - 1)u_2 + \frac{i\alpha J(\alpha^2 - 1)}{\mathbb{R}_1(W(1) - C)}u_2 = 0. \qquad (1e.27b)$$

System II was used in JRR and solved numerically with the Chebyshev-tau method [Orszag 1971]. We next comment on the conditions (1e.6) at $r = 0$ with respect to system II for the benefit of anyone contemplating the use of it. When eliminating w from the continuity equation (1e.2), there is a division by r: thus, even if we impose the condition that u and v are smooth at $r = 0$, we allow w to have an unphysical $\frac{1}{r}$-singularity. Using the method of Frobenius, the conditions at $r = 0$ can be stated more precisely as follows. The equation (1e.5) has a regular singular point at 0, and -1 is the root of the indicial equation precisely for $n = 1$. Since the second root is $+1$, the unbounded solution generally behaves like $\frac{1}{r} + ar \log r$ near $r = 0$. It can be shown that the coefficient a of the logarithmic term vanishes if and only if $C = W_1(0) - 3\alpha i/\mathbb{R}_1$. This mode appears in the computed list of eigenvalues as an extra eigenvalue for $n = 1$, and is simply dismissed.

VI.1(f) Pseudospectral Numerical Method

A collocation method using Chebyshev polynomials $T_k(y)$ was used to integrate System I. Following Orszag and Kells [1980], we expand $(u, v, w)(r)$ in terms of

$$T_k(y) = \cos(k \arccos y), \quad k = 0, 1, 2, ..., N \tag{1f.1}$$

where N is a truncation number. To use this representation for the discretization in the radial direction, we must map each of the regions occupied by the two fluids into $[-1, 1]$. In region 1, $r \to y$ where

$$r = \frac{y + 1}{2}, \tag{1f.2}$$

and in region 2, $r \to y$ where

$$r = \frac{(1 - a)y + 1 + a}{2}. \tag{1f.3}$$

The interface $r = 1$ maps into $y = 1$ for both regions.

In each region $i = 1, 2$, we define the following interpolation functions of y:

$$[I_N u, I_N v, I_N w] = \sum_{k=0}^{N} [\hat{u}_k, \hat{v}_k, \hat{w}_k] T_k(y). \tag{1f.4}$$

The collocation points are chosen to be

$$y_j = \cos \frac{\pi j}{N}, \quad j = 0, 1, ..., N \tag{1f.5}$$

where j = N is a boundary point and $j = 0$ is an interface point. In the core, the centerline conditions are imposed at the boundary point.

The interpolation functions must be determined by computing the coefficients ($\hat{u}_k$, $\hat{v}_k$, $\hat{w}_k$). The $N + 1$ coefficients $\hat{u}_k$ can be determined by

setting the discretized velocity (1f.4) evaluated at the collocation points equal to the original continuous velocity at those points:

$$I_N u(y_j) = u(r_j), \tag{1f.6}$$

where r_j is the point that is mapped into y_j. The coefficients $\hat{v}_k$ and $\hat{w}_k$ can be obtained in the same way. Thus, there are $3(N+1)$ velocity coefficients to be determined from the discretization of system I. The derivatives in the differential equation are discretized in the following way:

$$\left.\frac{d^p I_N u}{dy^p}\right|_{y_k} = \sum_{j=0}^{N} u(y_j)(D_p)_{kj}, \tag{1f.7}$$

where $u(y_j)$ is the function value evaluated at the collocation point [Canuto, Hussaini, Quarteroni and Zang 1988],

$$\left.\begin{aligned}
(D_1)_{kj} &= \frac{\bar{C}_k}{\bar{C}_j}\frac{(-1)^{j+k}}{y_k - y_j}, && k \neq j, \\
(D_1)_{jj} &= -\frac{y_j}{2(1-y_j^2)}, && 1 \leq k = j \leq N-1, \\
(D_1)_{00} &= \frac{2N^2+1}{6} = -(D_1)_{NN}, && \\
\bar{C}_N &= \bar{C}_0 = 2, && \\
\bar{C}_j &= 1, && 1 \leq j \leq N-1 \\
\text{and} \quad D_p &= (D_1)^p. &&
\end{aligned}\right\} \tag{1f.8}$$

There are $3(N-1)$ equations for u, v, w arising from (1e.2), (1e.12) and (1e.13) at interior points of collocation in the annulus and $3(N-1)$ equations in the core. There are three boundary conditions at the wall and three centerline conditions in the core and six interface conditions; hence $3(N+1)$ in each region and $6(N+1)$ in all. The $6N+6$ linear equations in $6N+6$ unknowns form a linear eigenvalue problem of the type

$$(\mathbf{A} + c\mathbf{B}) \cdot \mathbf{x} = 0 \tag{1f.9}$$

This eigenvalue problem was solved using the IMSL routine EIGZC.

The convergence of the discretization scheme was tested by increasing the truncation number N. Converged eigenvalues $C(N)$ would not change as N is increased, as opposed to any spurious eigenvalues. The convergence was satisfactory in our range of parameters when $N \geq 14$.

The numerical results were checked against those of JRR [1983] which are based on the Chebyshev-τ method (see section III.3 for this numerical scheme applied to the two-layer Benard problem). To compare the results with JRR, we put the density ratio $\zeta_2 = \rho_2/\rho_1$ to one, $S = 0$, the Reynolds number of JRR is Re and their complex wave speed is designated as C_R, related to our $\mathbb{R}_1$ and C by

$$Re = \frac{a^3}{(a^2+m-1)m}\mathbb{R}_1, \quad C_R = \frac{a^2+m-1}{a^2}C, \qquad (1f.10)$$

where $m = \mu_2/\mu_1 < 1$. The m used by JRR is $\mu_1/\mu_2 > 1$. Our results also agree with stability results for one fluid presented by Salwen and Grosch [1972] and Salwen, Cotton and Grosch [1980], which JRR reproduced.

Our numerical results for the longest and shortest waves were checked against the asymptotic formulas in section VI.1 (h) and section VI.1(i), respectively.

VI.1 (g) Axisymmetric and Nonaxisymmetric Disturbances

The pseudospectral numerical code handles both non-axisymmetric and axisymmetric disturbances, but we will present results only for $n = 0$ for the following reasons. In the range of parameters that was examined, PCJ did not find situations in which instability occurs for $n \neq 0$, with stability for $n = 0$.

Numerical results for a few discrete values of α were presented by JRR. In their work, the density difference is zero ($\zeta_2 = 1$) and surface tension is zero. Their results show that in some parameter ranges, the axisymmetric and the nonaxisymmetric modes can behave quite differently. For instance, when the less viscous fluid is in the core, it is possible for the $n = 0$ mode to be stable and the higher modes to be unstable. However, this type of viscosity stratification is not pursued here since we focus on having a thin layer of a much less viscous fluid at the wall. In our situation, numerical studies indicate that if the growth rates for $n = 0, 1, \ldots$ are compared for all wavenumbers, then the highest growth rate is achieved by the $n = 0$ mode. Short waves are stabilized by surface tension so that waves with $n >> 1$ tend to be stable: the larger the n, the greater the stability. In addition, experience has shown that it is the mode with the highest growth rate that is most likely to be observed in experiments. This does not, however, rule out the possibility or importance of an instability due to the $n = 1$ mode. In fact, the corkscrew waves pictured in figure V.1.3 are nonaxisymmetric. This area needs further study.

JRR found that the high azimuthal modes are unstable, but the magnitude of $\mathrm{Im}(C)$ decreases asymptotically with the mode number. This instability of the higher modes and also for large α is a manifestation of the short-wave instability (cf. sections IV.5, VI.1(i)) when surface tension is zero.

There is one type of instability (the capillary instability) for which the axisymmetric disturbance ought to be the most dangerous. The effect of surface tension appears only in the normal stress condition (1e.14) at the interface and is in the form $J(1 - \alpha^2 - n^2)$ where α is a positive real number and n is the azimuthal wave number. It is known that long waves are destabilized by surface tension; for example, there is instability even

with $n = \alpha = 0$. For long wave instability, $J(1 - \alpha^2 - n^2) > 0$: in order for this to be satisfied, we must have $n = 0$ and also $\alpha < 1$. This instability, it turns out, is analogous to a capillary instability and it is axisymmetric.

VI.1(h) Perturbation Solution for Long Waves

The stability problem has been solved explicitly in the limit of long waves ($\alpha \to 0$) by Hickox [1971] using the method of Yih [1967], in which the variables are expanded in a power series in α (see also sections III.4, where the method is used for the two-layer Benard problem, and IV.4, where the method is used for plane channel flows). The formulas in this section have been checked against Hickox's results.

The axisymmetric problem can be obtained from (1e.16a, c), (1e.17), (1e.19a), (1e.20), (1e.22), (1e.23). The v-problem (1e.16b), (1e.18), (1e.19b), (1e.21) is decoupled and gives rise only to stable eigenvalues. Thus,

$$u(r, \alpha) = u^{(0)}(r) + \alpha u^{(1)}(r) + O(\alpha^2), \tag{1h.1}$$

$$C(\alpha) = C^{(0)} + \alpha C^{(1)} + O(\alpha^2). \tag{1h.2}$$

At zeroth order, we get

$$C^{(0)} = \frac{a^2(a^2 - 1)}{a^4 + m - 1}. \tag{1h.3}$$

At first order,

$$C^{(1)} = i\mathbb{R}_1 \frac{1 - m}{m} \frac{(a^2 - 1)^2 G - (a^4 + m - 1)H}{(a^2 + m - 1)(a^4 + m - 1)}, \tag{1h.4}$$

where

$$G = -2(3a^2 + 2m - 3)\hat{\alpha}_1 - 3(8a^2 + 5m - 8)\hat{\beta}_1 + 2(a^6 + 3a^2 + 3m - 4)\hat{\alpha}_2$$
$$+3(a^8 + 8a^2 + 6m - 9)\hat{\beta}_2 + (2a^2 + m - 2)\hat{k},$$
$$H = (2a^6 - 3a^4 + 6a^2 - 5 - 12\ \ln a\hat{\alpha}_2 + (3a^8 - 4a^6 + 24a^2 - 23 - 48\ \ln a)\hat{\beta}_2$$
$$-6(a^2 - 1 - 2\ \ln a)(\hat{\alpha}_1 + 4\hat{\beta}_1 - \frac{\hat{k}}{3})$$
$$\hat{\alpha}_1 = \frac{a^2 + m - 1}{a^4 + m - 1} \frac{m}{24}, \qquad \hat{\alpha}_2 = \frac{2a^2 + 2m - 2 - ma^2}{(a^2 + m - 1)(a^4 + m - 1)} \frac{a^2}{24},$$
$$\hat{\beta}_1 = \frac{-m^2}{144(a^2 + m - 1)}, \qquad \hat{\beta}_2 = \frac{-1}{144(a^2 + m - 1)},$$

$$\hat{k} = \frac{(a^2 + m - 1)(a^4 + m - 1)S}{16(1 - m)}$$
$$- \frac{(\zeta_2 - 1)}{8} \frac{(a^2 - 1)^2(a^4 + 2(m - 1)a^2 - m + 1)}{(a^2 + m - 1)(a^4 + m - 1)}. \tag{1h.5}$$

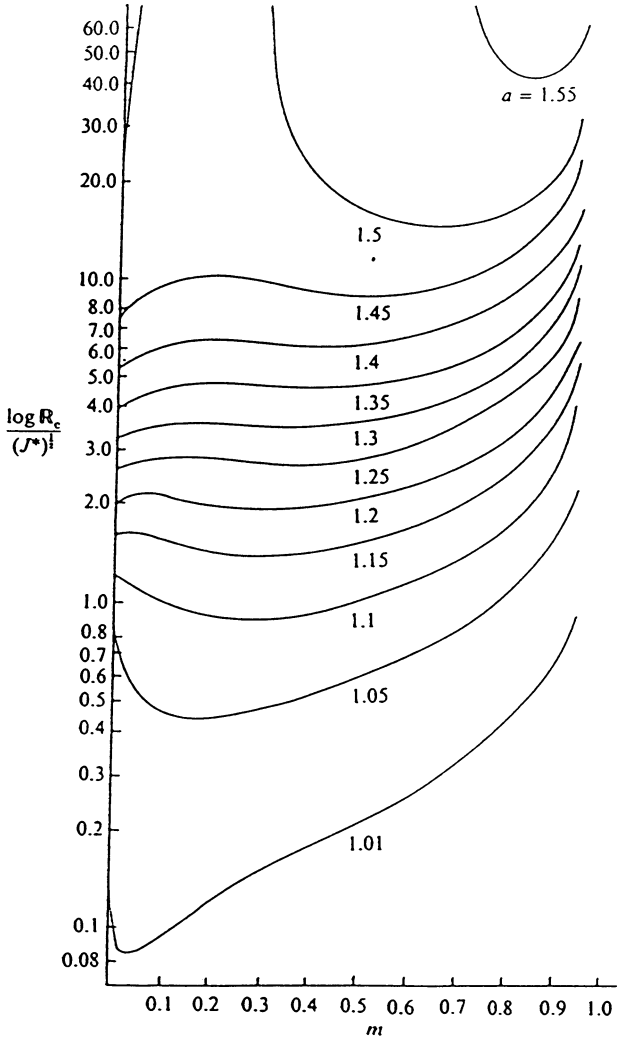

Fig. 1.1. [Preziosi, Chen and Joseph, 1989] $\mathbb{R}_c/(J^*)^{\frac{1}{2}}$ as a function of m for long waves ($\alpha \to 0$) with a as a parameter. The numbers on the vertical axis give values of $\mathbb{R}_c/(J^*)^{\frac{1}{2}}$.

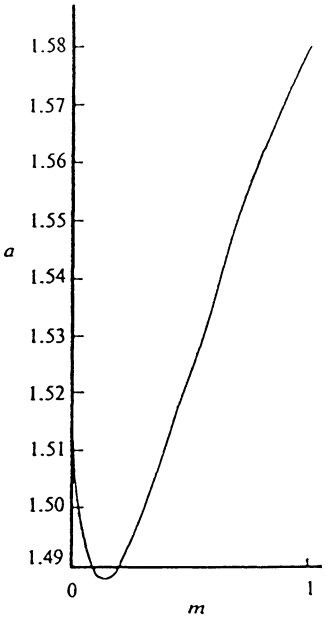

Fig. 1.2. [Preziosi, Chen and Joseph, 1989] The value $\hat{a}(m)$ for which $\mathbb{R}_c(a, m) \to \infty$. At $m = 0.9999$, $\hat{a} = 1.5805$. At $m = 0.15$, $\hat{a} = 1.4889$. The region above the curve is unstable at any $\mathbb{R}$.

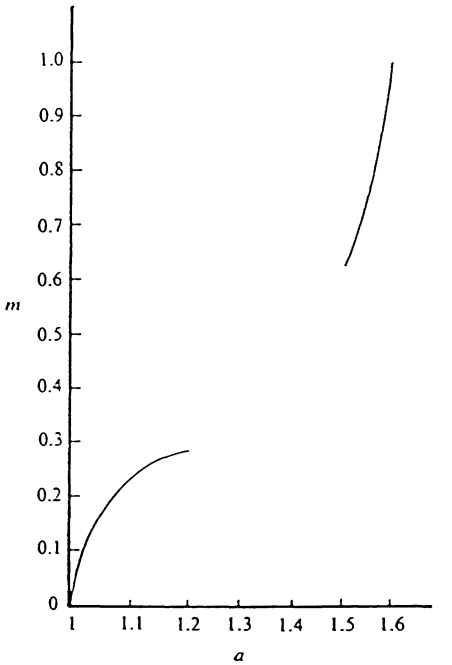

Fig. 1.3. [Preziosi, Chen and Joseph, 1989] The best viscosity ratio $\hat{m}(a)$ for minimizing instability to long waves ($\alpha \to 0$) according to (1h.12). For the gap in the curve, the values lie on the horizontal axis. This graph is obtained from figure 1.1 by seeking the critical Reynolds number for each curve.

To find points of the neutral curves for $\alpha \to 0$, put $C^{(1)}=0$ and solve for

$$\frac{J}{2\mathbb{R}_c^2(1-m)} =$$

$$8[(a^4+m-1)H_0-(a^2-1)^2G_0]/\Big((a^2+m-1)(a^4+m-1)$$

$$[(-4a^4+ma^2-3m+4)(a^2-1)+4\ \ln a(a^4+m-1)]\Big)$$

$$+\frac{(\zeta_2-1)(a^2-1)[a^4+2(m-1)a^2-m+1]}{(a^2+m-1)^2(a^4+m-1)^2}, \qquad (1h.6)$$

where H_0 and G_0 are the same as H and G after $\hat{k}$ is put to zero.

The flow is unstable for long waves $\alpha \to 0$ when

$$\frac{J^*}{a\mathbb{R}_1^2} = S > S_c = \frac{J^*}{a\mathbb{R}_c^2}. \tag{1h.7}$$

The coefficient of $\zeta_2 - 1$ in (1h.6) is positive whenever $a > 1$. Increasing the density of the liquid in the annulus stabilizes the flow against long waves when $m < 1$ and destabilizes when $m > 1$, but the effect is relatively weak. The effect of increasing the density of the liquid in the annulus destabilizes short waves when $m < 1$. Light lubricants are efficient against emulsification and heavy ones against capillarity.

We can write the criterion (1h.7) for instability as

$$\mathbb{R}_1 < \mathbb{R}_c. \tag{1h.8}$$

A greater than critical amount of shearing ($\mathbb{R}_1 > \mathbb{R}_c$) can stabilize capillary instabilities. We may express S_c as some function of a and m:

$$S_c = f^{-1}(a, m). \tag{1h.9}$$

Hence,

$$\mathbb{R}_c^2 = J^* f(a, m)/a. \tag{1h.10}$$

The lower critical Reynolds number varies with $(J^*)^{\frac{1}{2}}$. In figure 1.1, we show $\mathbb{R}_c/(J^*)^{\frac{1}{2}}$ as a function of m with a as a parameter. For each value of $a \leq 1.4889$, the values of $\mathbb{R}_c$ are finite for all $m \in [0, 1)$ and $\mathbb{R}_c \to \infty$ as $m \to 1$. When $a > 1.5805$, $\mathbb{R}_c = \infty$ for all $m \in [0, 1)$. When $1.4889 < a < 1.5805$, $\mathbb{R}_c(a, m)$ is finite for some m and is infinite for others. We may define $\hat{a}(m)$ as the a such that

$$\mathbb{R}_c(\hat{a}(m), m) \to \infty \tag{1h.11}$$

A graph of $\hat{a}(m)$ is shown as figure 1.2.

When $a < 1.5805$, there is a best viscosity ratio $m = \hat{m}(a)$ minimizing the region of instability to long waves:

$$\hat{\mathbb{R}}(a) = \min_{0 \leq m < 1} \mathbb{R}_c(a, m) = \mathbb{R}_c(a, \hat{m}(a)). \tag{1h.12}$$

The graph of $\hat{m}(a)$ is shown in figure 1.3 and the graph of $\hat{\mathbb{R}}(a)$ is figure 1.4.

VI.1(i) Perturbation Solution for Short Waves

Hooper and Boyd [1983] have considered the linear theory of stability of an unbounded plane Couette flow with constant shear rates above and below a flat interface, matched so that the shear stress is continuous. Their analysis is presented in section IV.5 and is relevant locally in the limit of short

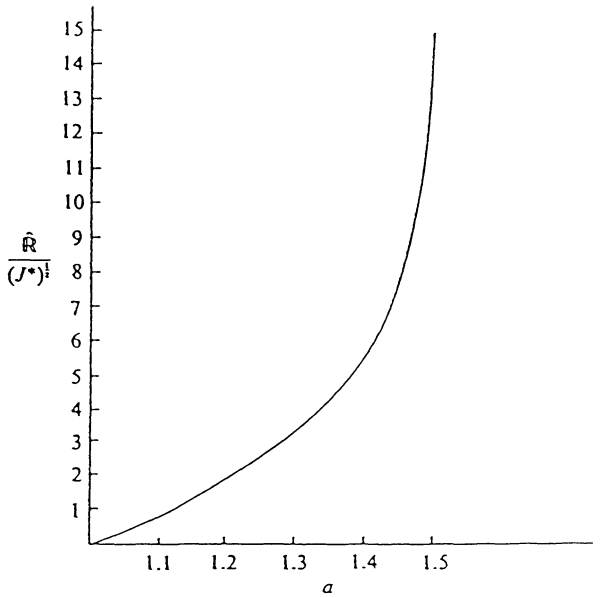

Fig. 1.4. [Preziosi, Chen and Joseph, 1989] Stability limit for long waves $\alpha \to 0$ defined by (1h.12). When $a = 1.5805$, $\hat{\mathbb{R}}(a) = +\infty$, and the interface will undergo a capillary instability to long waves ($\alpha \to 0$) at any $\mathbb{R}_1$. At $a = 1.55$, $\hat{\mathbb{R}}/(J^*)^{\frac{1}{2}} = 40.4$.

waves, $\alpha \to \infty$ or $n \to \infty$, and it predicts instability whenever surface tension vanishes. Surface tension can be included in their perturbation scheme provided that $\alpha^3 S \leq O(1)$ as $\alpha \to \infty$, or $n^3 S \leq O(1)$ as $n \to \infty$, and this stabilizes the short waves. Their perturbation scheme can be modified to apply to the situation where $S = O(1)$ (see equations (5.53) - (5.54) of section IV.5). The asymptotic expansion for core-annular flow (supplied to us by K. Chen) is:

$$C = W(1) - \frac{1}{\alpha^3} \frac{19m(1-m)}{(1+m)^2(a^2+m-1)},$$

$$+i\mathbb{R}_1 \left(\frac{2(1-m)^2}{\alpha^3(1+m)(a^2+m-1)^2} - \frac{S}{2(1+m)} \right) + O(\frac{1}{\alpha^4}) \qquad (1i.1)$$

as $\alpha \to \infty$ with $\alpha^3 S = O(1)$. For the case where $S = O(1)$ and $\alpha \to \infty$, we let

$$C = W(1) + c_0 + O(\frac{1}{\alpha}) \qquad (1i.2)$$

and find

$$c_0 = \frac{-i\mathbb{R}_1 S}{2(1+m)}.$$

(See Renardy and Joseph [1985 a] for the application of the short-wave perturbation scheme for $\alpha \to \infty$ and for $n \to \infty$ for circular Couette flow.)

In figure 7 of PCJ, the results of the psuedospectral code are compared with those of Hooper and Boyd exhibited as figure 5 of their 1987 paper. We present a list of conversion factors. We attach the subscript HB to the symbols used by HB [1987].

$$\left.\begin{aligned} \mathbb{R}_{\mathrm{HB}} &= \frac{2(a-1)^2}{m(a^2+m-1)}\mathbb{R}, \quad \mathbb{R} = \mathbb{R}_1, \\ S_{\mathrm{HB}} &= \frac{(a^2+m-1)^2}{4(a-1)^3} S, \\ m_{\mathrm{HB}} &= 1/m, \\ \alpha_{\mathrm{HB}} &= (a-1)\alpha, \\ \frac{C_{\mathrm{HB}}}{\mathbb{R}_{\mathrm{HB}}} &= \frac{m(a^2+m-1)^2}{4(a-1)^3}\frac{C}{\mathbb{R}}. \end{aligned}\right\} \qquad (1i.3)$$

There is an error in the last conversion factor of equations (9.3) of PCJ which has been corrected in equations (1i.3) above. With this correction, there is agreement with the results of HB for large α_{HB}.

VI.1(j) $m \to 0$ for $\mathbb{R}_1 \neq 0$ is a Singular Limit

We have already mentioned that $m = 0$ is an important limit for lubricated pipelining. Since $m = \mu_2/\mu_1$, we get very small m when lubricating viscous crudes $\mu_1 = 1000$ P with water $\mu_2 = 1/100$ p: $m = 10^{-5}$.

Consider the axisymmetric problem (1e.25), (1e.26) and (1e.27). The Reynolds number for the water $\mathbb{R}_2$ appears only in the water equation (1e.25) when $1 \leq r \leq a$ and $\mathbb{R}_2 = \mathbb{R}_1/m$. If $\mathbb{R}_1 \neq 0$ and $m \to 0$, the water equation is inviscid

$$r^4 u_2'' - r^3 u_2' + (\alpha^2 r^2 + 1) r^2 u_2 = 0, \qquad (1j.1)$$

and two derivatives are lost. To solve this singular perturbation problem at zeroth order, it is necessary to discard certain boundary and interface conditions. The no-slip condition $u_2'(a) = 0$ and (1e.27b) are set aside. The shear stress condition (1e.22) reduces to

$$u_1'' + u_1' + (\alpha^2 - 1) u_1 = 0, \qquad (1j.2)$$

which is an uncoupled condition on u_1. On the other hand, (1e.23) reduces to

$$u_1''' + 2u_1'' - (f_1 + 3\alpha^2 + 1)u_1' + f_1\zeta_2 u_2' + \{f_1(\zeta_2 - 1) - i\alpha \mathbb{R}_1 W_2'(1)\zeta_2 + 1 - \alpha^2\}u_1 + \frac{i\alpha J(\alpha^2 - 1)u_1}{\mathbb{R}_1(W(1) - C)} = 0, \tag{1j.3}$$

whereas (1e.24) reduces to

$$u_1''' + 2u_1'' - (3\alpha^2 + 1)u_1' + f_1(\zeta_2 - 1)u_2' + \{f_1(\zeta_2 - 1) - i\alpha \mathbb{R}_1(\zeta_2 - 1)W_2'(1) + 1 - \alpha^2\}u_1 + \frac{i\alpha J(\alpha^2 - 1)u_1}{\mathbb{R}_1(W(1) - C)} = 0. \tag{1j.4}$$

These two equations couple the flow in the water to the flow in the oil through terms proportional to u_2'. Equations (1j.3) and (1j.4) are equivalent when (1e.20), or the first of (1e.27*b*), holds. If (1e.20) is discarded *ab initio*, we are obliged to use (1j.3). This is the form of the normal stress when the outer fluid is regarded as inviscid from the start and the continuity of the axial component of velocity (1c.5), which leads to (1e.20) is omitted.

Equation (1j.3) decouples from the water when $\zeta_2 = 0$. Then (1e.25), (1j.2) and (1j.3) are enough to determine the family of eigenvalues given by Chandrasekhar [1961] in his study of capillary instability of a viscous jet. To identify our problem with his, we note that when $m = 0, W_1(r) = 1$. Then put $\mathbb{R}_1(1-C) = \hat{C}$, which is equivalent to rescaling the time. To complete the formal identification of this problem with Chandrasekhar's, put $W_0 = \nu/R_1$, where W_0 is the centerline velocity. In dimensionless variables, Chandrasekhar's problem can be written as

$$\mathbf{u}_t = -\nabla p/\rho + \nabla^2 \mathbf{u} \quad \text{on} \quad 0 \le r \le 1$$

with $u = \delta_t, \quad u_x + w_r = 0, \quad -p/\rho + 2u_r = J(\delta_{\theta\theta} + \delta_{xx} + \delta) \quad \text{on} \quad r = 1.$

It follows that $\hat{C}$ depends on a wave number α and the surface tension parameter J. The limit $\nu \to 0, \quad J \to \infty$, corresponds to an inviscid jet, leading to Rayleigh's theory with maximum growth rate at $\tilde{\alpha} = 0.697$. The wave number $\tilde{\alpha}(J)$, $0 \le \tilde{\alpha} \le 1$, which maximizes the growth rate $\sigma = \text{Im } \alpha\hat{C}(\alpha, J)$ is an increasing function with $\tilde{\alpha}(\infty) = 0.697$. For small J, Chandrasekhar [1961] showed that to a good approximation $\sigma = T(1 - \alpha^2)/6\mu_1 R_1$: hence, $\tilde{\alpha}(0) = 0$. Small J may be interpreted as large viscosity. In other words, the most dangerous wave for very viscous jets is very long.

VI.1(k) The Limit $\mathbb{R}_1 \to 0$ and $m \neq 0$

This is not a singular limit: $\mathbb{R}_2 = \mathbb{R}_1/m$ tends to zero with $\mathbb{R}_1$ and we get Stokes' linearized equations in the oil and in the water. We again calculate eigenvalues $C = \hat{C}/\mathbb{R}_1$. Then, when $\mathbb{R}_1 \to 0$, $f_1 = -\mathrm{i}\alpha\hat{C}$ and $f_2 = -\mathrm{i}\alpha\hat{C}/m$, (1e.27$b$) reduces to

$$u_1' = u_2' \quad \text{at} \quad r = 1$$

and the last term of (1e.27b) is replaced by

$$-\mathrm{i}\alpha J(\alpha^2 - 1)u_2/\hat{C}.$$

This problem is independent of $\mathbb{R}_1$ and also of $W_l(r), l = 1, 2$, as it should be in the Stokes' flow limit.

Surface tension J is stabilizing when $\alpha > 1$ and destabilizing when $\alpha < 1$. In all cases for which $\mathbb{R}_1 \to 0$, core-annular flow was found to be stable when $\alpha > 1$ and unstable when $\alpha < 1$. This is shown clearly in figure 1.9 and in the neutral curves exhibited in sections VI.1 (ℓ) and (m). Values of $\tilde{\alpha}(a, m, J)$ of the fastest growing wave show that the Stokes' flow limit $\mathbb{R}_1 \to 0$ depends on a, m, and J. We recover the capillary instability of Chandrasekhar [1961] numerically by fixing $m \ll \mathbb{R}_1 \to 0$, and the capillary instability of Rayleigh [1879] by putting $J \to \infty$ when $m/\mathbb{R}_1$ is small and $\mathbb{R}_1 \to 0$.

VI.1 (ℓ) Neutral Curves

Some representative types of neutral curves are shown in figures 1.5 - 1.7, and 1.10 - 1.14. The results given in section VI.1 (m) are a fairly complete representation of what linear theory has to say about the experiments depicted in figure V.1.1.

Figure 1.5 illustrates a typical situation, with disjoint neutral curves: each neutral curve consists of an upper branch and a lower branch. The lower branch is associated with long waves leading to an instability caused by surface tension at low Reynolds numbers. This region is in the bottom left-hand corner of the $(\alpha, \mathbb{R}_1)$-plane. It terminates on $\alpha = 1$ for $\mathbb{R}_1 = 0$. The values $\mathbb{R}_1 = \mathbb{R}_c$ as a function of a and m when $\alpha = 0$ were given in section VI.1 (h). When $a > 1.5805$, disturbances with $\alpha = 0$ are unstable at all $\mathbb{R}$. We may define a critical stability limit for the lower branch

$$\tilde{\mathbb{R}}_{\mathrm{L}}(a, m, J^*) = \max_{\alpha \geq 0} \mathbb{R}_{\mathrm{cL}}(a, m, J^*, \alpha). \qquad (1\ell.1)$$

The flow is unstable to generalized capillary instability when $\mathbb{R}_1 < \mathbb{R}_L$.

The upper branch of the neutral curve is associated with larger α, shorter waves and larger Reynolds number. We may define a critical stability limit for the upper branch:

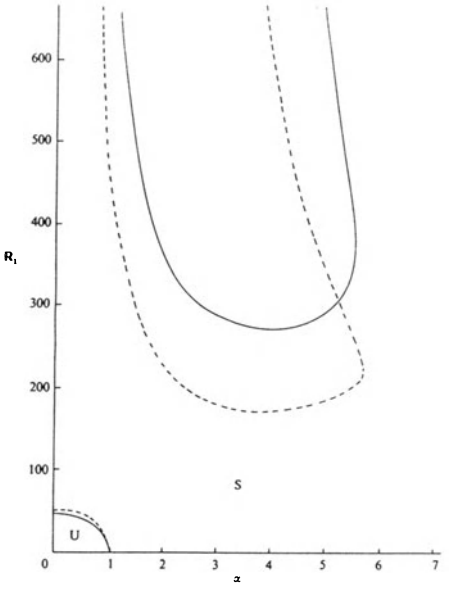

Fig. 1.5. [Preziosi, Chen and Joseph, 1989] Neutral curves $\mathbb{R}_c$ (a, m, J^*), $J^* = 930$, $a = 1.15$, $m = 0.05$ (– – –); $m = 0.1$ (——). The band of Reynolds numbers between the upper and lower critical branches is stable.

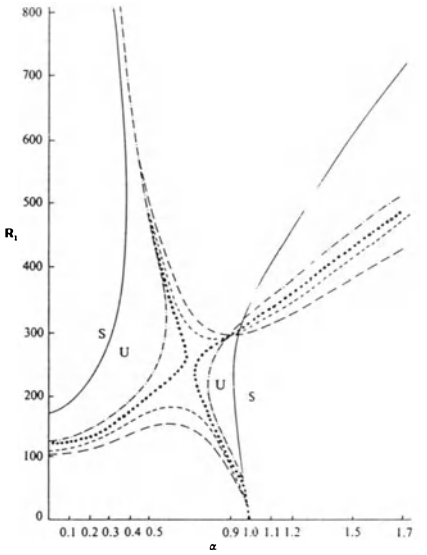

Fig. 1.6. [Preziosi, Chen and Joseph, 1989] Neutral curves $\mathbb{R}_c$ (a, m, J^*), $J^* = 930$, $a = 1.25$, $m = 0.9$ (——); $m = 0.8$ (–·–·–); $m = 0.78$ (○○○); $m = 0.75$ (- - - -); $m = 0.7$ (– – –). The stable band of Reynolds numbers disappears between $m = 0.78$ and $m = 0.75$.

$$\tilde{\mathbb{R}}_U(a, m, J^*) = \min_{\alpha \geq 0} \mathbb{R}_{cU}(a, m, J^*, \alpha). \tag{1\ell.2}$$

Core-annular flow (CAF) is unstable, evidently leading to emulsions, when

$$\mathbb{R}_1 > \tilde{\mathbb{R}}_U.$$

When

$$\tilde{\mathbb{R}}_L < \mathbb{R}_1 < \tilde{\mathbb{R}}_U \tag{1\ell.3}$$

we have stable CAF.

The topology of the neutral curves may change with the parameters. For instance, figure 1.6 shows a change of topology leading to the destruction of the upper and lower branches and the formation of the left and right neutral branches for $J^* = 930$, $a = 1.25$ for some m between 0.75 and 0.78. Left and right branches of the neutral curve $\mathbb{R}_c$ are also shown in figure 1.7.

Figure 1.8 is a graphical representation of $(1\ell.3)$ for $J^* = 930$, $a = 1.25$ for different values of m. CAF is stable in the enclosed region of the figure.

Figure 1.9 shows that increasing J^* stabilizes short waves ($\alpha >> 1$) and destabilizes long ones ($\alpha << 1$).

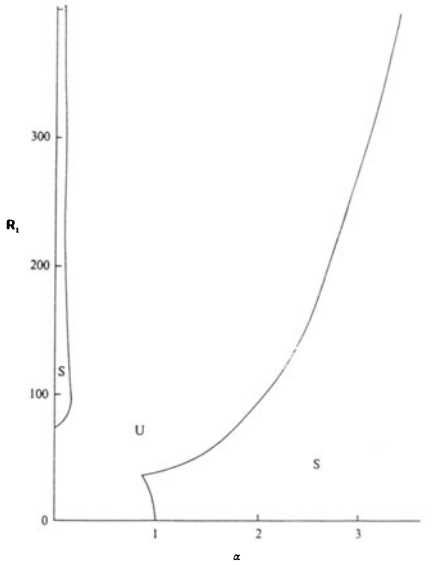

Fig. 1.7. [Preziosi, Chen and Joseph, 1989] Neutral curves $\mathbb{R}_c(a, m, J^*)$, $J^* = 930$, $a = 1.25$, $m = 0.01$. The lower critical condition and upper critical condition have merged. Stable core-annular flow is not possible.

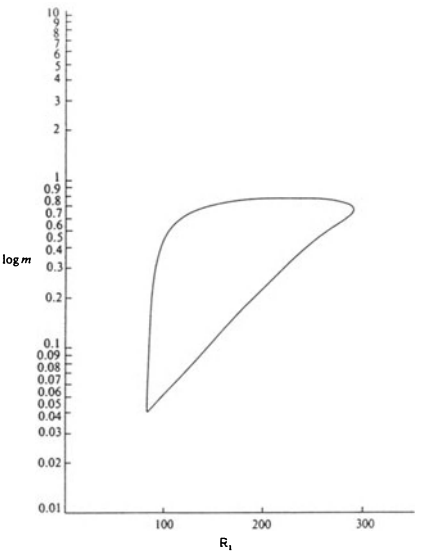

Fig. 1.8. [Preziosi, Chen and Joseph, 1989] Upper $\tilde{\mathbb{R}}_U(m)$ and lower $\tilde{\mathbb{R}}_L(m)$ critical Reynolds numbers for $a = 1.25$ and $J^* = 930$. Core-annular flow is stable in the enclosed region.

VI.1(m) Comparison with Experiments

Now we shall compare the results of the experiments of CGH with predictions based on the linear theory of stability applied to the axisymmetric mode. CGH presented pictures of the flow in eleven different cases (cf. figure V.1.1), for which we present the neutral curves and growth rates. The neutral curves are exhibited in figures 1.10 - 1.13 and the growth rates for the fastest growing waves are listed in the caption of figure 1.10, and in table 1.1.

The following three categories are used in the comparison and discussion to follow:

(1) Linear theory with the axisymmetric mode was used to predict the windows of the operating parameters for stable core-annular flow (CAF).
(2) The neutral curves were used to identify the nature of the instability which should be observed in the experiments. The aim was to discriminate between conditions in which they get bubbles and slugs of oil in water from those in which they got emulsions of water in oil.
(3) The length of the most rapidly growing wave was calculated in order to predict the length of slugs and bubbles which should arise from the capillary instability.

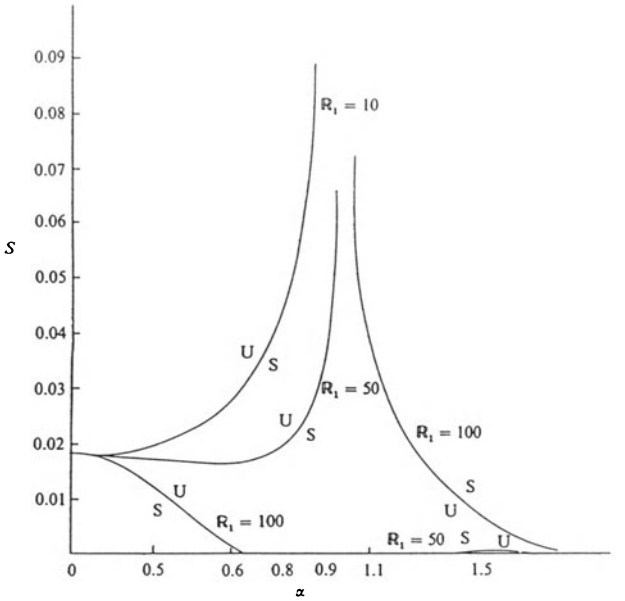

Fig. 1.9. [Preziosi, Chen and Joseph, 1989] Neutral curves in the (α, S)-plane for $a = 1.4$, $m = 0.5$. Increasing S at a fixed $\mathbb{R}_1$ is the same as increasing J. Increasing J at fixed α and $\mathbb{R}_c$ destabilizes long waves ($\alpha < 1$) and stabilizes short waves ($\alpha > 1$).

In all eleven experiments, except Experiment 2, CAF is unstable in the experiments and in the theory. In principle there is no reason why the flow observed under unstable conditions should correlate with the predictions of a linear theory. The bubbles, slugs and emulsions seen in the experiments are not small perturbations of CAF. Nevertheless, the predictions of the linear theory do seem to correlate with observations.

Table 1.1. Comparison of theory and experiment. The # refers to pictures shown in figure 1.1 of chapter V. $\sigma(\alpha) = \alpha \mathrm{Im}\ C(\alpha)$ is the growth rate and $\tilde{\alpha}$ is the wavenumber of the fastest growing wave. lR_2 is the length of a slug or the radius of a bubble.

Experiment			
#	a	$\mathbb{R}_1$	l_{exp}
3	1.42	69.80	4.5 (short slug)
			7.5 (long slug)
4	2.24	26.98	0.85 (bubble)
6	1.5	406.90	>15.75 (slug)
7	1.74	287.41	13.1 (slug)
8	2.80	134.50	0.69 (middle-most bubble)
9	1.81	795.97	6.0 or >15.75 (slug)
10	2.65	433.70	2.70 (longest slug)
11	4.63	221.69	0.3125 (largest bubble)

Theory			
#	$\tilde{a}$	$\sigma(\tilde{a})$	l
3	0.6	7.83518×10^{-2}	5.2665
4	0.66	2.91616×10^{-1}	0.8596
6	0.22	5.85969×10^{-3}	12.1856
7	0.08	2.34665×10^{-3}	21.4686
8	0.61	5.23881×10^{-2}	0.7060
9	0.32	6.8402×10^{-2}	4.7682
	0.023	5.39895×10^{-4}	66.3405
10	0.11	1.82720×10^{-2}	4.4199
11	0.64	2.41483×10^{-2}	0.4202

To apply the results of our stability calculation to the experiments, we need to convert the experimental data into parameters used in the analysis. Superficial velocity is defined as the volume flow rate divided by the area of the pipe. From the flow rates and the values of the material parameters, we may compute R_1 and W_0 for stable core-annular flow. This fixes all of the dimensional, hence, dimensionless, parameters used in the analysis. The solution is carried out in cgs units. The viscosity of water is given as 0.984 cP. For the oil viscosity (16.8 cp) listed in figure V.1.1, we get $m = 0.0532$. Carbon tetrachloride was added to the oil to increase the oil density. The density was matched ($\zeta_2 = 1$). The interfacial tension between the 16.8 cp oil and water was measured by the method of capillary rise and is given as 45 dyne/cm. (The capillary rise method is not accurate and the evaporation of carbon tetrachloride makes it likely that the surface tension value is not accurate and could have changed by as much as 5

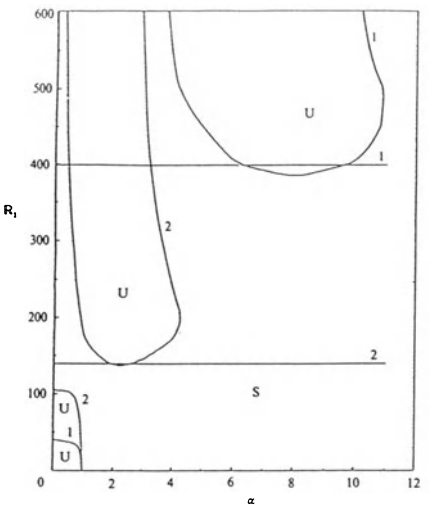

Fig. 1.10. [Preziosi, Chen and Joseph, 1989] Neutral curves corresponding to Experiments 1,2: $a = 1.08, 1.21$; $J^* = 2102$; $m = 0.0532$. The horizontal lines correspond to the Reynolds number of the experiments. For Experiment 2, the minimum value $\mathbb{R}_1 = 138.2$. Stable core-annular flow is observed with $\mathbb{R}_1 = 138.6$. The maximum growth rate $\hat{\alpha}\mathrm{Im}\, C = 2.747 \times 10^{-3}$ occurs at $\alpha = \hat{\alpha} = 2.24$. This flow is almost stable.

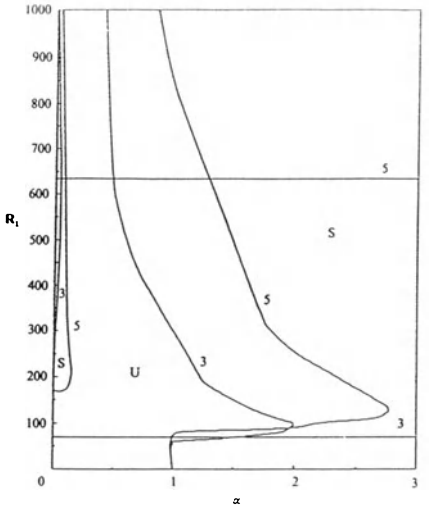

Fig. 1.11. [Preziosi, Chen and Joseph, 1989] Neutral curves corresponding to Experiments 3,5: $a = 1.42$, 1.31; $J^* = 2102$; $m = 0.0532$. Oil slugs in water are observed in Experiment 3. Water drops in oil are observed in Experiment 5.

dynes/cm from experiment to experiment.) In all the cases exhibited in figure V.1.1, water wets the wall of the cellulose acetate-butyrate. Let W_{1s} be the superficial velocity of the oil (called V in figure V.1.1) and W_{2s} the superficial velocity of water with $\xi = W_{1s}/W_{2s}$ from (1b.7) and

$$a = \left\{ \frac{1+\xi+(1+m\xi)^{\frac{1}{2}}}{\xi} \right\}^{\frac{1}{2}}, \quad W_0 = \frac{2W_{2s}}{m}(1+m\xi)^{\frac{1}{2}}[m-1+(1+m\xi)^{\frac{1}{2}}]. \tag{1m.1}$$

Then,

$$\left.\begin{aligned} \mathbb{R}_1 &= \frac{\rho_1 W_0 R_1}{\mu_1} = \frac{\rho_1 W_0 R_2}{a\mu_1}, \\ S &= \frac{T}{\rho_1 R_1 W_0^2} = \frac{aT}{\rho_1 R_2 W_0^2} = \frac{J^*}{a\mathbb{R}_1^2}. \end{aligned}\right\} \tag{1m.2}$$

The values of the superficial velocities are given in figure V.1.1.

The comparisons between theory and experiments are made in figures 1.10 - 1.13 (the neutral curves corresponding to the 11 drawings shown in figure V.1.1) and in table VI.1. The table gives the wavenumber $\alpha = \tilde{\alpha}$ corresponding to the maximum growth rate

$$\tilde{\alpha} C_{\mathrm{i}}(\tilde{\alpha}) = \max_{a \geq 0} \operatorname{Im} \alpha C(\alpha). \qquad (1m.3)$$

The dimensionless wavelength corresponding to $\tilde{\alpha}$ is $\tilde{\lambda} = 2\pi/\tilde{\alpha}$ and the dimensional one is $\tilde{\lambda} R_1$.

The window of parameters for stable CAF may be expressed as an interval

$$\tilde{\mathbb{R}}_{\mathrm{L}} < \mathbb{R}_1 < \tilde{\mathbb{R}}_{\mathrm{U}} \qquad (1m.4)$$

between the maximum $\mathbb{R}_1$ on the lower branch of the neutral branch and the minimum $\mathbb{R}_1$ on the upper branch. Such an interval exists when the lubricating layer is small but not when it is large. Recall that the flow is always unstable to long waves $\alpha \to 0$ when $a > 1.5805$.

The minimum $\tilde{\mathbb{R}}_{\mathrm{U}}$ decreases rapidly as a is increased. We may describe this result in terms of a critical Reynolds number

$$Re = \frac{(R_2 - R_1) W_0}{\nu_1} = \frac{\tilde{\mathbb{R}}_{\mathrm{U}}(a-1)}{m}$$

in the lubricating layer. The numerical results show that Re is a rather weak function of a and $Re \approx 660$. Hence, we get an approximation

$$\tilde{\mathbb{R}}_{\mathrm{U}} \approx \frac{m660}{(a-1)} = \frac{35.21}{a-1}.$$

On the other hand, the maximum value $\tilde{\mathbb{R}}_{\mathrm{L}}$ on the lower critical branch is an increasing function of $a - 1$ (see figure 1.4). Hence, as a increases, the interval (1m.4) shrinks; and the construction implied by the foregoing argument, shown in figure 1.14, indicates that CAF is always unstable under the experimental conditions ($m = 0.0532, J^* = 2102$) of CGH when $a > a_c$ where $a_c \approx 1.23$. The same argument shows that CAF is more stable when the lubricating layer is thinner with maximal intervals (1m.4) of stability as $a \to 1$.

CGH observed stable CAF in Experiment 2 and only in Experiment 2. The theoretical result for this experiment is shown in figure 1.10. The experiment lies very nearly in the stable band of Reynolds numbers with a weak short-wave instability (cf. growth rates, figure 1.11) in a narrow interval centered on $\alpha = 2.2$.

Very minor adjustments of the values of operating parameters, well within the errors expected of these experiments, would place the flow entirely within the stable band. All the other ten cases are unstable in the experiments and in the theory.

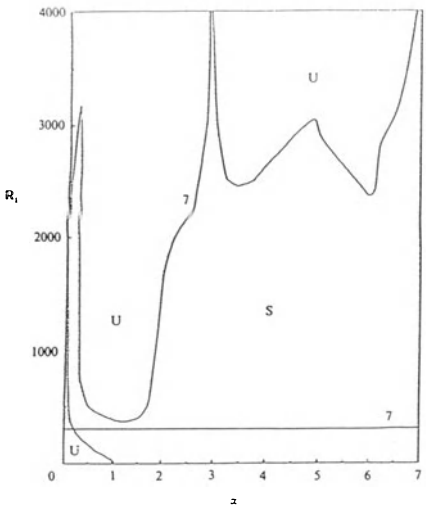

Fig. 1.12. [Preziosi, Chen and Joseph, 1989] Neutral curves corresponding to Experiment 7: $a = 1.74$, $J^* = 2102$, $m = 0.0532$. Oil slugs in water are observed. For Experiments 9, 4, 10, 8, 11 ($a = 1.84$, 2.24, 2.65, 2.80, 4.63, respectively) the neutral curves are very similar to the one shown here except for some scale changes. These other neutral curves are available from the authors PCJ on request.

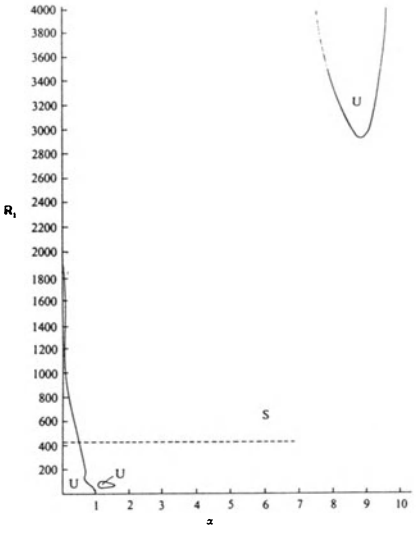

Fig. 1.13. [Preziosi, Chen and Joseph, 1989] Neutral curves corresponding to Experiment 6: $a = 1.50$, $J^* = 2102$, $m = 0.0532$. CAF plus water drops in oil are observed at $\mathbb{R}_1 = 407$.

We next consider category (2) of the comparison between theory and experiment. There are two cases and only two cases of emulsification of water into oil, shown in figure V.1.1 as experiments 1 and 5, with associated neutral curves in figures 1.10 and 1.11. In both cases, we get an instability for high Reynolds number $\mathbb{R}_1 > \tilde{\mathbb{R}}_U$ above the upper critical, short-wave branch.

The flows in all the other experiments (3, 4, 6, 7, 8, 9, 10, 11) of figure V.1.1 are unstable and the theory, exhibited in figures 1.11 - 1.15, show that the instability is due to long waves and not to short waves. For these long-wave instabilities, there is always a wavelength $\tilde{\lambda} = 2\pi/\tilde{\alpha}$ which maximizes the rate of growth (1m.3) of an unstable wave. The length of slugs and bubbles of oil in water can be compared with a theoretical value we get from computing $\tilde{\alpha}$. The procedure we use is to identify the volume of a cylinder

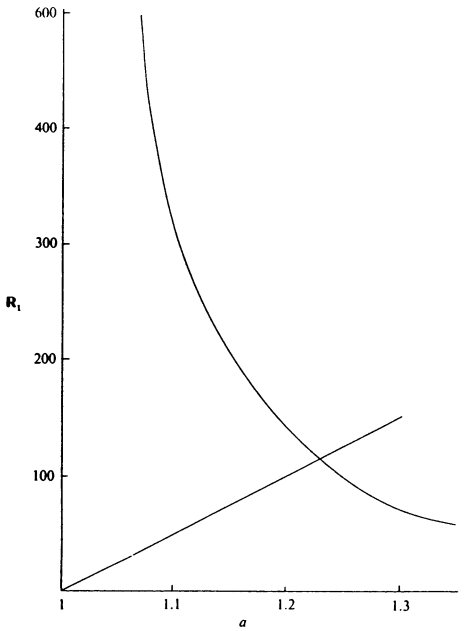

Fig. 1.14. [Preziosi, Chen and Joseph, 1989] Upper and lower stability limits as a function of a for J^*=2102, m=0.0532. The upper curve is derived from the critical Reynolds number from the upper branch of each neutral stability curve. The straight line is derived from the critical Reynolds number from the lower branch of each neutral stability curve. When the two lines meet, there is no stable region. CAF is never stable when a is larger than $a \approx 1.23$ at the point of intersection.

$$\pi R_1^2(\tilde{\lambda} R_1) = \frac{2\pi^2}{\tilde{\alpha}} R_1^3 \qquad (1m.5)$$

of radius R_1 and length $\tilde{\lambda} R_1$. We say that this volume is preserved in the nonlinear breakup of the oil, and hence is the same as the volume of slugs and bubbles observed in the experiments. (The words "oil drops" used by CGH in Experiment 11 is a sort of misnomer because the oil is lighter than the water. Perhaps a better expression would be *oil bubbles*). If $\tilde{\alpha}$ is very small, then the wavelength is many times the circumference of the core. The oil in such a long wave can gather together to form something like a spherical bubble only if the pipe is large enough. Otherwise the bubble cannot collect into a closed spherical shape: hence, it takes form as a cylinder, perhaps long, which we shall call *slug*. Slugs and bubbles, like CAF, seem well lubricated by water at a radius of approximately $a \approx 1.20$, as in Experiments 3, 6, 7 and 9. Hence, $R_1 \approx R_2/1.20$ and the volume (1m.5) is equal to the volume of the observed slug with area $\pi(R_2/1.2)^2$ and length lR_2 as follows:

$$\pi\left(\frac{R_2}{1.2}\right)^2 (lR_2) = \frac{2\pi^2}{\tilde{\alpha}} R_1^3. \qquad (1m.6)$$

Hence,

$$l = 1.44\tilde{\lambda}/a^3 = 2.88\pi/\tilde{\alpha}a^3. \qquad (1m.7)$$

The volume of the observed bubble is $\frac{4}{3}\pi b^3$ where b is the bubble radius. Equating this to (1m.5), we define

$$l = \frac{b}{R_2} = \left(\frac{3\pi}{2\tilde{\alpha}}\right)^{\frac{1}{3}} \frac{1}{a}. \qquad (1m.8)$$

The length $l_{\text{exp}}R_2$ of observed slugs was measured from the pictures in figure V.1.1. The l_{exp} gives the number of pipe radii in the length of one slug and it can be compared with the l in (1m.7). An identical measurement of the ratio of the bubble radius b to R_2 determines an l_{exp} to compare with the theoretical ratio in (1m.8).

Theory and experiment are compared in table 1.1, where we have identified the experiments with the numbers shown in figure V.1.1. In the table, we list the value $\mathbb{R}_1$, the wave number $\tilde{\alpha}$ of the fastest growing wave, the growth rate $\tilde{\sigma} = \tilde{\alpha}\text{Im}\, C(\tilde{\alpha})$ of this wave, the theoretical value l from (1m.7) (for Experiments 3, 6, 7, 9 and 10) or (1m.8) (for Experiments 4, 8 and 11) and the measured value l_{exp}. The size of bubbles and slugs which can be observed in figure V.1.1 under any particular operating condition is not unique. Since we compute a unique size based on the assumption of constant volumes, our comparison is only suggestive and not precise. Some remarks about the comparisons shown in table 1.1 are necessary. In the table, we have identified which slug or bubble has been used for comparison. We do not know if the size of slugs and bubbles, so identified, is representative. For example, there may be a longer or shorter slug upstream or downstream of the section showing the single long slug exhibited in Experiment 7 of figure V.1.1. In some of the experiments, like 6, 9 and 10, there is a great variability with different sizes and configurations occurring simultaneously. Only Experiment 2 of the three labeled *oil in water concentric* seems to be associated with stable CAF. The other two, Experiments 6 and 9, are unstable to very long waves leading to slugs whose lengths ($12.186R_2$, $66.340R_2$) are nearly as long or longer than the 15.75 R_2 length of frames shown in the pictures of figure V.1.1. We cannot distinguish such long slugs from *oil in water concentric*. A shorter slug can be identified in Experiment 9 of figure V.1.1 as the region between the narrow black lines running from top to bottom. The smaller water bubbles shown in Experiments 6 and 9 and the oil bubbles in Experiment 10 are unexplained by this analysis. They could arise as a reaction to turbulence in the water, or as a kind of secondary instability of the slugs.

VI.1(n) Conclusions

The analysis of the spectral problem of linear stability leads to the following conclusions:

(1) Core-annular flow (CAF) is stable to disturbances with infinitely long wavelengths ($\alpha \to 0$) for some $\mathbb{R}_1$ when the ratio $a = R_2/R_1$ of the radius of the pipe to the mean radius of the interface does not exceed a critical value $\hat{a}(m)$ which depends on the viscosity ratio $m = \mu_2/\mu_1 \leq 1$ alone (see figure 1.2) and

$$1.4889 = \hat{a}(0.15) \leq \hat{a} \leq \hat{a}(1) = 1.5805. \qquad (1n.1)$$

When $a > \hat{a}$, CAF is unstable to long waves at any $\mathbb{R}_1$.

(2) CAF is unstable to long waves when the core Reynolds number $\mathbb{R} = W_0 R_1/\nu$, where W_0 is the centerline velocity, is smaller than a critical value

$$\hat{\mathbb{R}}_L(a, m, J^*) = \max_{\alpha \geq 0} \mathbb{R}_{cL}(a, m, J^*, \alpha) \qquad (1n.2)$$

where $\mathbb{R}_{cL}$ is the lower branch of the neutral curve (see figures 1.5 - 1.8, 1.11 and 1.12). This long-wave instability is induced by surface tension and is a generalized capillary instability which leads to the formation of oil slugs and bubbles in water. When $a > 1.5805$, this instability is always present.

(3) The limit $m \to 0$, $\mathbb{R}_1 > 0$ is singular and leads to inviscid flow in the water whereas the flow in the core reduces to the problem of capillary instability of a viscous jet which was studied by Chandrasekhar [1961]. This problem depends on a surface tension parameter $J = J^*/a = TR_1/\rho_1\nu_1^2$. When $J \to 0$, the wavelength of the disturbance with maximum growth tends to infinity. When $J \to \infty$ then Chandrasekhar's problem reduces to Rayleigh's with a most dangerous wavenumber $\alpha = 0.697$.

(4) Increasing J^* stabilizes short waves ($\alpha >> 1$) and destabilizes long ones ($\alpha << 1$).

(5) The limit $m > 0$, $\mathbb{R}_1 \to 0$ is a Stokes flow limit. CAF is always unstable to long waves and is always stable to short waves in this limit when surface tension is present.

(6) CAF is unstable to short waves when

$$\mathbb{R}_1 > \tilde{\mathbb{R}}_U(a, m, J^*) = \min_{\alpha \geq 0} \mathbb{R}_{cU}(a, m, J^*, \alpha), \qquad (1n.3)$$

where $\mathbb{R}_{cU}$ is the upper branch associated with shorter waves (see figures 1.5 - 1.7, 1.10 - 1.12). Instability above the upper branch appears to lead to emulsions of water in oil. The emulsions may arise from a secondary capillary instability after water fingers into oil.

(7) There is a window of parameters (a, m, J^*) such that CAF is stable; that is, there is an interval

$$\tilde{\mathbb{R}}_{\mathrm{L}} \leq \mathbb{R}_1 \leq \tilde{\mathbb{R}}_{\mathrm{U}} \qquad (1n.4)$$

of stable CAF. In this interval, we may say capillary instability has been stabilized by shear. A section of such a window is shown in figure 1.9. This figure shows that there is an optimal value of $m \approx 0.5$ which maximizes the stable interval (1n.4) when $J^* = 930$ and $a = 1.25$.

(8) The density difference, without gravity, affects the stability of CAF, with opposite effects on the lower and upper branches. If we increase $\zeta_2 = \rho_2/\rho_1$ so that the fluid in the annulus is more dense, then $\mathbb{R}_{\mathrm{cL}}$ is decreased and there is a smaller region of generalized capillary instability; that is, the lower branch is more stable. The effect on the upper branch is opposite; increasing ζ_2 decreases $\mathbb{R}_{\mathrm{cU}}$, increasing the region ($\mathbb{R}_1 > \mathbb{R}_{\mathrm{cU}}$) of instability. The destabilizing effect of increasing ζ_2 on the upper branch is much greater than the stabilizing effect on the lower branch (see figure 1.10).

(9) The numerical results show that there is a critical Reynolds number in the water

$$Re = \tilde{\mathbb{R}}_{\mathrm{U}}(a-1)/m,$$

and for the experimental conditions, this is nearly independent of a: $Re \approx 660$ for $a \leq 1.42$. Hence,

$$\tilde{\mathbb{R}}_{\mathrm{U}} \approx \frac{35.2}{a-1}.$$

On the other hand, $\tilde{\mathbb{R}}_{\mathrm{L}}$ increases monotonically from zero when $a = 1$, to ∞ at some finite value of a (cf. figure 1.4). Thus, when $a \to 1$, we retrieve the maximal interval $0 < \mathbb{R}_1 < \infty$ for the interval (1m.4) of stable CAF, as we should.

(10) There is a critical value $a = \tilde{a}(m, J^*)$ such that when $a > \tilde{a}$, the interval (1n.4) of stable CAF closes up (see figure 1.6) and CAF is unstable. Note that

$$\tilde{a}(m, J^*) \leq \hat{a}(m).$$

For $m = 0.0532$, $J^* = 2102$, corresponding to the experiments of CGH

$$\tilde{a} \approx 1.23$$

(see figure 1.14). One of the most important parameters in lubricated pipelining is the volume fraction of oil to water

$$\phi = \frac{V_{\mathrm{w}}}{V_{\mathrm{O}}} = \frac{\pi(R_2^2 - R_1^2)}{\pi R_1^2} = a^2 - 1.$$

In the experiments, CAF is unstable when $\phi > 0.5376$. The pictures in figure V.1.1 suggest that long slugs are stable in a lubricated flow with $a \approx 1.2$.

(11) The linear theory of stability has shown that all the cases of emulsified water drops in oil seen in the experiments of CGH, and only these

cases, are at Reynolds numbers exciting the short waves on the upper branch (that is, $\mathbb{R}_1 > \tilde{\mathbb{R}}_U$) and long waves are not excited because $R_1 > \tilde{\mathbb{R}}_L$ (see figures 1.10 and 1.11).

VI.2 Energy Analysis of the Waves of Fastest Growth

This section is based on the paper of Hu and Joseph [1989 a].

VI.2(a) Introduction

We consider the linear stability of core-annular flow of two liquids with different densities and viscosities with surface tension included but gravity excluded. Results will be given for the problem with a water core, with oil on the wall, studied previously by Hickox [1971] for long waves, for all wavenumbers and Reynolds numbers, with effects of surface tension included. The extended analysis of this problem appears to be in good agreement with new experiments of Aul and Olbricht [1990] on water flow in an oil coated glass tube of small (54 μm) diameter. The application of such experiments is more related to oil recovery than to lubricated pipelining. Results will also be given for the lubricated flow of a viscous liquid when a layer of viscous fluid coats the pipe wall, modeling the situation in lubricated pipelining of oil when the pipe walls are hydrophobic. In this case, the pipe wall takes on oil, but the oil core is lubricated by water in a layer between the core and the oil coating the wall.

In section VI.1, we identified a window of parameters in which core-annular flow was stable to small disturbances. For stability, the water fraction cannot be too large, about 40 percent at most, and the Reynolds number for the core rests in an interval $\mathbb{R}_L < \mathbb{R} < \mathbb{R}_U$ where $\mathbb{R}_L$ is the lower critical value below which core-annular flow is unstable to capillary forces and $\mathbb{R}_U$ is the upper critical value. PCJ compared their results with the experiments of Charles, Govier and Hodgson [1961] (referred to as CGH), and they noticed that the cases of instability with $\mathbb{R} > \mathbb{R}_U$ were correlated with the emulsification of water into oil.

Many of the cases presented in section VI.1 and here are unstable. The utility of linear theory for understanding unstable flow is problematic, since the flows which arise from an instability are, in theory, a perturbation of core-annular flow only in some special circumstances involving stable bifurcations. The flows which actually arise from instability in practice seem in general not to be close to core-annular flow. In order to use linear stability theory to understand unstable flows, it is necessary to be guided by experiments.

In the experiments carried out by Joseph's group, we note three interesting observations. First, they are able to achieve a lubrication of a coal-oil dispersion (40 percent in SAE 30 motor oil) in water. The dispersion is very nearly density matched; and it could not be economically transported in a pipe without water because, at this high concentration of coal, the dispersion is a plastic fluid with an enormous viscosity. Secondly, they get a lubricated flow in three layers in glass pipes which are hydrophobic. Thirdly, they always see waves on thin oil films wetting glass when there is a shear driven by water. They argue that these waves are driven by interfacial friction associated with the viscosity difference. The waves on thin layers of oil driven by the shear flows of water remind us of water waves generated by wind. This problem was studied by Blennerhassett [1980] and Renardy [1989] from the point of view of nonlinear stability theory (see chapter IV). Of course, unstable interfacial waves driven by interfacial friction can be equilibrated by effects of gravity when the dense fluid is below, as in water waves driven by the wind. Travelling waves can be expected to arise from instability and bifurcation of stable core-annular flows [Renardy, M. and Joseph 1986]. The waves determined by Blennerhassett [1980] do not seem to fit the experimental data for water waves well, but we think this line of inquiry should not be closed.

A list of hydrodynamical structures which can be imagined to arise from the instability of core-annular flow are: (a) bubbles and slugs of oil in water; (b) drops of water in oil; (c) emulsions, mainly of water in oil; (d) wavy interfaces. Of these, it would seem that only some of the wavy interfaces could be regarded as arising out of stable bifurcation of core-annular flow. We might hope for a good agreement between the linear theory and experiments for this case.

In the cases (a, b, c) mentioned above, the comparison between linear theory and experiments is more problematic. We have basically three procedures which can be used.

(1) We can compute maximum growth rates and the wavelength of the fastest growing wave. This length can be compared with the size of bubbles and slugs which arise in experiments. The agreement between this type of calculation and experiments (cf. section VI.1) was better than we expected.

(2) We can calculate neutral curves and try to compare regions of parameter space in the stability diagrams with the corresponding regions in experiments. This procedure is global in the parameters and it appears to be promising.

(3) We can compute various terms which arise in the global balance of energy of the small disturbance with the largest growth rate. The energy analysis allows us to identify the three competing mechanisms under way: interfacial tension, interfacial friction and Reynolds stress. We get integrated Reynold stresses in the bulk fluid, as in the case of one fluid; but when there are two fluids, we can compare the contri-

butions to the total made by each of the fluids. There are boundary terms, one is proportional to interfacial tension, another to interfacial friction (proportional to the viscosity difference), and each of these contributions appears on every interface. All these terms take on positive and negative values as the parameters are varied, and they compete to determine whether or not the average energy of a disturbance will increase or decrease. For now, it will suffice to note that interfacial tension is always dominant and always destabilizing at the smallest Reynolds numbers. Interfacial friction can stabilize interfacial tension (capillary instability) and, in fact, is a major actor in the stabilization of core-annular flow with oil cores. In other circumstances, interfacial friction destabilizes and it always destabilizes the flow with water cores when the walls are wet by oil. The Reynolds stress in the core is not destabilizing; water cores are never destabilized by Reynolds stress. The Reynolds stress contribution in the water annulus lubricating the core will always lead to instability, whether or not water or oil is on the wall.

The results in this section were obtained with a finite element code which performs well even for small values less than 10^{-4} of the ratio of viscosity of water to oil where the problem is known to become singular (cf. section VI.3). The reader will find a summary of results at the conclusion of this section.

VI.2(b) The Basic Flow

Consider the problem of two liquids flowing down a circular pipe in three layers with the inner and outer layers occupied by liquid 1 and the middle layer by liquid 2. The interfaces between the liquids are $r = r_1(\theta, z, t)$ and $r = r_2(\theta, z, t)$, $(r_2 > r_1)$, where (r, θ, z) are cylindrical coordinates and t is time. Let $\mathbf{U} = (u_r, u_\theta, u_z)$ be the velocity and $\hat{p}$ be the pressure, μ_1 and ρ_1 be the viscosity and density of liquid 1, μ_2 and ρ_2 of liquid 2.

Assume that the pipe is infinitely long with radius R_3 and axis at $r = 0$, the mean value of r_1 (and r_2) over $\theta (0 \leq \theta \leq 2\pi)$ is R_1 (and R_2), a constant independent of time, and the gravity force can be neglected.

We scale the length with R_3, the velocity with the centerline velocity of the basic flow W_0, pressure with $\rho_1 W_0^2$, and time with R_3/W_0. We use the same symbols for dimensional and dimensionless variables.

The basic core-annular flow with constant pressure gradient $\partial P/\partial z = -F$ is

$$\mathbf{U} = (0, 0, W(r)) \tag{2b.1}$$

with

$$W(r) = \begin{cases} [(b^2 - \eta^2) + m(1 + \eta^2 - b^2 - r^2)]/A, & r \in [0, \eta], \\ [b^2 - r^2 + m(1 - b^2)]/A, & r \in [\eta, b], \\ [m(1 - r^2)]/A, & r \in [b, 1] \end{cases} \tag{2b.2}$$

where

$$W_0 = \frac{F}{4\mu_2}[m(R_1^2 + R_3^2 - R_2^2) + R_2^2 - R_1^2], \tag{2b.3}$$

$$A = b^2 - \eta^2 + m(1 + \eta^2 - b^2), \tag{2b.4}$$

and

$$m = \frac{\mu_2}{\mu_1}, \quad \eta = \frac{R_1}{R_3}, \quad b = \frac{R_2}{R_3}. \tag{2b.5}$$

VI.2(c) Perturbation Equations and Normal Modes

We perturb the core-annular flow with

$$\mathbf{U} = (u, v, w+W), \quad \hat{p} = P+p, \quad r_l = \eta \text{ (or } b) + \delta_l(\theta, z, t) \ (l = 1, 2) \tag{2c.1}$$

and introduce dimensionless parameters

$$\zeta = \frac{\rho_2}{\rho_1}, \quad \mathbb{R} = \frac{\rho_1 W_0 R_3}{\mu_1}, \quad J^* = \frac{TR_3\rho_1}{\mu_1^2}. \tag{2c.2}$$

Using the normal mode decomposition of solutions:

$$\left.\begin{array}{ll} & [u, v, w, p](r, \theta, z, t) = [\mathrm{i}u, v, w, p](r)\exp[\mathrm{i}n\theta + \mathrm{i}\beta(z - ct)] \\ \text{and} & [\delta_1, \delta_2](\theta, z, t) = [\delta_1, \delta_2]\exp[\mathrm{i}n\theta + \mathrm{i}\beta(z - ct)] \end{array}\right\} \tag{2c.3}$$

where $u(r), v(r), w(r), p(r)$ are complex-valued functions, and δ_1, δ_2 are complex constants. If we write $\delta_1 = |\delta_1|e^{\mathrm{i}\phi_1}, \delta_2 = |\delta_2|e^{\mathrm{i}\phi_2}$ then $\phi_2 - \phi_1$ indicates the phase shift of the two interfaces in the z-direction.

The linearized equations of motion are

$$\zeta_l\beta(W - c)u = p' - \frac{\mathrm{i}m_l}{\mathbb{R}}\left[\frac{d}{dr}\left(\frac{d(ru)}{rdr}\right) - \left(\beta^2 + \frac{n^2}{r^2}\right)u - \frac{2n}{r^2}v\right], \tag{2c.4}$$

$$\zeta_l\beta(W - c)v = -\frac{n}{r}p - \frac{\mathrm{i}m_l}{\mathbb{R}}\left[\frac{d}{dr}\left(\frac{d(rv)}{rdr}\right) - \left(\beta^2 + \frac{n^2}{r^2}\right)v - \frac{2n}{r^2}u\right], \tag{2c.5}$$

$$\zeta_l[\beta(W-c)w+W'u] = -\beta p - \frac{\mathrm{i}m_l}{\mathbb{R}}\left[\frac{1}{r}\frac{d}{dr}\left(r\frac{dw}{dr}\right) - \left(\beta^2 + \frac{n^2}{r^2}\right)w\right], \tag{2c.6}$$

$$\frac{d(ru)}{rdr} + \frac{n}{r}v + \beta w = 0. \tag{2c.7}$$

where $W' = dW/dr$, $m_l = (1,\ m,\ 1)$, $\zeta_l = (1, \zeta, 1), l = 1, 2, 3$ indicates the flow region Ω_1=[0,η), $\Omega_2 = (\eta, b)$, $\Omega_3 = (b,1]$ with $\rho_3 = \rho_1$ *and* $\mu_3 = \mu_1$. The boundary conditions are

$$r = 1: \qquad u = v = w = 0, \tag{2c.8}$$

$$r = 0: \qquad u, v, w, p \text{ and their derivatives are finite.} \tag{2c.9}$$

The linearized interface conditions are at $r = \eta$ and b (corresponds to $l = 1, 2$) :

$$u(r_l) = \beta(W - c)\delta_l, \tag{2c.10}$$

$$[\![u]\!]_l = [\![v]\!]_l = 0, \tag{2c.11}$$

$$[\![w]\!]_l + [\![W']\!]_l \delta_l = 0, \tag{2c.12}$$

$$[\![m_l(-\beta u + w')]\!]_l = 0, \tag{2c.13}$$

$$\left[\!\!\left[m_l \left(-\frac{nu + v}{r} + v' \right) \right]\!\!\right]_l = 0. \tag{2c.14}$$

$$[\![p]\!]_l - \frac{2\mathrm{i}}{\mathbb{R}}[\![m_l u']\!]_l = -\frac{J^*}{\mathbb{R}^2}\frac{1}{r_l^2}(1 - n^2 - r_l^2\beta^2)\delta_l, \tag{2c.15}$$

where for any function $G(r)$ in $\Omega = \Omega_1 \cup \Omega_2 \cup \Omega_3$, $[\![m_l G]\!]_l$ is defined as

$$[\![m_l G]\!]_l = m_l G(r_l^-) - m_{l+1} G(r_l^+).$$

We could eliminate δ_l in (2c.12) and (2c.15):

$$u[\![W']\!]_l - (W - c)[\![u']\!]_l = 0, \tag{2c.16}$$

$$[\![p]\!]_l - \frac{2\mathrm{i}}{\mathbb{R}}[\![m_l u']\!]_l = -\frac{J^*}{\mathbb{R}^2}\frac{1}{r_l^2}\frac{[\![u']\!]_l}{\beta[\![W']\!]_l}(1 - n^2 - r_l^2\beta^2). \tag{2c.17}$$

VI.2(d) Finite Element Formulation

Define functional spaces

$$V = \{u,\ v | u \in c^2(\Omega), v \in c^1(\Omega); \quad \text{at } r = 1, u(1) = u'(1) = v(1) = 0;$$

$$\text{at } r = 0,\ u, v \text{ and their derivatives are finite;}$$

$$\text{at } r = r_l, [\![u]\!]_l = [\![v]\!]_l = 0 \text{ and } u[\![W']\!]_l - (W - c)[\![u']\!]_l = 0\ \}.$$

Solving the equations (2c.4) to (2c.7) is equivalent to solving the following problem (weak solution):

Find $u, v \in V$ such that, for every $u^*, v^* \in V$,

$$\sum_{l=1}^{3} \int_{\Omega_l} \zeta_l \left\{ \left[\beta(W - c)uu^* + \frac{1}{\beta}(W - c)\frac{d(ru)}{rdr}\frac{d(ru^*)}{rdr} - \frac{W'}{\beta}u\frac{d(ru^*)}{rdr} \right] \right.$$

$$\left. + \frac{n}{\beta}\left[(W - c)\frac{v}{r}\frac{d(ru^*)}{rdr} \right] \right\} rdr$$

$$= \frac{\mathrm{i}}{\mathbb{R}\beta^2} \sum_{l=1}^{3} \int_{\Omega_l} m_l \left\{ \left[\frac{d}{dr} \left(\frac{d(ru)}{rdr} \right) \frac{d}{dr} \left(\frac{d(ru^*)}{rdr} \right) \right.\right.$$

$$+ \left(2\beta^2 + \frac{n^2}{r^2} \right) \frac{d(ru)}{rdr} \frac{d(ru^*)}{rdr} + \left(\beta^2 + \frac{n^2}{r^2} \right) \beta^2 uu^* \Big]$$

$$\left. + n \left[\frac{d}{dr} \left(\frac{v}{r} \right) \frac{d}{dr} \left(\frac{d(ru^*)}{rdr} \right) + \left(\beta^2 + \frac{n^2}{r^2} \right) \frac{v}{r} \frac{d(ru^*)}{rdr} + \frac{2\beta^2}{r^2} vu^* \right] \right\} rdr$$

$$+ \left[\left(p - \frac{\mathrm{i}m_l}{\mathbb{R}} \frac{d(ru)}{rdr} \right) ru^* + \frac{\mathrm{i}m_l}{\beta\mathbb{R}} w' \frac{d(ru^*)}{rdr} r \right]_{-0+\eta+b+1} \tag{2d.1}$$

and

$$\sum_{l=1}^{3} \int_{\Omega_l} \zeta_l \left\{ \frac{n}{\beta} \left[(W - c) \frac{d(ru)}{rdr} - W'u \right] \frac{v^*}{r} \right.$$

$$\left. + \frac{1}{\beta} (W - c) \left(\beta^2 + \frac{n^2}{r^2} \right) vv^* \right\} rdr$$

$$= \frac{\mathrm{i}}{\mathbb{R}} \sum_{l=1}^{3} \int_{\Omega_l} m_l \left\{ \frac{n}{\beta^2} \left[\frac{d}{dr} \left(\frac{d(ru)}{rdr} \right) \frac{d}{dr} \left(\frac{v^*}{r} \right) \right.\right.$$

$$+ \left(\beta^2 + \frac{n^2}{r^2} \right) \frac{d(ru)}{rdr} \frac{v^*}{r} + \frac{2\beta^2}{r^2} uv^* \Big]$$

$$+ \left[\frac{d(rv)}{rdr} \frac{d(rv^*)}{rdr} + \frac{n^2}{\beta^2} \frac{d}{dr} \left(\frac{v}{r} \right) \frac{d}{dr} \left(\frac{v^*}{r} \right) \right.$$

$$\left.\left. + \left(\beta^2 + \frac{n^2}{r^2} \right) \left(1 + \frac{n^2}{\beta^2 r^2} \right) vv^* \right] \right\} rdr$$

$$+ \left[\frac{\mathrm{i}m_l}{\mathbb{R}} \left(\frac{n}{r\beta} w' - \frac{d(rv)}{rdr} \right) rv^* \right]_{-0+\eta+b+1} \tag{2d.2}$$

where $[\ldots]_{-0+\eta+b+1} = -[\ldots]_{r=0} + [\![\ldots]\!]_1 + [\![\ldots]\!]_2 + [\ldots]_{r=1}$.

Using the boundary conditions and interface conditions, we evaluate two of the terms above:

$$\left[\left(p - \frac{\mathrm{i}m_l}{\mathbb{R}} \frac{d(ru)}{rdr} \right) ru^* + \frac{\mathrm{i}m_l}{\beta\mathbb{R}} w' \frac{d(ru)}{dr} \right]_{-0+\eta+b+1}$$

$$= \frac{\mathrm{i}}{\mathbb{R}} \{ [\![m_l u']\!]_1 \eta u^*(\eta) + (1-m) u(\eta) \eta u^{*\prime}(\eta) \} - \frac{J^* A}{2\beta\mathbb{R}^2} \frac{1 - n^2 - \eta^2\beta^2}{\eta^2(1-m)} [\![u']\!]_1 u^*(\eta)$$

$$+ \frac{\mathrm{i}}{\mathbb{R}} \{ [\![m_l u']\!]_2 b u^*(b) - (1-m) u(b) b u^{*\prime}(b) \} + \frac{J^* A}{2\beta\mathbb{R}^2} \frac{1 - n^2 - b^2\beta^2}{b^2(1-m)} [\![u']\!]_2 u^*(b), \tag{2d.3}$$

and

$$\left[\frac{im_l}{\mathbb{R}}\left(\frac{n}{r\beta}w' - \frac{d(rv)}{rdr}\right)rv^*\right]_{-0+\eta+b+1}$$

$$= \frac{i}{\mathbb{R}}[u(0)-v(0)]v^*(0) - \left[2(1-m)\frac{i}{\mathbb{R}}v(\eta)v^*(\eta)\right] + \left[2(1-m)\frac{i}{\mathbb{R}}v(b)v^*(b)\right]. \tag{2d.4}$$

In the finite element method, the domain Ω is divided into simple geometric subdomains or elements. u and v are approximated in each element by interpolation functions using values of u (and derivatives of u) and v at nodal points. The piecewise cubic Hermite interpolation fuctions are taken for u and the piecewise linear Lagrange interpolation functions are taken for v, since the governing equation for u after eliminating w is fourth order while the equation for v is second order. Thus the unknowns at each node are $(u, du/dr, v)$.

After discretization of (2d.1) and (2d.2), we combine them into matrix form

$$\mathbf{Ax} = c\mathbf{Bx}, \tag{2d.5}$$

where c is the eigenvalue in $(z - ct)$ in (2c.3), $\mathbf{A}$ and $\mathbf{B}$ are the global matrices with the forced boundary conditions (2c.8), (2c.11) and (2c.16) being applied, and $\mathbf{x} = [u_1, u'_1, v_1, u_2, u'_2, v_2, \ldots u_N, u'_N, v_N]^T$. N is the total number of nodes.

Using the IMSL routine EIGZC, the eigenvalues $c = c_r + ic_i$ of the problem (the eigenvalue of most interest is the one with the largest imaginary part c_i) and the corresponding eigenfunctions are computed. If the computed value $c_i < 0$, the perturbation will decay with time. The flow is stable to this mode of perturbation. If $c_i > 0$, then, in linear stability theory, this mode of perturbation will grow exponentially with the growth rate of βc_i. The basic flow is then unstable. Thus $c_i = 0$ indicates the neutral state.

VI.2(e) Energy Analysis

The method of energy is useful in the analysis of stability of flow of one fluid because certain limited nonlinear results can be obtained from the method by rigorous analysis. It is known that the utility of the method for the classical case of flow of one fluid is basically restricted to analysis of sufficient conditions for stability, though a recent approach of Galdi [1988] goes in another direction. The situation is more complicated for the case of two fluids. The main new feature is the appearance of new terms on the boundary. Hooper and Boyd [1983, 1987] and Hooper [1988] showed that the linearized energy equation can be used to analyze instability in the case of long and short waves. When the energy equation is evaluated on solutions,

we may determine the situations in which instability is introduced through the Reynolds stress, as in one fluid, or in the boundary terms, through the surface tension and viscosity difference. There are three instabilities which may be identified through the energy: due to interfacial tension, interfacial friction and Reynolds stress. Hu and Joseph [1989a] calculated these different terms on the most unstable eigenfunction corresponding to the wave whose length gives rise to the maximum rate of growth of a small disturbance. This procedure is based on Rayleigh's idea that the linear wave of maximum growth will be observed under nonlinear conditions. The analysis of the parameter dependence of these instabilities together with comparison with experiments gives this type of analysis a potential for uncovering the basic dynamics of the flow.

Mathematically, the energy analysis of the nonlinear stability of flow of two fluids is frustrated by the fact that the boundary terms cannot be estimated *a priori* in terms of the dissipation [Joseph 1987]. After multiplying equations (2c.4), (2c.5) and (2c.6) by u_*, v_* and w_*, the complex conjugates of u, v, w, we integrate and add the three equations using (2c.7) and boundary conditions (2c.8) , (2c.9) to obtain

$$\sum_{l=1}^{3}\int_{\Omega_l}\zeta_l\left[\beta(W-c)(|u|^2+|v|^2+|w|^2)+W'uw_*\right]rdr$$

$$=\frac{\mathrm{i}}{\mathbb{R}}\sum_{l=1}^{3}\int_{\Omega_l}m_l\left[\left|\frac{d(ru)}{rdr}\right|^2+\left|\frac{d(rv)}{rdr}\right|^2+\left|\frac{dw}{dr}\right|^2\right.$$

$$\left.+\left(\beta^2+\frac{n^2}{r^2}\right)(|u|^2+|v|^2+|w|^2)+\frac{4n}{r^2}uv_*\right]rdr$$

$$+\left[\!\!\left[pru_*-\frac{\mathrm{i}}{\mathbb{R}}m_l\left(\frac{d(ru)}{rdr}ru_*+\frac{d(rv)}{rdr}rv_*+\frac{dw}{dr}rw_*\right)\right]\!\!\right]_{\eta+b}$$

$$+\frac{\mathrm{i}}{\mathbb{R}}[|u(0)|^2+|v(0)|^2] \qquad (2e.1)$$

where $|u|^2=uu_*, |v|^2=vv_*, \ldots$. Each term in the equation is a type of energy; thus equation (2e.1) represents the energy balance for the perturbed flow. The imaginary part of (2e.1) governs the growth of the energy of the small perturbations and it can be separated into four terms

$$\dot{E}=I-D+B \qquad (2e.2)$$

where

$$\dot{E}=\beta c_{\mathrm{i}}\sum_{l=1}^{3}\int_{\Omega_l}\zeta_l(|u|^2+|v|^2+|w|^2)rdr,$$

$$I = \sum_{l=1}^{3} \int_{\Omega_l} \zeta_l W' \mathrm{Im}\{uw_*\} r dr,$$

$$D = \frac{1}{\mathbb{R}} \sum_{l=1}^{3} \int_{\Omega_l} m_l \left[\left| \frac{d(ru)}{rdr} \right|^2 + \left| \frac{d(rv)}{rdr} \right|^2 + \left| \frac{dw}{dr} \right|^2 + \left(\beta^2 + \frac{n^2}{r^2} \right) (|u|^2 + |v|^2 + |w|^2) + \frac{4n}{r^2} \mathrm{Re}\{uv_*\} \right] r dr + \frac{1}{\mathbb{R}} [|u(0)|^2 + |v(0)|^2], \tag{2e.3}$$

$$B = \mathrm{Im} \left\{ \left[\left[-pru_* + \frac{\mathrm{i}}{\mathbb{R}} m_l \left(\frac{d(ru)}{rdr} ru_* + \frac{d(rv)}{rdr} rv_* + \frac{dw}{dr} rw_* \right) \right] \right]_{\eta+b} \right\}.$$

$\dot{E}$ is the rate of change of kinetic energy of the perturbed flow; I is the rate at which energy is transferred from the basic flow to the perturbed flow through the Reynolds stress; $-D$ is the rate of viscous dissipation of the perturbed flow and B is the rate at which energy is being supplied at the two interfaces. Using the interface conditions (2c.10) to (2c.17), the energy B can be written as

$$B = B_{1\eta} + B_{1b} + B_{2\eta} + B_{2b} \tag{2e.4}$$

where

$$\left.\begin{aligned} B_{1\eta} &= c_{\mathrm{i}} \tfrac{J^*}{\beta \mathbb{R}^2} \tfrac{1-n^2-\eta^2\beta^2}{\eta(W(\eta)-c)^2} |u(\eta)|^2, \\ B_{1b} &= c_{\mathrm{i}} \tfrac{J^*}{\beta \mathbb{R}^2} \tfrac{1-n^2-b^2\beta^2}{b(W(b)-c)^2} |u(b)|^2, \end{aligned}\right\} \tag{2e.5}$$

$$\left.\begin{aligned} B_{2\eta} = \tfrac{2(1-m)}{\mathbb{R}} \Big[|v(\eta)|^2 - \mathrm{Re} \Big\{ \eta u'(\eta^+) u_*(\eta) + \tfrac{\eta^2(2-m)}{A(W-c)} |u(\eta)|^2 \\ + \tfrac{\eta^2 m}{A\beta(W-c)_*} w'(\eta^+) u_*(\eta) \Big\} \Big], \\ B_{2b} = -\tfrac{2(1-m)}{\mathbb{R}} \Big[|v(b)|^2 - \mathrm{Re} \Big\{ b u'(b^+) u_*(b) - \tfrac{b^2(1-2m)}{A(W-c)} |u(b)|^2 \\ + \tfrac{b^2}{A\beta(W-c)_*} w'(b^+) u_*(b) \Big\} \Big], \end{aligned}\right\} \tag{2e.6}$$

where $(W-c)_*$ indicates the complex conjugate of $(W-c)$.

$B_{1\eta}$ and B_{1b} are the energies supplied at the interfaces $r = \eta$ and $r = b$ due to surface tension. Surface tension destabilizes long axisymmetric ($n = 0$) waves $\beta < 1/b$ ($B_{1\eta} > 0$ and $B_{1b} > 0$) and stabilizes short waves $\beta > 1/\eta$ ($B_{1\eta}, B_{1b} < 0$). Surface tension always stabilizes nonaxisymmetric perturbations ($n \geq 1$). $B_{2\eta}$ and B_{2b} are the energies supplied at the interfaces $r = \eta$ and $r = b$, due to the difference of viscosity of the two fluids. Since the amplitude of velocities u, v, w (or eigenfunctions) is arbitrary, the value of each term of the energy is normalized with $D = 1$. From the values of $B_{1\eta}$, B_{1b}, $B_{2\eta}$, B_{2b}, I, and $\dot{E}$, we can determine which interface is more unstable, where the instability arises and what kind of instability it is.

VI.2(f) Comparison with Previous Results for Two-Layer Core-Annular Flow

To reduce the three-layer equations to two layers, we suppress all terms relating to the interface $r = b$. In the two-layer case, the basic flow is

$$W(r)\begin{cases}\{1-\eta^2+m(\eta^2-r^2)\}/A, & r\in[0,\eta],\\ (1-r^2)/A, & r\in[\eta,1]\end{cases} \tag{2f.1}$$

where

$$A = 1-\eta^2(1-m) \tag{2f.2}$$

and

$$m_l = (1,\ m),\quad \zeta_l = (1,\ \zeta),\quad (l=1,\ 2). \tag{2f.3}$$

We wish first to specify how many elements are needed to obtain reliable results. Table 1 of Hu and Joseph [1989 a] lists the influence of the number of elements on the eigenvalue of interest for three situations. This table shows that 10 elements (5 in Ω_1 and 5 in Ω_2) are sufficient for three-digit accuracy in the range of parameters we consider. Therefore, we present results with that number of elements. These results were frequently checked by using more elements. It was found that for larger Reynolds numbers and small viscosity ratios m, more elements are needed in the region outside the core which is occupied by the less viscous liquid. $m \to 0$ is a singular limit (cf. section VI.3). The calculations were compared with results of section VI.1 and JRR. Figure 1 of HJ_1 shows a comparison of both methods. The conversion of notation to those of section VI.1 [Preziosi, Chen and Joseph 1989] is as follows: PCJ defined

$$\left.\begin{array}{ll}\text{radius ratio } a = R_2/R_1: & a = 1/\eta,\\ \text{wavenumber based on } R_1: & \alpha = \beta\eta,\\ \text{Reynolds number } W_0R_1/v_1: & \mathbb{R}_1 = \mathbb{R}\eta.\end{array}\right\} \tag{2f.4}$$

The pseudospectral method of section VI.1 gives rise to spurious eigenvalues in the discretized system. This problem seems not to arise in the present finite element method. When numerical integration is done on the finite element matrices in (2d.1) and (2d.2), care must be taken at the first element because $r = 0$ is a singular point. This precaution is especially necessary when $n = 1$ because, in this case, $u(0)$ and $v(0)$ need not be zero.

VI.2(g) The Viscous Core: $m < 1$

The case $m < 1$, with a viscous core and lubricating annulus was treated in section VI.1. More results will be given for this case. Eigenfunctions are computed to evaluate the terms in the energy balance in an attempt to identify the mechanisms of instability and the finite-amplitude consequences of these mechanisms by comparing with experiments. The computational results, both for two-layer flow with $m < 1$ and $m > 1$ and for three-layer

flow, indicate that the axisymmetric mode of perturbation may be the most unstable, although the maximum growth rates for $n = 0$ and $n = 1$ are very close for large $\mathbb{R}$. Therefore, only the results for $n = 0$ are presented in this section.

VI.2(g)(i) The Fastest Growing Wave. When J^*, η, m, ζ and $\mathbb{R}$ are fixed, the growth rate βc_i varies with wave number β. There is a positive maximum growth rate at a certain wave number $\tilde{\beta}$ provided the flow is unstable.

Figure 2.1 shows the variation of the maximum growth rate $\tilde{\sigma} \stackrel{\text{def}}{=} \tilde{\beta} c_i(\tilde{\beta})$ and corresponding wavenumber $\tilde{\beta}$ with Reynolds number $\mathbb{R}$ when $J^* = 1000$, $\eta = 0.8$, $m = 0.1$ and $\zeta = 1$. Core-annular flow is stable when $\mathbb{R}_L < \mathbb{R} < \mathbb{R}_U$. In this interval, $\tilde{\sigma} = 0$ at $\tilde{\beta} = 0$. $\tilde{\beta}$ decreases slightly at first, then jumps to zero at $\mathbb{R} = \mathbb{R}_L$, remains zero in the stable region $\mathbb{R}_L < \mathbb{R} < \mathbb{R}_U$, and jumps up to a certain value at $\mathbb{R} = \mathbb{R}_U$, and finally decreases again. Figure 2.1 is typical for this case. When the stable interval of Reynolds number shrinks to nothing, the right and left branches of the curve giving the maximum growth rate merge at a certain value of $\mathbb{R}$ but the curve for $\tilde{\beta}$ may have one jump at such $\mathbb{R}$, indicating a switch from one mode of instability to another.

VI.2(g)(ii) Energy Analysis for Two Cases with $m < 1$. We have shown in section VI.1 that some neutral curves for $m < 1$ have two branches: a lower branch which is associated with long waves leading to capillary instability caused by surface tension at low $\mathbb{R}$ and an upper branch which is associated with shorter waves at large $\mathbb{R}$. The lower branch ends at wavenumber $\beta = 1/\eta$ in the notation of this section or $\alpha = 1$ in the notation of section VI.1. Neutral curves for $\eta = 0.8$ and $\eta = 0.7$ are shown in figure 2.2. For $\eta = 0.8$, the neutral curve has two branches, while for $\eta = 0.7$, the two branches have merged. In the present case, the energy equation (2e.2) is defined by (2e.3) with $\Omega = \Omega_1 \cup \Omega_2$. The boundary terms B_{1b} and B_{2b} at the second interface are suppressed. For simplicity, we write $B_{1\eta}$ and $B_{2\eta}$ as B_1 and B_2. All the terms were computed in the energy equation $\dot{E} = I - D + B_1 + B_2$ corresponding to the two cases shown in figure 2.2. The eigenfunctions in the integrals defining the energy balance are evaluated for $\beta = \tilde{\beta}$, corresponding to the disturbance of fastest growth.

The terms of the energy balance corresponding to $\eta = 0.8$ and $\eta = 0.7$ are plotted as a function of $\mathbb{R}$ in figure 2.3. Stable core-annular flow with $\mathbb{R}_L < \mathbb{R} < \mathbb{R}_U$ is possible for $\eta = 0.8$, but not for $\eta = 0.7$. Positive values mean energy is supplied by the disturbance, leading to instability, with the obvious opposite meaning for negative values. There are three different kinds of instability corresponding to:

$B_1 > 0$ (capillary instability due to interfacial tension);
$B_2 > 0$ (surface wave instability due to a difference of viscosity, interfacial friction);
$I - D(= I - 1) > 0$ (Reynolds stress instability. The production of energy in the bulk of the fluid exceeds its dissipation.).

It is known that B_1, which is proportional to the surface tension parameter J^*, produces capillary instability modified by shear. This instability is always dominant at low $\mathbb{R}$ when $m < 1$. The instability associated with interfacial friction B_2 is destabilizing at the lowest $\mathbb{R}$, but is not as important as capillarity. For larger but still small $\mathbb{R}$ (say, 100), the instability due to interfacial friction dominates interfacial tension. The Reynolds stress minus dissipation term $I - 1$ of the energy equation is stabilizing at small $\mathbb{R}$ and destabilizing at large $\mathbb{R}$. Eventually, at large $\mathbb{R}$, the flow is unstable by virtue of the production of energy in the bulk, with negligible contributions from the surface terms B_1 and B_2, as in one fluid. In the stable case $\eta = 0.8$, when there is less water, the Reynolds stress does not grow rapidly and is dominated by the dissipation. When $\mathbb{R}_L < \mathbb{R} < \mathbb{R}_U$, the term $I - D(= I - 1)$ is stabilizing and overcomes the destabilizing effect of the interfacial friction term B_2. We call this shear stabilization, though what actually happens is that the dissipation is large enough to dominate the other terms when $\mathbb{R}_L < \mathbb{R} < \mathbb{R}_U$. In the case $\eta = 0.8$, $\mathbb{R} > \mathbb{R}_L$, the surface terms are relatively small, but stabilizing.

The energy supplied by the production integral I is associated with the Reynolds stress in Ω and can be decomposed into two parts corresponding to the production of energy in oil in region Ω_1 and in water in region Ω_2. In Ω_1, $W' = 2mr/A$ is small when m is small, but $W' = 2\ r/A$ in Ω_2. This thought leads to the idea that the instability at moderately high $\mathbb{R}$ is associated with the water, not the oil. This is what happens in the two cases corresponding to figure 2.3, and is illustrated by computations shown in figure 2.4 which show that I_1, the Reynolds stress production in the oil, is entirely negligible.

VI.2(g)(iii) Comparison of the Energy Analysis with Experiments. In section VI.1, we describe the types of instability that are generated from linear theory and compare these with experimental results of CGH. The density of oil used in the experiments was matched with water by adding carbon tetrachloride. This eliminated gravity effects, so that conditions assumed in the theory (negligible gravity) are achieved in the experiment. The observed flows were far from core-annular flows but the linear stability results were in rather surprising agreement with regard to the type of instability and the size of bubbles and slugs, which were computed from the wavelength of the fastest growing disturbances.

The comparison of theory and experiment will be supplemented by computing all the terms in the energy equation, using the eigenfunction of the fastest growing mode, for each of the eleven cases shown in figure 1.1 of chapter V. The computed results are exhibited in table 2.1. The method used to convert data given for the experiments into the values needed for computation is explained in section VI.1. Two of the columns given in the table are not needed for the computations; the volume fraction of water is determined when $\eta = R_1/R_2$ is given, $V_w/V = \pi(R_2^2 - R_1^2)/\pi R_2^2$, and the Reynolds number $\mathbb{R}' = W_0(R_2 - R_1)\rho_2/\mu_2 = \mathbb{R}(1-\eta)\zeta/m$ in the water is

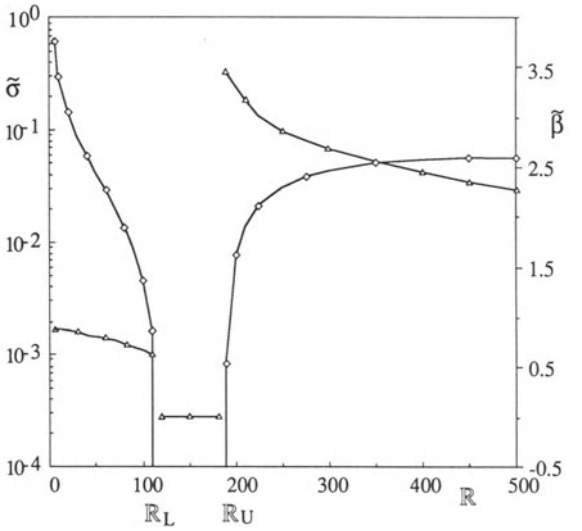

Fig. 2.1. [Hu and Joseph, 1989a] The wavenumber $\tilde{\beta}$ of maximum growth and the corresponding growth rate $\tilde{\sigma} = \tilde{\beta} c_i(\tilde{\beta})$ as a function of $\mathbb{R}$: $\diamond$ for $\tilde{\sigma}$, $\triangle$ for $\tilde{\beta}$.

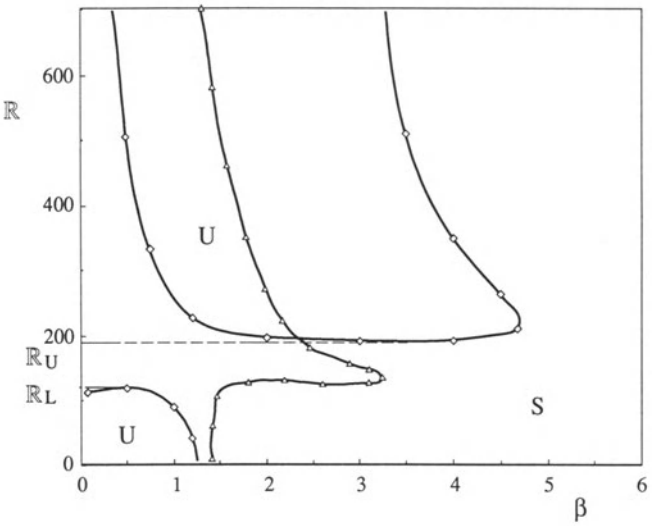

Fig. 2.2. [Hu and Joseph, 1989a] Neutral curves for $J^* = 1000$, $m = 0.1, \zeta = 1$: $\diamond$ for $\eta = 0.8$; $\triangle$ for $\eta = 0.7$. S and U indicate the stable and unstable regions.

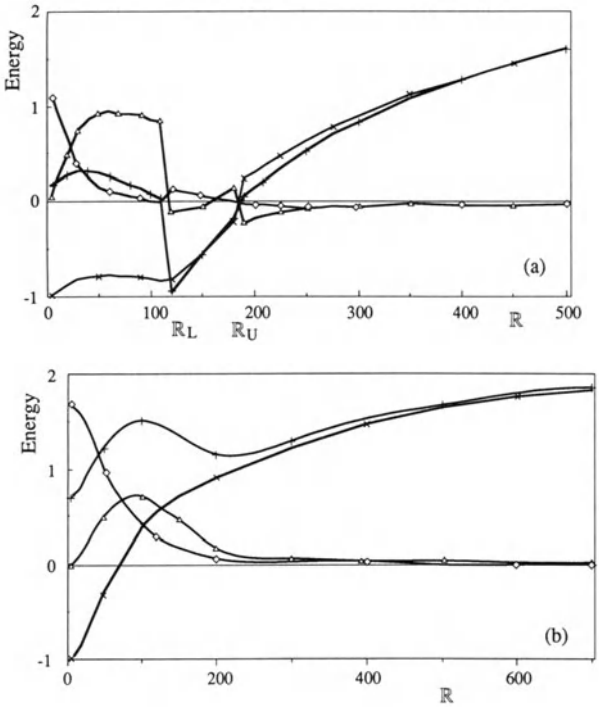

Fig. 2.3(a-b). [Hu and Joseph, 1989a] Variation with $\mathbb{R}$ of the terms $I - D = I - 1(\times)$, $B_1(\diamond)$, $B_2(\triangle)$, and $\dot{E}$ $(+)$ in the energy equation corresponding to the fastest growing disturbance with wavenumber β, $(J^*, m, \zeta) = (1000, 0.1, 1)$. (a) $\eta = 0.8$, (b) $\eta = 0.7$. Flows with negative $\dot{E}$ are stable. A discontinuity in these curves reflects a switch from one mode to another (mode jumping).

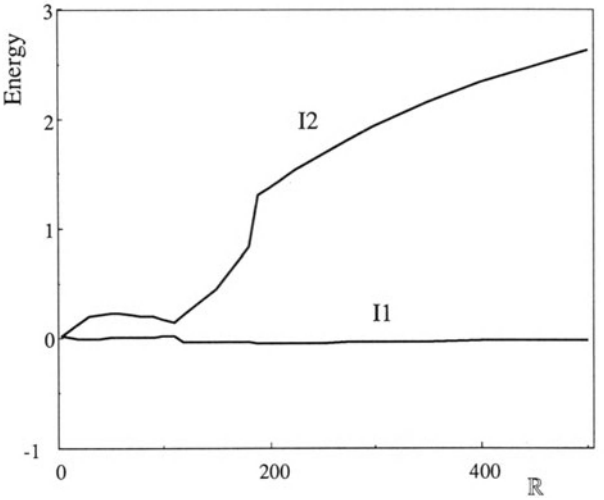

Fig. 2.4. [Hu and Joseph, 1989a] The Reynolds stress integral $I = I_1 + I_2$ is decomposed into an integral over Ω_1 and Ω_2 with conditions specified in figure 2.3 (a).

determined when the Reynolds number $\mathbb{R}$ and radius ratio are given.

Roughly speaking, two kinds of flow are observed in CGH: small water drops in oil and oil bubbles in water. Experiment 2 is an exception, it appears to be a stable core-annular flow but its stability parameters put it close to the border of stability leading to water drops in oil, as in experiment 1. The main factor controlling which phase appears is the water fraction (or radius ratio). There is a phase inversion at a value V_w/V around 0.45 (or η around 0.75) with water emulsions or stable core-annular flow for smaller water fractions and some form of oil bubbles in water for larger water fractions.

According to the linear theory, stable flows are those for which $\dot{E} < 0$. Table 2.2 shows that the least unstable flow among those in figure 1.1 of chapter V is experiment 2. This stable or nearly stable flow is achieved by balancing the destabilizing Reynolds stress minus dissipation $I - 1$ against the stabilizing effect of the interface term B_2 associated with the viscosity difference. Capillarity B_1 plays a secondary role.

Emulsions of water drops in oil are seen in experiments 1 and 5. The effect of surface tension B_1 is not important in the linear theory for these two flows. The instability is produced by the Reynolds stress in the water and is not introduced by effects at the interface which are stabilizing: $B_1 + B_2 < 0$. In section VI.1, we have noted that the emulsifying instability for experiment 1 was for $\mathbb{R} > \mathbb{R}_U$, above the upper critical branch of the neutral curve. The upper and lower critical branches have merged for the larger water fraction in experiment 5. In both experiments, the longest waves are stable.

High Reynolds numbers alone will not emulsify water into oil, as experiment 11 shows. Evidently, water-into-oil emulsions occur at higher Reynolds numbers, above critical, when the water fraction is smaller than a critical value of about 0.45.

At the other extreme, in all the flows where well-defined and fairly uniformly sized oil bubbles are observed, as in experiments 4, 8 and 11, table 2.2 shows that the dominant instability is due to surface tension: B_1 dominates. The instability of the shorter slugs shown in experiment 3 is still dominated by surface tension.

The interface term B_2, arising from friction, does not dominate when $m < 1$. It is an important term in the balance, giving rise to slugs and bubbles in experiments 3, 7, 8 and 10. It will be shown in the next section that when $m > 1$ (water inside, oil outside), the friction interface term B_2 is the dominant mode of instability giving rise to travelling waves on the interface.

Table 2.1. Terms of the energy equation $\dot{E} = I - 1 + B_1 + B_2$ evaluated for the most dangerous mode corresponding to experiment numbers in figure 1.1 of chapter V.

Exp. No.	η	$\mathbb{R}$	$\mathbb{R}'$	V_W/V	I−1	B_1	B_2	$\dot{E}$.
1	0.9245	432.2	613.4	0.145	0.361	−0.013	−0.229	0.119
2	0.8260	167.7	548.5	0.318	0.317	−0.008	−0.266	0.043
3	0.7026	99.4	555.4	0.494	0.952	1.408	0.642	3.000
4	0.4460	60.5	630.0	0.801	−0.802	5.784	−0.061	4.921
5	0.7614	833.1	3736.4	0.580	2.521	0.004	−0.015	2.510
6	0.6660	611.1	3836.6	0.556	1.746	0.026	0.034	1.805
7	0.5748	499.9	3995.4	0.670	1.531	0.119	0.241	1.890
8	0.3570	376.8	4554.2	0.873	0.223	4.383	0.275	4.880
9	0.5532	1439.0	12085.4	0.694	0.165	0.001	−0.001	0.165
10	0.3777	1148.2	13430.9	0.857	1.364	0.406	1.011	2.781
11	0.2160	1026.1	15121.5	0.953	−0.276	4.480	0.116	4.319

VI.2(h) The Viscous Liquid is on the Wall: $m > 1$

This case was considered by Hickox [1971] who used a perturbation scheme for long waves and showed that this flow is always unstable to long waves. In this section, it is shown that surface tension destabilizes long waves at the smallest $\mathbb{R}$ and the friction term B_2 at the interface destabilizes at larger $\mathbb{R}$. The instability takes form as a travelling wave of growing amplitude.

VI.2(h)(i) Neutral Curves, Parameters of the Fastest Growing Wave. Unlike the case $m < 1$, core-annular flow with $m > 1$ (the viscous liquid outside) is always unstable. The instability is always greatest for the axisymmetric mode and we shall present results for this case. Typical neutral curves are shown in figure 2.5. It shows that as $\mathbb{R} \to 0$, $\alpha \to 1$ and

$$\frac{d \log \mathbb{R}}{d\alpha} = \frac{1}{\mathbb{R}} \frac{d\mathbb{R}}{d\alpha} \to \infty.$$

The flow is unstable for small $\mathbb{R}$ when $\alpha < 1$. The results just given appear to be true for all positive values J, m, ζ, so long as $m > 1$.

Figure 2.6 shows the wavenumber $\tilde{\alpha}$ of the fastest growing wave and the maximum growth rate $\tilde{\sigma}$ as a function of $\mathbb{R}$ for different values η near 1 and $(J, m, \zeta) = (10^5, 10, 1)$. For small $\mathbb{R}$ the wavenumber of the fastest growing wave is independent of η and it is almost constant for $\mathbb{R} < 100$. From figure 2.6 (b) it is also evident that $\tilde{\sigma} \to 0$ as $\eta \to 1$. This means

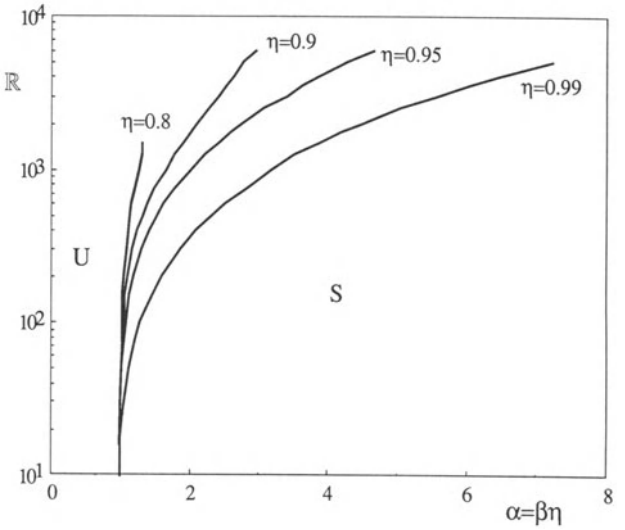

Fig. 2.5. [Hu and Joseph, 1989a] Neutral curves for different values of η near 1 when $(J^*, m, \zeta) = (10^5, 10, 1)$. U and S indicate the unstable and stable regions.

that core-annular flow with water in the core and oil outside is only weakly unstable if the thickness of the oil coating is thin.

VI.2(h)(ii) Energy Analysis. Figure 2.7 is a plot of the terms in the energy equation $\dot{E} = I - 1 + B_1 + B_2$ when $(J, m, \zeta) = (10^5, 10, 1)$ for $\eta = 0.7$ and 0.99. As in the case $m < 1$, surface tension plays an important role in instability at small values of $\mathbb{R}$, leading to the formation of water drops in oil. The main feature of the flows with m > 1 is that the friction term, which is proportional to the viscosity difference, is the dominant mode for instability at all but the smallest $\mathbb{R}$. The instability due to the Reynolds stress is not dominant when $m > 1$. In fact, $I - 1$ is often negative (stabilizing). This property of the Reynolds stress is compatible with the numerical evidence to date that Hagen-Poiseuille flow of one fluid in a round pipe is linearly stable. When the oil layer is very thin, the flow is only very weakly unstable. This fact, which we noted in our discussion of figure 2.6, is also evident in figure 2.7 (b).

VI.2(h)(iii) Comparison with Experiment. Aul and Olbricht [1990] have presented results of experiments corresponding to the analysis of this section. Their experimental apparatus is a glass capillary tube of round cross-section of radius 27 μm ($R_2 = 27\mu m$). The experiments were arranged so that the glass tube was wet by UCON oil of the same density as water. Water flows in the core. In the experimental results given to us, the film thickness of the oil is 1.8 μm. Hence $R_1 = 25.2\mu$m. The motion of the fluid

is monitored with a microscope. The values of material parameters are : $\rho_1 = \rho_2 = 10^6\,\mathrm{g/m^3}$, $\mu_1 = 1\,\mathrm{g/ms}$, $\mu_2 = 173\,\mathrm{g/ms}$, and $T = 3.5\,\mathrm{g/s^2}$. Hence $\eta = R_1/R_2 = 0.933$, $m = \mu_2/\mu_1 = 173$, $\zeta = 1$ and $J^* = TR_2\rho/\mu_1^2 = 94.5$.

The flow data are expressed as a superficial velocity based on the volume flux of water $U = Q_1/\pi R_2^2$. We compute the mass flux of water by integrating the basic velocity (2f.1) over the core.

$$Q_1 = W_0 \frac{1}{2}\pi R_1^2 \frac{m\eta^2 + 2(1-\eta^2)}{m\eta^2 + (1-\eta^2)}.$$

Thus

$$U = W_0 \frac{1}{2}\eta^2 \frac{m\eta^2 + 2(1-\eta^2)}{m\eta^2 + (1-\eta^2)} = 0.436 W_0.$$

We may now form expressions for the following quantities:

centerline velocity: $W_0 = \mathbb{R}\mu_1/\rho_1 R_2 = 3.704 \times 10^4 \mathbb{R}\mu\mathrm{m/s}$

superficial water velocity: $U = 0.436 W_0 = 1.615 \times 10^4 \mathbb{R}\mu\mathrm{m/s}$

wavelength: $L = 2\pi R_2/\tilde{\beta} = 169.6/\tilde{\beta}\mu\mathrm{m}$

growth rate: $\tilde{\sum} = \tilde{\sigma} W_0/R_2 = 1.372 \times 10^3 \tilde{\sigma}\mathbb{R}\mathrm{s}^{-1}$

wave speed: $\tilde{C} = c_\mathrm{r}(\tilde{\beta}) W_0 = c_\mathrm{r}(\tilde{\beta}) 3704 \times 10^4 \mathbb{R}\mu\mathrm{m/s}$

where $\tilde{\sigma} = \tilde{\beta} c_\mathrm{i}(\tilde{\beta})$.

The superficial water velocities U, which were specified in the experiments, range from 299 μm/s to 697 μm/s corresponding to $0.0185 < \mathbb{R} < 0.0432$, with an average $U = 448$ μm/s and an average $\mathbb{R} = 0.0277$. The wavelengths observed in the experiments ranged between $200\ \mu m < L < 280\mu$m, with an average $L = 225$ μm.

The theoretical predictions for the conditions specified in the experiments are given in table 2.2. It is found that the critical wavelength L does not depend on $\mathbb{R}$ for small $\mathbb{R}$. In table 2.3, the computed values for the terms in the energy balance are presented. These flows are unstable with small growth rates. The Reynolds stress minus dissipation $I - 1$ is always negative (stabilizing). At the smallest $\mathbb{R}$, the instability is due to a combination of capillarity and interfacial friction. At larger $\mathbb{R}$, in the region of the experiments, capillarity (B_1) has been suppressed and interfacial friction (B_2) supplies the destabilizing mechanism.

The following are points of comparison between theory and experiment:

(1) The theory predicts instability in all situations and no stable flows are observed.
(2) The theory predicts instability to axisymmetric disturbances and only these are observed.
(3) The theory predicts a travelling wave whose amplitude is increasing. This type of wave is observed.

(4) The theory predicts that the wavenumber of the fastest growing wave is independent of $\mathbb{R}$ in the range of small $\mathbb{R}$ in the experiments. This also appears to be true of the experiments though there is a non-systematic variation in the observed values of L, $200 < L < 280$ which does not correlate with $\mathbb{R}$.
(5) The value of $L = 224$ is predicted and a mean value $L = 225$ is observed.

Table 2.2. Predicted values of the lengths of the fastest growing wave L, the growth rate $\tilde{\sum}$ and the wave speed $\tilde{C}$ for the conditions in the experiments of Aul and Olbricht.

$\mathbb{R}$	$\tilde{\beta}$	$\tilde{\sigma}$	c_r	L(μm)	$\tilde{\sum}$(1/s)	$\tilde{C}$(μm/s)
0.005	0.757	$3.594\text{x}10^{-3}$	$9.900\text{x}10^{-4}$	224.0	$2.465\text{x}10^{-2}$	0.1833
0.01	0.757	$1.797\text{x}10^{-3}$	$9.900\text{x}10^{-4}$	224.0	$2.465\text{x}10^{-2}$	0.3667
0.0277	0.757	$6.488\text{x}10^{-4}$	$9.900\text{x}10^{-4}$	224.0	$2.466\text{x}10^{-2}$	1.016
0.05	0.757	$3.595\text{x}10^{-4}$	$9.900\text{x}10^{-4}$	224.0	$2.466\text{x}10^{-2}$	1.833
0.1	0.757	$1.799\text{x}10^{-4}$	$9.900\text{x}10^{-4}$	224.0	$2.468\text{x}10^{-2}$	3.667

Table 2.3. Values of the Reynolds stress minus dissipation $I - 1$, the interfacial tension surface term B_1, the frictional term at the interface due to the viscosity difference B_2, and the rate of change of disturbance energy $\dot{E}$ for the conditions in table 2.2.

$\mathbb{R}$	I−1	B_1	B_2	$\dot{E}$
0.005	$0.21\text{x}10^{-6}-1$	0.6605	0.3393	$0.2117\text{x}10^{-6}$
0.01	$0.41\text{x}10^{-6}-1$	0.3264	0.6733	$0.4173\text{x}10^{-6}$
0.0277	$0.55\text{x}10^{-6}-1$	0.05934	0.9402	$0.5816\text{x}10^{-6}$
0.05	$0.49\text{x}10^{-6}-1$	0.01899	0.9805	$0.6065\text{x}10^{-6}$
0.1	$0.16\text{x}10^{-6}-1$	$0.4819\text{x}10^{-2}$	0.9946	$0.6155\text{x}10^{-6}$

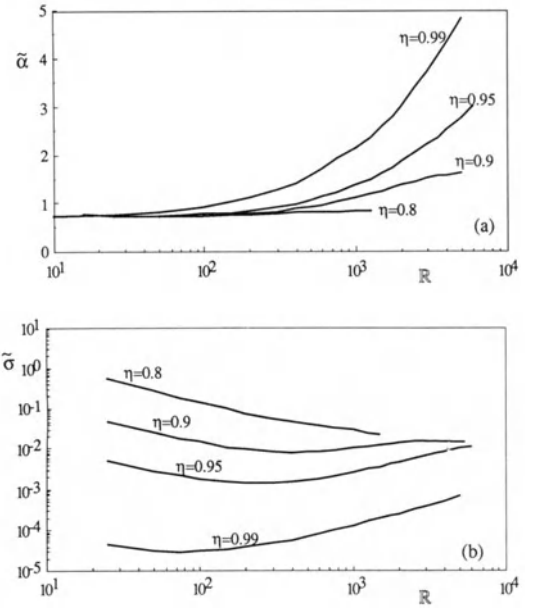

Fig. 2.6(a-b). [Hu and Joseph, 1989a] Maximum growth rate $\tilde{\sigma}$ and corresponding wavenumber $\tilde{\alpha} = \tilde{\beta}\eta$ against $\mathbb{R}$ for different values of η near 1 when $(J^*, m, \zeta) = (10^5, 10, 1)$. (a) $\tilde{\alpha}$, (b) $\tilde{\sigma}$.

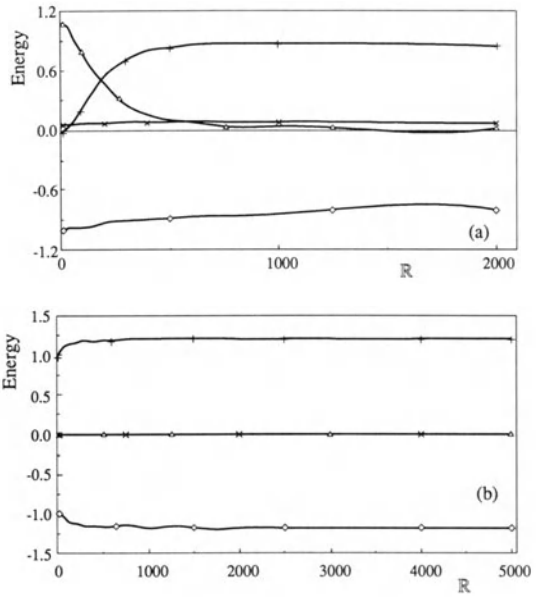

Fig. 2.7. [Hu and Joseph, 1989a] Variation of the terms of the energy equation $\dot{E} = I-1+B_1+B_2$ with $\mathbb{R}$ for $(J^*, m, \zeta) = (10^5, 10, 1)$. $\diamond, I-1; \triangle, B_1; +, B_2; \times, \dot{E}$. (a) η=0.7, (b) η=0.99. The flow is unstable if $\dot{E} > 0$. When η=0.99, $\dot{E}$ is very small, indicating neutral stability as $\eta \to 1$.

VI.2(i) Stability of Thin Liquid Threads

When η is sufficiently small, the core degenerates into a thin thread with a velocity profile

$$W(r) \sim \begin{cases} 1, & r \in [0, \eta], \\ 1 - r^2, & r \in [\eta, 1] \end{cases}$$

independent of m when $m\eta^2 \ll 1$. Moreover, both $W'(\eta^-)$ and $W'(\eta^+) \to 0$ with η. We may, therefore, expect limiting results, giving the instability of a uniform jet at the center of a Poiseuille flow of another liquid. The Poiseuille flow of a single liquid in a round pipe is always stable to small disturbances, and this stability does not appear to be disturbed by the small-diameter unstable jet. The jet itself cannot depend on W in this limit of small η and, if a new eigenvalue $\tilde{c} = \mathbb{R}(1-c)$ is defined, then it can be easily verified that the interface conditions are independent of $\mathbb{R}$. In fact, the numerical results yield eigenvalue c proportional to $1/\mathbb{R}$ and limiting values of the neutral curve and wavenumbers of the fastest growing wave which are independent of $\mathbb{R}$. In section VI.1 (k), we examined a capillary jet limit for a very viscous core, and it reduced to the one treated by Chandrasekhar [1961] in which $J(= TR_1\rho_1/\mu_1)$, rather than $\mathbb{R}$, appears as the controlling parameter. The thin jets studied here also have this property. The analysis of the energy of these jets shows clearly that when $\eta \to 0$, we are dealing exclusively with capillary instability. The disturbance energy associated with the Reynolds stress minus dissipation and with interfacial friction is stabilizing.

VI.2(i)(i) Neutral Curves, Parameters of the Fastest Growing Wave. The parameters used in this section are the wavenumber $\alpha = \eta\beta$ where $\eta = R_1/R_2$, the usual Reynolds number $\mathbb{R} = \rho_1 R_2 W_0/\mu_1$, and the surface tension parameter $J^* = TR_2\rho_1/\mu_1^2$. We shall give results for two representative values $m = 0.1$ and $m = 10$ and confine our attention to the case of matched density $\rho_2 = \rho_1$. If $\mathbb{R}$ and J^* are for $m = 0.1$, then $10\mathbb{R}$ and $100J^*$ are the Reynolds number and surface tension parameter when $m = 10$. The thin jet and its surrounding fluid have the same density and different viscosities: say oil is inside and water is outside or vice versa.

Figure 2.8 shows that the neutral curves are independent of $\mathbb{R}$ for small $\mathbb{R}$ and are also independent of m for small $\mathbb{R}$. The neutral curves begin at $\mathbb{R}$=0 and $\alpha = 1$, at which point the figure indicates that $\partial\mathbb{R}/\partial\alpha = \infty$. The flow is unstable for wavenumbers on the left of the neutral curves. Neutral curves of this sort are characteristic of capillary instability in which the main action of viscosity enters through J^* rather than $\mathbb{R}$.

Figure 2.9 is a log-log plot of the maximum growth rate $\tilde{\sigma}^* = \tilde{\alpha}c_i(\tilde{\alpha})$, as a function of $\mathbb{R}$ for different η. The straight lines show that $\tilde{\sigma}^*$ is proportional to $1/\mathbb{R}$, which indicates that the expression $\tilde{c} = \mathbb{R}(1 - c)$ is a natural grouping of terms. Figure 2.10 shows that the wavenumber of the fastest growing wave is basically independent of $\mathbb{R}$ for small η irrespective of whether the more viscous liquid is inside or outside.

Table 2.4 shows that the instability of a thin jet is due to capillarity. There are only weak effects of $\mathbb{R}$ and m through the stabilizing action of the Reynolds stress minus dissipation, $I-1$, and the interfacial friction B_2.

Table 2.4. Terms of the energy balance for thin liquid threads.

$\mathbb{R}$	B_1	B_2	$I-1$	$\dot{E}$
		$(J^*,m,\eta,\zeta)=(1000,0.1,0.05,1)$		
5	2.422	−0.05065	$0.1141\text{x}10^{-5}-1$	1.3717
50	2.422	−0.05063	$0.1140\text{x}10^{-3}-1$	1.3716
100	2.422	−0.05059	$0.4545\text{x}10^{-3}-1$	1.3723
250	2.422	−0.05026	$0.2793\text{x}10^{-2}-1$	1.3748
500	2.421	−0.04919	$0.1058\text{x}10^{-1}-1$	1.3829
		$(J^*,m,\eta,\zeta)=(10^5,10,0.05,1)$		
10	3.681	−0.2285	$0.4840\text{x}10^{-7}-1$	2.4523
100	3.681	−0.2285	$0.4840\text{x}10^{-5}-1$	2.4523
500	3.680	−0.2283	$0.1210\text{x}10^{-3}-1$	2.4522
2000	3.672	−0.2250	$0.1914\text{x}10^{-2}-1$	2.4490

Table 2.5. Capillary instability of a liquid jet in air $(J,\ m,\ \zeta,\ \mathbb{R}_1) = (10^{10},\ 10^{-3},\ 10^{-4},\ 10^{-3})$.

η	0.8	0.6	0.4	0.2	0.1	0.5
$\tilde{\alpha}$	0.6970	0.6969	0.6968	0.6968	0.6967	0.6965

VI.2(i)(ii) Capillary Instability. In the study of instability of jets, it is appropriate to use the radius of the jet R_1 as the scale of length. We have introduced dimensionless parameters $J = TR_1\rho_1/\mu_1^2$ and $\mathbb{R}_1 = W_0R_1\rho_1/\mu_1$ and the wavenumber α based on R_1.

Consider the capillary instability of a liquid jet in air. This corresponds to core-annular flow with a liquid core and an air annulus. Therefore, we take the viscosity ratio m and density ratio ζ to be very small. If the influence of the air is neglected and the jet is considered inviscid, this capillary instability leads to Rayleigh's result that the maximum growth rate occurs for the wavenumber $\tilde{\alpha}$=0.697. The jet presumably breaks into bubbles of length $2\pi R_1/0.697$ because of surface tension. Table 2.5 lists the results of computations, where J is taken very large and $\mathbb{R}_1$ very small to ensure that

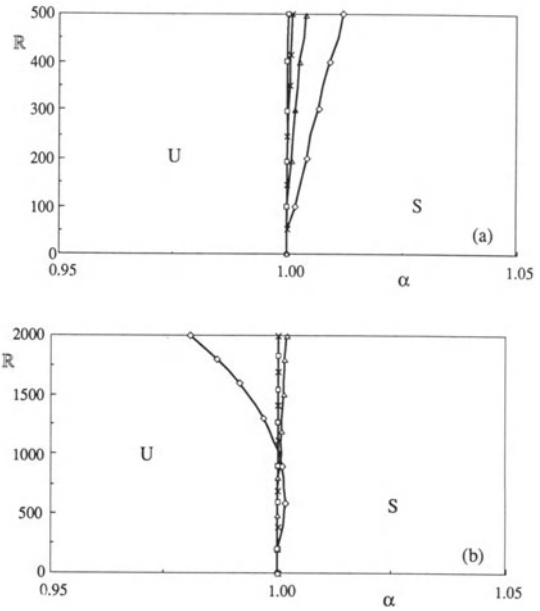

Fig. 2.8. [Hu and Joseph, 1989a] Neutral curves for different small values of η. $\diamond$, $\eta = 0.2$; $\triangle$, $\eta = 0.1$; $\times$, $\eta = 0.05$; $\square$, $\eta = 0.01$. (a) $(J^*, m, \zeta) = (10^3, 0.1, 1)$; (b) $(J^*, m, \zeta) = (10^5, 10, 1)$.

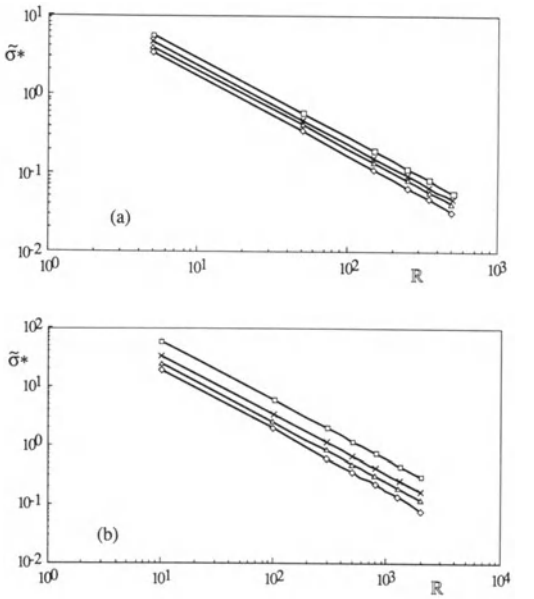

Fig. 2.9. [Hu and Joseph, 1989a] Maximum growth rate $\tilde{\sigma}^*$ as a function of $\mathbb{R}$ for $\eta = 0.2$, 0.1, 0.05 and 0.01. Symbols as in figure 2.8.

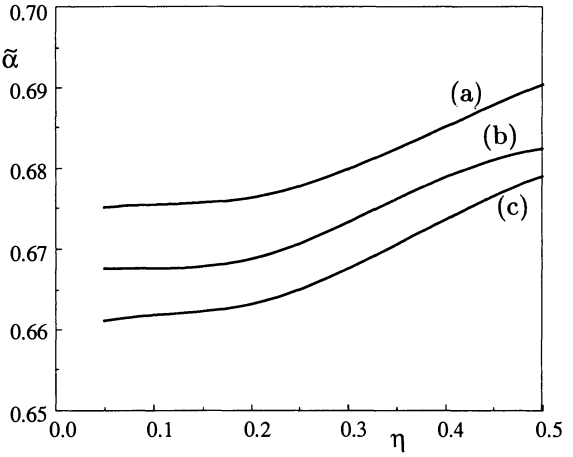

Fig. 2.10. [Hu and Joseph, 1989a] The wavenumber $\tilde{\alpha}$ of the fastest growing wave as a function of η when the density is matched, $\zeta = 1$, and capillary instability dominates. (a) $(J, \mathbb{R}_1, m) = (10^{10}, 0.1, 0.1)$; (b) $(J, \mathbb{R}_1, m) = (2 \times 10^9, 10^{-3}, 10^3)$; (c) $(J, \mathbb{R}_1, m) = (2 \times 10^3, 10^{-3}, 10^{-3})$.

surface tension dominates the instability. The agreement with Rayleigh's $\tilde{\alpha}$ = 0.697 is excellent.

In the above case, the inertia of the fluid outside the jet could be neglected. Now let us consider another extreme case: a jet of air injected into liquid. The capillary instability of such a 'hollow jet' was studied by Chandrasekhar [1961] with the result that the maximum growth rate is achieved at $\tilde{\alpha}$=0.484. It is obvious that in this situation the boundary of the pipe wall will have an effect on the instability, but this effect should become less as the core becomes thinner. In the computations here, m and ζ are both taken very large to simulate the situation. It is found that $\tilde{\alpha}$ = 0.489 at $\eta = 0.1$, and $\tilde{\alpha} = 0.487$ at $\eta = 0.05$ which are very close to the result of Chandrasekhar's 0.484.

For $\zeta = 1$, the inertia of both the fluid in the core and in the annulus cannot be neglected. Figure 2.10 presents results for three cases. For all the cases, the calculated limit of $\tilde{\alpha}$ as $\eta \to 0$ depends on the value of J and m. Computations show that for very large J, where surface tension plays a dominant role, the limiting value of $\tilde{\alpha}$ is almost the same for different viscosity ratios m regardless of whether $m < 1$ or $m > 1$. For fixed m, the limiting value increases with J and also tends to a unique J-independent limiting value when J is large.

VI.2(j) Stability of Core-Annular Flow in Three Layers (Hydrophobic Pipe Walls)

For some construction materials, it is impossible to make the water wet the pipe wall; the pipe wall is hydrophobic and takes on oil preferentially. Teflon is an example. It is, however, possible to get a lubricated flow in such a situation. There is an annulus of water between the oil in the core and the oil on the wall. In fact, it will be shown that core-annular flow of this type is always unstable. In these cases, waves are seen on the surface of the oil which wets the wall. It appears that such waves are equilibrated nonlinearly and that they are driven by an instability due to friction at the interface. In this section, we give the results from the linear theory of stability for the three-layer problem. The finite element code described earlier is used. A sample of results will be given, restricted to the case of density-matched fluids $\zeta = 1$ and compared with two representative two-layer problems. The representative problems are for $\eta = 0.6$ and $\eta = 0.8$. When $\eta = 0.8$, the neutral curve consists of two branches; whereas for $\eta = 0.6$ the neutral curve is continuous and not in separate branches.

VI.2(j)(i) Neutral Curves. In figure 2.11 we present neutral curves for the three-layer problem. The unstable region lies on the left side of each neutral curve and the stable region lies on the right. The flow is always unstable to long waves, as in the two-layer case with $m > 1$. The neutral curves all begin at the wavenumber $\beta = 1/\eta$. The neutral curves for b=0.90 and b=0.95 in figure 2.11 (a) have a corner at a certain β-value; the neutral curves for b= 0.8 and b= 0.9 in figure 2.11 (b) are rather strange. These unusual features will be explained in what follows.

For the cases considered in this section, it was found that three-layer core-annular flow may be regarded as the composition of one two-layer flow with $m < 1$ and another two-layer flow with $m > 1$, as shown in figure 2.12. In the decomposition, we define the dimensionless parameters $\mathbb{R}$, J^* based on one fluid (fluid 1), as in (2c.2), for all three cases. This decomposition will provide the explanation of the main features of the neutral curves. In figure 2.13, we compare two- and three-fluid neutral curves when η =0.8 and 0.6. The neutral curve for the three-layer case (1) begins at $\beta = 1/\eta$, first following the lower branch of the neutral curve for case (2), then following the neutral curve for case (3) until it meets the upper branch of the neutral curve for case (2). At this point, it makes a sharp turn to the right, roughly following the upper branch. Since the upper branch of the neutral curve corresponds to instability due to Reynolds stress in the water layer, the real characteristic length for this instability is the thickness of the water layer. When another layer of fluid is added near the pipe wall, this characteristic length decreases, and correspondingly the wavenumber β increases. Therefore, the position of this part of neutral curve for the three-layer case moves to larger β, as seen in figure 2.13 (a). The increase in the wavenumber for this part of the neutral curve is not linearly propor-

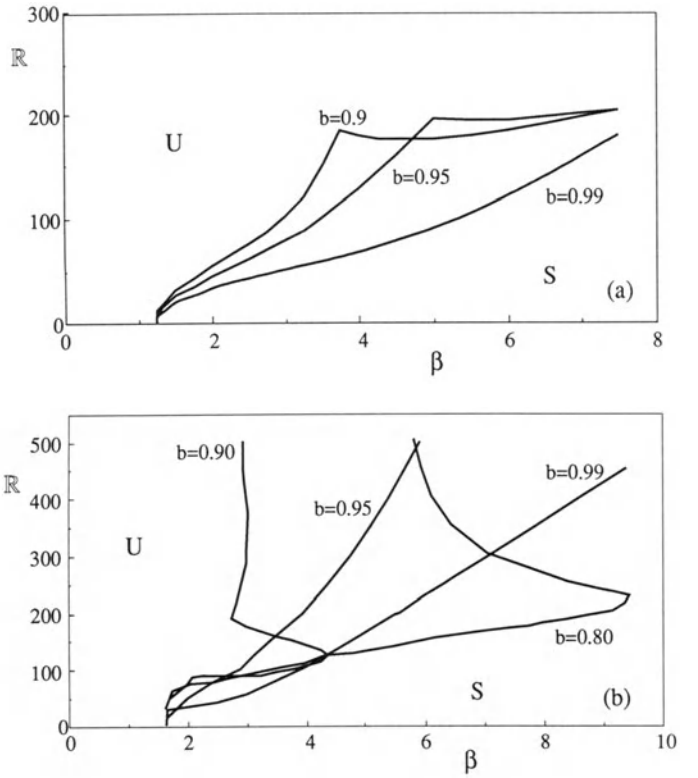

Fig. 2.11(a-b). [Hu and Joseph, 1989a] Neutral curves for different values of $b = R_2/R_3$ when $J^* = 10^3$, m=0.1 and (a) $\eta = 0.8$, (b) $\eta = 0.6$.

tional to the decrease in the thickness of the layer. Computations show that Reynolds stress near the pipe wall gives a relatively larger contribution to the total integrated Reynolds stress in the water. In figure 2.13 (b), curve (1) starts off following (2), then follows (3), and then deforms but swings back to follow what can be thought of as a deformed curve (2). It is expected that as the outer layer becomes thinner ($b \to 1$), this deviation of the neutral curve becomes less. Therefore, the neutral curve for the three-layer flow can be viewed as a combination of neutral curves for case (3) and the deformed neutral curve for case (2) in which the upper branch is moved to larger β.

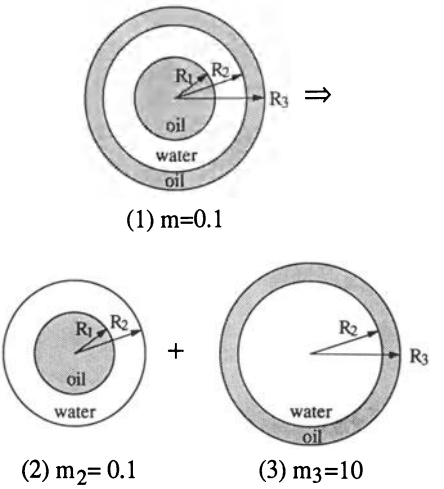

Fig. 2.12. [Hu and Joseph, 1989a] Diagram showing how three-layer core-annular flow could be understood from the composition of two two-layer flows.

VI.2(j)(ii) Parameters of the Fastest Growing Wave. In the three-layer problem, $b = R_2/R_3$ is the radius of the interface nearest the wall at $r = 1$ and $\eta = R_1/R_3$, $\eta \leq b \leq 1$, is the radius of the core. The case in which a thin oil-layer is on the wall, $b \to 1$, is of practical interest. Figure 2.14 shows the growth rate $\sigma(\beta)$ for $(J^*,\ m,\ \eta) = (10^3,\ 0.1,\ 0.8)$ for different $\mathbb{R}$ and (a) b= 0.9, (b) b= 0.99. Discontinuities in the slopes of the curve mean that the mode of instability has changed. For example, the growth-rate curve for $\mathbb{R} = 200$, shown in figure 2.14 (a), has two peaks: analysis of the energy shows that the first peak is associated with interfacial friction, the second with an instability due to the Reynolds stress in the middle (water) layer. As $\mathbb{R}$ increases, the second peak grows. The magnitude of the growth rates decreases as $b \to 1$. Figure (b) shows the growth rates on a logarithmic scale. The first peak on the curve for $\mathbb{R} = 50$ is due to instability induced by interfacial tension and friction on the interface at $r = \eta$. The high peak on the curve for $\mathbb{R} = 500$ corresponds to an instability due to the Reynolds stress in the water layer. The curve for $\mathbb{R} = 150$ is smooth because there is only one unstable mode due to interfacial friction; the corresponding two-layer

flow is stable when $\mathbb{R} = 150$ (see figure 2.2).

Figure 2.15 shows the maximum growth rate $\tilde{\sigma} = \tilde{\beta} c_i(\tilde{\beta})$ and wavenumber $\tilde{\beta}$ of the fastest growing wave as a function of $\mathbb{R}$ for the conditions specified in figure 2.14 when $\eta = 0.8$. The corresponding two-layer flow for $\eta = 0.8$ has an interval, shown in figure 2.2, in which core-annular flow is stable. The curves in figure 2.15 can be divided into three intervals. The first is an interval of small $\mathbb{R}$ where the growth rate for interfacial tension and friction is larger at the inner than at the outer interface. The second interval is for medium $\mathbb{R}$ where the growth rate for instability at the outer interface dominates. Actually, the inner interface is stable for most values of $\mathbb{R}$ in this section. The growth rate for the eigenvalue arising from the outer interface tends to zero as $b \to 1$. This is reflected in figure 2.15 (b) when $b = 0.99$ where the boundary of this interval is quite sharp and just fits the stable region of two-layer flow in figure 2.2. The third interval is for larger $\mathbb{R}$ where the growth rate of the eigenvalue arising from the inner interface again is the larger one and the flow is unstable due to the Reynolds stress. The jumps of $\tilde{\beta}$ indicate changes in the dominant mode of instability. The case $\eta = 0.6$ does not exhibit mode jumping, because the corresponding neutral curve for the two-layer problem shown in figure 2.2 does not have distinct branches. In all the cases, the growth rate for instability is larger at the inner than at the outer interface.

Figure 2.16 demonstrates that the difference between the two- and three-layer cases tends to zero as the outer layer gets thinner, $b \to 1$. Thus, a thin layer of oil on the wall of a pipe need not be a serious impediment to the lubrication of an oil core with water.

VI.2(j)(iii) Energy Analysis. In three-layer core-annular flow, there are two interfaces giving rise to two interfacial eigenvalues and using energy analysis, we can again determine the sources of the instabilities.

Figure 2.17 shows the graph of the terms in the energy equation, $\dot{E} = I - D + B_{1\eta} + B_{1b} + B_{2\eta} + B_{2b}$, corresponding to growth rate curves shown in figure 2.15. These curves are associated with mode jumping which is evident from figure 2.15. In the first interval, $B_{1\eta}$ and $B_{2\eta}$ are destabilizing. The instability is induced at the inner interface. As $\mathbb{R}$ increases, the first instability is a capillary instability due to interfacial tension ($B_{1\eta}$); then interfacial friction $B_{2\eta}$ becomes important. At higher $\mathbb{R}$, in the second interval, B_{2b} is largest; the instability is due to the interfacial friction at the outer interface (we believe this produces waves at the outer interface). At still higher $\mathbb{R}$, in the third interval, instability due to the Reynolds stress becomes dominant. This type of instability can be associated with the formation of emulsions of water in oil, at least in some cases.

In lubricated pipelining, the core-annular flow with capillary instability (oil bubbles or oil slugs in water) or surface waves is also effective for lubricated transport of very viscous oil, although not as effective as stable core-annular flow. The most undesirable situation is when water emulsifies in the oil. This leads to a breakdown of lubrication. The results of linear

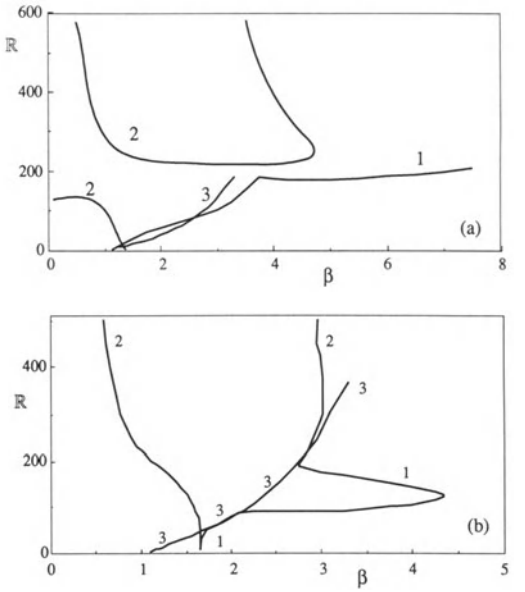

Fig. 2.13(a-b). [Hu and Joseph, 1989a] Neutral curves for two-layer and three-layer flows when $(J^*, m, b) = (10^3, 0.1, 0.9)$. (1) Three layers; (2) two layers with m=0.1; (3) two layers with m=10. (a) η =0.8, (b) $\eta = 0.6$.

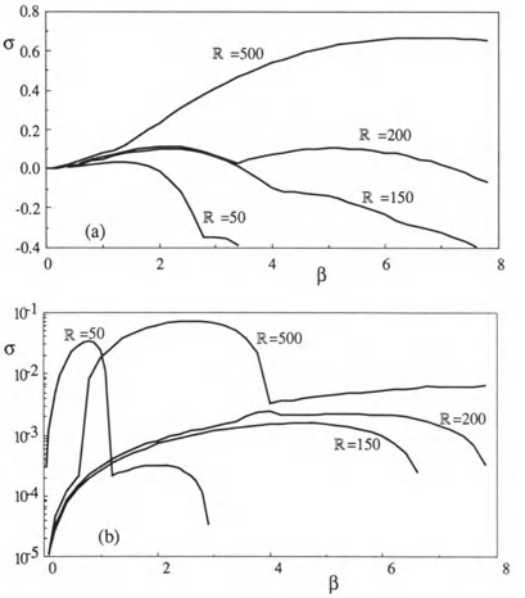

Fig. 2.14(a-b). [Hu and Joseph, 1989a] Growth rates $\sigma = \beta c_i$ for three-layer flows as a function of the wavenumber and different $\mathbb{R}$ when $(J^*, m, \eta) = (10^3, 0.1, 0.8)$. (a) $b = 0.9$, (b) $b = 0.99$.

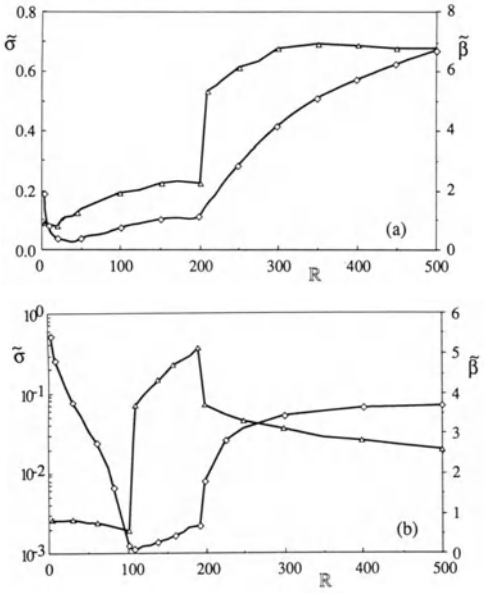

Fig. 2.15(a-b). [Hu and Joseph, 1989a] Maximum growth rate $\tilde{\sigma}$ and wavenumber $\tilde{\beta}$ for maximum growth as a function of $\mathbb{R}$ when $(J^*, m, \eta) = (10^3, 0.1, 0.8)$. $\diamond, \tilde{\sigma}$; $\triangle, \tilde{\beta}$. (a) $b = 0.90$, (b) $b = 0.99$.

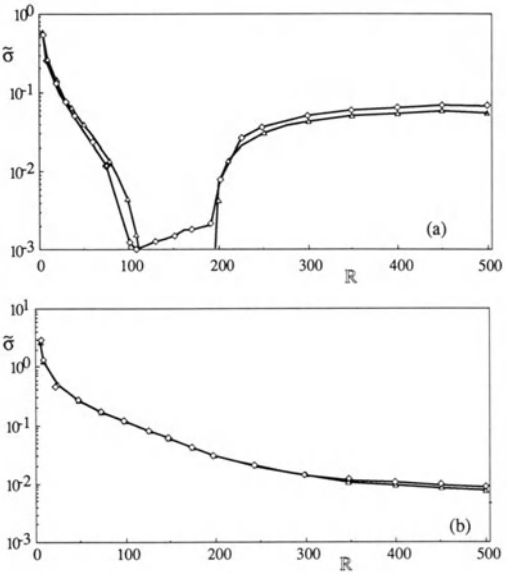

Fig. 2.16(a-b). [Hu and Joseph, 1989a] Comparison of the maximum growth rates $\tilde{\sigma}$ for two-layer and three-layer core-annular flow when the viscous layer on the outer wall is thin, $(J^*, m, b) = (10^3, 0.1, 0.99)$. $\diamond$, Two layers; $\triangle$, three layers. (a) η=0.8, (b) η=0.6.

stability theory suggest that the oil layer at the pipe wall does not have much influence on the operation of lubricated pipelining since it induces only slight changes on the onset of instabilities due to the Reynolds stress in the water.

Hooper and Boyd [1987] studied the instability of Couette flow of two superposed fluids of different viscosity when the depth of the lower less viscous fluid is bounded by a wall and the interface, while the depth of the upper viscous fluid is unbounded. They studied an instability at large Reynolds number (see also section IV.6b) revealed first in a numerical study of Renardy [1985] and suggested that the instability is due to the disturbance vorticity generated by the solid boundary. They showed that this instability is driven by the Reynolds stress in the water when m <1. In fact, the Reynolds stress is proportional to W' where $W(r)$ is the forward velocity of the basic flow. W' in the water is about $1/m$ times larger than W' in the oil core, leading to larger Reynolds stress in water than in oil. Figure 2.18 shows that the dominant instability at high $\mathbb{R}$ continues to be associated with the Reynolds stress in the water annulus even when there is an oil layer at the wall; the Reynolds stress contribution I_2 in the intermediate low-viscosity layer is clearly much larger than the Reynolds stress contribution I_1 in the oil core or I_3 in the oil layer on the pipe wall. The origin of this instability in the water when a layer of oil is on the wall needs clarification.

VI.2(j)(iv) Amplitude Ratio and Phase Shift of the Inner and Outer Interface. We recall that $\delta_1(z,t)$ is the deviation of the inner interface from a mean radius R_1 and $\delta_2(z,t)$ is the deviation of the outer interface from a mean radius R_2. In the linearized theory

$$[\delta_1(z,t);\delta_2(z,t)] = \exp[\mathrm{i}\beta(z-ct)][\delta_1;\delta_2],$$

where $\delta_1 = |\delta_1|e^{i\phi_1}, \delta_2 = |\delta_2|e^{i\phi_2}$ are complex constants. The amplitude ratio $|\delta_1|/|\delta_2|$ and phase shift $\phi_2 - \phi_1$ give the relative shape of the two interfaces in the linearized approximation.

Figure 2.19 shows the amplitude ratio and phase shift as a function of $\mathbb{R}$ for $(J^*, m, \eta) = (10^3, 0.1, 0.8)$ and $b = 0.99$. There are three distinct regions of Reynolds numbers. In the first and third regions, the flow of the corresponding two-layer problem is unstable (see figure 2.16 (a)). This means the main instability for low and high $\mathbb{R}$ in three-layer flow is associated with the core-lubricant interface or the water annulus. The magnitude of the amplitude ratio for these $\mathbb{R}$ is largely dependent on the thickness $1-b$ of the outer layer. The instability in these cases is reflected in the relatively large deformation of the inner interface. For $\mathbb{R}$ in the range $\mathbb{R}_L < \mathbb{R} < \mathbb{R}_U$, the two-layer core-annular flow is stable and the only instability is due to interfacial friction at the outer interface and $|\delta_1|/|\delta_2| < 1$, with only small variations with the thickness $1 - b$. There is always a phase shift between the two interfaces, except at the smallest $\mathbb{R}$ where interfacial tension is

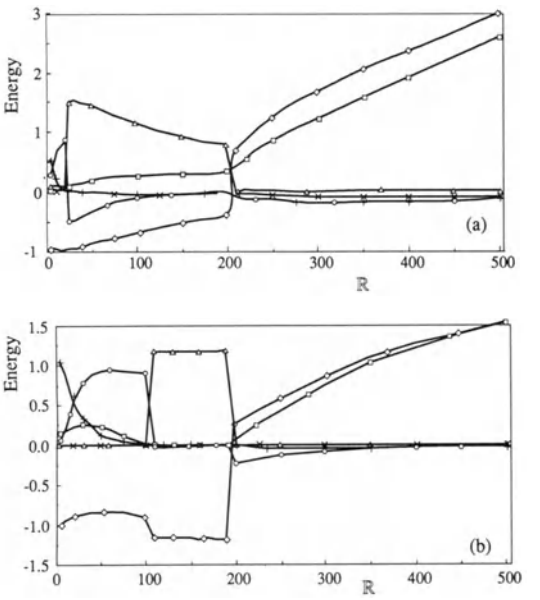

Fig. 2.17(a-b). [Hu and Joseph, 1989a] Variation with $\mathbb{R}$ of terms in the energy balance $\dot{E} = I + B_{1\eta} + B_{2\eta} + B_{1b} + B_{2b} - D$, normalized for $D = 1$ with $(J^*, m, \eta) = (10^3, 0.1, 0.8)$. (a) $b = 0.9$, (b) $b = 0.99$. $\diamond$, $I - 1$; $+$, $B_{1\eta}$; $\times$, B_{1b}; $\blacksquare$, $B_{2\eta}$; $\triangle$, B_{2b}; $\square$, $\dot{E}$.

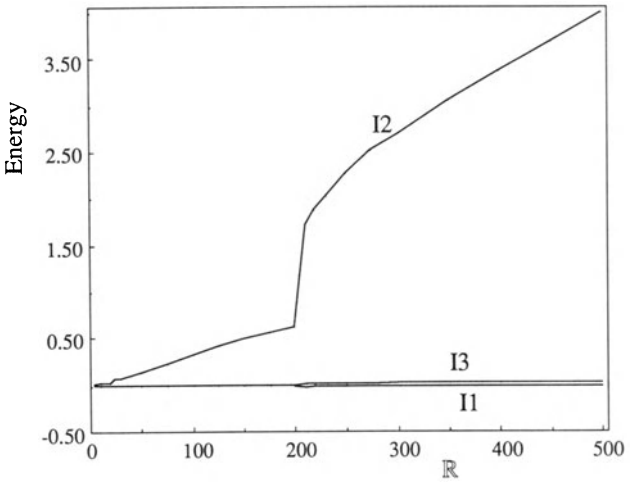

Fig. 2.18. [Hu and Joseph, 1989a] Variation with $\mathbb{R}$ of the energy due to Reynolds stresses I_1 in the oil core, I_2 in the water annulus and I_3 in the oil layer on the wall, $I = I_1 + I_2 + I_3$, $(J^*, m, \eta, b) = (10^3, 0.1, 0.8, 0.9)$.

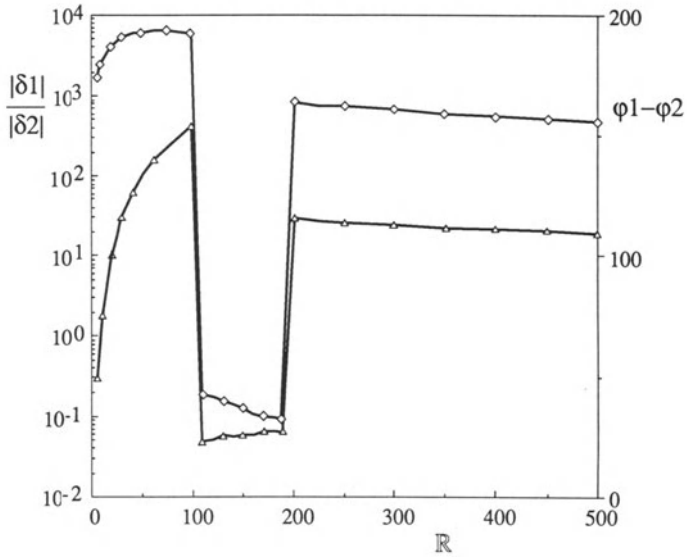

Fig. 2.19. [Hu and Joseph, 1989a] Amplitude ratio $|\delta_1|/|\delta_2|(\diamond)$, and phase shift $\phi_1 - \phi_2(\triangle)$. (J^*, m, η, b)=(10^3, 0.1, 0.8, 0.99).

dominant. The phase shift and amplitude ratio appear to tend to limiting values for large $\mathbb{R}$.

VI.2(k) Conclusions

Linear stability analysis of core-annular flow leads to the following conclusions:

(1) There are three different kinds of instability identified through the energy analysis: (a) an interfacial tension instability or capillary instability; (b) an interfacial friction instability due to the viscosity difference across the interface; (c) a Reynolds stress instability.

(2) At low Reynolds numbers, instability due to interfacial tension is dominant.

(3) Interfacial friction causes instability in two-layer flow with $m > 1$ when $\mathbb{R}$ is relatively large. It may also dominate the instability for three-layer flow at values of $\mathbb{R}$ in the range where two-layer core-annular flow with $m < 1$ would be stable if the water fraction were smaller.

(4) Instability due to the Reynolds stress is dominant in two-layer flow with $m < 1$ and the the three-layer flow when $\mathbb{R}$ is sufficiently large (corresponding to the upper branch of the neutral curve) and the core is not very thin.

(5) The Reynolds stress instability is always associated with the less viscous fluid layer. Even in the three-layer flow where a viscous layer of fluid is on the pipe wall, the Reynolds stress instability is induced by the less viscous fluid in the intermediate layer. The possibility raised by the work of Hooper and Boyd [1987] that this instability is due to the disturbance vorticity generated by the solid boundary needs to be reconciled with the observation that we have this type of instability in the water even when it does not touch the solid boundary.

(6) Comparison with the experiments of CGH suggests that bubbles or slugs of oil in water are associated with interfacial tension instability or capillary instability; the emulsification of water into oil is correlated with the Reynolds stress instability. The water fraction is an important factor in determining the phase inversion with water emulsions, in achieving stable core-annular flow for small water fraction, and in the formation of some types of oil bubbles in water for larger water fractions. Comparison with the experiments of Aul and Olbricht also suggests that interfacial friction instability generates interfacial waves which may equilibrate nonlinearly.

(7) Two-layer core-annular flow with $m < 1$ and η near 1 undergoes the following scenario of instabilities as $\mathbb{R}$ is increased: instability due to interfacial tension, stabilization of the instability of interfacial tension associated with the growth of instability due to interfacial friction, complete stabilization of core-annular flow, instability due to the growth of Reynolds stresses in the lubricating layer. If η is smaller than say 0.7, the stabilization of core-annular flow will not occur. When the core is very small ($\eta \to 0$), only the instability due to interfacial tension (capillary instability) will occur.

(8) Two-layer flow with $m > 1$ is always unstable. It is only weakly unstable if the thickness of the oil coating is very small (the maximum growth rate $\sigma \to 0$ as $\eta \to 1$).

(9) In two-layer flow with $m > 1$, there are two instabilities: interfacial tension at lower $\mathbb{R}$, and interfacial friction at higher $\mathbb{R}$. Instability due to Reynolds stresses does not occur because the flow with just one fluid would be linearly stable.

(10) Core-annular flow with a very thin core ($\eta \to 0$) undergoes instability due to interfacial tension alone, when $m > 1$ or $m < 1$. The disturbance energies associated with the Reynolds stress minus dissipation $I - D$ and with interfacial friction B_2 are stabilizing. The neutral curves and wavenumbers of the fastest growing wave are independent of $\mathbb{R}$; the maximum growth rate is proportional to $1/\mathbb{R}$. This is consistent with the fact that as $\eta \to 0$, the expression $\tilde{c} = \mathbb{R}(1 - c)$ is independent of $\mathbb{R}$, as in the theory of capillary instability.

(11) In general, the capillary instability of jets depends on parameters J^*, m and ζ. Rayleigh's capillary instability of an inviscid jet with $\tilde{\alpha} = 0.697$ emerges when the density ratio ζ and viscosity ratio m are very small.

Capillary instability of a 'hollow jet' with $\tilde{\alpha}$= 0.484 emerges when the density ratio ζ and viscosity ratio m are very large.

(12) Three-layer core-annular flow, denoted as flow (1), may in some instances be regarded as the composition of one two-layer flow with $m < 1$ (denoted by (2)) and another two-layer flow with $m > 1$ (denoted by(3)). The neutral curve for (1) can be viewed as a combination of the neutral curve for (3) and the deformed neutral curve for (2) in which the upper branch is moved to larger wavenumbers.

(13) The three-layer flow considered in this section is always unstable. Roughly speaking, as $\mathbb{R}$ increases, it undergoes the same sequence of instabilities as two-layer flow with $m < 1$ except that the stable core-annular flow region is destabilized by interfacial friction at the outer interface.

(14) As the viscous layer coating the pipe wall becomes thinner ($b \to 1$), the difference between two-layer flow with $m < 1$ and three-layer flow tends to zero. Thus, a thin layer of oil on the wall of a pipe need not be an impediment to lubricated pipelining.

(15) The amplitude ratio $|\delta_1|/|\delta_2|$ is largely dependent on the thickness of the outer layer $(1 - b)$, when the instability is induced at the inner interface or in the middle water annulus reflecting a relatively large deformation of the inner interface. Except at the smallest $\mathbb{R}$, there is always a phase shift between the two interfaces.

VI.2(ℓ) Comparison with Field Data: Scale-up, Transition to Water in Oil (w/o) Emulsions

Field Data. We were given field data by V. Kruka and G. Geiger of West-Hollow Research Center of the Shell Development Company in the following form.

Outline of the Test Cases

1. Lower limit of viscosity

Input: pipe D = 6.249 in.
pipe wall roughness ϵ=150×10^{-6}ft
oil flow rate $\dot{V}|_{\text{oil}}$=500 gpm
annular water flow rate $\dot{V}|_{\text{water}}$=165 gpm
interfacial tension 20 dynes/cm
oil viscosities 100000 cs, 10000 cs, 1000 cs, and lower to limit (i.e., core-flow breakup)
fresh water properties at 60°F

Output: frictional pressure gradient for each oil viscosity
wave characteristics such as wavelength and amplitude
lower limit of viscosity

2. Pipe diameter effects

Input: pipe D's 4.026, 6.249, 10, 14, 20, 26, 32, 40 and 48 in.
pipe wall roughness $\epsilon=150\times10^{-6}$ft
water to oil flow rate $\dot{V}|_{\text{oil}}/\dot{V}|_{\text{water}}=0.20$
interfacial tension 20 dynes/cm
oil viscosity 10000 cs
mean (bulk) velocity $\dot{V}|_{\text{total}}/A_{\text{total}}=5$ fps
fresh water properties at 60°F

Output: frictional pressure gradient for each pipe D
wave characteristics for each pipe D
maximum mean velocity at each pipe D

We were asked to obtain the output by inputting the given data into our theory. From the start, we knew that there was no way we could get the wave amplitude or frictional pressure gradient when the flow rates were prescribed from a linear theory. However, we evidently were successful in predicting wave lengths, wave speeds, and the conditions controlling the transition to w/o emulsions.

Transition to w/o Emulsions. We identified the transition to emulsions as a mode jump in which the fastest growing mode of the linear theory changes discontinuously as the viscosity is decreased, with the other parameters held constant. For the larger viscosities, the most dangerous disturbance is a short wave which gives rise to waves driven by interfacial friction. There is also a long wave mode of instability arising from Reynolds stresses in the water, as in figures 2.20-2.22, but the maximum growth rate for the long waves is smaller than for the short waves for the 100000 cs, 10000 cs and 1000 cs oil. At 500 cs, the situation is reversed, as in figure 2.23 and the maximum growth rate is for a long wave and is associated with the Reynolds stress in the water (see table 2.6). Perhaps this transition can be associated with a transition to turbulence in the water.

The transition to w/o emulsions depends also on the water fraction. You will never see water/oil emulsions in systems in which much more water than oil is present. This appears to be related to a problem of phase inversion for packing of liquid spheres.

We found that for each and every one of the test cases, the mechanism which produces instability is the interfacial friction B_2, proportional to the viscosity difference at the interface. The other two mechanisms, Reynolds stress in the water and interfacial tension, are stabilizing. In our previous work, we have always found that this instability profile corresponds to instability of PCAF, but stability of nonlinearly equilibrated interfacial waves which industry regards as stable core-flow. For all these, we produce a wavelength and a wave speed.

The last entry in table 2.6 shows sharply different stability properties than all the others. This case would correspond to 500 cs oil and the instability is produced by the Reynolds stress in the water: the interfacial

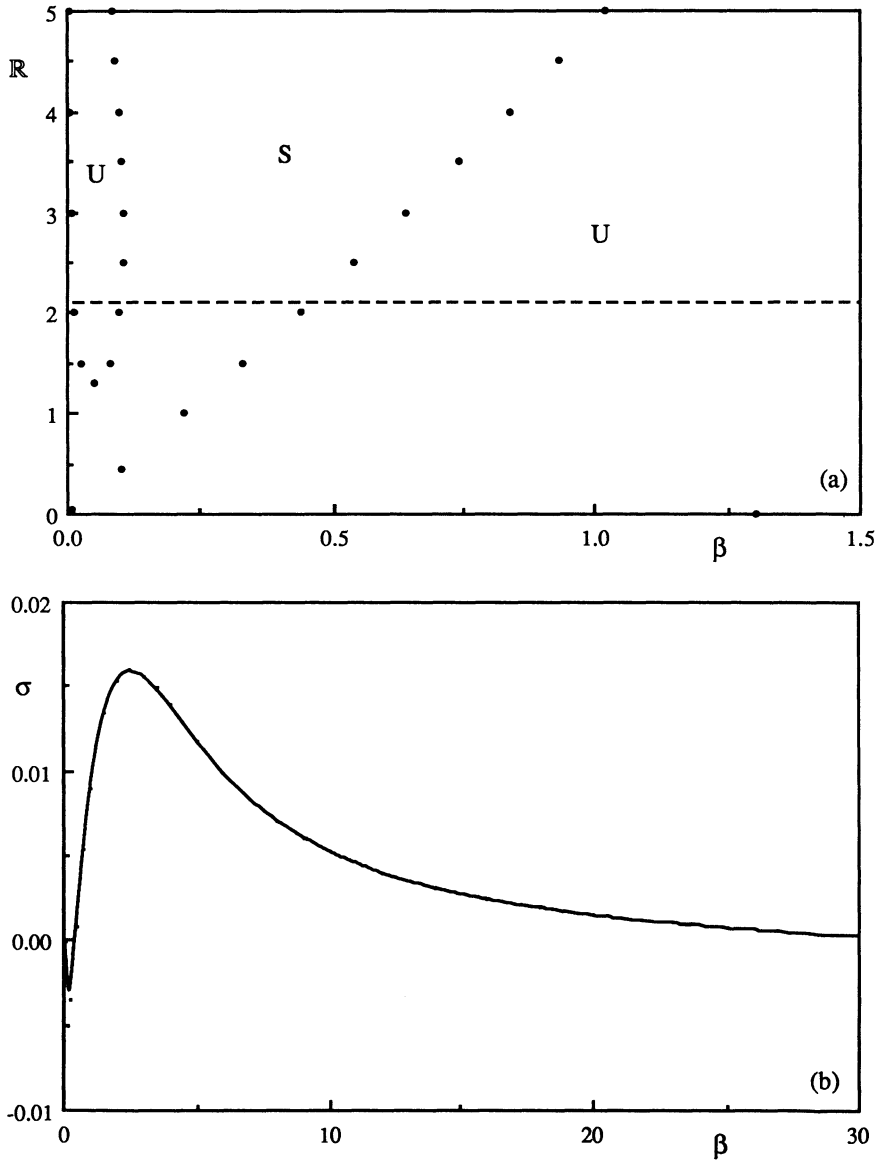

Fig. 2.20. Neutral curves (a) and growth rates (b) for the 100,000 cs oil in the test group on the lower limit of viscosity m=.000011, $\mathbb{R}$=2.1. The dashed line in (a) is at $\mathbb{R}$=2.1. The maximum growth (table 2.6) is at $\tilde{\beta} = 2.56$.

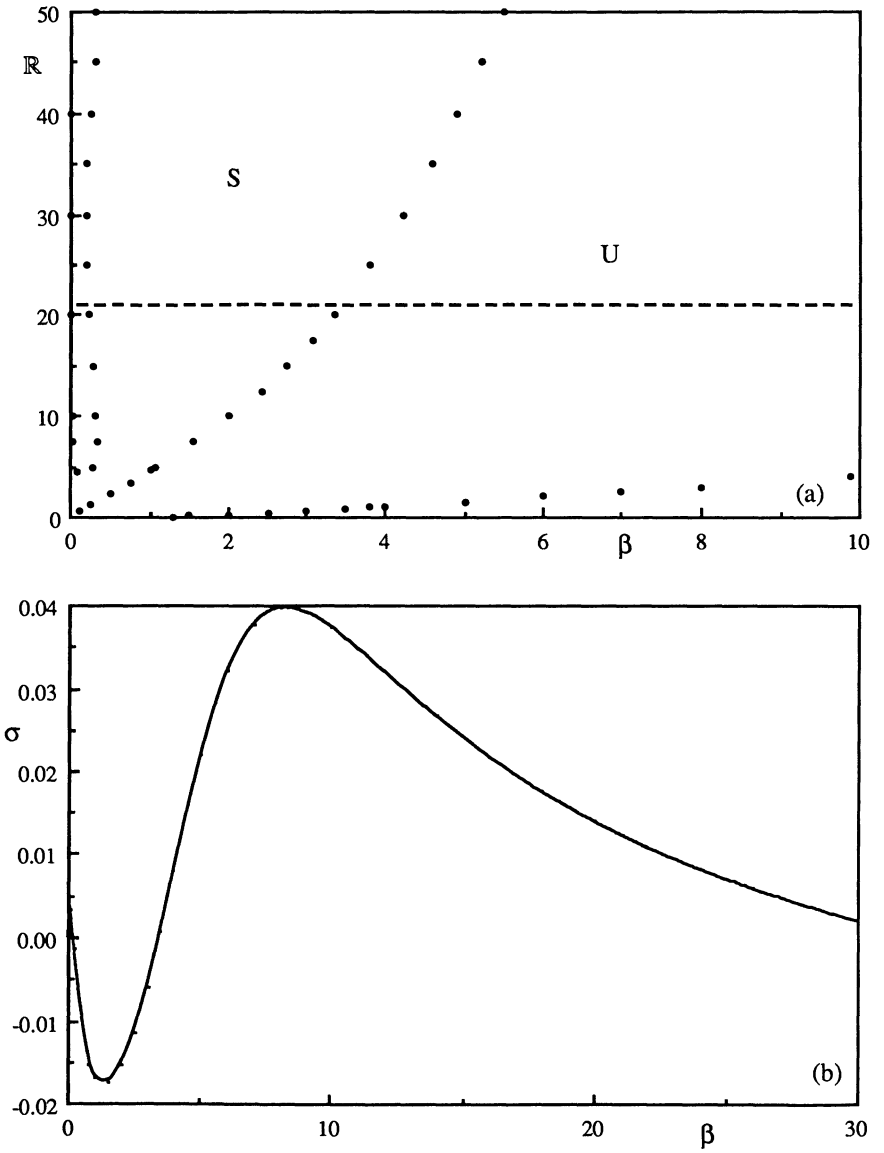

Fig. 2.21. Neutral curves (a) and growth rates (b) for the 10,000 cs oil in the test group on the lower limit of viscosity m=.00011, $\mathbb{R}$=21. The dashed line in (a) is at $\mathbb{R}$=21. The maximum growth (table 2.6) is at $\tilde{\beta} = 8.24$.

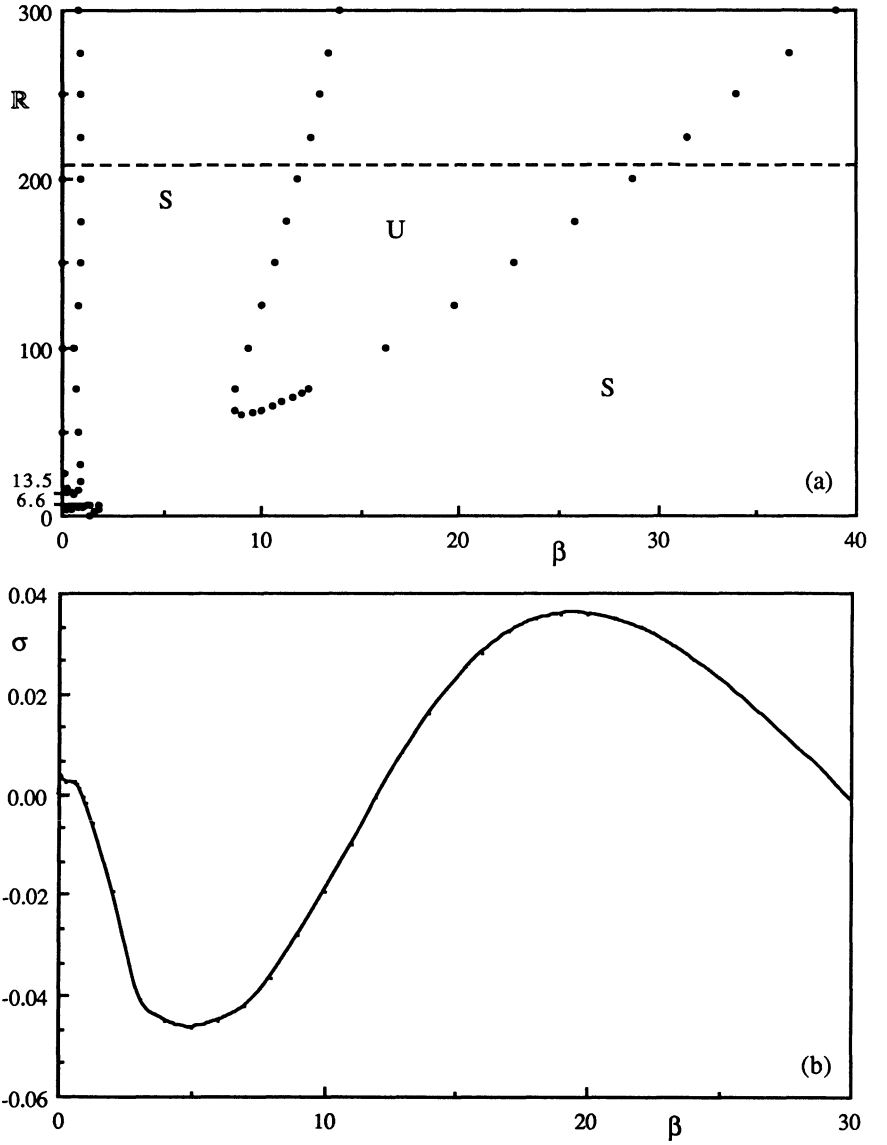

Fig. 2.22. Neutral curves (a) and growth rates (b) for the 1000 cs oil in the test group on the lower limit of viscosity m=.0011, $\mathbb{R}$=210. The dashed line in (a) is at $\mathbb{R}$=210. The maximum growth (table 2.6) is at $\tilde{\beta} = 19.54$. In this case there is a narrow band $\mathbb{R}$ for which it is possible to get stable core-annular flow without waves.

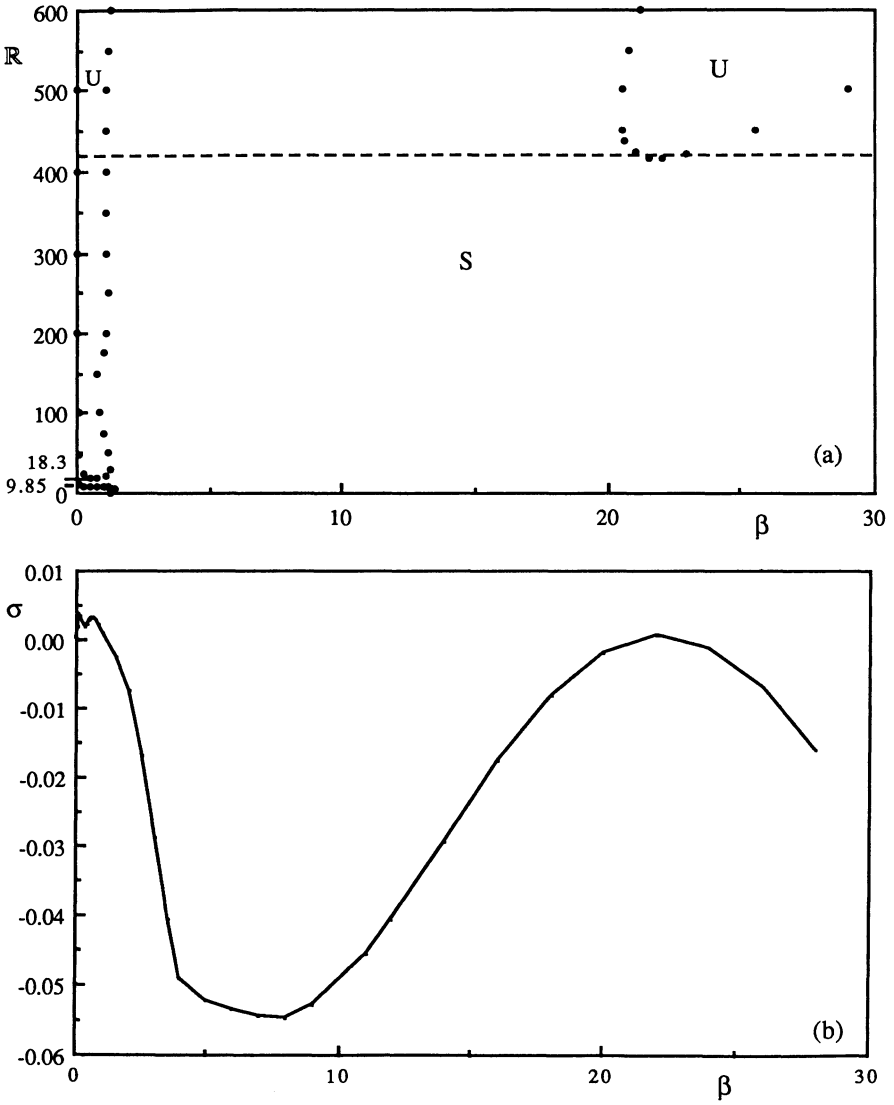

Fig. 2.23. Neutral curves (a) and growth rates (b) for the 500 cs oil; m=.0022, $\mathbb{R}$=421.05. The dashed line in (a) is at $\mathbb{R}$=421.05. The main feature is that the maximum growth is now in the unstable region on the left, with a much longer wave for the fastest growing disturbance. $\tilde{\beta} = 0.63$, $L = \pi D/0.63$. The analysis of energy shows that the Reynolds stress in the water is now the cause for instability and we expect emulsions of water in oil.

friction is now stabilizing (on this mode corresponding to the maximum wavelength). From our previous experience, comparing linear theory with experiments, we have come to associate this type of instability (and the associated neutral curve) with a kind of turbulence in water, leading to the emulsion of water in oil and the failure of core-flow.

Basic Quantities for the Computation. Since the basic flow (concentric core-annular) is given by (1b.7), the centerline velocity is then

$$W_0 = \frac{F}{4\mu_2} R_2^2 (m\eta^2 + 1 - \eta^2)$$

where $\eta = R_1/R_2$ is the radius ratio. From the velocity profile of the basic flow we can calculate the flow rate in the core (cf. equation VII.(18.10)-VII.(18.11))

$$Q_1 = 2\pi \int_0^{R_1} rW(r)dr = \frac{\pi}{2} W_0 R_1^2 \frac{m\eta^2 + 2(1-\eta^2)}{m\eta^2 + 1 - \eta^2},$$

the flow rate in the annulus

$$Q_2 = 2\pi \int_{R_1}^{R_2} rW(r)dr = \frac{\pi}{2} W_0 R_1^2 \frac{(1-\eta^2)^2}{m\eta^2 + 1 - \eta^2},$$

and the ratio of these flow rates

$$q = \frac{Q_1}{Q_2} = \eta^2 \frac{m\eta^2 + 2(1-\eta^2)}{(1-\eta^2)^2}.$$

From the above formula, we can solve for the radius ratio

$$\eta = \sqrt{\frac{1 + q - \sqrt{1 + mq}}{q + 2 - m}}.$$

If the flow rate Q_1 or Q_2 is given, we can calculate the Reynolds number for the flow by

$$\mathbb{R} = \frac{W_0 R_2}{\nu_1} = \frac{m\eta^2 + 1 - \eta^2}{\frac{\pi}{2}(m\eta^2 + 2(1-\eta^2))} \frac{Q_1}{\eta R_1 \nu_1} = \frac{m\eta^2 + 1 - \eta^2}{\frac{\pi}{2}(1-\eta^2)^2} \frac{Q_2}{R_2 \nu_1}.$$

If the mean bulk velocity V is given, then

$$V = \frac{Q_1 + Q_2}{\pi R_2^2} = \frac{W_0}{2} \frac{1 - (1-m)\eta^4}{m\eta^2 + 1 - \eta^2}, \quad \mathbb{R} = \frac{2(m\eta^2 + 1 - \eta^2) V R_2}{(1 - (1-m)\eta^4)\nu_1}.$$

Computation for the Lower Limit of Viscosity.

Input

Pipe radius R_2=3.124 in.=7.936 cm
Interfacial tension T=20 dynes/cm =20 g/s^2

Oil flow rate Q_1=500 gpm=0.03154 m^3/s
Water flow rate Q_2=165 gpm=0.01041 m^3/s
Oil/water flow ratio q=3.0303
Water viscosity ν_2=1.1 cs=$1.1\times10^{-6}m^2/s$ at 60°F
Oil viscosity ν_1=10^5, 10^4, 10^3 cs = 10^{-1}, 10^{-2}, 10^{-3} m^2/s
or lower limit
Density $\rho_1 = \rho_2 = 10^6$ g/m^3 (assumed to be matched)

Corresponding dimensionless parameters for the cases of our computations are:

Case a. $\nu_1 = 10^5$ cs $= 10^{-1}m^2/s$
$m = 1.1 \times 10^{-5}$, $\zeta = 1$, $\eta = 0.7761$,
$J^* = \frac{TR_2}{\nu_1^2\rho_1} = 1.587 \times 10^{-4}$, $\mathbb{R} = 2.10$.

Case b. $\nu_1 = 10^4$ cs $= 10^{-2}m^2/s$
$m = 1.1 \times 10^{-4}$, $\zeta = 1$, $\eta = 0.7761$,
$J^* = 1.587 \times 10^{-2}$, $\mathbb{R} = 21.0$.

Case c. $\nu_1 = 10^3$ cs $= 10^{-3}m^2/s$
$m = 1.1 \times 10^{-3}$, $\zeta = 1$, $\eta = 0.7761$,
$J^* = 1.587$, $\mathbb{R} = 210.3$

Case d. $\nu_1 = 500cs = 0.5 \times 10^{-3}$ m^2/s
$m = 2.2 \times 10^{-3}$, $\zeta = 1$, $\eta = 0.7759$,
$J^* = 6.348$, $\mathbb{R} = 421.05$

Table 2.6. We tabulate the terms in the energy balance for the lower limit of viscosity. The four entries in this table correspond to the four test cases specified above. These four cases fix all the parameters but the oil viscosity. The first three cases are all unstable to interfacial friction but stable to both interfacial tension and the Reynolds stress minus dissipation. This means that we will see nonlinearly stable travelling waves of length L and speed $\tilde{C} = c_r(\tilde{\beta})W_0$. We were asked to determine a lower limit of viscosity. Such a limit is given by the linear theory as the fourth entry in the table. In this case it is the Reynolds stress which destabilizes; interfacial friction is stabilizing. In all the cases we studied before with this theoretical profile, the actual flow gave way to an emulsion of water in oil. Hence, when the density is matched the emulsification occurs for a viscosity of about 500 cs.

m	$\tilde{\beta}$	$\tilde{\sigma}$	L(cm)	$\tilde{C}$(m/s)	$I-1$	B_1	B_2	$\dot{E}$
.000011	2.56	.01588	19.5	2.63	-.9513	-.0003	1.052	.1002
.00011	8.24	.03975	6.05	2.63	-.8901	-.0067	1.016	.1189
.0011	19.54	.03605	2.55	2.63	-.9318	-.0307	1.034	.0719
.0022	.63	.00327	79.1	1.10	1.111	.00002	-.0854	1.025

The results for the terms of the energy balance, wave length and wave speed of the fastest growing waves are listed in table 2.6. The neutral curves and the growth rates as a function of wave numbers for each case are plotted in figures 2.20-2.23. Our computation is consistent with the idea that the test cases for 100000, 10000 and 1000 cs oil are in wavy core-flow. We find that the 500 cs oil should emulsify.

Pipe Diameter Effects.

Input

Interfacial tension T=20 dynes/cm =20 g/s^2

Oil viscosity ν_1=10^4 cs = 10^{-2}m^2/s

Water viscosity ν_2=1.1 cs=1.1×10^{-6}m^2/s at 60°F

Water-to-total-flow ratio: $\frac{Q_2}{Q_1+Q_2}$ = 0.2 (or $q = \frac{Q_1}{Q_2}$=4.0).

Mean bulk velocity V=5 fps=1.524 m/s.

Pipe radius:

Case	a	b	c	d	e	f	g	h	i
D(in.)	4.026	6.249	10	14	20	26	32	40	48
R_2(m)	.0511	.0794	.127	.178	.254	.330	.406	.508	.610

Corresponding dimensionless parameters for the cases of our computations are:

$$m = 1.1 \times 10^{-4},\ \zeta = 1,\ \eta = 0.8165$$

Case	R_2 (m)	J^*	IR
a	.0511	.01023	9.351
b	.0794	.01588	14.51
c	.127	.02541	23.23
d	.178	.03557	32.52
e	.254	.05082	46.45
f	.330	.06607	60.39
g	.406	.08131	74.32
h	.508	.1016	92.90
i	.610	.1220	111.48

The data in table 2.7 shows that the stability properties are not changed qualitatively by scale-up. There is modest change in the wavelength of the fastest growing wave.

It is probably safe to extrapolate the data from small pipes to large ones, understanding at least the change in the wavelength. However, even if our linear analysis works well in relation to field data in small pipes, it could conceivably fail in large ones because of effects of gravity which have not yet been included in our analysis.

Table 2.7. We tabulate the effect of pipe radius. In these entries the viscosity ratio m, the flow ratio q and the radius ratio η and mean bulk velocity or maximum velocity W_0 are all fixed. Changing the radius is equivalent to scale-up. The only dimensionless parameters which change are $\mathbb{R}$ and J^*. The Reynolds stress minus bulk dissipation $I-1$ is negative (stabilizing). Interfacial tension B_1 is negative (stabilizing). Interfacial friction is positive (destabilizing) leading to $\dot{E}>0$ and hence the PCAF is unstable. We therefore expect to see interfacial waves of length $L=\pi D/\tilde{\beta}$. The crests of these waves would move forward with speed $\tilde{C}$, according to linear theory. The main effect of the scale-up is to change the wave length.

D(in.)	$\tilde{\beta}$	$\tilde{\sigma}$	L(in.)	$\tilde{C}$(m/s)	$I-1$	B_1	B_2	$\dot{E}$
4.026	6.24	.04899	2.03	1.81	-.9011	-.0055	1.019	.1128
6.249	7.70	.04916	2.55	1.81	-.8944	-.0069	1.017	.1160
10	9.58	.04901	3.28	1.82	-.8881	-.0088	1.016	.1188
14	11.2	.04855	3.93	1.82	-.8851	-.0103	1.015	.1197
20	13.2	.04754	4.76	1.82	-.8811	-.0117	1.012	.1194
26	14.8	.04644	5.52	1.82	-.8869	-.0132	1.016	.1159
32	16.2	.04530	6.21	1.82	-.8896	-.0141	1.016	.1126
40	17.9	.04382	7.02	1.82	-.8949	-.0150	1.018	.1077
48	19.4	.04243	7.77	1.82	-.9000	-.0157	1.019	.1028

VI.2(m) Stability of Rotating Core-Annular Flow

Linear stability theory for the rapid rotation of Poiseuille flow of one fluid in a pipe was studied by Pedley [1968,1969]. Joseph and Carmi [1969] did a nonlinear energy analysis which applies to the same flow and found a nearly identical result (see Joseph [1976]). They found that the flow is unstable to non-axisymmetric disturbances for Reynolds number greater than 82.9. This instability has been confirmed for slow rotation both numerically and experimentally by Mackrodt [1976]. Later, Cotton and Salwen [1981] did extensive numerical computations on the problem. They all found that the most unstable disturbance is non-axisymmetric ($|n|=1$).

Hu and Joseph [1989b] studied the stability of core-annular flow in a rotating pipe emphasizing the effect of rotation and the difference in the density of the two fluids. They computed neutral curves and formed the energy balance for unstable disturbances with the largest growth rates. Detailed results can be found in their paper and a summary is given below.

For two fluids of equal density, rotation stabilizes the axisymmetric (n =0) mode and destabilizes the non-axisymmetric ($|n|=1$) mode. Except for small Reynolds number $\mathbb{R}=\rho_1 W_0 R_2/\mu_1$, where capillary instability is dominant, the azimuthal mode $n=1$ is the most unstable. Even with slow rotation, the flow will be unstable to the $n=1$ mode. In this case we may observe spiral waves at the interface instead of stable core-annular flow. In fact, such spiral waves have been seen in nonlinear regimes of wavy core flow in which shearing stresses give rise to a turning torque.

If the heavier fluid is outside, the rotation of the pipe stabilizes the flow, and there exists a critical rotating speed Ω_c above which the flow is stable for a certain range of small $\mathbb{R}$. If the lighter fluid is outside, the flow of oil and water with the particular volume ratio studied in this section is unstable. If the annulus were thinner or if the viscosity difference were larger, it is possible to have shear-stabilization in the case of an adverse density stratification (see section IV.6 on the thin-layer effect in the presence of viscosity stratification).

VI.3 Stability of Core-Annular Flow with a Small Viscosity Ratio

This section is based on the paper of Hu, Lundgren and Joseph [1990]. The analysis is similar to the work of Miesen, Beijnon, Duijvestijn, Oliemans and Verheggen [1991]. Nonaxisymmetric disturbances have been investigated by Boomkamp and Miesen [1991] and shown to be of importance in some regimes: for instance, a situation with relatively low surface tension leads to an instability for the shorter waves and one would then expect the higher azimuthal modes to be important.

The viscosity of crude oil can be as high as 1000P at room temperature. Thus in actual applications, the ratio of viscosities of water to oil is usually extremely small, say 10^{-5}. The stability problem is then singular: the water annulus is nearly inviscid with boundary layers at the pipe wall and at the interface. In this section, we treat this problem by the method of matched asymptotic expansions. The results are confirmed with the finite element code described in section VI.2, modified to take into account the boundary layers at the pipe wall and at the interface between the water and oil.

VI.3(a) Formulation of the Problem

The equations governing this problem are given in sections VI.1 (b) - (d). The density of the two fluids are assumed to be the same: $\rho_1 = \rho_2 = \rho$.

The basic flow is given in equation (1d.2). It is a steady, fully developed core-annular flow driven by a constant pressure gradient. The velocity profile is parabolic in both the core and the annulus with a jump in slope at the interface due to the discontinuity in the viscosity of the two liquids.

We list the dimensionless parameters:

$$a = \frac{R_2}{R_1}, \qquad \text{the radius ratio,}$$

$$m = \frac{\mu_2}{\mu_1}, \qquad \text{the viscosity ratio,}$$

$$\mathbb{R} = \frac{\rho W_0 R_1}{\mu_1}, \qquad \text{the Reynolds number based on the core liquid,}$$

$$\hat{J} = \frac{T\rho R_1}{\mu_2^2} \qquad \text{the interfacial tension parameter based on liquid 2,}$$

where T is the coefficient of interfacial tension between the two liquids.

We will assume that the axisymmetric disturbance is the most dangerous. Thus, the disturbances to the velocity, the pressure and the interface radius are taken to be axisymmetric and proportional to $\exp[\,\mathrm{i}\alpha(x-ct)]$, where α is the dimensionless wavenumber. After eliminating the axial component w and pressure p, the linearized equation for u is given by equation (1e.25) (subscript 1 for the core, 2 for the annulus):

$$\frac{1}{\mathbb{R}\alpha}\left(D^2 + \frac{1}{r}D - \frac{1}{r^2} - \alpha^2\right)^2 u_1$$

$$-\mathrm{i}(W-c)\left(D^2 + \frac{1}{r}D - \frac{1}{r^2} - \alpha^2\right)u_1 = 0 \text{ for } 0 \le r \le 1, \tag{3a.1}$$

$$\frac{m}{\mathbb{R}\alpha}\left(D^2 + \frac{1}{r}D - \frac{1}{r^2} - \alpha^2\right)^2 u_2$$

$$-\mathrm{i}(W-c)\left(D^2 + \frac{1}{r}D - \frac{1}{r^2} - \alpha^2\right)u_2 = 0 \text{ for } 1 \le r \le a, \tag{3a.2}$$

where $D = \frac{d}{dr}$.

The boundary and interfacial conditions are, from equations (1e.26) - (1e.27):

$$u_2 = Du_2 = 0, \text{ at the pipe wall } r = a, \tag{3a.3}$$

$$u_1, Du_1, D^2u_1 \text{ are bounded at the origin } r = 0, \tag{3a.4}$$

and at the interface $r = 1$,

$$u_1 = u_2, \tag{3a.5}$$

$$\frac{2(1-m)}{a^2-1+m}u_1 - \left(\frac{a^2-1}{a^2-1+m} - c\right)(Du_1 - Du_2) = 0 \tag{3a.6}$$

$$(D^2 + D - 1 + \alpha^2)u_1 - m(D^2 + D - 1 + \alpha^2)u_2 = 0 \tag{3a.7}$$

$$\begin{aligned}&(D^3 + 2D^2 - (3\alpha^2+1)D + (1-\alpha^2))u_1\\ &\quad - m(D^3 + 2D^2 - (3\alpha^2+1)D + (1-\alpha^2))u_2\\ &\quad = \mathrm{i}m^2\frac{\hat{J}}{\mathbb{R}}\frac{\alpha(1-\alpha^2)}{\frac{a^2-1}{a^2-1+m} - c}u_1.\end{aligned} \tag{3a.8}$$

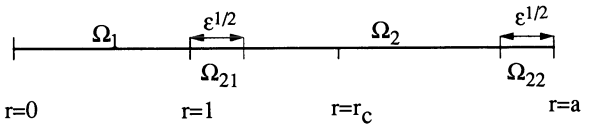

(a) Case I

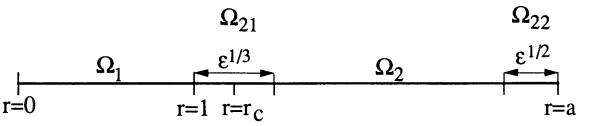

(b) Case II

Fig. 3.1. [Hu, Lundgren and Joseph, 1990, American Institute of Physics] Two cases considered. (a) Case I. The critical point $r = r_c$ is far away from the interface. (b) Case II. The critical point is close to the interface, within a distance of order $\varepsilon^{1/3}$.

The problem is to solve the eigen-system of ordinary differential equations (3a.1) and (3a.2) subject to the conditions (3a.3)-(3a.8), when the viscosity ratio $m \to 0$. After examining equation (3a.2) we choose

$$\varepsilon = \frac{m}{\mathbb{R}\alpha} \tag{3a.9}$$

as a small parameter, and use a matched asymptotic perturbation scheme to solve the problem.

As m or $\varepsilon \to 0$, equation (3a.1) is regular, and we can get a uniformly valid asymptotic expansion for u_1 in the core region. On the other hand equation (3a.2) is singular, since ε is the coefficient for the term which has the highest derivative. We therefore argue that within most of the annulus the viscous force corresponding to the first term is much less important than the inertial force corresponding to the second term and may be neglected. In some regions, however, the viscous force may be of the same order of magnitude as the inertial force. These regions are the viscous boundary layer at the pipe wall where the no-slip boundary condition is required, the viscous boundary layer at the interface where the interfacial conditions are prescribed, and the critical layer where the velocity of the disturbance is the same as the velocity $W(r_c)$ of the basic flow: $\mathrm{Re}(c) = W(r_c)$. The asymptotic expansions are different depending on the location of the critical point $r = r_c$. Two cases are treated: (a) the critical point is far away from the interface; and (b) the critical point is close to the interface, within a distance of order $\varepsilon^{1/3}$, as indicated in figure 3.1.

VI.3(b) Case I: The Critical Point is Far Away from the Interface

In this situation, an appropriate expansion for the eigenvalue c is

$$c \sim \sum_{n=0}^{\infty} \left(\varepsilon^{1/2}\right)^n c_n$$

In the present study, only two terms of the expansion are computed, that is

$$c \sim c_0 + \varepsilon^{1/2} c_1 + O(\varepsilon). \tag{3b.1}$$

The basic flow (1d.2) can be expanded in terms of ε as

$$W(r) = \begin{cases} 1 + O(\varepsilon) & 0 \le r \le 1, \\ (a^2 - r^2)/(a^2 - 1) + O(\varepsilon) & 1 \le r \le a. \end{cases} \tag{3b.2}$$

VI.3(b)(i) In the Core Ω_1. In Ω_1 as indicated in figure 3.1 (a), the velocity u_1 is expanded as

$$u_1(r) = u_1^{(0)}(r) + \varepsilon^{1/2} u_1^{(1)}(r) + O(\varepsilon). \tag{3b.3}$$

After substituting (3b.1), (3b.2) and (3b.3) into equation (3a.1), and collecting the coefficients for ε^0 and $\varepsilon^{1/2}$ terms in the equation, we have two equations for $u_1^{(0)}(r)$ and $u_1^{(1)}(r)$:

$$\left(D^2 + \frac{1}{r}D - \frac{1}{r^2} - \kappa^2\right)\left(D^2 + \frac{1}{r}D - \frac{1}{r^2} - \alpha^2\right) u_1^{(0)} = 0, \tag{3b.4}$$

$$\left(D^2 + \frac{1}{r}D - \frac{1}{r^2} - \kappa^2\right)\left(D^2 + \frac{1}{r}D - \frac{1}{r^2} - \alpha^2\right) u_1^{(1)} = -\mathrm{i}\mathbb{R}\alpha c_1 \left(D^2 + \frac{1}{r}D - \frac{1}{r^2} - \alpha^2\right) u_1^{(0)} \tag{3b.5}$$

where

$$\kappa^2 = \alpha^2 + \mathrm{i}\mathbb{R}\alpha(1 - c_0). \tag{3b.6}$$

Since the critical point is away from the interface, or $c_0 \neq 1$, we have $\kappa^2 \neq \alpha^2$.

The solutions to equations (3b.4) and (3b.5) with the conditions that the solutions are bounded at the origin are

$$u_1^{(0)}(r) = A_{11} I_1(\kappa r) + A_{12} I_1(\alpha r), \tag{3b.7}$$

$$u_1^{(1)}(r) = -\frac{\mathrm{i}\mathbb{R}\alpha c_1}{2\kappa} A_{11} r I_0(\kappa r) + B_{11} I_1(\kappa r) + B_{12} I_1(\alpha r), \tag{3b.8}$$

where $I_1(\cdot)$ and $I_0(\cdot)$ are the modified Bessel functions of the first kind with orders 1 and 0 respectively, A_{11}, A_{12}, B_{11} and B_{12} are arbitrary constants to be determined by the interfacial conditions. As $m \to 0$, the basic flow in

the core becomes uniform, and equations (3b.4) - (3b.5) can be integrated in terms of Bessel functions. Papageorgiou, Maldarelli and Rumschitzki [1990] use Kummer functions in integrating the core equations for general m.

VI.3(b)(ii) The Form of the Solution in the Annulus Ω_2. The outer expansions for velocity u_2 in Ω_2 is

$$u_2(r) = u_2^{(0)}(r) + \varepsilon^{1/2} u_2^{(1)}(r) + O(\varepsilon), \qquad \text{in } \Omega_2. \tag{3b.9}$$

After substituting the expansions into equation (3a.2), we find that they all satisfy

$$\left(D^2 + \frac{1}{r}D - \frac{1}{r^2} - \alpha^2\right) u_2^{(j)} = 0, \qquad \text{for } j = 0, 1. \tag{3b.10}$$

Thus the solutions are

$$u_2^{(0)}(r) = A_{21} I_1(\alpha r) + A_{22} K_1(\alpha r), \tag{3b.11}$$

$$u_2^{(1)}(r) = B_{21} I_1(\alpha r) + B_{22} K_1(\alpha r), \tag{3b.12}$$

where $K_1(\cdot)$ is the modified Bessel function of the second kind with order 1, and all the $A's$ and $B's$ are arbitrary constants. The solution to the outer Orr-Sommerfeld equation (3a.2) is not singular at the critical point $r = r_c$ for this case since $r(W'/r)'$ is zero (compares to equation (31.16) of Drazin and Reid [1982]). Thus, the outer expansion (3b.9) is smooth at r_c, and there is no need for a critical layer in this case as indicated in figure 3.1 (a).

VI.3(b)(iii) The Form of the Solution in the Boundary Layer at the Pipe Wall Ω_{22}. It can be easily verified that the proper choice of scaling for this wall boundary layer Ω_{22} is $\varepsilon^{1/2}$, the inner coordinate in the boundary layer is therefore introduced as

$$\eta = \frac{a - r}{\varepsilon^{1/2}}. \tag{3b.13}$$

The inner expansion for the velocity in this layer takes the form

$$u_2(r) = \varepsilon^{1/2} u_{22}^{(0)}(\eta) + \varepsilon u_{22}^{(1)}(\eta) + O(\epsilon^{3/2}). \tag{3b.14}$$

Since the basic flow is of order $\varepsilon^{1/2}$ in this layer, the order of the leading term in expansion (3b.14) is also taken to be $\varepsilon^{1/2}$.

By changing to the new variable in equation (3a.2), and using the expansion (3b.14), we obtain two equations for $u_{22}^{(0)}$ and $u_{22}^{(1)}$

$$D_\eta^4 u_{22}^{(0)} + \mathrm{i} c_0 D_\eta^2 u_{22}^{(0)} = 0, \tag{3b.15}$$

$$D_\eta^4 u_{22}^{(1)} + \mathrm{i} c_0 D_\eta^2 u_{22}^{(1)} = \frac{2}{a} D_\eta^3 u_{22}^{(0)} + \mathrm{i}\left[\frac{c_0}{a} D_\eta u_{22}^{(0)} + \left(\frac{2a}{a^2 - 1}\eta - c_1\right) D_\eta^2 u_{22}^{(0)}\right] \tag{3b.16}$$

where D_η stands for $\frac{d}{d\eta}$. The boundary condition (3a.4) transforms to

$$u_{22}^{(0)}(0) = D_\eta u_{22}^{(0)}(0) = u_{22}^{(1)}(0) = D_\eta u_{22}^{(1)}(0) = 0. \tag{3b.17}$$

As $\eta \to \infty$, $u_{22}^{(0)}$, $u_{22}^{(1)}$ are required to match the outer expansion (3b.10) as $r \to a$.

The solution to (3b.15) satisfying (3b.17) and the matching requirements is

$$u_{22}^{(0)}(\eta) = A_3^{(2)} \left[e^{p\eta} - p\eta - 1\right], \tag{3b.18}$$

where $A_3^{(2)}$ is a constant to be determined by the matching, and $p = \pm\sqrt{-\mathrm{i}c_0}$ with a negative real part.

Similarly, after substituting (3b.18) into (3b.16) we find the solution

$$\begin{aligned} u_{22}^{(1)}(\eta) = B_3^{(2)} \Bigg[& \left[e^{p\eta} - p\eta - 1\right] + \mathrm{i}A_3^{(2)} \Bigg\{ \frac{c_0\eta^2}{2ap} \\ & - \left(\frac{c_0}{a} + c_1 p\right) \frac{1}{2p^2} \left[\eta(e^{p\eta} + 1) - \frac{2}{p}(e^{p\eta} - 1)\right] \\ & + \frac{a}{2p(a^2-1)} \left[\eta^2 e^{p\eta} - \frac{\eta}{p}(5e^{p\eta} + 3) + \frac{8}{p^2}(e^{p\eta} - 1)\right] \Bigg\} \end{aligned} \tag{3b.19}$$

where $B_3^{(2)}$ is another constant to be determined by matching with the outer solution.

In order to determine the constants $A_3^{(2)}$ and $B_3^{(2)}$, we introduce an intermediate coordinate, for example $z = (a - r)/\varepsilon^{1/4}$. This method is used in Kevorkian and Cole [1980]. An alternative method is used in Van Dyke [1975]. In this way, we construct an intermediate layer where both the inner expansion (3b.14) and the outer expansion (3b.9) are valid. Note that since the outer expansion (3b.9) is a continuous function at $r = a$, we can represent it by a Taylor series around $r = a$. By equating these two expansions in the intermediate coordinate, we can obtain the following relations

$$u_2^{(0)}(a) = 0, \tag{3b.20}$$

$$Du_2^{(0)}(a) = A_3^{(2)} p, \tag{3b.21}$$

$$u_2^{(1)}(a) = -A_3^{(2)}, \tag{3b.22}$$

$$Du_2^{(1)}(a) = B_3^{(2)} p + \frac{\mathrm{i}A_3^{(2)}}{2p^2} \left(\frac{c_0}{a} + c_1 p + \frac{3a}{a^2 - 1}\right). \tag{3b.23}$$

$A_3^{(2)}$ in (3b.21) and (3b.22) can be eliminated giving

$$Du_2^{(0)}(a) = -u_2^{(1)}(a)p. \tag{3b.24}$$

VI.3(b)(iv) The Form of the Solution in the Boundary Layer at the Interface Ω_{21}. Following the procedure used above, an inner coordinate is defined

$$\xi = \frac{r-1}{\varepsilon^{1/2}}. \tag{3b.25}$$

The inner expansion for the velocity u_2 takes the form

$$u_2(r) = u_{21}^{(0)}(\xi) + \varepsilon^{1/2} u_{21}^{(1)}(\xi) + \varepsilon u_{21}^{(2)}(\xi) + O(\epsilon^{3/2}). \tag{3b.16}$$

Here we find it necessary to carry out the expansion to the third term.

At the leading order ε^0:

$$D_\xi^4 u_{21}^{(0)} - \mathrm{i}(1-c_0) D_\xi^2 u_{21}^{(0)} = 0, \tag{3b.27}$$

with boundary conditions at $\xi = 0$ (derived from the interfacial conditions (3a.5)-(3a.8)):

$$\begin{aligned} &u_{21}^{(0)}(0) = u_1^{(0)}(1), \\ &D_\xi u_{21}^{(0)}(0) = 0, \\ &D_\xi^2 u_{21}^{(0)}(0) = \frac{1}{\mathbb{R}\alpha}\left[D^2 + D - 1 + \alpha^2\right] u_1^{(0)}(1), \\ &D_\xi^3 u_{21}^{(0)}(0) = 0. \end{aligned} \tag{3b.28}$$

The solution to this order is a constant

$$u_{21}^{(0)}(\xi) = A_1^{(1)} = u_1^{(0)}(1). \tag{3b.29}$$

The third boundary condition in (3b.28) requires

$$\left[D^2 + D - 1 + \alpha^2\right] u_1^{(0)}(1) = 0. \tag{3b.30}$$

At the next order $\varepsilon^{1/2}$ we have

$$\begin{aligned} &D_\xi^4 u_{21}^{(1)} - \mathrm{i}(1-c_0) D_\xi^2 u_{21}^{(1)} \\ &= -2D_\xi^3 u_{21}^{(0)} + \mathrm{i}\left[(1-c_0) D_\xi u_{21}^{(0)} - \left(\frac{2\xi}{a^2-1} + c_1\right) D_\xi^2 u_{21}^{(0)}\right]. \end{aligned} \tag{3b.31}$$

The right hand side of the equation is zero after substituting for $u_{21}^{(0)}$. The boundary conditions at $\xi = 0$ are

$$\begin{aligned} u_{21}^{(1)}(0) &= u_1^{(1)}(1), \\ D_\xi u_{21}^{(1)}(0) &= D u_1^{(0)}(1) - \frac{2}{(a^2-1)(1-c_0)} u_1^{(0)}(1), \\ D_\xi^2 u_{21}^{(1)}(0) &= \frac{1}{\mathbb{R}\alpha}\left[D^2 + D - 1 + \alpha^2\right] u_1^{(1)}(1), \\ D_\xi^3 u_{21}^{(1)}(0) &= \frac{1}{\mathbb{R}\alpha}\left[D^3 + 2D^2 - (3\alpha^2+1)D + 1 - \alpha^2\right] u_1^{(0)}(1). \end{aligned} \tag{3b.32}$$

The solution is

$$u_{21}^{(1)}(\xi) = B_1^{(1)} + B_2^{(1)}\xi + B_3^{(1)}e^{q\xi}, \tag{3b.33}$$

where $q = \pm\sqrt{\mathrm{i}(1-c_0)}$ has a negative real part and the constants satisfy

$$B_1^{(1)} + B_3^{(1)} = u_1^{(1)}(1), \tag{3b.34}$$

$$B_2^{(1)} + qB_3^{(1)} = Du_1^{(0)}(1) - \frac{2}{(a^2-1)(1-c_0)}u_1^{(0)}(1), \tag{3b.35}$$

$$\mathbb{R}\alpha q^2 B_3^{(1)} = \left[D^2 + D - 1 + \alpha^2\right] u_1^{(1)}(1), \tag{3b.36}$$

$$\mathbb{R}\alpha q^3 B_3^{(1)} = \left[D^3 + 2D^2 - (3\alpha^2+1)D + 1 - \alpha^2\right] u_1^{(0)}(1). \tag{3b.37}$$

A similar derivation was carried out to order ε^1. The equation and boundary conditions are lengthy, so only the final result is presented here. We found that

$$\begin{aligned} u_{21}^{(2)}(\xi) =& D_1^{(1)} + D_2^{(1)}\xi + D_3^{(1)}e^{q\xi} - \frac{\mathrm{i}(1-c_0)}{2q^2}\left[B_2^{(1)} - (1+\alpha^2)A_1^{(1)}\right]\xi^2 \\ & - \mathrm{i}B_3^{(1)}\frac{1-c_0+c_1 q}{2q^2}\left(\xi - \frac{2}{q}\right)e^{q\xi} \\ & - \mathrm{i}B_3^{(1)}\frac{1}{2q(a^2-1)}\left(\xi^2 - 5\frac{\xi}{q} + \frac{8}{q^2}\right)e^{q\xi} \end{aligned} \tag{3b.38}$$

where $D_1^{(1)}, D_2^{(1)}$ and $D_3^{(1)}$ are constants, and $D_2^{(1)}$ can be determined by boundary conditions as

$$\begin{aligned} D_2^{(1)} =& B_3^{(1)}\left[1 - \frac{c_1}{1-c_0}q + \frac{2}{(a^2-1)(1-c_0)}\right] \\ & - \frac{1}{\mathbb{R}\alpha q^2}\left[D^3 + 2D^2 - \left(3\alpha^2 + 1 + \mathbb{R}\alpha q^2\right)D + 1 - \alpha^2\right]u_1^{(1)}(1) \\ & - \frac{2}{(a^2-1)(1-c_0)}\left[u_1^{(1)}(1) + \frac{c_1}{1-c_0}u_1^{(0)}(1)\right]. \end{aligned} \tag{3b.39}$$

Again the matching with the outer expansion (3b.9) as $r \to 1$ gives the relations:

$$u_2^{(0)}(1) = A_1^{(1)} = u_1^{(0)}(1), \tag{3b.40}$$

$$Du_2^{(0)}(1) = B_2^{(1)}, \tag{3b.41}$$

$$u_2^{(1)}(1) = B_1^{(1)}, \tag{3b.42}$$

$$Du_2^{(1)}(1) = D_2^{(1)}. \tag{3b.43}$$

VI.3(b)(v) The Secular Equations. At the zeroth order, we group four equations, equations (3b.20), (3b.30), (3b.40), and (3b.35) with $B_3^{(1)}$ and $B_2^{(1)}$

eliminated with (3b.27) and (3b.41), and write them explicitly using the properties of the Bessel functions

$$
\begin{aligned}
&A_{21}I_1(\alpha a) + A_{22}K_1(\alpha a) = 0,\\
&(\kappa^2+\alpha^2)A_{11}I_1(\kappa) + 2\alpha^2 A_{12}I_1(\alpha) = 0,\\
&A_{21}I_1(\alpha) + A_{22}K_1(\alpha) = A_{11}I_1(\kappa) + A_{12}I_1(\alpha),\\
&\alpha\left[A_{21}I_1'(\alpha) + A_{22}K_1'(\alpha)\right]\\
&-\frac{1}{\mathbb{R}\alpha q^2}\left\{A_{11}\left[(3\alpha^2-\kappa^2)\kappa I_1'(\kappa) - (\kappa^2-\alpha^2)I_1(\kappa)\right]\right.\\
&\left.+A_{12}\left[2\alpha^3 I_1'(\alpha)\right]\right\}\\
&=\left[\kappa A_{11}I_1'(\kappa) + \alpha A_{12}I_1'(\alpha)\right]\\
&-\frac{2}{(a^2-1)(1-c_0)}\left[A_{11}I_1(\kappa) + A_{12}I_1(\alpha)\right].
\end{aligned}
$$

Non-zero solutions A_{11}, A_{12}, A_{21} and A_{22} of this set of linear equations can be obtained only if the secular equation formed from the determinant of the coefficients is satisfied. This gives

$$
\begin{aligned}
&4\alpha^4\kappa\frac{I_1'(\kappa)}{I_1(\kappa)} - (\kappa^2+\alpha^2)^2\alpha\frac{I_1'(\alpha)}{I_1(\alpha)}\\
&+(\kappa^2-\alpha^2)^2\alpha Z + (\kappa^2-\alpha^2)\left(-2\alpha^2 + \frac{\mathrm{i}2\mathbb{R}\alpha}{a^2-1}\right) = 0,
\end{aligned}
\tag{3b.44}
$$

where

$$
Z = \frac{K_1(\alpha a)I_1'(\alpha)I_1(\alpha a)K_1'(\alpha)}{I_1(\alpha)K_1(\alpha a)I_1(\alpha a)K_1(\alpha)}. \tag{3b.45}
$$

At the next order, the equations used to derive the secular equation are (3b.24), (3b.34) with $B_1^{(1)}$ eliminated using (3b.42), (3b.36), and (3b.43) with $D_2^{(1)}$ given by (3b.39); the $B_3^{(1)}$ in these equations is given by (3b.37). After tedious manipulation of these equations and using (3b.44) to cancel some terms, the final result is simply

$$
c_1 = -\frac{\mathrm{i}}{\mathbb{R}\alpha}\frac{F}{G}, \tag{3b.46}
$$

where

$$
\begin{aligned}
F = &\frac{(\kappa^2-\alpha^2)^2}{2p}\frac{Y[K_1'(\alpha) - K_1(\alpha)Z]}{K_1(\alpha a)}\\
&+\frac{H}{q}\left[\left(\kappa^2-3\alpha^2\right)\left(\kappa^2-\alpha^2\right)\frac{Z}{2\alpha} - \frac{(\kappa^2-\alpha^4)}{2\alpha}\frac{I_1'(\alpha)}{I_1(\alpha)}\right.\\
&\left.-(\kappa^2-\alpha^2) + \frac{\mathrm{i}\mathbb{R}}{\alpha(a^2-1)}\left(\kappa^2-3\alpha^2\right)\right],
\end{aligned}
$$

$$G = -\left[1 + \frac{\kappa^2 - \alpha^2}{2\kappa}\frac{I_0(\kappa)}{I_1(\kappa)}\right]\frac{\kappa^2 - \alpha^2}{2\alpha}Z + \frac{\kappa^2 + \alpha^2}{2\alpha}\frac{I_1'(\alpha)}{I_1(\alpha)}\left[1 + \frac{\kappa^2 + \alpha^2}{2\kappa}\frac{I_0(\kappa)}{I_1(\kappa)}\right] - \frac{\mathrm{i}\mathbb{R}}{\alpha(a^2-1)}\frac{\kappa^2 - \alpha^2}{2\kappa}\frac{I_0(\kappa)}{I_1(\kappa)} - \alpha^2 + \frac{3(\kappa^2 - \alpha^2)}{2\kappa}\frac{I_0(\kappa)}{I_1(\kappa)} - H,$$

$$H = \frac{1}{\kappa^2 - \alpha^2}\left[(\kappa^2 - 3\alpha^2)\,\kappa\frac{I_1'(\kappa)}{I_1(\kappa)} + (\kappa^2 - \alpha^2) + (\kappa^2 + \alpha^2)\alpha\frac{I_1'(\alpha)}{I_1(\alpha)}\right],$$

$$Y = \frac{1}{\alpha a\,[I_1(\alpha)K_1(\alpha a) - I_1(\alpha a)K_1(\alpha)]}.$$

In the nonlinear equation (3b.44) the eigenvalue c_0 is embedded in $\kappa^2 = \alpha^2 + \mathrm{i}\mathbb{R}\alpha(1 - c_0)$. Inspection of (3b.44) and (3b.46) shows that there are three parameters in the equations, the radius ratio a, the dimensionless wave number α and the Reynolds number $\mathbb{R}$. The expansion (3b.1) shows that the eigenvalue depends also on the viscosity ratio m. It is interesting to notice that up to this order the interfacial tension parameter $\hat{J}$ does not come into play.

One obvious solution to the equation (3b.44) is $\kappa^2 = \alpha^2$, but since $c_0 \neq 1$ by the assumption in this section, this solution is rejected. Given a, α and $\mathbb{R}$, the nonlinear equation (3b.44) is solved numerically using the IMSL subroutine ZANLYT and checked on the Macintosh II with the software Mathematica. It is found that there is only one root for κ^2 (or c_0) to this equation in the range of interest. After obtaining κ^2 we can easily calculate c_1 from (3b.46), and eigenvalue c from

$$c = c_0 + \sqrt{\frac{m}{\mathbb{R}\alpha}}c_1. \tag{3b.47}$$

The neutral curves are computed by fixing a and m, and searching the $(\alpha, \mathbb{R})$ plane for the line on which the growth rate of disturbances $\mathrm{Im}(\alpha c) = 0$. Figure 3.2 presents the neutral curves obtained in this case, for radius ratio $a = 1.5$ and viscosity ratio $m = 10^{-3}$, 10^{-4} and 10^{-5}. The region to the right of these curves is stable, and to the left is unstable. These neutral curves are almost parallel straight lines in the log-log plot with a shift for different viscosity ratios m, and they seem to fit the relation α_c = constant $\times$ $(m\mathbb{R})^{1/3}$. In addition, the neutral curves exist at relatively small wavenumbers, or for long waves. Thus, an asymptotic analysis was carried out for the secular equations (3b.44) and (3b.46), for small α, under the condition that $\sqrt{m/(\mathbb{R}\alpha)}$ is still a small parameter. In this case the eigenvalue c can be expressed as

$$c = \frac{a^2 - 1}{a^2} - \mathrm{i}\frac{3\alpha(a^2 - 1)}{\mathbb{R}a^2} + \sqrt{\frac{m}{\mathbb{R}\alpha}}\frac{\sqrt{2}}{a^2(a^2 - 1)}\frac{1 + \mathrm{i}}{\sqrt{a^2 - 1}}. \tag{3b.48}$$

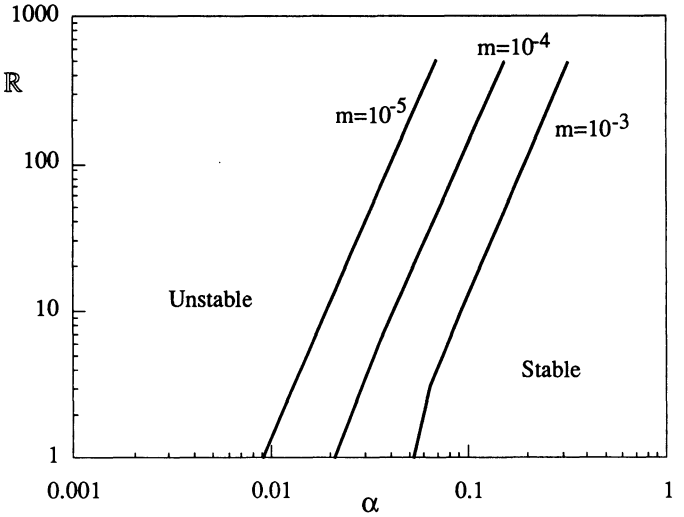

Fig. 3.2. [Hu, Lundgren and Joseph, 1990, American Institute of Physics] Neutral curves for the case I in which the critical point is far away from the interface. The radius ratio is $a = 1.5$ and the viscosity ratio $m = 10^{-3}$, 10^{-4} and 10^{-5}. The region to the right of the neutral curves is stable, and to the left is unstable. The asymptotic analysis for small α and small $\sqrt{m/(\mathbb{R}\alpha)}$ given by (3b.49) yields $\alpha_c = 0.4176(m\mathbb{R})^{1/3}$ in the present case. This formula almost exactly fits the curves in the figure.

The neutral curve is determined by $\mathrm{Im}(c) = 0$, that is

$$\alpha_c = \left(\frac{\sqrt{2}}{3}\right)^{2/3} \frac{(m\mathbb{R})^{1/3}}{(a^2-1)^{5/3}} = 0.6057 \frac{(m\mathbb{R})^{1/3}}{(a^2-1)^{5/3}}. \qquad (3b.49)$$

Equation (3b.49) gives the lines presented in figure 3.2 almost exactly.

VI.3(c) Case II: The Critical Point is Close to the Interface

In this section, we consider the case where the critical point is at a distance of order $\varepsilon^{1/3}$ from the interface, as shown in figure 3.1 (b). Unlike the previous case where the presence of the critical layer can be totally ignored, the critical layer in this case does play an important role. We consider the expansion

$$c = 1 + \varepsilon^{1/3} c_1 + \ldots \qquad (3c.1)$$

where $c_0 = 1$ and c_1 is the first order correction.

An analysis similar to the one carried out in the previous section is used to get the solutions in the core Ω_1, in the outer region of the annulus

Ω_2, and in the wall boundary layer Ω_{22}. Only one term of the expansion is computed. The results are listed below:

$$\text{in } \Omega_1 \begin{cases} u_1(r) = u_1^{(0)}(r) + O(\varepsilon^{1/3}), \\ u_1^{(0)}(r) = A_{11} I_1(\alpha r) + A_{12} r I_0(\alpha r), \end{cases} \tag{3c.2}$$

$$\text{in } \Omega_2 \begin{cases} u_2(r) = u_2^{(0)}(r) + O(\varepsilon^{1/3}), \\ u_2^{(0)}(r) = A_{21} I_1(\alpha r) + A_{22} K_1(\alpha r), \end{cases} \tag{3c.3}$$

$$\text{in } \Omega_{22} \begin{cases} u_2(r) = \varepsilon^{1/2} \left[u_{22}^{(0)}(\eta) + O\left(\varepsilon^{1/3}\right) \right], \\ u_{22}^{(0)}(\eta) = A_3^{(2)} \left[e^{p\eta} - p\eta - 1 \right]. \end{cases} \tag{3c.4}$$

We match the wall boundary inner expansion (3c.4) as $\eta = (a - r)/\varepsilon^{1/2} \to \infty$ with the outer expansion (3c.3) as $r \to a^-$ to find

$$u_2^{(0)}(a) = 0. \tag{3c.5}$$

Inside the critical layer Ω_{21} near the interface, we introduce an inner variable

$$z = \frac{r - 1}{\varepsilon^{1/3}}, \tag{3c.6}$$

and take a one term expansion for the velocity

$$u_2(r) = u_{21}^{(0)}(z) + O(\varepsilon^{1/3}). \tag{3c.7}$$

The equation (3a.2) at the leading order reduces to

$$D_z^4 u_{21}^{(0)} + \mathrm{i} \left(c_1 + \frac{2z}{a^2 - 1} \right) D_z^2 u_{21}^{(0)} = 0. \tag{3c.8}$$

The interfacial conditions (3a.5)-(3a.8), at $r = 1$ (or $z = 0$), become

$$u_{21}^{(0)}(0) = u_1^{(0)}(1), \tag{3c.9}$$

$$c_1 D_z u_{21}^{(0)}(0) = \frac{2}{a^2 - 1} u_1^{(0)}(1), \tag{3c.10}$$

$$0 = [D^2 + D - 1 + \alpha^2] u_1^{(0)}(1), \tag{3c.11}$$

$$\mathbb{R}\alpha D_z^3 u_{21}^{(0)}(0) = [D^3 + 2D^2 - (3\alpha^2 + 1)D + 1 - \alpha^2] u_1^{(0)}(1). \tag{3c.12}$$

Consider an equation of the form

$$\frac{d^2\omega}{dz^2} + \mathrm{i} \left(c_1 + \frac{2z}{a^2 - 1} \right) \omega = 0$$

which is solvable with Airy functions

$$Ai\left[-\left(\frac{2}{a^2-1}\right)^{1/3}\left(z+\frac{c_1}{2}(a^2-1)\right)e^{i\theta}\right],$$

where $\theta = \frac{\pi}{6}$, $\frac{5\pi}{6}$, or $-\frac{\pi}{2}$. If we require that ω should be matched with some outer expansion as $z \to \infty$, the solution must tend to some finite value as $z \to \infty$. This yields the only possible solution to be $\theta = \frac{5\pi}{6}$. Therefore the general solution of (3c.8) has a form similar to the one for plane shear flow computed by Hooper and Boyd [1983, 1987]:

$$u_{21}^{(0)}(z) = A_1^{(1)} + A_2^{(1)}z + A_3^{(1)}\chi(z) \tag{3c.13}$$

where

$$\chi(z) = \int_{\infty}^{z} dz \int_{\infty}^{z} Ai\left[-\left(\frac{2}{a^2-1}\right)^{1/3}\left(z+\frac{c_1}{2}(a^2-1)\right)e^{i5\pi/6}\right] dz. \tag{3c.14}$$

The boundary conditions (3c.9), (3c.10), (3c.12) require that

$$A_1^{(1)} + A_3^{(1)}\chi(0) = u_1^{(0)}(1), \tag{3c.15}$$

$$c_1\left[A_2^{(1)} + A_3^{(1)}\chi'(0)\right] = \frac{2}{a^2-1}u_1^{(0)}(1), \tag{3c.16}$$

$$\mathbb{R}\alpha A_3^{(1)}\chi'''(0) = \left[D^3 + 2D^2 - (3\alpha^2+1)D + 1 - \alpha^2\right]u_1^{(0)}(1). \tag{3c.17}$$

The matching of this inner with the outer expansion (3c.3) requires that

$$A_2^{(1)} = 0, \tag{3c.18}$$

$$A_1^{(1)} = u_2^{(0)}(1). \tag{3c.19}$$

Equation (3c.16) with $A_2^{(1)} = 0$ and $A_3^{(1)}$ eliminated by (3c.17) may be written as

$$\frac{2\mathbb{R}\alpha}{(a^2-1)c_1}\frac{\chi'''(0)}{\chi'(0)}\left[A_{11}I_1(\alpha) + A_{12}I_0(\alpha)\right] = -2\alpha^3\left[A_{11}I_1'(\alpha) + A_{12}I_1(\alpha)\right]. \tag{3c.20}$$

This, together with equation (3c.11) written as

$$A_{11}2\alpha^2 I_1(\alpha) + A_{12}2\alpha\left[I_1(\alpha) + \alpha I_0(\alpha)\right] = 0 \tag{3c.21}$$

leads to the secular equation

$$\frac{1}{c_1}\frac{\chi'''(0)}{\chi'(0)} = \frac{\alpha(a^2-1)}{\mathbb{R}}\left[1 + \alpha^2 - \alpha^2\frac{I_0^2(\alpha)}{I_1^2(\alpha)}\right]. \tag{3c.22}$$

If we define a constant E independent of the unknown c_1

$$E = 1 - i\frac{\alpha(a^2-1)}{\mathbb{R}}\left[1 + \alpha^2 - \alpha^2\frac{I_0^2(\alpha)}{I_1^2(\alpha)}\right], \tag{3c.23}$$

and use

$$x = \left(\frac{a^2-1}{2}\right)^{2/3} e^{-i\pi/6}\frac{c_1}{2} \tag{3c.24}$$

as the new variable, we may use the properties of Airy functions to write the secular equation (3c.22) in a very simple form

$$\int_0^\infty (z+Ex)Ai(x+z)dz = 0. \tag{3c.25}$$

It is interesting to notice that the unknown x in the equation depends only on E, a combination of three parameters: a, α and $\mathbb{R}$. Therefore, in the computation of neutral curves, we need to find only one neutral point at $E = E_c$ and $x = x_c$ which satisfies $\mathrm{Im}(c_1)$=0. Then, using (3c.23) we can extend this point to a whole curve in the (α, $\mathbb{R}$) plane valid for different values of a. The equation for this neutral curve is

$$\mathbb{R}_c = i\frac{(a^2-1)}{1-E_c}\alpha\left[1+\alpha^2-\alpha^2\frac{I_0^2(\alpha)}{I_1^2(\alpha)}\right].$$

We note that although the total eigenvalue c depends on the viscosity ratio m, the neutral curve on which $\mathrm{Im}(c)$=$\mathrm{Im}(c_1)$=0 is independent of m.

The Airy functions of complex argument were computed using an algorithm developed by Schulten, Anderson and Gordon [1979]. The integration in (3c.25) was transformed into one for the interval [0,1] and integrated numerically using an adaptive scheme given by Robinson [1976], which was modified to handle the complex-valued functions. The equation solver is subroutine ZANLYT on IMSL. The results were again checked on the Macintosh II with the software Mathematica. In solving the nonlinear equation (3c.25), we choose only the root c_1 that has a negative real part since the velocity of the disturbance equals the basic flow velocity at the critical point which is always less than 1. The root with the largest imaginary part, or the most unstable mode with the largest growth rate, is chosen.

It is found numerically that $E_c = 1 + 0.425i$; thus, the neutral curves are given by

$$\mathbb{R}_c = 0.294(a^2-1)\alpha\left[-1-\alpha^2+\alpha^2\frac{I_0^2(\alpha)}{I_1^2(\alpha)}\right]. \tag{3c.26}$$

Figure 3.3 shows (3c.26) for $a = 1.5$. The region to the right of the neutral curve is unstable, and the region to the left is stable. The short waves (disturbances with large wavenumber α) are unstable, since the effect of interfacial tension is suppressed in the present study. If the effect of interfacial tension is to be included (we need to make some assumptions about the magnitude of the combination $m^2\alpha\hat{J}/\mathbb{R}$ in the equation (3a.8)), we expect the shortest waves to be stabilized.

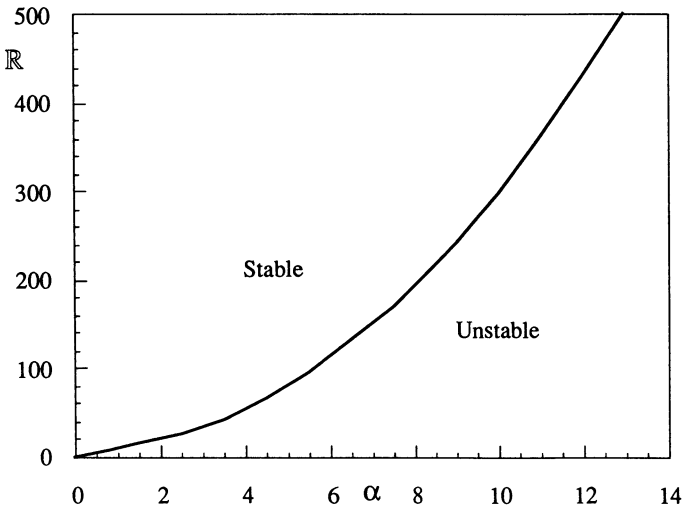

Fig. 3.3. [Hu, Lundgren and Joseph, 1990, American Institute of Physics] Neutral curves for case II in which the critical point is close to the interface, when the radius ratio $a = 1.5$. The region to the right of the neutral curves is unstable, and to the left is stable (see equation (3c.26)).

VI.3(d) Numerical Results

The finite element code described in section VI.2 is modified to take into account the effect of the boundary layers near the pipe wall and near the interface between the two liquids.

In the core region $0 \leq r \leq 1$, since the equation is regular, 10 uniform elements are used. The annulus $1 \leq r \leq a$, is divided into 8 equal intervals. In the first interval (closest to the interface) and in the last interval (closest to the pipe wall), the size of the elements increases gradually with a magnification rate of 2. The size of the smallest element is kept less than $0.1\sqrt{m/(\mathbb{R}\alpha)}$. Thus, the number of the elements used in the program varies automatically according to the values of $m, \mathbb{R}$ and α.

The results obtained using this modified finite element code were compared with those obtained by the matched asymptotic expansions method. Figure 3.4 shows the comparison of neutral curves at relatively small α, corresponding to the case in which the critical point is far away from the interface or the velocity of the disturbances is not close to one. There is good agreement at one end of the curves. At the other end, the finite element code predicts another branch of neutral curves, while the matched asymptotic expansions method fails since $\sqrt{m/(\mathbb{R}\alpha)}$ is no longer a small parameter when α or $\mathbb{R}$ is extremely small.

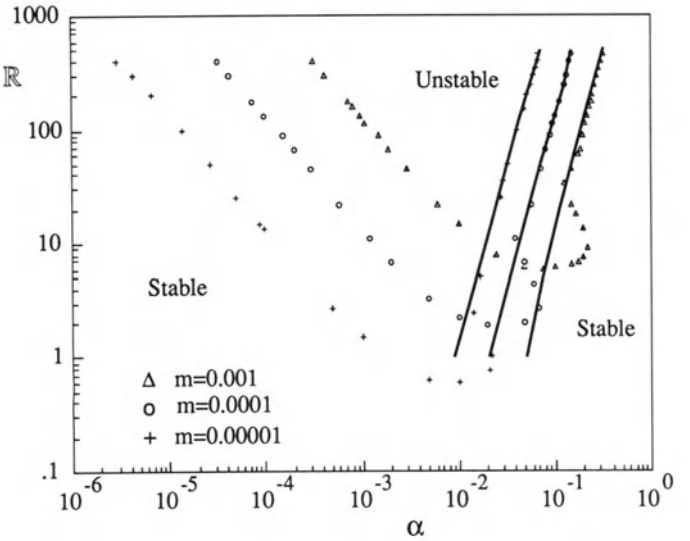

Fig. 3.4. [Hu, Lundgren and Joseph, 1990, American Institute of Physics] Comparison of neutral curves corresponding to case I obtained by the matched asymptotic expansions (solid lines) with that obtained by the modified finite element code (dots). The radius ratio $a = 1.5$, surface tension parameter $J = 0$ and viscosity ratio $m = 10^{-3}$, 10^{-4} and 10^{-5}.

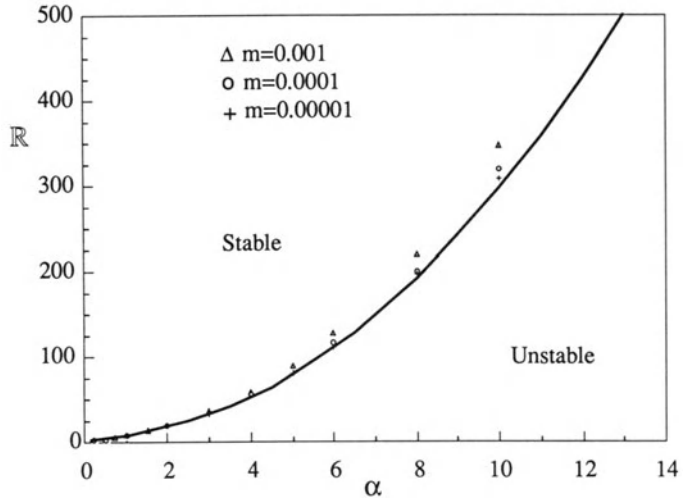

Fig. 3.5. [Hu, Lundgren and Joseph, 1990, American Institute of Physics] Comparison of neutral curves corresponding to case II obtained by the matched asymptotic expansions (solid line given by equation (3c.26)) with that obtained by the modified finite element code (dots). The radius ratio $a = 1.5$, surface tension parameter $J = 0$ and viscosity ratio $m = 10^{-3}$, 10^{-4} and 10^{-5}. The agreement is increasingly better as $m \to 0$.

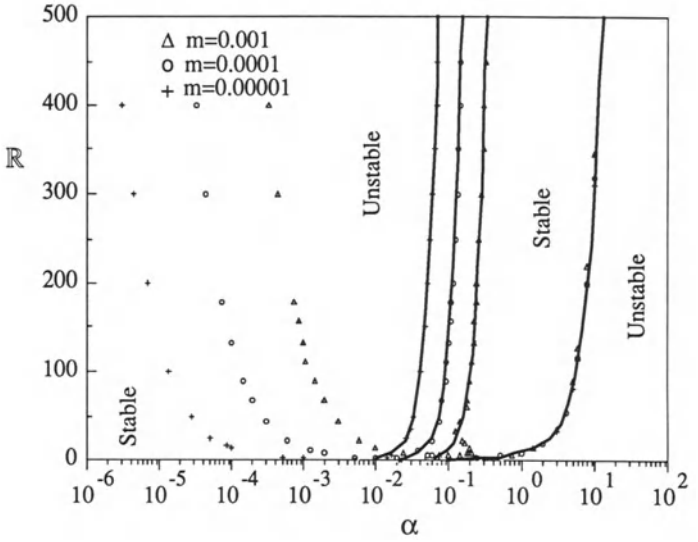

Fig. 3.6. [Hu, Lundgren and Joseph, 1990, American Institute of Physics] Combination of figures 3.4 and 3.5. This gives an overall view of the neutral curves for both cases I and II.

Figure 3.5 presents the comparison of neutral curves corresponding to the case in which the critical point is near the interface or the velocity of the disturbances is close to one. There is an increasingly better agreement as $m \to 0$. Figure 3.6 combines the neutral curves in figures 3.4 and 3.5, giving an overall view of the neutral curves in the $(\alpha, \mathbb{R})$ plane.

Figure 3.7 demonstrates the changes of the neutral curves in the $(\alpha,\mathbb{R})$ plane as m increases when $\hat{J}$ is not zero (a=1.25, $\hat{J}$=1000). The numerical solutions shown in figure 3.7 (a) for $m = 0.001$ is similar to the neutral curves in figure 3.6 except that in figure 3.7 (a), there exists an extra branch for $\alpha > 1$ at small $\mathbb{R}$, which corresponds to the stabilizing effect of the interfacial tension for short waves. Since the effect of interfacial tension scales according to the parameter $J^* = T\rho R_1/\mu_1^2 = \hat{J}m^2$, as m increases, the influence of the interfacial tension increases. In figure 3.7 (b) ($m = 0.01$), the extra branch gets connected with the branch corresponding to the case II in the asymptotic analysis, and forms another U-shape branch at large α. At the left-hand side corner, the small unstable bubble is caused by the capillary instability due to the interfacial tension. When $m = 0.1$ (figure 3.7 (c)), the interfacial tension further stabilizes the short waves (pushes up the U-shape branch at large α) and destabilizes the long waves (blows the bubble at the left-hand side corner). If the $\hat{J}$ is large enough, the U branch at large α can be pushed out of sight. Then the U-shaped branch at small α and the bubble at the left-hand side corner are the familiar upper and lower branches of the neutral curves displayed in section VI.1 for finite but small m.

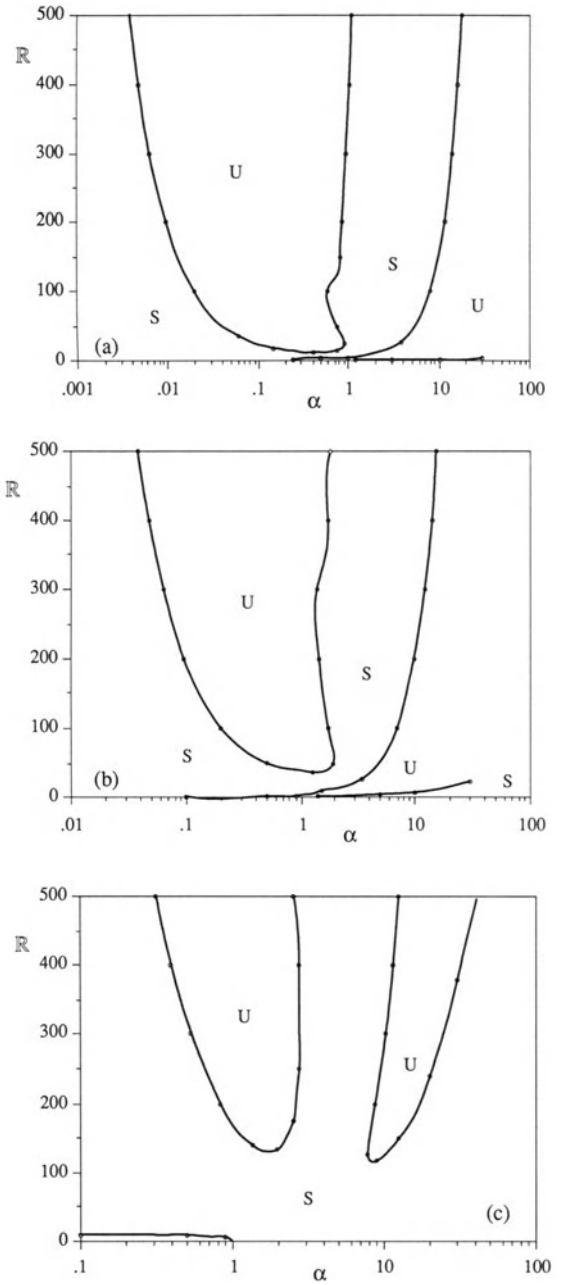

Fig. 3.7. [Hu, Lundgren and Joseph, 1990, American Institute of Physics] Changes in the neutral curves as the viscosity ratio m increases. The radius ratio $a = 1.25$, surface tension parameter $\hat{J}$=1000 and (a) m=0.001; (b) m=0.01; (c) m=0.1. Here U and S indicate unstable and stable regions respectively.

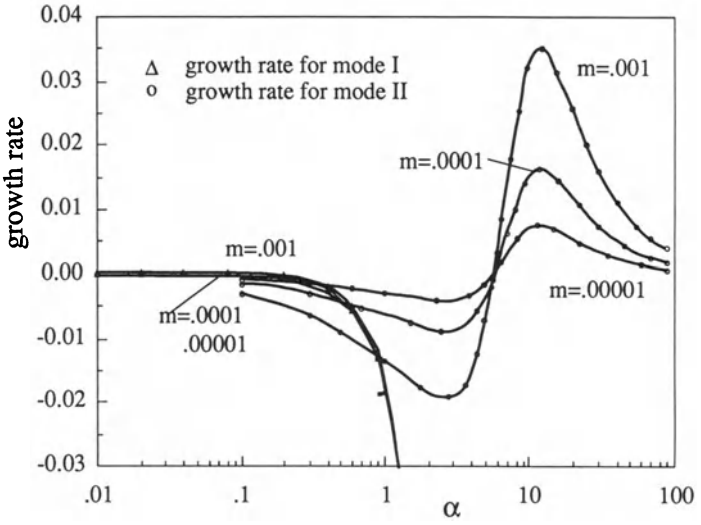

Fig. 3.8. [Hu, Lundgren and Joseph, 1990, American Institute of Physics] Growth rates $\mathrm{Im}(\alpha_c)$ vs wavenumber α for two modes of instability when $\mathbb{R}$=100, $a = 1.5$ and $m = 0.001, 0.0001, 0.00001$. Δ is the growth rate for mode I corresponding to case I, and o is the growth rate for mode II corresponding to case II. Except at small α where the growth rate of mode I is slightly positive and the growth rate of mode II is negative, the growth rate of mode II is much larger than that of mode I. The maximum growth rate occurs on the curve for mode II at $\alpha = 12.1$, and tends to zero (neutrally stable) as m tends to zero.

VI.3(e) Growth Rate and Wave Velocity

$\mathrm{Im}(\alpha c)$ is the growth rate and $\mathrm{Re}(c)$ is the wave velocity for small disturbances. The two modes of instability corresponding to case I and case II have different growth rates. For $\mathbb{R}$=100, $a = 1.5$ and $m = 0.001$, 0.0001 and 0.00001, the growth rates for both modes are plotted in figure 3.8. The results are obtained using the method of matched asymptotic expansions. This figure shows that the growth rate for mode I, corresponding to case I, is small and positive at small α. It reaches a maximum at α about 0.1, which varies for different m, then decreases rapidly as α increases. The growth rate for mode II, corresponding to case II, has a peak at $\alpha = 12.1$ which is independent of m, and decays to zero at both ends of small and large α. Except at small α, the growth rate of mode II is much larger than that of mode I. Combining these two modes of instability the maximum growth rate for the whole range of α occurs on the curve for mode II at $\alpha = 12.1$. This maximum growth rate tends to zero (neutrally stable) as m tends to zero because the growth rate is proportion to $m^{1/3}$ as shown in expansion (3b.49).

The energy analysis described in section VI.2 shows that for the sec-

ond mode of instability the B_2 term due to the difference of viscosity and interfacial friction is dominant in the energy balance. The comparison with experiments discussed in section VI.2 shows that this type of instability leads interfacial waves.

The wave velocities for the same parameters as in figure 3.8 at the maximum growth rates are 0.9961, 0.9982, 0.9991 for $m = 0.001, 0.0001$ and 0.00001 respectively. The expansion (3b.49) also shows that the interfacial wave tends to be stationary. The wave velocity is equal to the velocity of the core, as m tends to zero.

VI.3(f) Conclusions

(a) As the ratio of viscosities of water to oil m tends to zero ($\varepsilon = m/(\mathbb{R}\alpha)$ as a small parameter), the equation that governs the linear stability of the core-annular flow is regular in the core; and is singular in the annulus of water, with boundary layers near the pipe wall and the interface, and with a critical layer whose position is not predetermined.

(b) Depending on the position of the critical point in the annulus, there are two modes of instability. One is when the critical point is far away from the interface, or the velocity of the disturbance is much less than one, corresponding to case I. The other is when the critical point is close to the interface within a distance of order $\varepsilon^{1/3}$, corresponding to case II.

(c) In case I, the eigenvalue c is determined by (3b.44) and (3b.46). For small values of α and $\sqrt{m/(\mathbb{R}\alpha)}$ the eigenvalue can be expressed explicitly by equation (3b.48), and the neutral curve by equation (3b.49). In case II, the eigenvalue c can be determined by solving the nonlinear equation (3c.25), while the neutral curve is simply given by equation (3c.26) explicitly.

(d) The instability of the core-annular flow, when the viscosity ratio m is small, leads to an interfacial wave with wave velocity slightly less than the velocity of the interface. As m tends to zero, the interfacial wave tends to a standing wave convected with the velocity of the flow at the interface and the maximum growth rate tends to zero. This leads to a neutrally stable standing wave in a coordinate system moving with the velocity of the interface.

Chapter VII
Core-Annular Flow in Vertical Pipes

VII.1 Introduction

A linear stability analysis is given in sections VII.2 - VII.9 for Poiseuille flow in a vertical pipe in the presence of gravity [Chen, Bai and Joseph 1990], and sections VII.10 - 21 are based on Bai, Chen and Joseph [1992]

and Arney, Bai, Joseph and Liu [1992]. The analysis will be restricted to the axisymmetric mode. We include the effect of an applied pressure gradient which can reinforce or oppose the body force due to gravity. The physical effects treated are associated with gravity, density difference, viscosity difference, surface tension and Reynolds number. It is shown that a heavy lubricant should be used to stabilize capillary instability in slow flows in the direction of gravity and a light lubricant should be used for slow flow against gravity. The results also show that there is an optimal value of density ratio that maximizes the interval of Reynolds numbers for which CAF is stable.

Before we investigate the stability of vertical pipe flow, it is instructive to look at the two-dimensional analogue of this problem. Renardy [1987b] considered the linear stability of three-layer vertical plane Poiseuille flow in the presence of gravity. The layers next to the walls are assumed to be of the same thickness and to be the same fluid. The two fluids have different viscosities and densities. Since the problem is symmetric across the centerline, the interfacial mode is composed of an axisymmetric one and an antisymmetric one. We refer to the symmetric mode as being 'varicose' and the antisymmetric one as 'snake'. Numerical results, as well as formulas for short and long waves, were obtained.

The plane problem may be expected to model pipe flow in some sense; for instance, if the layers at the walls are thin. For viscosity stratification, the arrangement with a thin layer of the less viscous fluid at the walls is stable in both flows. For density stratification, intuition suggests that the fluids should arrange themselves in order to flow most easily; that is, to maximize the flow rate for a given pressure gradient. This leads one to expect that the heavier fluid should tend to stay at the center of the pipe for down flow and to stay at the walls for up-flow. The numerical results of Renardy [1987] support this idea if the density difference is large. The picture is not so simple if the densities are similar, as in the case of water and oil. Let r denote the ratio ρ_{outer}/ρ_{core}. For lubricated pipelining, we have r slightly greatly than 1. The numerical results for the plane problem indicate that for down flow, if r is a little larger than 1, there is a snake mode instability (see her figure 8). For up flow, there is a varicose mode instability (see her figure 16). We report experimental results in the latter part of this chapter [Bai, Chen and Joseph 1992], including observations of axisymmetric 'bamboo' waves for up-flow, and the non-axisymmetric 'corkscrew' waves in down flow.

It is essential that the predictions of linearized theory be tested against experiments. Two devices were constructed to study the flow of two liquids in a vertical pipe, one for free fall under gravity and the other for forced flow. The linear theory was used to predict the parameters necessary to enter into the window of stability of perfect core-annular flow in the free-fall apparatus and obtained agreement between theory and experiment. With these two devices, the parameters which appear in the analysis were monitored. The

vertical pipe seems to be the instrument of choice in this field because the experiments and the analysis are well-matched, and because of the relevance to industrial applications (cf. chapter V). In fact, the use of water as a lubricant for pumping crude oil from underground wells appears to be a possible technology in down-hole situations with shallow wells, or when the oil viscosity is very large as in cold wells. For such applications, pumping up against gravity is the relevant case.

In the latter half of this chapter, experimental results are given for water-lubricated pipelining of 6.01 poise cylinder oil in a vertical apparatus in up and down flows in regimes of modest flow rates, less than 3 ft/sec. Measured values of flow rates, hold-up ratios (cf. section VII.14), pressure gradients and flow types are presented and compared with theoretical predictions based on the linear theory of stability of the laminar flow. New types of flow, such as bamboo waves in up-flow and corkscrew waves in down-flow, are observed. These are consistent with the results on varicose and snake instabilities of Renardy [1987b]. Nearly perfect core-annular flows are observed in down-flows and these transport the oil very efficiently with measured values close to those of the idealized problem. The hold-up ratios in up-flow and fast down-flow are constant independent of the value, and the ratio of values, of the flow rates of oil and water. A vanishing hold-up ratio can be achieved by fluidizing a long lubricated column of oil in the down-flow of water. In some regimes, there is satisfactory agreement between the experiments and theory for the celerity and diagnosis of flow type. Since the oil is very viscous, waves are observed to be nearly stationary, convected with the oil core. These results are robust with respect to moderate changes in the viscosity and surface tension. The computed wavelengths are somewhat smaller than the average length of bamboo waves which are observed. This is explained by stretching effects of buoyancy and lubrication forces induced by the wave. Other points of agreement and disagreement are reviewed. All the data are reduced and plotted on a master curve using two different formulations of the Reynolds number and friction factor.

VII.2 Basic Flow

Two immiscible liquids are flowing up or down a vertical pipe of radius R_2. The interface between the two liquids is given by $r = R(\theta, x, t)$, where (r, θ, x) are cylindrical coordinates chosen in such a way that gravity is acting in the positive x-direction, as shown in figure 2.1, and $\mathbf{u} = (u, v, w)$ are the corresponding velocity components. The region $0 \leq r \leq R(\theta, x, t)$ is occupied by the first liquid with viscosity μ_1 and density ρ_1 and the second liquid with viscosity μ_2 and density ρ_2 is located in $R(\theta, x, t) \leq r \leq R_2$. The pipe is infinitely long and the mean value of $R(\theta, x, t)$ is R_1, a constant fixed by prescribing the volumes of each liquid, independent of t.

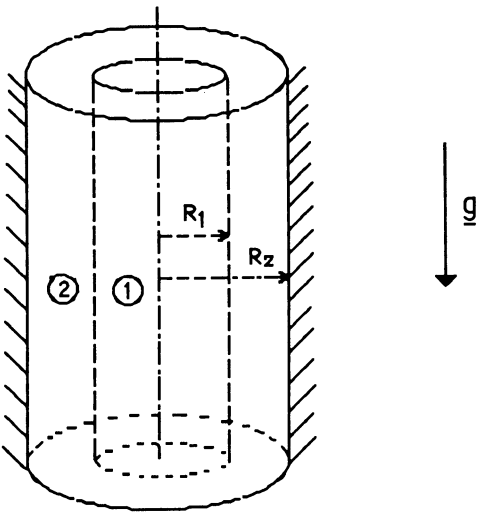

Fig. 2.1. [Chen, Bai and Joseph, 1990] Sketch of vertical core-annular flow.

We are interested in the perfect core-annular flow solution of the governing equations given in section VI.1 (b), with the addition of gravity (the gravity term in the equations of motion cannot be absorbed into the pressure: cf. equation (4.8)), satisfying

$$\mathbf{U} = (0, 0, W_i(r)), \quad i = 1, 2,$$

and

$$R(\theta, x, t) = R_1.$$

On the cylindrical interface $r = R_1$,

$$[\![\hat{P}]\!] = T/R_1, \tag{2.1}$$

where T is the interfacial tension and the jump across the interface is defined by

$$[\![\cdot]\!] = (\cdot)_1 - (\cdot)_2.$$

It follows that the pressure satisfies

$$\frac{d\hat{P}_1}{dx} = \frac{d\hat{P}_2}{dx} = -f \text{ (constant)}.$$

The axial velocities are

$$W_1(r) = \frac{f + \rho_1 g}{4\mu_1}(R_1^2 - r^2) + \frac{f + \rho_2 g}{4\mu_2}(R_2^2 - R_1^2)$$

$$+\frac{R_1^2[\![\rho]\!]g}{2\mu_2}\ln\frac{R_2}{R_1}, \quad 0\le r\le R_1, \tag{2.2a}$$

$$W_2(r)=\frac{f+\rho_2 g}{4\mu_2}(R_2^2-r^2)-\frac{R_1^2[\![\rho]\!]g}{2\mu_2}\ln\frac{r}{R_2}, \quad R_1\le r\le R_2. \tag{2.2b}$$

We scale length with R_1, velocity with gR_1^2/ν_1, time with ν_1/gR_1 and pressure with $\rho_1 g^2 R_1^4/\nu_1^2$. The dimensionless parameters are defined as follows:

$$m=\frac{\mu_2}{\mu_1}, \quad a=\frac{R_2}{R_1}, \quad \zeta_i=\begin{cases} 1, & 0\le r\le R_1, \quad i=1,\\ \rho_2/\rho_1, & R_1\le r\le R_2, \quad i=2,\end{cases}$$

$$\mathbb{R}=\mathbb{R}_1=\frac{gR_1^3}{\nu_1^2}, \quad \mathbb{R}_2=\frac{\zeta_2}{m}\mathbb{R}, \quad F=\frac{f}{\rho_1 g},$$

$$J^*=\frac{aTR_1}{\rho_1\nu_1^2}=\frac{TR_2}{\rho_1\nu_1^2}.$$

We also introduce $\mathbb{R}_g$:

$$\mathbb{R}_g=\frac{R_1(gR_1)^{\frac{1}{2}}}{\nu_1}=\mathbb{R}^{\frac{1}{2}}.$$

The parameter F is the ratio of the driving forces: the pressure gradient and gravity. The Reynolds number $\mathbb{R}_g$ is based on gravity and is zero in a forced flow when gravity is entirely neglected, a case not considered here. Forced flows with a fixed value of $\mathbb{R}_g$ characterize the experiments of this section well. Strong forcing is then obtained when $|F-1|\gg 1$ for a fixed value of $\mathbb{R}_g$. Free fall without forcing means $F=0$. The pressure gradient and gravity act in the same direction when the driving force ratio $F>0$, and in opposition when $F<0$.

When written in terms of the dimensionless quantities, the velocities (2.2) of CAF become

$$W_1(r)=\frac{F+1}{4}(1-r^2)+\frac{F+\zeta_2}{4m}(a^2-1)+\frac{1-\zeta_2}{2m}\ln a, \quad 0\le r\le 1, \tag{2.3a}$$

$$W_2(r)=\frac{F+\zeta_2}{4m}(a^2-r^2)-\frac{1-\zeta_2}{2m}\ln\frac{r}{a}, \quad 1\le r\le a. \tag{2.3b}$$

Examination of the formulas (2.3a, b) shows that we may determine the range of F for which the flow goes up and when it goes down in terms of F_1 and F_2 defined by

$$F_1=-\frac{\zeta_2(a^2-1)+1}{a^2}$$

and

$$F_2 = -\frac{m + 2\ln a + \zeta_2(a^2 - 1 - 2\ln a)}{m + a^2 - 1}.$$

Each one of these is negative. There are three types of flows:

$$\text{down} - \text{flow in the core and annulus,} \quad F > F_u \tag{2.4}$$

$$\text{mixed flow, up in some places, down in others,} \quad F_u > F > F_l \tag{2.5}$$

$$\text{up} - \text{flow in the core and annulus,} \quad F_l > F \tag{2.6}$$

where $(F_l, F_u) = (F_1, F_2)$ if $\zeta_2 > 1$ and $(F_l, F_u) = (F_2, F_1)$ if $\zeta_2 < 1$.

The situation of interest in pumping against gravity is (2.6), and also possibly $F < F_1$ when the water is heavier and outside. Free flow corresponds to downward flow in both core and annulus. The size of the $F-$interval for which mixed flows are possible is

$$|F_1 - F_2| = \frac{|1 - \zeta_2|}{a^2 - 1}\left\{\frac{2a^2 \ln a - a^2 + 1}{a^2} + \frac{m(a^2 - 1 - 2\ln a)}{m + a^2 - 1}\right\}.$$

When the densities are matched $F_1 = F_2$, and mixed flows are not possible.

VII.3 Experiments

Two devices were built to study lubricated vertical core-annular flow. The first setup is a free-fall apparatus (see plate VII.3.1). The fluids are introduced into the pipe in the core and annulus. The entrance for the core is a centrally located stand pipe through which oil is introduced. The water enters through an annulus surrounding the stand pipe. The flow is driven by gravity alone acting on the density difference, care being taken not to introduce large differences in the static heads of oil and water at the entrance. The water and oil are kept separated by the stand pipe wall for a few centimeters before the two streams merge into the test plastic pipe of inner radius of 0.3175 cm and 120 cm long. The two fluids empty into the atmosphere simultaneously. CBJ constructed the free-fall apparatus in a rough and ready way solely to demonstrate that a perfect core-annular flow, i.e. the basic flow given by (2.3) with $F = 0$, could be achieved in experiments designed so that the system parameters are in the window identified as stable by the linear theory. Theory and experiment are compared in section VII.8.

The second apparatus shown in figure 3.3 is a much more carefully designed inverse U loop whose long legs are pipes for up and down flows. These pipes are plastic and are of inner radius 0.48 cm. The second apparatus is used to study forced flows, up when the pressure gradient and gravity are in opposition and down when the pressure and gravity are in the

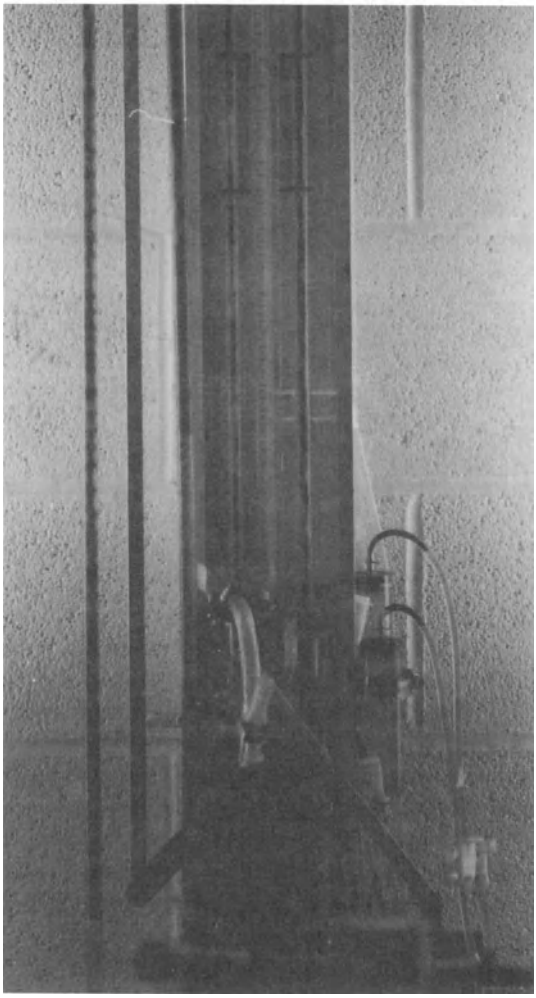

Fig. 3.3. [Chen, Bai and Joseph, 1990] Forced-flow apparatus. The sections indicated by arrows are test sections and they are surrounded by boxes filled with glycerine to eliminate visual distortion. The left test section is for up-flow and the right is for down-flow. The two extra sections on the far left are only used for demonstration purposes. The inner radius of the pipe is 0.48 cm.

same direction. Sections VII.10 - VII.20 show data on the flow rates, pressure drops and hold-up ratios (ratio of the input oil-water ratio to the *in situ* ratio) for several oil-water systems, and comparison between the linear theory and experimental results. A part of these results, documenting the prediction of perfect CAF in free fall, is presented in the following sections. We also present some representative results for the linear theory to provide the reader with an understanding of the range of phenomena which may be expected from the instabilities of CAF in vertical pipes.

Table 3.1. Material parameters at 23°C.

Fluid	Density (gm/cc)	Viscosity (P)	Interfacial tension (dyne/cm)
80% - 20% glycerine-water	1.18	0.34	
			12.27
SAE 30	0.85	1.03	

VII.3(a) Free Fall

In free fall, there is no pressure gradient ($F = 0$) and the two fluids run down the pipe under the influence of gravity alone. As we will see later in section VII.8, the linear theory predicts that it is possible to choose parameters so as to achieve a perfect core-annular flow in free fall. It is very important to test this prediction because linearly stable pipe flows of a single fluid are known to be destabilized by finite amplitude disturbances. The flows which the oil companies call 'lubricated' are wavy core flows, not perfect core-annular flows. At one point, CBJ thought that it might be possible that wavy core flows can arise out of a subcritical bifurcation of perfect core-annular flow. Until they carried out these experiments, they had never seen a perfect core-annular flow, though the sketch of experiment 2 by CGH (see figure 1.1 of chapter V) called 'oil in water concentric' is close to perfect and the data for this experiment is nearly in the region of stability (see figure 1.12 of section VI.1). In the experiments reported below, based on the predicted parameters for stable CAF, CBJ built an apparatus and selected fluids to match the prediction and were successful. Now it is established that it is possible to run a perfect core-annular flow, robustly stable to finite amplitude disturbances if the operating conditions are stable according to linearized theory.

In section VI.1, it is shown that the values of the viscosity ratio m for which stable CAF is possible lie in a bounded interval (see figure 1.10 of section VI.1, for example) and there is a certain m, near 0.5, which maximizes the size of the interval of Reynolds numbers for which CAF is stable.

The calculations in section VII.8 show that heavy lubricants are beneficial, and we can minimize capillary instability by choosing two fluids with a small interfacial tension. To sum up, we need small interfacial tension, a relatively heavy lubricant, a viscosity ratio which is somewhat close to 0.5 and Reynolds number large enough to avoid capillary instability but not too high. These conditions are met by choosing a pipe with inner radius 0.3175 cm, using 80% glycerine and 20% water (by weight) mixture as the lubricant for the transport of Tropic Artic (Phillip) SAE 30 core fluid (see table 3.1). With these design parameters, $\zeta_2 = 1.4$, m=0.33 and CBJ were able to realize stable CAF for various values of a. The example in plate VII.3.2 corresponds to $a = 1.86$, $\mathbb{R}_g = 1.82$ and $J^* = 2.26$. The neutral curves for these parameters are exhibited in section VII.8 and it will be shown that the linear theory agrees with experiment.

We think it is important to draw attention to the effects of the material of construction of the pipe on the problem of lubrication. In fact, it was necessary to thoroughly wash the pipe with the glycerine-water mixture. If the pipes were not so prepared, we might see flow with oil deposited on the plexiglass wall. There is an instability which we call 'chugging' which is associated with this failure of lubrication. We really have nothing in our equations to tell us whether the oil or the glycerine-water mixture will be on the wall. This appears to be a problem of adhesion which goes beyond the usual discussion about contact lines.

VII.3(b) Forced Flows

As explained earlier, we shall only describe some of the qualitative behaviors of forced flow here. A photograph of the U loop, used to study forced flows, is shown in figure 3.3. The working fluids are water and heavy Mobil oil with $\rho = 0.881$ gm/cc, $\mu = 13.32$ poise. This gives $\zeta_2 = 1.135$, $m = 0.00067$. Water is introduced in an annulus by small nozzles evenly distributed on a circle on the outer wall of the annulus. The oil is introduced through a thin-walled pipe at the center of the annulus. After a few centimeters, the water in the annulus merges with the flow of oil. The applied pressure gradient in the water and oil tanks, and the volume flow rates of both water and oil, are adjustable; they are dials with which the experiments are controlled. Pressure drops and hold-up ratios can be measured in the two test sections to monitor up- and down-flow. The test sections are seen in figure 3.3 as the portions of the U loop surrounded by boxes filled with glycerine designed to remove the visual distortion which is created by the circular tube. A high-speed video system is used to detect different flow configurations in these boxes, and to measure the size of bubbles and slugs.

A sequence of photographs of the flows which are realized as the superficial water velocity $V_{\rm w} = Q_{\rm w}/A$ and the superficial oil velocity $V_o = Q_o/A$ are varied is shown in figure 3.4. Here $Q_{\rm w}$, Q_o are the volume flow rates of water and oil respectively and $A = \pi R_2^2$ ($R_2 = 0.48$ cm) is the area of the

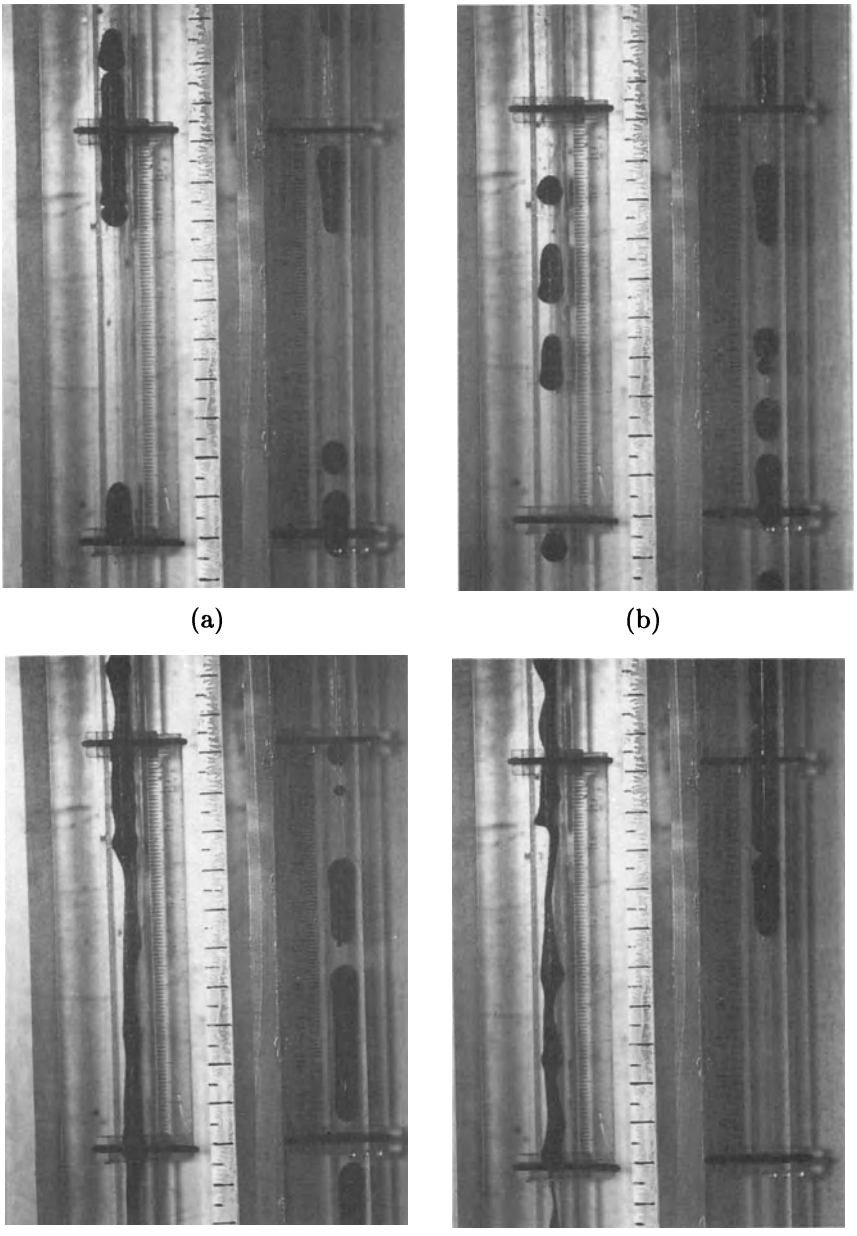

Fig. 3.4(a-k). [Chen, Bai and Joseph, 1990] Core-annular flow of heavy Mobil oil and water. The left panel is up-flow; gravity opposes the applied pressure gradient. The right panel is down-flow; gravity aids the applied pressure gradient. V_w and V_o are the superficial velocities of water and oil respectively. (a) $(V_w, V_o) = (0.436, 0.283)$ ft/s; (b) (1.56, 0.256) ft/s; (c) (0.436, 0.542) ft/s; (d) (1.56, 0.582) ft/s; (e) (1.56, 0.906) ft/s; (f) (0.413, 0.426) ft/s; (g) (0.413, 0.426) ft/s; (h) (0.554, 0.739) ft/s; (i) (0.330, 0.909) ft/s; (j) (0.436, 1.766) ft/s; (k) (1.116, 1.241) ft/s.

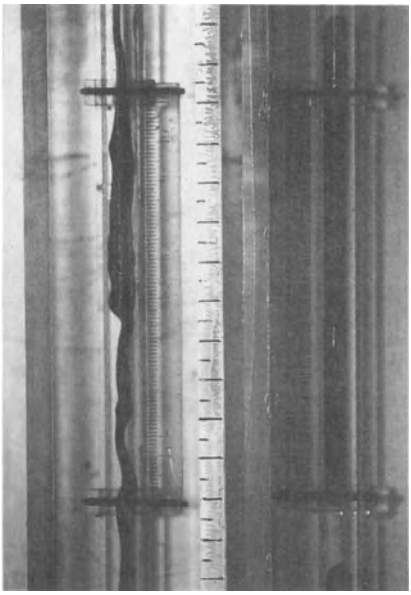

(e)

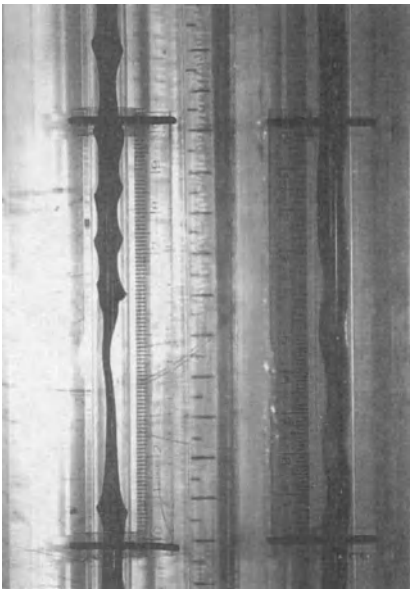

(f)

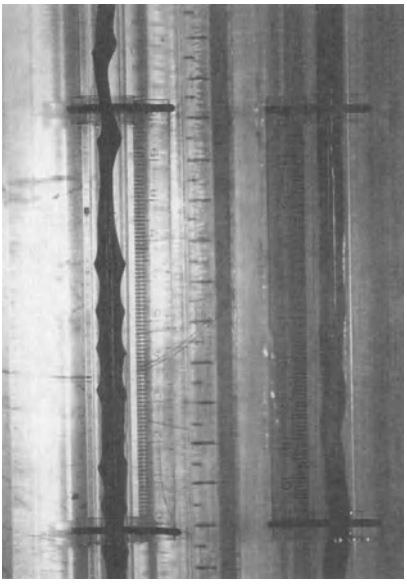

(g)

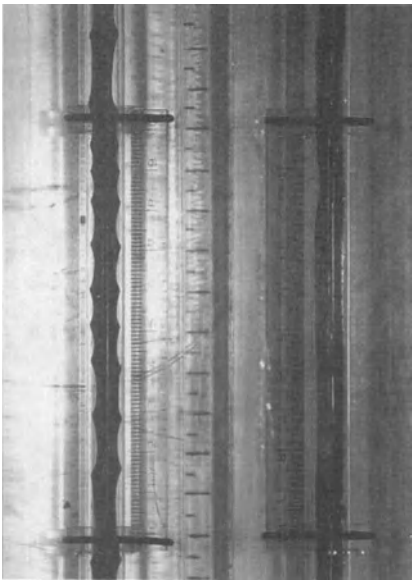

(h)

Fig. 3.4(e-h). Continued.

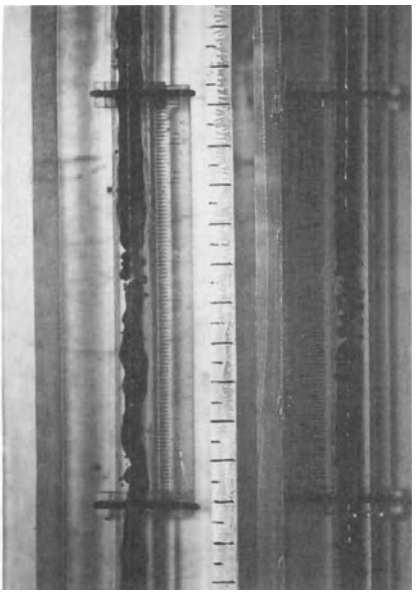

(i)

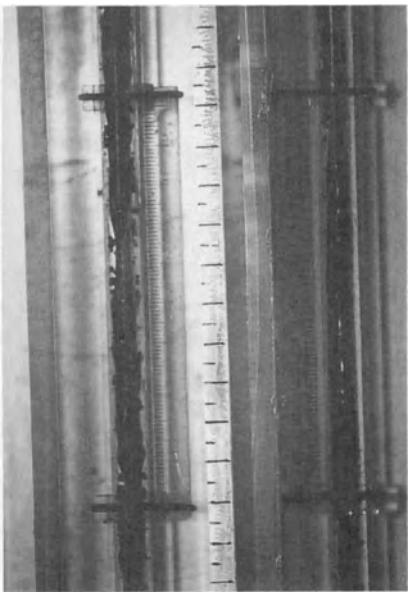

(j)

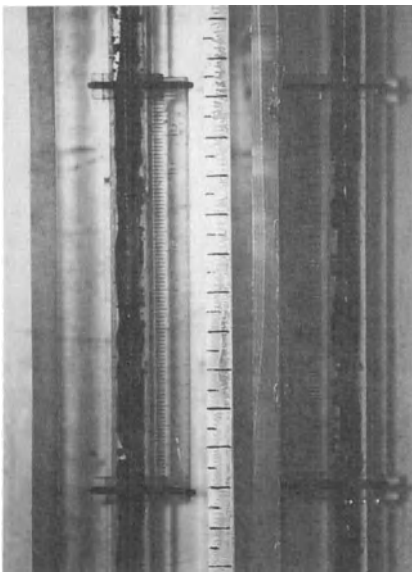

(k)

Fig. 3.4(i-k). Continued.

cross-section of the whole pipe. There are two panels in each photograph. Up-flow with the pressure gradient pushing the fluid up against gravity is on the left. Down-flow with the pressure gradient pushing the fluid down in the same direction as gravity is on the right. When the oil velocity V_o is small, as in figure 3.4 (a) and (b), oil bubbles are formed both in the up- and down-flows. These bubbles are a consequence of capillary instability in the unstable left hand side of the $F - \alpha$ plane of neutral curves shown in section VII.9; for example, figure 9.1 (b). As V_o is increased, wavy core flow is first observed in up-flow on the left, while the down-flow takes form in the bubbles and slugs as in (c) and (d) or in long slugs as in (e). This trend can be explained as follows in terms of the hold-up ratio used by CGH in a similar experiment (see figure 1.1 of chapter V and section VI.1 (m) for the work of CGH). In general, the input oil-water ratio, $R_{o/w} = Q_o/Q_w$, and the *in situ* ratio, which is the ratio of the volume of the pipe occupied by oil to the volume occupied by water, are different because one of the components will tend to accumulate in the pipe. The hold-up ratio, defined as the ratio of the input oil-water ratio to the *in situ* oil-water ratio, is thus an important parameter for core-annular flow. For a given input ratio $R_{o/w}$, if oil accumulates in the pipe, the hold-up ratio will be less than unity, and greater than unity if water accumulates in the pipe. When the flow rates are moderate, the accumulation of water in up-flow is greater than in down-flow because the effective gravity accelerates oil (buoyancy) and decelerates water. For down-flow, the opposite is true: gravity decelerates oil and accelerates water. This leads to an accumulation of oil in the down-flow. The *in situ* ratio was examined in both up- and down-flows simultaneously, and the results confirm that if the flow rates are not too large, the *in situ* ratio in the down-flow test section is larger than that in the up-flow test section. At higher speeds, this difference is negligible. Mathematically, the above statement is equivalent to the statement that for a given input ratio $R_{o/w}$, the parameter a in our analysis has different values for up- and down-flows: a is larger for up-flow than that for down-flow. For water and heavy Mobil oil, the parameters are not in the window of stable CAF because m is too small, ζ_2 is not large enough, etc. In section VII.9, it will be shown that with other parameters fixed, the unstable region will expand as a is increased: typically, the upper branch of neutral curves which is associated with wavy core flows will sink. The instability on the upper branch is responsible for the wavy flows observed in up-flow while stable slugs occur in down-flow. For faster flows, the effect of gravity is small and there is less difference between the up- and down-flows. The differences which can be observed in figure 3.4 (f) through (j) are again well-correlated with the argument about the hold-up ratio which leads to a larger water fraction, and less stability, in up-flow.

Many different and interesting nonlinear waves of large amplitude develop in vertical core-annular flow. There is as yet no coherent theory for these waves. We shall make a few casual observations. First, wakes are im-

portant. We see the drafting of slugs and bubbles, in which the rear bubble accelerates in the wake of the bubble preceding it, eventually forming a bubble train held together by pressure deficits behind the blunt body. Such trains can be seen at the top of the up-flow panel in figure 3.4 (a) and the down-flow panel in (d). This type of wake-effect is present also in the wavy core behind the large crests as in the draining of up-flow jets shown in (c), (d), (e) and (f). Large-amplitude axisymmetric waves in up-flow with peaked crests like those shown at the top and the bottom of the left panel of (f) more typically take a corkscrew form in down-flow as is evident in the right panels of (f) and (g). The pictures in (f) and (g) show that the waves are slowly modulated and are not strictly periodic. It may be argued that all non-axisymmetric waves will be forced to rotate by hydrodynamic couples associated with shear between oil and water.

VII.4 Disturbance Equations

The linear stability of CAF is analyzed as in section VI.1 (e). The governing equations, and the boundary and centerline conditions are the same. The interfacial conditions, (1e.7), (1e.8), (1e.10) and (1e.11) in section VI.1 (e) are unchanged, but (1e.9) which arises from the balance of shear tractions, has to be replaced by

$$\left[\!\left[\frac{\zeta}{\mathbb{R}}W''(1)\right]\!\right]u(1)+\left[\!\left[\frac{\zeta}{\mathbb{R}}(w'-\alpha u)\right]\!\right]\alpha(W(1)-C)=0. \tag{4.1}$$

This change is solely due to the presence of the density difference because

$$\left[\!\left[\frac{\zeta}{\mathbb{R}}W''(1)\right]\!\right]=\frac{\zeta_2-1}{\mathbb{R}}. \tag{4.2}$$

The condition (4.1) is better understood when written in dimensional form. It arises originally from the statement that the shear stress τ_{rx} is continuous across the interface $r=R_1+\delta$:

$$(1-\delta_x^2)[\![\mu(W'(r)+w_r+u_x)]\!]+2\delta_x[\![\mu(u_r-w_x)]\!]=0. \tag{4.3}$$

The continuity of the shear stress for the basic flow ($\delta=0$) is in the form

$$[\![\mu W'(R_1)]\!]=0 \tag{4.4}$$

and

$$[\![\mu W''(R_1)]\!]=-[\![\rho]\!]g. \tag{4.5}$$

To leading order, (4.3) reduces to

$$[\![\mu W''(R_1)]\!]\delta+[\![\mu(w_r+u_x)]\!]=0. \tag{4.6}$$

This shows that the jump in the shear stress on $r = R_1$ is balanced by the effective gravity

$$[\![\rho]\!] g\delta = [\![\mu(w_r + u_x)]\!]. \tag{4.7}$$

The instability associated with (4.7) is induced by gravity. The only stable equilibrium of two fluids in a gravitational field is vertically stratified. Hence, when the velocity is reduced to zero, the heavy fluid will fall into a stratified configuration with heavy fluid below. Experiments (cf section VII.3) and analysis show that this fall-down instability can be stabilized by shear. The gravity term in this system of equations is not conservative, and cannot be written as a gradient, because

$$\text{curl } \rho\mathbf{g} = \nabla\rho \times \mathbf{g} \neq 0, \tag{4.8}$$

where $\nabla\rho$ is distributional (a delta function) across the interface.

It is shown in section VI.2 (e) that the linearized energy equation may be used to identify sources of instability. The growth rate of the energy of small disturbances is given by equation (2e.2) of section VI.2 (e), together with equation (2f.4) for the notation. We have

$$\dot{E} = I - D + B, \tag{4.9}$$

where

$$\dot{E} = \alpha c_{\mathrm{i}} \int_\Omega \zeta_j r(|u|^2 + |v|^2 + |w|^2)dr,$$

$$I = \int_\Omega \zeta_j r W'(r)\mathrm{Im}(uw_*)dr,$$

$$D = \int_\Omega \frac{\zeta_j}{\mathbb{R}_j}\left\{\frac{1}{r}\left(\left|\frac{d(ru)}{dr}\right|\right)^2 + \frac{1}{r}\left(\left|\frac{d(rv)}{dr}\right|\right)^2 + r\left(\left|\frac{dw}{dr}\right|\right)^2 \right.$$

$$\left. + r\left(\alpha^2 + \frac{n^2}{r^2}\right)(|u|^2 + |v|^2 + |w|^2) + \frac{4n}{r}\mathrm{Re}(u_* v)\right\} dr$$

$$+ \frac{1}{\mathbb{R}}(|u(0)|^2 + |v(0)|^2),$$

$$B = B1 + B2 + B3$$

$$B1 = \frac{J^*}{\alpha\mathbb{R}^2}\frac{1-\alpha^2-n^2}{\alpha}\frac{c_{\mathrm{i}}}{|W(1)-C|^2}|u(1)|^2,$$

$$B2 = \frac{1-m}{\mathbb{R}}\left\{2(|u|^2 + |v|^2) + 2\alpha\mathrm{Re}(u_* w_2) + 2n\mathrm{Re}(uv_*)\right.$$

$$\left. - \frac{f+1}{2}\frac{1}{\alpha}\mathrm{Re}\left(\frac{u_* w_2'}{(W(1)-C)^*}\right) - \frac{F+1}{2m}\frac{(2-m)(W(1)-c_{\mathrm{r}})}{|W(1)-C|^2}|u(1)|^2\right\},$$

$$B3 = -(\zeta_2 - 1)\frac{1}{\alpha}\mathrm{Re}\left(\frac{vw_{2*}}{W(1) - C}\right)$$
$$+\frac{1-m}{\mathbb{R}}\frac{F+1}{\alpha^2|W(1)-C|^2}\frac{\zeta_2 - 1}{2m}|u(1)|^2. \tag{4.10}$$

$$c_\mathrm{r} = \mathrm{Re}(C), \quad c_\mathrm{i} = \mathrm{Im}(C),$$

$c_\mathrm{i} > 0$ for instability,

$$\int_\Omega (\cdot)dr = \int_0^1 (\cdot)_1 dr + \int_1^a (\cdot)_2 dr,$$

and an asterisk denotes the complex conjugate. To compare with the equations in (2e.3) of section VI.2, replace β and r of that section by α/η and $r\eta$ respectively, where $\eta = 1/a$.

$\dot{E}$ and D may be further decomposed into a part in the water and a part in the oil. $B1$ is the energy supplied at the interface due to interfacial tension. It originates from the normal stress balance at the interface and arises from a perturbation of the curvature of the interface. It can be seen from the expression for B1 that interfacial tension stabilizes short waves and all asymmetric waves ($n \geq 1$), and destabilizes long axisymmetric waves.

$B2$ is the energy supply due to the viscosity jump which is called 'interfacial friction' in section VI.2. It comes from perturbing the condition expressing the continuity of velocity. This leads to a jump in the shear rate which can be reduced to a viscosity jump. Instability due to interfacial friction is a viscous generalization of the Kelvin-Helmholtz instability. It has been found that when the densities are matched, $B2$ stabilizes the flow at low Reynolds numbers, destabilizes at high Reynolds numbers and causes wavy core flows. The term $B3$ in the energy supply is proportional to the jump of the density, with gravity as a constant of proportionality. We have used gR_1^2/ν_1 as the velocity scale so that the gravity effect is implicit. The last term in $B3$ also contains a factor proportional to the viscosity difference, indicating the coupling of the effect of the viscosity jump and the effect of the density jump. We call $B3$ 'interfacial gravity'.

It is clear from the energy equation that even when viscosities are matched ($m = 1$) and $J^* = 0$, there is still an interfacial energy supply $B = B3$ due to interfacial gravity which can induce instability.

VII.5 Numerical Method

The Chebyshev pseudospectral method of section VI.1 (f) is modified and applied to the eigenvalue problem.

Convergence tests were performed by increasing the truncation number N of the interpolation functions (see table 2 of CBJ [1990]). $N = 20$ yielded

sufficient accuracy for the calculations of this section. The code was checked against JRR, PCJ and HJ. If we take $\zeta_2 = 1$ and

$$F = \frac{4m}{m + a^2 - 1} - 1,$$

then our problem is identical with that of section VI.1.

In section VI.1 (g), we discuss reasons for analyzing the axisymmetric mode and not the nonaxisymmetric modes when gravity is neglected. When gravity is included, we cannot confine ourselves to the axisymmetric modes. If the lubricant at the wall is in a very thin annulus, then the two-dimensional analogue of our problem is the lubricated vertical Poiseuille flow [Renardy 1987b]. For the plane problem, it is found that when the densities are similar, either the axisymmetric or the antisymmetric mode is unstable, and that the densities have to be very different in order to have a linearly stable flow. It appears, however, that for the pipe flows presented in this chapter, the data on the axisymmetric mode suffices for the neutral curves. Growth rates were computed for the axisymmetric mode ($n = 0$) and the asymmetric modes $n = 1$ and 5 for $a = 1.1$, $m = 0.95$, ζ_2=0.2, $J^* = F = 0$, $\mathbb{R}_g = 10$, which is a free flow under gravity: the axisymmetric mode has the largest growth rate. Similar mode comparisons have been carried out for other ranges of parameters, including up-flows, and the axisymmetric mode happened to be the most unstable. In the rest of this chapter, only the axisymmetric disturbances are pursued.

VII.6 Density Stratification and Interfacial Gravity

Interfacial gravity plays an important role in the disturbance energy budget. Density stratification could either stabilize or destabilize the basic flow, depending on the parameters. To illustrate the effect of density stratification, we consider the following two examples.

In the first example, we have calculated the growth rates for $a = 1.1$, $m = 1$, $J^* = F = 0$, $\mathbb{R}_g = 10$, corresponding to free fall with matched viscosities and zero interfacial tension. Figure 6.1 shows that the flow is stable when the lubricant is heavier than the core fluid and unstable when lighter. The interfacial mode degenerates to the neutral mode $C = W(1)$ when the densities are also matched. This example indicates that density stratification could cause instability even in the absence of interfacial tension and interfacial friction.

We next consider the lubricated case, $m = 0.5$. JRR showed that for horizontal pipe-flow with matched density, in the absence of interfacial tension, CAF is stable to long waves if the lubricating layer is very thin. But if the lubricating layer is thick, CAF is unstable to long waves, even in the limit $\mathbb{R} \to 0$. This long-wave instability is due to interfacial friction.

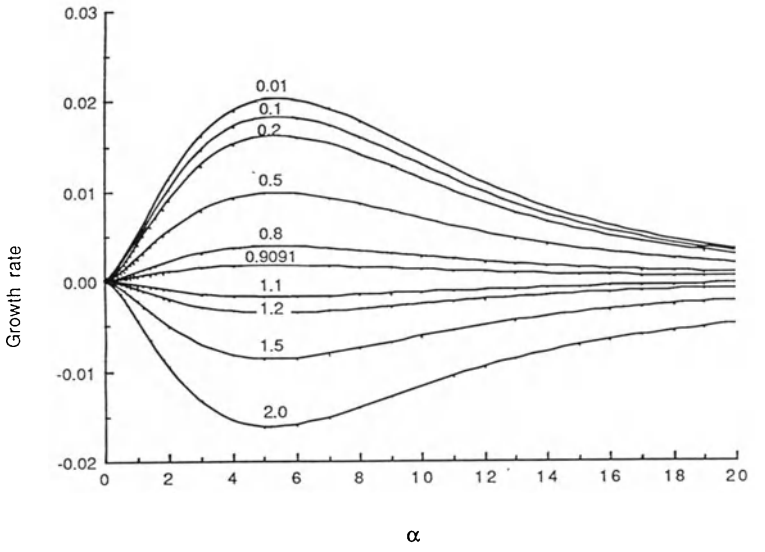

Fig. 6.1. [Chen, Bai and Joseph, 1990] Growth rates for a=1.1, m=1, J^*= F=0, $\mathbb{R}_g$ =10. Values of ζ_2 are indicated above each curve. The flow is stable when $\zeta_2 > 1$ and unstable when $\zeta_2 < 1$.

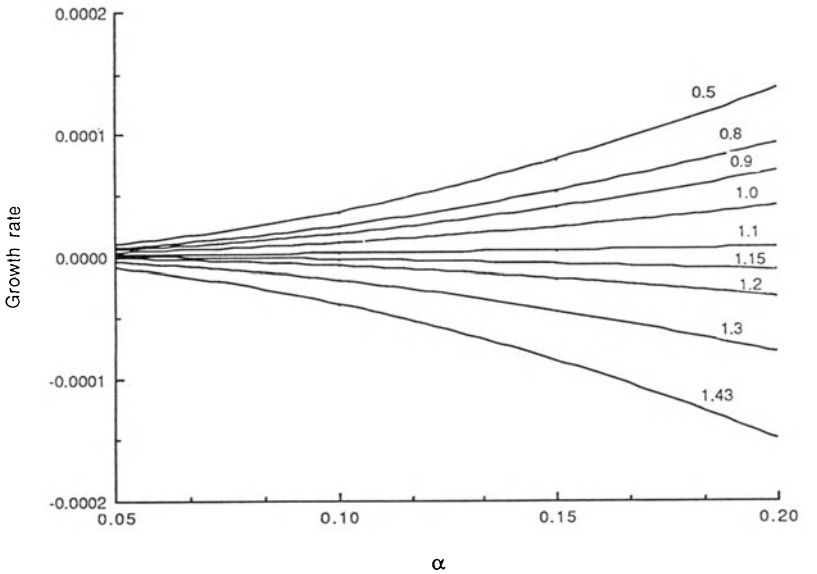

Fig. 6.2. [Chen, Bai and Joseph, 1990] Growth rates for a=1.86, m = 0.5, J^* = F = 0, $\mathbb{R}$=1; ζ_2 is indicated above each curve. The long-wave instability for ζ_2 =1 is reinforced when $\zeta_2 < 1$, suppressed when $\zeta_2 > 1$, and stabilized when $\zeta_2 \geq 1.15$.

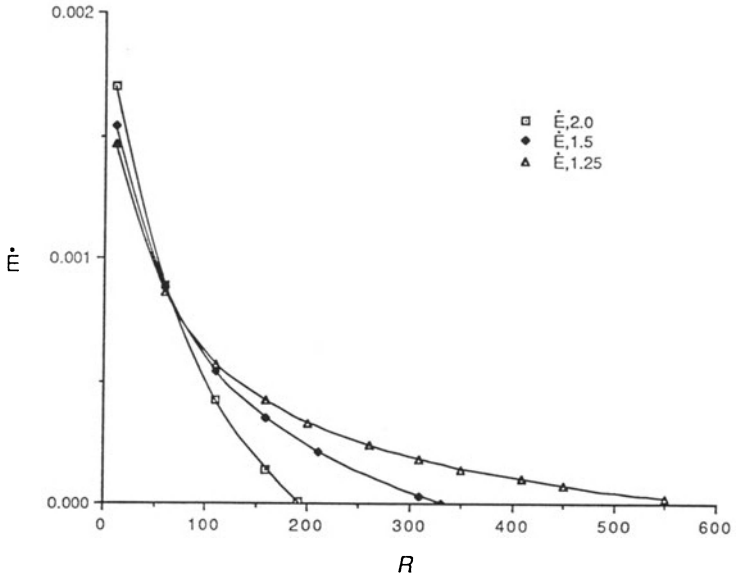

Fig. 6.3. [Chen, Bai and Joseph, 1990] The rate of change of disturbance energy $\dot{E}$ versus Reynolds number $\mathbb{R}$ for a=1.1, m=1, F=0, J^*= 2000, ζ_2 =2.0, 1.5, 1.25. The flow is stable when $\mathbb{R}> \mathbb{R}_c(\zeta_2)$: $\mathbb{R}_c(2.0) = 190$, $\mathbb{R}_c(1.5) = 330$, $\mathbb{R}_c(1.25)$=550.

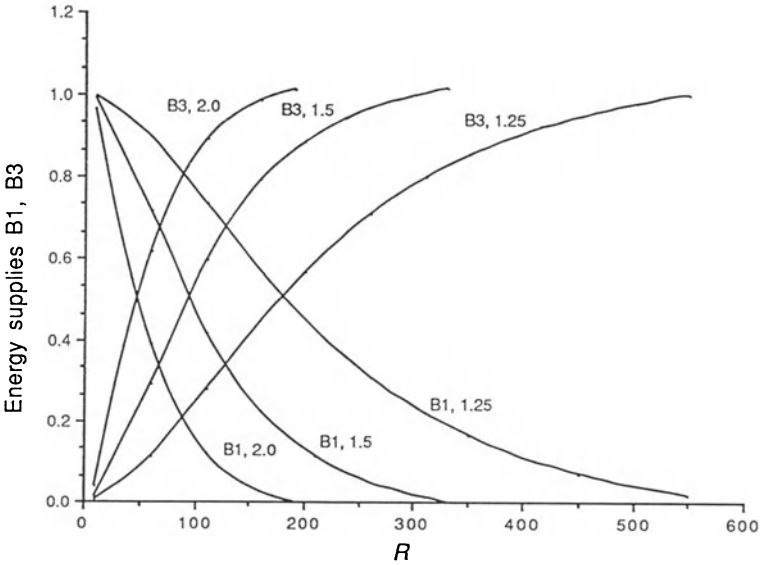

Fig. 6.4. [Chen, Bai and Joseph, 1990] Energy supplies $B1$ and $B3$ for a =1.1, m=1, F = 0, J^* = 2000, ζ_2 =2.0, 1.5, 1.25. Interfacial gravity $B3$ is always positive, destabilizing the flow.

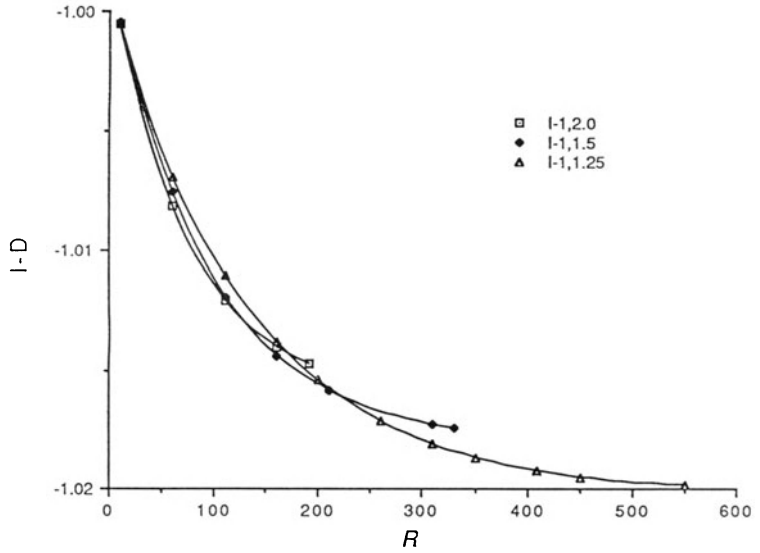

Fig. 6.5. [Chen, Bai and Joseph, 1990] $I - D$ for $a = 1.1$, $m = 1$, F =0, $J^* = 2000$, $\zeta_2 = 2.0, 1.5, 1.25$.

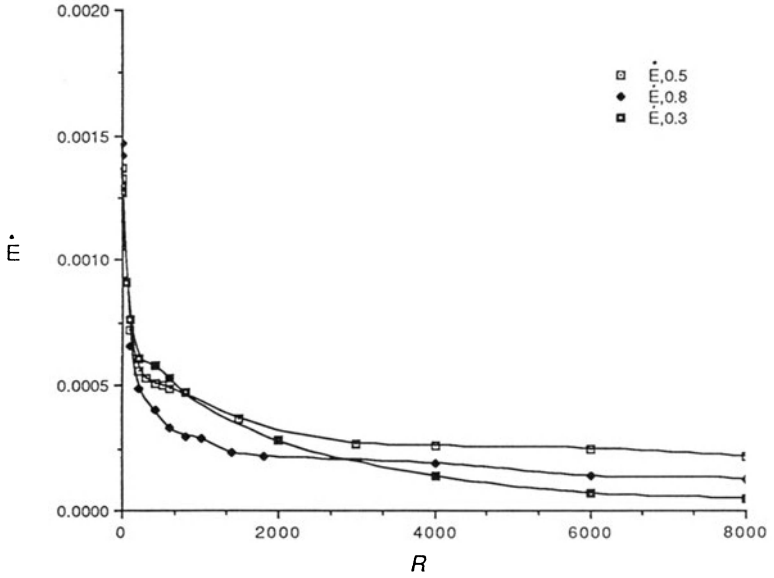

Fig. 6.6. [Chen, Bai and Joseph, 1990] Rate of change of disturbance energy $\dot{E}$ for $a = 1.1$, $m = 1$, $F = 0$, $J^* = 2000$, and $\zeta_2 = 0.8, 0.5, 0.3$. The flow is always unstable.

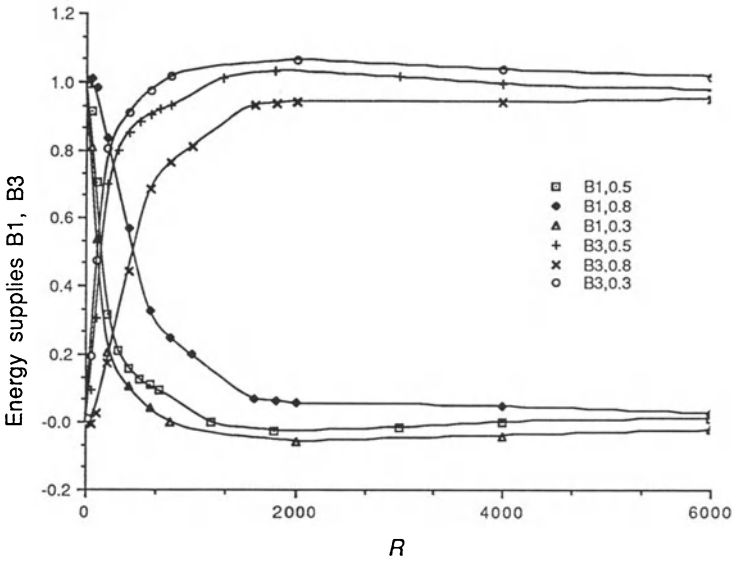

Fig. 6.7. [Chen, Bai and Joseph, 1990] Energy supplies $B1$ and $B3$ for $a = 1.1$, $m = 1$, $F = 0$, J^*=2000 and $\zeta_2 = 0.8, 0.5, 0.3$. At large Reynolds numbers, interfacial gravity $B3$ is the main source of instability.

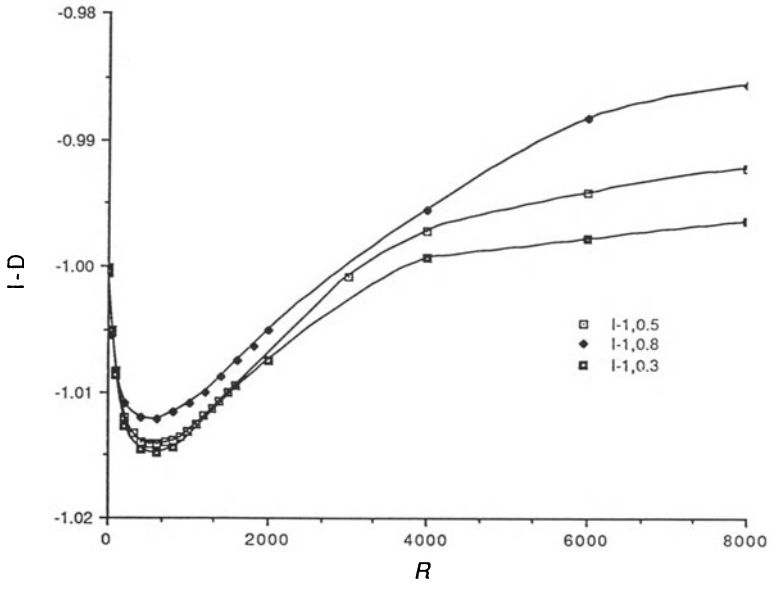

Fig. 6.8. [Chen, Bai and Joseph, 1990] $I - D$ for $a = 1.1$, $m = 1$, $F = 0$, $J^* = 2000$ and $\zeta_2 = 0.8, 0.5, 0.3$.

Interfacial tension can also induce a long-wave instability. For vertical pipe flow studied here, say free fall, the same type of long-wave instability due to interfacial friction will be present if the radius ratio a is large, the densities are matched and interfacial tension is neglected. We want to determine if this long-wave instability can be stabilized by density stratification. We have computed the case $a = 1.86$, $m = 0.5$, $J^* = F = 0$, $\mathbb{R}_g = 1$, and various values of density ratio ζ_2, for the long waves $a \ll 1$. The results are shown as plots of growth rates αc_i vs ζ_2 in figure 6.2. From these plots it is clear that the long-wave instability (ζ_2=1) is reinforced when $\zeta_2 < 1$, suppressed when $\zeta_2 > 1$ and completely stabilized when $\zeta_2 > \zeta_J (> 1)$. In our case, ζ_J is about 1.15.

The stabilizing effect of using heavy lubricant seems to work generally. When interfacial tension is included, short waves ($\alpha > 1$) are stabilized and there is a battle in the long-wave range $0 < \alpha < 1$ between the destabilizing effect of surface tension and the stabilizing effect of density stratification. In the rest of this section, we will include interfacial tension and monitor the terms in the energy budget corresponding to the most unstable mode as the Reynolds number is varied. In performing such calculations, we will normalize our eigenfunction with $D = 1$. We choose the following parameters: $a = 1.1$, $J^* = 2000$, $F = 0$, $m = 1$ and various values of ζ_2, as one example of free flow under gravity. By matching the viscosities we make the $B2$ term in the energy budget vanish so that we can isolate and study the interfacial gravity $B3$.

We start with $\zeta_2 > 1$: the heavy fluid is outside. In figure 6.3, the rate of change of the disturbance energy $\dot{E}$ is plotted against Reynolds number $\mathbb{R}$ for three different values of ζ_2. As $\mathbb{R}$ is increased to $\mathbb{R}_c(\zeta_2)$, $\dot{E}$ monotonically decays to zero. The flow is stable when $\mathbb{R} > \mathbb{R}_c(\zeta_2)$. The fact that $\mathbb{R}_c(2.0) < \mathbb{R}_c(1.5) < \mathbb{R}_c(1.25)$ indicates that increasing the density of the lubricating fluid can stabilize the flow. Water is a good lubricant for oil. A heavier fluid (at the same viscosity ratio) might have a wider window of stability in parameter space. For instance, see figure 6.4, where we compare the interfacial energy supply $B1$. Capillary instability is rapidly stabilized by using a heavy lubricant. This result could be used for preventing the formation of slugs and bubbles in slow flows.

Figure 6.4 also shows that interfacial gravity $B3$ is always positive and destabilizes the flow. In fact, $B3$ is a monotonically increasing function of $\mathbb{R}$ and levels off at large $\mathbb{R}$. Although the interfacial gravity is always destabilizing, the flow is stable when $\mathbb{R} > \mathbb{R}_c(\zeta_2)$. The larger the ζ_2, the faster $B1$ decays and the faster $B3$ increases. The Reynolds stress $I - D$ in the bulk of the fluids is plotted in figure 6.5. It is always stabilizing. This result indicates that the stabilizing effect of using a heavy lubricant is achieved through increasing viscous dissipation, not through interfacial gravity $B3$.

When $\zeta_2 < 1$, the heavy fluid is in the core and the results are very different. The density stratification helps instability and the flow is always

unstable for all the Reynolds numbers that were used. Figure 6.6 shows that for $\zeta_2 = 0.8$, 0.5 and 0.3, the rate of change of the disturbance energy $\dot{E}$ is positive and is a monotonically decreasing function of the Reynolds number. Figure 6.7 is a plot of the energy supply $B1$ and interfacial gravity $B3$ against Reynolds number. At low Reynolds numbers, interfacial tension is the main source of instability and at large Reynolds numbers the interfacial gravity is the main source of instability. The value of the Reynolds number for this transition in the type of instability decreases as ζ_2 decreases.

Figure 6.8 shows that $I - D$ is stabilizing for all Reynolds numbers. The following conclusions can be drawn for flows falling freely under gravity ($F = 0$):

(1) A heavy lubricant suppresses the long-wave instability caused by interfacial tension and prevents the formation of slugs and bubbles.
(2) Heavy lubricants can also stabilize the long-wave instability due to interfacial friction which occurs when a is large.
(3) Capillary instability is dominant at low Reynolds numbers and is stabilized by shear at large Reynolds numbers.
(4) Interfacial gravity is always destabilizing and increasingly so at higher Reynolds numbers. When the viscosities are matched and the lubricant is lighter, interfacial gravity is responsible for instability at large Reynolds numbers.

VII.7 Long Waves

In the long-wave limit $\alpha \to 0$, the eigenvalue problem can be solved explicitly with a series of powers of α using the method of Yih [1967]. The general method is described in section IV.4 in the context of plane flows. The solution was first given by Hickox [1971], in terms of a different set of parameters than ours. The surface tension parameter used by Hickox is

$$S = \frac{T}{\rho_1 R_1 W_1^2(0)},$$

where $W_1(0)$ is the centerline velocity. See equations (1d.9)- (1d.10) of section VI.1 for a discussion of this parameter.

The formula thus obtained for the eigenvalue C can be written as

$$C = c^{(0)} + \alpha c^{(1)} + O(\alpha^2), \tag{7.1}$$

where $c^{(0)}$ is a real constant and thus does not affect stability and $c^{(1)}$ is purely imaginary and therefore determines the stability at the lowest order. In fact, $c^{(1)}$ can be written as

$$c^{(1)} = \mathrm{i}\left\{\frac{J^*}{\mathbb{R}} f_1(a,m) + \mathbb{R} f_2(a,m,\zeta_2,F)\right\}, \tag{7.2}$$

where $f_1(a,m)$ is positive definite, measuring the capillary instability modified by shearing. For details, the reader is referred to the appendix of the paper by CBJ. The function $f_2(a,m,\ \zeta_2,\ F)$ indicates the effects of interfacial shearing and interfacial gravity on the long-wave stability, since $f_2(a,m,\zeta_2,F)$ can be expressed as

$$f_2(a,m,\zeta_2,F) = (1-m)q_1(a,m,\zeta_2,F) + (1-\zeta_2)q_2(a,m,\zeta_2,F). \quad (7.3)$$

We also note that $f_2(a,m,\zeta_2,F)$ is a quadratic polynomial in ζ_2. These functions are given in the appendix of CBJ.

Consider free flow under gravity ($F=0$). If $f_2(a,m,\zeta_2,0)$ is negative, then there exists a critical Reynolds number $\mathbb{R}_0$, defined in the same way as $\mathbb{R}_g$ in section VII.2, determined by

$$\frac{\mathbb{R}_0^4}{J^*} = -\frac{f_1(a,m)}{f_2(a,m,\zeta_2,0)}, \quad (7.4)$$

such that we have stability to long waves when $\mathbb{R}_g > \mathbb{R}_0$ and instability when $\mathbb{R}_g < \mathbb{R}_0$. It can be seen from (7.2) that shear stabilizes capillary instability when $\mathbb{R}_g > \mathbb{R}_0$.

In figure 7.1, we have plotted $\mathbb{R}_0/J^{*\frac{1}{4}}$ vs ζ_2 for $m=0.5$ and different values of a. The function $f_2(a,m,\zeta_2,F)$ is a parabola on the $f_2-\zeta_2$ plane for any given value of a, m and F and $f_1(a,m)$ is a constant for given a and m. For the parameters we chose to use, f_2 is a concave-up parabola. For the ζ_2-range of interest, say $0<\zeta_2<5.5$, there are three distinct cases, depending on the values of a:

(1) For small a (say $a=1.1$) there is a region of stability $\mathbb{R}_g > \mathbb{R}_0\ (\zeta_2)$, for $0<\zeta_2<5.5$.

(2) Define ζ_0 to be one of the two zeros of the parabola $f_2(a,m,\zeta_2,0)$ in the ζ_2-range considered. Then $\mathbb{R}_0\ (\zeta_2) \to \infty$ as $\zeta_2 \to \zeta_0$. There is one and only one ζ_0 in this range. An example of this is the curve for $a=1.2$. When $\zeta_2<\zeta_0$, the flow is unstable to long waves at every $\mathbb{R}_g > \mathbb{R}_0 = 0$; when $\zeta_2>\zeta_0$ and $\mathbb{R}_g > \mathbb{R}_0$ the flow is stable to long waves, when $\zeta_2>\zeta_0$ and $\mathbb{R}_g < \mathbb{R}_0$ the flow is unstable to long waves.

(3) Define two critical density ratios ζ_{01} and ζ_{02} to be the two zeros of $f_2(a,m,\zeta_2,0)$ and they are both in the range $0<\zeta_2<5.5$. Then $\mathbb{R}_0(\zeta_2)\to\infty$ as $\zeta_2\to\zeta_{01}$ or ζ_{02}. The flow is unstable to long waves when $\zeta_{01}<\zeta_2<\zeta_{02}$ at all $\mathbb{R}_g > \mathbb{R}_0(\zeta_2)$ and is stable when $\mathbb{R}_g > \mathbb{R}_0$. When $\zeta_2<\zeta_{01}$ or $\zeta_2>\zeta_{02}$ the flow is unstable at all values of $\mathbb{R}_0$. The curves for $a=1.4$ and 1.6 are of this type.

The above classification only makes sense in the range of ζ_2 considered, i.e. $0<\zeta_2<5.5$. In fact, type (3) is the generic case. But for smaller values of a, one or both of the zeros ζ_{01} and ζ_{02} of $f_2(a,m,\zeta_2,0)$ may be either negative or too large and out of the range of interest.

For forced flow ($F\neq 0$), we can determine $\hat{F}_u$ and $\hat{F}_l$ for given values of $\mathbb{R}_g$ and the other parameters such that when $\hat{F}_l < F < \hat{F}_u$, long waves

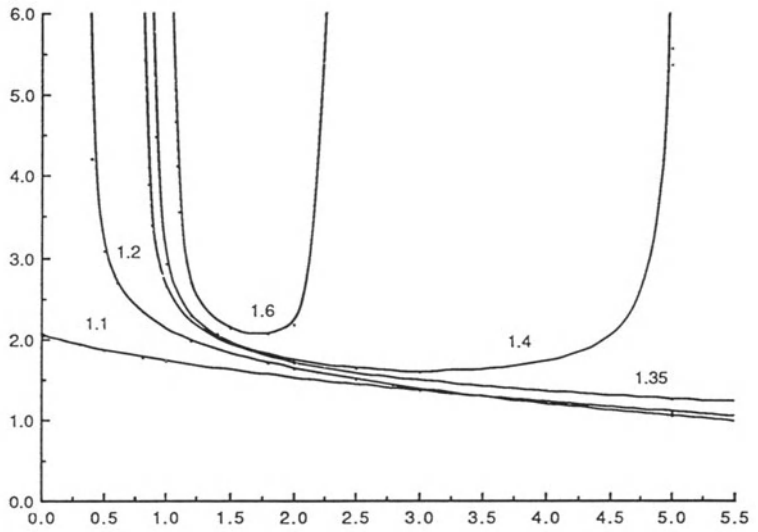

Fig. 7.1. [Chen, Bai and Joseph, 1990] Critical $\mathbb{R}_0/J^{*\frac{1}{4}}$ vs ζ_2 for $\alpha = 0$, $m = 0.5$, $F = 0$ and a as a parameter with values given above each curve.

are unstable. This corresponds to capillary instability. Some examples are given in section VII.9.

It has been shown (cf. section VI.1, PCJ, Renardy [1987b]) that maximum growth rates often occur when the wavenumbers are of order 1 rather than for long waves. It is therefore never sufficient to discuss the stability of CAF to long waves alone.

VII.8 Neutral Curves: Free Fall Under Gravity

The simplest vertical CAF is free fall under gravity ($F = 0$). This flow can be realized physically by slowly pouring fluids into a vertical pipe (cf. section VII.3 (a)). The effect of density stratification in free fall can be determined by comparing neutral curves in the $(\mathbb{R}_g, \alpha)$ plane.

Figures 8.1-8.4 are neutral curves for $a = 1.1$, 1.2, 1.3, $m = 0.5$, $J^* = 2000$, and $\zeta_2 = 0.5$, 1.0, 1.2, 1.4, 1.6, 2.0.

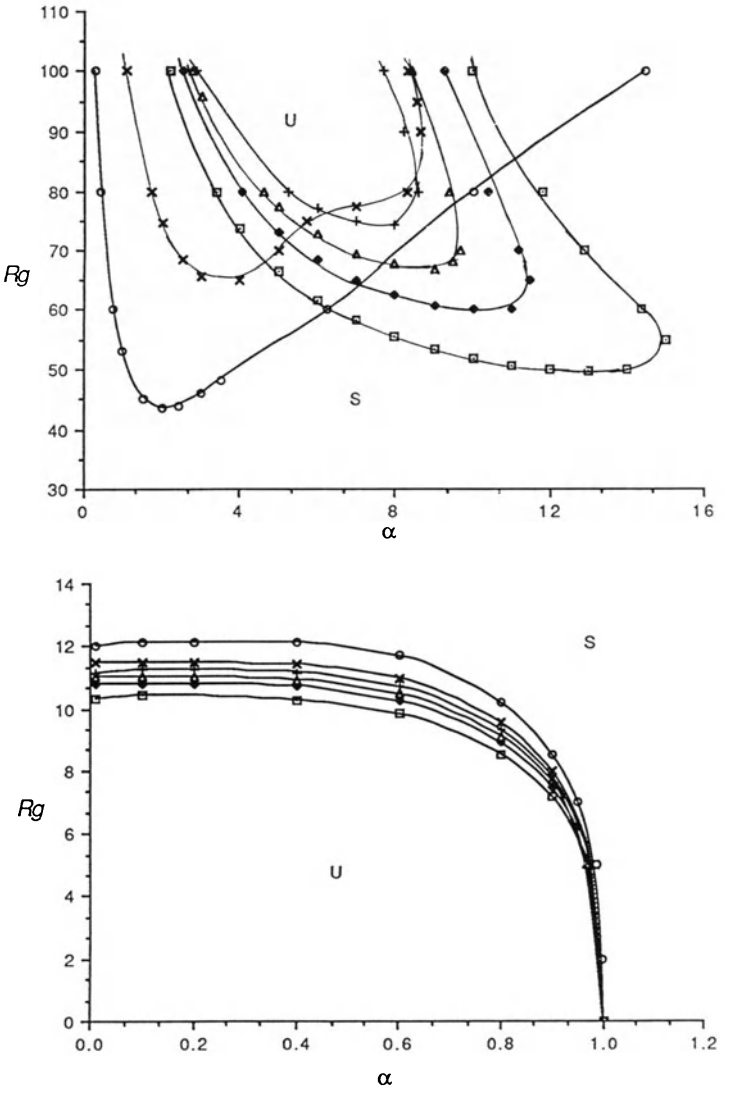

Fig. 8.1. [Chen, Bai and Joseph, 1990] Lower and upper branches of the neutral curves for a =1.1, m=0.5, F =0, J^*=2000. ζ_2 = 2.0, 1.6, 1.4, 1.2, 1.0, 0.5. Stable and unstable regions are marked by S and U respectively. The plotting symbols for ζ_2 are: □, 2.0; ◇, 1.6; △, 1.4; +, 1.2; ×, 1.0; ○, 0.5.

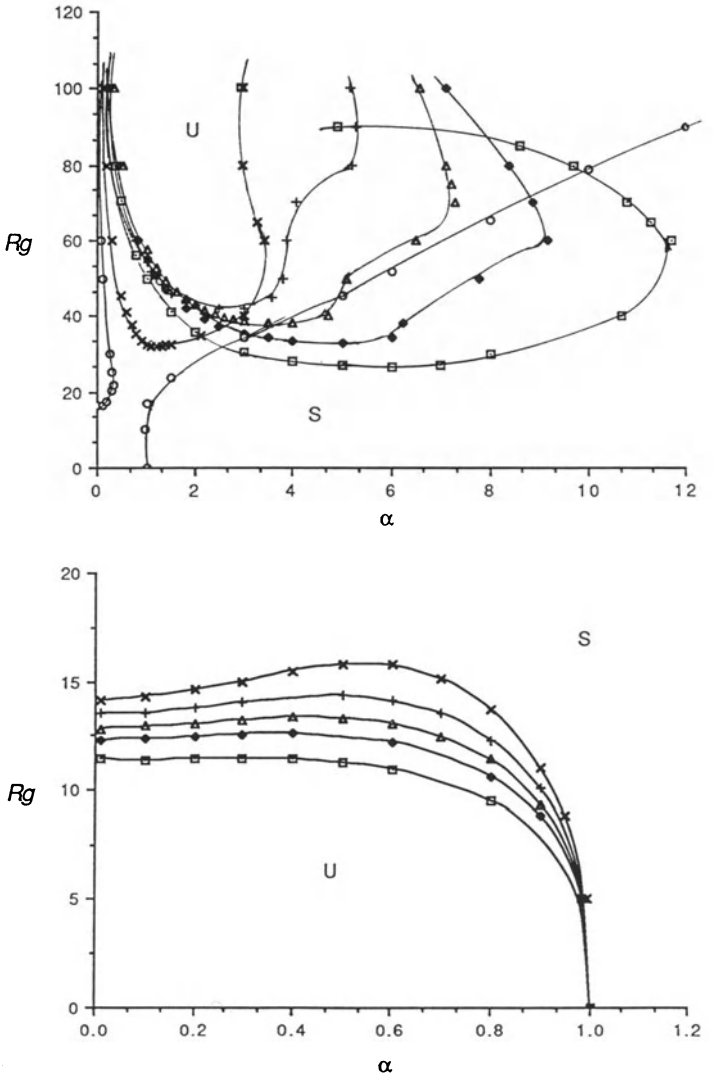

Fig. 8.2. [Chen, Bai and Joseph, 1990] Neutral curves for $a = 1.2$, m=0.5, $F = 0$, J^*=2000, $\zeta_2 = 2.0, 1.6, 1.4, 1.2, 1.0, 0.5$. Symbols as for figure 8.1.

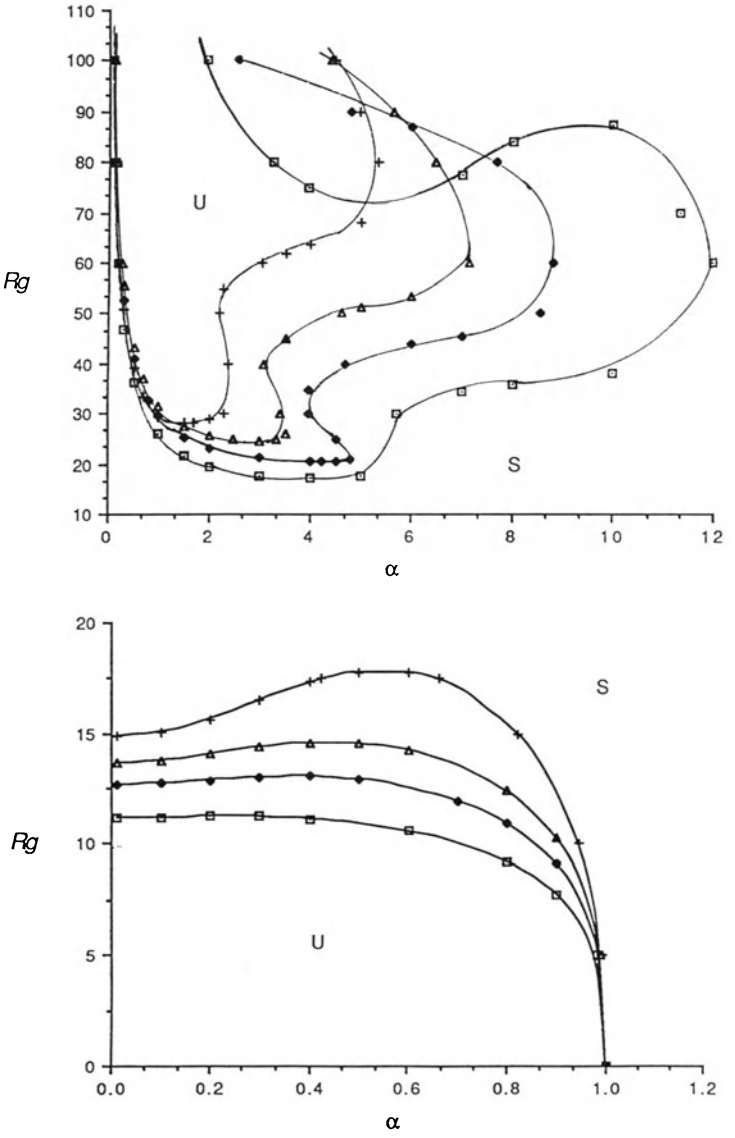

Fig. 8.3. [Chen, Bai and Joseph, 1990] Neutral curves for $a = 1.3$, m=0.5, F=0, $J^* = 2000$, $\zeta_2 = 2.0, 1.6, 1.4, 1.2$. Symbols as for figure 8.1.

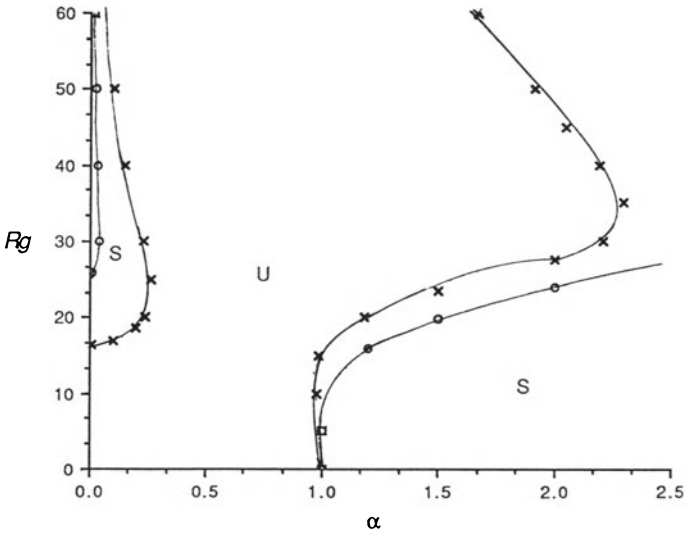

Fig. 8.4. [Chen, Bai and Joseph, 1990] Left and right branches of neutral curves for $a = 1.3$, $m = 0.5$, F=0, $J^* = 2000$, $\zeta_2 = 1.0, 0.5$. CAF is always unstable for these density ratios. Symbols as for figure 8.1.

The following observations can be obtained from inspecting the neutral curves for $n = 0$, $a = 1.1$:

(1) There is an interval

$$\mathbb{R}_L < \mathbb{R}_g < \mathbb{R} \tag{8.1}$$

in which CAF is stable for the six values of ζ_2. Here, $\mathbb{R}_L$ and $\mathbb{R}_U$ are the maximum and minimum Reynolds numbers on the lower and upper branches, respectively.

(2) $\mathbb{R}_L(\zeta_2)$ is a monotonically decreasing function of ζ_2 in the range of ζ_2 considered. The heavier the lubricant, the smaller is the maximum Reynolds number below which CAF is unstable to capillary instability induced by interfacial tension.

(3) $\mathbb{R}_U(\zeta_2)$ is not monotonic in ζ_2:

$$\mathbb{R}_U(1.2) > \mathbb{R}_U(1.4) > \mathbb{R}_U(1.0) > \mathbb{R}_U(1.6) > \mathbb{R}_U(2.0) > \mathbb{R}_U(0.5)$$

There is an optimal value of ζ_2 , around 1.2, that maximizes $\mathbb{R}_U(\zeta_2)$.

(4) The change of $\mathbb{R}_L(\zeta_2)$ with respect to the density ratio ζ_2 is relatively small compared to that of $\mathbb{R}_U(\zeta_2)$.

(5) The stable interval (8.1) is larger when the heavy fluid is outside ($\zeta_2 > 1$), than when the lighter fluid is outside ($\zeta_2 < 1$), and reaches a maximum when $\zeta_2 = 1.2$.

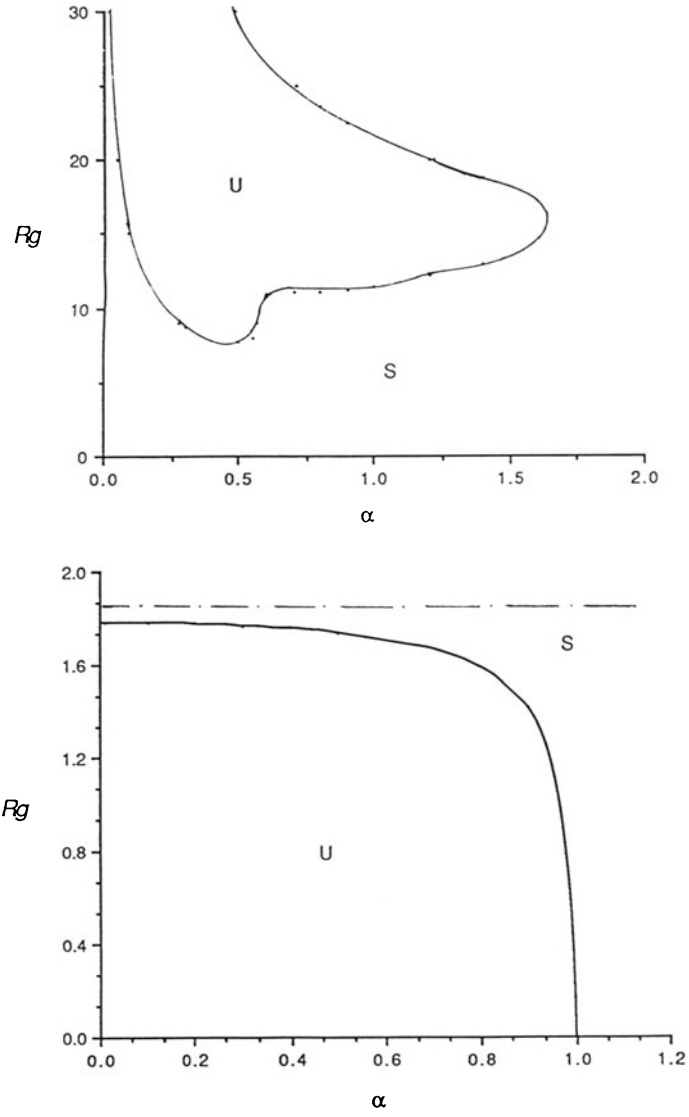

Fig. 8.5. [Chen, Bai and Joseph, 1990] Neutral curves for free fall, $a = 1.86$, $m = 0.33$, $\zeta_2 = 1.4$, $J^* = 2.26$, $F = 0$. Stable and unstable regions are marked by S and U respectively. The dashed straight line corresponds to the experiment $\mathbb{R}_g = 1.82$, which is shown in plate VII.3.2. Stable perfect core-annular flow is observed.

(6) Increasing the density of the lubricating fluid moves the upper branch towards shorter waves.

Similar conclusions can be drawn from figure 8.2 - 8.4 for $a = 1.2$ and 1.3, but there are some new features:

(7) When $a = 1.2$, linearly stable CAF is no longer possible for $\zeta_2 = 0.5$, while there still exists a stable window of $\mathbb{R}_g$ in which CAF is stable for other density ratios $\zeta_2 = 1.0$, 1.2, 1.4, 1.6 and 2.0. When $a = 1.3$, not only $\zeta_2 = 0.5$ but also $\zeta_2 = 1.0$ become unstable, while others are still stable.

(8) The optimal value of ζ_2 which maximizes $\mathbb{R}_U(\zeta_2)$ is still about $\zeta_2 = 1.2$ for both a=1.2 and 1.3.

(9) Comparing figures 8.1, 8.2 and 8.3, we found that, for those ζ_2 values with which there is a stable $\mathbb{R}_g$ window, and therefore $\mathbb{R}_L(\zeta_2)$ and $\mathbb{R}_U(\zeta_2)$ could be defined, the following relations hold:

$$\mathbb{R}_L(\zeta_2)|_{a=1.1} < \mathbb{R}_L(\zeta_2)\,|_{a=1.2} < \mathbb{R}_L(\zeta_2)|_{a=1.3}\,, \tag{8.2}$$

$$\mathbb{R}_U(\zeta_2)|_{a=1.1} > \mathbb{R}_U(\zeta_2)\,|_{a=1.2} > \mathbb{R}_U(\zeta_2)|_{a=1.3}\,. \tag{8.3}$$

In other words, for a fixed value of ζ_2 , the size of the $\mathbb{R}_g$ window, in which CAF is stable, is a decreasing function of a.

The main results obtained in the study of the neutral curves for $n = 0$, $m = 0.5$, $J^* = 2000$ can be summarized as

(a) for a fixed value of a, there exists an optimal value of density ratio ζ_m which maximizes the size of the stability window of $\mathbb{R}_g$. For our cases, ζ_m is about 1.2 for $a = 1.1$, 1.2 and 1.3.

(b) for a fixed value of ζ_2, increasing a (increasing the volume of lubricant) will decrease the size of the stable window of $\mathbb{R}_g$, or even destroy the stability of the flow, like the cases $a = 1.2$, $\zeta_2 = 0.5$ and $a = 1.3$, $\zeta_2 = 0.5$, 1.0.

In section VI.1, it was shown that with other parameters fixed, there is an optimal value of the viscosity ratio m which maximizes the size of the interval of Reynolds number for which CAF is stable. Using this result and those obtained above as a guideline, perfect and stable core-annular flows were realized in the free-fall experiment described in section VII.3 (a). The neutral curves corresponding to the example of plate VII.3.2 is given in figure 8.5, where the parameters are $m = 0.33$, ζ_2=1.4, $a = 1.86$, $J^* = 2.26$, and the Reynolds number for the experiment $\mathbb{R}_g$ =1.82 is shown as a dashed line. Clearly, the Reynolds number for the experiment falls in the stability window of $\mathbb{R}_g$.

VII.9 Neutral Curves: Forced Flows

In this section, neutral curves are calculated for forced flows. The effect of varying the density ratio is explored for lubricating layers $a = 1.1$, 1.2, 1.3 and 1.4 for the sample set of parameters $m = 0.5$, $J^* = 2000$, $\mathbb{R}_g = 10$.

Neutral curves for $a = 1.1$ are shown in figure 9.1. For each value of ζ_2, there are three branches of neutral curves. A region of capillary instability to long waves is formed for slow motions around $F = -1$. This region is shown in (b). When $\zeta_2 = 1$, all the neutral curves are symmetric about the axis $F = -1$. Since the basic flow is symmetric about $F = -1$, changing the value of F from F_1 to $-F_1 - 2$ will only reverse the flow without changing the dynamics. Figure 9.1 (b) shows that a heavier lubricant will shift the region of capillary instability downward without changing its shape. Therefore, for a given pressure gradient, one way to overcome the capillary instability is to use a heavy lubricant for down-flows (say $F > 0$) and a light lubricant for up-flows (say $F < -1$). When the densities are markedly different, one might expect that the heavier fluid should stay at the center of the pipe for down-flows and the light fluid stays at the center for up-flows, but this heuristic idea is just a guide and need not always be true (Renardy [1987b]).

The upper branches (a) of the neutral curves correspond to fast flow. The effect of increasing ζ_2 on the upper branch of figure 9.1 (a) is interesting. We may confine our remarks to the positive upper branch (F being positive) since the negative upper branch (F being negative) is dynamically similar to the positive one with the sign of F reversed. Let $F_U(\zeta_2)$ denote the minimum value of $F(\alpha)$ on the upper neutral curve over a for each fixed value of ζ_2. Similar to the case of free fall under gravity, for a given value of a, there is an optimizing value ζ_m of the density ratio ζ_2, for which $F_U(\zeta_m)$ is a maximum. For $a = 1.1$, ζ_m is about 1.5. The upper branch (a) is more sensitive than the capillary branch (b) to changes of ζ_2. When ζ_2 is increased, the unstable wavenumbers on the upper branches (a) are shifted to shorter waves (larger α).

Figure 9.2 gives the neutral curves for $a = 1.2$. For each given value of ζ_2, the size of stable regions for CAF is rapidly reduced as the water fraction is increased. For $\zeta_2 = 0.5$, stable CAF is impossible for $a = 1.2$, while for $a = 1.1$ there is still a region of stability. The main effect of increasing a is to move the upper branches downward reducing the region of stability. The lower branch of the neutral curve is less sensitive to changing a. The upper branch sinks as a is increased until it connects with the lower branch at a critical value of a. Then stable CAF is not possible. The critical value of a depends strongly on all the other parameters.

The neutral curves for negative values of F in figure 9.2 (a) are nearly mirror reflections of the upper branches of neutral curves for positive F across the line $F = -1$. We call these 'negative-F upper branches'. The negative-F upper branches shift to short waves as ζ_2 is increased more strongly than the positive branches (see figure 9.2 (a)). There is again a

density ratio which maximizes stability.

Figure 9.3 shows that when the density is matched, stable CAF is possible when the radius ratio $a \leq 1.2$, but is not possible for $a = 1.3$. Stable CAF can be achieved when a is large by choosing a lubricant which brings the density ratio close to the optimal one: for example, there is stability for $a = 1.3$ when $\zeta_2 = 2$ but instability when $\zeta_2 = 0.5$.

There are similarities with the free-fall situation discussed in section VII.8. For a given a, the largest window of stable CAF can be achieved by choosing a favorable density ratio ζ_m, and for a given density ratio ζ_2, the size of the stable region can be reduced by increasing the radius ratio a. For example, the stabilization of the flow for $a = 1.3$, achieved by increasing the density ratio to $\zeta_2 = 2$ (figure 9.3(a)), is nearly lost when a is increased to 1.4 (figure 9.4 (d)). The figures show that the destabilization with increasing lubricant fraction (or radius ratio a) acts on the upper branch of the neutral curve and can to some extent be countered by a suitable choice of ζ_2.

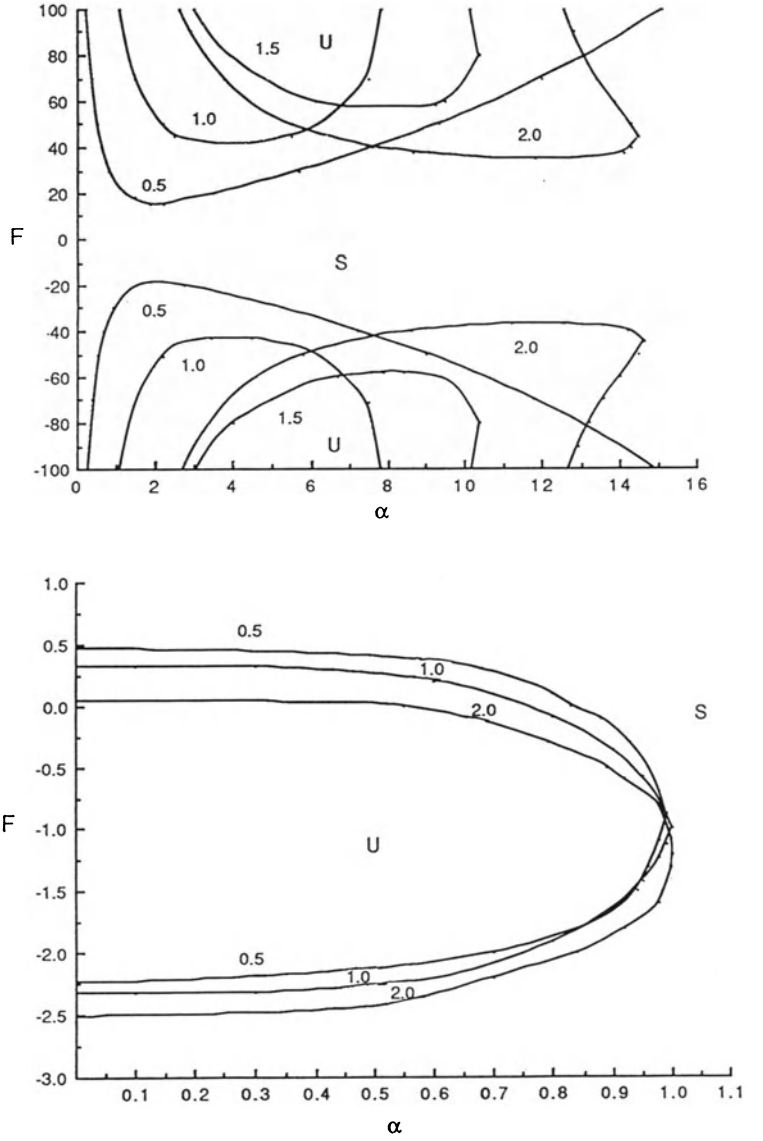

Fig. 9.1. [Chen, Bai and Joseph, 1990] Neutral curves for $a = 1.1$, $m = 0.5$, $J^* = 2000$, $\mathbb{R}_g = 10$, and different values of ζ_2 given by the numbers above each curve. (a) Positive- and negative-F upper branches. The negative branches are similar to the positive ones. The band of stability is maximized for a certain value ζ_m of ζ_2, and ζ_m is close to 1.5. (b) Regions of capillary instability.

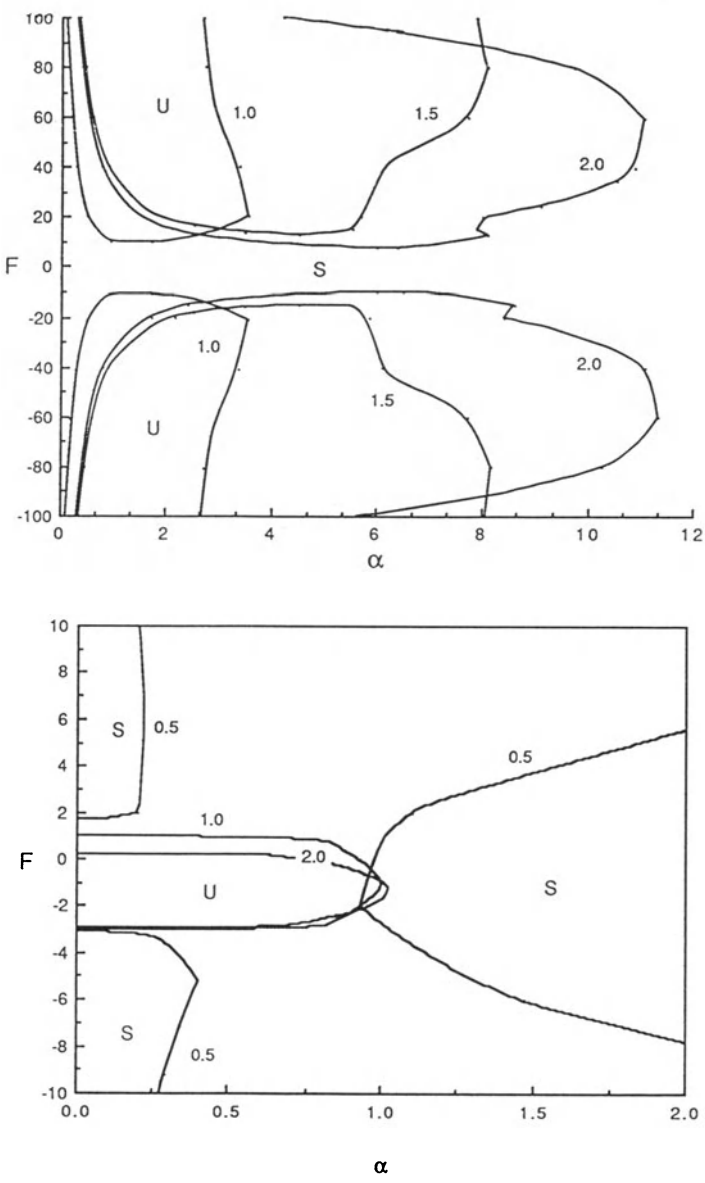

Fig. 9.2. [Chen, Bai and Joseph, 1990] Neutral curves for $a = 1.2$, $m = 0.5$, $J^* = 2000$, $\mathbb{R}_g = 10$, and different values of ζ_2 given by the numbers above each curve. (a) Positive and negative-F upper branches. The stability regions are largest when the density ratio ζ_2 is close to 1.5. (b) Detailed view near the capillary instability region. The neutral curves for $\zeta_2 = 0.5$ are also shown here. CAF is unstable for $\zeta_2 = 0.5$.

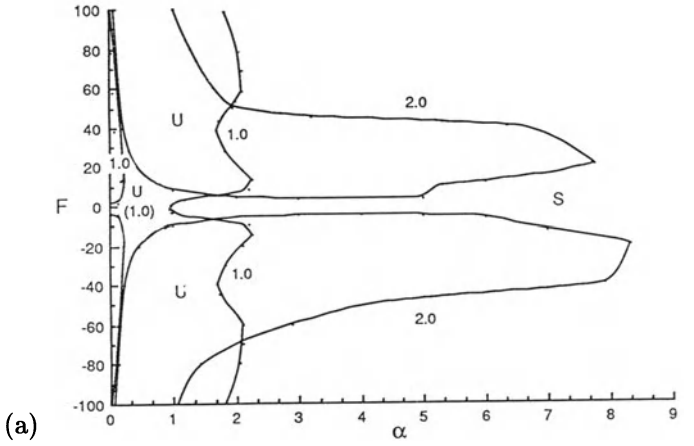

(a)

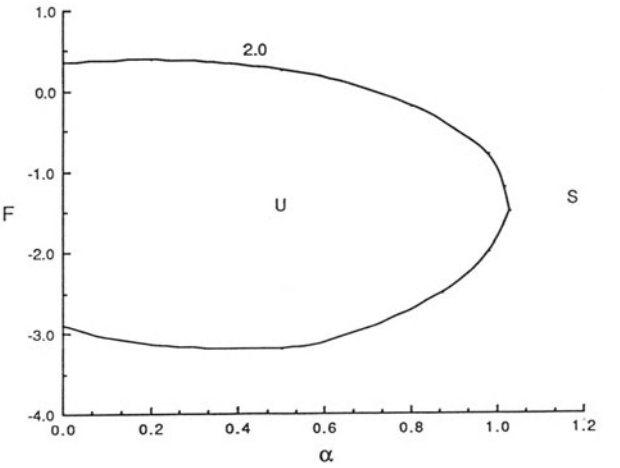

(b)

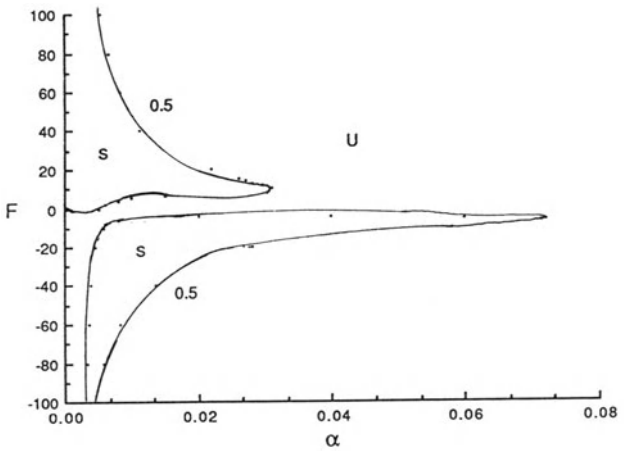

(c)

Fig. 9.3(a-d). [Chen, Bai and Joseph, 1990] Neutral curves for $a = 1.3$, m=0.5, $J^* = 2000$, $\mathbb{R}_g = 10$, and different values of ζ_2. Stable CAF is hard to achieve. (a) A global view. (b) Region of capillary instability for $\zeta_2 = 2.0$. (c) Left branch for $\zeta_2 = 0.5$: it consists of two parts. (d) Right branch for $\zeta_2 = 0.5$.

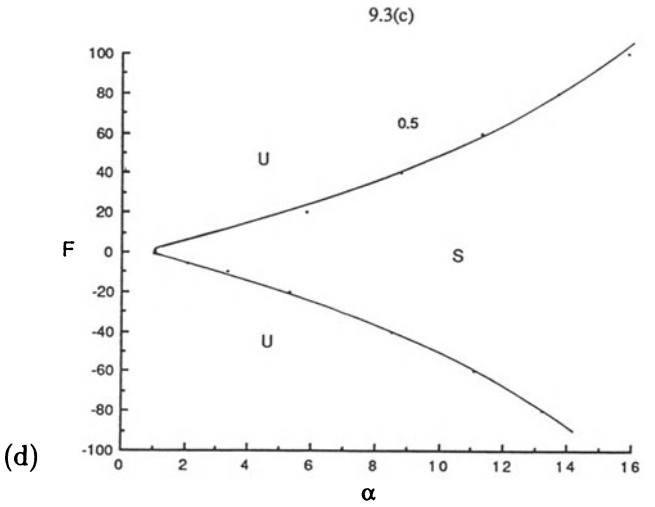

Fig. 9.3(d). Continued.

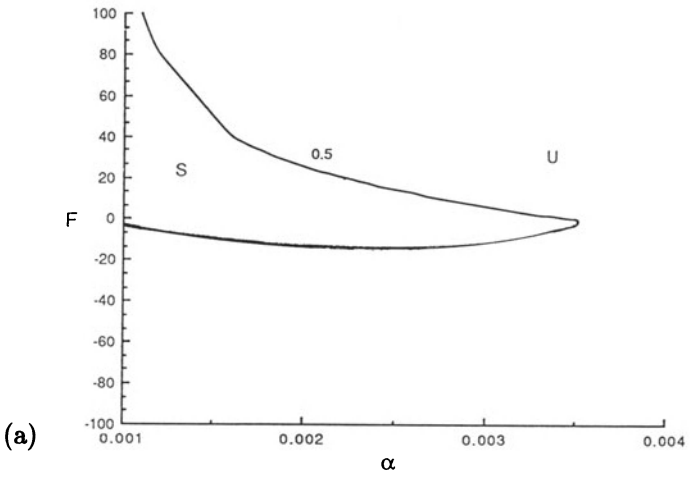

Fig. 9.4(a-e). [Chen, Bai and Joseph, 1990] Figure 9.4 shows neutral curves for $a = 1.4$, $m = 0.5$, $J^* = 2000$, $\mathbb{R}_g = 10$, and various ζ_2. (a) Left branch for $\zeta_2 = 0.5$. (b) Right branch for $\zeta_2 = 0.5$. CAF is unstable. (c) $\zeta_2 = 1$. CAF is unstable. (d) Positive- and negative-F upper branches for $\zeta_2 = 2$. There is a narrow band of stability. (e) Region of capillary instability for $\zeta_2 = 2$.

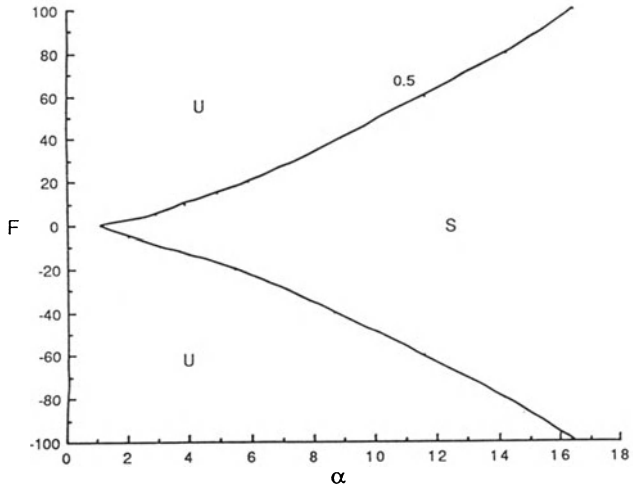

(b)

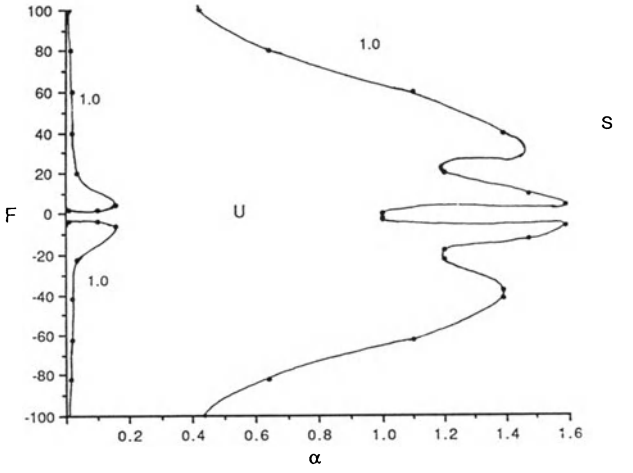

(c)

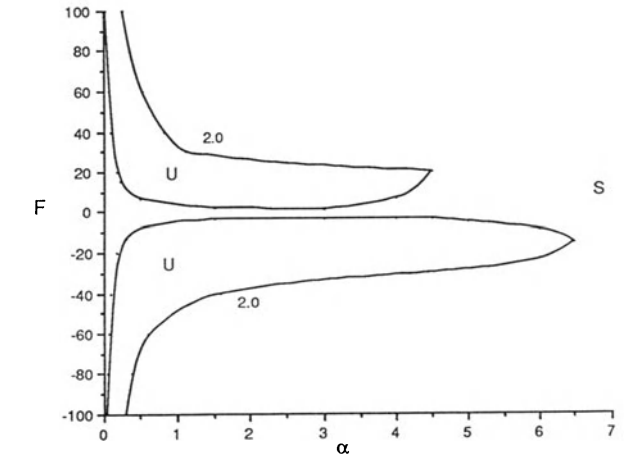

(d)

Fig. 9.4(b-d). Continued.

(e)

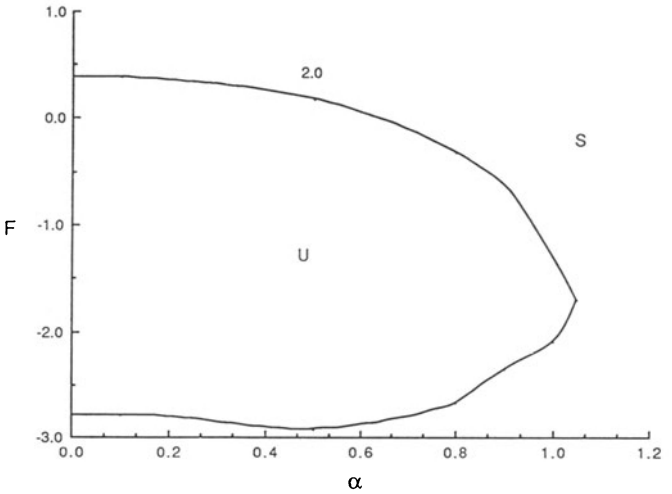

Fig. 9.4(e). Continued.

VII.10 Conclusions on Linear Stability

We have analyzed the effect of the density difference on the stability of vertical core-annular flow. The density difference changes the basic flow of chapter VI and introduces an effective gravity $[\![\rho]\!]g$ in the balance equation for the shear stress at the interface.

First, we summarize the main results for free fall when the lubricating layer is thin and the viscosities are matched, emphasizing the effect of the density ratio. As a typical example, we take $(F, a, m) = (0, 1.1, 1)$, $n = 0$.

(1) Energy analysis shows that interfacial gravity is destabilizing, for heavy and light lubricants and at all Reynolds numbers.
(2) The Reynolds stress minus the dissipation is stabilizing in the cases studied in this chapter.
(3) The stabilizing effects just mentioned are in opposition to capillary instability and to the destabilizing effect of gravity at the interface which drive the fluids to vertical stratification. The flow may be stabilized by dissipation for $\mathbb{R} > \mathbb{R}_c(\zeta_2)$ if the lubricant is heavy, but not if it is light.

Now we allow for different viscosities with the more viscous fluid inside, and set $m = 0.5$.

(4) Heavy lubricants suppress capillary instability. Increasing the density of the lubricant shifts the upper branch of the neutral curves toward shorter waves.
(5) When the lubricating layer is thin and the density ratio is not too small, there is an interval of Reynolds numbers between the lower and upper branches in which CAF is stable.
(6) For a given value of a, we can maximize the interval of Reynolds numbers on which CAF is stable by choosing the best $\zeta_2 = \zeta_m, 0 < \zeta_m < \infty$, the other parameters being fixed. The destabilization of the upper branch due to increasing a (thick lubricating layers) can be countered by using lubricants with ζ_2 close to ζ_m.

We next summarize the results for forced flow: $F \neq 0$ and F can be positive or negative. When $\zeta_2 = 1$, $F = -1$ implies that the gravity force and the pressure gradient are in balance and the neutrally buoyant core flow will break up by capillary instability. Large positive F means down-flow and large negative F means up-flow. There are two branches of neutral curves for up-flow and two branches for down-flow: the capillary branch and the upper branch. In order to have linear stability for a given density ratio, the lubricating layer must be sufficiently thin. The following summarizes the results for the parameter range addressed in the preceding sections.

(7) To achieve stable CAF for slow flow, use a heavy lubricant for down-flow and a light one for up-flow.
(8) The difference in the nature of the response between up-flow and down-flow is due only to the effect of gravity, and the two flows would be equivalent if the basic speeds involved were very fast. Thus, if $|F|$ is very large, the flows are very fast, either upward or downward, and the response of the system in both types of flows are the same.
(9) The upper branch for either up-flow or down-flow is more sensitive to changes in the density of the lubricant than the capillary branch. Increasing the density of the lubricant will shift all the upper branches to shorter waves.
(10) If the lubricating layer is sufficiently thin, it is possible to have linear stability for some range of density ratios, and there is an optimizing density ratio $\zeta_2 = \zeta_m$ which gives the largest interval of Reynolds numbers for stability.

The experiments described here on free fall have established that it is possible to run a perfect core-annular flow, robustly stable to finite amplitude disturbances, if the operating conditions are stable according to linearized theory. Some results are given for forced flows to show the range of flows which can be expected from a heavy motor oil and water. The experimental results are pursued in more depth in the next sections.

VII.11 Notation for Sections VII.12-21

a $=R_2/R_1$ radius ratio
A = area of the pipe (πR_2^2 where R_2 =3/16 in is the inside radius of the pipe)
A_o = cross-sectional area of the core (πR_1^2 where R_1 is the radius of the core)
A_{w} = cross-sectional area of the annulus ($\pi(R_2^2 - R_1^2)$)
BW = bamboo waves (see figures 15.3, 19.1-19.9)
CW = corkscrew wave (see figures 14.1, 19.4)
D_1 $=2R_1$
D_2, d $=2R_2$
DBW = disturbed bamboo waves (see figure 15.6)
DCAF = disturbed core-annular flow (see figures 15.7, 19.9)
η = $R_1/R_2 = 1/a$ radius ratio
λ = friction factor (19.4)
f_1, f_2 = pressure gradients (18.8)
g = gravity constant 9.81 m/s^2
H_1 = H_o height of oil head
H_2 = H_{w} height of water head
$\hat{H}, \hat{H}_1, \hat{H}_2$ = heights of water columns in the manometer tube (see figure 13.2)
h = hold-up ratio (14.1)
θ = dimensionless pressure drop
J = $TR_2/a\rho_1\nu_1^2$ capillary number of Chandrasekhar
J^* = aJ
L = pipe length, also = $H_o + H_{\mathrm{w}}$
m = μ_2/μ_1 viscosity ratio (oil inside corresponds to $m < 1$). In the experiments m =1/601 at 22°C)
μ_1 = μ_o oil viscosity
μ_2 = μ_{w} water viscosity
ν = kinematic viscosity μ/ρ, $\nu_1 = \nu_{\mathrm{w}}$, $\nu_2 = \nu_o$
Ω_o = $L\pi R_1^2 = LA_o = H_o\pi R_2^2 = H_oA$ volume of oil
Ω_{w} = $L\pi(R_2^2 - R_1^2) = LA_{\mathrm{w}} = H_{\mathrm{w}}\pi R_2^2 = H_{\mathrm{w}}A$ volume of water
Ω = $\Omega_o + \Omega_{\mathrm{w}}$ total volume
Δp = pressure drop
$\hat{P}$ = piezometric pressure
p = dynamic pressure
p' = constant pressure gradient
PCAF = perfect core-annular flow
Q_1 = Q_o volume flow rate of oil
Q_2 = Q_{w} volume flow rate of water
R_1 = mean radius of the core
R_2 = inside radius of the pipe
$\mathbb{R}$ = Reynolds number (see W_o)
$\mathbb{R}e$ = Vd/ν Reynolds number (see V)
$\mathbb{R}_g(R_1)$ = $R_1\sqrt{gR_1}/\nu_1$ Reynolds number

$\mathbb{R}_A$ $= U_w(D_2 - D_1)/\nu_1$
ρ_1 $= \rho_o$ oil density
ρ_2 $= \rho_w$ water density
$[\![\rho]\!]$ $= \rho_1 - \rho_2$
T = interfacial tension
τ_w = shear stress at the wall
U_o = average velocity of the oil
U_w = average velocity of the water
$(V, V_1, V_2) = (V,\ V_o,\ V_w) = (Q,\ Q_o,\ Q_w)/A$ are superficial velocities
$W(r)$ = axial velocity of PCAF
W_o $= W(0)$ centerline velocity
$W(1)$ = velocity of the oil/water interface in PCAF

VII.12 Properties of Fluids Used in Experiments

The Mobil cylinder oil was repeatedly recycled, in contact with water, during the two-year course of experiments reported here. After the two years, the recycled oil had taken on water in a relatively stable emulsion. The viscosity of the emulsified oil is less than half that of the pure oil. It is well known that emulsification of water into oil will increase the viscosity, as evident in Einstein's formula (cf. §4.11, Batchelor [1970]; Happel and Brenner [1983]) and in the measurements of Tipman and Hodgson [1956] for water emulsified in oil in concentrations ranging up to 30%. Except for an observed small decrease in viscosity at a water fraction of 2.5%, the emulsions of water in oil had increasingly larger viscosities. Both our fresh oil and our recycled oil are Newtonian (see Bai, Chen and Joseph [1992] for shear stress versus shear rate plots and viscosity versus temperature plot). We do not have an explanation for the decrease in viscosity of the water-emulsified oil. The decrease is even greater than for an ideal mixture computed as follows. If ε is the water fraction, the density ρ_e of the emulsion is the weighted sum $\varepsilon\rho_w + (1-\varepsilon)\rho_o$ of the densities of water and oil. The viscosity of the emulsion is $\mu_e = \varepsilon\mu_w + (1-\varepsilon)\mu_0$. The density $\rho_e = 0.905$ g/cm^3 and $\rho_o = 0.885$ g/cm^3. Hence $\varepsilon = 2/11.5$. At 22°C, μ_0=13.8p and $\mu_e \sim 9.5(13.8)/11.5$=11.4 poise. This is much larger than the measured value μ_e=6.01 poise. It is possible that the emulsified oil contains air. Another possibility is that the oil has undergone chemical change in two years, possibly due to attack by bacteria.

The viscosity of the pure oil and the used oil was measured on a Rheometrics System 4 rheometer and on a parallel plate Deer rheometer with consistent results. The water used in the experiments was a 0.4% aqueous solution of sodium silicate. The density of this solution is ρ_w=0.995 g/cm^3 and the viscosity is taken at $\mu_w = 10^{-2}$ poise. The sodium silicate was added to promote wettability of the glass walls of the pipe with water, to promote lubrication. This works if the glass is clean. After two years without cleaning (yuck!), the dirty walls are less hydrophilic to aqueous sodium silicate solution than clean walls to pure water. The nature of absorbed lay-

ers, and the history of wetting are important; wetting is not just a property of materials but depends on the history and dynamics of fluid motions near a surface (see (vi) of section VII.15 for more discussion).

The interfacial tension was measured with a spinning rod tensiometer which is basically a spinning drop tensiometer with a centrally located rod of small diameter designed to improve spin up and stability. The interfacial tension between the emulsified oil and pure water is $T = 22.50 \pm 1.86$ dyn/cm. The interfacial tension between the emulsified oil and the aqueous sodium silicate solution is $T = 8.54 \pm 0.157$ dyn/cm.

For our computations we have used measured values for the emulsified oil and sodium silicate solution at $T = 22°$.

$$\begin{aligned} &(\mu_{\mathrm{w}},\ \mu_0) = (10^{-2},\ 6.01)\text{poise}, \\ &(\rho_{\mathrm{w}},\ \rho_o) = (0.995,\ 0.905)\ \mathrm{g/cm^3}, \\ &T = 8.54\ \mathrm{dyn/cm}. \end{aligned} \tag{12.1}$$

The values for pure oil are as follows, but they do not characterize the fluids for which the flow data were taken. However, we present some computations in section VII.19 for this oil.

$$\begin{aligned} &(\mu_{\mathrm{w}},\ \mu_0) = (10^{-2},\ 13.32)\text{poise}, \\ &(\rho_{\mathrm{w}},\ \rho_o) = (1,\ 0.881)\ \mathrm{g/cm^3}, \\ &T = 20\ \mathrm{dyn/cm}. \end{aligned} \tag{12.2}$$

VII.13 Experimental Set-Up and Procedures

The flow system is shown in figure 13.1. The pipeline is a $\cap$ loop which is mounted on the wall with its long legs vertical, aligned with gravity. The flow of oil and water to the pipeline is established by the pressure of compressed air in the oil and water tanks. The flow rates Q_o and Q_{w} for oil and water are controlled by valves at the outlet of the oil and water tanks. Q_{w} is measured by a Dwyer rotameter and Q_o by a positive displacement gearmeter (FTB-1000, manufactured by Omega Engineering Co.) which is particularly suited for high-viscosity liquids. The oil and water are injected into the pipeline concentrically, with the oil in the core and water in an annulus, by means of a nozzle fitted centrally in the pipe. The oil is delivered through the nozzle. The flow is first pushed up against gravity in the left leg of the $\cap$ loop. The flow turns around at the top of the loop and flows down in the right leg. There are test sections on the left and right legs which are enclosed in boxes filled with glycerine to remove lens distortion from the round walls of the pipe. The height of the test sections is 93″. The total height of the $\cap$ loop is 180″.

The ∩ loop system is closed: the oil and water are recirculated. Oil and water are stored in separate pressurized tanks. The pressure levels in the two tanks are adjustable and drive the liquids to the ∩ loop without pulses. The oil and water are ejected into a large tank and separated under gravity. After separation, the two liquids are driven back into the inlet storage oil tanks by compressed air.

Pressure drops are measured in the up- and down-flow legs of the ∩ loop. In each leg, there are two pressure taps connected to a manometer. The pressure taps are designed to facilitate the separation of oil from the water so that only water will enter the manometer. The pressure gradient cannot simply be read off the manometer when there are two fluids in the pipe. Let $\hat{P}_A$ be the piezometric pressure at the bottom tap in figure 13.2 and $\hat{P}_B$ is the piezometric pressure at the top tap. The pressure difference

$$\hat{P}_A - \hat{P}_B = \rho_{\mathrm{w}} g H_{\mathrm{w}} + \rho_o g H_o + \Delta p \tag{13.1}$$

where $\rho_{\mathrm{w}} g H_{\mathrm{w}}$ is the weight of the water, $\rho_o g H_o$ the weight of the oil per unit area and

$$\Delta p = p_A - p_B \tag{13.2}$$

is the dynamic pressure producing the flow. Now consider the manometer in figure 13.2 (a) and let $\hat{P}_C$ be the air pressure in the column of air separating the two legs of the manometer. The pressure at A balances P_C plus the pressure of the water column of height $\hat{H}_1$,

$$\hat{P}_A = \hat{P}_C + \rho_{\mathrm{w}} g \hat{H}_1. \tag{13.3}$$

The pressure $\hat{P}_C$ balances $\hat{P}_B$ plus the pressure of the column of water of $L - \hat{H}_2$ where L is the distance A to B

$$\hat{P}_C = \hat{P}_B + \rho_{\mathrm{w}} g (L - \hat{H}_2). \tag{13.4}$$

Combining now (13.1), (13.3), (13.4) and

$$L = H_o + H_{\mathrm{w}} \tag{13.5}$$

we find that

$$\Delta p = \rho_{\mathrm{w}} g \hat{H} + (\rho_{\mathrm{w}} - \rho_o) g H_o \tag{13.6}$$

is the pressure drop due to the motion in up-flow.

In down-flow, where the pressure gradient and relative buoyancy are opposed, the difference in height of the manometer legs is proportional to Δp plus the hydrostatic contribution so that

$$\Delta p = \rho_{\mathrm{w}} g \hat{H} - (\rho_{\mathrm{w}} - \rho_o) g H_o. \tag{13.7}$$

We may have flow, due to relative buoyancy alone, for which $\hat{H} = 0$.

Formulas (13.6) and (13.7) require measured values of $\hat{H}$ and H_o. The height difference $\hat{H}$ is read directly but H_o depends on the volume of oil between the pressure taps in the pipe and it cannot be determined directly.

To determine H_o, we measure the volumes of oil and water between the pressure taps directly. This is done by means of two valves, called hold-up valves, which cut off the flow between the taps simultaneously. There is a third safety valve which opens at the same time that the hold-up valves are closed, releasing the high pressure in the system. After the hold-up valves are closed, the oil rises and the volumes of oil and water are read easily. Actually, the distance between the hold-up valves is 93 inches so that the measured heights must be reduced by 90/93. Since the diameter ($d = 3/8$ inches) of all pipes is the same, we may easily compute volumes by measuring heights. There are two sets of hold-up valves, one for up-flow and one for down-flow.

All the data taken in our experiments is recorded on our Kodak Spin Physics2000 Motion Analysis System or on a high resolution video camera. The only quantities that can be controlled after an experiment is in place are the flow rates of oil and water. One of these flow rates is fixed, and the other is varied. Then we wait for transients to decay. The slower flow rates have long transients. After steady conditions are established, video recordings are made. The high-speed recordings have the raw data for the analysis of the flow; they allow us to measure the distances, say between crests of waves, and their phase speed (celerity). We present average wave lengths and wave speeds, which are simple averages obtained by summing values and dividing by the number of trials.

To correlate the experimental observations with the linear theory of stability, we need to specify whether we are in up- or down-flow, the two flow rates and the water fraction in the pipe. The water fraction is a functional of the solution determined by the hold-up ratio in the manner described below.

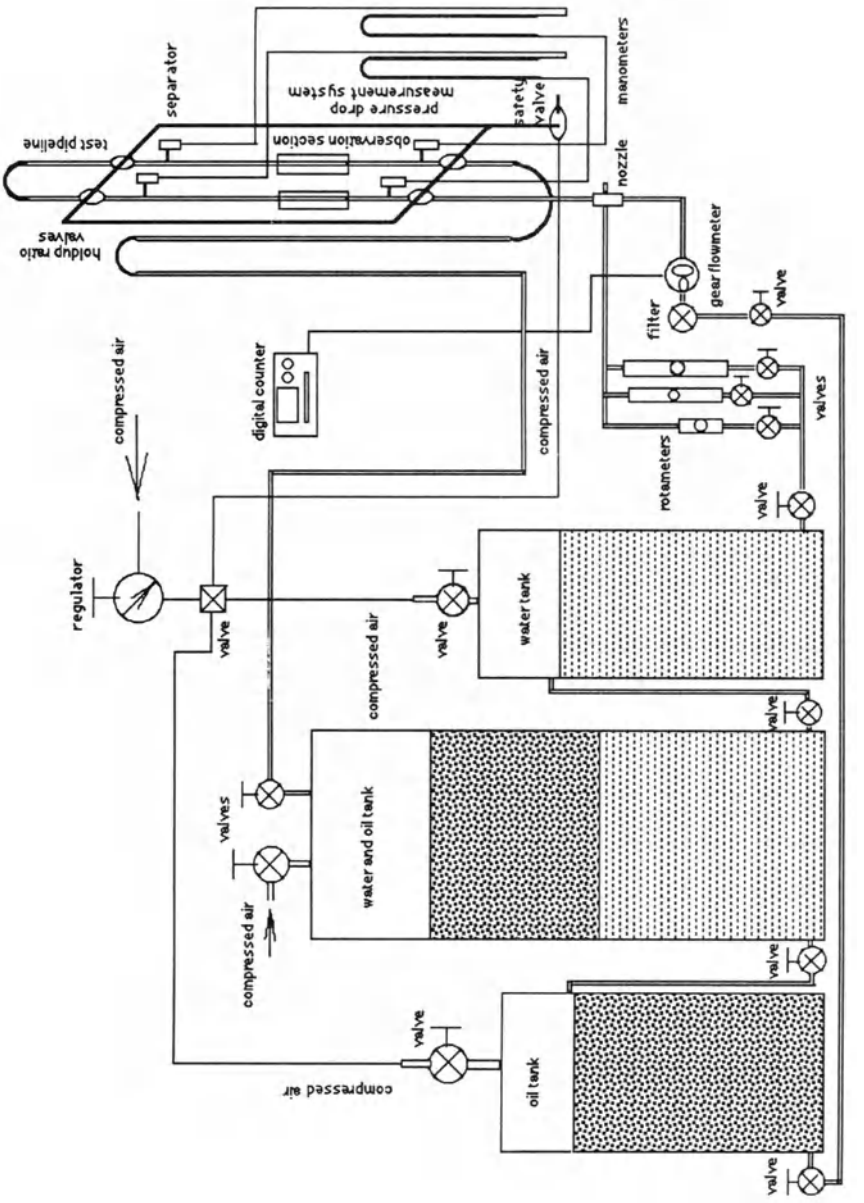

Fig. 13.1. [Bai, Chen and Joseph, 1992] The experimental system.

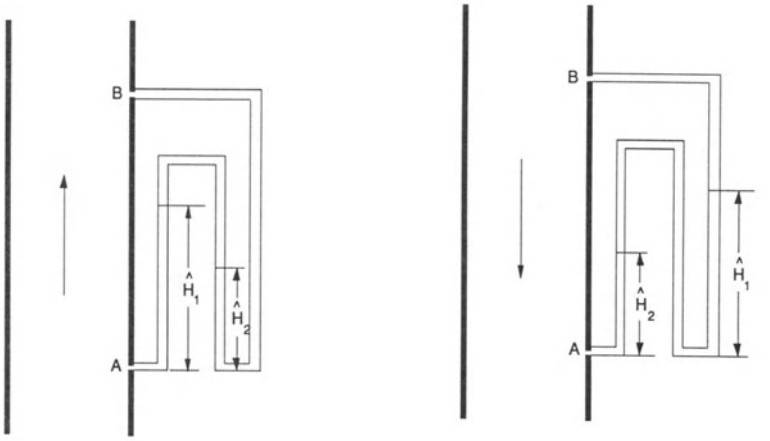

Fig. 13.2. [Bai, Chen and Joseph, 1992] Manometer tubes in up-flow (a) and down-flow (b). The distance from A to B is L and $\hat{H}_1 - \hat{H}_2 = \hat{H}$. In flows driven by buoyancy alone, without pressure gradients, $\hat{H} < 0$.

VII.14 Hold-Up Ratio

Conventional wisdom about hold-up ratios in lubricated pipelining needs to be amended for effects of buoyancy in vertical pipes. The *hold-up ratio* is the ratio of ratios (14.1), the ratio of volume flow rates to the ratio of volumes. These two ratios would be the same in a perfectly mixed flow, say a well-emulsified solution of water in oil. In the perfectly mixed flow, the hold-up ratio h is one. In general, and certainly in lubricated pipelining, the two fluids are not well-mixed, and the hold-up ratio differs from unity. The conventional wisdom is that the liquid in contact with the pipe wall tends to be held back. Thus the hold-up ratio will tend to be greater than unity when the water is the component in contact with the pipe wall and to be less than unity when oil is in contact with the pipe wall. This idea is not correct in vertical flow where the effects of buoyancy are important. Gravity makes the water flow faster than the oil in down-flow.

Because the up- and down-flow legs of our $\cap$ loop apparatus are connected, the pressure drop is established over the whole pipe with a continuous loss of pressure due to friction. The reader may be helped by thinking that to a first approximation, the pressure gradient is a constant, the same constant in the up- and down-legs of the $\cap$ apparatus. Gravity aids the

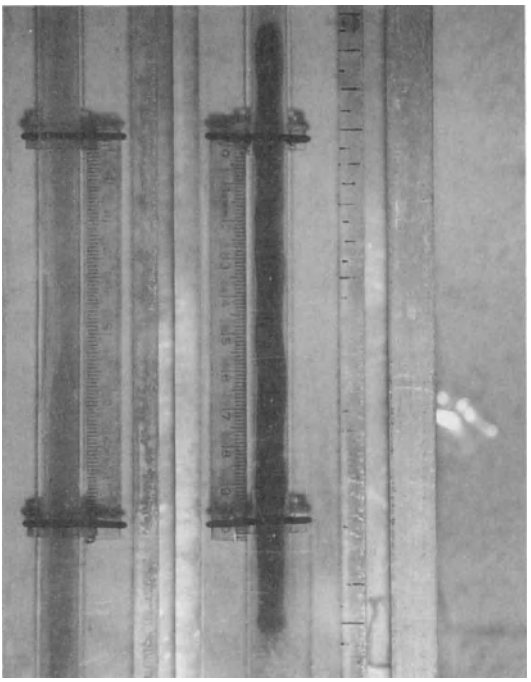

Fig. 14.1. [Bai, Chen and Joseph, 1992] Long oil slug suspended by gravity in down-flow of water when the water flow rate is about 0.04 ft./sec. The slug is fluidized, in equilibrium under weight and drag. The hold-up ratio is zero. Transient traveling spiral waves, called corkscrews, can be seen on different segments of the core. It is easy to fluidize much longer slugs, even to have a continuous core of oil fill the entire down-flow pipe.

applied pressure gradient in accelerating the oil relative to water in the up-flow and decelerating the oil relative to the water in the down-flow legs of the apparatus. This means that more oil accumulates in down-flow than in up flow. The water fraction is greater in up-flow than in down-flow. This implies that the $a-1=(R_2-R_1)/R_1$ is smaller in down-flow and that the hold-up ratio

$$h=(Q_o/Q_{\rm w})/(\Omega_o/\Omega_{\rm w})=(V_o/V_{\rm w})/(H_o/H_{\rm w}) \tag{14.1}$$

is smaller in down-flow where the oil volume $\Omega_o=\pi R_2^2 H_o$ is larger.

The value $h=0$ of the hold-up ratio can never be achieved in up flow or horizontal flow, but it can be realized in down-flow. We get $h=0$ when there is already oil in the pipe, ($\Omega_o\neq 0$) but no new oil supply is forthcoming ($Q_o=0$). An experimental realization of this in down-flow is shown in figure 14.1 where a long slug of oil with aspect ratio in excess of 20 is exhibited. This slug is perfectly lubricated by water. Basically,

we can say that the slug is fluidized: it is lifted by gravity against the oncoming downward flow of water, suspended in the lubricating stream in an equilibrium of weight and drag. It is possible to suspend truly large slugs with aspect ratios greater than 100 in this way.

The volume ratio $\Omega_o/\Omega_w = H_o/H_w$ is per unit length of pipe, and is hence equal to the area ratio A_o/A_w of oil to water in a perfect core-annular flow. This ratio may be expressed in terms of the radius ratio $a = R_2/R_1$ by the formula $a^2 - 1 = A_w/A_o$. After replacing Ω_w/Ω_o with $a^2 - 1$ in (14.1), we get

$$a = \sqrt{1 + hQ_w/Q_o} = \sqrt{1 + hV_w/V_o} \tag{14.2}$$

This formula is relevant to experiments which show that h is constant in up-flow and fast flows.

In figure 14.2 we present the volume ratio $\Omega_o/\Omega = H_o/L$, $L = H_o + H_w$, where $\Omega = \Omega_o + \Omega_w = \pi R_2^2(H_o + H_w)$ is the total volume, against the input flow ratio $Q_o/Q_w = V_o/V_w$. We can fit the data for up-flow to the empirical curve

$$\frac{H_o}{L} = 1 - \frac{1}{(1 + 0.72V_o/V_w)}. \tag{14.3}$$

Hence $H_w/\Omega = 1/(1 + 0.72V_o/V_w)$ and

$$h = \frac{Q_o}{Q_w}\frac{\Omega_w}{\Omega_o} = \frac{V_o}{V_w}\frac{H_w}{H_o} = 1/0.72. \tag{14.4}$$

This shows that h is constant in up-flow of cylinder oil in water and is independent of any input ratio or flow condition.

Figure 14.3 is for down-flow. The data points are more scattered in down- than in up-flow, especially for moderate input ratios. The empirical formula (14.3) which works for up-flow does not work as well in down-flow. The difference between up-flow and down-flow is more clearly expressed in figure 14.4.

One major conclusion implied by the data shown in figures 14.2 and 14.4 is that the hold-up ratio h in *up-flow* does not depend on the flow rates of oil and water, nor on the ratio of flow rates. The hold-up ratio in *down-flow* depends strongly on these parameters, as is shown in figures 14.3 and 14.4. These figures show that when the flow rates are large, the effect of gravity is suppressed, as the up- and down-flows can be treated equivalently. Hence, in fast flows, the hold-up ratios are the same and equal to approximately 1.39 in both up- and down-flows. This result agrees with conventional wisdom (the water is being held up), but disagrees with results of Charles, Govier and Hodgson [1961] who found that in horizontal pipes, when the densities of oil and water are matched, the hold-up ratio does depend on the input ratio and flow velocity, even at large flow rates.

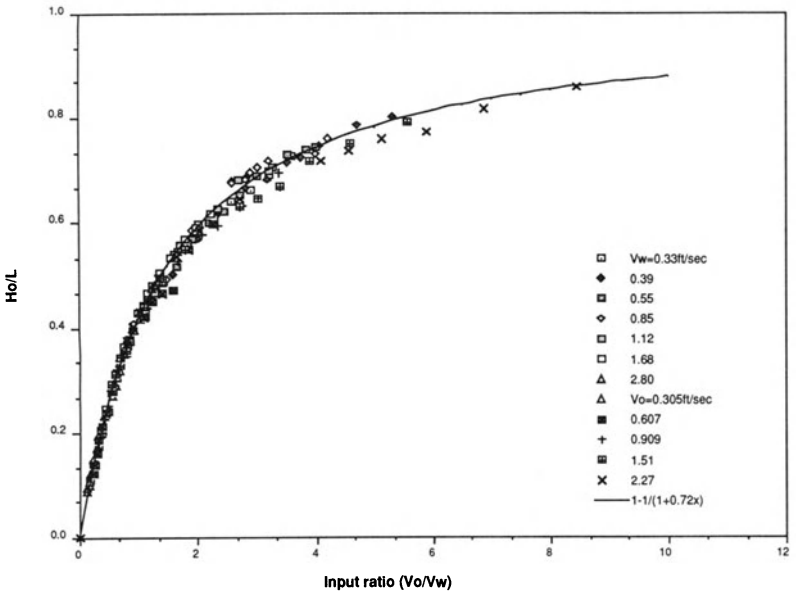

Fig. 14.2. [Bai, Chen and Joseph, 1992] The volume ratio $\Omega_o/\Omega = H_o/L$ versus the input ratio V_o/V_w for up-flow . The data falls close to the solid line given by (14.3). The data points are given by the superficial velocity of water V_w in ft/sec.

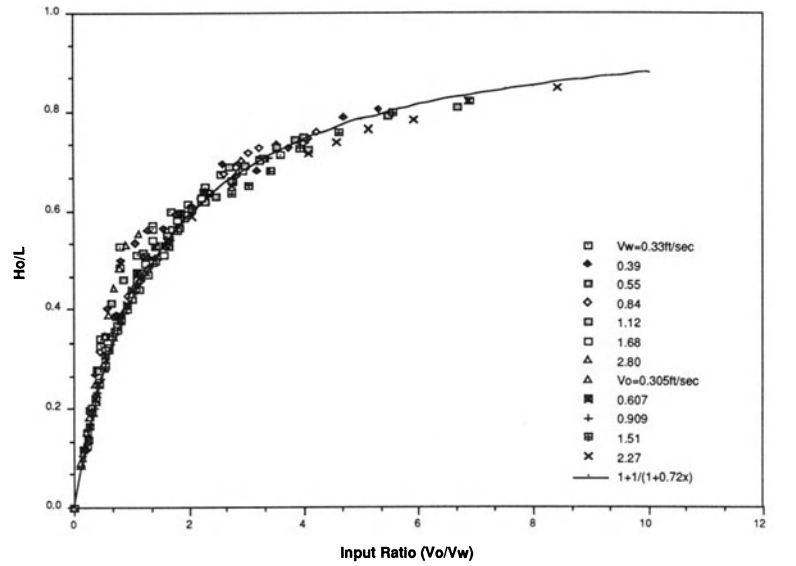

Fig. 14.3. [Bai, Chen and Joseph, 1992] The volume ratio versus input ratio for down-flow. The formula (14.3) is plotted. The data points are designated as in figure 14.2.

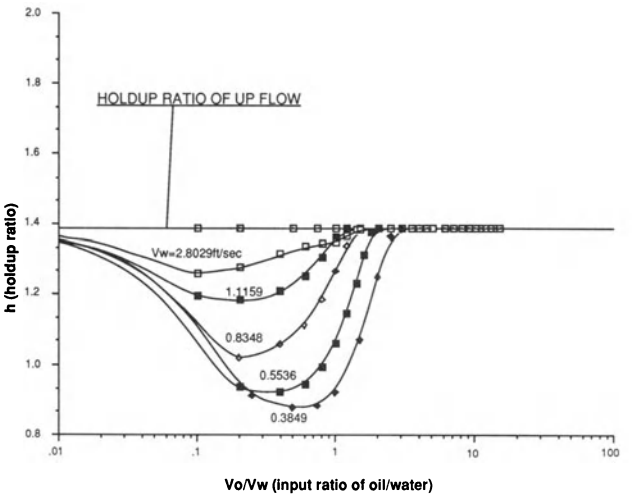

Fig. 14.4. [Bai, Chen and Joseph, 1992] Hold-up ratio in down-flow as a function of V_o/V_w with V_w as a parameter.

VII.15 Flow Types

Several qualitatively different regimes of flow can be distinguished in our experiments. There is some subjectivity involved in the delineation of differences which might be labeled qualitative or merely quantitative, so that the exact number of qualitatively different regimes may differ slightly from observer to observer. The flow regimes which appear in horizontal pipes under conditions of matched density have been already identified in the paper by CGH (figure V.1.1) who studied concurrent flow of water and oil-carbon tetrachloride solution in a 1.04 inch diameter pipe. Some of the different regimes observed by them have been studied in chapter VI. Many of these regimes, and some new ones, for example, bamboo waves, appear in vertical flow. We were not able to study the regime in which water emulsifies into the oil, called 'water droplets' by CGH, because our apparatus is not strong enough to withstand the high pressure gradients generated in this condition.

(a) 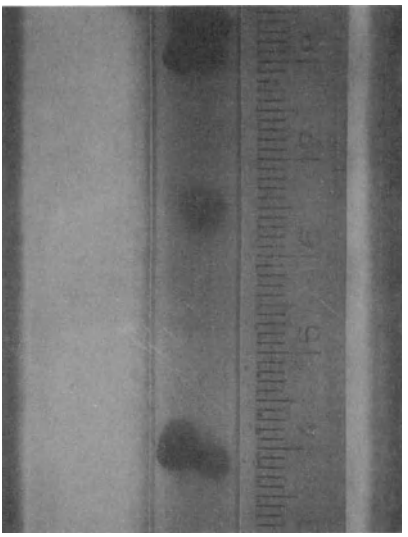 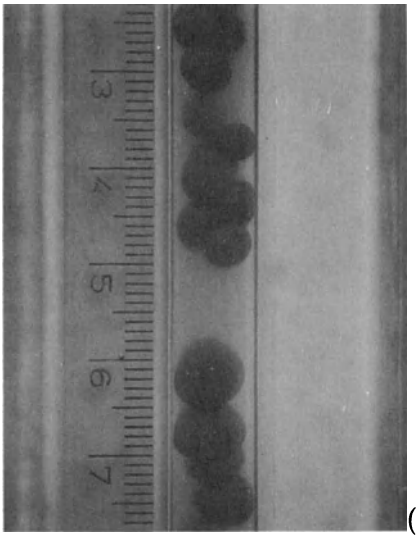 (b)

Fig. 15.1(a-b). [Bai, Chen and Joseph, 1992] Oil bubbles in water. (a) Up-flow. The bubbles do not aggregate. Wake forces are weak. (b) Down-flow. Bubbles aggregate in bubble-trains held together by wake forces.

In this section, we shall give a qualitative description of the types of flow we encounter, together with illustrative photographs and a discussion of some underlying physical mechanisms associated with them. In the next section, the regimes are depicted as regions on a flow chart, whose coordinates may be chosen as the superficial velocities of oil and water.

(i) Oil bubbles in water. These bubbles arise from capillary instabilities in the presence of shear. Oil bubbles in water are produced by capillarity but the size of the bubbles is determined by other factors, like shear, as well. The range of sizes of the bubbles which are observed is fairly well predicted by the linear theory of stability using Rayleigh's idea (cf. §1.5, Drazin and Reid [1982]) that the mode that would be observed is the one with the maximum growth rate. In our situation, this means that the size of the bubble which would be observed corresponds to one-half of the wavelength of the mode with the maximum growth rate. Rayleigh's idea originated in his work on the stability of an incompressible inviscid jet in air with surface tension at the free surface. In contrast, the presence of shear in our problem has a strong influence on the length of maximum growth. A comparison of calculations from the linear theory of stability with the size of bubbles observed in the experiments of CGH is shown in table 1.1 of chapter VI and shows agreement.

(a) 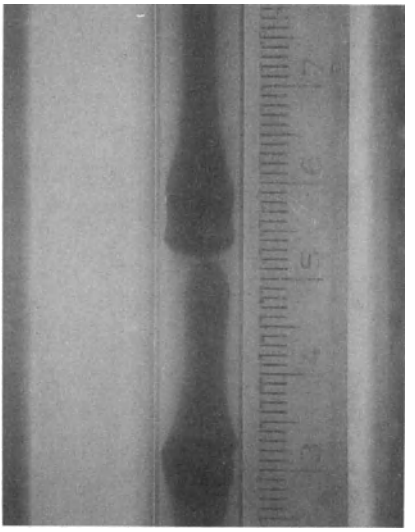 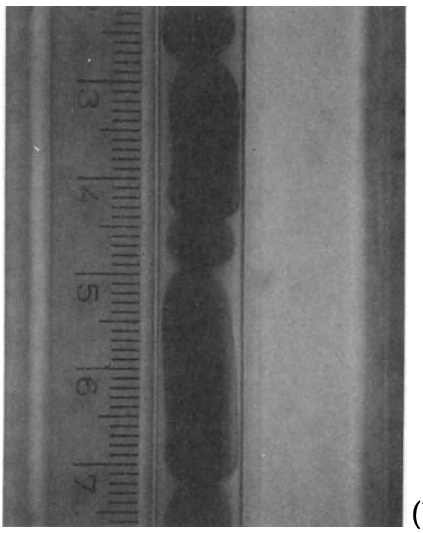 (b)

Fig. 15.2(a-b). [Bai, Chen and Joseph, 1992] Oil slugs in water. (a) Up-flow. The larger bubbles are stretched out under the action of shear and buoyancy. This is shear-stabilization of slugs and bubbles leading to long bamboo waves. (b) Down-flow. The oil is held up by buoyancy and slugs held together by wakes forming long trains.

As a rule of thumb, we can say that we will always have oil bubbles in water if there is a large amount of water. Dispersions of oil in water, rather than bubbles, appear when the water velocity is much larger than the oil velocity. Dispersions will be discussed under (vii) below.

There is a marked difference in the distribution of bubbles in up-flow and in down-flow, even when they are of approximately the same size. In up-flow, the bubbles tend to spread and distribute themselves uniformly in the pipe. The wake interactions are weak because the velocity of the oil relative to the water is small. The oil is lifted by gravity relative to a forced stream of water moving in the same direction. Bubbles in down-flow tend to aggregate. Wake forces between bubbles in down-flow are much greater than in up flow because the bubbles are lifted against the forced stream of water, producing larger relative velocities and stronger wakes.

The tendency of bubbles to disperse in up-flow and to aggregate in down-flow is evident in the photograph shown in figure 15.1.

(ii) Slugs of oil in water. Suppose we use Rayleigh's idea mentioned in (i) above and determine a natural diameter for an oil bubble in water. If this diameter is larger than the pipe diameter, it will not fit in the pipe. One

way to get the entire volume into the pipe is to squash it into a capsule shape. These capsule shapes are dynamically possible because they are shear-stabilized by water. They move through the pipe freely lubricated on all sides by water in a manner reminiscent of capsule transport in pneumatic tubes.

Slugs form readily from bubble aggregates in down-flow when the oil fraction is increased. The bubble aggregates collapse to form longer slugs which have a relatively large diameter lubricated by a thin layer of water. Long slugs are like segments of PCAF, but they support corkscrew waves. Corkscrew waves look like a periodically buckled wimpy rod which rotates in the water due to hydrodynamic torques. Corkscrew waves on a long shear stabilized slug are shown in figure 14.1 and many of them can be seen in the down-flow side on the right hand sides of the photographs of section VII.20, say figure 20.5.

It seems to be impossible to create capsule slugs and corkscrew waves in up-flow. In up-flow bubbles do not aggregate to form slugs as the oil input is increased. Instead, filaments are pulled out and the bubbles are stretched, as shown in the photograph of figure 15.2, under the combined action of buoyancy and lubrication forces described in the caption of figure 15.5. This filamentation gives rise to the bamboo waves which are described next.

(iii) Bamboo waves (BW). The shear-stabilization of capillary instabilities in up-flow leads to a regime of wavy flow in trains of sharp crests connected by long filaments. We call these bamboo waves. Superficially, they resemble Stokes waves except that they perturb a cylinder. They appear to be axisymmetric but there may be slight imperfections, such as that the crests may not be exactly axisymmetric. Many photographs of bamboo waves under different conditions are shown in section VII.20. The filaments which connect the crests thicken as the oil velocity V_o is increased for a fixed V_w and the average length of a wave decreases. These effects are evident in the photographs exhibited in figure 15.3 and are documented in the graphs of data assembled in figure 15.4. These waves are nearly stationary in a coordinate system moving with the undisturbed interface velocity so that the wave speed relative to laboratory coordinates also increases with increasing oil input.

Bamboo waves are a very robust regime of up-flow, occupying a large area in the up-flow charts shown in figures 16.1 - 16.4. They seem to maintain well-defined average wave lengths and wave speeds, but they are not perfectly periodic. The overtaking of one crest by another and the transient stretching of filaments between the waves is a frequent occurrence.

The stability analysis of Renardy [1987b] for vertical plane Poiseuille flow has shown that a varicose instability arises in up-flow and a snake instability (analogous perhaps to corkscrew waves) arises in down-flow. Something like a varicose instability might give rise to bamboo waves. A heuristic reasoning for the shape of the bamboo waves in up-flow is that they are

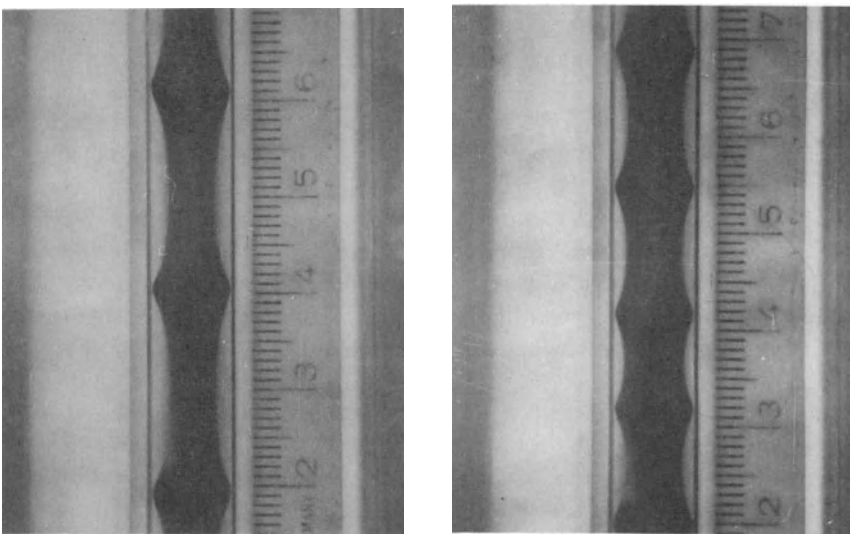

Fig. 15.3. [Bai, Chen and Joseph, 1992] Thin and thick bamboo waves. The bamboo thickens and the average length of a wave decreases when the oil velocity increases at a fixed value of the water velocity. Some very short bamboo waves associated with high input velocities are shown in figure 15.6.

stretched due to the combined action of buoyancy and lubrication forces. The buoyancy part of this mechanism is simply that the oil is lifted by gravity relative to the heavy water which in any event is stationary on the pipe wall. The crest of a wave on the oil must move forward relative to the water. We noted already that the wave is nearly stationary, convected with the oil, unable to move fast on the oil core because the oil is so viscous. This means that there will be a positive build-up of pressure on the up side and a decrease of pressure on the down side of every crest in up-flow, as shown in figure 15.5 The pressure associated with this lubrication effect will push the water from plus to minus and this will induce stretching in the same sense as buoyancy, elongating the wave, stretching the stems. On the other hand, the effects of buoyancy and lubrication are opposed in down flow. This tends to compress, even to eliminate, bamboo waves and may lead to the form of buckling which we have called corkscrew.

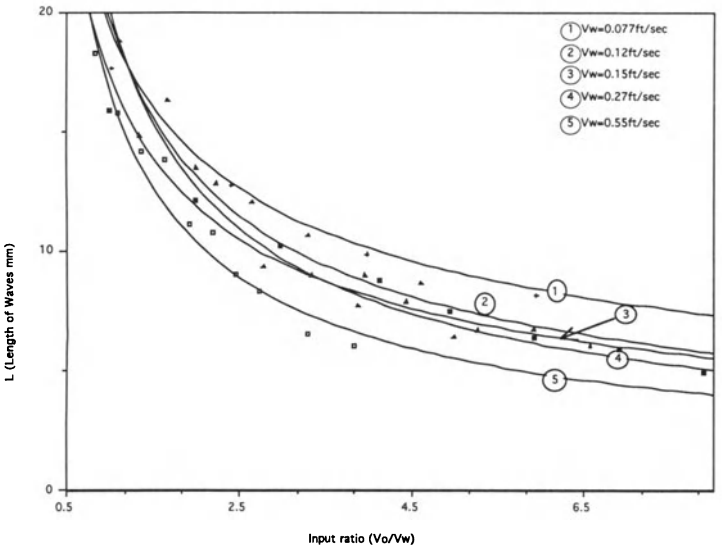

Fig. 15.4. [Bai, Chen and Joseph, 1992] The average length of a bamboo wave decreases monotonically as the oil input is increased for fixed flow rate of water.

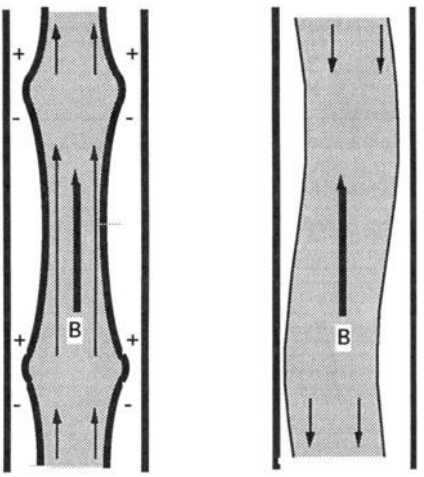

Fig. 15.5(a-b). [Bai, Chen and Joseph, 1992] Lubrication forces arise from bamboo waves which in the first approximation are connected with the oil relative to stationary walls. The pressures which develop in the water in the front and back of crests are designated by (+−) and buoyancy of oil relative to water is designated by B. The pressure forces and buoyancy work together in up-flow (a) where they lead to stretching and are opposed in down-flow (b) where they lead to compression and buckling.

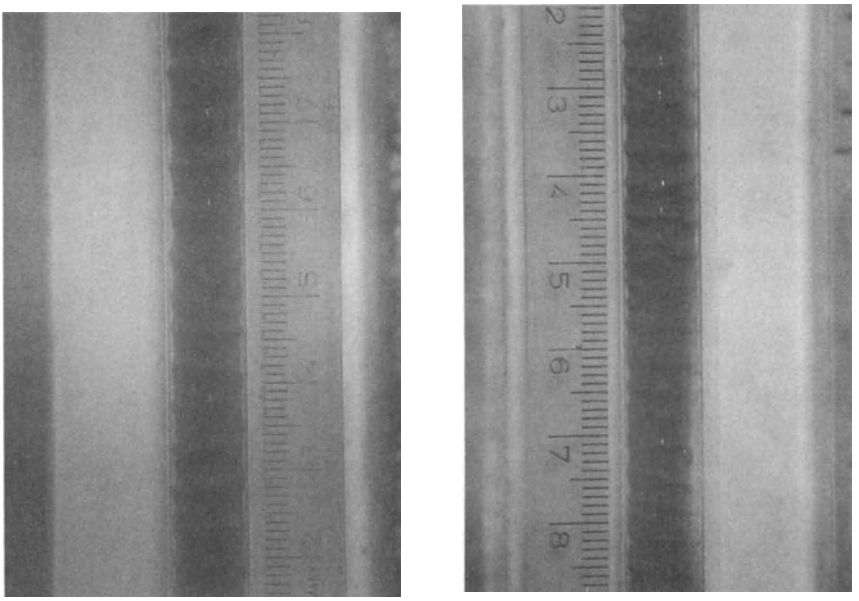

Fig. 15.6(a-b). [Bai, Chen and Joseph, 1992] Disturbed bamboo waves. When the pressure gradient is much larger than buoyancy, the difference between up-flow (a) and down-flow (b) is suppressed. One sees short, thick-stemmed waves. The effect of stretching in up-flow and compression in down-flow is still active in producing longer waves in up-flow.

(iv) Disturbed bamboo waves (DBW). We have already mentioned that when the driving pressure gradients are relatively large and the flow is fast, the difference between up- and down-flow vanishes. In particular, the asymmetric effect of buoyancy on the hold-up ratio is relatively less important when the pressure gradient is large. This can be seen in the disturbed up- and down-flow bamboo waves shown in figure 15.6. Some effect of buoyancy on the wave length is still in evidence, with stretched waves in up-flow and compressed ones in down-flow. At a lower speed, the up-flow waves would elongate and the bamboo stems would thin, while in down-flow the stems thicken into columns of oil which support perfect core-annular flow which is perturbed by corkscrew waves from place to place. At a faster speed, the oil core cannot keep its integrity and various kinds of dispersions of oil in water and water in oil will form.

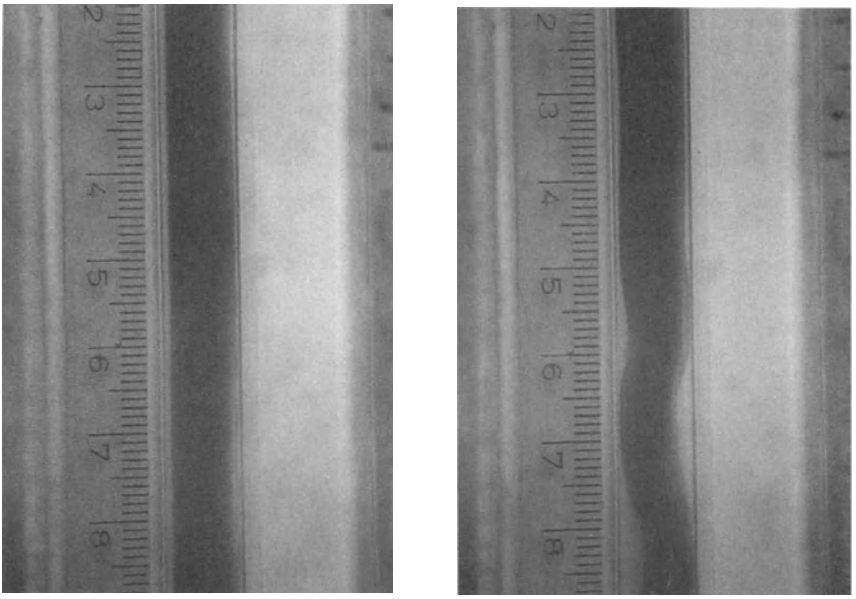

(a) (b)

Fig. 15.7(a-b). [Bai, Chen and Joseph, 1992] Disturbed core annular flow (DCAF). Some portions of the oil column in down-flow are nearly perfect (a) while others are buckled and rotate as a corkscrew (b).

(v) Disturbed core-annular flow (DCAF) and corkscrew waves. In PCAF, the core has a perfectly cylindrical interface of uniform radius which is perfectly centered on the pipe axis with an annulus of lubricating water outside. See earlier sections of this chapter for photographs. Figure 15.7 shows PCAF disturbed by transient spiral waves which we call corkscrew. This is reminiscent of the snake instability found in down-flow of vertical plane Poiseuille flow [Renardy 1987b]. We call this regime of flow disturbed core-annular flow (DCAF). Actually, the motion of a corkscrew as it is screwed forward in the cork is an accurate description of the waves we see. These waves are not understood by us but they are perhaps associated with the buckling of a very soft rubber when loaded with shear tractions, which in our experiments are generated by the motion of water in the annulus. The apparent velocity of advance of the turning corkscrew is larger than the superficial velocity of oil or water. When the water flow rate is fixed in the small-to-moderate range where corkscrew waves appear, the pitch of the screw will increase with increasing rates of flow of oil leading to an apparent slowing of the wave. In this way, one can obtain a nearly perfect core annular flow.

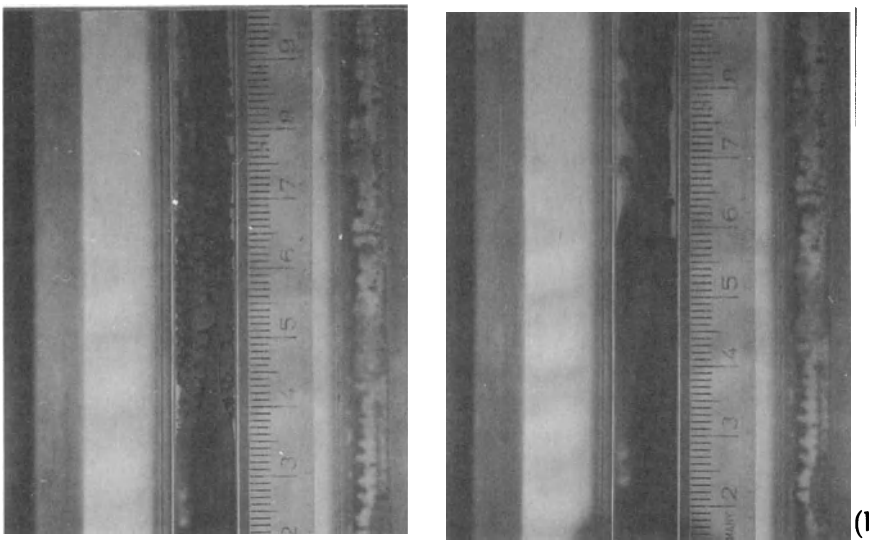

(a) (b)

Fig. 15.8(a-b). [Bai, Chen and Joseph, 1992] Deposition of oil on the wall. Oil seizes the hydrophilic glass wall when the oil flow rate is increased at a small fixed water flow rate (see 'oil sticks to the wall' on the flow charts in section VII.16). After the oil seizes the wall, the pipe is blocked and the blockage is relieved by an 'oil-core water-annulus oil-sheath' configuration. (a) A bubble cloud around an internal core. (b) A clearer picture of the ejected core.

(vi) Oil sticks to the wall. The glass wall of the pipe is wet preferentially by water. However, when the water flow rate is small and the oil flow rate is large, oil can displace the water on the wall of the pipe. This usually happens first in the up-flow leg of the loop. At still higher values of the oil flow rate, water will disperse or emulsify into oil. This dispersion is discussed under (vii) below.

The deposition of oil on the pipe wall can sometimes be observed as a slow propagation of the wetting front with oil on the wall behind the front and water on the wall before the front. We call this phenomenon *chugging*. Two chugging configurations in up-flow are exhibited in figure 15.8. To achieve chugging, we increase the oil flow rate, keeping the water rate constant. In (a) and (b), an oil core plus oil bubbles are ejected from the sheath of oil on the wall. Evidently, there is an annulus of water between the sheath and the core. There is a blockage when the oil seizes the wall which is relieved by an 'oil-core water-annulus oil-sheath' configuration. Shearing forces tear away many oil bubbles which form a cloud around an oil core in (a), more clearly seen in (b). If the oil flow rate is increased

(a) 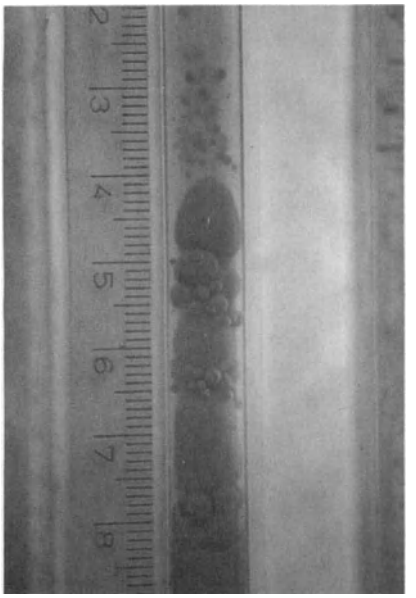 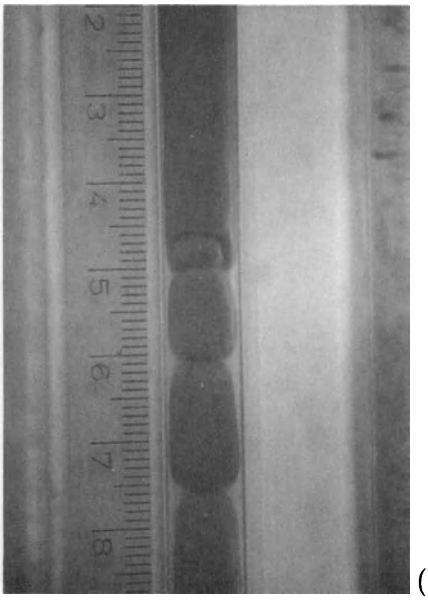 (b)

Fig. 15.9(a-b). [Bai, Chen and Joseph, 1992] (a) Removal of oil from the hydrophilic wall in down-flow. Look at the bottom of the photograph. Oil is being removed from the wall. Slugs and bubbles are entering the oil sheath where they are lubricated by water. (b) Oil is deposited on the wall in down-flow. Slugs and bubbles are ejected from the sheath.

further, more oil bubbles than in (a) will be formed followed by a phase inversion in which water droplets emulsify and oil becomes the continuous phase. This leads to a loss of the lubricated arrangement of the fluids and to huge increases in the pressure gradient.

The fact that oil replaces water on a hydrophilic wall under certain repeatable dynamical conditions is of wide interest because the complete solution of the problem of wetting and spreading [Dussan V. 1979] cannot be solved by thermodynamic and generalized energy considerations; it is not only a problem of finding good constitutive models. The answer to the question "When two fluids flow, which one will be on the wall?" depends on the history of the motion as well as the properties and interactions of the two fluids and the wall.

In figure 15.9, we see that oil may be deposited or removed from the hydrophilic glass pipe. In figure 15.10, the oil is deposited on one part of the glass wall, and water on the other. This is reminiscent of figure II.5.3, where it is shown that oil can stick on the plexiglass wall of a Taylor apparatus at the downflow cell boundary of a Taylor cell of an emulsified oil, but not elsewhere. This 'painted' configuration remains 'forever' even after the motion is put to rest. People who actually work for a living know they have

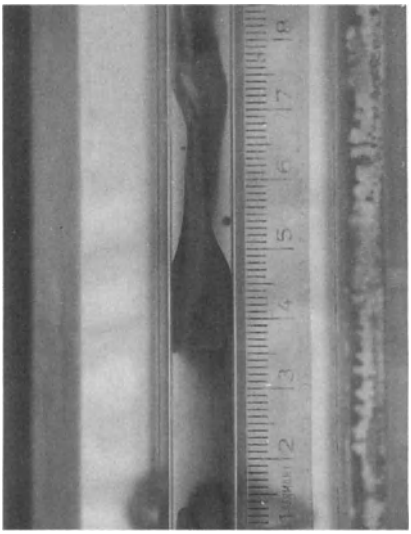

Fig. 15.10. [Bai, Chen and Joseph, 1992] Some oil sticks on the wall, water flowing through. In a static tube filled with water one can see stationary slugs of oil clinging to the wall which do not move even though they are buoyed up.

to wash their hands to get them clean.

CGH got water lubrication for three different oils (6.29, 16.8 and 65.0 centipoise) in a 1.04″ cellulose acetate-butyrate pipe which is *hydrophobic*. This shows that water lubrication is mainly a dynamical effect, with a secondary role played by wettability. To more fully understand this, we need to consider the problem of *phase inversion* which is considered in the next subsection.

Hasson, Mann and Nir [1970] studied core flow of water in a heavier (density 1.02 g/cm^3) organic liquid (kerosene-perchlorthylene solution). They were not aware that their flow is unstable because the organic solution has a higher viscosity. Their pipe was made of glass, preferentially wet by water, and they studied film rupture. They say that

"The mechanism whereby the preferentially wall-wetting core liquid causes film rupture is not sufficiently clear. Accidental wetting of the glass wall by water is apparently insufficient in itself to disintegrate the organic film. The observed reproducibility in the break-up location (Figure 8) in spite of the wavy interface and the occasional water drops adhering to the pipe wall, suggests that the criterion governing the occurrence of film rupture must also involve a film momentum resisting break-up. It may be of significance that break-up film-thicknesses measured from enlarged

photographs for the data plotted in Figure 8, were all roughly equal. The mean value of the break-up thickness was 500 micron, with a random scatter in the range of 300 to 700 micron while the interfacial velocities in the vicinity of the break-up point were of the order of 20 cm/sec."

(vii) Dispersions, Phase inversion. There is evidently a *dispersion* limit in which large bubbles, slugs, sheets, and other coherent bodies of a single fluid are broken up by forces associated with the motion. A dispersion of immiscible liquids, one of which is polar, the other non-polar, is often called an *oil and water dispersion* or *emulsion.* An emulsion is a stable dispersion, but stability here is defined in a time frame so that a dispersion over a long time can be considered an emulsion over a short time. There are water in oil (w/o) dispersions and oil in water dispersions (o/w). There are conditions under which an o/w dispersion will change to w/o dispersion. This is called a *phase inversion.* It is also possible for o/w and w/o dispersions to coexist. The formation of dispersions, their properties, and phase inversion may be studied in different systems; for example, see section II.5 for dispersions in a Taylor-Couette apparatus.

Dispersions will always form in motions of two immiscible liquids which are sufficiently intense. CGH gave data for them; w/o dispersions were called 'water drops in oil' and o/w dispersions were called 'oil drops in water.'

This distinction between small bubbles of oil in water and o/w dispersions can be fuzzy. In section VI.1, the size of a small bubble which would arise in the experiment of CGH on 'oil drops in water' was computed and found to be 4/3 the size of the largest oil bubble in the dispersion. The other bubbles in the dispersion were much smaller. Perhaps the study of the size of single drops and bubbles in different flows is fundamental in distinguishing between bubbles and dispersions.

The o/w dispersions are a lubricated regime of flow, which is of practical interest since they burn with reduced nitrous oxide (NOx) and particulate emissions (and is better for the environment) than the oil would on its own.

Water in oil dispersions have a higher viscosity than oil alone; the resulting pressure gradients are greater than the apparatus could withstand. The w/o dispersions have higher oil flow rates than the one in which oil seizes the wall. If we tried to increase the flow of oil in a case like figure 15.1 (a), the pressure gradient would shoot up, and if we could run the apparatus at the high pressure, a phase inversion to a w/o dispersion would likely result. The w/o dispersions, and similarly phase inversion from o/w dispersions, are undesirable for industrial pipelining.

CGH gave flow charts for oils of viscosities 6.29, 16.8 and 65 cp, and identified a phase inversion boundary in the region of dispersions. This boundary does not seem to depend strongly on the viscosity or interfacial tension, but the water fraction is important. They observed w/o dispersions

for water fractions ranging from 10 to 67% at sufficiently high oil velocities. The importance of the water fraction is also mentioned in laboratory and field tests of Charles [1963], who reports that:

"Very substantial reductions in pressure gradient are again evident. For water contents up to about 20 per cent the pressure gradient was affected very little by the addition of the water and these conditions probably correspond to the water-in-oil emulsion flow pattern. At a water content of approximately 20 per cent a sudden decrease in pressure gradient was observed which was probably coincident with the transition of the flow pattern to stratified flow. For water contents greater than 40 per cent the pressure gradient was reduced by factors in excess of 10. The results obtained with the field pipeline indicated that optimum reduction of pressure gradients was obtained when the water was added to the extent of 30 to 50 per cent of the total liquid flow."

Topological considerations, like the packing fractions of monodisperse (bubbles of uniform size) and polydisperse (bubbles of different sizes) spheres, are of importance in emulsion rheology and are probably important for the problem of the phase inversion of dispersions in lubricated pipelining. The rhomboidal packing point for monosized spheres is the closest possible packing of spheres and the volume fraction of the spheres in this packing is 74.08%. Imagine that we have a dispersion of monosized spheres of oil; for example, many spheres of oil are shown in figure 15.8(a), but they are polydisperse. A monodisperse dispersion of such oil spheres could not exist if the water fraction were less than 25.92% because there would be no room for the oil spheres. Either we get polydisperse oil spheres, sphere distortions which are energetically unstable, or phase inversions.

VII.16 Flow Charts

A flow chart is a graph in the $(V_w,\ V_o)$ plane in which regions of different flow types are designated. The hold-up ratio h for each $(V_w,\ V_o)$ point may be obtained from figure 14.4 and the corresponding value of the water fraction given by $a = R_2/R_1$ from (14.4). The determination of a for a given $(V_w,\ V_o)$ is simplified by the fact that $h = 1.38$ universally in up-flow and for fast down-flows.

Figure 16.1 is a chart showing the types of up-flow of oil and water (0.4% aqueous sodium silicate solution). The flow condition is identified by points in the $(V_w,\ V_o)$ plane, where $V_w = Q_w/A$ is the superficial velocity of the water and V_o is the superficial velocity of the oil.

Figure 16.2 is a flow chart for up-flow using the same oil with pure water in a freshly cleaned pipe.

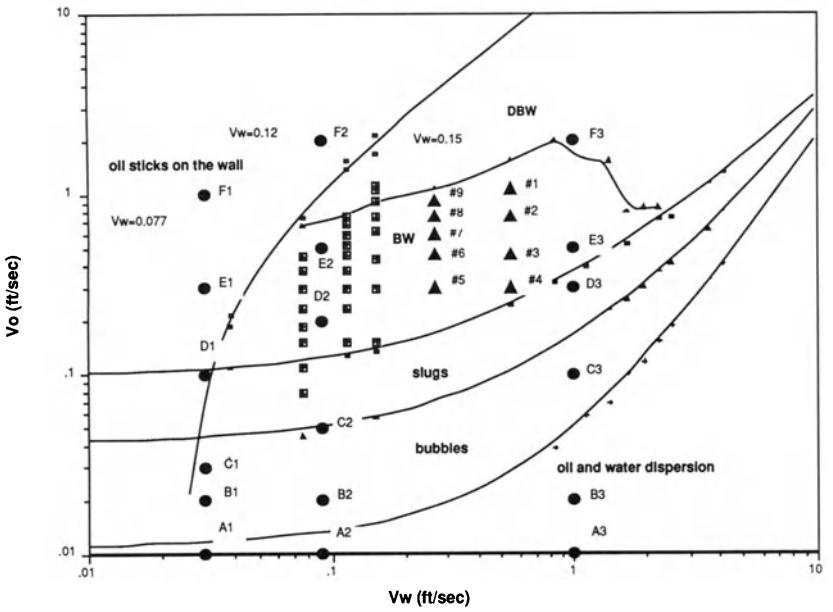

Fig. 16.1. [Bai, Chen and Joseph, 1992] This flow chart shows the types of flow that arise in up-flow as a function of the superficial water (with sodium silicate) velocity $V_w = Q_w/A$ and oil velocity $V_o = Q_o/A$. The hold-up ratio is universally $h = 1.38$ (see figure 14.4) and the value of $a = R_2/R_1$ can be obtained from (14.2) for each and every point. The labeled circles and triangles are identified for comparison with the theory in section VII.19.

Figure 16.3 is a flow chart for down-flow under the conditions specified in figure 16.1. Figure 16.4 is the down-flow chart using fresh water in a freshly cleaned pipe.

The figures may be compared with the flow charts of CGH. The flow types are not the same; they did not have bamboo waves or disturbed core-annular flow with corkscrew waves and we could not achieve the pressure gradients necessary for emulsification of water into oil. Nevertheless, the interested reader will find the way to identify similar regimes. There is a regularity in the pattern with which flow types fall on the flow charts.

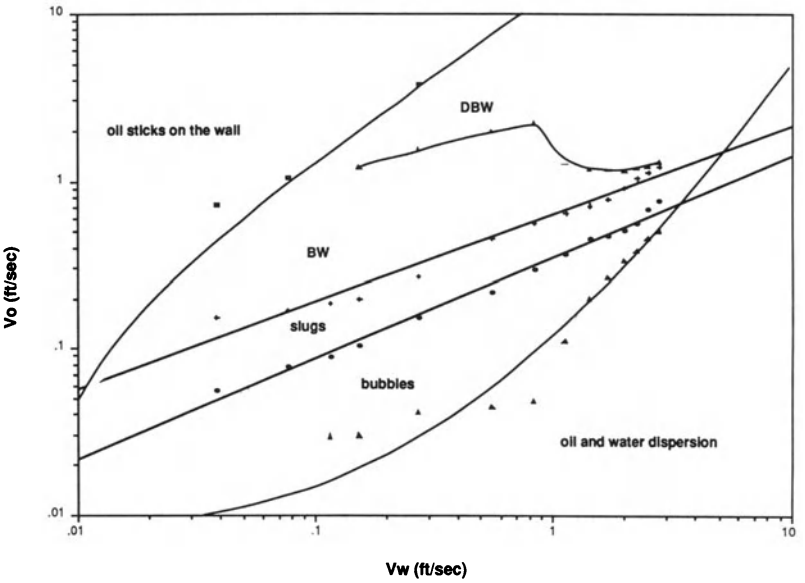

Fig. 16.2. [Bai, Chen and Joseph, 1992] Flow chart in up-flow as in figure 16.1 except that fresh water is used in a freshly cleaned pipe. There is a small upward shift probably due to a decrease in the water fraction, $h = 1.38$ for this flow.

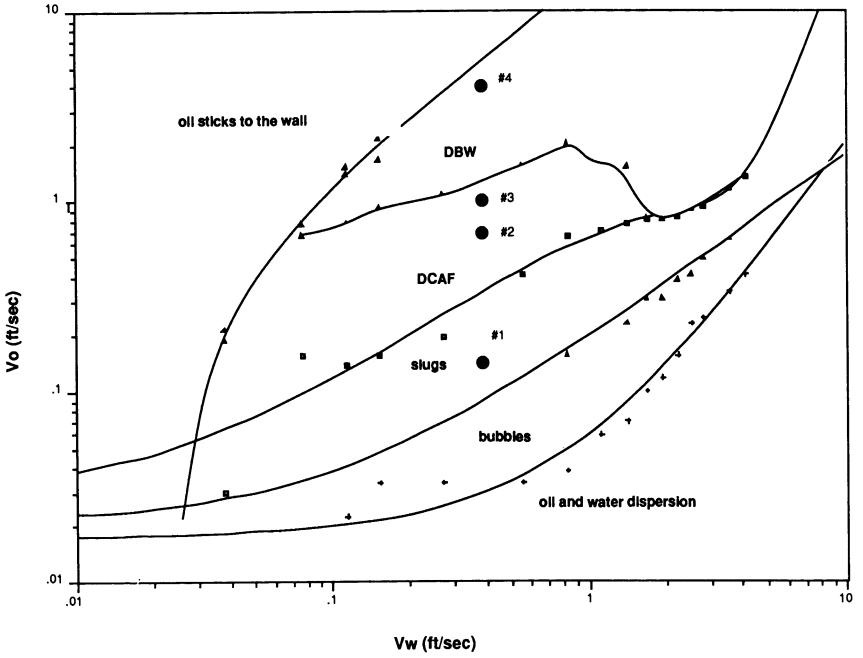

Fig. 16.3. [Bai, Chen and Joseph, 1992] This flow chart shows the types of flows that occur in down-flow as a function of the superficial velocities. The value of $a = R_2/R_1$ can be determined from (14.2) when the hold-up ratio h is found experimentally as in figure 14.4. The disturbance in disturbed core-annular flow (DCAF) are corkscrew waves near the slugs boundary and immature bamboo waves near the DBW boundary. The four circles are for reference to the linear theory of stability discussed in section VII.19.

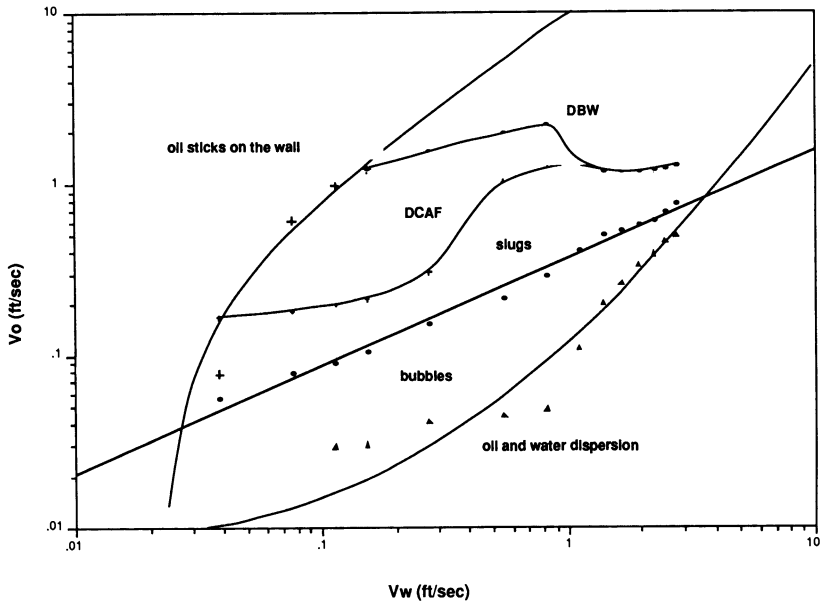

Fig. 16.4. [Bai, Chen and Joseph, 1992] Flow chart for down-flow using fresh water in a newly cleaned pipe.

VII.17 Pressure Drop Measurements

Data on pressure drops and hold-up ratios were obtained for different flow rates of oil and water. We are expressing the flow rates Q_w, Q_o in terms of superficial velocities $(V_w, V_o) = (Q_w, Q_o)/A$ in ft/sec where $A = \pi d^2/4$ and $d = 3/8$ inch. Data were taken for six values of V_w = .329, .385, .554, .834, 1.116, 1.678, 2.803 and five values of V_o = .305, .607, .909, 1.513 and 2.269. We fix V_w (or V_o) and take measurements for all V_o (or V_w). We measure Δp for the motion with the manometers using equations (13.6) and (13.7). The pressure gradient due to the motion is $\Delta p/L$. We define a dimensionless pressure gradient

$$\Theta = \Delta p/\rho_w g L \tag{17.1}$$

which is expressed as feet of water/foot. Measured values of the pressure drop versus the flow rate ratio with V_w as a parameter are given in figure 17.1.

Measured values of the pressure drop vs. the flow rate ratio with V_o as a parameter are given in figure 17.2. The reader's attention should focus on the following practical result: for a fixed flow rate of oil there is an optimal flow rate V_w of water, with V_w/V_o between 0.2 and 0.8 in the experiments, for which Θ is minimized. This means the flow rates of water and oil can be adjusted to minimize energy expenditure while transporting the same amount of oil. The minimum Θ point moves toward lower values of V_w/V_o as V_o is increased. All the minimum points in up-flow are located in regions of bamboo waves.

The minimum pressure gradients fall in the region of disturbed core-annular flow. In this region, one finds corkscrew waves, perfect or nearly perfect core-annular flow with disturbances in the form of immature corkscrew waves, or bamboo waves.

In figure 17.3 we compare the pressure gradients in up-flow and down-flow as a function of the input ratio. The difference in the pressure gradients depends mainly on the rate of flow of the lubricating water. For high pressure gradients, the effect of buoyancy is relatively small and the differences between up- and down-flows are suppressed. In general, the pressure gradients in down-flow are smaller because of buoyancy which leads to greater accumulations of oil and more energy efficient flow regimes in down-flow.

The manner in which the oil is introduced into the pipe has some effect on the pressure drops. Tests were done with two different diameters for the nozzle used to deliver the oil centrally into the pipe (see figure 17.4). Their inside diameters were 0.2" and 0.17". Smaller nozzles were rejected because they give rise to higher pressure gradients, especially when oil flow rates are large. The reason is that when the nozzle is small, for one reason or another, many small oil bubbles are formed at the exit lip. Although the flow will soon tend to a steady state compatible with a particular set of operating conditions, the small bubbles persist and produce an additional

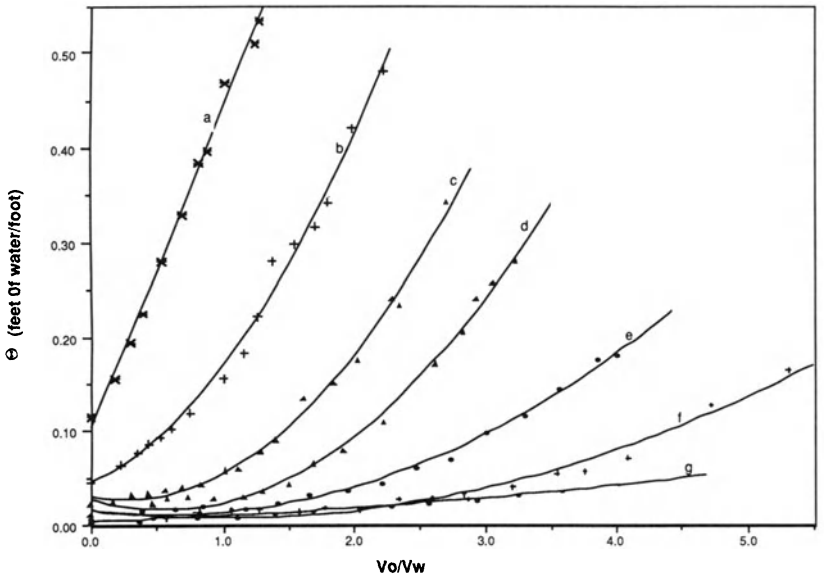

(a)

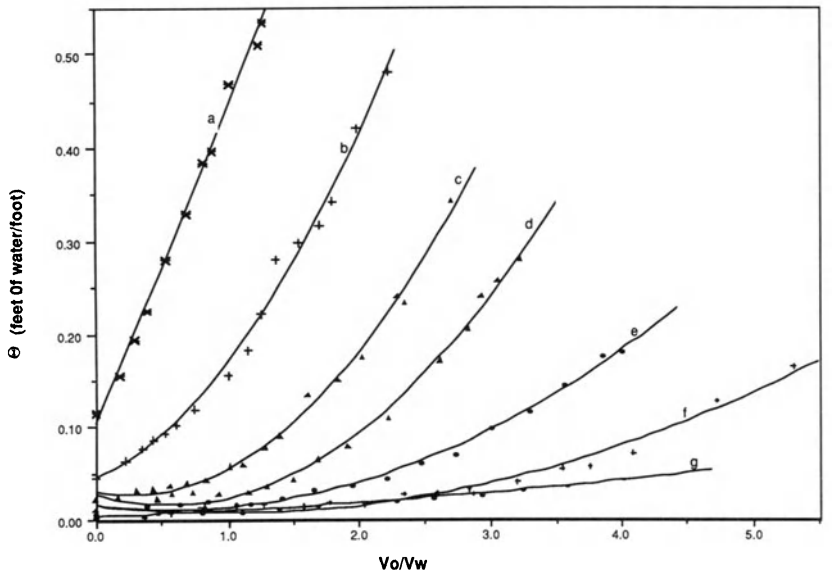

(b)

Fig. 17.1(a-b). [Bai, Chen and Joseph, 1992] Pressure drop per unit length as a function of the input ratio for various values of water flow velocity V_w in ft/sec: (a)2.80, (b)1.08, (c)1.12, (d)0.83, (e)0.55, (f)0.38, (g)0.33. For each V_w, Θ is an increasing function of V_o, with larger increases for larger values of V_w and no increases, even decreases, for small value of V_w. (a) Up-flow, (b) Down-flow.

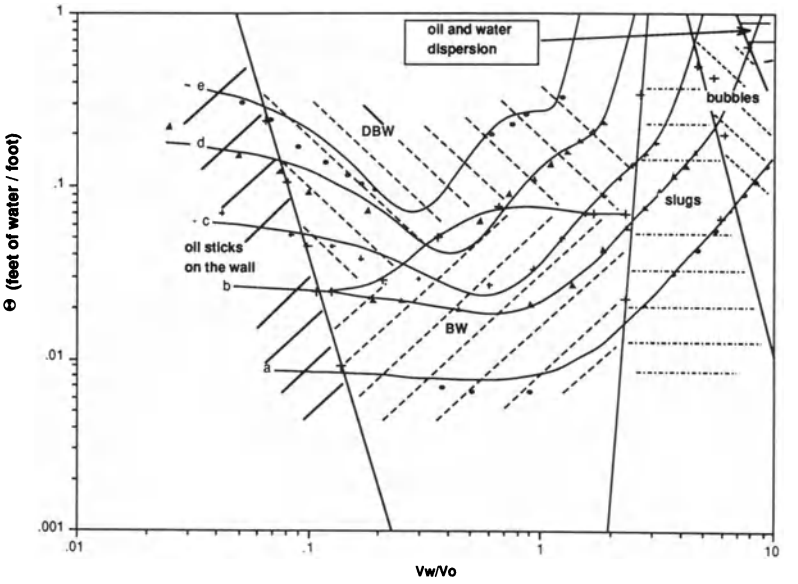

(a)

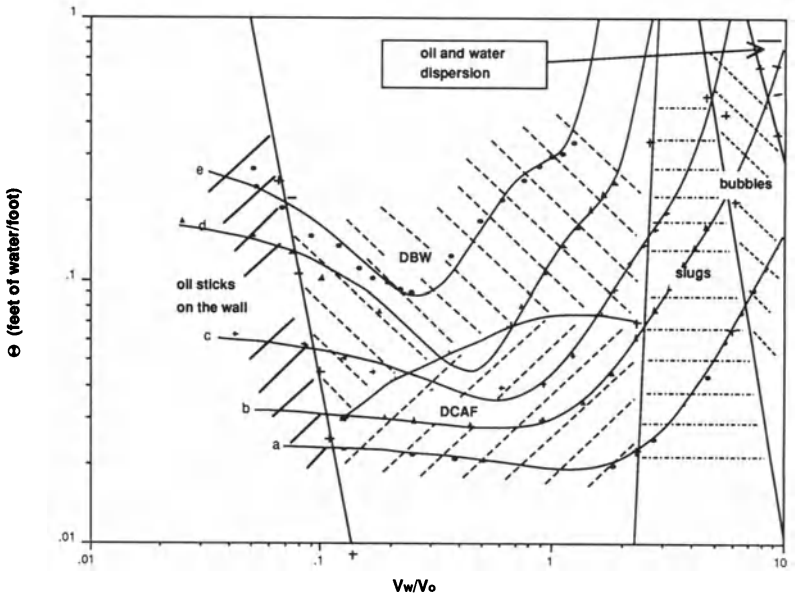

(b)

Fig. 17.2(a-b). [Bai, Chen and Joseph, 1992] Dimensionless pressure gradient versus the inverse input ratio for different values of the oil velocity in ft/sec: (a)0.31, (b)0.61, (c)0.91, (d)1.51, (e)2.27. (a) Up-flow, (b) Down-flow.

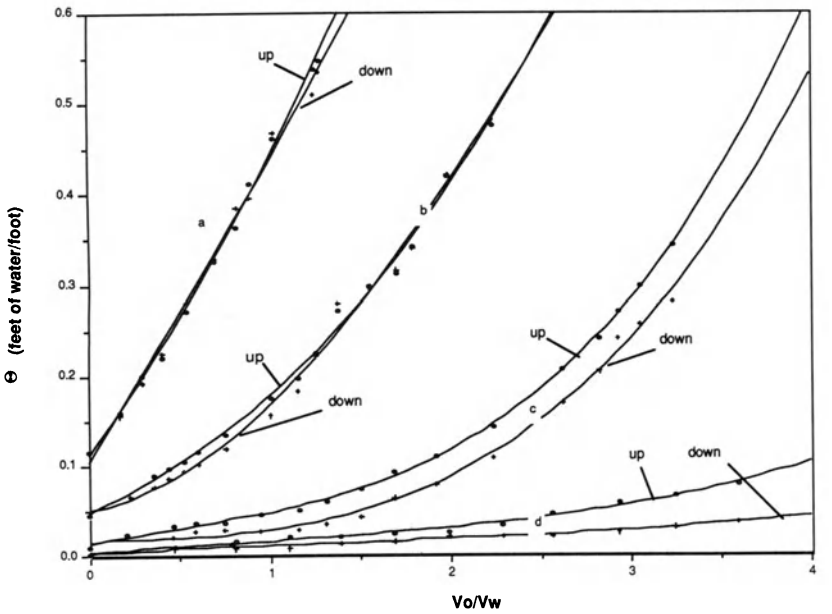

Fig. 17.3. [Bai, Chen and Joseph, 1992] Comparison of the pressure drop per unit length as a function of the input ratio for four values of V_w in ft/sec: (a) 2.80, (b)1.68, (c) 0.83, (d) 0.33.

pressure drop. This effect is greatly enhanced by increasing the flow rate of oil.

VII.18 Ideal and Measured Efficiency of Lubrication

To assess the energy saving due to water lubrication in vertical flow, a comparison was made of the measured values for the flow rates, hold-up ratio and pressure gradients with ideal values which are described below. The ideal values are determined by the solutions of the equations (cf. VI.(1b.1))

$$-\hat{P}' + \rho_l g + \mu_l \left(W'' + \frac{1}{r} W' \right) = 0 \tag{18.1}$$

for $W = W_l(r)$ which holds for up-flow in the region $l = 1$ of the core $0 < r < R_1$ and the region $l = 2$ of the annulus $R_1 < r < R_2$ when

$$\frac{d\hat{P}_1}{dx} = \frac{d\hat{P}_2}{dx} = \hat{P}'$$

is one and the same constant pressure gradient.

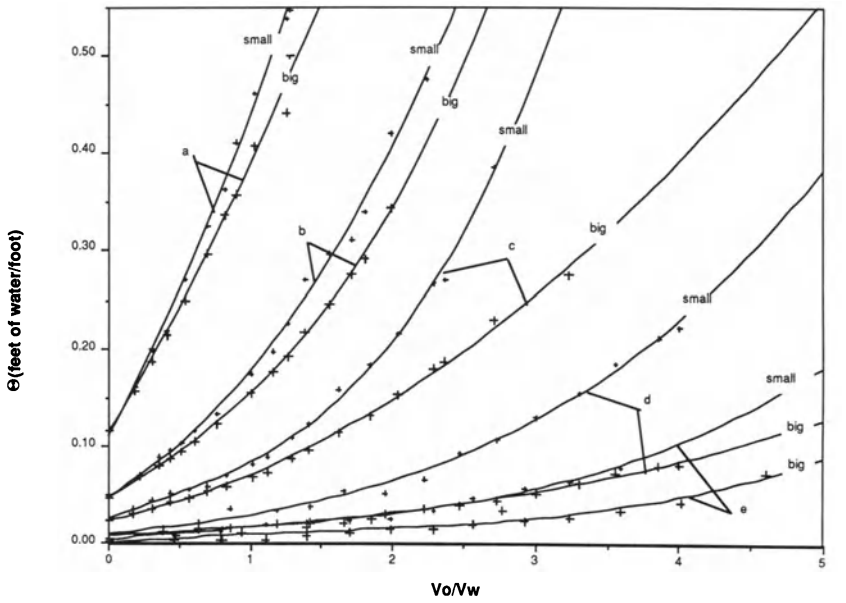

(a)

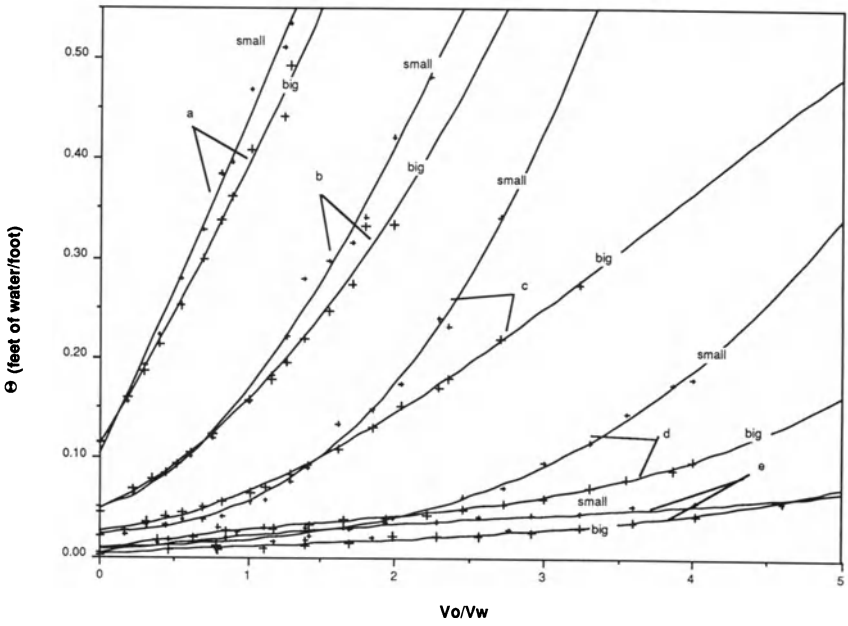

(b)

Fig. 17.4(a-b). [Bai, Chen and Joseph, 1992] The effect of the nozzle diameter on the pressure drop as a function of the input ratio for different values of the water velocity V_w in ft/sec: (a) 2.80, (b) 1.68, (c) 1.12, (d) 0.55, (e) 0.33. The nozzle 'big' has an inside diameter of 0.2, 'small' has an inside diameter of 0.17. (a) up-flow, (b) down-flow.

To compare this ideal flow with experiments, we must remove the part of the pressure associated with the composite density of the mixture

$$\rho_c = \frac{\rho_w H_w + \rho_o H_o}{H_w + H_o}$$

where $L = H_o + H_w$, and H_o and H_w are the heights of the oil and water in the pipeline which were described in section VII.13. We may determine H_o and H_w in terms of $\eta = 1/a = R_1/R_2$ and L by the conservation of volume

$$H_o \pi R_2^2 = \pi R_1^2 L,$$
$$H_w \pi R_2^2 = \pi (R_2^2 - R_1^2) L.$$

Hence

$$H_o = \eta^2 L, \qquad H_w = (1 - \eta^2) L \tag{18.2}$$

and

$$\rho_c = (1 - \eta^2)\rho_2 + \eta^2 \rho_1 \tag{18.3}$$

where $\rho_2 = \rho_w$ and $\rho_1 = \rho_o$.

The dynamic pressure p which is measured by the method of section VII.13 is then given by

$$\hat{P} = p + \rho_c g x$$

and

$$-\hat{P}' + \rho_l g = -p' + (\rho_l - \rho_c) g \tag{18.4}$$

where, using (18.3), we find that

$$\begin{aligned} \rho_1 - \rho_c &= (1 - \eta^2)[\![\rho]\!], \\ \rho_2 - \rho_c &= -\eta^2 [\![\rho]\!]. \end{aligned} \tag{18.5}$$

Then, we have

$$\begin{aligned} &-p' + (1 - \eta^2)[\![\rho]\!] g + \mu_1 \left(W'' + \frac{1}{r} W' \right) = 0, \quad 0 \le r \le R_1, \\ &-p' - \eta^2 [\![\rho]\!] g + \mu_2 \left(W'' + \frac{1}{r} W' \right) = 0, \quad R_1 \le r \le R_2. \end{aligned} \tag{18.6}$$

Equations (18.6) show that core-annular flow in a vertical pipe depends on the density through the density difference and only through the density difference. These terms disappear entirely from the governing equation (18.5) when the flow is all oil ($\eta = 1$) or all water ($\eta = 0$).

If we think of x increasing in the same direction as the pressure drop, we have the same equation (18.5) in down-flow but with gravity reversed. The equations derived below are for up-flow. To get the equations for down-flow, change the sign of g.

The solution of (18.6) together with appropriate boundary and interface conditions (see section VII.2) is

$$W_1(r) = \frac{f_1}{4\mu_1}(R_1^2 - r^2) + \frac{f_2}{4\mu_2}(R_2^2 - R_1^2) + \frac{R_1^2[\![\rho]\!]g}{2\mu_2}\ln\frac{R_2}{R_1} \tag{18.7}$$

where

$$\begin{aligned} f_1 &= -p' + (1-\eta^2)[\![\rho]\!]g \\ f_2 &= -p' - \eta^2[\![\rho]\!]g \end{aligned} \tag{18.8}$$

in up-flow and

$$W_2(r) = \frac{f_2}{4\mu_2}(R_2^2 - r^2) - \frac{R_1^2[\![\rho]\!]g}{2\mu_2}\ln\frac{r}{R_2}. \tag{18.9}$$

The oil flow rate is given by

$$\begin{aligned} Q_1 &= 2\pi\int_0^{R_1} rW_1(r)dr \\ &= 2\pi\left\{\frac{f_1}{16\mu_1}R_1^4 + \frac{f_2}{8\mu_2}(R_2^2R_1^2 - R_1^4) + \frac{R_1^4[\![\rho]\!]g}{4\mu_2}\ln\frac{R_2}{R_1}\right\}. \end{aligned} \tag{18.10}$$

The water flow rate is given by

$$\begin{aligned} Q_2 &= 2\pi\int_{R_1}^{R_2} rW_2(r)dr \\ &= 2\pi\left\{\frac{f_2}{16\mu_2}(R_2^2 - R_1^2)^2 + \frac{[\![\rho]\!]g}{8\mu_2}\left[R_1^2R_2^2 + 2R_1^4\ln\frac{R_1}{R_2} - R_1^4\right]\right\} \end{aligned} \tag{18.11}$$

When there is only oil in the pipe, $R_1 = R_2$, $Q_2 = 0$, $f_1 = -p'$. When there is only water in the pipe, $R_1 = 0$ and $Q_1 = 0$, $f_2 = -p'$. Hence in both cases, the flow rate is

$$Q = -\frac{p'}{8\mu}\pi R_2^4. \tag{18.12}$$

When $g = 0$, such as in the case of matched densities studied by CGH, we have

$$Q_1 = -\frac{p'\pi R_1^4}{8\mu_1}\left\{1 + 2\frac{\mu_1}{\mu_2}\left(\frac{R_2^2}{R_1^2} - 1\right)\right\} \tag{18.13}$$

and

$$Q_2 = \frac{-p'\pi}{8\mu_2}(R_2^2 - R_1^2)^2. \tag{18.14}$$

Some people have tried to explain why the two fluids end up in the lubricated arrangement by resorting to various optimization problems (cf. section I.3). For example, we found in section I.3 (f) the water fraction, or the value of R_1, such that the total volume flux Q_1+Q_2 is maximized among all the flows satisfying (18.13) and (18.14) for a given pressure gradient p'. Another problem is to maximize the oil flow rate Q_1 alone under the same conditions. This is a payoff calculation in which the water fraction is chosen

to maximize the throughput of oil. This problem was solved when $[\![\rho]\!]g = 0$ by Russell and Charles [1959] (cf. Joseph, Nguyen and Beavers [1984]).

The slightly more difficult case of vertical flow is considered below. First we rewrite (18.10) and (18.11) in a more convenient form in which we introduce the superficial velocities $V_o = Q_1/\pi R_2^2$ and $V_w = Q_2/\pi R_2^2$. Thus

$$\frac{4V_o\mu_2}{R_2^2 g} = \frac{-p'}{g}\left\{\frac{m}{2}\eta^4 + \eta^2 - \eta^4\right\} + [\![\rho]\!]\left\{\frac{m}{2}(\eta^4 - \eta^6) - \eta^4 + \eta^6 - 2\eta^4 \ln \eta\right\} \tag{18.15}$$

and

$$\frac{4V_w\mu_2}{R_2^2 g} = -\frac{p'}{2g}(1-\eta^2)^2 + \frac{[\![\rho]\!]}{2}\left\{\eta^2 - \eta^6 + 4\eta^4 \ln\eta\right\} \tag{18.16}$$

Equations (18.15) and (18.16) each depend on two dimensionless parameters. The right sides of both depend on one parameter $p'/g[\![\rho]\!]$ which is positive because $p' < 0$ and $[\![\rho]\!] \leq 0$ in our flows. The same formulas hold in down-flow with the sign of g reversed.

A theoretical formula for the hold-up ratio can be derived from (14.1), (18.2), (18.15) and (18.16)

$$h = V_o H_w / V_w H_o$$

$$= 2\frac{(1-\eta^2)\left\{\Theta\left(\frac{m}{2}\eta^4 + \eta^2 - \eta^4\right) + \frac{[\![\rho]\!]}{\rho_w}\left[\left(\frac{m}{2} - 1\right)(\eta^4 - \eta^6) - 2\eta^4 \ln\eta\right]\right\}}{\eta^2\left\{\Theta(1-\eta^2)^2 + \frac{[\![\rho]\!]}{\rho_w}(\eta^2 - \eta^6 + 4\eta^4 \ln\eta)\right\}} \tag{18.17}$$

where

$$\frac{-p'}{\rho_w g} \stackrel{\text{def}}{=} \Theta \tag{18.18}$$

is a dimensionless pressure gradient which can be compared with $\Delta p/\rho_w g L$ measured in experiments.

The maximization problem solved by Russel and Charles [1959] is to maximize V_o with respect to η, for fixed p' when $[\![\rho]\!] = 0$. They found that V_o is the maximum when

$$\eta = \left(\frac{1}{2-m}\right)^{1/2}.$$

In our experiments

$$m \approx 1/601, \quad [\![\rho]\!]g = -0.090g$$

and the oil flow-pressure gradient relation (18.15) for up-flow becomes

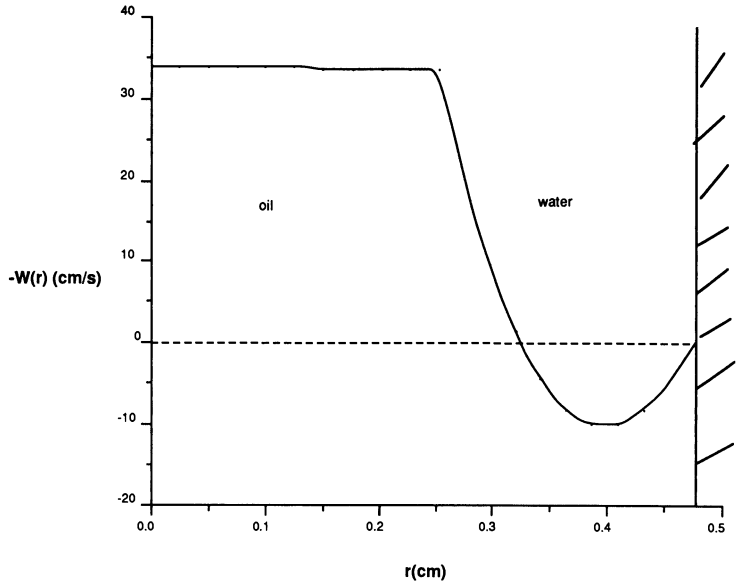

Fig. 18.1. [Bai, Chen and Joseph, 1992] Up-flow with negative flow of water, V_o=0.305 ft/sec, V_w=-0.046 ft/sec.

$$\frac{4V_0\mu_2}{R_2^2 g\rho_w} = -\frac{p'}{g\rho_w}(\eta^2-\eta^4) - \frac{0.090}{\rho_w}(\eta^6-\eta^4-2\eta^4\ln\eta) \tag{18.19}$$

where $\rho_w = 0.995$, to within a small error. The same formula holds in down-flow with the sign of g reversed.

In the first five rows of table 18.1 we compare experimental and ideal results for five cases of up-flow, and in rows 6 through 10 for five cases of down-flow. The columns of this table are as follows: V_{oe} is the superficial velocity from experiments, V_{we} the prescribed water velocity, h_e is the hold-up ratio from figure 14.4, $\eta_e = R_{1e}/R_2$ is the experimental ratio of the mean radius of the interface to the pipe radius which is computed from h_e using (14.4), and Θ_e is the measured value of dimensionless pressure gradient. We may define an ideal flow as PCAF satisfying (18.15) and (18.16). Subscript L is used for parameters of the idealized laminar flow. Then η and $\Theta_L(\eta)$ are computed from (18.15) and (18.16) when $(V_o,\ V_w) = (V_{oe},\ V_{we})$ and (18.17) determines $h_L(\eta)$. $\Theta_L(\eta_e)$, $V_{wL}(\eta_e)$ and $h_L(\eta_e)$ are computed from the formulas when $(\eta,\ V_o) = (\eta_e,\ V_{oe})$ are given. The value $\eta = 1/\sqrt{2}$ is a good approximation to the value of η which minimizes $\Theta(\eta) = -p'/g\rho_w$ for a fixed value of V_o. We can prove this when η is close to one by noting that

$$\eta^6-\eta^4-2\eta^4\ln\eta = \eta^6-\eta^4-\eta^4\ln[1-(1-\eta^2)] = \eta^6-\eta^4+\eta^4(1-\eta^2)+O[(1-\eta^2)^2]$$
$$= O[(1-\eta^2)^2] \tag{18.20}$$

Table 18.1. Comparision of experimental and ideal values in up-flow (#1-5) and down flow (#6-10) for the same oil flow. V is given in ft/sec. The other quantities are dimensionless. Subscript e denotes experimental and L denotes theoretical data. *The velocity profile for this case of negative V_w is shown in figure 18.1.

	V_{oe}	V_{we}	η_e	flow type	h_e	Θ_e	η	$\Theta_L(\eta)$	$h_L(\eta)$
1.	0.305	0.554	0.52	BW	1.39	0.019	0.34	0.0013	4.18
2.	0.607	0.272	0.78	BW	1.39	0.020	0.56	- 0.004	4.83
3.	0.909	0.554	0.74	BW	1.39	0.027	0.58	0.003	3.31
4.	1.513	0.554	0.82	BW	1.39	0.052	0.72	0.016	2.53
5.	2.269	0.494	0.88	DBW	1.39	0.096	0.82	0.044	2.19
6.	0.305	0.554	0.53	DCAF	1.39	0.020	0.61	0.026	1.59
7.	0.607	0.154	0.86	DCAF	1.39	0.025	0.85	0.028	1.59
8.	0.909	0.154	0.90	DCAF	1.39	0.033	0.88	0.038	1.78
9.	1.513	0.554	0.82	DCAF	1.39	0.052	0.78	0.050	1.72
10.	2.269	0.554	0.86	DBW	1.39	0.090	0.83	0.071	1.86

	$Q_L(\eta_e)$	$V_{wL}(\eta_e)$	$h_L(\eta_e)$	$\eta_m(\Theta_e)$	$V_{oL}(\Theta_e)$	$V_{wL}(\Theta_e)$
1.	-0.011	-0.046*	-16.7	0.67	1.68	0.82
2.	-0.00013	0.11	3.89	0.67	1.73	0.84
3.	0.0038	0.25	2.97	0.67	2.04	1.01
4.	0.026	0.31	2.29	0.68	3.17	1.60
5.	0.062	0.31	2.11	0.69	5.16	2.61
6.	0.027	0.64	0.91	0.89	0.34	0.06
7.	0.028	0.14	1.61	0.86	0.50	0.11
8.	0.04	0.12	1.84	0.82	0.81	0.24
9.	0.051	0.45	1.76	0.77	1.61	0.65
10.	0.076	0.41	1.90	0.74	3.31	1.53

	$h_L(\eta_m)$	$\Theta_L(1)$	$\Theta_L(o)$
1.	2.53	2.34	.0095
2.	2.51	4.65	.0097
3.	2.41	6.96	.016
4.	2.24	11.6	.023
5.	2.141	7.4	.031
6.	1.55	2.34	.0095
7.	1.57	4.65	.0084
8.	1.62	6.96	.012
9.	1.72	11.6	.023
10.	1.84	17.4	.031

The result $\eta = 1/\sqrt{2}$ follows from (18.19) when the second term of the right hand side is zero. $\eta_{\rm m}(\Theta_e)$ is the value of η which maximizes $V_o = V_{oL}(\Theta_e)$ in (18.15) when $\Theta = \Theta_e$ and $h_L(\eta_{\rm m})$ is calculated from (18.17) with $(\eta,\ \Theta) = (\eta_{\rm m},\ \Theta_e)$.

The value $\Theta(1)$ is the dimensionless pressure gradient required to transport oil alone in the same pipe with the same oil throughput. We obtain

$$\Theta(1) = 8V_o\mu_1/gR_2^2\rho_{\rm w} \tag{18.21}$$

from (18.15) with η =1.

Another measure of efficiency which is used in the oil industry is to compare the observed pressure gradient Θ_e with the pressure drop $\Theta(0)$ required to transport water alone with a volume flux $Q_{o+w} = Q_o + Q_{\rm w}$ equal to the total flux. We can compute $\Theta_L(0)$ for the laminar flow of water from (18.12)

$$\Theta_L(0) = \frac{8V_{o+{\rm w}}\mu_2}{gR_2^2\rho_{\rm w}} \quad \text{(laminar)} \tag{18.22}$$

where $V_{o+{\rm w}} = V_o + V_{{\rm w}e} = Q_{o+{\rm w}}/A$ can be obtained from tables. Table 18.1 shows correlation between experimental and theoretical data for the DCAF cases.

In table 18.2 we have various pressure gradient ratios, which are measures of efficiency together with the values of the Reynolds number

$$\mathbb{R}e = \frac{V_{o+{\rm w}}d}{\nu_{\rm w}}, \quad \nu_{\rm w} = \mu_2/\rho_{\rm w}$$

where $d = 3/8$ in and $\mu_2 = 10^{-2}$ poise. Hence

$$\mathbb{R}e = V_{o+{\rm w}}\frac{12(2.54)^2300}{8} \cong 2903V_{o+{\rm w}}. \tag{18.23}$$

From experimental data, the water is turbulent when $\mathbb{R}e > 2300$ in which case we should not compare Θ_e with $\Theta_L(0)$ for laminar flow. For these, we should compute $\Theta_T(0)$, the pressure gradient for turbulent flow at a superficial velocity of $V_{o+{\rm w}}$. It requires a greater pressure gradient, $\Theta_T(0) = k\Theta_L(0)$ with $k > 1$ (for example, $k = 3/2$), to transport a given mass flux in turbulent flow. So, as a rough measure, the reader should multiply the number $\Theta_L(0)/\Theta_c$ by 3/2 when $\mathbb{R}e > 2300$.

Table 18.2. Comparison of the ratio of ideal to the experimental pressure gradients for the same oil flow. The Reynolds number $\mathbb{R}e = (V_o + V_w)d/\nu_w$. $\mathbb{R}e > \mathbb{R}e_c$ where $\mathbb{R}e_c \approx 2000$, the flow is turbulent. In the turbulent case we should replace $\Theta_L(o)$ with $\Theta_T(o) > \Theta_L(o)$ because a greater pressure gradient is required for the same volume flux in turbulent flow.

	flow type	$\Theta_L(1)/\Theta_e$	$\Theta_L(\eta)/\Theta_e$	$\Theta_L(\eta_e)/\Theta_e$	$\Theta_L(o)/\Theta_e$	$\mathbb{R}$
1.	BW	122.93	0.068	-0.58	0.49	2481
2.	BW	232.46	-0.20	-0.0065	0.49	2599
3.	BW	257.88	0.11	0.14	0.60	4226
4.	BW	222.87	0.31	0.50	0.44	5656
5.	DBW	180.97	0.46	0.65	0.32	7981
6.	DCAF	116.79	1.30	1.35	0.47	2481
7.	DCAF	185.97	1.12	1.12	0.34	2198
8.	DCAF	210.99	0.85	1.21	0.36	3071
9.	DCAF	222.88	0.96	0.98	0.44	5971
10.	DBW	193.04	0.79	1.07	0.35	8155

From our comparisons of ideal and measured values of the pressure gradients we may draw the following conclusions.

(1) The pressure drops required to transport a given flux of oil with water lubrication are about 200 times less than pressure drops required to transport the same flux of 601 cp oil without lubrication. In vertical pipes we have found a reduction of the order k/m where $m = \mu_2/\mu_1$ and k is a fraction, say about 1/3 (see second column of table 18.2).

(2) The pressure drops required to transport a given flux of oil and water with water lubrication are of the same order as the pressure drop necessary to transport water alone at a superficial velocity V_{o+w} corresponding to the total flux provided that the water is turbulent.

(3) Bamboo waves require a much greater pressure gradient to transport a given volume flux of oil at low oil velocity and fixed water velocity than in the ideal case (see fifth column of table 18.2). The significance of this comparison is diminished by the fact that oil is being transported mainly by buoyancy.

(4) Disturbed core-annular flow with corkscrew waves is energy efficient, with pressure gradients only moderately greater, sometimes even less than those required for perfect core-annular flow with the same water fraction. In this sense, DCAF is close to PCAF.

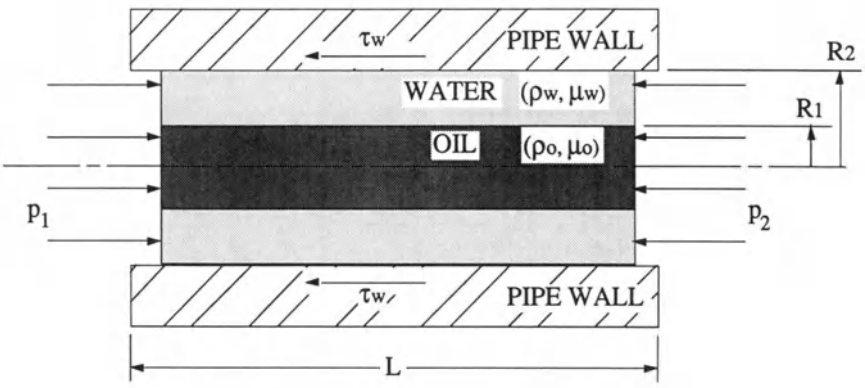

Fig. 19.1. Force balance.

VII.19 Friction Factor and Reynolds Number for Lubricated Pipelining

The Reynolds number and friction factors can, from a theoretical standpoint, be defined in any convenient way. We have chosen a definition which yields the most meaningful compression of data from different authors.

The force balance in figure 19.1 shows that

$$\pi R_2^2(p_1 - p_2) = 2\pi R_2 L\tau_w. \tag{19.1}$$

Hence,

$$\frac{\Delta p}{\rho_w g} = \frac{2L\tau_w}{R_2\rho_w g} \tag{19.2}$$

and

$$-p' = \frac{2\tau_w}{R_2} \tag{19.3}$$

where $\Delta p = p_1 - p_2$ and p' is the dynamic pressure gradient $-p' = \Delta p/L$. We may eliminate τ_w with the friction factor (resistance coefficient) λ defined in the usual way (see, for example, p505 of Schlichting [1960]).

$$\frac{8\tau_w}{\rho_c V^2} = \lambda(\mathbb{R}) \tag{19.4}$$

where ρ_c is the composite density defined by (18.3), and

$$V = V_o + V_w = (Q_o + Q_w)/\pi R_2^2 \tag{19.5}$$

is an average superficial velocity and $\mathbb{R}$ is a to-be-determined Reynolds number. We next eliminate V_o and V_w in terms of p', using (18.5) and (18.16) giving rise to a relation between p' and V. Then p' is eliminated in favor of τ_w using (19.3) and τ_w is then eliminated in favor of λ and V using (19.4). After solving for λ, we get

$$\lambda = \frac{p' 2D_2}{\rho_c V^2} = \frac{64}{\mathbb{R}} - B \tag{19.6}$$

where $\xi = \rho_o/\rho_w$, $m = \mu_w/\mu_o$, $\rho_c(\eta)$ is the composite density (18.3),

$$\mathbb{R} = \frac{\rho_c D_2 V}{\mu_w}(1+\eta^4(m-1)) = \frac{\rho_w D_2 V}{\mu_w}[1+\eta^2(\xi-1)](1+\eta^4(m-1)) \tag{19.7}$$

and

$$B = \frac{2[\![\rho]\!] g D_2 (1-\eta^2)\eta^2(1+\eta^2(m-1))}{\rho_w V^2(1+\eta^2(\xi-1))(1+\eta^4(m-1))}. \tag{19.8}$$

If $[\![\rho]\!] < 0$, $B < 0$. This applies in down-flow. For up-flow, we change the sign of the two velocities and the pressure gradient so that $-p' > 0$ and

$$\lambda = \frac{64}{\mathbb{R}} - B \qquad \text{for down flow}$$

$$\lambda = \frac{64}{\mathbb{R}} + B \qquad \text{for up flow.}$$

Of course $B = 0$ when there is no gravity. We may evaluate the friction factor in special situations. For a horizontal pipe, $\mathbf{g}$=0, and $[\![\rho]\!] = 0$, so $\xi = 1$. Then $\lambda = 64/\mathbb{R}$ and

$$\mathbb{R} = \frac{\rho_c D_2 V}{\mu_w}(1+\eta^4(m-1)) = \frac{\rho_w D_2 V}{\mu_w}(1+\eta^4(m-1)). \tag{19.9}$$

If $Q_o = 0$, $\eta = 0$ and we retrieve the friction factor and Reynolds number for water alone.

If $Q_w = 0$, η=1 and we retrieve the formulas for oil alone.

For $Q_o > 0$ and $\eta < 1$, the velocity profile has a back flow as in figure 19.2.

When $Q_o + Q_w \geq 0$ and $p_1 - p_2 \leq 0$: this condition occurs only for up-flow in a vertical pipe when Reynolds number is small, so that the buoyancy contribution B dominates the friction factor. In fact, the oil's buoyancy drives the flow and an external pressure gradient is not needed.

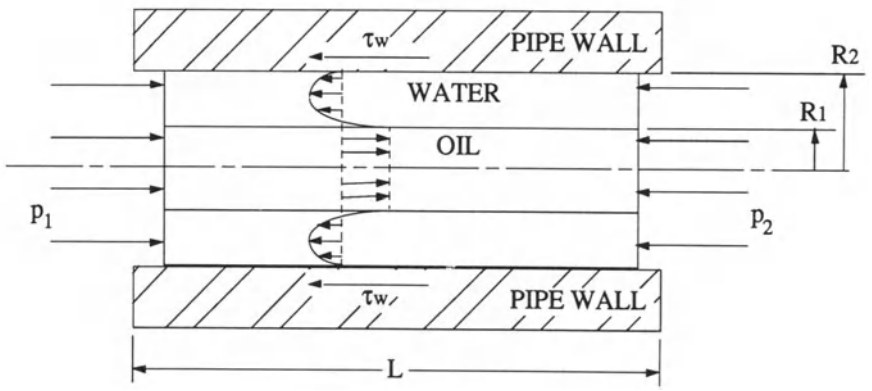

Fig. 19.2. Back flow.

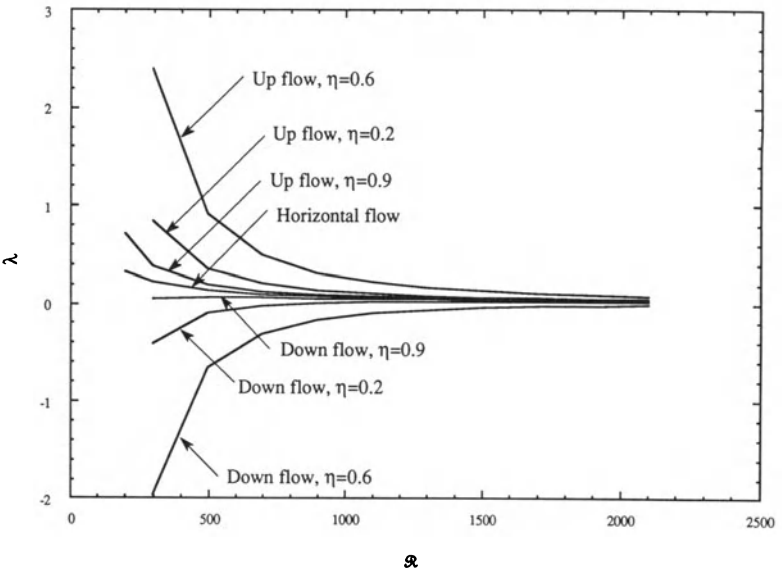

Fig. 19.3. Theoretical friction factor.

Our definition is suitable whenever $Q_o + Q_w \geq 0$, regardless of the sign of Q_w. The case of back flow of water is rare.

Figure 19.3 shows that the friction factor depends strongly on η. The maximum friction factor occurs at $\eta \approx 0.5, 0.6$ for down-flow. For up-flow, the minimum friction factor occurs around $\eta \approx 0.5, 0.6$. When the Reynolds

number or η increases, the friction factor will tend to $64/\mathbb{R}$. If η decreases to zero, the friction factor will also tend to $64/\mathbb{R}$. The friction factor also depends on the difference of the densities of water and oil. In figure 19.3, we put $[\![\rho]\!]$=0.09. If the density difference were smaller, the friction factor would be close to the curve of $64/\mathbb{R}$.

Generally speaking, the density of water is greater than that of oil and $[\![\rho]\!] < 0$. However, if $[\![\rho]\!] > 0$, $B > 0$. Therefore, the down-flow equations for $[\![\rho]\!] < 0$ are the same as the up-flow equations for $[\![\rho]\!] > 0$, and the up-flow equations for $[\![\rho]\!] < 0$ are the same as the down-flow equations for $[\![\rho]\!] > 0$.

Comparison with Experiments. In this section, we reduce the data from the experiments of different authors into a friction factor versus Reynolds number plot. This is an effective way to gather all the data originating from a wide range of pipeline shapes and sizes, with vastly different core fluids. Thus, a simple and complete procedure for predicting pressure drop for a given core-annular flow situation is introduced and evaluated.

The holdup volume fraction H_w was measured as a function of the input fraction C_w, following the convention first used by Oliemans [1986]:

$$H_w = \frac{V_w}{V_o + V_w}, \qquad C_w = \frac{Q_w}{Q_w + Q_o},$$

where V_w is the volume of water, V_o is the volume of oil, Q_w is the volume flow rate of water and Q_o is the volume flow rate of oil. C_w and H_w are related to the holdup ratio h of Charles *et al.* [1961] (cf. (14.1)) defined as

$$h = \frac{V_o Q_w}{V_w Q_o}$$

so that

$$C_w = \frac{H_w}{h(1 - H_w) + H_w}. \tag{19.10}$$

The definitions for the friction factor and Reynolds number which we have given were designed to compress the data in a meaningful way. The Reynolds number $\mathbb{R}$ for an experiment can be determined from (19.7) when V and h are known. V is the composite superficial velocity (19.5) which is determined from the prescribed flow rate and an average radius ratio $\eta = R_1/R_2$ can be determined from measured values of the pressure drop using $\lambda = (R_2 \Delta p)/(\rho_c V^2 2L)$ where $\rho_c(\eta)$ is slightly less than ρ_w, $\rho_c/\rho_w \approx 0.92$, and slowly varying in the interval $\rho_o \leq \rho_c \leq \rho_w$. This definition of λ and $\mathbb{R}$ allows us to reduce our correlations to what they should be when $\eta \to 1$, in the case of pure oil. In the lubricated case, it may be more natural to replace ρ_c with ρ_w, and $(\lambda, \mathbb{R})$ with $(\tilde{\lambda}, \tilde{\mathbb{R}})$, where $\tilde{\lambda} = \lambda(\rho_c/\rho_w)$ and $\tilde{\mathbb{R}} = \mathbb{R}(\rho_w/\rho_c)$. This has the effect of shifting all experimental points down and to the right. This brings the points from the experiments of BCJ closer to the theoretical values in figure 19.4. The theoretical results are the same as in figure 19.3 except for the difference in scales.

The data of Sinclair [1970], Charles, Govier and Hodgson [1961], Russell, Hodgson and Govier [1959] and Oliemans [1986], CBJ[1991] and Arney, Bai, Joseph and Liu [1992] are represented in figures 19.5 - 19.6 and table 19.1. Points in the data of CGH which are labeled *water drops in oil* are omitted. These points represent a failure of lubrication in which very small water drops are dispersed in oil, forming a single emulsified fluid with a viscosity much greater than that of the oil alone. Sinclair [1970] looked at vertical flow and remarked that '...in the laboratory tests no measurable difference was found in the friction losses in horizontal and vertical test sections' ... and he shows results for horizontal flow for three different pipeline diameters. Charles *et al.* used one value for the diameter, but with three different oils. Also featured are data from pilot plant processes which are contributed by INTEVEP, Caracas, Venezuela, and Shell Oil Development Company, Houston, Texas. INTEVEP used a core oil that was really an emulsion of crude oil and water. Table 19.1 features a wide variety of situations regarding the viscosity of the oil, pipe diameter and pipe length.

The data of Arney *et al.* [1992] was taken for waxy crude oil in water and #6 fuel oil lubricated by water in a horizontal pipe made of glass. Details of the experimental set-up and fluid properties are presented in their paper (see table 19.1 for a summary). The water preferentially wets the glass wall.

Figure 19.5 contains the holdup data for literature sources listed in table 19.1. The holdup volume fraction is plotted as a function of the input fraction achieving good agreement among all of the data sources. The points that show the most scatter, which are for the emulsified waxy crude oil and for the data from INTEVEP, the core fluid is non-Newtonian, but all of the data for Newtonian oils show excellent agreement. The holdup data is fitted to the empirical formula:

$$H_w = C_w^*(1 + 0.35(1 - C_w)). \tag{19.11}$$

A line corresponding to this formula is also shown in the figure. This formula is comparable to the one found in Oliemans [1986], but more closely fits the available data. Until the work of Oliemans [1986], a useful prediction of the holdup was missing from the literature. When the input fraction for a process is known, equation (19.11) can be used to predict the holdup fraction and the average core diameter can be estimated by

$$D_c = D_p\sqrt{1 - H_w}, \tag{19.12}$$

where D_c is the diameter of the core and D_p is the diameter of the pipe. The Reynolds number is similar to (19.9):

$$\Re = \frac{\rho_c \bar{V} D_p(1 + \eta^4(m - 1))}{\mu_w}. \tag{19.13}$$

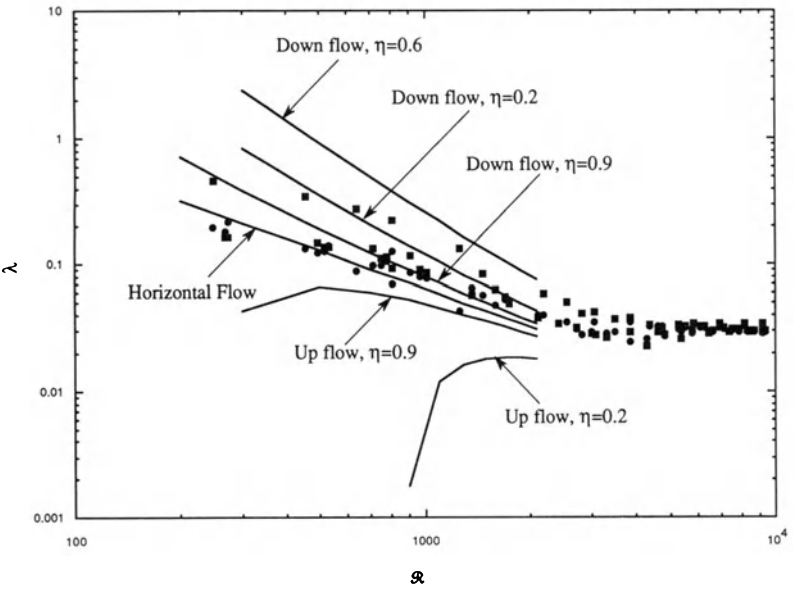

Fig. 19.4. Theoretical friction factor and a comparison with the data from the vertical pipeline of Bai, Chen, Joseph. • up-flow, ▪ down-flow.

The friction factor is (19.6):

$$\lambda = \frac{2p' D_p}{\bar{\rho}\bar{V}^2} \tag{19.14}$$

where

$$\bar{\rho} = \eta^2 \rho_o + (1 - \eta^2)\rho_w$$

is the average density,

$$\eta = \frac{D_c}{D_p},$$

$$\bar{V} = \frac{4(Q_o + Q_w)}{D_p^2}$$

is the overall velocity, and p' is the pressure drop per unit length of pipe.

Figure 19.6 is the result of applying equations (19.13) - (19.14) to the pressure drop −− flow rate data listed in table 19.1. For comparison, we drew lines corresponding to the theoretical formula for laminar flow

$$\lambda = \frac{64}{\mathbb{R}}$$

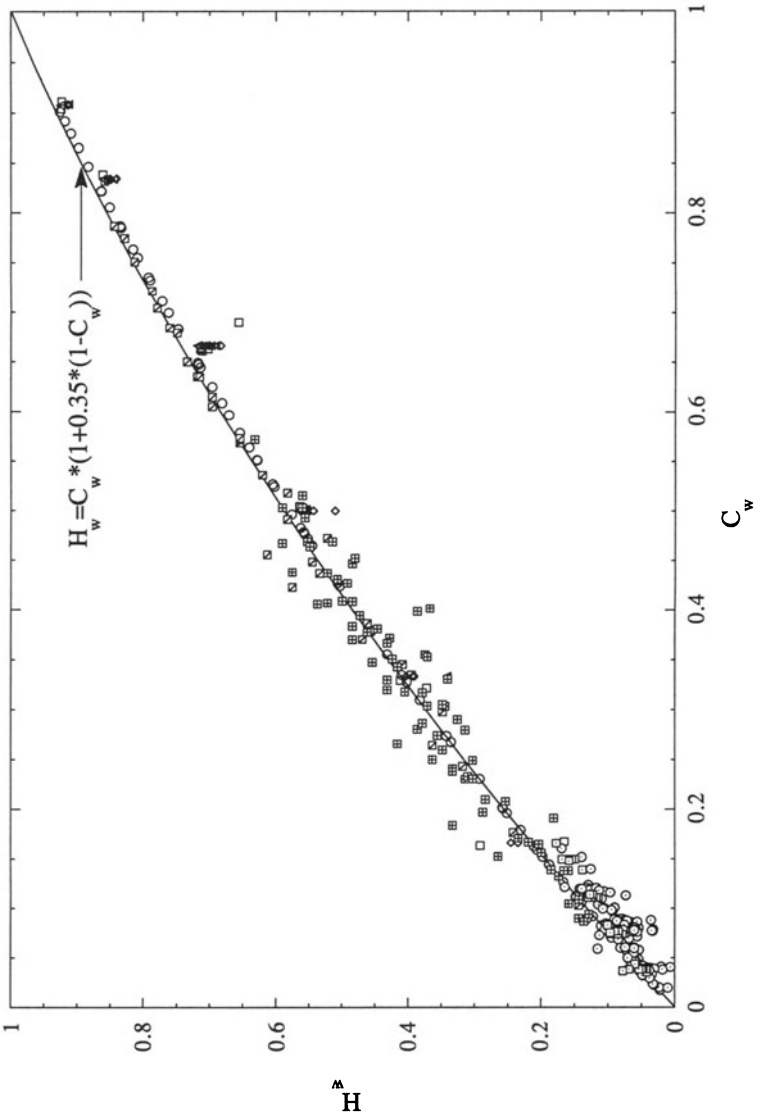

Fig. 19.5. Holdup data for sources listed in table 19.1

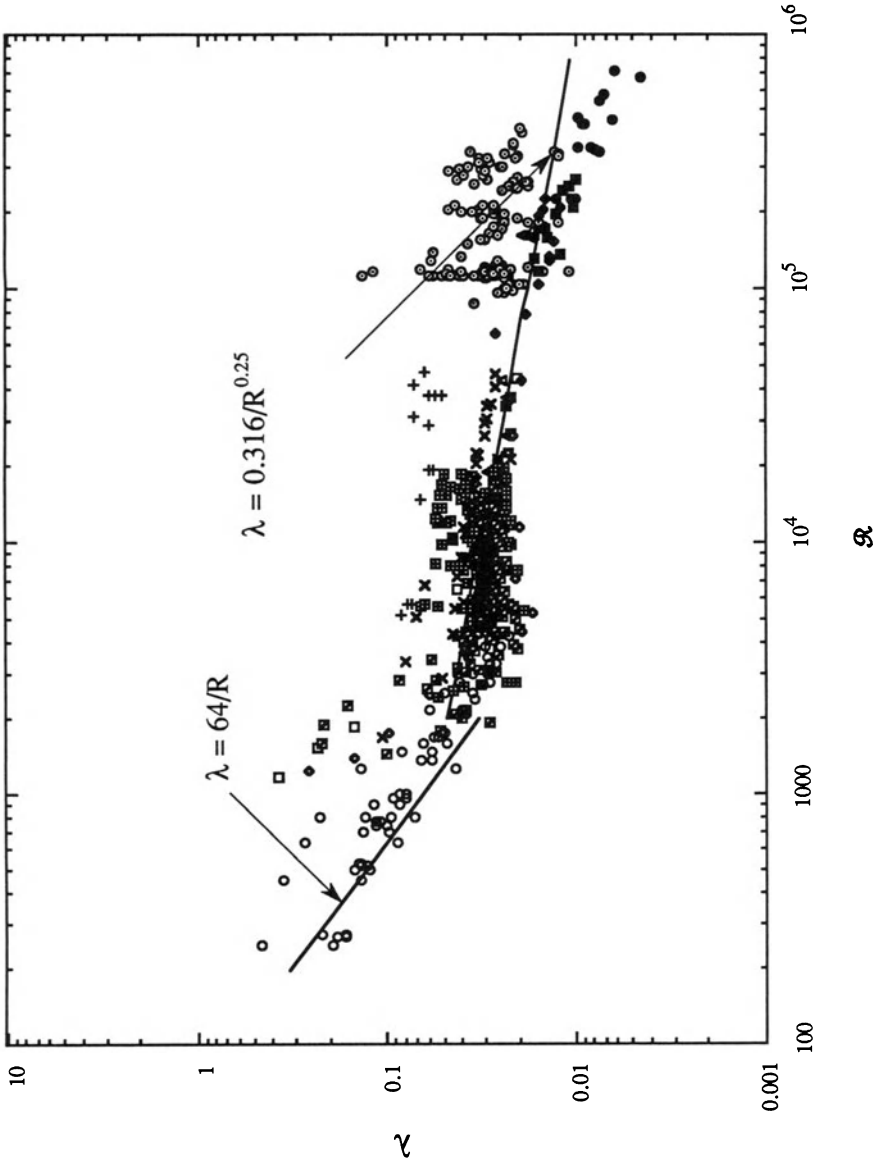

Fig. 19.6. Friction factor versus Reynolds number for sources listed in table 19.1.

and the Blasius formula for turbulent flow

$$\lambda = \frac{0.316}{\mathbb{R}^{0.25}}.$$

Two authors, Sinclair [1970] and the pilot plant data from Shell Oil Co. of Houston did not give holdup data, so we used equation (19.11) to calculate the Reynolds number and friction factor.

The data appears to be scattered for low Reynolds numbers. This is expected since, for slow flow rates, the core becomes very eccentric, causing the friction between the core and the wall to rise, yielding an increased friction factor. This increase in the friction has been predicted by Oliemans [1986]. For high Reynolds numbers, the data is smoother, with data from the non-Newtonian waxy crude oil and INTEVEP oil measurements showing the most scatter. It is reasonable to expect that the wavyness of the core will influence the pressure drop, much like the roughness of the pipe influences regular single-fluid pipe flow. The main strength of the results in figures 19.5 - 6 lies in the fact that it works very well for the high Reynolds numbers which are of interest in most industrial situations.

Figure 19.6 is the *Moody Chart* for lubricated pipelining since, together with figure 19.5, it can be used to predict pressure drops for any lubricated pipeline of any size.

Table 19.1. Comparison of the experimental parameters relevant to figures 19.5 - 6.

Author/group	Pipe Length Inches	Pipe Diameter inches	Core Fluid	Annulus fluid	Oil Density gm/cm^3	Oil Viscosity (poise)	Water Density gm/cm^3	Water Viscosity Poise	Plot Symbol
Bai, Chen, Joseph [1989]	90	0.375	20-30% water in Mobile® Cylinder Oil	0.4% Sodium Silicate in Water	0.905	6.01	0.995	0.0100	○
Charles, Govier and Hodgson [1961]	288	1.04	20.6% Carbon TetraChloride in Marcol GX	Water	0.998	0.0629	0.998	0.0089	□
Charles, Govier and Hodgson [1961]	288	1.04	18.7% Carbon Tetrachloride in Wyrol J	Water	0.998	0.168	0.998	0.0089	◇
Charles, Govier and Hodgson [1961]	288	1.04	16.7 Carbon Tetrachloride in Teresso 85	Water	0.998	0.63	0.998	0.0089	△
INTEVEP (Venezuela)	1.009 km	8" sch 40	Heavy crude oil	Water	.99-1.01	50-1200	1.000	0.0100	○
Minnesota (#6 fuel oil)	780	0.625	#6 fuel oil	Water	0.995	20	0.998	0.0089	◙
Minnesota (Waxy crude oil)	780	0.620	27% water in waxy crude oil emulsion	Water	0.985	>600	0.995	0.0090	⊞
Oliemans [1986]	354	2	"high viscosity oil"	Water	0.97	23	1.000	0.0089	×
Oliemans [1986]	354	8	"high viscosity oil"	Water	0.97	23	1.000	0.0089	+
Shell Oil (Houston)	24.24 miles	6	Crude oil	Water	0.992	120	1.000	0.0100	▲
Sinclair [1970]	600	3/4" sch 40	Humble Fractol oil, water, emulsifier	Sea Water	0.97	10	1.030	0.0100	◆
Sinclair [1970]	600	1" sch 40	Humble Fractol oil, water, emulsifier	Sea Water	0.97	10	1.030	0.0100	■
Sinclair [1970]	600	2 1/2" sch 40	Humble Fractol oil, water, emulsifier	Sea Water	0.97	10	1.030	0.0100	●

VII.20 Comparison of Experiments with Theory

In the linear theory of stability presented in sections VII.2-10, the Reynolds number is defined as $\mathbb{R}_g(R_1) = W_g R_1/\nu_1$ where $W_g = gR_1^2/\nu_1$ and $F = -\hat{P}'/\rho_1 g$. Lengths are scaled with R_1, velocity with W_g and time with $R_1/|W_g|$. In those sections, x increases in the direction of gravity so that $W(r)$ in up-flow here is $-W(r)$ there.

Two kinds of comparisons were made between theory and experiments. First, we calculated wave lengths and wave speeds in the regions of parameter space in which waves were observed and compared the calculated and measured values. Secondly, we tried to determine the regions of parameter space where different flow types could be found by analysis of the energy of the most dangerous disturbance.

It is useful here to draw attention again to the fact that we are trying to compare results of a linear theory of stability of PCAF with flow types in deeply nonlinear regions of flow. There are different ways to make this comparison corresponding to different choices of the laminar flow which is supposed to be relevant for the nonlinear flow which is observed. We shall give a more precise characterization of the possible choices below.

A laminar flow is determined by two parameters, say V_w and V_o or V_o and $a = 1/\eta = R_2/R_1$ or V_w and a. For example, given V_o and V_w we may compute η and p' from (18.15) and (18.16). We may conclude that other types of flow, say bamboo waves, are determined by prescribing two parameters plus the flow type. We compare flow types having

(1) the same oil and water inputs; that is, V_o and V_w are prescribed and equal to measured values

(2) the same oil input, V_o and the same water fraction expressed by $a = a_e$ where a_e is taken from the measured hold-up $h = h_e$ in figure 14.4. Bamboo waves trap water between the crests (see figure 15.5) and sweep it through the system faster than in laminar flow: less water is held up. The $\eta_e > \eta$ or $a_e < a$ in up-flow. In down-flow, this trapping does not operate and the experimental hold-up is nearly the same as the laminar one (see table 18.1).

VII.20(a) For Fixed Values of V_o and V_w

Calculations were carried out for the emulsified oil used in the experiments at a temperature of 22°C with material parameters given by (12.1). The dimensionless parameters which can be computed from the parameters given by (12.1) are

$$m = 1/601, \quad \rho_w/\rho_o = 0.995/0.905 = 1.10, \quad J^* = \frac{TR_2}{\rho_o \nu_o^2} = 0.102. \quad (20.1)$$

In our first comparison of linear theory with experiments, we select nine arbitrary cases of bamboo waves from experiments and compare observed and calculated wave lengths and wave speeds. Bamboo waves are imperfectly periodic but it is easy to identify average values, taken as simple averages from video recordings using scaled reticle and automatic lapsed-timer features. To compute wave lengths and wave speed from linear theory, we need to identify the unstable wave of maximum growth. For this we need to prescribe dimensionless parameters a, F and $\mathbb{R}_g$ which can be obtained from PCAF formulas in section VII.18; values of the oil and water volume flow rates $Q_o = V_o/A$ and $Q_{\rm w} = V_{\rm w}/A$ are prescribed. The values of these parameters at the labeled flow points in the chart of figure 16.1 are listed in table 20.1.

VII.20(a)(i) Up-flow. The comparison of computed and measured values of the wave speed and wave length of bamboo waves for points 1 through 9 of figure 16.1 is given in table 20.2. The measured values of the wave length are on the average slightly larger than computed values, probably due to the nonlinear stretching associated with the lubrication and buoyancy effects described in figure 15.5.

The speed $W(1)$ of the undisturbed interface is on the average slightly larger than the computed value of c. This shows that the bamboo wave is on the average basically stationary in a frame moving with velocity $W(1)$. As a further check we computed $c = 8.03$ cm/s, $W(1) = 9.84$ cm/s at point $D2$ and $c = 16.96$ cm/s, $W(1) = 18.95$ cm/s at $E2$. The viscosity of the oil is too large to support any but slowly propagating waves, so the wave is convected with the oil. Analysis of the singular problem $m \to 0$ (section VI.3) shows that $c \to W(1)$ in the limit $m \to 0$. The discrepancy between the computed and measured values of the wave speed is consistent with the idea that the wave is convected with the oil. The reason for the discrepancy can be traced to the fact that the water fraction for laminar flow with V_o and $V_{\rm w}$ prescribed is larger than the measured water fraction in up-flow; $\eta < \eta_e$ in the first five columns of table 18.1. Since V_o is prescribed to be the same in laminar flow and bamboo waves, the oil in a core with $R_1 < R_{1e}$ must flow faster. We speculate that the speed discrepancy between c in theory and experiments is due to the reduction of the water fraction due to sweep-out effects of bamboo waves.

Table 20.1. Specification of parameters used to calculate theoretical values from the linear theory of stability at the labeled flow points in the flow chart of figure 16.1.

	Experiment		Basic flow (18.7), (18.9) with the same V_o, V_w				
	V_o(ft/sec)	V_w (ft/sec)	a	W_0(cm/sec)	$W(1)$(cm/sec)	$\mathbb{R}_g(R_1)$	F
1	1.06	0.55	1.61	83.91	83.69	0.5749	-1.067
2	0.76	0.55	1.90	83.90	83.73	0.3475	-1.0737
3	0.46	0.55	2.44	83.03	82.91	0.1646	-1.0835
4	0.31	0.55	2.93	80.03	79.94	0.0951	-1.0893
5	0.31	0.27	2.58	62.15	62.05	0.1390	-1.0807
6	0.46	0.27	2.11	61.83	61.69	0.2563	-1.0722
7	0.61	0.27	1.78	58.66	58.49	0.4262	-1.0635
8	0.76	0.27	1.54	54.78	54.58	0.6595	-1.0556
9	0.91	0.27	1.38	53.23	53.01	0.9045	-1.0509
A1	0.01	0.03	8.03	19.68	19.67	0.0046	-1.0969
B1	0.02	0.03	6.41	25.04	25.02	0.0091	-1.0953
C1	0.03	0.03	5.59	28.62	28.59	0.0137	-1.0940
D1	0.1	0.03	3.63	40.09	40.04	0.0504	-1.0869
E1	0.3	0.03	2.18	43.39	43.27	0.2327	-1.0690
F1	1.0	0.03	1.03	32.80	31.91	2.1952	- 1.1127
A2	0.01	0.09	8.52	22.14	22.13	0.0039	-1.0980
B2	0.02	0.09	6.72	27.57	27.55	0.0079	-1.0965
C2	0.05	0.09	4.87	36.21	36.18	0.0207	-1.0931
D2	0.2	0.09	2.82	48.50	48.41	0.1071	- 1.0808
E2	0.5	0.09	1.48	33.27	33.09	0.7472	- 1.0459
F2	2.0	0.09	1.04	67.16	65.93	2.1045	-1.1605
A3	0.01	1.0	14.95	68.98	68.97	0.0007	- 1.1108
B3	0.02	1.0	10.91	73.51	73.50	0.0018	- 1.0509
C3	0.1	1.0	5.42	90.68	90.65	0.0151	-1.1063
D3	0.3	1.0	3.41	106.16	106.09	0.0607	-1.0996
E3	0.5	1.0	2.72	112.95	112.85	0.1190	-1.0943
F3	2.0	1.0	1.49	135.06	134.74	0.7292	-1.0832

Table 20.2. Comparison of computed and measured values of the wave speed c and wave length λ of bamboo waves at the flow points #1 through #9 of the flow chart in figure 16.1 for up-flow. The first column shows the experiment number #. The speed $W(1)$ of the undisturbed interface is also listed for convenience. The computations are for the most unstable mode. The values listed in the parentheses are those computed when V_0, $a = a_e$ are prescribed.

	Experiments		Computations		
#	λ (cm)	c (cm/sec)	λ (cm)	c(cm/sec)	$W(1)$(cm/sec)
1	1.21	57.70	0.82 (0.79)	79.84 (52.02)	83.69 (55.64)
2	1.31	43.28	0.92 (0.96)	80.21 (42.54)	83.73 (46.24)
3	1.41	35.65	1.22 (1.22)	79.76 (33.51)	82.91 (37.26)
4	1.22	27.81	1.65 (1.33)	77.00 (29.42)	79.94 (32.66)
5	1.374	19.16	1.56 (1.25)	58.91 (17.94)	62.05 (20.75)
6	1.79	22.90	1.23 (1.16)	58.12 (22.17)	61.69 (25.35)
7	1.34	28.22	1.05 (1.02)	54.80 (26.68)	58.49 (29.95)
8	1.17	31.06	0.95 (0.87)	50.85 (31.33)	54.58 (34.53)
9	0.90	36.25	0.86 (0.79)	49.38 (35.71)	53.01 (39.12)

We turn next to analysis of the equation governing the evolution of the kinetic energy E of the most unstable disturbance of PCAF. This may be written as

$$\dot{E} = I - D + B1 + B2 + B3 \tag{20.2}$$

where $I - D$ is the Reynolds stress minus the dissipation (and we normalize with $D = 1$), $B1$ is a boundary term associated with interfacial tension, $B2$ is a boundary term associated with the viscosity difference which we call interfacial friction and $B3$ is a boundary term in the energy supply which is proportional to gravity times the jump in density. All the terms in (20.2) are derived and explicit formulas for them are given in section VII.4. It has been shown in section VI.2 that terms of the energy equation should be computed on the most unstable disturbance to help diagnose the mechanism producing instability. Table 20.3 shows that bamboo waves are driven by interfacial friction, the other terms in the energy equation are stabilizing with an ever so slight destabilizing effect from interfacial tension in experiments 4 and 5.

Table 20.3 (a). Energy equation (20.2) evaluated on the most unstable mode at each of 9 labeled points in figure 16.1. The first column shows the experiment number #. Positive $\dot{E}$ means that PCAF is unstable.

#	$\dot{E}$	$I-D$	$B1$	$B2$	$B3$
1	0.1836	-0.7932	-0.01419	0.9944	- 0.00359
2	0.2142	-0.7680	-0.01080	0.9983	- 0.00544
3	0.2759	-0.7081	0	0.9950	-0.01123
4	0.3480	-0.6332	0.01423	0.9873	- 0.02057
5	0.3837	-0.5869	0.00830	0.9800	- 0.01781
6	0.3133	-0.6485	-0.00321	0.9754	- 0.01062
7	0.2640	-0.6996	-0.00968	0.9802	- 0.00700
8	0.2244	-0.7405	-0.01329	0.9833	- 0.00514
9	0.1829	-0.7881	-0.01554	0.9903	-0.00378

Table 20.3(b). The values listed here are those computed when V_o, $a = a_e$ are prescribed. The flows are all unstable to interfacial friction $B2 > 0$ leading to bamboo waves.

#	$\dot{E}$	$I-D$	$B1$	$B2$	$B3$
1	0.1552	-0.8214	-0.01659	0.9961	- 0.00284
2	0.2117	-0.7511	-0.01409	0.9818	- 0.00497
3	0.3352	-0.6131	-0.00851	0.9659	- 0.00915
4	0.4186	-0.5502	-0.00451	0.9848	- 0.01150
5	0.3491	-0.6323	-0.01078	1.0013	- 0.00918
6	0.2463	-0.7165	-0.01238	0.9828	- 0.00772
7	0.1805	-0.7826	-0.01422	0.9829	- 0.00558
8	0.1402	-0.8303	-0.01603	0.9902	- 0.00371
9	0.1203	-0.8487	-0.01584	0.9876	- 0.00271

Table 20.4. Energy budget (20.2) evaluated on the most unstable mode at labeled points in figure 16.1. $\hat{\lambda}$ is the dimensional wave length based on the most unstable mode.

Points	$\dot{E}$	I-D	B_1	B_2	B_3	$\hat{\lambda}$(cm)	Flow region in the chart
A1	0.2450	-0.8982	0.4145	0.7341	-0.0060	1.5519	O/W dispersion
B1	0.2852	-0.8791	0.2085	0.9702	-0.0148	1.7295	oil bubble
C1	0.3052	-0.8610	0.1362	1.0485	-0.0189	1.7833	oil bubble
D1	0.4116	-0.6853	0.0388	1.0816	- 0.0237	1.8341	BW/slug
E1	0.4264	-0.5353	0.0011	0.9798	-0.0141	1.4624	oil sticks on the pipe wall
F1	0.0032	-0.9954	-0.0021	0.9978	- 0.0001	0.2342	oil sticks on the pipe wall
A2	0.2291	-0.9038	0.4840	0.6532	- 0.0053	1.5268	O/W dispersion
B2	0.2719	-0.8862	0.2387	0.9331	-0.0143	1.7116	oil bubble
C2	0.3424	-0.8050	0.0909	1.0806	-0.0243	1.9188	oil slug
D2	0.4566	-0.5449	0.0167	1.0068	-0.0220	1.7690	BW
E2	0.2814	-0.6791	-0.0120	0.9799	-0.0075	1.1267	BW
F2	0.0552	-0.9261	-0.0115	0.9968	-0.0001	0.2604	oil sticks on the pipe wall
A3	0.0742	-0.9778	1.1728	-0.1204	-0.0012	1.0009	O/W dispersion
B3	0.1353	-0.9530	0.7341	0.3618	-0.0084	1.3061	O/W dispersion
C3	0.2721	-0.8208	0.1095	1.0203	-0.0373	2.1226	oil bubble
D3	0.2983	-0.7031	0.0221	1.0022	-0.0231	1.6892	oil slug
E3	0.2457	-0.7436	0.0030	0.9980	- 0.0119	1.2353	BW
F3	0.1371	-0.8506	-0.0158	1.0049	- 0.0014	0.6096	DBW

Table 20.5. Specification of parameters used to calculate theoretical values from the linear theory of stability at the labeled flow points in the flow chart of figure 16.3.

	Experiment		Basic flow (18.7), (18.9) with the same V_o, V_w				
	V_o(ft/sec)	V_w (ft/sec)	a	W_0(cm/sec)	W(1)(cm/sec)	$\mathbb{R}_g(R1)$	F
1	0.105	0.40	1.59	10.70	10.82	0.5965	- 1.0356
2	0.70	0.40	1.34	37.33	37.37	1.0010	-1.0094
3	1.0	0.40	1.27	49.38	49.36	1.1638	-0.9964
4	4.0	0.40	1.09	145.74	144.54	1.8480	-0.8288

Photographs of the nine cases considered in tables 20.2 and 20.3 are shown in figures 20.1-9. The close-up photograph is taken from the TV monitor and shows an actual frame used in constructing the average wave length and wave speed. The still photograph from a distance shows both the up-flow bamboo waves and down-flow disturbed core-annular flow with corkscrew waves.

Terms of the energy budget for the other labeled points in the up-flow chart of figure 16.1 are displayed in table 20.4. In addition, we have given the value of the wave length $\hat{\lambda} = 2\pi/\hat{\alpha}$ of the fastest growing wave. It is shown in section VI.1 that the length of the slugs and bubbles which are observed correlate well with $\hat{\lambda}/2$. We would not get this kind of agreement here, because the slugs are stretched and stringy due to buoyancy and shear (see figures 15.2, 20.4).

There is agreement between theory and experiment with regard to selection of flow type in a sense which needs explanation. In all the entries the Reynolds stress term $I - D$ is stabilizing. In section VI.2, it is shown that when the flow is unstable ($\dot{E} > 0$) and $I - D > 0$ is destabilizing, with all other terms negative, there is correlation with transitions to w/o (water into oil) emulsions. We did not encounter this situation when evaluating the energy budget and, correspondingly, no w/o dispersions are observed. In every case where slugs, bubbles and o/w dispersions are observed, PCAF is unstable both to interfacial tension $B1$ and interfacial friction $B3$; the other terms are stabilizing. The size of the bubbles in the o/w dispersions is much smaller than $\hat{\lambda}/2$ and is probably associated with the breakup of large bubbles in shear flow.

The energy budgets for the cases of bamboo waves (BW) and disturbed bamboo waves (DBW) that are observed are all alike. The instability producing these waves is due to a strongly positive $B2$, with all other effects stabilizing or at least only weakly destabilizing. Interfacial friction is driving these interfacial waves.

VII.20(a)(ii) Down-flow. For down-flow, we reverse the sign of g. We are going to compare theory and experiment at four arbitrarily chosen points on the down-flow chart in figure 16.4. The flows at points in the region DCAF are essentially PCAF as the theory predicts (see table 20.6) The point #4 in the region DBW is unstable to interfacial friction. The point #1 in the region of slugs is unstable also to interfacial tension. This gives perfect agreement at all four points. The neutral curves for experiments labeled as # 1 and #3 of down flow are shown in figure 20.10-12. The dashed straight lines correspond to the experimental points and it is obvious that # 1 is unstable to capillary instability (modified by shear) and # 3 is linearly stable.

Table 20.6. Energy budget (20.2) evaluated on the most unstable mode at labeled points in figure 16.3. $\hat{\lambda}$ is the dimensional wave length based on the most unstable mode.

Points	$\dot{E}$	$I-D$	B_1	B_2	B_3	$\hat{\lambda}$ (cm)	Flow region in the chart
1	0.1690	-0.8327	0.0035	1.2220	- 0.2238	13.4382	slugs
2	stable						DCAF
3	stable						DCAF
4	0.0854	-0.9105	-0.0126	1.0085	0.0002	0.2887	DBW

Table 20.7. Specification of parameters used to calculate theoretical values from the linear theory of stability at the labeled flow points in the flow chart of figure 16.1.

	Experiment			Basic flow (18.7), (18.9) with the same V_o, V_w			
	V_o(ft/sec)	V_w (ft/sec)	a	W_0(cm/sec)	W(1)(cm/sec)	$\mathbb{R}_g(R1)$	F
1	1.06	0.55	1.31	55.89	55.64	1.0592	-1.0510
2	0.76	0.55	1.42	46.44	46.24	0.8396	-1.0491
3	0.46	0.55	1.64	37.43	37.26	0.5452	-1.0530
4	0.31	0.55	1.88	32.80	32.66	0.3633	-1.0589
5	0.31	0.27	1.50	20.91	20.75	0.7156	-1.0422
6	0.46	0.27	1.35	25.53	25.35	0.9697	-1.0382
7	0.61	0.27	1.27	30.15	29.95	1.1605	-1.0377
8	0.76	0.27	1.22	34.75	34.53	1.3077	-1.0394
9	0.91	0.27	1.19	39.37	39.12	1.4242	-1.0428

VII.20(b) For Fixed Values of V_o and a

We remarked that the discrepancy between the theoretical and measured values of c in table 20.2 was due to the sweeping out of trapped water between the crests of bamboo waves leading to a reduced water fraction. To check this idea, we decided to compute stability results when V_o is prescribed as in the experiment and $a = a_e$ is given by experiment. This idea is completely consistent with results shown in the parentheses listed in table 20.2. The energy decomposition shown in table 20.3(b) is also completely consistent with the idea that bamboo waves are produced by interfacial friction.

Table 20.8. Specification of parameters used to calculate theoretical values from the linear theory of stability at the labeled flow points in the flow chart of figure 16.1 (pure oil).

	Experiment			Basic flow (18.7), (18.9) with the same V_o, V_w			
	V_o(ft/sec)	V_w (ft/sec)	a	W_0(cm/sec)	$W(1)$(cm/sec)	$\mathbb{R}_g(R_1)$	F
1	1.06	0.55	1.31	55.69	55.53	0.2043	-1.0577
2	0.76	0.55	1.42	45.67	45.52	0.1620	-1.0587
3	0.46	0.55	1.64	37.43	37.27	0.1052	-1.0668
4	0.31	0.55	1.88	32.83	32.69	0.0701	-1.0760
5	0.31	0.27	1.50	20.90	20.79	0.1381	-1.0541
6	0.46	0.27	1.35	25.41	25.30	0.1871	-1.0469
7	0.61	0.27	1.27	30.00	29.88	0.2239	-1.0443
8	0.76	0.27	1.22	34.59	34.46	0.2523	-1.0444
9	0.91	0.27	1.19	39.33	39.19	0.2748	-1.0464

We carried out a similar computation, with V_o, a_e prescribed, but with parameters appropriate to pure oil as given in (12.2). We get satisfactory agreement again between theory and experiments even though the oil used in the experiments is not pure oil. In fact many results are insensitive to small changes of viscosity when the water fraction is fixed because the viscosity of the oil is so much larger.

(a)

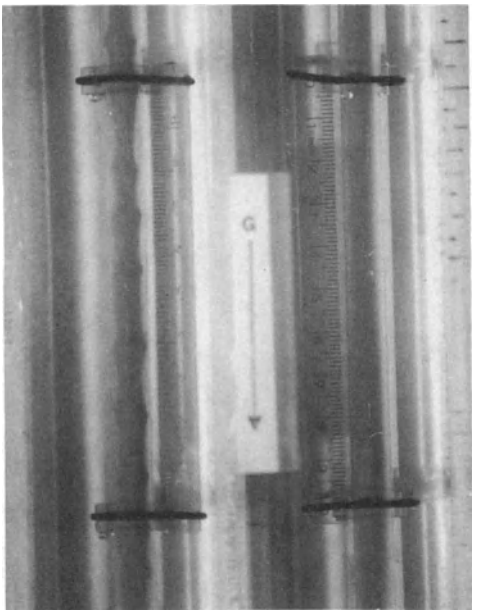

(b)

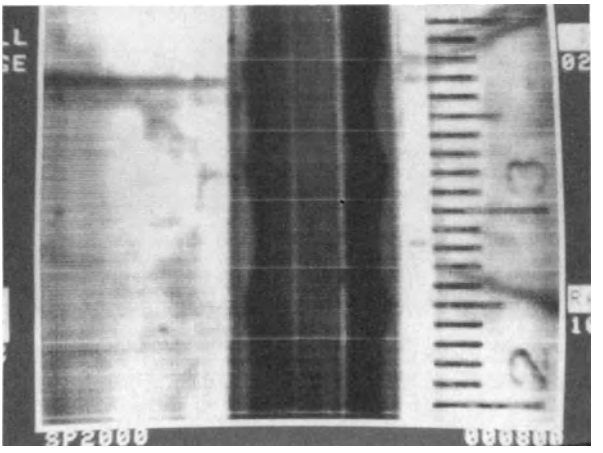

Fig. 20.1(a-b). [Bai, Chen and Joseph, 1992] Flow condition at #1 (V_w, V_o) = (0.55, 1.06) ft/sec of figure 16.1. Upper photo (a) Bamboo waves in up-flow on the left, and disturbed core annular flow with immature bamboo and corkscrew waves in down flow on the right. Lower photo (b) Bamboo waves on the video monitor.

(a)

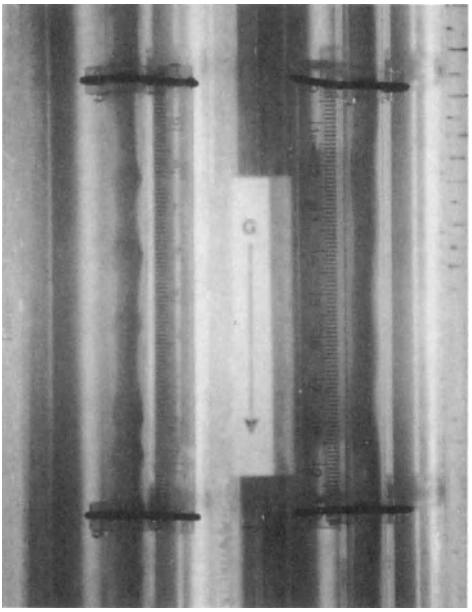

(b)

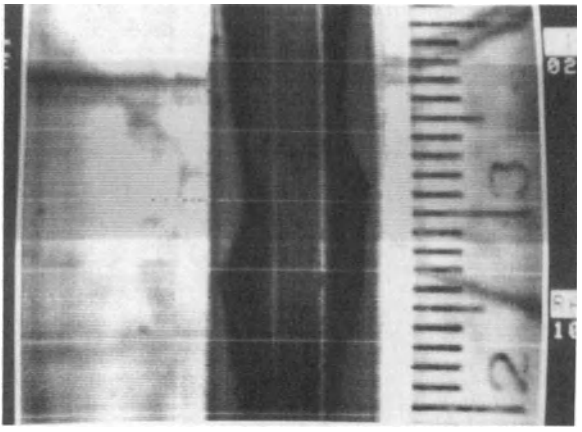

Fig. 20.2(a-b). [Bai, Chen and Joseph, 1992] Flow condition at #2 (V_w, V_o) = (0.55, 0.76) ft/sec of figure 16.1. Upper photo (a) Bamboo waves in up-flow on the left, and DCAF with mild corkscrew waves on the right. Lower photo (b) Bamboo waves on the video monitor.

(a)

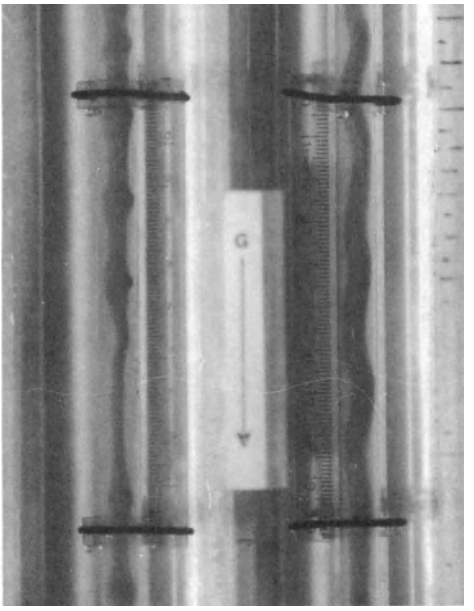

(b)

Fig. 20.3(a-b). [Bai, Chen and Joseph, 1992] Flow condition at #3 (V_w, V_o) = (0.55, 0.46) ft/sec of figure 16.1. Upper photo (a) Bamboo waves arising from shear stabilization of slugs in up flow on the left, corkscrew waves on the right. Lower photo (b) Bamboo waves on the video monitor.

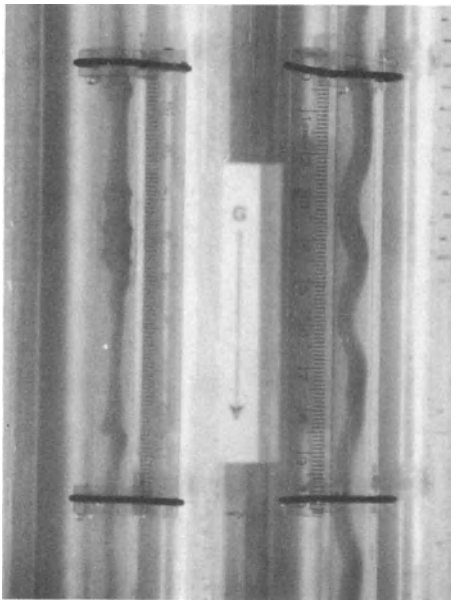

(a)

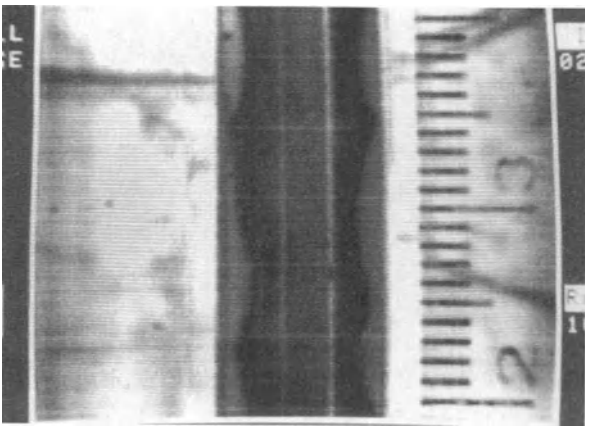

(b)

Fig. 20.4(a-b). [Bai, Chen and Joseph, 1992] Flow condition at #4 (V_w, V_o) = (0.55, 0.35) ft/sec of figure 16.1. The flows are like those in figure 20.3, but exaggerated.

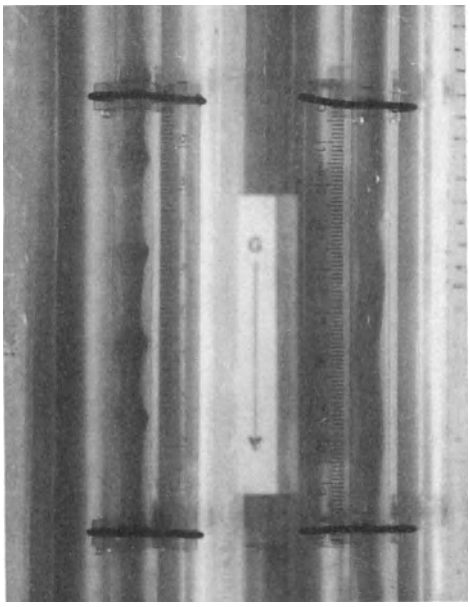

(a)

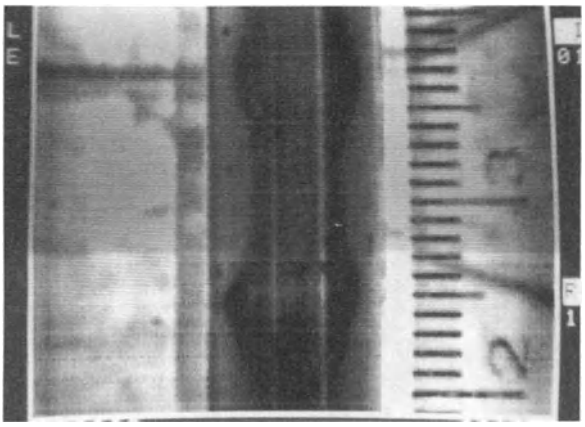

(b)

Fig. 20.5(a-b). [Bai, Chen and Joseph, 1992] Flow condition at #5 (V_w, V_o) = (0.27, 0.31) ft/sec of figure 16.1. Upper photo (a) Bamboo waves in up-flow on the left, DCAF with corkscrew waves on the right. Lower photo (b) Bamboo waves on the video monitor.

(a)

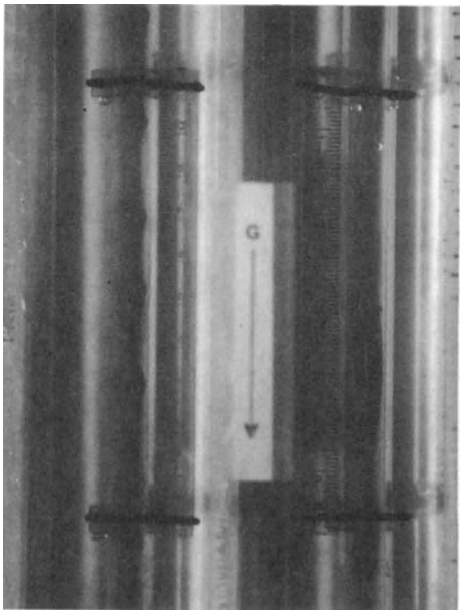

(b)

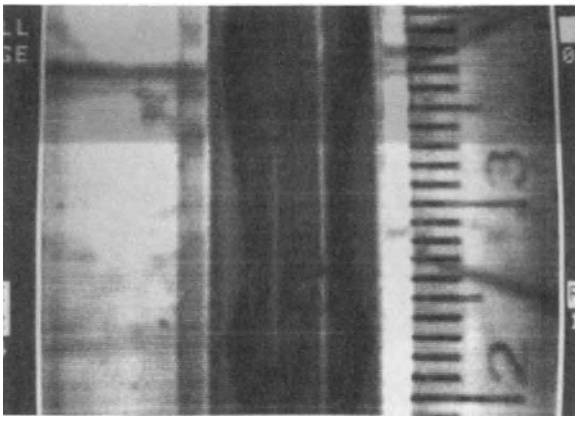

Fig. 20.6(a-b). [Bai, Chen and Joseph, 1992] Flow condition at #6 (V_w, V_o) = (0.27, 0.46) ft/sec of figure 16.1. Upper photo (a) Bamboo waves in up-flow on the left, corkscrew waves on the right. Lower photo (b) Bamboo waves on the video monitor.

(a)

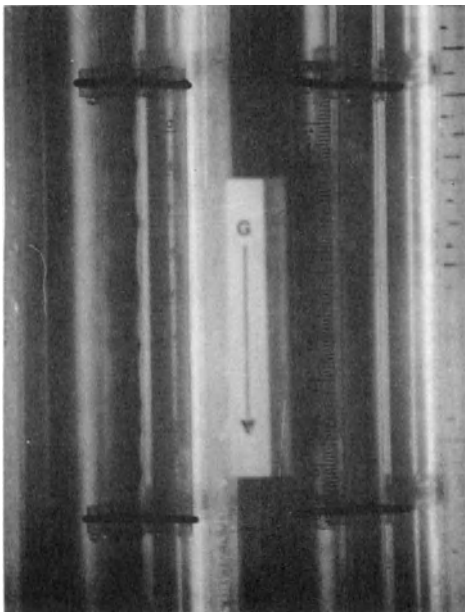

(b)

Fig. 20.7(a-b). [Bai, Chen and Joseph, 1992] Flow condition at #7 (V_w, V_o) = (0.27, 0.61) ft/sec of figure 16.1. Upper photo (a) Bamboo waves in up-flow on the left, mildly disturbed core annular flow in down-flow on the right. Lower photo (b) Bamboo waves on the video monitor.

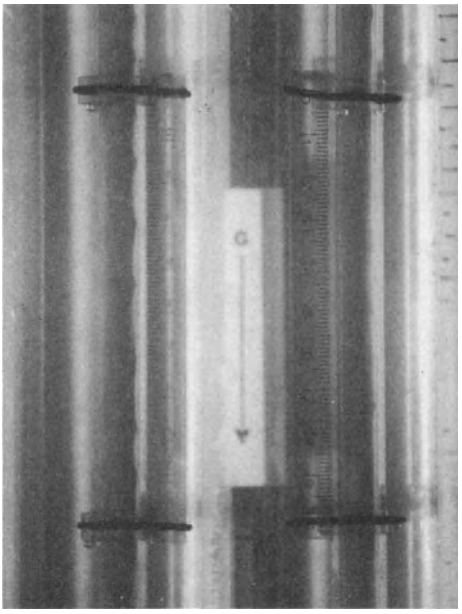

(a)

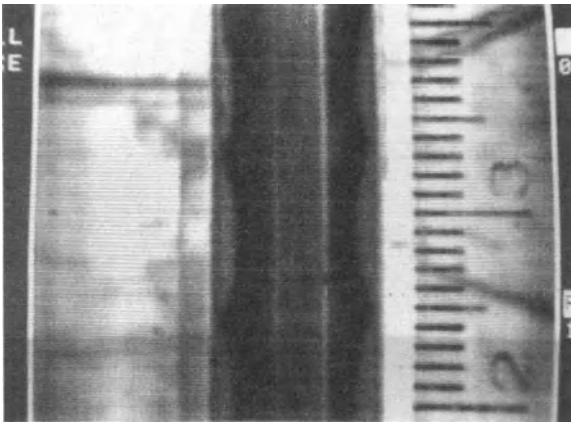

(b)

Fig. 20.8(a-b). [Bai, Chen and Joseph, 1992] Flow condition at #8 (V_w, V_o) = (0.27, 0.76) ft/sec of figure 16.1. Upper photo (a) Bamboo waves in up-flow on the left, DCAF with immature bamboo waves on the right. Lower photo (b) Bamboo waves on the video monitor.

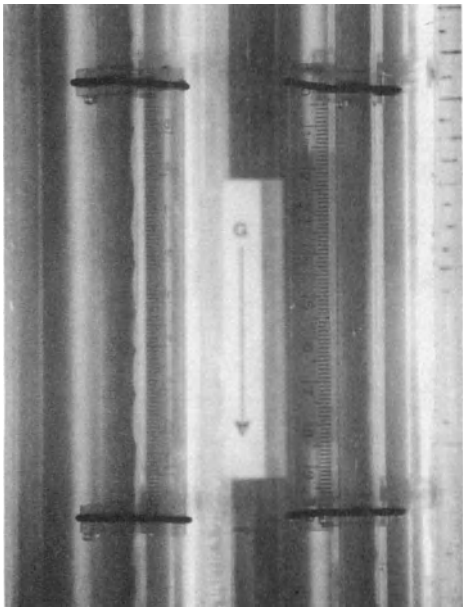

(a)

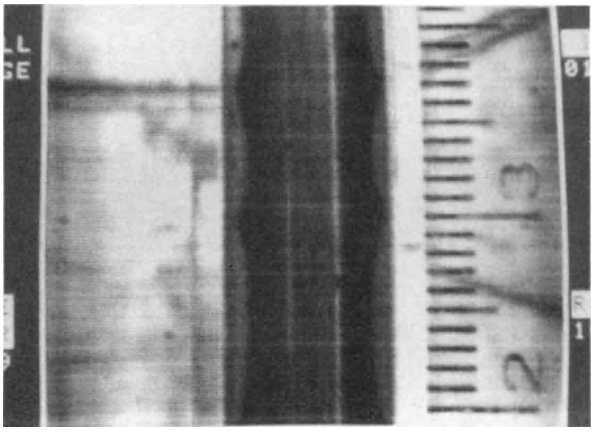

(b)

Fig. 20.9(a-b). [Bai, Chen and Joseph, 1992] Flow condition at #9 (V_w, V_o) = (0.27, 0.91) ft/sec of figure 16.1. Upper photo (a) Bamboo waves in up-flow on the left, DCAF with immature bamboo and corkscrew waves on the right. Lower photo (b) Bamboo waves on the video monitor.

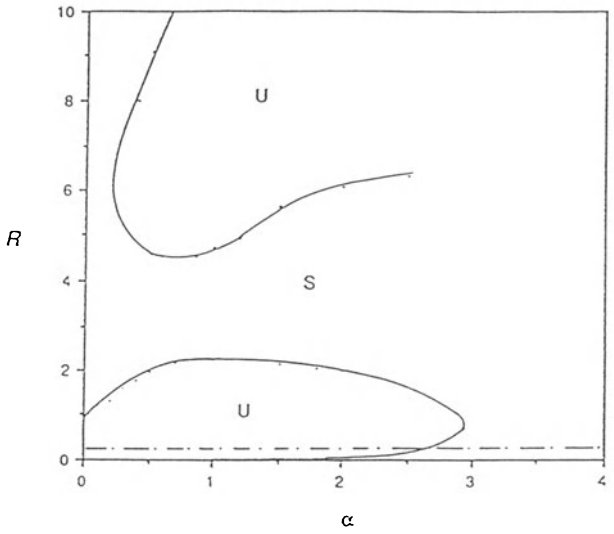

Fig. 20.10. [Bai, Chen and Joseph, 1992] Neutral curves for down-flow experiment labeled # 1.

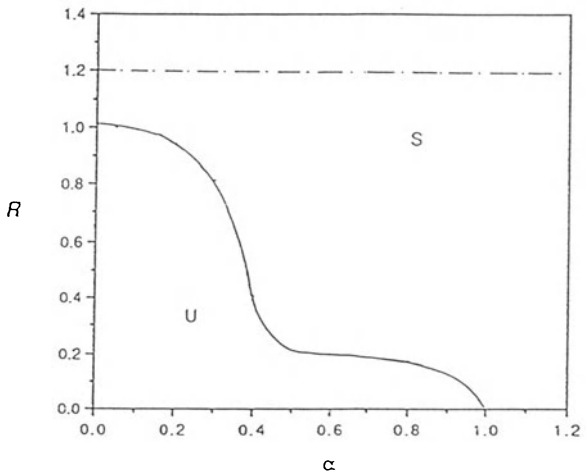

Fig. 20.11. [Bai, Chen and Joseph, 1992] Neutral curves for down-flow experiment labeled # 3. Lower branch.

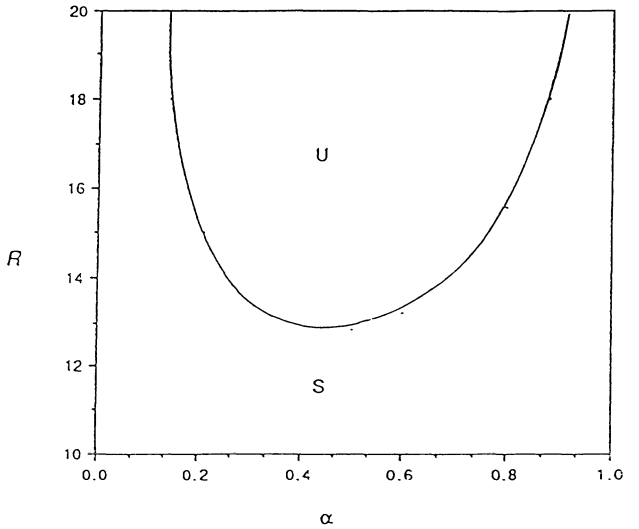

Fig. 20.12. [Bai, Chen and Joseph, 1992] Neutral curves for down-flow experiment labeled # 3. Upper branch.

VII.21 Summary and Discussion

In sections VII.11-20, we reported the results of experiments on water lubricated pipelining of 6.01 poise cylinder oil in a vertical apparatus with up and down-flow. The measurements were compared with theoretical predictions (sections VII.2-10) based a linear stability analysis of the axisymmetric mode in ideal laminar flow (PCAF).

Flow rates for the oil and water, pressure gradients and hold-up ratios for up and down-flow over a wide range of velocities less than 3 ft/sec were recorded.

The oil is buoyed up in water by gravity. In up-flow the pressure gradient and buoyancy are in the same direction. Waves develop in up-flow and the lubrication forces together with the buoyancy tend to stretch wave troughs. In down-flow the pressure gradient and buoyancy are opposed. This compresses the oil column, suppresses bamboo waves, and leads to straight or buckled columns of oil. The differences between up and down-flow are suppressed in fast flow when the pressure gradient dominates buoyancy.

The stretching of oil in up-flow and its compression in down-flow implies that less oil will accumulate in up-flow than in down-flow. It is possible to fluidize hugely long slugs of oil in down-flow. The ratio of the input ratio to the volume ratio is called the hold-up ratio h; h is one in a well-mixed

flow and larger than one in a laminar lubricated flow without gravity. Buoyancy changes this; zero and even negative hold-ups are possible (see figure 18.1).

Different types of flow were observed and located on flow charts in a V_w, V_o plane. The flow types change with the oil flow at a fixed water flow.

First we describe changes in up-flow as the oil flow is increased. For slow oil flow with enough water, oil bubbles will form by capillary instability; if the water flow is fast enough the large bubbles are torn apart, leaving o/w dispersions. When the water flow is slow enough to support capillary bubbles, increasing oil flow will cause the bubbles to connect into longer structures, called slugs, which are like segments of bamboo with bamboo swells connected by long thin bamboo stems. Further increases in the oil flow cause the segments to connect into a definite bamboo train. The stems of the bamboo thicken and the distance between the cells decreases with increasing oil flow. Bamboo waves seem to be imperfect monochromatic waves with a very well defined average length, speed and amplitude. Yet further increases in the oil throughput lead to much thicker and shorter stems and the bamboo crests become very jagged, irregular, and not axisymmetric. These are called disturbed bamboo waves (DBW). BW and DBW are robust regimes of up-flow.

In a region of the up-flow chart where the superficial velocity of water is low compared with that of oil, the oil sticks to the wall. This is a flow-induced adhesion, and it can be reversed. This flow induced *change of adhesion* results either in blockage with a loss of lubrication or in a three-layer configuration with oil on the outer wall, water in an annulus beneath and oil in the core. Our apparatus could not withstand the pressures needed to produce larger rates of oil than the ones in which oil sticks to the wall. We believe that water in oil emulsions would arise if the oil flow could be increased.

Now we describe down-flow after the flow turns around at the upper end of the pipe, first for high oil flows with DBW in up-flow and then as the oil flow is decreased. When DBW are observed at high oil flow rates in up-flow, they are also observed in down flow. However, the wave lengths of DBW are shorter in down-flow than in up-flow because of stretching in up-flow and compression in down flow. When the oil input is decreased, the waves disappear leading to disturbed core annular flow. This flow can be almost a perfect core annular flow. At higher flow rates of oil, it is disturbed by immature bamboo waves, at lower flow rates by rotating buckled structures which we call corkscrews. At yet lower oil inputs the oil column will break into trains of long slugs and then into trains of large bubbles which seem tied together by wake forces.

For a fixed flow of oil, there is an optimum flow rate of water for which the pressure gradient is a minimum. The minimum pressure gradient is in a region of bamboo waves in up-flow and in a region of disturbed core annular flow in down-flow. The pressure gradients in down-flow are less than in up-

flow. This shows that disturbed core annular flow is more efficient than bamboo waves.

We compared ideal lubrication theory with experiments and obtained some measures of energy efficiency. To calculate the dynamic pressure gradient, it is necessary to take account of the composite water-oil density. The properties of the flow can be evaluated on the PCAF solution when two parameters, such as the flow inputs of oil and water, are prescribed. A theoretical formula for the hold-up is derived and evaluated. We calculate the water fraction for the PCAF flow which maximizes the oil flow when the pressure gradient is fixed.

We compared measured pressure gradients with different ideal pressure gradients in five cases of up-flow and five cases of down flow. The pressure gradient required to move a given flow rate of 6.01 poise oil is on the average 200 times greater when there is no water lubrication. This improvement is roughly one-third of the ratio $\mu_o/\mu_w = 1/m$. We can guess that drag reductions of the order $\mu_o/3\mu_w$ are possible in a vertical pipeline. For a viscous crude, water lubrication would reduce the pressure gradient by a factor of more than 10,000.

We compared measured pressure gradients with the gradients required to move water alone with a flow rate equal to the measured total flow (oil plus water). For laminar flow, the measured gradients in lubricated flow are roughly three times larger than the theoretical gradients required for laminar flow of water alone. However, at the given flow rates, water would be turbulent and the ratio of measured to theoretical values would be much closer to one.

The measured values of the pressure gradient and water fraction were compared with theoretical values computed for PCAF with the same oil and water input. The computed water fraction expressed by the radius ratio $a = R_2/R_1$ is larger than the mean values $a_e = R_2/R_{1e}$ measured in the experiments. This reduction in the water fraction in the experiments is due to the transport of water trapped between bamboo waves, flushing out water, leaving a smaller water fraction behind. The computed pressure gradients in up flow at low oil flow rates is much smaller than the measured values. This comparison must be interpreted in the light of the fact that under these conditions the main force of transport is buoyancy. At higher oil flow rates, the ratio of computed to measured pressure gradients is of order one, between 0.1 and 0.5.

Theoretical and measured values of the water fraction and pressure gradients in down-flow are very close for the disturbed core-annular flows. These are practically optimally efficient, with pressure gradient reductions of the same value as PCAF with the same water fraction. This indicates that DCAF is only a slight perturbation of PCAF.

We compared measured values of the speed and wave length of bamboo waves with two different theoretical values computed from the linear theory of stability. In the first comparison we compared all flows with the same

oil and water input, the same V_o and V_w, as in our experiments. In the second comparison we compared all flows with the same oil input and water fraction, the same V_o and a, where a was put equal to the measured value for that V_o. The second comparison was introduced to validate the following conclusion: the wave on a very viscous oil, which basically must travel with nearly uniform velocity (see figure 18.1), must be very nearly a standing wave, convected with the flow. At 6.01 poise, it is too viscous to support fast wave propagation. In every case, the computed wave speed c of the most unstable disturbance was nearly the same as the speed W of the oil core in the basic PCAF.

The average wave length of bamboo waves is slightly larger than the wave length of the most unstable disturbance of a $PCAF_1$, with the same V_o and V_w and also of the $PCAF_2$, with the same V_o and a as in the experiments. Nonlinear effects are responsible for this discrepancy.

There is a larger discrepancy between the measured and theoretical wave speeds for PCAF, with theoretical speeds up to three times faster. We attribute this discrepancy to a systematic difference $a - a_e > 0$ between the experiments and $PCAF_1$. The wave speed must be greater for flows with more water because the oil core with superficial oil velocity V_o has to rise faster when a is larger. Since the wave is convected with the oil, a comparison of computation with one a with another computation or experiment with another will give rise to a systematic discrepancy of the observed type. In fact this systematic discrepancy disappears when the measured speeds are compared with the ones computed for the $PCAF_2$ which has the same a.

We attempted to correlate the flow types observed in experiments by identifying the source of instability in the energy equation evaluated for the most dangerous disturbance of $PCAF_1$ and $PCAF_2$. For $PCAF_1$ we found that when oil bubbles and slugs occur in water, the instability arises from the boundary through a combination of interfacial tension and interfacial friction. When bamboo waves and disturbed bamboo waves are observed, the destabilizing factor is only interfacial friction. For $PCAF_1$, energy analysis of down-flows yields the same consistent identification of the sources of instability for slug flow and disturbed bamboo waves. In addition, for the two arbitrarily chosen points near the center of the DCAF area, where nearly perfect core-annular flows are actually observed, the linear theory shows $PCAF_1$ to be stable. In sections VI.1-2, it is shown that when oil in water dispersions were observed, instability of PCAF arises from the Reynolds stress in the water, and not from terms at the boundary. We did not observe o/w dispersion in the experiments and no term with a Reynolds stress-induced instability was identified from the theory.

Future work correlating stability calculations with experiments using more viscous and less viscous oils in vertical flow ought to be undertaken. It would be worthwhile to build a robust apparatus in which the pressure gradients needed to create o/w emulsions could be attained. The transition

to o/w emulsions is a practical problem of considerable importance because it leads to a loss of lubrication in the field.

Chapter VIII
Nonlinear Stability of Core-Annular Flow

VIII.1 Introduction

In this chapter, we will discuss nonlinear theories of the Ginzburg-Landau type [Chen and Joseph 1991a] and various long-wave equations [Chen and Joseph 1991b].

Surprisingly, the linear theory of stability performs better than expected for predicting wave lengths, wave speeds and flow types in flows which are far from the perfect core-annular flow which the linear theory is supposed to perturb only slightly (chapter VII). However, there are some

situations for which the linear theory fails and it is of interest here to see what understanding can be achieved from nonlinear theory. For instancce, an effort is made here to correlate the 'bamboo' waves, shown in plate V.1.2 to the weakly nonlinear analysis, but it is found that these waves cannot be obtained from this theory.

The analysis of sections VIII.1 - VIII.9 applies to situations in which there is a threshold for instability; this means cases in which stable PCAF (perfect core-annular flow) is possible and the neutral curves are separated as in figures 5.1 - 5.2. For these cases, we apply an amplitude equation which allows for slow modulations of wavy flow in space and time. The amplitude evolution equation has now come to be known as the Ginzburg-Landau equation.[1] As discussed in section IV.8(b), there is more than one way of deriving the Ginzburg-Landau equation, and depending on the assumptions made, the Landau coefficient turns out to be different. For instance, the stability analysis can be performed with the pressure gradient fixed, or with the combined volume flux fixed. Both are treated for the plane flow in chapter IV where it is shown that the sign of the Landau constant computed both ways can have opposite signs. The volume flux is chosen fixed for the pipe flow in sections VIII.1-9. Another place where we have to make a decision is in the calculation of the second-order correction to the mean flow. The method adopted here is that of section IV.8 (b), and an alternative way is that of Blennerhassett [1980]. Thus, the analysis can be carried out in a variety of ways, and the final Landau constant is numerically different depending on the path that leads to it. We have to choose the path which we feel is the best description of our experimental procedure.

There are regimes of flow which give rise to separated neutral curves for which the Ginzburg-Landau equation may be applied. There are, however, even more regimes in which PCAF is not possible and analytical approaches to the nonlinear problem seem to be unknown. The neutral curves shown in figures 1.8 and 1.12 of section VI.1 and figure 8.4 of section VII.8 where the upper and the lower branches have merged to form left and right branches, will not allow for bifurcation analysis. Unfortunately, the case $m \ll 1$ which is typical of applications in which the oil is very viscous is one of these cases (cf. section VI.3).

Amplitude equations are derived under restricted conditions. Once derived, they take on a life of their own and may be applied in all sorts of situations for which they were never intended. For example, the Ginzburg-Landau equation presumably applies only to small-amplitude waves which modulate a monochromatic wave of wavelength $2\pi/\alpha_c$ where α_c is the critical wavenumber at the nose of the neutral curve. A modulated wave solv-

[1] Our 'Ginzburg-Landau' equation actually follows from the work of Newell [1974] and Stewartson and Stuart [1971] who extended the work of Newell and Whitehead [1969] and Segel [1969] to the unsteady case in which the marginally stable eigenvalue at criticality is purely imaginary, as in Hopf bifurcation. Ginzburg and Landau [1950] wrote down, but did not derive, a differential amplitude equation with slow modulation for the theory of superconductivity.

ing the Ginzburg-Landau equation (3.12) has a slowly varying amplitude $A(\xi,\tau)$, $\xi = \epsilon(x - c_g t)$, $\tau = \epsilon^2 t$ (see (3.3)), where ϵ (given by (3.1)) is small and determines the bandwidth of excited waves centered on the wavelength $2\pi/\alpha_c$ of the monochromatic wave. $A(\xi,\tau)$ is the envelope of amplitudes of this monochromatic wave. The length of the periodic wave solution may be computed from the Ginzburg-Landau equation. It is of interest to see what kinds of effects may be described by solutions lying in the full solution set of Ginzburg-Landau equations. The formation of solitons and chaos are two such effects which have been examined in a qualitative way in the works of Moon, Huerre and Redekopp [1983] and Bretherton and Spiegel [1983]. There are many recent works in which the coefficients of the Ginzburg-Landau equations are selected so as to give apparent agreement between computer simulations and experiments. What we need are the explicit coefficients for the Ginzburg-Landau equation which apply to the experiments. With this information, we may hope to answer the question of "where is the modulation?", and to look for structures which can be described as modulations of monochromatic waves.

In sections VIII.2-9, we compute the coefficients of the Ginzburg-Landau equations for different situations of interest and we make some comparisons with experiments. The singular value decomposition method is used to compute the coefficients of the amplitude equation and normal forms. This is described in section VIII.4. Our comparison of Ginzburg-Landau theory with experiments is limited by the fact that the theory applies to a small set of situations in which there are stable flows. Even in these cases, we see no evidence of modulation, so that our calculations are rather more in the way of an application of Ginzburg-Landau equations to the bifurcation of nonlinear monochromatic waves than to any kind of modulation of these waves. In this restricted application, we do see some agreement between the weakly nonlinear theory and the experiments. In the problem of water-lubricated pipelining, we have obtained many useful results from the linearized theory of stability but only limited success with the nonlinear theories.

In sections VIII.10-17, we present some of the weakly nonlinear long-wave equations applicable to core-annular flows. We show that lubrication theory sometimes fails to capture the destabilizing effect of the inertia of the core or of the annulus, particularly when the outer lubricating layer is not thin enough or when the viscosity ratio is small. However, there is a place for theories in which the waves are long with respect to the gap width, but not necessarily long with respect to the inner core radius, and lubrication theory is one way to tackle this situation. These aspects are summarized in section VIII.17.

VIII.2 Nonlinear Evolution of Axisymmetric Disturbances

Two immiscible fluids are flowing inside a pipe of radius R_2. The interface between the two fluids is cylindrical at $r = R_1$. Fluid 1 is located in the core and fluid 2 in the annulus. We are interested in the stability of this core-annular flow.

There are five independent controlling parameters: a, m, ζ_2, J^* and $\mathbb{R}_1$ for horizontal core-annular flow and six for vertical core-annular flow: a, m, ζ_2, J^*, $\mathbb{R}_g$ and F (see below for definitions). Although a multi-parameter bifurcation analysis is possible, we restrict our attention here to the simplest case in which a single parameter is varied for fixed values of the other five. We prefer a parameter that we can control in our experiments once the working fluids and the pipe are chosen. For horizontal flow, the Reynolds number $\mathbb{R}_1$ defined below can be used as the bifurcation parameter. For vertical flow, a good dynamical parameter is the forcing ratio

$$F = \frac{f}{\rho_1 g},$$

where

$$f = -\frac{d\hat{P}_1}{dx} = -\frac{d\hat{P}_2}{dx}$$

is the applied pressure gradient. For the concentric basic flows considered here, f is the same constant in both the core and the annulus. In this chapter, we shall use a different equivalent set of parameters incorporating both horizontal and vertical flows.

We shall choose the magnitude of the center-line velocity $|W(0)|$ as the velocity scale, R_1 the length scale and $R_1/|W(0)|$ the time scale. We define the following parameters:

$$a = \frac{R_2}{R_1}$$

$$(m_1, m_2) = (1, m) = \left(1, \frac{\mu_2}{\mu_1}\right),$$

$$(\zeta_1, \zeta_2) = (1, \zeta) = \left(1, \frac{\rho_2}{\rho_1}\right),$$

$$\mathbb{R} \overset{\text{def}}{=} \mathbb{R}_1 = \frac{|W(0)|\rho_1 R_1}{\mu_1}, \qquad \text{Reynolds number},$$

$$\mathbb{R}_2 = \frac{|W(0)|\rho_2 R_1}{\mu_2} = \frac{\zeta_2}{m}\mathbb{R},$$

$$\mathbb{R}_g = \frac{gR_2^3}{\nu_1^2} = \frac{gR_1^3 a^3}{\nu_1^2}, \qquad \text{Reynolds number based on gravity},$$

(This is different from $\mathbb{R}_g = \frac{gR_1^3}{\nu_1^2}$ used in sections VII.2 - VII.10.)

$$J^* = \frac{TR_2}{\rho_1 \nu_1^2},$$

$$K = \frac{f + \rho_1 g}{f + \rho_2 g} \qquad \text{(ratio of driving forces in core and annulus)}$$

where T is the interfacial tension. The cylindrical polar coordinate system is chosen in such a manner that gravity is acting in the positive x-direction. We choose the Reynolds number $\mathbb{R}$ as our bifurcation parameter. When the density is matched, $K = 1$ and gravity does not enter into the problem. $\mathbb{R}_g$ and J^* are known constants once the working fluids and pipe radius are given, independent of flow conditions.

The basic flow in dimensional form is given in (2.2) of section VII.2. The velocity at the centerline of the pipe is

$$W(0) = \frac{f + \rho_1 g}{4\mu_1} R_1^2 + \frac{f + \rho_2 g}{4\mu_2} \left(R_2^2 - R_1^2\right) + \frac{[\![\rho]\!] g R_1^2}{2\mu_2} \ln \frac{R_2}{R_1}.$$

Using this relation, we can show that the parameter K can be expressed in terms of $\mathbb{R}_g$ and $\mathbb{R}$. To do this, we need to distinguish between the cases $W(0) > 0$ and $W(0) < 0$. For convenience, we will loosely refer to flows with $W(0) > 0$ as down-flows and $W(0) < 0$ as up-flows, although mixed flows are also possible for both cases, depending on the magnitude of $W(0)$ or f, as shown in chapter VII. Then the dimensionless basic flow can be expressed as:

(a) down-flow: $W(0) > 0$

$$K(\mathbb{R}) = \frac{4ma^3\mathbb{R} + [\![\zeta]\!]\mathbb{R}_g(a^2 - 1 - 2l\ln a)}{4ma^3\mathbb{R} - [\![\zeta]\!]\mathbb{R}_g(m + 2l\ln a)}, \tag{2.1a}$$

$$W_1(r, \mathbb{R}) = 1 - \frac{mK(\mathbb{R})r^2}{mK(\mathbb{R}) + a^2 - 1 + 2(K(\mathbb{R}) - 1)l\ln a}, \quad 0 \le r \le 1 \tag{2.1b}$$

$$W_2(r, \mathbb{R}) = \frac{a^2 - r^2 - 2(K(\mathbb{R}) - 1)l\ln\frac{r}{a}}{mK(\mathbb{R}) + a^2 - 1 + 2(K(\mathbb{R}) - 1)l\ln a}. \quad 1 \le r \le a \tag{2.1c}$$

(b) Up-flow: $W(0) < 0$

$$K(\mathbb{R}) = \frac{4ma^3\mathbb{R} - [\![\zeta]\!]\mathbb{R}_g(a^2 - 1 - 2l\ln a)}{4ma^3\mathbb{R} + [\![\zeta]\!]\mathbb{R}_g(m + 2l\ln a)} \tag{2.2a}$$

$$W_1(r, \mathbb{R}) = -1 + \frac{mK(\mathbb{R})r^2}{mK(\mathbb{R}) + a^2 - 1 + 2(K(\mathbb{R}) - 1)l\ln a}, \quad 0 \le r \le 1 \tag{2.2b}$$

$$W_2(r, \mathbb{R}) = -\frac{a^2 - r^2 - 2(K(\mathbb{R}) - 1)l\ln\frac{r}{a}}{mK(\mathbb{R}) + a^2 - 1 + 2(K(\mathbb{R}) - 1)l\ln a}. \quad 1 \le r \le a \tag{2.2c}$$

In the above formulas, the jump $[\![\cdot]\!]$ is defined as

$$[\![\cdot]\!] = (\cdot)_1 - (\cdot)_2.$$

It can be seen from these expressions that the up-flow velocity is formally the negative of the down-flow velocity except that the parameter $K(\mathbb{R})$ is different. However, both down-flow and up-flow can be analyzed using the velocity profile (2.1), with $\mathbb{R}_g > 0$ for down-flows and $\mathbb{R}_g < 0$ for up-flows since any up-flow can be obtained from a down-flow by simply reversing the direction of gravity. The basic flow (2.1) depends on the Reynolds number $\mathbb{R}$ through the parameter $K(\mathbb{R})$.

The perfect core-annular flow (2.1) can be realized if the controlling parameters fall in a certain range. Experiments in a vertical pipe with parameters in this range were described in chapter VII. It is also possible to realize the concentric core-annular flow in a horizontal pipe if the densities of oil and water are matched. The experiment 2 of CGH (see figure V.1.1) called 'oil in water concentric', can be regarded as an example of perfect core-annular flow in a horizontal pipe.

Numerical experiments using linear theory have indicated that for our range of parameters in horizontal flows, and for some vertical flows, it may be sufficient to consider axisymmetric disturbances (cf. chapter VII). Therefore, the analysis here is restricted to them. Nevertheless, nonaxisymmetric waves arise in practice. The photograph of 'corkscrew' waves exhibited in figure 1.3 of chapter V is a good example. These corkscrew waves may result from the instabilities due to finite nonaxisymmetric disturbances.

For axisymmetric disturbances, the disturbance velocity is of the form $\mathbf{u} = (u, 0, w)$ in the cylindrical coordinates (r, θ, x) and $\frac{\partial(\cdot)}{\partial\theta} = 0$.

The full nonlinear evolution equations for $\mathbf{u}$ in dimensionless form are

$$\frac{1}{r}\frac{\partial}{\partial r}(ru) + \frac{\partial w}{\partial x} = 0, \tag{2.3a}$$

$$\frac{\partial u}{\partial t} + W\frac{\partial u}{\partial x} + u\frac{\partial u}{\partial r} + w\frac{\partial u}{\partial x} = -\frac{\partial p}{\partial r} + \frac{1}{\mathbb{R}_l}\left[\nabla^2 u - \frac{u}{r^2}\right], \tag{2.3b}$$

$$\frac{\partial w}{\partial t} + W\frac{\partial w}{\partial x} + W'u + u\frac{\partial w}{\partial r} + w\frac{\partial w}{\partial x} = -\frac{\partial p}{\partial x} + \frac{1}{\mathbb{R}_l}\nabla^2 w \tag{2.3c}$$

where

$$\nabla^2 f = \frac{1}{r}\frac{\partial}{\partial r}\left(r\frac{\partial f}{\partial r}\right) + \frac{\partial^2 f}{\partial x^2}.$$

W is the basic flow and p is the perturbation pressure. These equations hold both in the core, $l = 1$ when $0 \le r \le 1 + \delta(x,t)$, and in the annulus, $l = 2$ when $1 + \delta(x,t) \le r \le a$. $\delta(x,t)$ is the dimensionless deviation of the interface from the $r = 1$. The primes denote derivatives with respect to the coordinate r. On the pipe wall $r = a$, we have the no-slip condition

$$u = w = 0, \tag{2.4}$$

and at the center of the pipe, $r = 0, u, w, p$ are bounded.

At the interface, $r = 1 + \delta(x,t)$, we have the kinematic condition

$$u = \frac{\partial \delta}{\partial t} + (W_1 + w_1)\frac{\partial \delta}{\partial x} = \frac{\partial \delta}{\partial t} + (W_2 + w_2)\frac{\partial \delta}{\partial x}, \tag{2.5}$$

and the continuity of velocity

$$[\![u]\!]_\delta = [\![W + w]\!]_\delta = 0 \tag{2.6}$$

where the subscript δ refers to the deformed interface $r = 1 + \delta(x,t)$.

The shear stress and normal stress balances on the interface are

$$[\![m\{(1-\delta_x^2)(W' + u_x + w_r) + 2\delta_x(u_r - w_x)\}]\!]_\delta = 0 \tag{2.7}$$

$$\begin{aligned} -[\![\zeta p]\!]_\delta + \frac{2}{\mathbb{R}_1(1+\delta_x^2)}[\![m\{u_r - \delta_x(W' + u_x + w_r) + \delta_x^2 w_x\}]\!]_\delta \\ = \frac{J^*}{a\mathbb{R}_1^2}\left\{\frac{\delta_{xx}}{(1+\delta_x^2)^{3/2}} - \frac{1}{(1+\delta)(1+\delta_x^2)^{1/2}} + 1\right\}. \end{aligned} \tag{2.8}$$

where, the subscripts r and x refer to differentiations with respect to r and x, respectively.

To simplify these equations further, we can introduce a perturbation stream function ψ in each region:

$$u = -\frac{\psi_x}{r}, \qquad w = \frac{\psi_r}{r}.$$

Then the field equations can be reduced to a single equation for the stream function ψ by eliminating the pressure p :

$$\begin{aligned} (L\psi)_t - \left(W'' - \frac{W'}{r}\right)\psi_x + \left(W + \frac{1}{r}\psi_r\right)(L\psi)_x \\ -\frac{1}{r}\psi_x(L\psi)_r + \frac{2}{r^2}\psi_x L\psi = \frac{1}{\mathbb{R}_l}L^2\psi \end{aligned} \tag{2.9}$$

where the operator L is defined as

$$L = \frac{\partial^2}{\partial r^2} - \frac{1}{r}\frac{\partial}{\partial r} + \frac{\partial^2}{\partial x^2}.$$

$$\text{At } r = a: \qquad \psi = \psi_r = 0. \tag{2.10}$$

$$\text{At } r = 0: \qquad \psi = \psi_r = 0. \tag{2.11}$$

All the interface conditions can be expressed in terms of the perturbation stream function ψ, resulting in a system of differential equations for $\psi_1(r,x,t)$, $\psi_2(r,x,t)$ and $\delta(x,t)$.

To study weakly nonlinear stability, we expand the interfacial conditions around the unperturbed interface $r = 1$ and truncate the Taylor series

at order $O(\delta^3)$. For this purpose we notice that from the linear theory, we have

$$u \sim w \sim \delta. \tag{2.12}$$

The resulting interface conditions up to the third order can be summarized as:
Kinematic condition:

$$L_{i1}(\psi_l, \delta) = Q_{i1}(\psi_l, \delta) + C_{i1}(\psi_l, \delta), \tag{2.13a}$$

Continuity of velocity:

$$[\![L_{i2}(\psi)]\!] = Q_{i2}(\psi_1, \psi_2, \delta) + C_{i2}(\psi_1, \psi_2, \delta), \tag{2.13b}$$

$$[\![L_{i3}(\psi, \delta)]\!] = Q_{i3}(\psi_1, \psi_2, \delta) + C_{i3}(\psi_1, \psi_2, \delta), \tag{2.13c}$$

Shear stress balance:

$$[\![mL_{i4}(\psi, \delta)]\!] = Q_{i4}(\psi_1, \psi_2, \delta) + C_{i4}(\psi_1, \psi_2, \delta), \tag{2.13d}$$

Normal stress balance:

$$[\![L_{i5}(\psi, \delta)]\!] - \frac{J^*}{a\mathbb{R}_1^2}(\delta_{xxx} + \delta_x) = Q_{i5}(\psi_1, \psi_2, \delta) + C_{i5}(\psi_1, \psi_2, \delta). \tag{2.13e}$$

In the above expressions, the jump $[\![(\cdot)]\!]$ without subscript δ refers to the jump evaluated at the undeformed interface $r = 1$ and all the quantities are evaluated at $r = 1$ as well. The symbols L, Q, C refer to linear, quadratic and cubic differential operators respectively. The subscripts i indicate that all these operators are defined on the interface $r = 1$ only.

These interfacial operators are listed below [Chen 1990].

$$L_{i1}(\psi_l, \delta) = \delta_t + W(1)\delta_x + \psi_x,$$

$$Q_{i1}(\psi_l, \delta) = -\left\{W'(1)\delta\delta_x + \delta_x\psi_r + \delta(\psi_{rx} - \psi_x)\right\},$$

$$C_{i1}(\psi_l, \delta) = -\left\{\frac{1}{2}W''(1)\delta^2\delta_x + \delta\delta_x(\psi_{rr} - \psi_r) + \delta^2\left(\frac{1}{2}\psi_{rrx} - \psi_{rx} + \psi_x\right)\right\};$$

$$L_{i2}(\psi) = \psi_x,$$

$$Q_{i2}(\psi_1, \psi_2, \delta) = -\delta[\![\psi_{rx}]\!],$$

$$C_{i2}(\psi_1, \psi_2, \delta) = -\frac{1}{2}\delta^2[\![\psi_{rrx}]\!];$$

$$L_{i3}(\psi, \delta) = W'(1)\delta + \psi_r,$$

$$Q_{i3}(\psi_1,\psi_2,\delta) = -\frac{1}{2}\delta^2[\![W''(1)]\!] - \delta[\![\psi_{rr}-\psi_r]\!],$$

$$C_{i3}(\psi_1,\psi_2,\delta) = -\frac{1}{6}\delta^3[\![W'''(1)]\!] - \delta^2[\![\frac{1}{2}\psi_{rrr}-\psi_{rr}+\psi_r]\!],$$

$$L_{i4}(\psi,\delta) = \psi_{rr}-\psi_r-\psi_{xx}+W''(1)\delta,$$

$$\begin{aligned} Q_{i4}(\psi_1,\psi_2,\delta) = -\Big[\!\Big[m\Big\{&\frac{1}{2}\delta^2 W'''(1)+\delta(\psi_{rrr}-\psi_{rr}+\psi_r-\psi_{rxx})\Big] \\ &+2\delta_x(-2\psi_{rx}+\psi_x)\Big\}\Big], \end{aligned}$$

$$\begin{aligned} C_{i4}(\psi_1,\psi_2,\delta) = -\Big[\!\Big[m\Big\{&\frac{1}{6}\delta^3 W''''(1)-\delta\delta_x^2 W''(1) \\ &+\delta^2\left(\frac{1}{2}\psi_{rrrr}-\frac{1}{2}\psi_{rrr}+\psi_{rr}-\psi_r\right. \\ &\left.-\frac{1}{2}\psi_{rrxx}\right) \\ &-\delta_x^2(\psi_{rr}-\psi_r-\psi_{xx})+2\delta\delta_x(-2\psi_{rrx}+\psi_{rx}-\psi_x)\Big\}\Big], \end{aligned}$$

$$\begin{aligned} L_{i5}(\psi,\delta) =&\zeta\left\{\psi_{rt}+W(1)\psi_{rx}-W'(1)\psi_x\right\} \\ &+\frac{m}{\mathbb{R}_1}\left\{-\psi_{rrr}+\psi_{rr}-\psi_r-3\psi_{rxx}+2\psi_{xx}-2\delta_{xx}W'(1)\right\}, \end{aligned}$$

$$\begin{aligned} Q_{i5}(\psi_1,\psi_2\delta) = -\,&[\zeta\{\delta[\psi_{rrt}-\psi_{rt}+W(1)(\psi_{rrx}-\psi_{rx}) \\ &+(W'(1)-W''(1))\psi_x] \\ &-\delta_x[\psi_{xt}+W(1)\psi_{xx}]+[-\psi_x(\psi_{rr}-\psi_r)+\psi_r\psi_{rx}]\} \\ &+\frac{m}{\mathbb{R}_1}\{-\delta[-\psi_{rrrr}+2\psi_{rrr}-3\psi_{rr}+3\psi_r-3\psi_{rrxx} \\ &+5\psi_{rxx}-4\psi_{xx}-2\delta_{xx}W''(1)]-2\delta_{xx}[\psi_{rr}-\psi_r-\psi_{xx}] \\ &+\delta_x[-3\psi_{rrx}+5\psi_{rx}-4\psi_x+3\psi_{xxx}-2\delta_x W''(1)]\Big\}\Big] \\ &+\frac{J^*}{a\mathbb{R}_1}\delta_x(\delta_{xx}-2\delta), \end{aligned}$$

$$
\begin{aligned}
C_{i5}(\psi_1,\psi_2,\delta) = -\Big[\Big[\zeta\Big\{&\delta^2\Big[\frac{1}{2}\psi_{rrrt}-\psi_{rrt}+\psi_{rt}\\
&+W(1)\Big(\frac{1}{2}\psi_{rrrx}-\psi_{rrx}+\psi_{rx}\Big)\\
&+W'(1)\Big(\frac{1}{2}\psi_{rrx}-\psi_x\Big)+W''(1)\Big(-\frac{1}{2}\psi_{rx}+\psi_x\Big)\\
&-\frac{1}{2}W'''(1)\psi_x\Big]\\
&+\delta[\psi_x(-\psi_{rrr}+3\psi_{rr}-3\psi_r)+\psi_r(\psi_{rrx}-\psi_{rx})]\\
&-\delta\delta_x\Big[\psi_{rxt}-\psi_{xt}+W(1)\psi_{rxx}+\Big(W'(1)-W(1)\Big)\psi_{xx}\Big]\\
&+\delta_x\left[\psi_x(\psi_{rx}-\psi_x)-\psi_r\psi_{xx}\right]\}\\
&+\frac{m}{\mathbb{R}_1}\Big\{\delta^2\Big[-\frac{3}{2}\psi_{rrrxx}+4\psi_{rrxx}-7\psi_{rxx}\\
&+6\psi_{xx}-\delta_{xx}W'''(1)\\
&-\frac{1}{2}\psi_{rrrrr}+\frac{3}{2}\psi_{rrrr}+\frac{17}{2}\psi_{rrr}+6\psi_{rr}-6\psi_r\Big]\\
&-2\delta\delta_x[\psi_{rrr}-2\psi_{rr}+2\psi_r-\psi_{rxx}+\psi_{xx}]\\
&+4\delta_x\delta_{xx}\left[2\psi_{rx}-\psi_x\right]+6\delta_x^2\delta_{xx}W'(1)\\
&+\delta\delta_x[-3\psi_{rrrx}+8\psi_{rrx}-14\psi_{rx}+12\psi_x-3\psi_{xxx}\\
&+3\psi_{rxxx}-2\delta_xW''(1)]\\
&+2\delta_x^2\left[-\psi_{rrr}+2\psi_{rr}-2\psi_r+3\psi_{rxx}-2\psi_{xx}\right]\}\Big]\\
&+\frac{J^*}{a\mathbb{R}_1^2}\Big(3\delta_x\delta_{xx}^2-\frac{3}{2}\delta_{xxx}\delta_x^2-\frac{1}{2}\delta_x^3-\delta\delta_x\delta_{xx}+3\delta^2\delta_x\Big).
\end{aligned}
$$

The reduced system (2.9), (2.10), (2.11) and (2.13) is used to derive the amplitude equation.

VIII.3 Multiple Scales, Wave Packets and Ginzburg-Landau Equations

The derivation of the amplitude equation near criticality, using the techniques of multiple scales is now well known and the details can be found in Newell [1974] or Stewartson and Stuart [1971]. We introduce a small perturbation parameter ε, defined by

$$\varepsilon^2 = |d_{1r}(\mathbb{R}-\mathbb{R}_c)|, \tag{3.1}$$

where we have adopted the notation of Stewartson and Stuart [1971] for d_{1r}

$$d_{1r} = \text{Real}\,\{d_1\},$$
$$d_1 = -i\left\{\frac{\partial(\alpha c)}{\partial \mathbb{R}}\right\}(\alpha_c, \mathbb{R}_c). \tag{3.2}$$

Here $-i\alpha c$ is the linear complex growth rate for the linear instability of the basic flow and $(\alpha_c,\ \mathbb{R}_c)$ is the point at the nose of the neutral curve. This critical point is a minimum on the upper branch of the neutral curve and a maximum on the lower branch. Here, 'upper' and 'lower' refer to the bifurcation parameter $\mathbb{R}$, not the wave number α as traditionally assigned. The basic flow loses stability as $\mathbb{R}$ is increased past $\mathbb{R}_c$ on the upper branch. Here, $d_{1r} > 0$ on the upper branch, and $d_{1r} < 0$ on the lower branch. We may consider the first case $d_{1r} > 0$, $\mathbb{R} > \mathbb{R}_c$ and then generalize to cover all the possibilities.

Introduce the slow spatial and time scales

$$\xi = \varepsilon(x - c_g t),$$
$$\tau = \varepsilon^2 t, \tag{3.3}_1$$

where c_g is the group velocity at criticality. These scales are appropriate for a wave packet centered at the nose of the neutral curve and the long time behavior of this wave train is examined in the frame moving with its group velocity c_g. The perturbation stream function ψ and the interface deviation δ are assumed to be slowly varying functions of $\xi,\ \tau$:

$$\psi \to \psi(\xi, \tau; r, x, t),$$
$$\delta \to \delta(\xi, \tau; x, t),$$
$$\frac{\partial}{\partial t} \to \frac{\partial}{\partial t} - \varepsilon c_g \frac{\partial}{\partial \xi} + \varepsilon^2 \frac{\partial}{\partial \tau}, \tag{3.3}_2$$
$$\frac{\partial}{\partial x} \to \frac{\partial}{\partial x} + \varepsilon \frac{\partial}{\partial \xi}.$$

We then define the traveling wave factor of the amplitude

$$E \overset{\text{def}}{=} \exp\left[\mathrm{i}\alpha_c(x - c_r t)\right], \tag{3.4}$$

where c_r is the phase speed at criticality. For a wave packet centered around the critical state, we can assume that ψ and δ have the following form:

$$\psi = \psi_0(r, \xi, \tau) + \{\psi_1(r, \xi, \tau)E + c.c\} + \{\psi_2(r, \xi, \tau)E^2 + c.c\} + h.h.$$

$$\delta = \delta_0(\xi, \tau) + \{\delta_1(\xi, \tau)E + c.c\} + \{\delta_2(\xi, \tau)E^2 + c.c\} + h.h., \tag{3.5}$$

where $c.c$ stands for complex conjugate and $h.h.$ for higher harmonics. We assume that the fundamental wave $\psi_1(r, \xi, \tau)E$ is of order ε and expansions in ε yield

$$\begin{aligned}\psi_1 &= \varepsilon\psi_{11}(r,\xi,\tau) + \varepsilon^2\psi_{12}(r,\xi,\tau) + \epsilon^3\psi_{13}(r,\xi,\tau) + O(\varepsilon^4),\\ \psi_2 &= \varepsilon^2\psi_{22}(r,\xi,\tau) + O(\varepsilon^4),\\ \psi_0 &= \varepsilon^2\psi_{02}(r,\xi,\tau) + O(\varepsilon^4),\end{aligned} \tag{3.6}$$

and similarly,

$$\begin{aligned}\delta_1 &= \varepsilon\delta_{11}(\xi,\tau) + \varepsilon^2\delta_{12}(\xi,\tau) + \varepsilon^3\delta_{13}(\xi,\tau) + O(\varepsilon^4),\\ \delta_2 &= \varepsilon^2\delta_{22}(\xi,\tau) + O(\varepsilon^4),\\ \delta_0 &= \varepsilon^2\delta_{02}(\xi,\tau) + O(\varepsilon^4).\end{aligned} \tag{3.7}$$

Substitute the above expansions into the nonlinear system of equations and identify different orders $(k,n) \Leftrightarrow (E^k, \varepsilon^n)$ to obtain a sequence of differential equations. To obtain the amplitude equation at the lowest order, we only need to consider $k = 0, 1, 2$ exponentials (3.4) and $n = 1, 2, 3$ powers of the small parameter ε.

At order (1, 1) we have the linear eigenvalue problem at criticality and if we denote the eigenfunction at criticality to be $\varphi(r)$, then

$$\begin{aligned}\psi_{11}(r,\xi,\tau) &= A(\xi,\tau)\varphi(r),\\ \delta_{11}(\xi,\tau) &= A(\xi,\tau)\eta_{11},\end{aligned} \tag{3.8}$$

where η_{11} is a constant which can be expressed in terms of the value of φ at $r = 1$ and $A(\xi,\tau)$ is the slowly varying amplitude of the fundamental wave. The equations which arise at orders (0, 2), (2, 2), (1, 2) support separated product solutions of the following type

$$\begin{aligned}\psi_{02}(r,\xi,\tau) &= |A(\xi,\tau)|^2 F(r),\\ \delta_{02}(\xi,\tau) &= |A(\xi,\tau)|^2\eta_{02};\\ \psi_{22}(r,\xi,\tau) &= A^2(\xi,\tau)G(r),\\ \delta_{22}(\xi,\tau) &= A^2(\xi,\tau)\eta_{22};\\ \psi_{12}(r,\xi,\tau) &= \frac{\partial A(\xi,\tau)}{\partial\xi}H(r) + A_2(\xi,\tau)\varphi(r),\\ \delta_{12}(\xi,\tau) &= \frac{\partial A(\xi,\tau)}{\partial\xi}\eta_{12} + A_2(\xi,\tau)\eta_{11}.\end{aligned} \tag{3.9}$$

We need to be careful with the calculation of the (0,2) term, since there is more than one way of handling it, and this influences the final value of the Landau constant. The method employed here is the one discussed around equation IV.(8b.31) for the χ function. An alternative method was used by Blennerhassett [1980]. This concerns the fact that at order (0,2), the kinematic condition at the interface does not give any equation for the interface deviation η_{02}, since the condition contains terms such as η_t and η_x, whereas $\eta_{02} = \eta_{02}(\xi,\tau)$. Thus, we look for another condition to use. Since the oil volume is conserved, we have

$$\int_0^L \int_0^{1+\delta(x,t)} 2\pi r \, dr dx = (\text{volume})_{\text{oil}} \text{ of 1 period}$$

$$= \int_0^L \int_0^1 2\pi r \, dr dx.$$

Therefore,

$$\int_0^L 2\delta(x,t) + \delta^2(x,t) \, dx = 0.$$

Into this equation, we substitute the following:

$$\delta(x,t) = \eta_0(\xi,\tau) + \eta_1(\xi,\tau)E + \bar{\eta}_1(\xi,\tau)E^{-1} + \ldots,$$

$$E = e^{i\alpha_c(x-c_r t)},$$

$$\eta_0(\xi,\tau) = \epsilon^2\eta_{02}(\xi,\tau) + O(\epsilon^4),$$

$$\eta_1(\xi,\tau) = \epsilon\eta_{11}(\xi,\tau) + \epsilon^2\eta_{12}(\xi,\tau) + O(\epsilon^3),$$

$$\eta_2(\xi,\tau) = \epsilon^2\eta_{22}(\xi,\tau) + O(\epsilon^4).$$

Any term multiplied by E, E^{-1}, E^{-2}, ..., will be integrated to zero, and the left-over, to $O(\epsilon^2)$, is

$$L\big(2\eta_{02}(\xi,\tau) + 2\eta_{11}(\xi,\tau)\bar{\eta}_{11}(\xi,\tau)\big) = 0$$

and this yields

$$\eta_{02}(\xi,\tau) = -|\eta_{11}(\xi,\tau)|^2.$$

The other equations for the problem at order (0,2) are:

$$\nabla_0^2\psi_{02} = 2\frac{\zeta_i}{m_i}\alpha_c \mathbb{R}_c \, \mathrm{Im}\Big\{\frac{1}{\mathrm{r}}\psi_{11\mathrm{r}}\nabla_1^2\bar{\psi}_{11} + \frac{1}{\mathrm{r}}\psi_{11}\frac{\partial}{\partial \mathrm{r}}\nabla_1^2\bar{\psi}_{11} + \frac{2}{\mathrm{r}^2}\bar{\psi}_{11}\nabla_1^2\psi_{11}\Big\}$$

where $\nabla_0^2 = \frac{\partial^2}{\partial r^2} - \frac{1}{r}\frac{\partial}{\partial r}$, and at the interface,

$$\eta_{02} = -\eta_{11}\bar{\eta}_{11},$$

$$[\![\psi_{02}]\!] = 2\,\mathrm{Re}\big\{[\![\psi_{11r}]\!]\bar{\eta}_{11}\big\} = 0,$$

$$[\![W'(1)]\!]\eta_{02} + [\![\psi_{02r}]\!] = -[\![W''(1)]\!]\eta_{11}\bar{\eta}_{11} - 2\,\mathrm{Re}\big\{\eta_{11}[\![\bar{\psi}_{11rr} - \bar{\psi}_{11r}]\!]\big\},$$

$$\begin{aligned}[\![m_i(\psi_{02rr} - \psi_{02r} + W''(1)\eta_{02}]\!] &= -[\![m_i\big(W''(1)\eta_{11}\bar{\eta}_{11} \\ &\quad + 2\,\mathrm{Re}\big\{\eta_{11}(\bar{\psi}_{11rrr} - \bar{\psi}_{11rr} + (1-3\alpha_c^2)\bar{\psi}_{11r} + 2\alpha_c^2\bar{\psi}_{11})\big\}\big)]\!],\end{aligned}$$

$$\begin{aligned}&[\![m_i(-\psi_{02rrr} + \psi_{02rr} - \psi_{02r})]\!] \\ &\quad = 2\alpha_c\mathbb{R}_c \,\mathrm{Im}\big\{[\![\zeta_i\big(\bar{\eta}_{11}[(\mathrm{W}(1) - \mathrm{c_r})(\psi_{11\mathrm{r}} - \psi_{11\mathrm{r}}) \\ &\quad + (W'(1) - W''(1) - \alpha_c(W(1) - c_r))\psi_{11}] \\ &\quad + \bar{\psi}_{11}(\psi_{11rr} - \psi_{11r})\big)]\!]\big\} \\ &\quad + 2\alpha_c^2\,\mathrm{Re}\big\{[\![m_i\eta_{11}\big(-\bar{\psi}_{11rrrr} + 2\bar{\psi}_{11rrr} + (3\alpha_c^2 - 2)\bar{\psi}_{11rr} \\ &\quad - 5\alpha_c^2\bar{\psi}_{11r} + (5\alpha_c^2 + 4)\bar{\psi}_{11} + 2(\alpha_c^2 + 1)W''(1)\bar{\eta}_{11}\big)]\!]\big\}.\end{aligned}$$

Then at orders (1, 2) and (1, 3), we have

$$L_1(H, \eta_{12}) = F(\varphi(r), c_g),$$
$$L_1(\psi_{13}, \delta_{13}) = J_1 \frac{\partial A}{\partial \tau} + J_2 \frac{\partial^2 A}{\partial \xi^2} + J_3 A + J_4 |A|^2 A + J_5 \frac{\partial A_2}{\partial \xi} \quad (3.10)$$

where L_1 is the linear Orr-Sommerfeld operator at criticality and $J_i, i = 1, \cdots, 5$ are functions of $\varphi(r)$, $F(r)$, $G(r)$ and $H(r)$. Applying the Fredholm alternative at order (1, 2), we can obtain a formula determining the group velocity c_g. At order (1, 3), the application of the Fredholm alternative yields the Ginzburg-Landau equation governing the amplitude $A(\xi, \tau)$ of the fundamental wave,

$$\frac{\partial A}{\partial \tau} - a_2 \frac{\partial^2 A}{\partial \xi^2} = \frac{d_1}{d_{1r}} A - l|A|^2 A. \quad (3.11)$$

The term $\frac{\partial A_2}{\partial \xi}$ does not appear because its coefficient vanishes when the group velocity c_g is properly expressed using the Fredholm alternative. The complementary part of the solution of the singular problem at order (1, 2) has no effect on the final amplitude equation. The coefficient of the cubic term, l, is called the first Landau constant and it depends on all the lower order solutions. The coefficients a_2 , d_1 and l are complex in general and can be computed using the Fredholm alternative. For the upper branch of the neutral curve $d_{1r} > 0$ and for the lower branch $d_{1r} < 0$. For non-degenerate cases, the real part of a_2 is always positive for both the upper and the lower branch because the growth rate reaches a maximum at the critical point, the nose of the neutral curve ($a_{2r} = 0$ if the neutral curve has a higher order (> 2) contact with $\mathbb{R} = \mathbb{R}_c$).

We may write a uniform form of the Ginzburg-Landau equation, valid for both the upper and lower branch of the neutral curves

$$\frac{\partial A}{\partial \tau} - a_2 \frac{\partial^2 A}{\partial \xi^2} = \mathrm{sgn}(d_{1r})\mathrm{sgn}(\mathbb{R} - \mathbb{R}_c) \frac{d_1}{d_{1r}} A - l|A|^2 A, \quad (3.12)$$

by taking proper account of the various sign possibilities offered by (3.1). Here the parameter $\mathrm{sgn}(d_{1r})\ \mathrm{sgn}(\mathbb{R} - \mathbb{R}_c)$ measures the distance from the bifurcation threshold (linear growth or damping), $\mathrm{sgn}(d_{1r})\ \mathrm{sgn}(\mathbb{R} - \mathbb{R}_c)\ \frac{d_{1i}}{d_{1r}}$ corresponds to the frequency shift due to the linear dispersion, a_{2r}, a_{2i}, l_r, l_i are associated with diffusion($a_{2r} > 0$), dispersion, nonlinear saturation(l_r) and nonlinear renormalization of the frequency respectively.

The Landau constant l depends on the normalization of the eigenvector $\varphi(r)$ of the spectral problem but is independent of the normalization of the adjoint eigenvector. If we use a different normalization for the eigenvector $\varphi(r)$ such that

$$\varphi(r) \to q\varphi(r), \quad A(\xi, \tau) \to qA(\xi, \tau)$$

where q is any non-zero constant, we find, using (3.12), that

$$\frac{\partial A}{\partial \tau} - a_2 \frac{\partial^2 A}{\partial \xi^2} + \operatorname{sgn}(d_{1r})\operatorname{sgn}(\mathbb{R} - \mathbb{R}_c)\frac{d_1}{d_{1r}} A - l|q|^2|A|^2 A. \tag{3.13}$$

The Landau constant will become unique if a well-defined amplitude is introduced. This is especially important when pursuing higher order Landau constants [Joseph and Sattinger 1972; Herbert 1980; Sen and Venkateswarlu 1983]. In the lowest order case, represented by the Ginzburg-Landau equation (3.12), we can simply rescale the amplitude function $A(\xi, \tau)$

$$A(\xi, \tau) \to \frac{A(\xi, \tau)}{|q|\sqrt{|l_r|}} \tag{3.14}$$

where $l = l_r + il_i$, to get a Ginzburg-Landau equation with coefficients independent of q:

$$\frac{\partial A}{\partial \tau} - a_2 \frac{\partial^2 A}{\partial \xi^2} = \operatorname{sgn}(d_{1r})\operatorname{sgn}(\mathbb{R} - \mathbb{R}_c)\frac{d_1}{d_{1r}} A - (\operatorname{sgn}(l_r) + iC_n)|A|^2 A, \tag{3.15}$$

where $C_n = \frac{l_i}{|l_r|}$ is a parameter independent of the normalization condition for $\varphi(r)$.

Another useful rescaled form of (3.13) can be obtained by introducing the following transformations:

$$A(\xi, \tau) = \frac{\hat{A}(\xi, \tau)}{|q|\sqrt{|l_r|}} \exp\left[i \operatorname{sgn}(d_{1r})\operatorname{sgn}(\mathbb{R} - \mathbb{R}_c)\frac{d_{1i}}{d_{1r}}\right],$$

$$\hat{\xi} = \frac{\xi}{\sqrt{|a_{2r}|}}, \qquad C_d = \frac{a_{2i}}{|a_{2r}|}, \qquad C_n = \frac{l_i}{|l_r|}. \tag{3.16}$$

After dropping the roofs, we get

$$\frac{\partial A}{\partial \tau} - (\operatorname{sgn}(a_{2r}) + iC_d)\frac{\partial^2 A}{\partial \xi^2} = \operatorname{sgn}(d_{1r})\operatorname{sgn}(\mathbb{R} - \mathbb{R}_c)A - (\operatorname{sgn}(l_r) + iC_n)|A|^2 A. \tag{3.17}$$

The form (3.17) was first introduced by Moon, Huerre and Redekopp [1983] in their study of transition to chaos in solutions of the Ginzburg-Landau equation. Since $a_{2r} > 0$ we can replace $\operatorname{sgn}(a_{2r})$ by $+1$.

Equation (3.17) can be regarded as the canonical form of the Ginzburg-Landau equation. It admits a traveling wave solution of the form $A(\xi, \tau) = A_0 \exp[i(\beta_0 \xi - \gamma_0 \tau)]$ where A_0, β_0, and γ_0 are all real constants defined in terms of the coefficients of (3.17). The stability of the traveling wave solution was studied by Newell [1974], Stuart and DiPrima [1978] and Moon [1982]. Their analysis provides a unified treatment of the well-known Eckhaus instability and Benjamin-Feir instability, and their results are also framed in terms of the coefficients of (3.17). When the real part of the Landau coefficient, l_r, is positive, there are soliton-like solutions of the Ginzburg-Landau equation which have been discussed by Hocking and Stewartson [1972]. These solutions have been called 'breathers' by Holmes

Color Insert

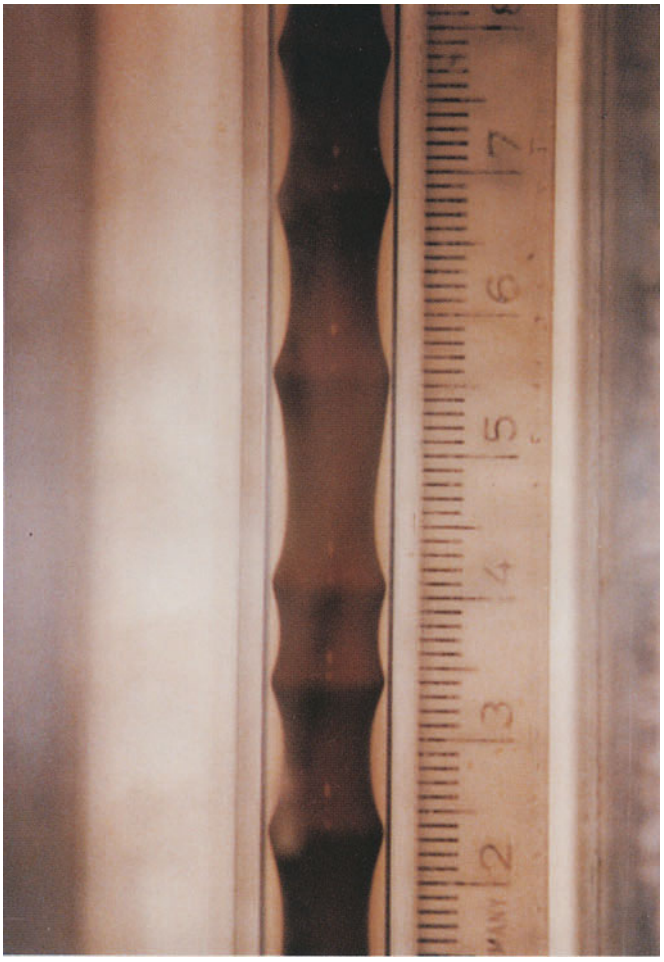

Plate V.1.2. [Bai, Chen and Joseph, 1992] Bamboo waves observed in up-flows of motor oil and water. The oil has a viscosity of 6.01 poise and a density of 0.881 g/cm^3 at room temperature T = 22°C. The volume flow rates are Q_o = 0.11332 GPM, Q_w = 0.05284 GPM.

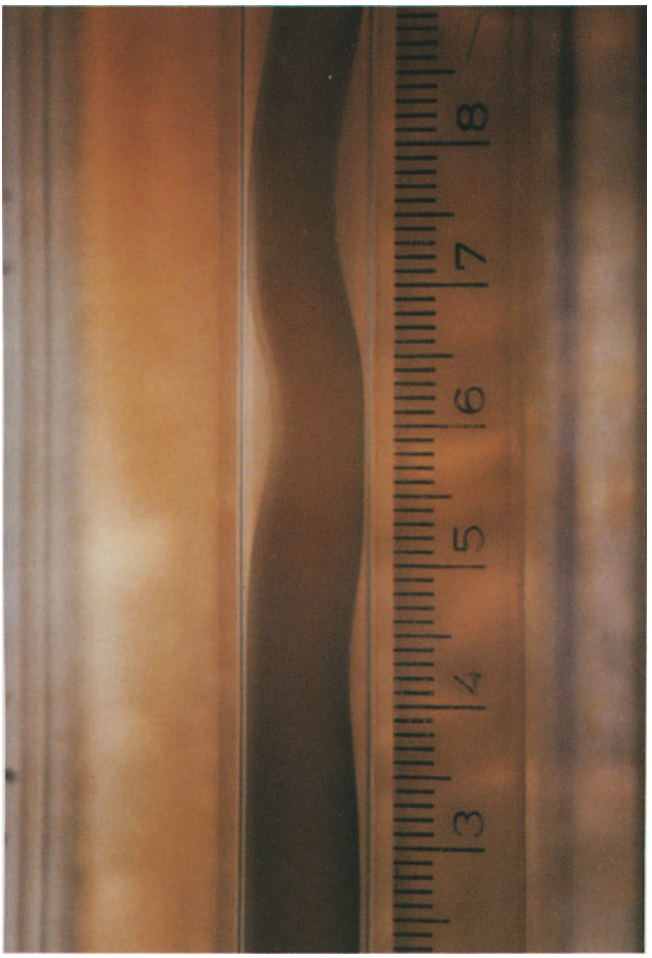

Plate V.1.3. [Bai, Chen and Joseph, 1992] Corkscrew waves observed in downflows of motor oil and water. The oil has a viscosity of 6.01 poise and a density of 0.881 g/cm^3 at room temperature T = 22°C. The volume flow rates are Q_o = 0.08312 GPM, Q_w = 0.05284 GPM.

Plate V.2.3. Core-annular flow of oil lubricated by water in a pipe of diameter 8" and test loop of length 1km at San Tome, Venezuela. The water fraction is approximately 10%. The oil is Zuata. At 30°C, the viscosity is 80,000 mPa.s. This photograph was supplied by INTEVEP, SA.

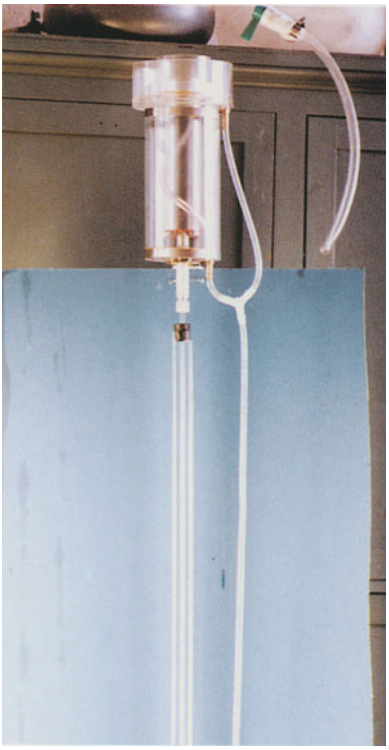

Plate VII.3.1. [Chen, Bai and Joseph, 1990] Free-fall apparatus. The test section of the pipe is surrounded by a square box filled with glycerine to remove the visual distortion created by the circular pipe. The inner radius of the pipe is 0.3175 cm and the pipe is 120 cm long.

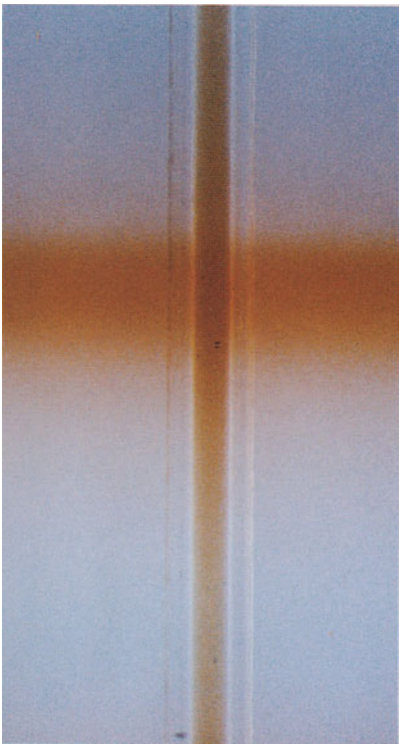

Plate VII.3.2. [Chen, Bai and Joseph, 1990] Stable perfect core-annular flow of SAE 30 oil and glycerine/water mixture. a=1.86, m=0.33, ζ_2=1.4, J^* = 2.26, F = 0, $\mathbb{R}_g$=1.82.

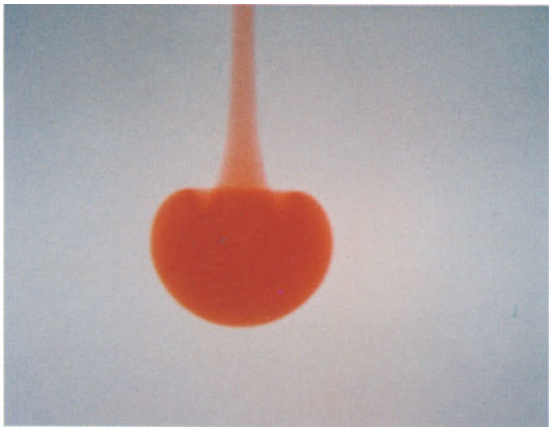

(a)

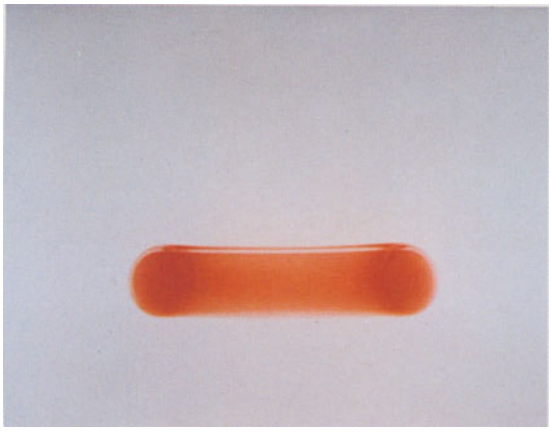

(b)

Plate IX.2.2(a-b). [Kojima, Hinch and Acrivos, 1984, American Institute of Physics] Falling drops of aqueous corn syrup of density 1.329 g/cm^3 and viscosity 3.9 P into aqueous corn syrup of density 1.26 g/cm^3 and viscosity 0.51 P. (a) The low viscosity mixture intrudes into the drop at the trailing edge near the tail. (b) A vortex ring forms. Continued.

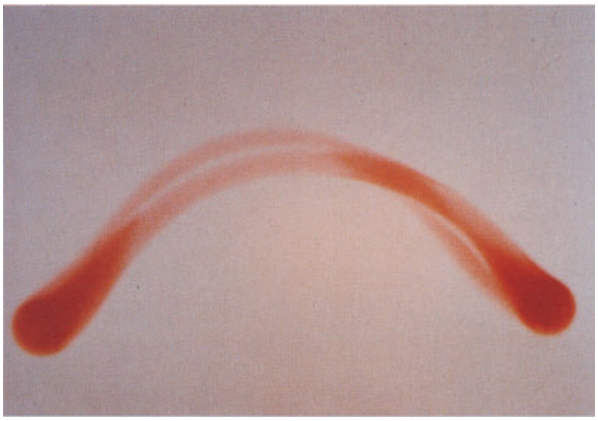

(c)

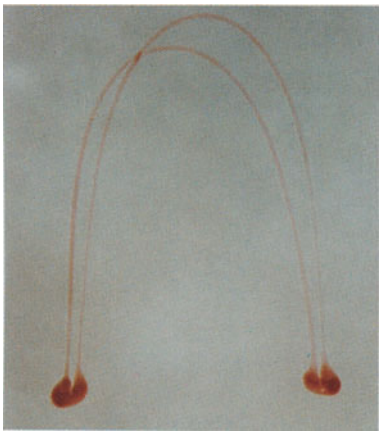

(d)

Plate IX.2.2(c-d). [Kojima, Hinch and Acrivos, 1984, American Institute of Physics] (c) Vortex ring (Rayleigh-Taylor) instability. (d) Cascade of new rings begins to form.

(a)

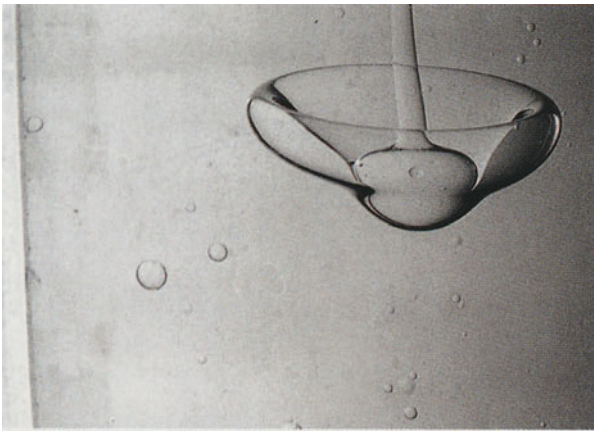

(b)

Plate IX.7.5(a-c). [Baumann, Joseph, Mohr and Renardy, 1992, American Institute of Physics] Failure of poke-through of captured drop of 1000 cS silicone oil in an indented oblate drop of the same silicone oil falling through contaminated safflower oil. (a) The captured drop is sucked strongly into the wake behind the oblate drop. There is a tail drawn out of the captured drop by the motion of safflower oil in the wake which reminds one of the tail behind drops in miscible liquids (cf. figure IX.2.2 (c)). (b) The drops are sucked into strong contact. (c) The captured drop decelerates under the restraining action of the silicone oil membrane on the oblate drop which never breaks.

(c)

Plate IX.7.5(c). Continued.

(a)

Plate IX.7.6(a-d). [Baumann, Joseph, Mohr and Renardy, 1992, American Institute of Physics] Crisco rising in a column of water with surfactant (Alconox). The value of interfacial tension has been reduced from 3.39 dyn/cm to 0.158 dyn/cm by the surfactant. The membrane does not break, despite the low tension. (a) A torus is formed inside the water bag. (b) The water in the torus is dragged out in the wake.

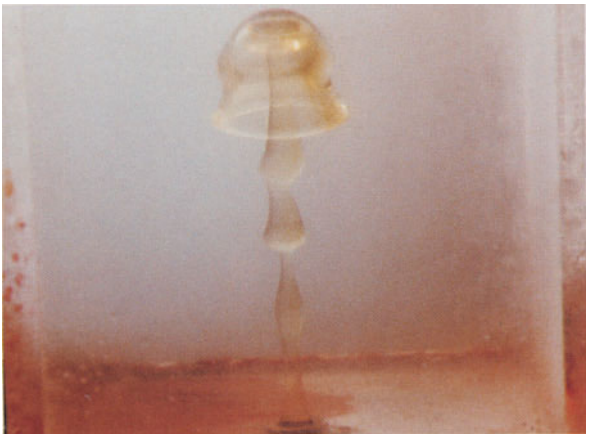

(b)

(c)

Plate IX.7.6(b-c). Continued.

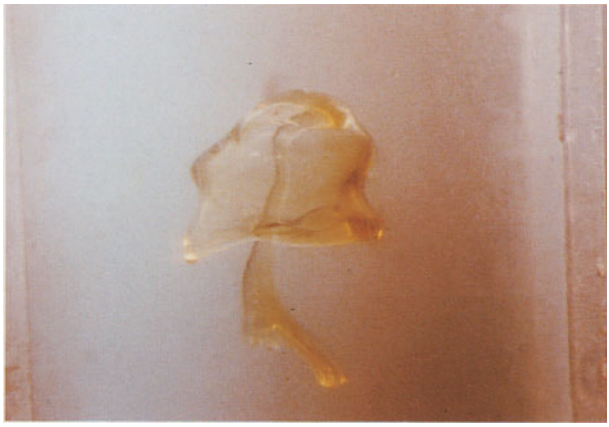

(d)

Plate IX.7.6(d). Continued.

(a) (b)

Plate IX.8.3(a-f). [Baumann, Joseph, Mohr and Renardy, 1992, American Institute of Physics] Ring formation in 1000 cS silicone oil with a surfactant falling in soy bean oil. The surfactant is a trace amount of 97% dye with 3% Rhodamine B base powder. (a) One indented oblate sphere accelerates in the wake of another; (b) they come close. (c) Poke-through: the large ring loses its membrane. (d) The small ring never pokes through; it retains the oblate indented shape. (e) Beginning of the two-lobe instability of the Rayleigh-Taylor type. (f) The instability can be compared with 8.2 (b) where the membrane does not break and with the miscible ring in figure IX.2.2 (d).

(c)

(d)

(e)

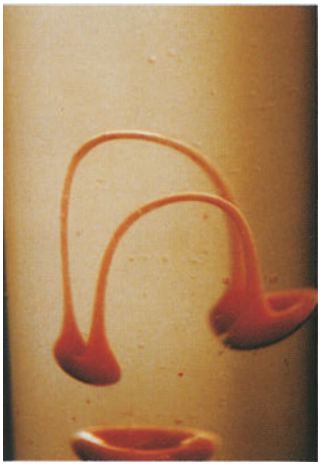

(f)

Plate IX.8.3(c-f). Continued.

Plate IX.8.4. [Baumann, Joseph, Mohr and Renardy, 1992, American Institute of Physics] Vortex ring of 1000 cS silicone oil with trace amounts of surfactant (Igepal) falling in soy bean oil after blow-out.

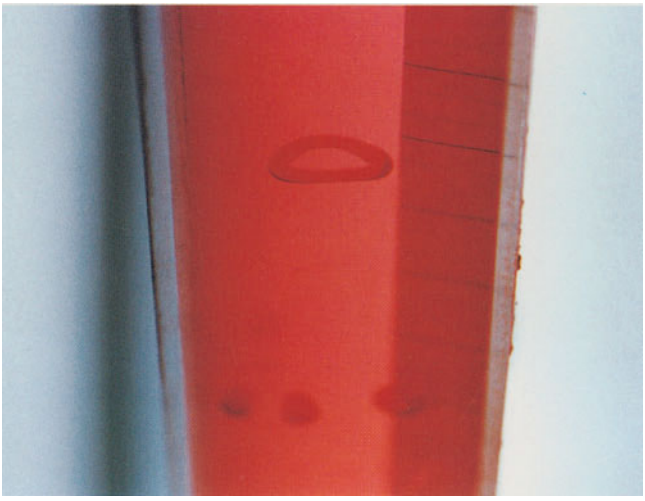

Plate IX.8.5. [Baumann, Joseph, Mohr and Renardy, 1992, American Institute of Physics] Vortex ring of dyed glycerine falling in soy bean oil after blow-out.

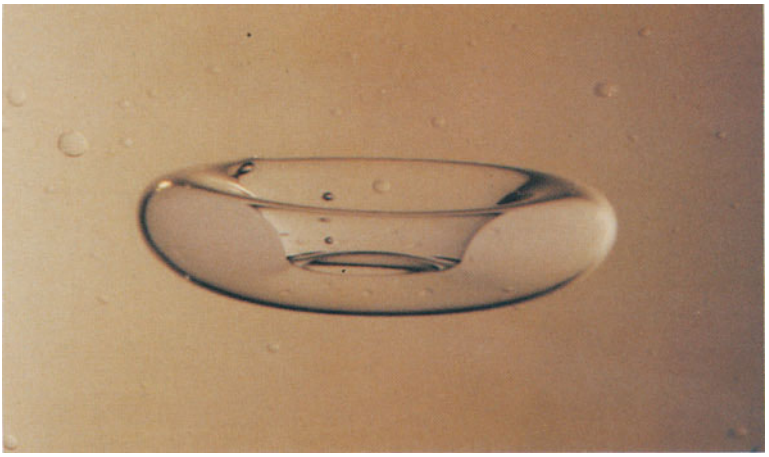

(a)

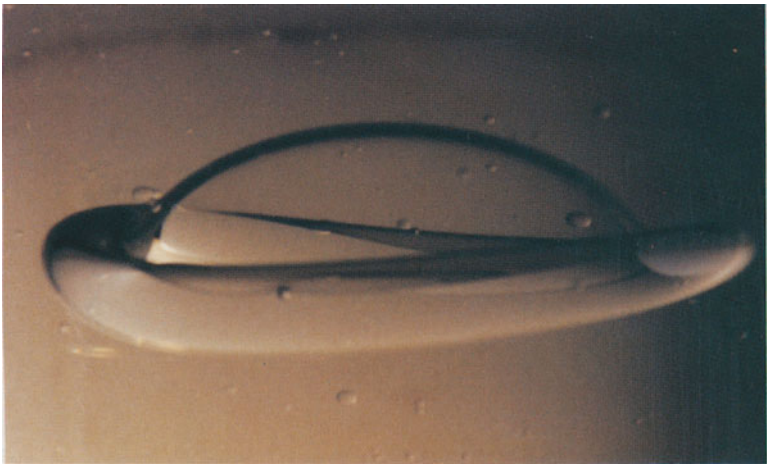

(b)

Plate IX.10.1(a-b). [Baumann, Joseph, Mohr and Renardy, 1992, American Institute of Physics] (a) The center-spanning membrane has ruptured while still at the bottom of this 2ml drop of pure silicone oil. (b) Here, the membrane has bulged up through the center of the 5ml, pure silicone drop, forming a large dome.

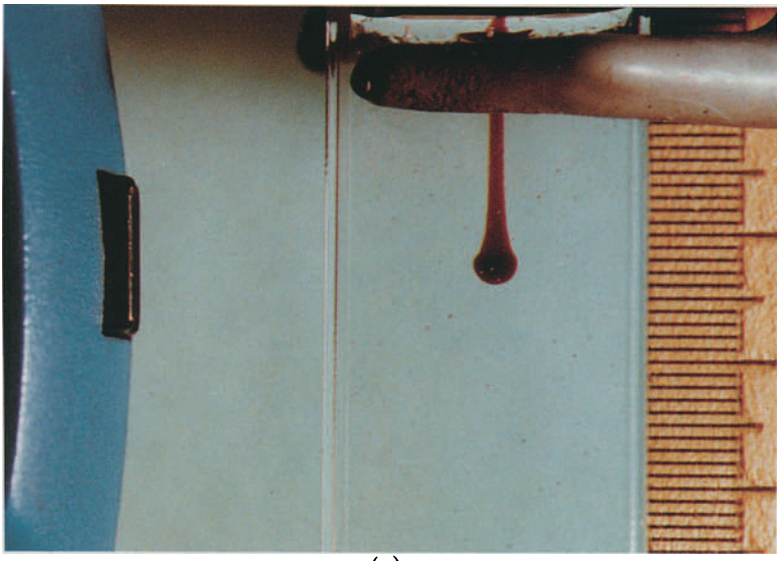

(a)

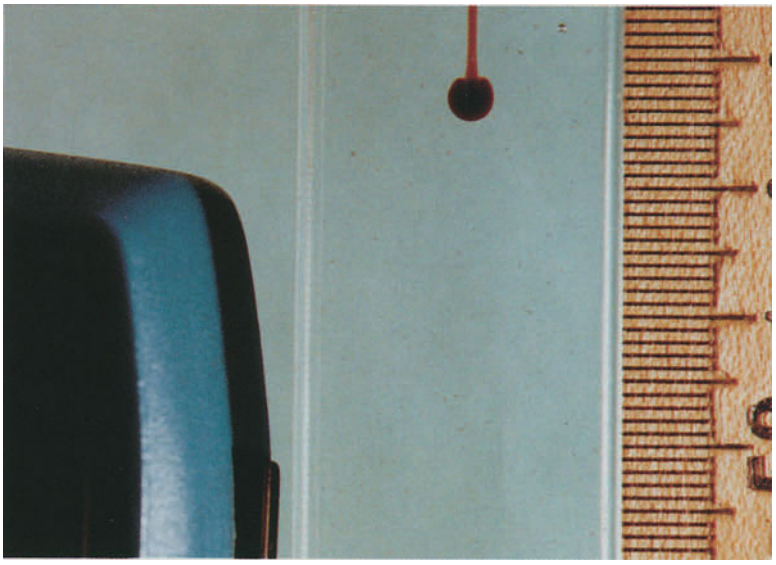

(b)

Plate X.1.3(a-f). [Joseph, 1990, Gauthier-Villars] Molasses drops falling in glycerin. The fall is timed in seconds. Frictional drag on the falling drop creates circulation. The drop eats the thread in (a), (b), (c). In (d), the tail of the drop is breaking. It breaks, then reforms. In (e) a small 'capillary bubble' forms on the molasses thread. In (f), the drop at the bottom has reformed. Continued.

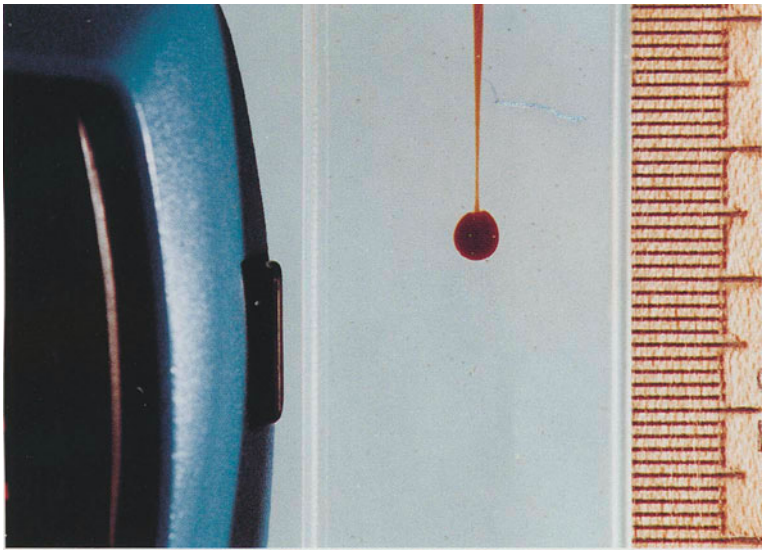

(c)

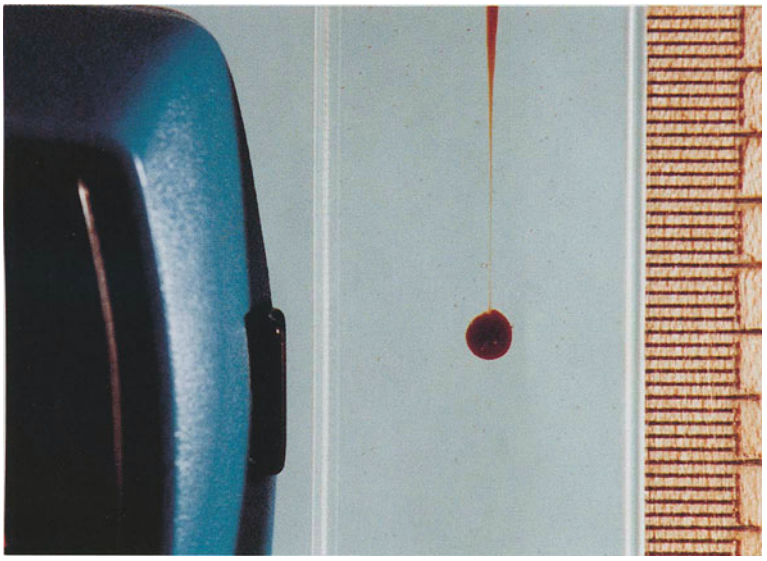

(d)

Plate X.1.3(c-d). Continued.

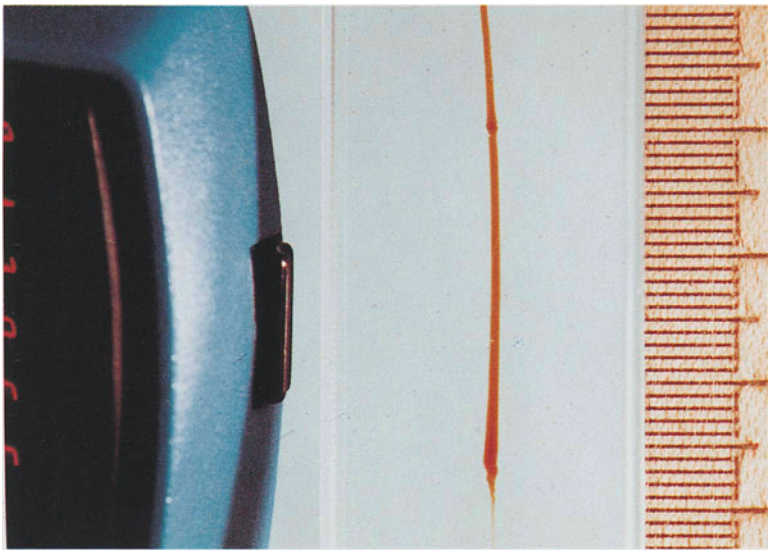

(e)

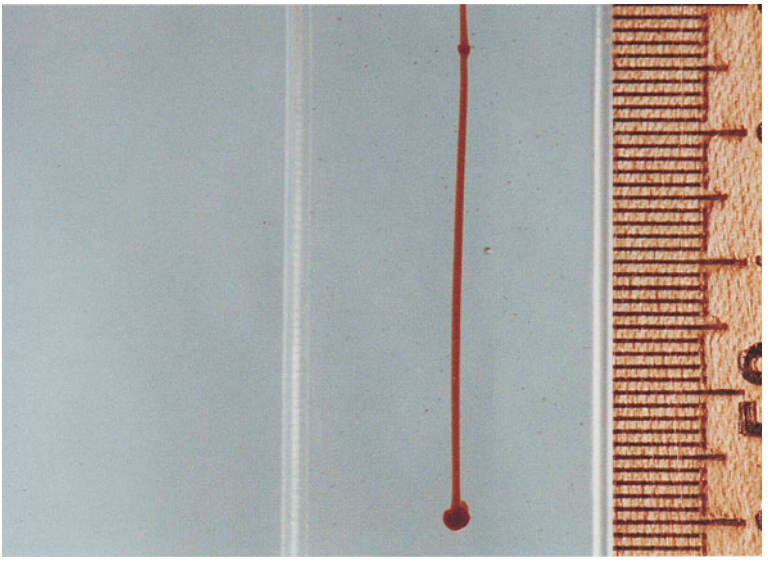

(f)

Plate X.1.3(e-f).

(a)

(b)

(c)

Plate X.3.2(a-c). [Joseph, 1990, Gauthier-Villars] Mobil 1 synthetic motor oil (0.83 g/cc at 77°) in mineral oil (0.82 g/cc at 77°). This looks like a pendant drop due to surface tension (see figure X.2.2). The three frames were photographed at four-second intervals. We think that the side drift of the drop is due to convection and other temperature effects induced by the hot lights used for illumination.

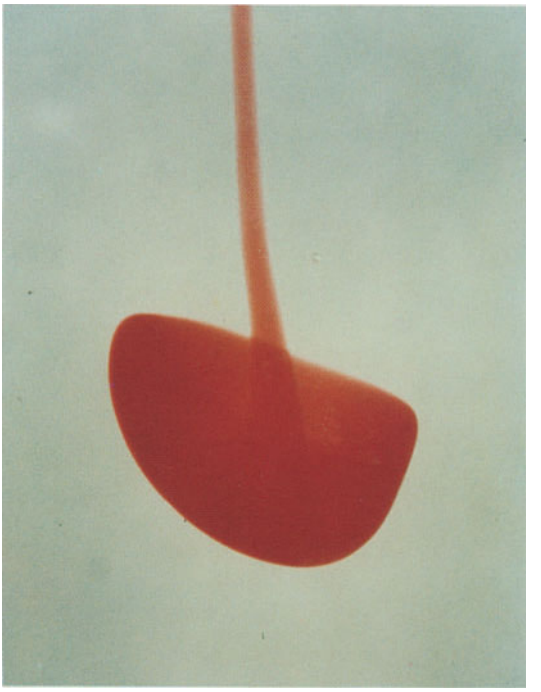

Plate X.6.2. [Kojima, Hinch and Acrivos, 1984, American Institute of Physics] Cold drop initially -7°C falls into the same liquid initially at 21°C.

[1986]. The soliton-like solutions can also be described in terms of the coefficients in (3.17).

The spectral problem (1, 1) and the boundary value problems at orders (0, 2), (2, 2), (1, 2) which are needed to compute the coefficients of the Ginzburg-Landau equation (3.12) are listed in Chen [1990]. We note that at each order the interface parameter η can be eliminated. All the algebraic operations are carried out by the symbolic manipulator REDUCE2 and independently checked by hand. An efficient method to compute the coefficients of the Ginzburg-Landau equation is presented in the next section. Interested readers may apply the theory of modulated plane wave and soliton-like structures to the problem of water-lubricated pipelining using these coefficients. Large-amplitude waves (such as the bamboo waves) have been observed in our experiments, but we have concluded that they are not modulated monochromatic waves and that they seem not to be described by the Ginzburg-Landau equation.

VIII.4 Numerical Scheme

There are many universal equations used as model equations for the study of various physical processes. These equations arise as an asymptotic solvability condition which is a condition on the leading order approximation to the solution of a more complicated set of equations which ensures that the later iterates of the approximation remain uniformly bounded. Examples of these equations are the Korteweg-de Vries equation and its generalizations, the Ginzburg-Landau equation and its generalizations and the Davey-Stewartson equations [Craik 1983; Newell 1985]. For parallel shear flows, the coefficients of these model equations are in general given by very lengthy domain integrals expressing solvability conditions, commonly known as the Fredholm alternative.

The Fredholm alternative requires that the inhomogeneous terms in the underlying system of differential equations, which contain the unknown coefficients, be orthogonal to the independent eigenvector spanning the null space of the adjoint system of differential equations. Typically the underlying system of the inhomogeneous differential equation is discretized and solved as an inhomogeneous matrix-valued problem. We find that the solvability conditions which lead to values of the unknown coefficients are conveniently and economically computed by application of the singular value decomposition directly to the matrix formulation.

The singular value decomposition (SVD) is one of the most important decompositions in matrix algebra and is widely used for statistics and for solving least squares problems (see Golub and Van Loan [1983]). The decomposition theorem can be stated as follows: each and every $M \times N$ complex valued matrix $\mathbf{T}$ can be reduced to diagonal form by unitary transformations $\mathbf{U}$ and $\mathbf{V}$,

$$\mathbf{T} = \mathbf{U}\ \mathrm{diag}\,[\sigma_1, \sigma_2, \cdots\cdots, \sigma_N]\,\mathbf{V}^H, \tag{4.1}$$

where $\sigma_1 \geq \sigma_2 \geq \cdots\cdots \geq \sigma_N \geq 0$ are real-valued scalars, called the singular values of $\mathbf{T}$. Here $\mathbf{U}$ is an $M \times N$ column orthonormal matrix, $\mathbf{V}$ an $N \times N$ unitary matrix and $\mathbf{V}^H$ is the Hermitian transpose of $\mathbf{V}$. The columns of $\mathbf{U}$ and $\mathbf{V}$ are called the left and right singular vectors of $\mathbf{T}$ respectively.

When $M = N$, $\mathbf{T}$ is a square matrix and

$$\mathbf{U}\,\mathbf{U}^H = \mathbf{U}^H\mathbf{U} = \mathbf{I} \tag{4.2}$$

$$\mathbf{V}\,\mathbf{V}^H = \mathbf{V}^H\mathbf{V} = \mathbf{I}. \tag{4.3}$$

Consider the generalized matrix eigenvalue problem

$$(\mathbf{A} - c\mathbf{B})\mathbf{x} = 0, \tag{4.4}$$

where $\mathbf{A}$, $\mathbf{B}$ are both square $N \times N$ complex matrices. Assume that c is an semi-simple eigenvalue of (4.4) with algebraic and geometric multiplicity K. Then applying SVD to the matrix $\mathbf{A} - c\mathbf{B}$, we get

$$\mathbf{A} - c\mathbf{B} = \mathbf{U}\ \mathrm{diag}\,[\sigma_1, \sigma_2 \cdots\cdots, \sigma_{N-K}, 0, 0, \cdots\cdots, 0]\,\mathbf{V}^H, \tag{4.5}$$

where $\sigma_1 \geq \sigma_2 \geq \cdots\cdots \geq \sigma_{N-K} > 0$ are real constants (see Wilkinson [1977]).

Let

$$\mathbf{U} = [\mathbf{u}_1, \mathbf{u}_2, \cdots, \mathbf{u}_{N-K}, \mathbf{u}_{N-K+1}, \cdots, \mathbf{u}_N], \tag{4.6}$$

$$\mathbf{V} = [\mathbf{v}_1, \mathbf{v}_2, \cdots, \mathbf{v}_{N-K}, \mathbf{v}_{N-K+1}, \cdots, \mathbf{v}_N], \tag{4.7}$$

where $\mathbf{u}_j$, $\mathbf{v}_j (j = 1, \cdots, N)$ are the column vectors of matrices $\mathbf{U}$ and $\mathbf{V}$, respectively. From (4.4) and (4.5) we see that diag $[\sigma_1, \sigma_2, \cdots, \sigma_{N-K}, 0, 0, \cdots, 0]\ \mathbf{y} = \mathbf{0}$, where $\mathbf{V}^H\mathbf{x} = \mathbf{y}$ and $\mathbf{x}$ is the eigenvector corresponding to the eigenvalue c. Therefore we have

$$\mathbf{V}^H\mathbf{x} = \mathbf{y} = [0, 0 \cdots, 0, y_{N-K+1}, \cdots, y_N], \tag{4.8}$$

where $y_{N-K+1}, \cdots, y_N$ are K arbitrary constants. Then $\mathbf{x} = \mathbf{V}\mathbf{y}$ is an eigenvector of $\mathbf{A} - c\mathbf{B}$. We find, in this way, that the column vectors $\mathbf{v}_j, j = N - K + 1, \cdots, N$, are the K independent eigenvectors corresponding to c, normalized with

$$\mathbf{v}_j^* \mathbf{v}_j^T = 1, \quad j = N - K + 1, \cdots, N,$$

where the asterisk * denotes the complex conjugate and superscript T denotes the transpose. Similarly the column vectors $\mathbf{u}_j, j = N - K + 1, \cdots\cdots, N$, are the K independent eigenvectors of the problem adjoint to (4.4):

$$(\mathbf{A} - c\mathbf{B})^H\mathbf{x} = 0. \tag{4.9}$$

They are the corresponding adjoint eigenvectors, normalized with

$$\mathbf{u}_j^* \mathbf{u}_j^T = 1, \ j = N - K + 1, \cdots, N.$$

The application of SVD to solve the inhomogeneous system of algebraic equations

$$(\mathbf{A} - c\mathbf{B})\mathbf{x} = \mathbf{f} \tag{4.10}$$

is straight forward. Suppose c is an semi-simple eigenvalue of (4.4) of multiplicity K. We use SVD to decompose $\mathbf{A} - c\mathbf{B}$ in the form (4.5). We then compute

$$\text{diag}[\sigma_1, \sigma_2, \cdots\cdots, \sigma_{N-K}, 0, 0, \cdots\cdots, 0]\mathbf{V}^H \mathbf{x} = \mathbf{U}^H \mathbf{f}. \tag{4.11}$$

The last K components of the vector on the left of (4.11) are identically zero and so must be those on the right. This defines the Fredholm alternative, the solvability conditions

$$\mathbf{u}_j^* \mathbf{f}^T = 0, \quad j = N - K + 1, \cdots\cdots, N, \tag{4.12}$$

for the inhomogeneous matrix problem (4.10). The conditions (4.12) are necessary and sufficient for solvability of the inhomogeneous problem (4.10) in which c is an eigenvalue of $\mathbf{A}$ relative to $\mathbf{B}$.

The solution to the inhomogeneous equation (4.10) is given by

$$\mathbf{x} = \mathbf{V}_s \mathbf{g} + \sum_{j=N-K+1}^{N} \beta_j \mathbf{v}_j, \tag{4.13}$$

where the $N \times (N - K)$ matrix $\mathbf{V}_s$ is given by

$$\mathbf{V}_s = [\mathbf{v}_1, \mathbf{v}_2, \cdots, \mathbf{v}_{N-K}],$$

with $\mathbf{v}_1, \mathbf{v}_2, \cdots\cdots, \mathbf{v}_{N-K}$ given by (4.7) and the vector $\mathbf{g}$ has $N - K$ components given by

$$\mathbf{g} = [\sigma_1^{-1} \mathbf{u}_1^* \mathbf{f}^T, \sigma_2^{-1} \mathbf{u}_2^* \mathbf{f}^T, \cdots\cdots, \sigma_{N-K}^{-1} \mathbf{u}_{N-K}^* \mathbf{f}^T],$$

where the $\mathbf{u}_j$'s are those given by (4.6). The β_j's are constants and can be determined by the K normalization conditions.

Applications of the above SVD algorithm to bifurcation theory is studied in detail by Chen and Joseph [1990]. Independently, Newell, Passot and Souli [1989] applied the same algorithm to the bifurcation study of convection at finite Rayleigh numbers in large containers. The algorithm takes advantage of the matrix formulations of the perturbation problems stated in section VIII.3. Specifically, the problems (0, 2), (2, 2) are invertible and (1, 2), (1, 3) are singular. For these singular problems, a singular system of algebraic equations of the form (4.10) arises after discretization and the techniques described above are readily applicable. For the spectral problem, we have

$$(\mathbf{A} - c_r \mathbf{B})\varphi = 0,$$

where the matrix $\mathbf{A} - c_r\mathbf{B}$ and the vector φ result from the discretization of the Orr-Sommerfeld operator at criticality and the eigenfunction $\varphi(r)$ respectively. At orders (1, 2) and (1, 3), we have the following singular algebraic equations

$$(\mathbf{A} - c_r\mathbf{B})\mathbf{h} = \mathbf{f}(\varphi, c_g), \tag{4.14}$$

$$(\mathbf{A} - c_r\mathbf{B})\psi_{13} = \frac{\partial A}{\partial \tau}\mathbf{f}_1 + \frac{\partial^2 A}{\partial \xi^2}\mathbf{f}_2 + \frac{A}{d_{1r}}\mathbf{f}_3 + |A|^2 A\mathbf{f}_4. \tag{4.15}$$

Assume at criticality c_r is semi-simple with multiplicity $K = 1$. Then (4.14) can be solved by first using the solvability condition (4.12) to evaluate the group velocity c_g and then using the formula (4.13) without the complementary part ($\beta_j = 0$) because of the fact that the complementary part has no contribution to the final amplitude equation. Application of the solvability condition (4.12) to (4.15) generates the coefficients of the Ginzburg-Landau equation (3.12):

$$\begin{aligned} a_2 &= -\mathbf{u}_N^* \mathbf{f}_2^T / \mathbf{u}_N^* \mathbf{f}_1^T, \\ d_1 &= -\mathbf{u}_N^* \mathbf{f}_3^T / \mathbf{u}_N^* \mathbf{f}_1^T, \\ l &= \mathbf{u}_N^* \mathbf{f}_4^T / \mathbf{u}_N^* \mathbf{f}_1^T, \end{aligned}$$

and

$$\mathbf{u}_N^* \mathbf{f}_1^T \neq 0.$$

The above procedure was applied to the problem of one-fluid plane Poiseuille flow and compared with values obtained by Reynolds and Potter [1967] and Davey, Hocking and Stewartson [1974]. The comparison is presented in table 1 of Chen and Joseph [1991 a], showing that the present algorithm gives accurate results. A Chebychev psuedospectral method (cf. section VI.1) is used for the discretization of the differential equations. We normalize the eigen-streamfunctions φ_1 and φ_2 such that the discrete L_2 norms satisfy $\|\varphi_1\|^2 + \|\varphi_2\|^2 = 1$.

VIII.5 Nonlinear Stability of Core-Annular Flows

The nature of the bifurcation of core-annular flows is determined by the real part of the Landau constants l in (3.12). If $l_r > 0$, the bifurcation is supercritical and a finite amplitude equilibrium solution exists. On the other hand, if $l_r < 0$, the bifurcation is subcritical; the bifurcating solution of (3.12) will burst in finite time and a higher-order theory is needed.

The coefficients of Ginzburg-Landau equations for different parameters are listed in tables 5.1 - 5.6. Since we are mainly interested in the direction of the bifurcations here, we have only listed the values of the critical states $(\alpha_c, \mathbb{R}_c(\alpha_c))$, $\mathrm{sgn}(l_r)$, C_d and C_n in these tables, corresponding to the

canonical form (3.17). The values of c_r, c_g, d_1, a_2 and l are documented in Chen [1990]. The first thing to look at in these tables is the next to the last column labeled sgn(l_r). A plus sign here means that the bifurcation is supercritical, subcritical for the minus sign.

The cases studied in tables 5.1 - 5.6 are for the purpose of exploring the general features of bifurcation of core-annular flow. The cases with parameters corresponding to some of the experiments of CGH (figure V.1.1) and those of chapter VII are discussed in section VIII.8. As mentioned earlier, our bifurcation analysis is only valid near the nose of the neutral curves. This means that such analysis is applicable only when the upper branch and the lower branch of the neutral curve are separated, i.e. there exists a Reynolds number window within which core-annular flow is linearly stable, as in figures 5.1 - 5.2. In other words, we can only study those cases where linearly stable core-annular flow is possible. The reader may easily understand how the subcritical and supercritical solutions fit in with the upper and lower branches of the neutral curves by looking at figure 5.3. It has been shown in section VI.1 and also in chapter VII that such a stable CAF occurs only when the parameters a, m, ζ, J^* fall into a certain subspace of the parameter space. Typically, there is a 'thin layer effect': that is, a thin lubricating layer with a small $a - 1 (= R_2/R_1 - 1)$ tends to stabilize core-annular flow. It is also shown in section VI.3, that if the oil is too viscous, $m = m_2/m_1 \ll 1$, stable core-annular flow is very difficult to achieve. We have thus restricted our studies in tables 5.1 - 5.6 to the typically small values of $a - 1$ and values of m of order 10^{-1}, which stabilize core-annular flows.

The parameter $|\mathbb{R}_g| = 0.5$ is used for all the cases considered in the tables. This parameter enters into the equations only as a product $(\zeta_2 - 1)\mathbb{R}_g$, hence plays no role when the densities of the two fluids are the same ($\zeta_2 = 1$). We can vary the effective gravity $(\zeta_2 - 1)\mathbb{R}_g$ by varying the value of ζ_2 for a fixed value of $\mathbb{R}_g$.

We are going to divide the tables into two groups according to the value of capillary number J^*. The first group is for $J^* = 1$, corresponding to weak capillary effects typical for our experiments. The results for $J^* = 1$ are summarized in tables 5.1 - 5.4. The second group is for $J^* = 2000$, corresponding to strong capillary effects. This case is of interest for low viscosity cores for which the capillary number is large.

There is an important difference in the lower branch of the neutral curves when $J^* = 1$ and $J^* = 2000$ that is evident from a comparison of figures 5.1 - 5.2. When $J^* = 1$, the maximum value of $\mathbb{R}(\alpha)$ on the lower branch of the neutral curve occurs near $\alpha = 0$. When $J^* = 2000$, the maximum value of $\mathbb{R}(\alpha)$ on the lower branch of the neutral curve occurs at a finite value near 0.6.

The lower branch of the neutral curve for $J^* = 1$ has a region in the neighborhood of $(\alpha, \mathbb{R}(\alpha)) = (0, \mathbb{R}(0))$ in which the analysis of long waves may be relevant. In the case of very long waves, it may be impossible to

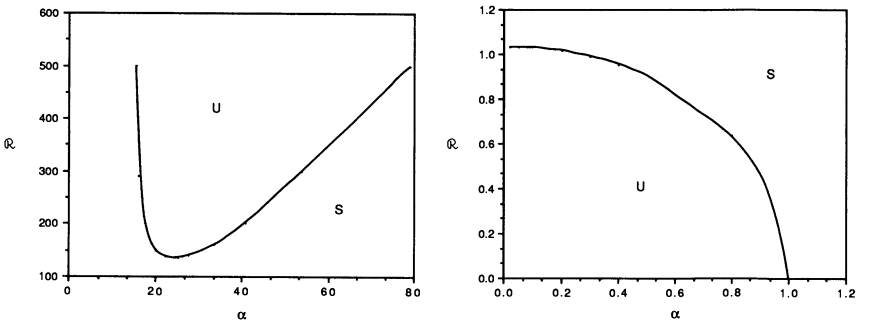

Fig. 5.1. [Chen and Joseph, 1991a] Neutral curves for a=1.1, m=0.5, $\zeta_2 = 1.2$, $J^* = 1.0$, $\mathbf{R}_g$= 0.5, down-flow. U and S stand for unstable and stable. The upper and lower branches are well separated. Surface tension is weak and the critical Reynolds number for the lower branch occurs at α=0.09.

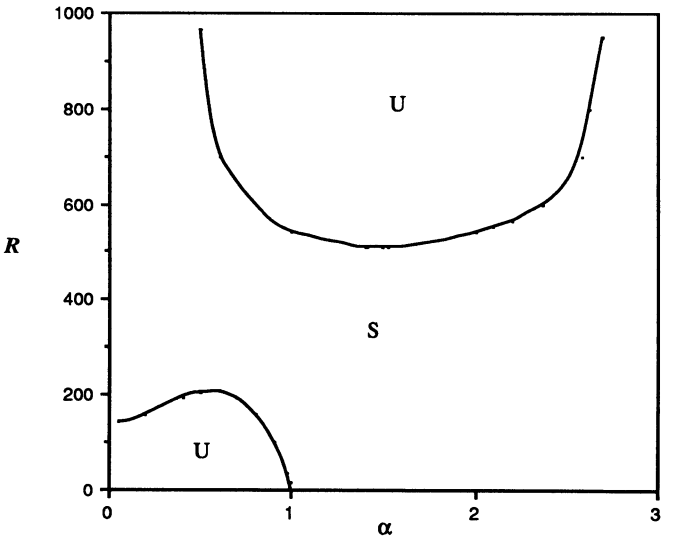

Fig. 5.2. [Chen and Joseph, 1991a] Neutral curves for $a = 1.3$, $m = 0.5$, $\zeta_2 = 1.2$, $J^* = 2000$, $\mathbf{R}_g = 0.5$, down-flow. U and S stand for unstable and stable. For this case of strong surface tension, the critical Reynolds number for the lower branch occurs at a wavenumber $\alpha = 0.56$ away from zero.

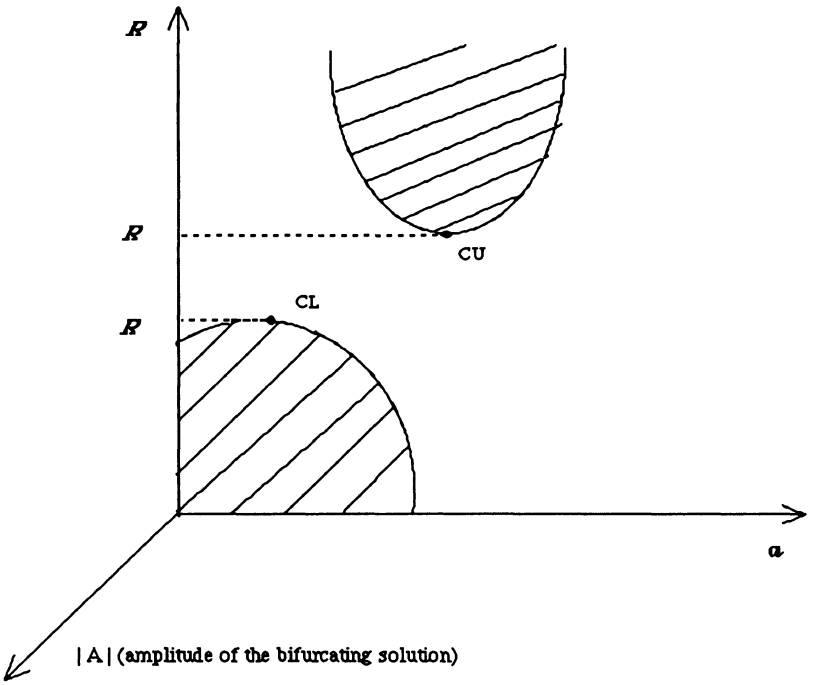

Fig. 5.3. [Chen and Joseph, 1991a] An example of neutral curves for which PCAF can be stable. The region of linear stability is $\mathbb{R}_{cL} < \mathbb{R} < \mathbb{R}_{cU}$. The regions above the upper curve and below the lower curve are linearly unstable. The critical Reynolds numbers for the curves are denoted by $\mathbb{R}_{cU}$ and $\mathbb{R}_{cL}$. Bifurcation theory can be used for $\mathbb{R}$ close to $\mathbb{R}_{cU}$ or $\mathbb{R}_{cL}$. Bifurcating branches of solutions with $\mathbb{R}$ in the linearly unstable region are supercritical and with $\mathbb{R}$ in the linearly stable region are subcritical. Thus, when $\mathbb{R} > \mathbb{R}_{cU}$ and $|A| > 0$, or when $\mathbb{R} < \mathbb{R}_{cL}$ and $|A| > 0$, the flow is supercritical. The shaded regions are supercritical. When $\mathbb{R}_{cL} < \mathbb{R} < \mathbb{R}_{cU}$ and $|A| > 0$, the flow is subcritical.

obtain an amplitude equation of the Ginzburg-Landau type. The critical wave number at the nose of the neutral curve tends to zero so that the wave you are supposed to modulate is already hugely long.

Table 5.1. Coefficients of the Ginzburg-Landau equation for $a = 1.25$, $\zeta_2 = 1$, $J^* = 1$, down-flow

(a) Upper branch of the neutral curve

m	α_c	$\mathbb{R}_c$	C_d	sgn(l_r)	C_n
0.9	2.99	175.033	5.0054	+	-11.4151
0.85	3.2	162.23	5.0375	+	-197.3133
0.8	3.3	150.71	4.9972	-	-6.7538
0.7	3.6	128.72	4.3832	-	-1.2640
0.5	9.1	55.61	-0.7895	-	-1.3827
0.2	5.8	16.24	-1.0769	-	-0.8101
0.1	4.4	9.985	-0.4983	-	-0.1714

(b) Lower branch of the neutral curve

m	α_c	$\mathbb{R}_c$	C_d	sgn(l_r)	C_n
0.9	0.09	5.6047	7.0	+	-5.6021
0.85	0.06	4.7010	4.3030	+	-3.9426
0.8	0.04	4.0821	6.7899	+	-5.5512
0.7	0.03	3.3751	42.8759	+	-31.0698
0.5	0.05	2.78	23.3539	-	20.4787
0.2	0.029	2.6341	245.4459	-	254.3165
0.1	0.06	2.707	71.4207	-	78.8215

Table 5.2. Coefficients of the Ginzburg-Landau equation for $a = 1.25$, $m = 0.7$, $J^* = 1$, $\mathbb{R}_g = 0.5$, down-flow

(a) Upper branch of the neutral curve

ζ_2	α_c	$\mathbb{R}_c$	C_d	sgn(l_r)	C_n
1.0	3.6	128.72	4.3832	-	-1.2640
1.2	1.95	1592.3	4.1387	+	0.1952
1.4	2.7	1060.74	1.2524	+	-0.1585
1.6	3.28	791.31	1.0583	+	-0.2605

(b) Lower branch of the neutral curve

ζ_2	α_c	$\mathbb{R}_c$	C_d	sgn(l_r)	C_n
1.0	0.03	3.3751	42.8759	+	-31.0698
1.2	0.04	3.1830	35.5138	+	-19.6098
1.4	0.01	3.071	1.5466	+	-1.6507
1.6	0.01	2.93	1.4688	+	-1.4710

Table 5.3. Coefficients of GL equation for $a = 1.25$, $m = 0.5$, $J^* = 1$, $\mathbb{R}_g = 0.5$, down-flow

(a) Upper branch of the neutral curve

ζ_2	α_c	$\mathbb{R}_c$	C_d	sgn(l_r)	C_n
1.0	9.1	55.61	-0.7895	-	1.3827
1.2	1.9	543.6	11.2156	+	0.7736
1.4	2.71	568.68	1.6348	+	-0.1513
1.6	3.1	469.25	1.4034	+	-0.4332

(b) Lower branch of the neutral curve

ζ_2	α_c	$\mathbb{R}_c$	C_d	sgn(l_r)	C_n
1.0	0.05	2.78	23.3539	-	20.4787
1.2	0.08	2.523	14.9791	-	13.8764
1.4	0.04	2.3228	61.18	-	51.4451
1.6	0.08	2.1801	9.2344	-	8.4382

Table 5.4. Coefficients of the GL equation for $a = 1.1$, $m = 0.5$, $J^* = 1$, $\mathbb{R}_g = 0.5$, down-flow

(a) Upper branch of the neutral curve

ζ_2	α_c	$\mathbb{R}_c$	C_d	sgn(l_r)	C_n
0.5	7.26	140.871	5.7827	-	-2.4054
0.8	8.91	235.084	4.7197	-	-0.8352
1.0	24.77	156.451	1.1180	-	5.2623
1.2	24.36	136.034	1.1141	-	12.0131
1.4	24.05	121.916	1.0833	-	273.0102
1.5	23.92	116.355	1.0514	+	44.9198
1.6	23.82	111.522	1.0179	+	24.6314

(b) Lower branch of the neutral curve

ζ_2	α_c	$\mathbb{R}_c$	C_d	sgn(l_r)	C_n
0.5	0.1	1.08	-11.9596	-	-7.2965
0.8	0.15	1.051	-9.3205	-	-6.5107
1.0	0.05	1.044	-58.0376	-	-28.6788
1.2	0.09	1.034	-15.1812	-	-10.8792
1.4	0.14	1.0202	-9.5561	-	-7.2649
1.5	0.06	1.019	-21.2016	-	-0.8362
1.6	0.1	1.0	-23.6511	-	-14.7862

Table 5.5. Coefficients of GL equation for $a = 1.1, m = 0.5, J^* = 2000, \mathbb{R}_g = 0.5$, down-flow

(a) Upper branch of the neutral curve

ζ_2	α_c	$\mathbb{R}_c$	C_d	sgn(l_r)	C_n
0.5	2.03	619.53	-0.2407	+	-1.7274
0.6	2.16	706.80	-0.1143	+	-2.6185
0.7	2.31	824.45	0.0196	+	-6.3772
0.8	2.53	994.30	0.1235	-	-5.0004
1.0	3.56	1490.16	0.3926	-	-0.3405
1.2	7.67	2025.59	-0.2422	-	-6.9622
1.4	8.80	1700.47	-0.4030	-	-2.6566
1.5	9.55	1537.17	-0.5902	-	-34.1854
1.6	10.36	1390.44	-0.8053	+	0.8573
1.8	11.91	1162.06	-1.1776	+	1.0673

(b) Lower branch of the neutral curve

ζ_2	α_c	$\mathbb{R}_c$	C_d	sgn(l_r)	C_n
0.5	0.26	47.91	-5.9844	-	-0.7709
0.6	0.24	47.70	-7.0583	-	-0.8770
0.7	0.22	47.50	-8.2410	-	-0.9921
0.8	0.22	47.30	-7.7273	-	-0.9799
1.0	0.20	46.92	-8.3867	-	-1.0912
1.2	0.16	46.564	-11.6444	-	-1.4088
1.4	0.1	46.22	-21.4375	-	-2.2710
1.5	0.11	46.053	-16.9091	-	-2.0493
1.6	0.11	45.89	-16.0870	-	-2.0335
1.8	0.09	45.56	-18.9375	-	-2.4719

Table 5.6. Coefficients of GL equation for $a = 1.1, m = 0.9, J^* = 2000, \mathbb{R}_g = 0.5$, down-flow

(a) Upper branch of the neutral curve

ζ_2	α_c	$\mathbb{R}_c$	C_d	sgn(l_r)	C_n
0.5	1.55	1347.87	-0.7492	+	1.0261
1.0	2.63	2701.37	-0.3912	+	0.1679
1.2	4.18	7126.05	0.0020	-	104.0321
1.5	3.87	6503.75	0.6476	-	-0.3164
2.0	6.81	3202.31	0.1169	-	-1.9525
3.0	13.46	1381.32	-1.3575	-	-5.8459
4.5	15.50	990.06	-1.1833	+	0.2410

(b) Lower branch of the neutral curve

ζ_2	α_c	$\mathbb{R}_c$	C_d	sgn(l_r)	C_n
0.5	0.52	150.26	-0.7910	+	0.5327
1.0	0.51	145.26	-0.7624	+	0.5031
1.2	0.503	143.47	-0.7740	+	0.5048
1.5	0.50	140.95	-0.7473	+	0.4812
2.0	0.49	137.17	-0.7418	+	0.4657
3.0	0.47	130.79	-0.7500	+	0.4516
4.5	0.45	123.25	-0.7345	+	0.4175

VIII.6 Small Capillary Numbers

When the capillary parameter J^* is small, the maximum growth rate for capillary instability does not differ much from the value as $\alpha \to 0$ which maximizes $\mathbb{R}(\alpha)$ on the lower branch of the neutral curve in figure 5.1. We have selected the value $J^* = 1$ to represent weak surface tension and our results are displayed in tables 5.1 - 5.4 and in figure 5.1. Tables 5.1 - 5.3 are for $a = 1.25$, corresponding to the water-to-oil volume ratio $V_w/V_o = a^2 - 1 = 0.5025$. The coefficients of the Ginzburg-Landau equations in the case in which the densities of the core and the lubricating fluids are the same ($\zeta_2 = 1$) are exhibited in table 5.1. We know from energy analysis of the linear problem that PCAF in the region above the upper branch of the neutral curve is unstable to interfacial friction (cf. section VI.2 and the latter half of chapter VII). We expect that wavy core flow will arise from this instability. The entries in table 5.1 show that the bifurcating waves are supercritical when the viscosity ratio $\mu_2/\mu_1 = m \geq 0.85$ and subcritical when $m \leq 0.8$. Stable small-amplitude shear waves are expected in the

supercritical case and something else far from PCAF, perhaps large waves, in the subcritical case. Small viscosity differences can lead to stable wavy flow at the interface.

Turning next to the lower branch of the neutral curve which is prey to modified capillary instability, we note that the bifurcation is supercritical when $m \geq 0.7$ and subcritical when $m \leq 0.5$. We expect to see small-amplitude capillary waves in the supercritical case. This can be interpreted to mean that linear capillary instability is nonlinearly shear-stabilized when $m \geq 0.7$. The flows which bifurcate subcritically ($m \leq 0.5$) would be far from PCAF. These more viscous cores probably break into slugs or bubbles far from PCAF connected by thin threads. The results in table 5.1 indicate that when the densities of the fluids are matched, a large viscosity difference leads to subcritical bifurcation while a small viscosity difference can result in supercritical bifurcation.

We next study the effect of changing the density of the lubricant for the same fixed $a = 1.25$. If the lubricant is heavier than the core, say water and oil, then $\zeta_2 > 1$. Can we change the nature of the bifurcations, i.e. change the dynamics of lubrication, by varying ζ_2? Table 5.2 shows that for fluids with $m = 0.7$, the bifurcation of the upper branch for $\zeta_2 = 1$ can be changed from sub to supercritical by increasing the density ratio to $\zeta_2 = 1.2$. We can stabilize small-amplitude bifurcating waves driven by interfacial friction by increasing the density of the lubricant. The change of density does not destabilize the supercritical bifurcating solution on the lower branch. Table 5.3 gives results for a smaller viscosity ratio $m = 0.5$. The same manner of bifurcation holds also when $m = 0.2$. The only difference is that the wavy solutions below the lower branch of the neutral curve are all stable when the viscosity ratio is large ($m = 0.7$) and are all unstable when $m = 0.5$ and $m = 0.2$. These results suggest that for a given surface tension, the bifurcation of the upper branch is sensitive to changes in the density ratio, while the lower branch is sensitive to changes of the viscosity ratio but not to changes of the density ratio.

In table 5.4, we look at fluids with $m = 0.5$ for the effect of varying ζ_2 . The difference here is that there is much less water: $a = 1.1$, and water-to-oil volume ratio $V_w/V_o = a^2 - 1 = 0.21$. The lubricating layer is quite thin. The bifurcation of the periodic solution from the lower branch of the neutral curve is subcritical for ζ_2 between 0.5 and 1.6, as in the case $a = 1.25$. The bifurcation of a periodic solution from the upper branch of the neutral curve can be changed from sub to supercritical by increasing the density of the lubricant. However the transition density ratio for $a = 1.1$ occurs between $\zeta_2 = 1.4$ and $\zeta_2 = 1.5$, a larger transition ratio than for $a = 1.25$, $m = 0.5$, which is between $\zeta_2 = 1.0$ and $\zeta_2 = 1.2$ (see table 5.3). Suppose the density ratio of the fluids is between 1.2 and 1.5 and the viscosity ratio is $m = 0.5$. If the lubricating layer is relatively thick ($a = 1.25$), then the upper branch will bifurcate supercritically. However, if the lubricating layer is thin, say $a = 1.1$, then the upper branch will

bifurcate subcritically. This indicates some kind of nonlinear break-down of the 'thin layer effect': in order to achieve a linearly stable core-annular flow, we need to have a thin lubricating layer. However, if the layer is too thin, the bifurcation of the upper branch will become subcritical. The exact physical implication of this subcritical bifurcation is not clear to us. However, in the experiments of chapter VII, in a region where the superficial oil velocity is large and superficial water velocity is relatively small, corresponding to very small values of a, oil sticks to the pipe wall.

The role that a density difference plays in the stability of core-annular flow is interesting. The effect of the density difference on the neutral stability curves of core-annular flow is studied in chapter VII. The calculations there, as well as the weakly nonlinear ones presented here, show that the upper branch of the neutral curves are more sensitive to the changes of density ratio ζ_2 than the lower branch. For the upper branch, the Reynolds number is large and the effect of the effective gravity $[\![\zeta]\!]\mathbb{R}_g$ is negligible. The only place that the density ratio ζ_2 enters into the equations is through the jump in the perturbation pressure in the normal stress balance equation at the interface, (2.8). Relatively small changes in ζ_2 can cause a large perturbation of the pressure jump when the Reynolds number is large. This changes the stability of the upper branch considerably. When the Reynolds number is large, the pressure jump is basically equal to the jump in the inertia of the fluids which is large in this case. On the other hand, when the Reynolds number is small, density stratification manifests itself mainly through the effective gravity term $[\![\zeta]\!]\mathbb{R}_g$ in the basic flow. This term is not too large for the small pipes we have considered and the change of the lower branch is relatively small for the moderate changes in ζ_2.

We have also computed a few cases of up-flow, for $a = 1.1$, with $\mathbb{R}_g = -0.5$. After comparing these results with relevant entries in the previous tables, we found that there are only slight changes in the values of coefficients and the type of bifurcation remains the same for both upper and lower branches. This is expected for the case of not too large $|\mathbb{R}_g|$ and *fixed value* of a. Effective gravity $[\![\zeta]\!]\mathbb{R}_g$ has little effect on the stability, and particularly for the upper branch, there is almost no difference between up- and down-flows for both the neutral curves and bifurcation. For the lower branch, there is a slight shift of the neutral curves between the up- and down-flows, but the type of bifurcation is not affected. The large difference between up- and down-flows at moderate flow rates observed in experiments is due to the accumulation of oil in down flow and its depletion in up-flow due to buoyancy. The water fraction is therefore greater and a is larger in up- than in down-flow.

VIII.7 Large Capillary Numbers

As the surface tension parameter J^* is increased, the wave number corresponding to the most unstable mode of the lower branch tends to the capillary limit $\alpha = 0.69$. It has been shown in section VI.1 that linearly stable CAF is possible only when the lubricating fluid is heavy and ζ_2 is large enough. The neutral curve for $a = 1.3$, $m = 0.5$, $J^* = 2000$, $\mathbb{R}_g = 0.5$ and $\zeta_2 = 1.2$ is shown in figure 5.2. For this set of parameters $a, m, J^*, \mathbb{R}_g$, linearly stable CAF is only possible when $\zeta_2 \geq 1.2$. A heavy lubricant will stabilize capillary instability, and the critical Reynolds number below which the flow is unstable to capillarity is decreased as ζ_2 is increased. However, increasing the density of the lubricant does not appear to change the nature of the bifurcation from the capillary branch, which is subcritical at least for the case $a = 1.3$, $m = 0.5$ and $J^* = 2000$ which we calculated. The subcritical bifurcation here may lead to the capillary break-up of the oil core and the formation of oil slugs and bubbles. Bifurcations from the upper branch when $(a, m, J^*) = (1.3, 0.5, 2000)$ are always supercritical, leading to the finite travelling waves at the interface.

The second example of large capillary number is exhibited in table 5.5 for the parameters $a = 1.1$, $m = 0.5$, $J^* = 2000$ and $\mathbb{R}_g = 0.5$. Linearly stable CAF is possible for a much wider range of ζ_2 because of the stabilization effect of thin lubricating layer. However, the bifurcation of the capillary branch remains subcritical for all the density ratios considered. These results for $J^* = 2000$ and those for $J^* = 1$ show that the bifurcation of the lower branch is insensitive to the changes in density difference and water fraction. For the upper branch, from table 5.5 (a), we see that there is a range of density ratios within which the bifurcation of the upper branch is subcritical. Outside of this range, i.e. for small and large density ratios, the bifurcation becomes supercritical. This result also holds when $J^* = 1$, as shown in section VIII.6, but the subcritical range is different. The break-down of the 'thin-layer effect' for $J^* = 1$ also occurs for $J^* = 2000$.

How do changes in the viscosity ratio m change the bifurcation of core-annular flows when J^* is large? Table 5.6 gives results for $a = 1.1$, $m = 0.9$, $J^* = 2000$, $\mathbb{R}_g = 0.5$ and down-flow. The remarkable difference between $m = 0.9$ and $m = 0.5$ is that for the smaller viscosity stratification, the lower capillary branch bifurcates supercritically for all the density ratios considered, even for a lighter lubricant ($\zeta_2 < 1$). This means that finite amplitude capillary waves are saturated nonlinearly by the action of a small viscosity difference (m near one). This nonlinear saturation by small viscosity difference also occurs when J^* is small (cf. section VIII.6). For the upper branch, there is still a range of density ratios within which the bifurcation is subcritical, as in the case of weak capillarity.

VIII.8 Experiments

In the somewhat restricted situation of Hopf bifurcation of strictly periodic waves at a simple eigenvalue, we could say that the supercritical waves are stable whilst the subcritical waves are unstable. To compare bifurcation analysis with experiments, we must first identify a flow with a critical Reynolds number $\mathbb{R}_c$. There are then upper and lower critical values, $\mathbb{R}_{cU}$ and $\mathbb{R}_{cL}$ (see figure 5.3). If the operating Reynolds number $\mathbb{R}$ is in a region of instability of PCAF near criticality, then supercritical bifurcating solutions are in this same region of instability of PCAF. Under restrictive hypotheses, the supercritical bifurcating solution is stable. We say that bifurcation theory is consistent with experiments when the observed supercritical solution is just a small perturbation of PCAF (we would need to compare details of the bifurcated solution with experiments to test the theory, and we have not done this). On the other hand, if the bifurcation is subcritical when $\mathbb{R}$ is in the unstable region for PCAF (shaded region in figure 5.3), then the bifurcating solution is unstable when its amplitude is small, but may recover stability for large amplitudes. In this case the observed flows would be far from PCAF. If $\mathbb{R}$ is in a region of stability of PCAF, $\mathbb{R}_{cL} < \mathbb{R} < \mathbb{R}_{cU}$, and both bifurcations are supercritical, we might expect to see stable PCAF, stable both to small and finite disturbances. If, on the other hand, one or both bifurcations are subcritical and $\mathbb{R}_{\mathrm{cL}} < \mathbb{R} < \mathbb{R}_{\mathrm{cU}}$, then the conclusion of bifurcation theory is ambiguous. Without ambiguity, we may conclude that if a flow different than stable PCAF is seen in the linearly stable range, then one or both bifurcations should be subcritical with large deviations (with an ambiguous 'large') from PCAF.

In table 8.1, we have compared bifurcation theory with experiments. The comparisons exhibited in rows one and two can be said to show agreement between theory and experiments. Less can be concluded from rows three through seven, but in all cases, there is no obvious inconsistency between experiments and bifurcation theory.

We wish to draw attention to a possible interpretation of bamboo waves as a structure far from PCAF. When the waves are large, they are clearly far from PCAF. In one interpretation, bamboo waves arise from shear stabilization of capillary instability which in pure form leads to spheres of oil, far from PCAF. There is no stable capillary figure close to a cylinder.

We turn next to a discussion of theory and experiments in which the entries in table 8.1 are explained in a wider context. We first consider the experiment labeled as 2 in figure V.1.1. One sees a slightly perturbed PCAF which is labeled as 'oil in water concentric'. The neutral curve for this case is shown as figure 1.10 in section VI.1. The operating condition, $a = 1.21$, $J^* = 2102$, $m = 0.0532$, $R_1 = 138.6$, is just above the nose $(\alpha_c, \mathbb{R}_c) = (2.24, 138.2)$ of the upper neutral curve; hence PCAF is unstable. For this case the coefficients of the amplitude equation (3.17) are

$$C_d = -1.3967,$$
$$C_n = -0.02393,$$
$$\text{sign}(l_r) = +1.$$

Since $l_r > 0$, the bifurcation is supercritical and only a small perturbation of PCAF is expected and is realized. The remaining ten cases in figure 1.1 of chapter V are either always unstable or with operating conditions (operating Reynolds numbers) far away from the critical conditions (see section VI.1 for the neutral curves). Thus bifurcation analysis can not be applied.

In chapter VII, the linear theory of stability is correlated with experimental data. The fluids and the size of the pipe were chosen with the guidance of the linear theory and a stable perfect core-annular flow was achieved in the free-fall apparatus, as predicted by the theory. The neutral curve for that experiment is given in figure VII.8.5. The experiment falls in the linearly stable region and is not too far away from the critical condition of the lower branch. After converting the parameters to the ones used in the present paper, we have, for the experiment, $a = 1.86$, $m = 0.33$, $\zeta_2 = 1.4$, $J^* = 2.26$, $\mathbb{R}_g = 21.31$, $\mathbb{R} = 8.22$. The bifurcation near the critical state of the lower branch, $(\alpha_c, \mathbb{R}_c) = (0.04, 6.31)$, is supercritical:

$$C_d = 89.65,$$
$$C_n = 21.31,$$
$$\text{sign}(l_r) = +1.$$

The upper branch, although far away with $(\alpha_c, \mathbb{R}_c) = (0.5, 153.0)$, also bifurcates supercritically. Perfect core-annular flow was observed in the experiment, as predicted by theory.

The difficulty in applying the above theory to the practical situations of lubricated pipelining lies in the fact that, when the viscosity ratio of water to oil ($m = \mu_2/\mu_1$) is very small, say m of order 10^{-5} which is typical for crude oil and water, PCAF is always linearly unstable and thus there is no critical state for bifurcation analysis. This restriction severely limits the parameter range for which this analysis can be applied.

The experiments of chapter VII reveal many interesting features of nonlinear waves in lubricated pipelining. For these experiments, we have

$$m = 1.66 \times 10^{-3}, \quad \zeta_2 = 1.0994, \quad J^* = 0.1019, \quad \mathbb{R}_g = 2.4.$$

For this value of m, linearly stable CAF can be obtained only when a is very small (say $a < 1.15$). The flow charts in chapter VII show how the flow regimes change with respect to the superficial velocities of water and oil, V_w, V_o . In the up-flow chart, there is a region in the (V_w, V_o) plane called 'wavy CAF', which corresponds to the bamboo waves observed (see plate V.1.2). For the points marked #1 through #9, and D_2, E_3 in the bamboo wave regime, the upper and lower neutral curves are connected and they are

linearly unstable at all Reynolds numbers. This is because of the large values of a for these points. For point E_2, $a = 1.12$, $R_1 = 1.2283$. The upper and lower branches of the neutral curves are separated. The experimental line $R_1 = 1.2283$ is cutting through the upper branch, linearly unstable and is not too far away from the nose of the neutral curve $(\alpha_c, \mathbb{R}_c) = (2.41, 0.501)$. The bifurcation at this point is found to be subcritical with

$$C_d = 0.9623,$$
$$C_n = -0.9657,$$
$$\text{sign}(l_r) = -1.$$

This subcritical bifurcation indicates that in order to achieve the experimentally observed stable bamboo waves at E_2, higher order theory is needed.

The examples discussed above show that the current lowest order bifurcation theory is hopeless for the prediction of bamboo waves, either because the corresponding linear theory predicts linear instability for all Reynolds numbers, or because of the subcriticality of the bifurcation. For the latter case, we may supplement a higher order theory. Nevertheless, the above examples suggest that bamboo waves are flows far from PCAF and fully numerical simulations may be required for their characterizations.

The flow regime called 'oil sticking on the wall' in the up-flow chart is a region where V_w is small and V_o is large. In this region, there is little water in the pipe and thus the value of a is small. We found that for these small values of a, the upper and lower branches of the neutral curves are separated, due to the strong stabilization of the thin lubricating layer ('thin-layer effect'). The experimental lines $R_1 = R_E$ cut through the upper branch. However, the bifurcations of the upper branch are found to be all subcritical. This is the nonlinear break-down of the thin-layer effect discussed in section VIII.6. An example in this region is the point F_1, where $a = 1.03$, $R_1 = 2.2838$. The nose of the upper branch is $(\alpha_c, \mathbb{R}_c) = (12.0, 2.04)$ and we have a subcritical bifurcation with

$$C_d = -0.1479,$$
$$C_n = -0.7556,$$
$$\text{sign}(l_r) = -1.$$

Whether these subcritical bifurcations correlate to the losses of lubrication observed in the experiments remains to be resolved, either by higher order theory or numerical solution. Obviously the phenomena observed in the experiments are very nonlinear.

We next examine the down-flow chart of chapter VII. The points #2, #3 fall in a region called 'disturbed CAF', corresponding to 'corkscrew' waves as in plate V.1.3. The linear theory predicts that #2 , #3 are linearly stable to infinitesimal disturbances, axisymmetric and nonaxisymmetric. The bifurcations of the upper and lower branches are all subcritical. It is

obvious that these 'corkscrew' waves are nonaxisymmetric and due to finite nonaxisymmetric disturbances which are not considered in this paper.

The point marked #4 in the down-flow chart falls in a region called 'disturbed CAF', which corresponds to axisymmetric, very short stem bamboo waves. For point #4, $a = 1.09$, $R_1 = 9.59$, the upper and lower branches are separated, and $\mathbb{R}_1 = 9.59$ cuts through the upper branch. In this case, the bifurcation at the nose of upper branch, $(\alpha_c,\ \mathbb{R}_c) = (3.6, 1.36)$ is supercritical with

$$C_d = 0.6590,$$
$$C_n = -0.5718,$$
$$\text{sign}(l_r) = +1.$$

However, the experimental point $\mathbb{R}_1 = 9.59$ is far away from the nose and the information on the bifurcation at the nose may be not relevant to the observed equilibrium waves.

A summary of the results testing bifurcation theory are in table 8.1. It is evident from the above discussions that the usefulness of the bifurcation analysis is restricted. For the situations of practical interest, $m \ll 1$, the bifurcation analysis is either not applicable or fails to provide useful information relevant to the experimentally observed phenomena. On the other hand, in all these cases we have obtained useful information from the study of the linear theory of stability. It seems to us that, unlike linear theory, weakly nonlinear theory is valid in a too narrowly defined set of conditions to be of much use in our problem. Perhaps direct numerical approaches have more to offer.

Table 8.1. Comparison of bifurcation theory and experiments. Among the experiments, there is only a small number to which the Ginzburg-Landau theory would apply. They are listed in this table. sgn(l_r)=+1 for supercritical, sgn(l_r)=-1 for subcritical bifurcations. Subscripts U and L refer to the upper and lower branch respectively.

Experiment	Operating $\mathbb{R}$	sgn$(l_r)_U$	sgn$(l_r)_L$	Observations and Comments
fig.V.1.1 #2	$\mathbb{R} > \mathbb{R}_{cU}$	+1		The bifurcation is supercritical and the flow is near PCAF.
sec.VII.3 Free fall	$\mathbb{R} > \mathbb{R}_{cU}$	+1	+1	PCAF is observed. Perfect agreement between experiments and theory.
* #E2 up-flow	$\mathbb{R} > \mathbb{R}_{cU}$	-1		Bamboo waves, far from PCAF
* #F1 up-flow	$\mathbb{R} > \mathbb{R}_{cU}$	-1		Oil sticks to the pipe wall.
* #2 down-flow	$\mathbb{R}_{cL} < \mathbb{R} < \mathbb{R}_{cU}$	-1	-1	Intermittent corkscrew waves are observed.
* #3 down-flow	$\mathbb{R}_{cL} < \mathbb{R} < \mathbb{R}_{cU}$	-1	-1	Intermittent corkscrew waves are observed.
* #4 down-flow	$\mathbb{R} >> \mathbb{R}_{cU}$	+1		Disturbed bamboo waves, perhaps not far from PCAF, are observed.

* fig. VII.16.1

VIII.9 Summary and Discussion of the Application of Ginzburg-Landau Equations to Core-Annular Flow

(1) There are regions of parameter space in which PCAF is possible and the neutral curves consist of an upper branch and a lower branch. For these parameters we can write two Ginzburg-Landau equations, one near the minimum point of the upper branch and another near the maximum point of the lower branch. At the upper branch, PCAF loses stability to waves generated by interfacial friction. At the lower branch PCAF loses stability to capillary waves.

(2) There are many regions of parameter space in which PCAF is not possible, and bifurcation analysis is not applicable.

(3) The singular value decomposition is a useful numerical method for computing all the coefficients of Ginzburg-Landau equation.

(4) The stability of wavy flows near the upper branch of the neutral curve can be controlled by varying the density ratio ζ_2 . For example, when the other parameters are fixed we can choose a best ζ_2 (say $\hat{\zeta}_2$,) to maximize the minimum critical value $\mathbb{R}_U(\zeta_2)$ of the linear theory on the upper branch of the neutral curve (chapter VII). The bifurcation of waves from the upper branch $\mathbb{R}_U(\zeta_2)$ of the neutral curve will be supercritical if ζ_2 is large enough. For smaller values of ζ_2 the bifurcation is subcritical.

(5) The lower branch is less sensitive to changes in ζ_2 than the upper branch. The critical Reynolds number above which down-flow is linearly stable decreases with increasing ζ_2. In up-flow, smaller values of ζ_2 lead to larger regions of linear stability (chapter VII). The bifurcation of the lower branch is controlled by the viscosity difference and surface tension. Changes of ζ_2 do not change the directions of bifurcation of the lower branch.

(6) The viscosity ratio, m, plays a key role in determining both the linear and nonlinear stability of core-annular flows. When m is small, linearly stable PCAF cannot be achieved (chapter VI). Stable PCAF can be achieved only when the viscosity difference $1 - m$ is small.

(7) Other things being equal, the linear theory tells us that we will get larger intervals of the Reynolds number in which PCAF is stable if the lubricating layer is thin ($a \to 1$). We can say that this stability will be realized practically even when PCAF is unstable, if the bifurcating solutions of small amplitude are stable. This means that a robust form of lubricated pipelining with thin lubricating films is expected when the bifurcations are supercritical, but nonlinear failures may occur when the bifurcations are subcritical. On the other hand, there are cases for which increasing the thickness of the lubricating layer can change subcritical to supercritical bifurcation.

(8) When the flows are slight perturbations of PCAF, experiments agree perfectly with both linear and nonlinear theories. One example is the experiment #2 of figure V.1.1. The operating Reynolds number of the experiment is slightly above the nose of the upper branch of the neutral curve where the bifurcation is found to be supercritical. An even more convincing example is the free-fall experiment of chapter VII in which PCAF is predicted and observed.

(9) The finite amplitude bamboo waves (plate V.1.2) are evidently too far from PCAF to be described by our Ginzburg-Landau equation. In many practical situations described in chapter VII, the bifurcation theory can not be applied because the corresponding PCAF is linearly unstable at all Reynolds numbers. In other cases, the bifurcations near the nose of the upper branch are subcritical. These results suggest that bamboo waves and other flows far from PCAF perhaps may be best treated by direct numerical methods.

VIII.10 Nonlinear Amplitude Equations for Long Waves

In the case of very long waves, it would be impossible to obtain an amplitude equation of the Ginzburg-Landau type. The critical wave number at the nose tends to zero so that the wave you are supposed to modulate is already hugely long.[2] In this situation, there are other types of approximations which give rise to nonlinear amplitude equations describing a slowly varying waveform rather than the slowly varying envelope of a modulated wave as in the Ginzburg-Landau equation. This type of approach was pioneered by Benney [1966]. For core-annular flow in a pipe, a similar approach based on the lubrication approximation in the annulus has been developed by Frenkel , Babchin, Levich, Shlang and Sivashinsky [1987], Frenkel [1988] and Papageorgiou, Maldarelli and Rumschitskii [1990]. Inertia of the fluid in the annulus is completely neglected in the derivation of the nonlinear amplitude equation which arises at lowest order. This means that such theories automatically rule out motions in which secondary flows are involved. It is thought that such theories are particularly relevant to very thin films in situations in which the most amplified wave of linear theory is very long.

In general, the inertia term in the Navier-Stokes equation $\rho(\mathbf{u} \cdot \nabla)\mathbf{u}$ induces wave number multiplication which produces shorter and shorter waves. A monochromatic linear wave proportional to $\exp(i\tilde{\alpha}x)$, where $\tilde{\alpha}$ is the wave number of maximum linear growth, undergoes multiplications leading to $\exp(\pm 2i\tilde{\alpha}x)$ and mean terms: the nonlinear interactions of these lead to $\exp(\pm 4i\tilde{\alpha}x)$, and so on. The nonlinear terms therefore rapidly produce short waves from long ones. This type of generation of short waves from long ones due to inertia is automatically removed by assuming the scales used in lubrication-based theories which allow inertia to be treated only as a perturbation, if at all. The amplitude equation which appears at lowest order has a nonlinear, wave-shortening term $\eta\ \partial\eta/\partial x$ which is controlled at the interface by surface tension. But we do not know if the neglected inertia terms in the fluid can be controlled by surface tension. Maybe the dynamics will not allow the assumed slow scales. If the dissipative terms do not dissipate the short waves, they will begin to dominate the dynamics, but their effects will not be captured by the amplitude equation. For this reason, we think that if the problem is to follow the evolution of the amplitude of a wave under conditions in which the wave number of maximum growth is bounded strictly away from zero, the application of a long wave equation could lead to irrelevant results. Solutions of a hierarchy of equations (the higher-order equations in the perturbation series) pinned on the amplitude equation which converge and preserve slow scales may fail

[2] We are indebted to A. Frenkel for this remark. He noted that to have a Ginzburg-Landau equation the sideband width $\Delta\alpha$ ought to be small relative to the wave number α on which it centers.

to satisfy the Navier-Stokes equations. This problem appears not to have been studied with the tools of analysis, numerical analysis or by comparison with experiments.

We have been trying to determine the conditions under which the predictions of the lubrication-based amplitude equations for lubricated pipelining may be realized in an experiment. These amplitude equations are appropriate when there is a thin lubricating film of water on the pipe. Very thin water films have not yet been seen in experiments in which the flow rates of oil and water are prescribed. In these cases, the film thickness is a functional of the solution. If the water flow rate is reduced or the flow rate of oil is increased, the oil will stick to the wall and/or the water will emulsify into the oil, leading to a failure of lubrication. It may be hard to achieve the conditions required to test the predictions of the nonlinear amplitude equations based on the lubrication approximation. On the theoretical side, we have studied the conditions of validity for the amplitude equations based on lubrication theory. For water-lubricated pipelining, the oil in the core is typically 100 times more viscous than the lubricating water. For the lubrication-based theory to be applicable even under the moderate operating condition of order one core Reynolds number, the water film has to be extremely thin. If it is not thin, the inertia of the water film will not be negligible. Indeed, examination of the special case of long waves in section VIII.14 shows that the lubrication-based theory applies only when the dimensionless film thickness is small compared to $m^{2/3}$, where $m = \mu_{water}/\mu_{oil}$, which is typically 10^{-2} or smaller.

VIII.11 Amplitude Equation of Hooper and Grimshaw

Hooper and Grimshaw [1985] derive a nonlinear amplitude equation (the Kuramoto-Sivashinsky equation) which we describe in section IV.8(a). The flow is Couette-Poiseuille between parallel plates with an undisturbed interface at $y = 0$ with $\mathbf{u} = \mathbf{e}_x u_l(y)$, $u_l(y) = A_l y^2 + a_l y + 1$, $l = 1$ for $y < 0$, $l = 2$ for $y > 0$, $A_l = G/2\mu_l$ where G is the pressure gradient. The viscosities of the fluids are μ_l. The dispersion relation for the linear problem when the disturbance wavelength is long compared with the depth of either fluid is given by IV.(8a.66):

$$c = c_o + i\alpha R\{J(m, n, r, A_1) - \alpha^2 S(m, n)\} + O(\alpha^2) \qquad (11.1)$$

where c is the complex wavespeed, α is the disturbance wavenumber, and c_0 is real. The viscosity, density and depth ratios are denoted by $m = \mu_2/\mu_1$, $r = \rho_2/\rho_1$ and $n = d_2/d_1$, respectively. $R = U_0 d_1/\nu_1$ is the Reynolds number. J and S are rational functions of the parameters defined by IV.(8a.64 - 65). $S(m, n)$ is proportional to surface tension.

Hooper and Grimshaw did a weakly nonlinear long-wave analysis assuming IV.(8a.19 - 20):

$$\eta = \varepsilon A(\xi, \tau), \quad \xi = \varepsilon(x - c_0 t), \quad \tau = \varepsilon^2 t \tag{11.2}$$

where ε is a small parameter, otherwise unspecified, and η is the deviation of the fluid interface from its flat position.

The perturbed streamfunction is expanded as IV.(8a.20):

$$\psi(x, y, t; \varepsilon) = \varepsilon\psi_0(\xi, y, \tau) + \varepsilon^2\psi_1(\xi, y, \tau) + \dots \tag{11.3}$$

At $O(\varepsilon^0)$, they recover the basic flow. At $O(\varepsilon)$, they get Yih's stability result. The eigenfunctions are expressed in terms of the unknown amplitude $A(\xi, \tau)$ which is determined by solvability conditions at second order. These conditions yield the amplitude equation IV.(8a.62):

$$A_\tau + RJ(m, n, r, A_1)A_{\xi\xi} + \varepsilon^2 RS(m, n)A_{\xi\xi\xi\xi} = -l(m, n)AA_\xi \tag{11.4}$$

where the subscripts are partial derivatives with respect to the corresponding variables, and $l(m, n)$ is a rational function found by analysis.

We can deduce the left-hand side of (11.4) from (11.1) formally by replacing α with $-i\frac{\partial}{\partial x}$ and αc by $i\frac{\partial}{\partial t}$. Then $\alpha cA = \alpha c_0 A + i\alpha^2 R(J - \alpha^2 S)A$ to within terms of order α^3 and

$$i\frac{\partial A}{\partial t} = -ic_0\frac{\partial A}{\partial x} - iRJ\frac{\partial^2 A}{\partial x^2} - iRS\frac{\partial^4 A}{\partial x^4}. \tag{11.5}$$

They say that "... retention of the surface tension term requires that $\varepsilon^2 S$ is 0(1) in their perturbation expansion.... When S is 0(1) and the term S is ignored, the evolution equation is Burger's equation. When J is positive this equation (with S ignored) describes unstable behavior, and disturbances grow without limit with the shortest wavelengths having the greatest growth rates. It is for this reason that we have included the effects of surface tension in the analysis to ensure that unstable waves possess a high wave number cut-off."

The linear part of the amplitude equation (11.4) is exact in the sense that, linearization of it results in the exact dispersion relation (11.1). Thus, the linear stabilization or destabilization mechanism for the longest waves are preserved in the amplitude equation (11.4). It is important to note that, although the linear instability caused by viscosity stratification persists at arbitrarily small Reynolds numbers, it is necessary to maintain all the inertia terms in the governing equations when performing the stability analysis, as is evident in the dispersion relation (11.1). The second term on the right hand side of equation (11.1), excluding the surface tension contribution, is the sum of the contributions from the inertias of both fluids, and it is the term determining the linear instability or stability of the problem to the leading order.

An amplitude equation similar to (11.4) can be derived for core-annular flow of two fluids in a circular pipe by following the procedure of Hooper and Grimshaw when the wave is long relative to both the core radius and annulus thickness. This amplitude equation has the same linear part as that

of the linearization of the full problem in the same limit, which includes both the contributions from the core and the annulus, but only up to and not including terms of $O(\alpha^2)$. This equation should not be used to describe the nonlinear evolution of systems like those driven by capillary instability, in which the wavenumber $\alpha = \alpha_c$ of maximum growth is bounded strictly away from zero. In such a case, the expression for α_c would involve terms of order α^2 neglected in the analysis (cf. equation (12.16)). Other types of amplitude equations which do not produce the same dispersion relation as the exact linear theory can also be derived for core-annular flow, as well shall see in section VIII.13, but extra conditions must be imposed for the validity of such theories.

VIII.12 Rupture of Thin Films

Theories like those of Hooper and Grimshaw are called long-wave theories. They could be called very long-wave theories since they restrict attention to waves which are longer than all of the physically relevant length scales. In the case of core-annular flow, these very long waves are much longer than the core radius. To get nonlinear descriptions, these theories inevitably introduce restrictions which go beyond the linear long-wave analysis for the exact problem. The usual practice is to choose scales so that the linearization of the amplitude equation agrees at leading order in α with the first term of the expansion of the dispersion relation of the exact problem. If the wavenumber of maximum growth in the exact problem is surpassingly small, then there is perhaps hope for this method. If, on the other hand, the wavenumber of maximum growth is bounded strictly away from zero, then it is not likely that the amplitude equations for the longest waves can represent the observed dynamics.

It is sometimes possible to restrict the values of given parameters in the problem in such a way as to drive the wavenumber of maximum growth toward zero. This formal procedure, proposed for example for the problem of film rupture by A. Frenkel at the end of this section, has many advantages. The expansion may be framed in terms of physically identifiable, externally given parameters with which we can control the wavenumber and force it to zero. We have no control over wave-shortening due to the part of inertia which is quadratic in $\mathbf{u}$, but the linear parts are well-represented.

To illustrate the points just raised, we shall consider the problem of film rupture posed by Williams and Davis [1982] using their notation.

A thin film of mean thickness h_0 lies above a horizontal solid plate. The x-axis is horizontal and the z-axis is vertical. The velocity components are u and w, respectively. The dimensionless equations are

$$u_t + uu_x + wu_z = \nabla^2 u - p_x - \phi_x,$$

$$w_t + uw_x + ww_z = \nabla^2 w - p_z - \phi_z,$$
$$u_x + w_z = 0,$$
$$\phi = \frac{A}{h^3}, \tag{12.1}$$

where ϕ is the potential of the van der Waals forces, A is the dimensionless Hamaker constant and $h(x,t)$ is the dimensionless film thickness. At $z = 0$,

$$u = w = 0. \tag{12.2}$$

At $z = h(x,t)$, we have the following free surface conditions:

$$w = h_t + uh_x,$$
$$(u_z + w_x)(1 - h_x^2) + 2h_x(w_z - u_x) = 0,$$
$$-p + 2\frac{(1 - h_x^2)w_z - h_x(u_z + w_x)}{(1 + h_x^2)} = \frac{3Sh_{xx}}{(1 + h_x^2)^{3/2}}, \tag{12.3}$$

where S is a dimensionless surface tension parameter.

The basic state is static with

$$\hat{h} = 1, \quad \hat{p} = \text{constant},$$
$$\hat{u} = \hat{v} = \hat{w} = 0, \quad \hat{\phi} = A. \tag{12.4}$$

The linearized stability of this basic state is governed by

$$u_t = \nabla^2 u - p_x - \phi_x,$$
$$w_t = \nabla^2 w - p_z - \phi_z,$$
$$u_x + w_z = 0,$$
$$\phi = -3A\delta,$$

where u, w, p and ϕ are perturbed quantities and δ is the deviation of the free surface from $\hat{h} = 1$. At $z = 0$, $u = w = 0$. At $z = 1$,

$$w = \delta_t, \quad u_z + w_x = 0, \quad -p + 2w_z = 3S\delta_{xx}. \tag{12.5}$$

We introduce normal modes $(u,\ w,\ p,\ \delta) = (U(z),\ W(z),\ P(z),\ \eta)$ $\exp i\alpha(x - ct)$.

VIII.12(a) Long Waves

For long waves, we can expand U, W, P, c and η in powers of α. To compare the long-wave analysis with the lubrication theory of Williams and Davis in the linearized case, we need to carry out the analysis to order α^4. We eliminate P and U throughout the equations.

Zeroth order: $W_0 = 0$, c_0 and η_0 undetermined.

Order α: $W_1 = 0$, $c_0 = 0$.

Order α^2: $W_2 = -\frac{A}{2}\eta_0(z^3 - 3z^2)$, $c_1 = iA$.
Order α^3: $W_3 = -\frac{A}{2}\eta_1(z^3 - 3z^2)$, $c_2 = 0$.
Order α^4: $W_4 = -\frac{A}{2}\eta_0(-2 + ic_1)(\frac{-z^5}{20} + \frac{z^6}{120}) + \frac{B_1 z^3}{6} + \frac{B_2 z^2}{2}$,
$c_3 = i(-S + \frac{A}{12} + \frac{A^2}{24})$,
where

$$B_1 = 3S\eta_0 - 3A\eta_2 + A\eta_0(5/2 - ic_1/2),\ B_2 = -3S\eta_0 + 3A\eta_2 - A\eta_0(3/4 - ic_1/8),$$

and η_2 is undetermined.

Therefore, the eigenvalue up to $O(\alpha^3)$ is given by

$$c = i(\alpha A - \alpha^3 S + \alpha^3 A/12 + \alpha^3 A^2/24). \tag{12.9}$$

VIII.12(b) Lubrication Theory

We return now to the nonlinear problem. Williams and Davis expanded the variable u and w in powers of α as before, but p is expanded differently:

$$p = \frac{1}{\alpha}(p_0 + \alpha p_1 + O(\alpha^2)), \tag{12.10}$$

and $h = 1 + \delta$ is not expanded at all. Clearly, even at this stage, there is a big difference between the lubrication theory and that of long waves.

To justify (12.10), Williams and Davis assume that $(12.5)_3$ gives, at zeroth order,

$$-p_0 = 3\bar{S}h_{\xi\xi}, \tag{12.11}$$

where $\bar{S} = O(1)$ and $\xi = \alpha x$. This implies that

$$\bar{S} = \alpha^3 S = O(1). \tag{12.12}$$

Otherwise, you don't get (12.10). This is the typical assumption (see Atherton and Homsy [1975]) used to retain surface tension at the lowest order.

In the same spirit, Williams and Davis assumed

$$\bar{A} = \alpha A = O(1). \tag{12.13}$$

Then $\bar{A}$ and $\bar{S}$ appear in their problem at zeroth order.

The amplitude equation of Williams and Davis is

$$h_t + A(h_x/h)_x + S(h^3 h_{xxx})_x = 0. \tag{12.14}$$

After linearization around $h = 1$, this gives the dispersion relation

$$c = i(\alpha A - \alpha^3 S). \tag{12.15}$$

This can be compared to (12.9), and (12.15) is correct when (12.12) and (12.13) hold. The long-wave expression (12.9) is correct up to order α^3 for all bounded values of A and S, without further restrictions.

The most interesting α is the one which gives rise to the maximum growth rate. Ideally, for long waves, α=0 would be best. In the present case, the α giving maximum growth is

$$\alpha_m = \sqrt{\frac{A}{2S - \frac{A}{12} + \frac{A^2}{24}}}. \tag{12.16}$$

Williams and Davis cite the values $A = 10^{-4}$ and $S = 0.1$ as typical. For these values, $\alpha_m \approx \sqrt{A/2S} = 1/\sqrt{2000}$. This is small, so that we might expect to see agreement with the long-wave analysis.

We could hope that for the typical values of A and S which give a small α_m, the order conditions (12.12)-(12,13) for the lubrication theory would hold. However,

$$\bar{A} = \alpha_m A = \frac{1}{10^4\sqrt{2000}}, \qquad \text{and} \qquad \bar{S} = \alpha_m^3 S = \frac{1}{10(2000)^{3/2}}$$

are not of order one. Obviously, you need special conditions, beyond long waves, to get equation (12.14).

One problem of the lubrication theory just reviewed is that the specification of the condition beyond long waves for which the theory applies, is not framed in terms of the parameters of the problem: the wavenumber α is in some sense a functional of the solution. Frenkel (1990) in a personal communication has suggested to us that the region of validity of the equation derived by Williams and Davis can be greatly extended by discarding conditions like $\alpha^3 S = O(1)$ and replacing them with conditions on parameters which insure the length $2\pi/\alpha_m$ of the wave that grows fastest is large. Frenkel in particular has carried out the analysis, based on *two* small parameters $\sqrt{A/2S}$ and A^2/S without placing any restrictions on α. These restrictions can be regarded as an alternative to the thin-film assumption.

VIII.13 Amplitude Equations of Frenkel et al. and Papageorgiou et al.

Frenkel *et al.* [1987] considers a core-annular flow of two fluids with matched viscosities and densities. Unlike the long-wave analysis of the Hooper-Grimshaw type, this analysis does accomodate capillary instability. It predicts that in a certain range of parameters, capillary instabilities saturate nonlinearly, producing chaotic waves rather than film rupturing. Since the viscosity difference is neglected, the linear mechanism of shear stabilization through interfacial friction which is routinely observed in experiments is absent from the analysis. Besides requiring that the layer thickness be small relative to the core radius, the analysis requires small Reynolds numbers in the annulus, as well as other conditions. They derive a Kuramoto-Sivashinsky equation of the form (13.6) below with $DI = 0$. This equation

gives rise to bounded but chaotic solutions which are said to saturate the linear instability.

Frenkel, responding to results of the analysis of the stabilizing effect of interfacial friction, found a method for dealing with the dynamical effects of the core in which lubrication approximations are inappropriate. He used lubrication theory in the gap and a different approximation which is basically not restricted to long waves in the core. He obtained a nonlinear amplitude equation with additional linear terms, equivalent to the term DI in (13.6), which gave rise to dispersion and dissipation. Smooth rather than chaotic waves then saturate unstable core-annular flow (see Papageorgiou *et al.* [1990]). He identified four parameters

$$\varepsilon_1 = \frac{J\varepsilon^2}{\mathbb{R}_1}, \quad \varepsilon_2 = \frac{\mathbb{R}_1}{\varepsilon J}, \quad \varepsilon_3 = \frac{1}{m-1}, \quad \varepsilon_4 = \mathbb{R}_1 \tag{13.1}$$

which must each be small (and positive) for his theory to be valid. ϵ in (13.1) is defined as $(R_2 - R_1)/R_1$ where R_2 and R_1 are the radius of the pipe and the oil core, respectively. $\mathbb{R}_1$ and J are the core Reynolds number and dimensionless surface tension parameter defined in section VI.1. Since $\varepsilon_1\varepsilon_2 = \varepsilon$, the film thickness must be small.

Frenkel also uses his equation to discuss the case of lubricated pipelining in which $m < 1$ and $\varepsilon_3 < 0$, but he does not give the justification of his theory for this case. He notes that his equations give rise to shear stabilization due to viscosity stratification (interfacial friction) without nonlinear effects when

$$\mathbb{R}_1\alpha \ll 1 \quad \text{and} \quad \frac{mJ\varepsilon}{\mathbb{R}_1^2} \ll 1. \tag{13.2}$$

This can be interpreted as shear stabilization for small gaps ($\varepsilon \ll 1$) and long waves ($\alpha \ll 1$). We shall see that this shear stabilization is correct in the case of very thin films to which the lubrication theory applies.

Frenkel's idea was further developed and systematized in the work of Papageorgiou *et al.* [1990]. They obtain a nonlinear equation for the evolution of the interface from the analysis of a solution of the problem in powers of the film thickness $\varepsilon \ll 1$. They found that the inertia of the water in the thin annulus may be neglected at leading order and they took into account the dynamics of the core in an approximation introduced by Frenkel. They found that in addition to the requirement that $\varepsilon \ll 1$ it was also necessary to guarantee that

$$\frac{\varepsilon J}{\mathbb{R}_1} = 0(1). \tag{13.3}$$

This condition can be satisfied in two ways:

$$\mathbb{R}_1 = \varepsilon, \quad J = 0(1) \tag{13.4}$$

which gives rise to a low Reynolds number approximation, and

$$\mathbb{R}_1 = 0(1), \quad J = 1/\varepsilon \tag{13.5}$$

which is a large surface tension approximation. The condition $(13.5)_2$ may be written as $R_1 = (\rho\nu_1^2)/(T\epsilon)$ where T is surface tension. For heavy crudes, $T = 20$ dyn/cm, $\mu_1 = 10^3$ p, and if $\epsilon = 0.1$ ($J = 10$) say, then $R_1 = 0(10^6\text{cm})$ which is not a reasonable size. Obviously, (13.5) is a very restrictive condition.

If $\varepsilon \ll 1$ and (13.3) is satisfied, then they find an amplitude equation in the form

$$\eta_\tau - \frac{2}{m}\eta\eta_z + \frac{J\varepsilon}{3\mathbb{R}_1 m}(\eta + \eta_{zz})_{zz} + DI = 0 \tag{13.6}$$

where t, x are physical variables such that

$$\tau = \varepsilon^2 t, \quad z = \varepsilon(x - W(1)t), \tag{13.7}$$

$W(1)$ being the interfacial velocity of the basic flow. The term DI is a linear term which depends globally on the wave number. Equation (13.6) was given by Frenkel [1988] but the term DI was expressed in an abstract rather than explicit manner.

In the small Reynolds number case (13.4) Papageorgiou *et al.* find that the core dynamics is governed by Stokes flow

$$\begin{aligned} &\nabla^2 U_0 - \frac{1}{r^2}U_0 = \varepsilon\mathbb{R}_1\partial_r P_0, \qquad \nabla^2 W_0 = \varepsilon\mathbb{R}_1\partial_z P_0, \\ &\partial_r(rU_0) + \partial_z(rW_0) = 0. \end{aligned} \tag{13.8}$$

The stream function for (U_0, W_0) satisfies a partial differential equation of fourth order which is solved by the method of Fourier transforms. The transform of the stream function satisfies an ordinary differential equation which can be solved by Bessel functions. The stream function for the core can be expressed by the inversion integral which is a global expression in wave number space and not restricted to long waves. The core quantities on the interface can be expressed in terms of this inversion integral and they appear in the term DI as follows:

$$DI = \frac{i}{\pi m}\left(1 - \frac{1}{m}\right)\int_{-\infty}^{\infty} \aleph_B(k) \int_{-\infty}^{\infty} \eta(y,\tau)\exp\{ik(z-y)\}\,dydk, \tag{13.9}$$

where

$$\aleph_B = \frac{k^2 I_1^2(k)}{kI_1^2(k) - kI_0^2(k) + 2I_0(k)I_1(k)}, \tag{13.10}$$

and $I_0(k)$ and $I_1(k)$ are Bessel functions.

The linear term DI given above is purely dispersive so that it cannot stabilize the capillary instability. In fact, shear stabilization is associated with the inertia of the basic flow, which is neglected here both in the core and the annulus. You don't have much shear stabilization at very low Reynolds numbers, so the analysis and the physics are not incompatible.

In the second case (13.5), where the surface tension is supposed to be large, a Stokes flow approximation in the core is not appropriate. The core inertia of the basic flow must be taken into account and this can lead to shear stabilization [Frenkel 1988]. In the analysis of Papageorgiou *et al.* [1990], the inertia of the core is explicitly represented. The core equations are given by

$$\begin{aligned}(1-r^2)\frac{\partial U_0}{\partial z} &= -\frac{\partial P_0}{\partial r} + \frac{1}{\mathbb{R}_1}\left(\frac{\partial^2}{\partial r^2} + \frac{1}{r}\frac{\partial}{\partial r} + \frac{\partial^2}{\partial z^2} - \frac{1}{r^2}\right) U_0 \\ &\quad - 2rU_0 + (1-r^2)\frac{\partial W_0}{\partial r} \\ &= -\frac{\partial P_0}{\partial z} + \frac{1}{\mathbb{R}_1}\left(\frac{\partial^2}{\partial r^2} + \frac{1}{r}\frac{\partial}{\partial r} + \frac{\partial^2}{\partial z^2}\right) W_0 \end{aligned} \tag{13.11}$$

The neglected terms $\frac{\partial U_0}{\partial t}$ and $\frac{\partial W_0}{\partial t}$ are rigorously zero in a coordinate system which moves with the speed c_0 of the wave.

The solution of (13.11) together with the continuity equation can be obtained by the method of Fourier transforms, as indicated already, and the stream function can be expressed by the inverse transform. This leads again to (13.6) but now with

$$DI = \frac{-i}{2\pi m}\left(1 - \frac{1}{m}\right)\int_{-\infty}^{\infty} \aleph_K(k) \int_{-\infty}^{\infty} \eta(y,\tau)\exp\{k(z-y)\}\, dydk, \tag{13.12}$$

where

$$\aleph_K(k) = \frac{I_1(k)\exp[-\lambda]M(\Lambda, 2, 2\lambda)}{N_1(k)I_0(k) - N_2(k)I_1(k)}, \tag{13.13}$$

with

$$\lambda = \frac{1}{2}\sqrt{k\mathbb{R}}\,\exp[-i\frac{\pi}{4}], \qquad \Lambda = 1 + \frac{k^2}{8\lambda} - \frac{\lambda}{2},$$

$$N_1(k) = \int_0^1 \left(I_1(k)K_1(kt) - I_1(kt)K_1(k)\right) t^2\, \exp[-\lambda t^2]M(\Lambda, 2, 2\lambda t^2)dt,$$

$$N_2(k) = \int_0^1 \left(I_o(k)K_1(kt) + I_1(kt)K_0(k)\right) t^2 \exp[-\lambda t^2]M(\Lambda, 2, 2\lambda t^2)dt$$

and M is the confluent hypergeometric function (the Kummer function). The functions I and K are the modified Bessel functions.

The analyses of Frenkel and Papageorgiou *et al.* and the calculation in the next section show that DI given by (13.9) or (13.12) gives rise to dissipation as well as to dispersion. We get shear stabilization from (13.12) which represents the contribution from the inertia of the core. The amplitude equation (13.6) is quite general in the sense that it is capable of describing waves with wavelengths comparable to the core radius, although the wavelengths are required to be long compared to the thickness of the

annulus. On the other hand, the contribution from the inertia of the annulus is totally neglected. Under what circumstances can this omission of the annulus inertia be compatible with the underlying physics, so that equation (13.6) can be applied? This question has not been adequately addressed. For the special case of long waves, with wavelengths long relative to both the core radius and annulus thickness, we will give a critical assessment of the validity of the amplitude equation (13.6) in section VIII.15.

VIII.14 Long-Wave Expansions for the Amplitude Equation (13.6) when =O(1)

We want to compare the stability criteria for long waves which arise from linearizing the nonlinear amplitude equation (13.6) around $\eta = 0$ with stability criteria for long waves for the linearized full problem when $\mathbb{R}_1 = O(1)$.

We first substitute normal modes

$$\eta(z,\tau) = \hat{\eta}\, \exp\left[i\alpha(z - ct)\right] \tag{14.1}$$

into the linearized version of (13.6)

$$\eta_\tau + \frac{J\varepsilon}{3\mathbb{R}_1 m}(\eta + \eta_{zz})_{zz}$$

$$-\frac{i(m-1)}{2\pi m^2}\int_{-\infty}^{\infty} \aleph_K(k) \int_{-\infty}^{\infty} \eta(y,\tau)\exp\left\{ik(z-y)\right\} dydk = 0. \tag{14.2}$$

After using Fourier transforms in the form

$$\aleph_K(\alpha)e^{i\alpha z} = \frac{1}{2\pi}\int_{-\infty}^{\infty}\int_{-\infty}^{\infty} \aleph_K(k)e^{ikz}e^{i(k-\alpha)y}dkdy,$$

we find that

$$i\alpha c = (\alpha^4 - \alpha^2)\frac{J\varepsilon}{3\mathbb{R}_1 m} - i\frac{m-1}{m^2}\aleph_K(\alpha). \tag{14.3}$$

Asymptotic development of the Kummer function for small α leads to

$$\aleph_K(\alpha) = -4\alpha - i\alpha^2\mathbb{R}_1/12. \tag{14.4}$$

Combining (14.3) and (14.4) and writing $c = c_0 + \alpha c_1$ we find that

$$c = 4\frac{m-1}{m^2} + i\alpha\left[\frac{J\varepsilon}{3\mathbb{R}_1 m} + \frac{m-1}{m^2}\frac{\mathbb{R}_1}{12}\right] = c_0 + \alpha c_1. \tag{14.5}$$

Finally we note that the stability of the solution $\eta = 0$ of (13.6) to long waves depends on the sign of the growth rate $\alpha Im\ c$ corresponding to (14.1). To leading order in α, we have

$$\alpha Im\ c = \alpha^2 \left[\frac{J\varepsilon}{3\mathbb{R}_1 m} + \frac{m-1}{m^2} \frac{\mathbb{R}_1}{12} \right]. \tag{14.6}$$

The eigenvalue c given by (14.5) is related to the eigenvalue C of the exact linearized theory by

$$C - W(1) \sim \varepsilon^2 c + O(\varepsilon^3). \tag{14.7}$$

In the next section we will show that the result (14.6) of lubrication theory is exact in the limit $\varepsilon \to 0$, to which it is said to apply provided that $J = 1/\varepsilon$ and $\mathbb{R}_1 = 0(1)$. Equation (14.6) shows that perfect core-annular flow is always unstable when $\mathbb{R}_1$ is small or the less viscous fluid is inside ($m > 1$). We get shear stabilization when the more viscous fluid is inside and $\mathbb{R}_1$ is increased past a critical value defined by the first zero of (14.6). This shear stabilization is solely due to the inertia of the core which is maintained in the analysis leading to equation (13.6) when $\mathbb{R}_1$=O(1).

VIII.15 Exact Stability Results for Long Waves

Now we shall study the stability of perfect core-annular flow to long waves ($\alpha \approx 0$) without using the approximations (one of which is $\varepsilon \to 0$) of lubrication theory. We will show that the two theories give rise to the same result in the limit $\alpha \to 0$ and $\varepsilon \to 0$. However, the results of lubrication are not robust; they change qualitatively when ε is finite. In particular, for larger values of ε, greater than say $\tilde{\varepsilon}(m)$, the core is destabilizing, and we have $\tilde{\varepsilon}(m) \to 0$ as $m \to 0$. Moreover, the inertia of the lubricating fluid in the annulus which is negligible (of order ε^3) when $\varepsilon \to 0$ becomes important when $\varepsilon > \tilde{\tilde{\varepsilon}}(m)$ and $\tilde{\tilde{\varepsilon}}(m) \to 0$ as $m \to 1$.

We may hope that an asymptotic theory is actually applicable under less restricted conditions than are required for its strict mathematical validity. We do not appear to have such good luck in the present case.

The analysis of long-wave solutions of the equations of the linearized theory of stability of perfect core-annular flow in a series of powers of the wave number α was done for horizontal flow (section VI.1) and for vertical flow (section VII.7). Here we are going to carry the analysis to a more explicit conclusion suitable for comparison with nonlinear theories, based on lubrication-type approximations. We shall confine our attention to axisymmetric solutions $n = 0$, $v = 0$ for the case in which $\zeta = \rho_2/\rho_1 = 1$, with fluid 1 in the core and fluid 2 in the annulus. We may eliminate the pressure and streamwise perturbations $w(r)$ of velocity and height function η from the governing equations. Then we get an eigenvalue problem for the radial component of velocity $u(r)$ which satisfies VI.(1e.25), $u(0) = 0$ and $u'(0)$

is bounded. At the solid wall $r = a$, $u(a)$ satisfies VI.(1e.26). The interface conditions at $r = 1$ are given by VI.(1e.27), with the last equation replaced by the following equivalent condition:

$$-\left[\!\left[\alpha\Big((W(1)-C)(u'+u)-W'(1)u\Big)\right.\right.$$
$$\left.\left.+\frac{i}{\mathbb{R}}\Big(u'''+2u''-(1+\alpha^2)u'+(1-\alpha^2)u\Big)\right]\!\right]+\frac{2i\alpha^2}{\mathbb{R}_1}[\![mu']\!]$$
$$=\frac{J\alpha(1-\alpha^2)}{\mathbb{R}_1^2}\frac{[\![u']\!]}{[\![W']\!]}. \tag{15.1}$$

Long-wave solutions may be obtained by substituting the series

$$u(r,\ \alpha)=u^{(0)}(r)+\alpha u^{(1)}(r)+O(\alpha^2),\quad C=C^{(0)}+\alpha C^{(1)}+O(\alpha^2) \tag{15.2}$$

into the above equations. $u^{(0)}$ and $C^{(0)}$ satisfy

$$\frac{d}{dr}\left(\frac{1}{r}\frac{d}{dr}\left[r\frac{d}{dr}\left\{\frac{1}{r}\frac{d}{dr}(ru^{(0)})\right\}\right]\right)=0 \tag{15.3}$$

in the core $0 < r < 1$ and in the annulus $1 < r < a$,

$$u^{(0)}(a)=u^{(0)'}(a)=0, \tag{15.4}$$

$$u^{(0)}(0)=0\quad\text{and } u^{(0)'}(0)\text{ is bounded.} \tag{15.5}$$

At the interface $r = 1$,

$$[\![W']\!]u^{(0)}-(W(1)-C^{(0)})[\![u^{(0)'}]\!]=0, \tag{15.6}$$

$$[\![u^{(0)}]\!]=0, \tag{15.7}$$

$$[\![m(u^{(0)''}+u^{(0)'}-u^{(0)})]\!]=0, \tag{15.8}$$

$$[\![m(u^{(0)''''}+2u^{(0)''}-u^{(0)'}+u^{(0)})]\!]=0. \tag{15.9}$$

The first-order problem is an inhomogeneous form of the zeroth order problem

$$\frac{1}{\mathbb{R}_l}\frac{d}{dr}\left(\frac{1}{r}\frac{d}{dr}\left[r\frac{d}{dr}\left\{\frac{1}{r}\frac{d}{dr}(ru^{(1)})\right\}\right]\right)=f_l(r) \tag{15.10}$$

where $f_1(r)$ is for the core $0 \le r < 1$ and $f_2(r)$ is for the annulus $1 \le r \le a$,

$$u^{(1)}(a)=u^{(1)'}(a)=0, \tag{15.11}$$

$$u^{(1)}(0)=0,\quad u^{(1)'}(0)\text{ is bounded.} \tag{15.12}$$

At the interface $r = 1$

$$[\![W']\!]u^{(1)}-[W(1)-C^{(0)}][\![u^{(1)'}]\!]=g_1, \tag{15.13}$$

$$[\![u^{(1)}]\!]=0 \tag{15.14}$$

$$[\![m(u^{(1)''} + u^{(1)'} - u^{(1)})]\!] = 0, \tag{15.15}$$

$$[\![m(u^{(1)'''} + 2u^{(1)''} - u^{(1)'} + u^{(1)})]\!] = g_2, \tag{15.16}$$

where

$$f_l = i[W_l(r) - C^{(0)}](u_l^{(0)'}(r) + u_l^{(0)}(r)/r)', \tag{15.17}$$

$$g_1 = -C^{(1)}[\![u^{(0)'}]\!], \tag{15.18}$$

$$g_2 = i\left\{\frac{J}{\mathbb{R}_1}\frac{[\![u^{(0)'}]\!]}{[\![W']\!]} + \mathbb{R}_1\left[\!\!\left[(W(1) - C^{(0)})(u^{(0)'} + u^{(0)}) - W'(1)u^{(0)}\right]\!\!\right]\right\}. \tag{15.19}$$

The problem adjoint to (15.3) through (15.9) is satisfied by $q(r)$ and $C^{(0)}$. The function $q(r)$ satisfies (15.3)- (15.5), (15.7), (15.8) and

$$\begin{aligned} &[\![q']\!] = 0 \\ &[\![m(q''' + 2q'' - q' + q)]\!] - \frac{[\![W']\!]}{W(1) - C^{(0)}}m(q_1'' + q_1' - q_1) = 0 \end{aligned} \tag{15.20}$$

The adjoint eigenfunction will be used to obtain solvability conditions for the inhomogeneous problem (15.10) - (15.16). One disadvantage of the usual procedure is that, in the final dispersion relation, the contributions from the core inertia and the annulus inertia are not explicitly distinguishable. We notice however that $C^{(1)}$ can be obtained by invoking the Fredholm alternative without actually solving the $O(\alpha)$ problem. The contributions from the inertia of the core and the annulus to $C^{(1)}$ are explicit in the formula obtained by this method and this allows us to not only track the origin of the instability, but also evaluate the relative importance of each contribution. The solvability condition is found in the form

$$\begin{aligned} &\int_0^1 rq_1(r)f_1(r)dr + \int_1^a rq_2(r)f_2(r)dr \\ &\qquad = \frac{1}{\mathbb{R}_1}\left\{q_1^{(1)}g_2 - \frac{q_1''(1) + q_1'(1) - q_1(1)}{W^{(1)} - C^{(0)}}g_1\right\}. \end{aligned} \tag{15.21}$$

We satisfy this condition with an appropriate choice of $C^{(1)}$.

Now we shall list all the parameters and functions which are involved in the determination of $C^{(1)}$ from (15.21).

$$W_1(r) = 1 - \frac{mr^2}{a^2 + m - 1}, \tag{15.22}$$

$$W_2(r) = \frac{a^2 - r^2}{a^2 + m - 1}, \tag{15.23}$$

$$[\![W']\!] = \frac{2(1-m)}{a^2+m-1}, \tag{15.24}$$

$$u_1^{(0)}(r) = \left[(a^2-1)^2 - m\right] r + mr^3, \tag{15.25}$$

$$u_2^{(0)}(r) = (a^2-r^2)^2/r, \tag{15.26}$$

$$C^{(0)} = a^2(a^2-1)/(a^4+m-1), \tag{15.27}$$

$$q_1(r) = D_1 r^3 + F_1 r, \tag{15.28}$$

$$q_2(r) = D_2 r^3 + E_2 r(2ln\ r - 1) + F_2 r + \frac{G_2}{r}, \tag{15.29}$$

$$D_1 = m(a^2-1)^2,$$

$$F_1 = (2a^2+m-2)(2a^2+m-1) + (1-m)(a^2-1)^2 \\ -(a^4+m-1)(4lna+1+m),$$

$$D_2 = -(2a^2+m-2)$$

$$E_2 = 2(a^4+m-1)$$

$$F_2 = 2\{a^2(2a^2+m-2) - 2(a^4+m-1)lna\}$$

$$G_2 = (1-m)(a^2-1)^2 + a^4 + m - 1.$$

Using these formulas, we may evaluate (15.21) and find that

$$C^{(1)} = i\frac{[W(1)-C^{(0)}]^2}{[\![W']\!]u_1^{(0)}(1)[q_1''(1)+q_1'(1)+q_1(1)]} \\ \times \left\{ \mathbb{R}_1(I_c + B_c + I_a + B_a) - \frac{J}{\mathbb{R}_1}\frac{u_1^{(0)}(1)q_1(1)}{W(1)-C^{(0)}} \right\} \tag{15.30}$$

where

$$I_c = \int_0^1 rq_1(r)[W_1(r)-C^{(0)}]\left(u_1^{(0)\prime} + \frac{u_1^{(0)}}{r}\right)' dr \\ = 8m\int_0^1 r^2 q_1(r)[W_1(r)-C^{(0)}]dr, \tag{15.31}$$

$$B_c = q_1(1)\left\{[W(1)-C^{(0)}](u_1^{(0)\prime}(1) + u_1^{(0)}(1)) - W'(1)u_1^{(0)}(1)\right\}, \tag{15.32}$$

$$I_a = \int_1^a rq_2(r)[W_2(r) - C^{(0)}] \left(u_2^{(0)\prime} + \frac{u_2^{(0)}}{r} \right)' dr$$

$$= 8 \int_1^a r^2 q_2(r)[W_2(r) - C^{(0)}] dr, \tag{15.33}$$

$$B_a = q_1(1) \left\{ [W(1) - C^{(0)}](u_2^{(0)\prime}(1) + u_2^{(0)}(1)) - W_2'(1) u_2^{(0)}(1) \right\}. \tag{15.34}$$

Since the disturbances are proportional to $e^{i\alpha(x-ct)}$ and $C^{(0)}$ given by (15.27) is real, the question of stability to long waves is resolved by the sign of Im $C^{(1)}$ given by (15.30). We have $e^{i\alpha(x-ct)} = e^{i(\alpha x - C_0 t)} e^{\alpha^2 Im C^{(1)} t}$ so that we have instability when Im $C^{(1)} > 0$.

We want to trace effects of different terms in the growth rate formula (15.30). The letters I_c and I_a stand for 'integrals' in the core and in the annulus respectively, while B_c and B_a are interface or boundary terms in the core and in the annulus. Actually, using (15.6) and (15.7), we can show that

$$B_a + B_c = 0. \tag{15.35}$$

However, we want to assess the effect of inertia in the core $I_c + B_c$ and inertia in the annulus $I_a + B_a$ on stability.

It can be shown that:

$$[\![W']\!] = \frac{2(1-m)}{a^2 + m - 1} > 0 \quad \text{for } m < 1, \tag{15.36}$$

$$u^{(0)}(1) = (a^2 - 1)^2 > 0, \tag{15.37}$$

$$q_1''(1) + q_1'(1) - q_1(1) = 8m(a^2 - 1)^2 > 0, \tag{15.38}$$

$$W(1) - C^{(0)} = \frac{[\![W']\!](a^2 - 1)^2}{2(a^4 + m - 1)} > 0, \quad \text{for } m < 1 \tag{15.39}$$

$$q_1(1) = (2a^2 + m - 2)(2a^2 + m - 1) + (a^2 - 1)^2 - (a^4 + m - 1)(4ln\ a + 1 + m)$$

$$< 0, \ \forall m, \ a > 1. \tag{15.40}$$

We may use the expressions (15.36) - (15.40) to put (15.30) in a more explicit form:

$$C^{(1)} = i \left\{ \mathbb{R}_1 \frac{1-m}{16m(a^2+m-1)(a^4+m-1)^2} (I_c + B_c + I_a + B_a) + \frac{J}{\mathbb{R}_1} \times \right.$$

$$\left. \frac{-[(2a^2+m-2)(2a^2+m-1)+(a^2-1)^2-(a^4+m-1)(4ln\ a+1+m)]}{16m(a^4+m-1)} \right\}. \tag{15.41}$$

When the viscosities are matched ($m = 1$), only capillary instability is possible.

In figures 15.1 through 15.4 we have plotted the values of the integrals which lead to shear stabilization or shear destabilization in (15.41) as a function of a for different values of m.

Figure 15.1 shows that the inertia $I_c + B_c$ of the oil core is stabilizing when $\varepsilon = a - 1$ is small and is destabilizing when ε is greater than a critical value $\tilde{\varepsilon}(m)$ which depends strongly on m and tends to zero with m.

Figure 15.2 shows that the inertia $I_a + B_a$ of the water annulus is stabilizing when $\varepsilon = a - 1$ is small and $m < 0.8$; otherwise it is destabilizing. The inertia of the annulus is negligible for small ε when m is small, but not when $1 - m$ is small.

Figure 15.3 gives a direct comparison of the contributions of inertia due to the oil and water. The core contributions are dominant for the very smallest values of ε, but not for larger values.

Figure 15.4 shows how the combined action of inertia $I_a + B_a + I_c + B_c = I_a + I_c$ in the core and annulus produces shear stabilization or destabilization. Though the core contribution and the annulus contribution are separately sensitive to the value of m, the combined contribution depends only weakly on m. The flow is stabilized by interfacial friction when $\varepsilon < 0.4$, say, independent of m and is destabilized when ε is larger. The comparison shows that inertia can not be neglected in the annulus when ε is large or when ε is small and m is near 1.

A quantitative estimate for the range of ϵ within which the core contribution dominates and thus the annulus contribution can be safely neglected, can be obtained by examining the asymptotic expansions for the contributions of inertia in the core and the annulus when the annulus is thin. When $\epsilon << 1$, we have

$$I_c + B_c = \frac{-4}{3} m^2 \epsilon^2 + O(\epsilon^3), \quad I_a + B_a = \frac{128}{15}(-4 + 5m)\epsilon^5 + O(\epsilon^6). \tag{15.42}$$

For the lubricated case ($m < 1$) and a thin annulus ($\epsilon << 1$), the contribution $I_c + B_c$ of the core is always negative and stabilizing, while the contribution $I_a + B_a$ of the annulus is negative and stabilizing only when $m < 0.8$. Thus, when $m < 0.8$, both the core and the annulus are stabilizing, and the contribution from the annulus is negligible if $-(128/15)(-4 + 5m)\epsilon^5 << (4/3)m^2\epsilon^2$. This leads to

$$\epsilon << \left(\frac{5}{32} \frac{m^2}{4 - 5m}\right)^{1/3}. \tag{15.43}$$

When m is small, this reduces to

$$\epsilon << 0.34 m^{2/3}. \tag{15.44}$$

When $m = 0.05$, (15.44) indicates that the inertia in the annulus can be safely neglected when $\epsilon << 0.046$, which is consistent with figure 15.1(b).

We may derive a criterion like (15.44) by quantitative arguments when $m < 1$. The film Reynolds number is defined by

$$\mathbb{R}_f = \frac{W(1)(R_2 - R_1)}{\nu_2}. \tag{15.45}$$

$\mathbb{R}_f$ is related to the core Reynolds number $\mathbb{R}_1$ by the relation

$$\mathbb{R}_f = \mathbb{R}_1 \frac{\epsilon}{m} \frac{\epsilon(2+\epsilon)}{\epsilon(2+\epsilon)+m}. \tag{15.46}$$

The expansion scheme leading to the omission of inertia in the annulus and to the amplitude equation (13.6) is actually an expansion in the parameter $\epsilon\mathbb{R}_f$. For the inertia of the annulus to be negligible, one requires that $\epsilon\mathbb{R}_f << 1$. When ϵ is also small, (15.46) reduces to $\mathbb{R}_f = \mathbb{R}_1(\epsilon^2/m^2)$. Hence

$$\epsilon << m^{2/3}, \tag{15.47}$$

when $\mathbb{R}_1 = O(1)$. This is consistent with the criterion (15.44).

When $0.8 < m < 1$, inertia in the core is stabilizing but inertia in the annulus is destabilizing when ϵ is small. In this situation, the contribution from the annulus is negligible if

$$\epsilon << (\frac{5}{32}\frac{m^2}{5m-4})^{1/3}. \tag{15.48}$$

When the core fluid is less viscous ($m > 1$), and the multiplier in the first term on the right hand side of (15.30) is negative, the asymptotic formula (15.42) indicates that when $\epsilon << 1$ the core inertia is destabilizing and the annulus inertia is stabilizing. When (15.48) is satisfied, however, the stabilizing effect of the annulus can be neglected, as in the numerical studies for the case $m > 1$ by Papageorgiou *et al.*

VIII.16 Comparison of Lubrication Theory with Exact Theory

The lubrication theory is in perfect agreement with the exact theory in the long-wave case $\alpha \to 0$ when the assumption $\varepsilon \to 0$ of the lubrication theory is valid. This may be demonstrated analytically by setting $a = 1+\varepsilon$ in the expressions (15.27), (15.39), and (15.41), giving $C^{(0)}$ and $C^{(1)}$, then expanding in powers of ε. After comparing the result with the expression from lubrication theory (14.5), we find first that

$$W(1) - C^{(0)} \to \frac{4(m-1)}{m^2} = c_0\varepsilon. \tag{16.1}$$

Then, after setting $B_c + B_a = 0$ in (15.41) we find that

$$I_c = -\frac{4}{3}m^2\varepsilon^2 + 0(\varepsilon^3) \tag{16.2}$$

and

$$I_a = 0(\varepsilon^3). \tag{16.3}$$

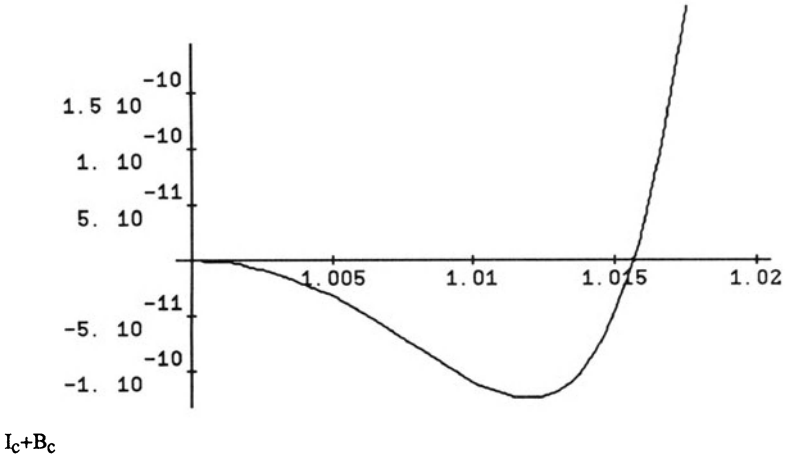

(a)

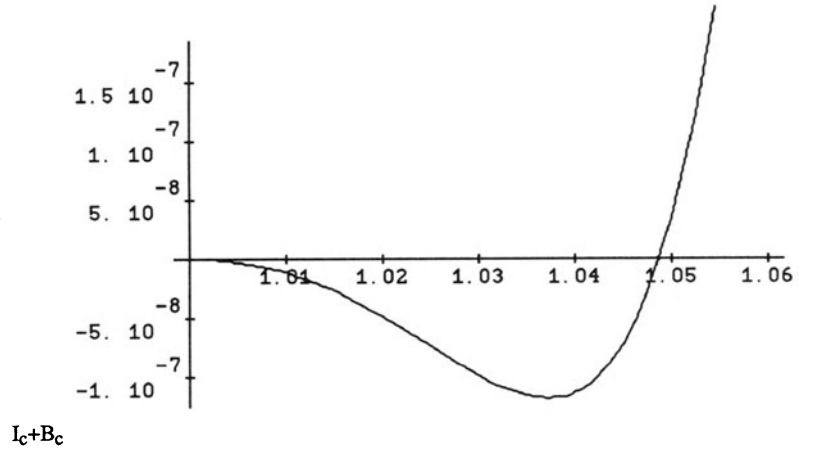

(b)

Fig. 15.1(a-d). [Chen and Joseph, 1991b, American Institute of Physics] The inertia contribution $I_c + B_c$ of the oil core to instability of perfect core-annular flow as a function of $a = R_2/R_1 \geq 1$: (a) $m = 0.001$, (b) $m = 0.01$, (c) $m = 0.1$, (d) $m = 0.95$. The core contribution is stabilizing when $\varepsilon = a - 1$ is small and is destabilizing when ε is larger than a critical value $\tilde{\varepsilon}(m)$ which tends to zero with m. For small m the core is effectively destabilizing for all but the smallest ε.

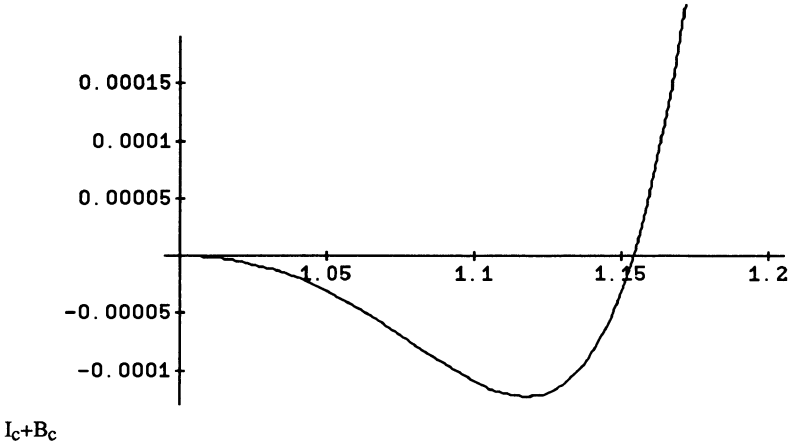

(c)

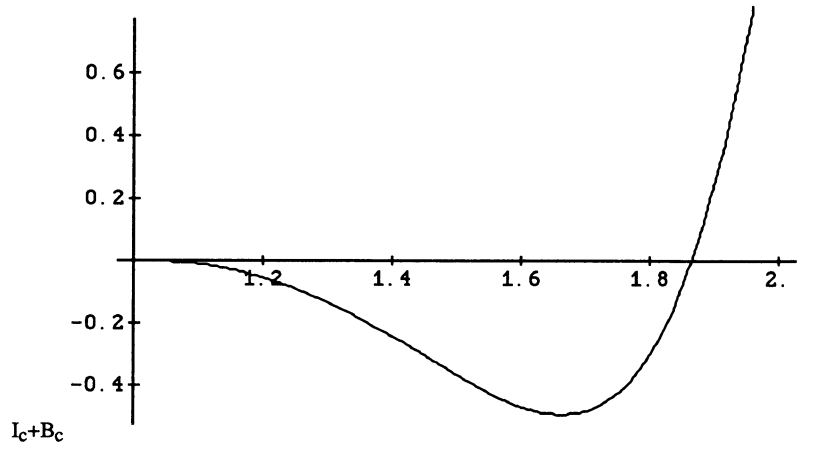

(d)

Fig. 15.1(c-d). Continued.

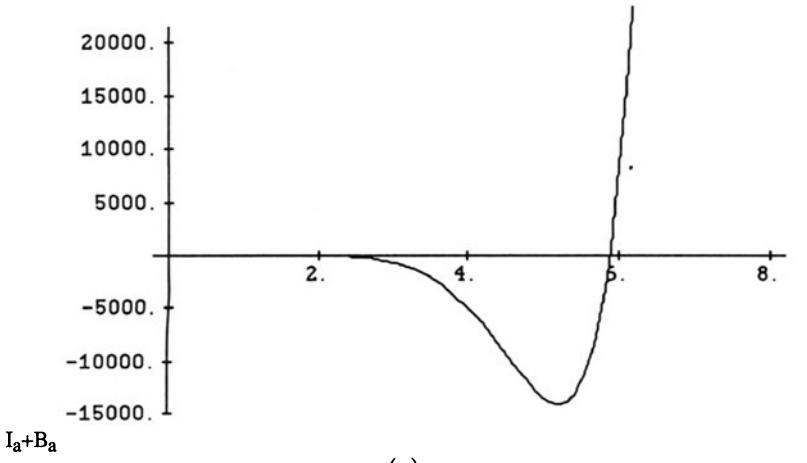

(a)

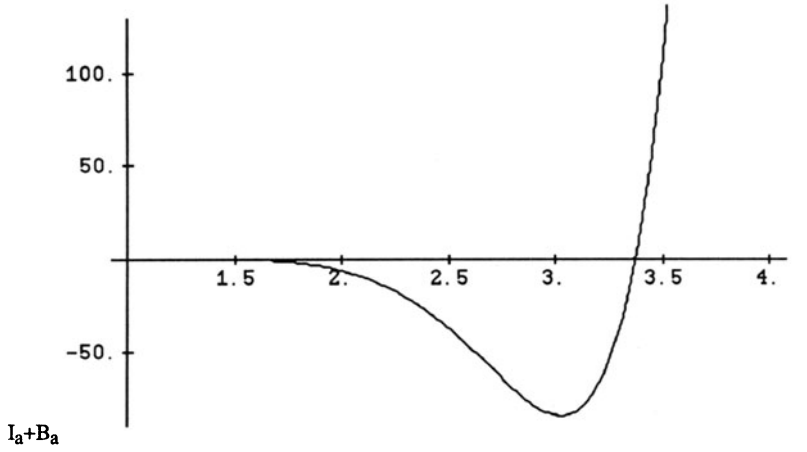

(b)

Fig. 15.2(a-b). [Chen and Joseph, 1991b, American Institute of Physics] The inertial contribution $I_a + B_a$ of the water annulus to the instability of core-annular flow as a function of a: (a) m=0.001, (b) m=0.5. The inertia in the annulus is stabilizing for small ε when $m < 0.8$ and is destabilizing for all ε when $m \geq 0.8$ (see also figure 15.3).

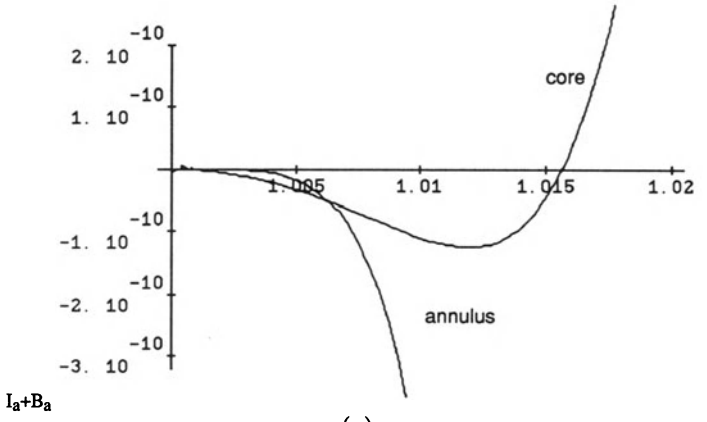

(a)

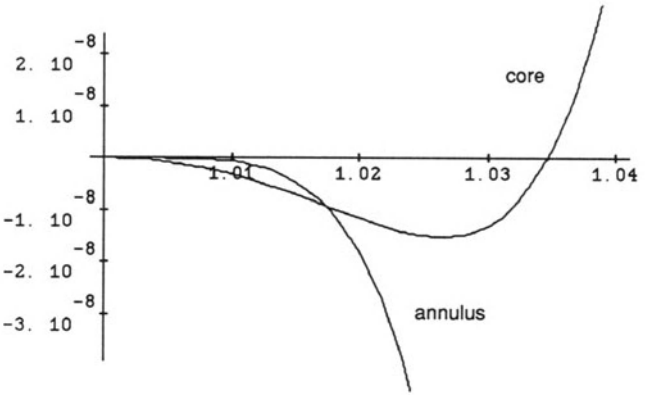

(b)

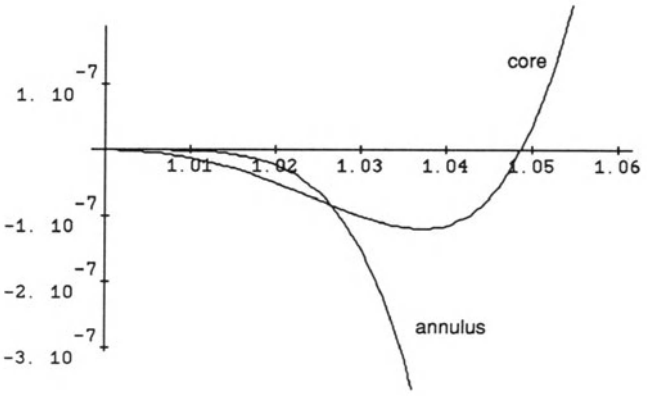

(c)

Fig. 15.3(a-j). [Chen and Joseph, 1991b, American Institute of Physics] Comparison of the contributions of inertia of the water annulus $I_a + B_a$ and oil core $I_c + B_c$ to the long-wave instability of core-annular flow as a function of a: (a) m=0.001, (b) m=0.005, (c) m=0.01, (d) m=0.05, (e) m=0.1, (f) m=0.3, (g) m=0.5, (h) m=0.7, (i) m=0.8, (j) m=0.95. The inertia in the annulus is stabilizing for small ε when $m < 0.8$, destabilizing for $m \geq 0.8$.

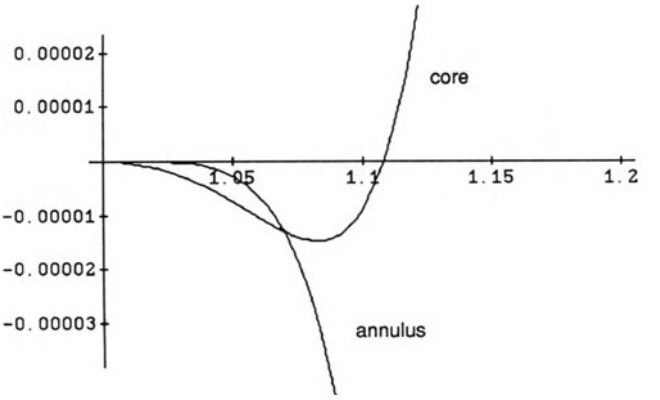

(d)

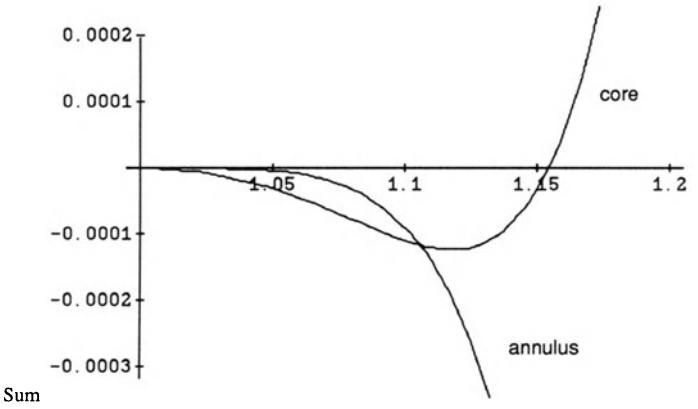

(e)

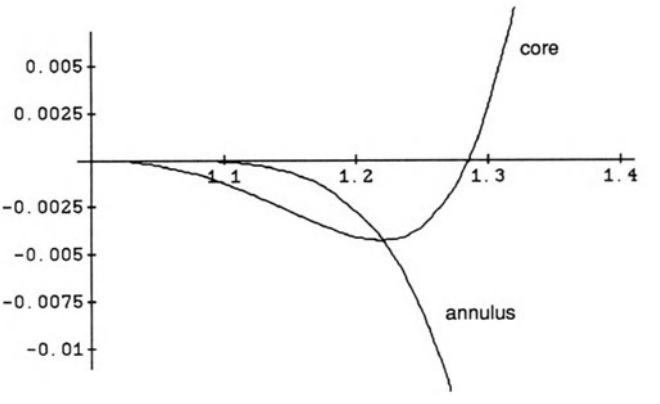

(f)

Fig. 15.3(d-f). Continued.

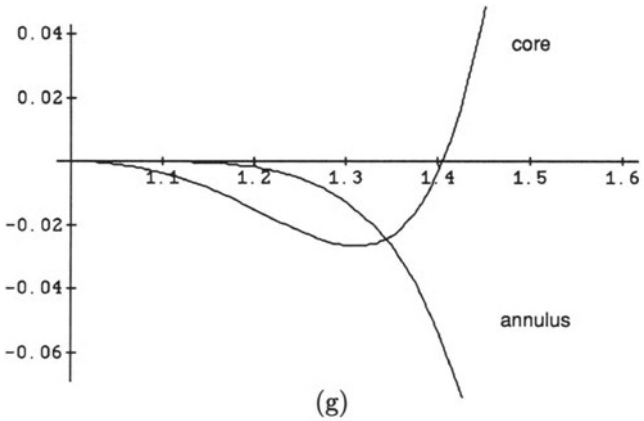

(g)

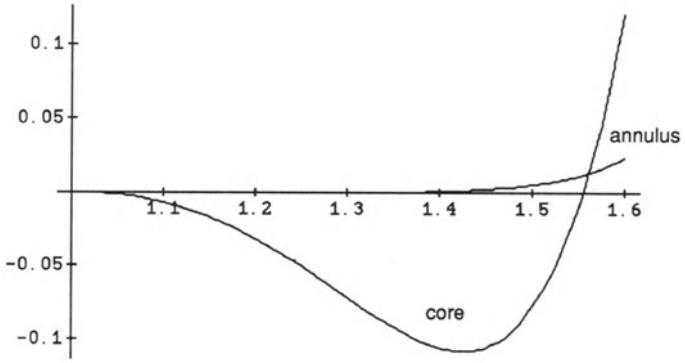

(h)

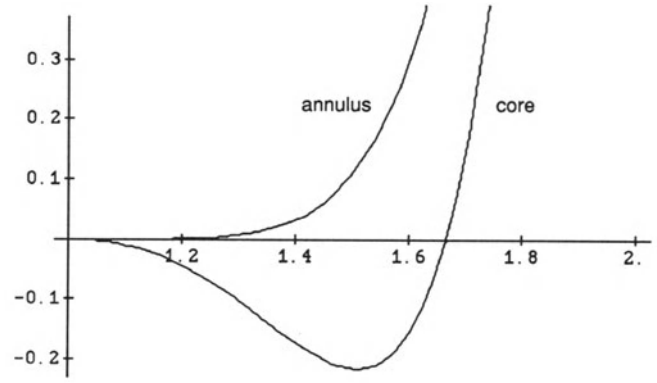

(i)

Fig. 15.3(g-i). Continued.

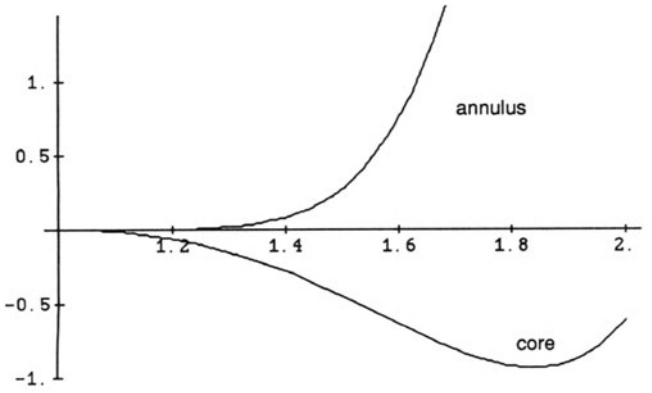

(j)

Fig. 15.3(j). Continued.

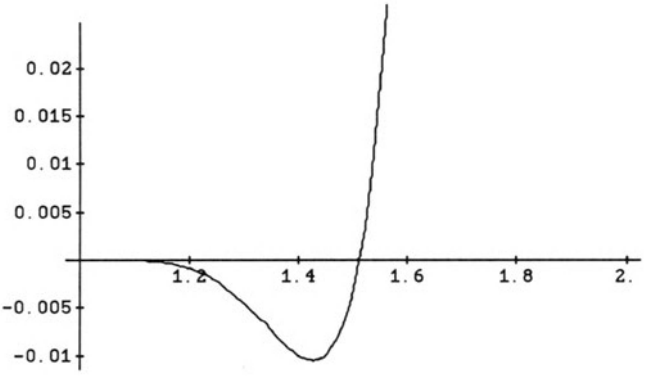

(a)

Fig. 15.4(a-c). [Chen and Joseph, 1991b, American Institute of Physics] Total contribution of inertia of the core plus the annulus $I_a + B_a + I_c + B_c = I_a + I_c$ to instability of core-annular flow for $m < 1$. Though the separate contributions of the core and the annulus are sensitive to the values of m, the total contribution is insensitive. (a) m=0.001, (b) m=0.5, (c) m=0.95.

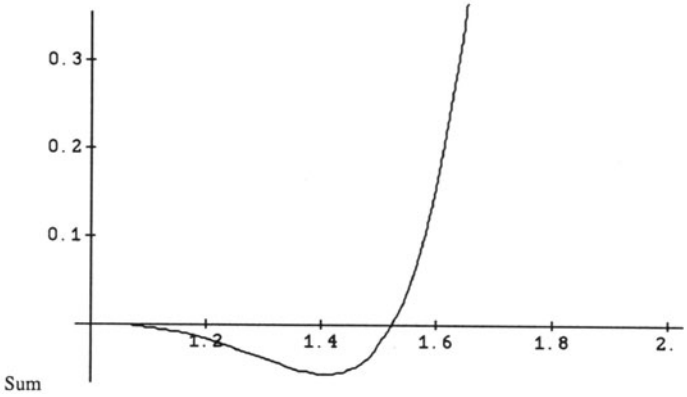

(b)

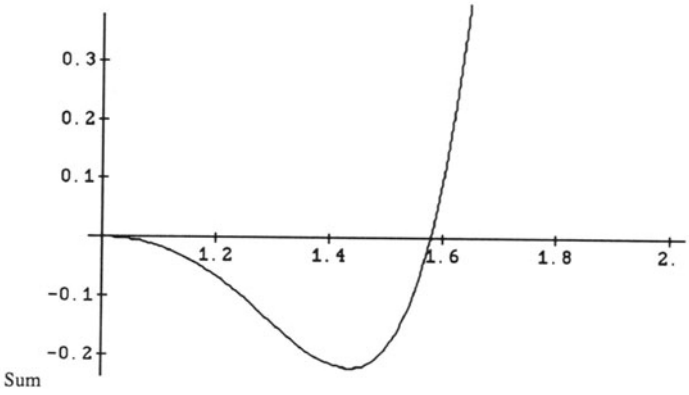

(c)

Fig. 15.4(b-c). Continued.

The term $J/\mathbb{R}_1$ also occurs at order ε^3:

$$C^{(1)} = i\varepsilon^2 \left\{ \frac{m-1}{12m^2}\mathbb{R}_1 + \frac{\varepsilon J}{3m\mathbb{R}_1} \right\} + 0(\varepsilon^3). \tag{16.4}$$

Comparing this with (14.5), we find that

$$C^{(1)} = \varepsilon^2 c_1$$

proving that the two theories agree in the stated limit.

VIII.17 Discussion

For the lubricated case $m < 1$, the linear dispersion relation resulting from the amplitude equation (13.6) in the limit $\alpha \to 0$ approaches that of the exact problem when (15.43) is satisfied. This follows from the asymptotic formula (15.42). We have seen that when (15.43) is satisfied, the contribution from inertia in the annulus $I_a + B_a$ can be neglected and we have the following expansion for the eigenvalue C of the exact theory:

$$C - W(1) = \epsilon^2 4\frac{m-1}{m^2} + i\alpha\epsilon^2\left(\frac{J\epsilon}{3\mathbb{R}_1 m} + \frac{m-1}{m^2}\frac{\mathbb{R}_1}{12}\right) + O(\epsilon^3).$$

Comparing this to the dispersion relation (14.5), we have found that $C - W(1) = \epsilon^2 c + O(\epsilon^3)$.

At least two types of weakly nonlinear amplitude equations can be obtained for core-annular flow when the annulus is thin. The first is the one analogous to that of Hooper and Grimshaw. The wavelength is required to be long compared with both the core radius and the annulus thickness. The linear part of this amplitude equation is exact in the sense that the linear dispersion relation reduces to that of the full problem in the same limit. The linear mechanism of shear stabilization or destabilization is fully preserved in this amplitude equation, but the dynamics is retricted to the longest waves which, as in the case of capillary instability, are not the most strongly amplified. The second approach is that of Frenkel and Papageorgiou *et al.* Their amplitude equation is more general, because the wavelength is required to be long only compared with the annulus thickness and waves with wavelength comparable to the core radius are incorporated in the analysis. The trade-off of this is that, on top of the strict restriction $\epsilon J/\mathbb{R}_1$=O(1), the contribution of the inertia in the annulus is completely neglected and the linear part of the amplitude equation is only an approximation to the exact linear problem. When certain additional conditions are not satisfied, some of the important physics could be missed. In the case of lubricated pipelining ($m < 1$), the theory is restricted to cases where the annulus thickness ($\epsilon = a - 1$) is very small: specifically, we require that (15.43) hold for $m < 0.8$. If m is sufficiently small, then (15.44) holds. This condition may be hard to achieve for lubricated pipelining for which typical values of m are of the order of 0.01 or smaller.

Chapter IX
Vortex Rings of One Fluid in Another in Free Fall

IX.1 Introduction

This chapter is based on the paper by Baumann, Joseph, Mohr and Renardy [1992]. We present and interpret experiments in which vortex rings of one immiscible liquid are created in another from drops falling from rest under gravity. These rings are associated with circulations generated by viscosity and, unlike classical vortex rings which occur in miscible liquids at high Reynolds numbers, they can exist even at very low Reynolds numbers. Since the rings do not diffuse, they are well-defined. Nonetheless, there are many similarities in the dynamics of formation and flow of miscible and immiscible rings. We are going to identify parameters which appear to correlate our observations and to show photographs of some of the more interesting events we have seen.

IX.2 Classical Vortex Rings

By way of comparison, it is instructive to recall that in classical hydrodynamics, it is usual to consider vortical regions embedded in an otherwise irrotational flow. In the case of the ring, a cross-section (figure 2.1(a)) is like the "potential vortex" (figure 2.1 (b)): the flow outside a cylinder which rotates rigidly. This is the Taylor problem (flow between two concentric cylinders with the inner one rotating and the outer one fixed) with the outer cylinder moved to infinity. The streamfunction ψ of the flow, with $(\psi_y, -\psi_x)$ for the velocity in the $x-y$-plane, and $r = (x^2 + y^2)^{1/2}$, is then $\psi = c\ ln\ r$. Thus, $\Delta\psi = 0$ and the flow is irrotational. The potential vortex satisfies the no slip boundary condition at the cylindrical boundary, and it is one of only a few potential flow solutions of the Navier-Stokes equations.

In the classical theory of vortex rings, viscosity is absent, diffusion is absent and surface tension is absent. For the classical case, we think of a smoke ring. Many beautiful photographs of vortex rings in miscible liquids can be found in the photograph album of Van Dyke [1982].

Vortex rings can be generated in a number of ways. One way is to impulsively eject a puff of fluid from a circular opening into a bath of the same fluid, as in the smoke ring [Baird, Wairegi and Loo 1977]. Another is to let a drop of liquid fall into a pool of the same liquid [Chapman and Critchlow 1967]. A third method is to force a buoyant fluid into a tank of water (see section 6.3.2 of Turner [1979]) [Simons and Larson 1974]. These experiments do not involve immiscible liquids. Rings are more easily created in miscible rather than immiscible liquids. Thomson and Newall [1885] did an interesting study of ring formation and their stability in miscible and immiscible liquids. They say that:

"It is not every liquid, however, which, when dropped into water, gives rise to rings, for if we drop into water any liquid which does not mix with it, such as chloroform, the drop in consequence of the surface tension remains spherical as it descends. In fact, we may say that, with some few exceptions to be noticed later, rings are formed only when a liquid is dropped into one with which it can mix. This is important, because surface tension has been supposed to play an important part in the formation of these rings; it is difficult, however, to see how any appreciable surface tension can exist between liquids that can mix, and as far as our experiments go they tend to show that it is only the absence of surface tension which is necessary for their production."

Most of the experimental studies of vortex rings are for rings generated impulsively or otherwise in a single fluid or between miscible liquids. Many theoretical studies proceed from the inviscid equations of motion in which the vorticity is confined to certain regions, say rings, in an otherwise potential flow. These are models of flows at high Reynolds numbers. Low Reynolds number studies of the settling and break-up of miscible drops

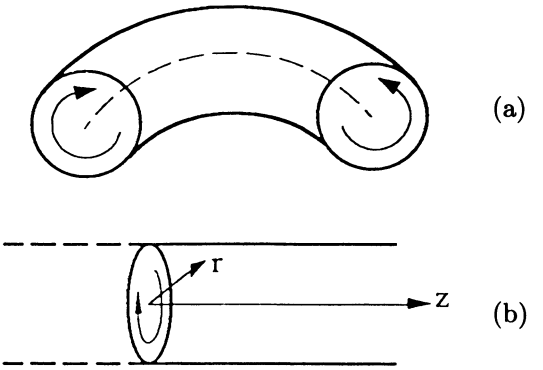

Fig. 2.1(a-b). [Baumann, Joseph, Mohr and Renardy, 1992, American Institute of Physics] (a) The two circular cross-sections of a ring vortex are shown. The flow is as indicated. The dashed line denotes the axis at the center of the ring. The ring as a whole turns about this axial line. The continual turning of the ring is analogous to the rigid-body rotation of a straight cylinder shown in (b) if the ring were cut and straightened. (b) An infinitely long solid cylinder is rotating with azimuthal velocity Ωr, where Ω is the angular speed. The flow outside the cylinder is irrotational and given by the streamfunction $\psi = c \ln r$.

and the formation of rings have been given by Kojima, Hinch and Acrivos [1984] (plate IX.2.2) and by Arecchi, Buah-Bassuah, Francini, Pérez-Garcia and Quercioli [1989] (figure 2.3). To explain the discrepancies between their experimental observations and their Stokes flow calculations, Kojima *et al.* introduced some notions of transient interfacial tension (cf. chapter X).

Most of the studies of vortex rings in immiscible liquids are for water and air at high Reynolds numbers. One example is to let a bubble of air rise through water [Walters and Davidson 1963; Pedley 1968], and another is to let a drop of water fall through the air [O'Brien 1961]. The latter method leads to large deformations from the original drop, and the formation of bags which look very different from rings even though these are related. In the former study, it is necessary to inject the air impulsively to create a strong circulation in order to get a ring to form. A recent analysis of this problem has been given by Lundgren and Mansour [1990].

On the whole, it is not surprising that a phenomenon which occurs at zero interfacial tension also occurs at small values of interfacial tension. And *small* here means *with respect to viscous effects*, so that the actual numerical value of the coefficient of interfacial tension does not have to be small. The processes are similar whether miscible or immiscible liquids are involved, up to the ring stage. However, interfacial tension does affect the

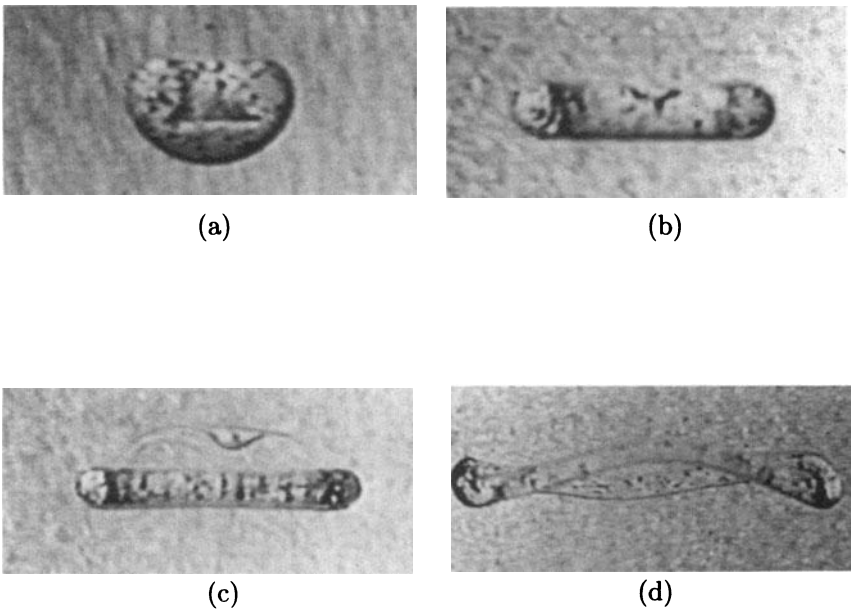

Fig. 2.3(a-d). [Figure 1 of Arecchi *et al.*, 1989, Editions de Physique] [1989]) Evolution of a falling drop of 9/10 glycerin-water (r = 0.29 cm) seeded with small carbon particles into a 3/2 glycerin-water solution of nearly matched density ($\Delta\rho = 0.0789$ g/cc). (a) - (d) is a sequence of lateral views of the drop motion taken at the following positions from the free surface and times from the deposition: (a) 6.0 cm, 3.03 s; (b) 10.0cm, 5.2s; (c) 13.0 cm, 7.34s; and (d) 16.0 cm, 10.0 s. (c) shows the appearance of the turban instability (the change of sign in the curvature of the bottom membrane is the onset of what is called a turban instability, since the deformed drop looks like a turban), and (d) the torus breaking by Rayleigh-Taylor instability.

break-up pattern: for example [O'Brien 1961], it can prevent the smaller-sized drops from repeating the sequence of ring formation and break-up: this limits the vortex-cascade (Thomson and Newall [1885] describe this cascade for the case of an ink drop in water, with their figures 1 and 2 as illustrations) to one or two stages. Membrane *rupture* is another form of break-up. The rupture strength or breaking strength of membranes is not well-understood but it may be related to surface tension. We know that the rupture strength generally decreases with surface tension. When the surface tension parameter is small but the surface tension is large, a vortex ring spanned by a tough permanent membrane can form. In other cases in which interfacial tension has been reduced by surfactants, the membrane is blown out and an unstable vortex ring of the type shown in our photographs forms. The difference between strong and weak interfacial tension is illustrated in plates IX.7.5 and IX.8.3. In plate IX.7.5, a smaller drop of 1000 cS silicone oil is sucked into the wake of an oblate ring-like cap of the same silicone oil falling in a contaminated soy bean oil. The membrane in this system is too tough to break. On the other hand, if a surfactant (97 % dye, 3% Rhodamine B base powder, Aldrich Chem. Co., Milwaukee, WI) is added (as in plate IX.8.3) the membrane breaks readily. Figure 2.3 (e) illustrates this well. The existence of a spanning membrane in miscible liquids is hard to understand without invoking the idea of transient interfacial tension induced by momentarily strong gradients of composition. Such notions were introduced by Kojima *et al.* [1984], and considered in more detail in chapter X.

IX.3 The Normal Stress Balance

It is probable that the parameters which control the deformations of drops to rings in free fall are associated with the stress balance at the interface (cf. section I.2):

$$-[\![p]\!]\mathbf{n} + 2[\![\mu \mathbf{D}[\mathbf{u}]]\!]\mathbf{n} + S^*\mathbf{n}2H = 0. \tag{3.1}$$

H is the mean curvature at a point on the interface Σ and $\mathbf{D}[\mathbf{u}]$ is the rate of strain:

$$2H = \frac{1}{R_1} + \frac{1}{R_2}, \qquad \mathbf{D}[\mathbf{u}] = \frac{1}{2}(\nabla \mathbf{u} + (\nabla \mathbf{u})^T),$$

where R_1 and R_2 are the local radii of curvature at a point of Σ; $\mathbf{n}$ is the outward normal on the interface.

We denote

$$[\![\cdot]\!] = (\cdot)_d - (\cdot)_o,$$

to be the jump in the quantity $\cdot$ across the interface, where the subscript d stands for drop and o stands for the outer fluid. In the equilibrium case

(that is, no flow), the drop or bubble pulls into a sphere with radius $R_1 = R_2 = a$ and equilibrium pressures satisfying

$$[\![p^e]\!] = p_d^e - p_o^e = \frac{2S^*}{a}.$$

Equation (3.1) may be decomposed into normal and tangential parts. The tangential part says that shear stress is continuous. By using the condition that the velocity is continuous at the interface

$$[\![\mathbf{u}]\!] = 0 \tag{3.2}$$

and the continuity equation, we will show that

$$[\![D_{nn}]\!] = 0, \tag{3.3}$$

where we denote

$$D_{nn} = \mathbf{n} \cdot \mathbf{D}[\mathbf{u}] \cdot \mathbf{n}.$$

This result will be used in equations (3.8) and (4.4).

For the proof, we write the continuity equation

$$\nabla \cdot \mathbf{u} = (\mathbf{n}\frac{\partial}{\partial n} + \nabla_{\|}) \cdot \mathbf{u} = 0 \tag{3.4}$$

where $\partial/\partial n = \mathbf{n} \cdot \nabla$, $\nabla_{\|}$ is the surface gradient $\mathbf{t_1}(\mathbf{t_1} \cdot \nabla) + \mathbf{t_2}(\mathbf{t_2} \cdot \nabla)$, and $\mathbf{t_1}$ and $\mathbf{t_2}$ are the two tangents to the interface. Then on the interface,

$$\begin{aligned} 0 = [\![\nabla \cdot \mathbf{u}]\!] &= [\![\mathbf{n} \cdot \frac{\partial \mathbf{u}}{\partial n} + \nabla_{\|} \cdot \mathbf{u}]\!] \\ &= [\![\mathbf{n} \cdot \frac{\partial \mathbf{u}}{\partial n}]\!] + \nabla_{\|} \cdot [\![\mathbf{u}]\!] \\ &= [\![\mathbf{n} \cdot \frac{\partial \mathbf{u}}{\partial n}]\!]. \end{aligned} \tag{3.5}$$

We note next that

$$D_{nn} = n_i \frac{\partial u_i}{\partial x_j} n_j = \mathbf{n} \cdot \frac{\partial \mathbf{u}}{\partial n}. \tag{3.6}$$

We take the jump of (3.6) and use (3.5) to prove (3.3).

The next step in the reduction of the normal component of the stress balance on the interface Σ is the decomposition of the pressure into an equilibrium part p^e, a hydrostatic part $p^s = \rho g z$, with $p^s = \rho_d g z$ in the drop, and a dynamic part Π due to the motion. We use a coordinate system where the origin is the center of the spherical drop, and we denote the parametrization for the surface of the drop by $z = z_\Sigma(x, y)$. Thus, $[\![p^s]\!] = [\![\rho]\!] g z_\Sigma$, and

$$\begin{aligned} [\![p]\!] &= [\![p^e]\!] + [\![p^s]\!] + [\![\Pi]\!] \\ &= \frac{2S^*}{a} + [\![\rho]\!] g z_\Sigma + [\![\Pi]\!]. \end{aligned} \tag{3.7}$$

Combining now (3.3) and (3.7) with (3.1), we find that

$$-[\![\Pi]\!] + 2D_{nn}[\![\mu]\!] + [\![\rho]\!]gz_\Sigma + S^*(\frac{1}{R_1} + \frac{1}{R_2} - \frac{2}{a}) = 0. \tag{3.8}$$

The dynamic pressure is of course an unknown which must be determined from the solution. This equation will be used in (4.4).

IX.4 Stokes Flow Around a Drop or Bubble

It is of interest here to consider the solution due to Hadamard and Rybczynski [Clift, Grace and Weber 1978; Happel and Brenner 1983] for the problem of a falling drop when the Reynolds numbers are small enough so that inertia may be neglected. The solution is also discussed in §4.9 of Batchelor [1970]. For numerical simulations on the problem at finite Reynolds numbers, see Dandy and Leal [1989] and Tryggvason and Unverdi [1991].

When inertia is negligible, if we assume that the drop is spherical and is falling at its terminal speed, and match the shear stress and velocities at the interface, then the normal stress condition will be seen a posteriori to be automatically satisfied. Thus, a spherical drop falling at its equilibrium speed is a steady solution.

We begin by supposing that interfacial tension is large enough to keep the drop spherical against the deforming effect of the viscous forces. We use spherical polar coordinates $(r,\ \theta,\ \phi)$, with the spherical interface Σ being $r = a$. On Σ, $z = z_\Sigma = a\cos\theta$. We assume axisymmetry: $\partial/\partial\phi = 0$. It is convenient to introduce a stream function ψ such that

$$u_r = \frac{-1}{r^2\sin\theta}\frac{\partial\psi}{\partial\theta}, \quad u_\theta = \frac{1}{r\sin\theta}\frac{\partial\psi}{\partial r}. \tag{4.1}$$

The velocity and shear stress are made continuous at the interface and the kinematic condition is satisfied. Let U be the speed of the drop. It can be shown (see equation (4.9.5) of Batchelor [1970]) that the required solution is in the form

$$\psi = f(r)\sin^2\theta, \quad r \geq a, \tag{4.2}$$

$$\psi_d = f_d(r)\sin^2\theta, \quad r \leq a,$$

where

$$f(r) = Ar + Br^2 + \frac{D}{r},$$

$$f_d(r) = Er^4 + Fr^2,$$

$$A = -\frac{3Ua}{4}\frac{(\mu_d + \frac{2}{3}\mu)}{\mu_d + \mu}, \quad B = \frac{1}{2}U,$$

$$D = \frac{Ua^3}{4}\frac{\mu_d}{\mu_d+\mu}, \quad E = \frac{U}{4a^2}\frac{\mu}{\mu_d+\mu}, \quad F = \frac{-U}{4}\frac{\mu}{\mu_d+\mu}.$$

The pressure for Stokes flow is harmonic $\nabla^2\Pi = 0$ and the solution is given by

$$\Pi = \frac{aU\cos\theta}{r^2}\frac{\mu(\mu+\frac{3}{2}\mu_d)}{\mu_d+\mu}, \quad r \geq a, \tag{4.3}$$

$$\Pi_d = \frac{-5Ur\cos\theta}{a^2}\frac{\mu}{\mu_d+\mu}, \quad r \leq a.$$

The solution (4.2) and (4.3) is obtained by satisfying all the required conditions except the normal stress equation (3.8). It can be shown that the solution automatically satisfies the normal stress condition. Equation (3.8) may be written on $z_\Sigma = a\cos\theta$ and $R_1 = R_2 = a$ as

$$-[\![\Pi]\!] + 2D_{rr}[\![\mu]\!] + [\![\rho]\!]ga\cos\theta = 0, \tag{4.4}$$

where

$$D_{rr} = \frac{\partial u_r}{\partial r}_{(r=a)} = \frac{-2\cos\theta}{a^2}f'(a) = \frac{-2U\cos\theta}{a}\frac{\mu}{\mu_d+\mu}, \tag{4.5}$$

and

$$[\![\Pi]\!] = (\Pi_d - \Pi)_{r=a} = \frac{-U\cos\theta}{a}\left(\frac{13\mu}{2} + \frac{\mu^2}{\mu_d}\right). \tag{4.6}$$

In equation (4.4), the interfacial tension term vanishes, so that it is not necessary to assume a priori that the effect of surface tension must be enough to keep the drop spherical. For example, a large air bubble rising in tar can take a spherical shape, even when the effect of interfacial tension cannot be dominant. Putting this all together, we get

$$\left(\frac{-3U\mu}{a}\frac{\mu+\frac{3}{2}\mu_d}{\mu_d+\mu} + [\![\rho]\!]ga\right)\cos\theta = 0. \tag{4.7}$$

This yields

$$U = \frac{1}{3}\frac{a^2g}{\mu}(\rho_d - \rho)\frac{\mu+\mu_d}{\mu+\frac{3}{2}\mu_d}. \tag{4.8}$$

The analysis just given shows that if the flow is very slow, so that inertia may be neglected, the sphere is a solution for the shape of a drop falling at its terminal speed. At low Reynolds number, a solution is a slightly perturbed sphere [Taylor and Acrivos 1964]. There is numerical and experimental evidence to suggest that these solutions are stable to small disturbances [Koh and Leal 1990; Pozrikidis 1990] but not to large disturbances.

The same result holds for the case in which a drop falls from rest under gravity. In this situation, we have the unsteady Stokes equation with gravity as the body force for the flows inside and outside the drop. Suppose the drop has a speed $U(t)$ in the direction of gravity. Then in a coordinate system moving with the drop, the governing equations are the continuity equation (3.4) and

$$\rho\frac{\partial \mathbf{u}}{\partial t} = -\nabla p - \rho(g - \dot{U}(t))\mathbf{e_z} + \mu\nabla^2\mathbf{u}. \tag{4.9}$$

We divide the pressure into three parts: $p = p^a + \Pi + p^s$, where p^s is the static pressure satisfying $[\![p^s]\!] = 2/a$, p^a is the pressure due to the body force, which can be found from $\nabla p^a = -\rho(g - \dot{U})\mathbf{e_z}$, and Π is the dynamic pressure, which will be determined with the solenoidal velocity $\mathbf{u}$ by

$$\rho\frac{\partial \mathbf{u}}{\partial t} = -\nabla\Pi + \mu\Delta\mathbf{u}. \tag{4.10}$$

Equation (4.10) holds in both fluids.

Assuming now that the flow is axisymmetric, we introduce a stream function as in (4.1). Equations (3.1) and (3.7) imply that $[\![u_\theta]\!]$, $[\![u_r]\!]$, $[\![\mu D_{r\theta}]\!]$ all vanish, and

$$-[\![\Pi]\!] + 2[\![\mu D_{rr}]\!] + [\![\rho]\!](g - \dot{U}(t))a\cos\theta + S^*(\frac{1}{R_1} + \frac{1}{R_2} - \frac{2}{a}) = 0, \tag{4.11}$$

where S^* is the surface tension coefficient and $\frac{1}{R_1} + \frac{1}{R_2}$ is the mean curvature of the surface.

It is concluded that the spherical bubble does not need interfacial tension to retain its shape when it is accelerating because the weight is momentarily greater than the drag. The proof will be as follows. First, we suppose that the surface tension is large enough to keep the spherical shape of the bubble: that is, we ignore equation (4.11) and enforce the other boundary conditions on the sphere. Then we show that this equation will automatically be satisfied without any condition on S^*.

Taking the curl of (4.10), we get the equation for the stream function $\psi(r, \theta, t)$:

$$\rho\frac{\partial}{\partial t}E^2\psi = \mu E^4\psi, \tag{4.12}$$

where

$$E^2 = \frac{\partial^2}{\partial r^2} + \frac{\sin\theta}{r^2}\frac{\partial}{\partial\theta}(\frac{1}{\sin\theta}\frac{\partial}{\partial\theta}).$$

We can separate variables:

$$\psi(r, \theta, t) = f(r, t)\sin^2\theta. \tag{4.13}$$

Then u_r can be written as $\tilde{u}_r(r, t)\cos\theta$, $u_\theta = \tilde{u}_\theta(r, t)\sin\theta$. From the equation

$$\frac{\partial\Pi}{\partial r} = \mu(\nabla^2 u_r - \frac{\partial u_r}{\partial r} - \frac{2}{r^2}\frac{\partial u_r}{\partial\theta} - \frac{2u_\theta}{r}\cot\theta) - r\frac{\partial u_r}{\partial t},$$

where

$$\nabla^2 = \frac{1}{r^2}(\frac{\partial}{\partial r}(r^2\frac{\partial}{\partial r})) + \frac{1}{r^2\sin\theta}\frac{\partial}{\partial\theta}(\sin\theta\frac{\partial}{\partial\theta}),$$

we see that $\Pi(r, \theta, t)$ is of the form

$$\Pi(r, \theta, t) = \tilde{\Pi}(r, t)\cos\theta.$$

Hence,

$$D_{rr}(r,\theta,t) = \frac{\partial u_r}{\partial r} = \tilde{D}_{rr}(r,t)\cos\theta,$$

$$D_{r\theta} = \frac{1}{2}(r\frac{\partial}{\partial r}(\frac{u_\theta}{r}) + \frac{1}{r}\frac{\partial u_r}{\partial \theta}) = \tilde{D}_{r\theta}(r,t)\sin\theta.$$

Now let us compute the force acting on the spherical bubble by the outside fluid which, because of the symmetry, must be along $\mathbf{e_z}$. By Newton's law, the magnitude of this force is equal to the force acting on the outside fluid by the bubble. Hence,

$$\int \mathbf{e_z}\cdot[\![\mathbf{T}]\!]\cdot\mathbf{n}\,ds = 0, \tag{4.14}$$

where

$$[\![\mathbf{T}]\!] = (-[\![\Pi]\!] + [\![\rho]\!](g - \dot{U}(t))a\cos\theta))\mathbf{I} + 2[\![\mu\mathbf{D}(\mathbf{u})]\!],$$

$\mathbf{e_z} = \cos\theta\mathbf{e_r} - \sin\theta\mathbf{e}_\theta$, $\mathbf{n} = e_r$, and $\mathbf{I}$ is the unit matrix, and the integral is executed on the spherical surface.

Using all the above equations and $ds = 2\pi a^2\sin\theta\,d\theta$, we get

$$2\pi a^2\big(-[\![\tilde{\Pi}(a,t)]\!] + [\![\rho]\!](g - \dot{U}(t)a) + 2[\![\mu\tilde{D}_{rr}(a,t)]\!]\big)\int_0^\pi \cos^2\theta\sin\theta\,d\theta = 0. \tag{4.15}$$

Therefore,

$$-[\![\tilde{\Pi}(a,t)]\!] + [\![\rho]\!](g - \dot{U}(t)a) + 2[\![\mu\tilde{D}_{rr}(a,t)]\!] = 0.$$

This is just the sum of the first three terms of equation (4.11). Thus, if we can find a solution for $f(r,t)$, the proof is finished.

We introduce $V = a^2g\rho/\mu$, a and V/g as scales for the velocity, length and time respectively, and Va^2 for $f(r,t)$. Then, using the same notation for the dimensionless variables, the initial value problem becomes

$$\frac{\partial}{\partial t}L^2 f = L^4 f, \qquad \text{for } r > 1;$$

$$\frac{\partial}{\partial t}L^2 f_d = L^4 f_d, \qquad \text{for } 0 < r < 1;$$

$$f(r,0) = f_d(r,0) = U(0) = 0,$$

$$f(1,t) = f_d(1,t) = 0,$$

$$[\![\frac{\partial f}{\partial r}]\!] = 0,$$

$$\frac{1}{r}\frac{\partial^2 f}{\partial r^2} - \frac{2}{r^2}\frac{\partial f}{\partial r} = m(\frac{1}{r}\frac{\partial^2 f_d}{\partial r^2} - \frac{2}{r^2}\frac{\partial f_d}{\partial r}),$$

$$f(r,t) \to -\frac{1}{2}r^2U(t) \quad \text{as } r\to\infty,$$

and

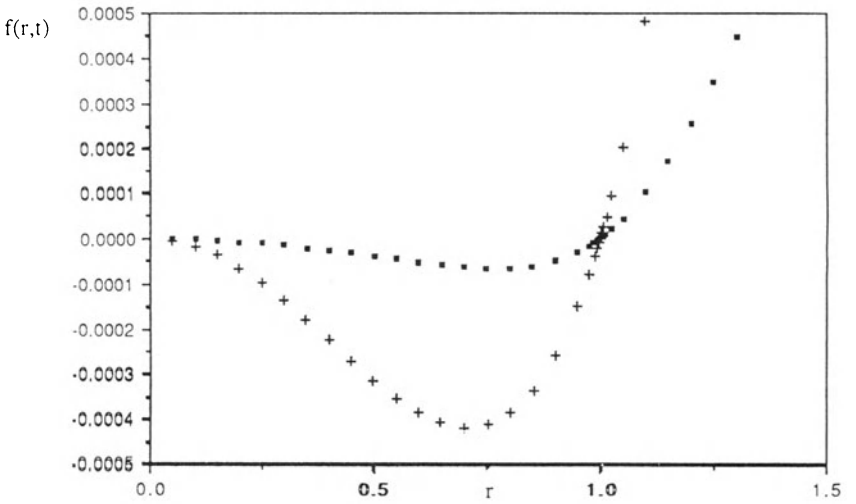

Fig. 4.1. $f(r,t)$ vs r, $m = 0.9$ and $d = 0.95$: (•) $t = 0.11$, (+) $t = 0.27$.

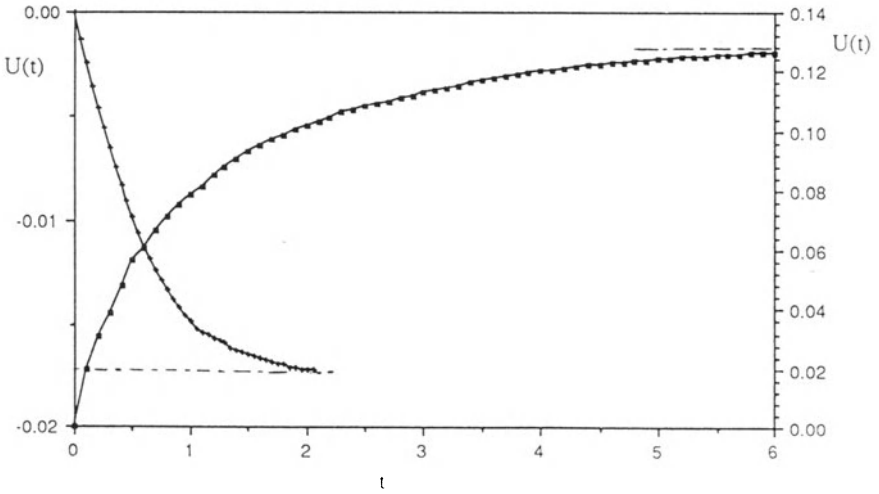

Fig. 4.2. $U(t)$ vs t: (+) $m = 0.9$, $d = 0.95$, $\tilde{U} = -0.0172$; (•) $m = 0.4$, $d = 1.3$, $\tilde{U} = 0.1273$. Positive values of $U(t)$ are for falling drop and negative are for rising bubble.

$$d\dot{U}(t) = (-\frac{\partial^3 f}{\partial r^3} + \frac{2}{r}\frac{\partial^2 f}{\partial r^2} + \frac{2}{r^2}\frac{\partial f}{\partial r} + d - 1)|_{r=1} + \frac{\partial^2 f}{\partial r \partial t}|_{r=1},$$

where

$$d = \frac{\rho_d}{\rho} \quad \text{and} \quad m = \frac{\mu_d}{\mu}.$$

The system was solved for $f(r,t)$ and $U(t)$ by a finite element method. Graphs of $f(r,t)$ versus r for $m = 0.9$, $d = 0.95$ at two different times are given in figure 4.1. Graphs of the dimensionless $U(t)$ versus t for different parameters are given in figure 4.2. The terminal velocity of the drop is given by

$$\tilde{U} = \frac{2(1+m)(d-1)}{3(2+3m)}.$$

This is the dimensionless form of equation (4.8). Figure 4.2 shows that the unsteady solution $U(t)$ converges to $\tilde{U}$ as t approaches infinity.

IX.5 Dimensionless Parameters

To identify dimensionless parameters, we scale lengths with a, the radius of the equivalent spherical drop or bubble with the same volume, and velocity with U to be specified later (see section IX.6). The normal stress balance at the interface (see section IX.3) shows that there are four forces at work: gravity, surface tension, inertia and viscosity.

The viscosity ratio

$$M = \frac{\mu_d}{\mu}, \tag{5.1}$$

where μ_d is the viscosity of the drop and μ is the viscosity of the ambient fluid, is very important.

The ratio of inertia to viscous forces is measured by the Reynolds numbers

$$R = \frac{Ua}{\nu}, \quad R_d = \frac{Ua}{\nu_d}, \tag{5.2}$$

where $\nu = \mu/\rho$, $\nu_d = \mu_d/\rho_d$. To form immiscible vortex rings, inertia is important because the drop will be close to a sphere if R and R_d are sufficiently small [Clift, Grace and Weber 1978].

The viscous part of the normal stress in the drop is scaled by $U\mu_d/a$ and in the exterior fluid by $U\mu/a$. The interfacial tension term in the stress balance is scaled by S^*/a. The ratio of the stress associated with interfacial tension to the viscous part of the normal stress in the outer fluid is

$$\frac{S^*}{\mu U} = \frac{J}{R}, \tag{5.3}$$

where

$$J = \frac{S^* a}{\nu^2 \rho}, \tag{5.4}$$

is Chandrasekhar's capillary number (used in his study of the capillary instability of a jet; see §111 of his book [1981]) for the outer fluid. Similarly, for the inner fluid we have

$$\frac{S^*}{\mu_d U} = \frac{J_d}{R_d}, \tag{5.5}$$

where

$$\frac{M J_d}{R_d} = \frac{J}{R}. \tag{5.6}$$

For a ring to form, the tendency for interfacial tension to keep the drop spherical should be overcome by the effect of viscosity to distort it. Thus, we expect to see rings when $J/R << 1$. In our experiments, we got ring formation only when $M >> 1$. We did not observe rings in immiscible liquids when $M < 5$. The condition $M >> 1$ may not be universal. Certainly it is easier to form vortex rings in miscible liquids; for these $J/R = 0$ but evidently when $M \approx 1$, it is possible to form vortices from ink drops falling in water.

We have already mentioned that inertial effects are always important in deforming the drop away from a sphere. These effects can be measured by the Weber number, the ratio of interfacial tension to inertia.

The inertial part of the dynamic pressure for the outer fluid is scaled with ρU^2 and the drop with $\rho_d U^2$. The ratio of interfacial tension to inertia in the outside fluid is

$$\frac{(S^*/a)}{\rho U^2} = \frac{J}{R^2} = \frac{1}{W}, \tag{5.7}$$

and in the drop is

$$\frac{(S^*/a)}{\rho_d U^2} = \frac{J_d}{R_d^2} = \frac{1}{W_d}, \tag{5.8}$$

where W is the Weber number. Obviously,

$$\frac{\rho_d}{\rho} \frac{J_d}{R_d^2} = \frac{J}{R^2}. \tag{5.9}$$

Since ρ and ρ_d do not differ greatly in our experiments, the Weber number is nearly the same in the outside fluid and the drop. The Weber number W_d for systems that do form rings ranged between 330 and 9600 whereas the W_d for systems that do not form rings ranges between 0.3 and 11000. The low Weber number drops are spherical.

IX.6 Physical and Other Properties

The physical properties are density, viscosity and interfacial tension. Other properties used in our discussion are the velocity U and the drop size a. First, we discuss the fluid properties.

Table 6.1 lists the fluids used in the experiments. The densities were measured using a Curtin Scientific hydrometer at approximately 21 degrees Celsius. The viscosities were measured using standard Cannon Fenske tube viscometers. The interfacial tension S^* was measured with the spinning rod tensiometer.

Table 6.1. Fluid properties are tabulated. .95 Gly = 95 percent glycerin in 5 percent water. Sil = Silicone oil with indicated viscosity. Canola oil is also termed rapeseed oil. The glycerin listed is .99 pure USP glycerin. The percentages listed for golden syrup and glycerin are dilutions with water. Alconox is an industrial glass cleaner and is used as a surfactant with water.

Fluid	Density (g/cm^3)	Kinematic Viscosity (cstokes)	Viscosity (g/cm sec)
Canola Oil	0.915	67	0.61
Glycerin	1.265	656	8.29
.95 Gly	1.245	244	3.03
.91 Gly	1.240	113	1.40
.92 Golden Syrup	1.400	2606	36.49
Lyle's Golden Syrup	1.440	20804	299.58
Motor Oil 30W	0.886	316	2.80
Olive Oil	0.914	69	0.63
Palmolive Soap	1.05	238	2.50
Safflower Oil	0.920	51	0.47
Sesame Oil	0.920	64	0.59
Shell Research Oil	0.895	2037	18.23
Sil 5cS	0.930	5	0.05
Sil 100cS	0.960	100	0.96
Sil 200cS	0.970	200	1.94
Sil 300cS	0.970	300	2.91
Sil 400cS	0.970	400	3.88
Sil 500cS	0.971	500	4.86
Sil 600cS	0.971	600	5.83
Sil 1000cS	0.971	1000	9.71
Sil 10000cS	0.975	10000	97.50
Sil 30000cS	0.975	30000	292.50
Soy Bean Oil	0.922	53	0.49
Water	1.000	1	0.01
Water+Alconox	1.080	33	0.36
Walnut Oil	0.925	51	0.47

Our early experiments on vortex rings were carried out in a plexiglass box three inches square and eight feet long. The top of the box is open to allow introduction of the drop and the bottom is closed by a valve. The valve holds the host fluid in and allows the removal of the dropped fluids that collect at the bottom. The plexiglass is clear to allow good visualization and photographic recording. The apparatus is back-lighted by reflecting incandescent light off of a translucent plexiglass sheet. The most recent experiments were carried out in a tube, which differed from the earlier apparatus in that it is made of glass and has a circular rather than square cross-section. The tube is four feet long, and like the plexiglass box, it is open at the top, and closed at the bottom with a valve.

The method for introducing the drop into the vortex ring box is as follows. A 10 cc drop of the more dense fluid was carefully placed on top of the host fluid with a calibrated beaker. This gives

$$\frac{4}{3}\pi a^3 = 10\ cc \quad \text{or} \quad a = (2.39)^{1/3}\ cm\ = 1.34\ cm.$$

Care was taken to insure that the drop was not splashed or accelerated into the host fluid.

A parametric study of drop size was also carried out with volumes other than 10 cc. The results of these studies are summarized in figure 9.1.

The velocity scale we use to calculate the Reynolds numbers is U given by (4.8). Using this U, $R_d = Ua/\nu_d$ depends only on measurable quantities and may be interpreted as the ratio between the buoyancy and viscous foces. The assumptions leading to (4.8) are that the fluid is a sphere falling at constant speed in Stokes flow, and that if the shear stress and velocity are matched at the interface, then the normal stress is automatically matched. The analysis does not say anything about what the drop would do if it were not falling at the terminal speed; for example, in the experiments, the drop starts at rest, some drops do not attain any steady speed, and moreover appear not to reach the speed predicted by this formula. It is difficult to decide *a priori* on a velocity scale because we do not have a formula for predicting the velocity as the drop changes shape. For each experiment, one could measure the maximum speed attained by the drop and use that as U, and this type of data is available for some of the experiments.

The velocity of the drop as it falls in the vortex ring box has been measured for some situations and found to be much smaller than the value from (4.8). Measurements of the velocity of a falling drop were made by recording the time it took for the drop to cross a six inch region of the box. Five such regions were selected to best capture the rate of fall at critical sections. The records were taken ten times for each region and the average velocity was calculated. Figure 6.1 shows the average velocity versus distance down the tube for three types of glycerin (e.g. 90% glycerin means 90% glycerin in 10 % water) and silicone oil falling in soy bean oil. (Rings

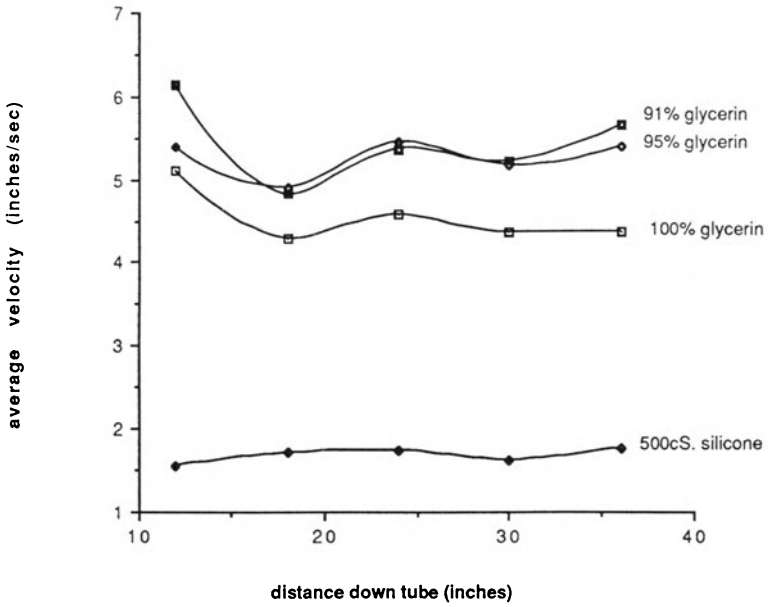

Fig. 6.1. [Baumann, Joseph, Mohr and Renardy, 1992, American Institute of Physics] The average velocity versus distance down the vortex ring tube for the designated liquids falling in soy bean oil.

were observed in the 100% glycerin case, but not in the other two cases, which happen to have higher velocities in the figure.)

Take, for example, the data in this figure. Compared with this, the value of U from (4.8) is approximately 110 inches per second, which is about twenty times the actual average velocity. This is consistent with the notion that a spherical drop would fall faster than a flattened spheroid or a ring. The swings in the measured speed reflect the changes in the shape of the drop as it evolves into a ring and decays. We should therefore keep in mind when looking at the tables that the true Reynolds numbers are probably an order of magnitude less than those tabulated.

There are also situations where U from (4.8) turns out to be large which is inconsistent with one of the assumptions in the derivation of (4.8); but since Stokes drag is less than the actual drag at higher Reynolds numbers, we expect that the U is an upper bound on the actual maximum velocity. Thus, our tabulated values of J_d/R_d and J/R in the sequel underestimate the importance of surface tension, but consistently, so that they should probably be an order of magnitude larger than they are. This would imply that the switch in the behavior from ring formation to no ring is actually occurring at a value of J/R of order 1. This, in fact, is what one would expect.

It is interesting that the condition for ring formation (on M and J/R) appears to hold for the entire wide range of Reynolds numbers encountered in the experiments. Why? In the normal stress condition at the interface, the only term we have not really commented on above is the pressure term, which is multiplied by the Reynolds number R. It appears that this term does not affect the ability to give birth to a ring: indeed, the factor R appearing there can be made to disappear just by changing the way the pressure is non-dimensionalized.

The formation of vortex rings always involves the breaking of a membrane, by poke-through or blow-out, and the breaking strength (toughness) of a membrane is very difficult to control, especially in silicone-vegetable oil systems. Our early experiments were recently repeated with good success except for the breaking of silicone-vegetable oil membranes. Some experiments were carried out with a contaminated safflower oil with various additives. We could never break a membrane in a silicone-contaminated safflower oil system (plate IX.7.5 and figure 8.2). The breaking strength of a membrane may be related to interfacial tension since we could get tough membranes to break by adding certain types of surfactants to the silicone oil (trace amounts of 97% dye, 3% Rhodamine B base powder in plate IX.8.3; trace amounts of Igepal in plate IX.8.4). We also had difficulty breaking membranes in a silicone-soy bean oil system, even when uncontaminated fluids were used. However, the oils used in the most recent experiments were not exactly the same as those used earlier, and it is possible that the newer oils had an interfacial tension large enough to prohibit vortex ring formation. As was the case for the contaminated oil system, rings were formed when the above mentioned surfactants were added to the silicone oil.

The low values of surface tension in the silicone oil-vegetable oil systems may indicate the possibility of small-scale activity at the interface. This activity could affect the boundary conditions involved, but more research must be done before any definitive statements may be made.

IX.7 Distortion of the Spherical Drop

When viscous effects win over the effect of interfacial tension, a falling drop cannot maintain a spherical shape. Numerical solutions have been obtained by Dandy and Leal [1989] for steady streaming flow past an axisymmetric drop over a wide range of Reynolds numbers, interfacial tension, viscosity ratios and density ratios. Their results indicate that at lower Reynolds numbers, the shape of the drop tends toward an indented oblate shape with decreasing interfacial tension, and at higher Reynolds numbers the drop becomes more disk shaped with decreasing interfacial tension.

In our experiments, the drop is released at zero speed and undergoes accelerations and decelerations, so that the results mentioned above concerning steady motions cannot strictly be used to infer anything about what

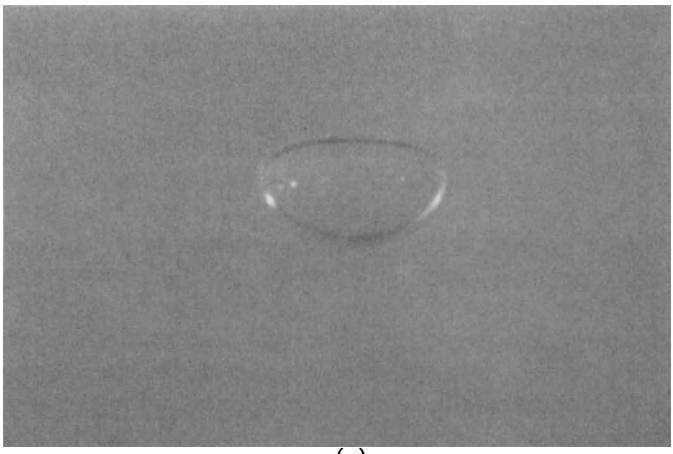

(a)

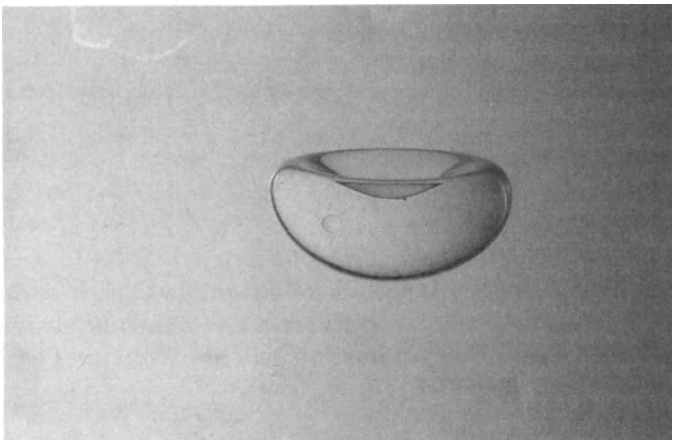

(b)

Fig. 7.1(a-b). [Baumann, Joseph, Mohr and Renardy, 1992, American Institute of Physics] Indented oblate drops falling in safflower oil. (a) Water $M = 0.02$, $J = 4530$, $S^* = 3.39$ dyn/cm. Indentation never develops in water and oil systems without surfactants. (b) 500 cS silicone oil. These are the most common shapes when falling. The high viscosity drop develops a circulation which brings it closer to a vortex ring.

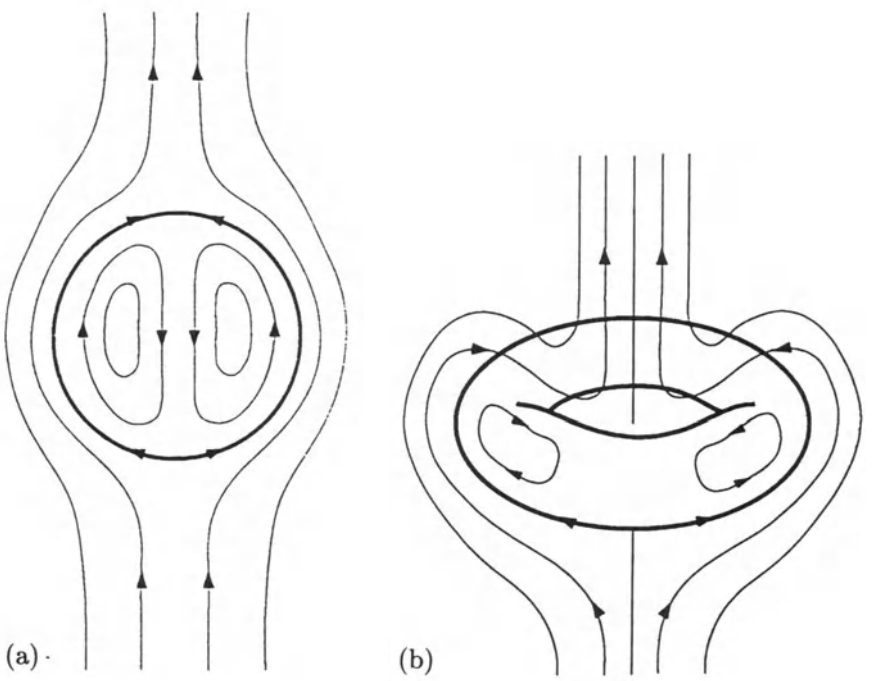

Fig. 7.2(a-b). [Baumann, Joseph, Mohr and Renardy, 1992, American Institute of Physics] Development of vorticity in a drop falling from rest. The streamlines are sketched in a frame moving with the drops: (a) from experimental observations at sufficiently small velocity, (b) larger velocity.

our drop is doing. Moreover, as mentioned in section IX.6, measurements of the drop speed indicate that it often does not reach the steady speed predicted by the formula (4.8). However, there are similarities with these analyses and what we have seen.

Figure 7.1 shows an indented oblate drop like those computed by Dandy and Leal at low Reynolds numbers (see, for example, their figure 3). Experimental observations suggest that the streamline pattern on the concave side of the cap is probably like that of figures 7.2; there are no points of separation or vortices in this guess about the underlying fluid dynamics. The suction in the cap, call it a wake, is large and small drops and even large drops are easily captured by the indented drop, as shown in figures 7.3 - 7.4 and 8.1(a) and plate IX.7.5 (a). If the conditions are right, the drop in the wake will poke through the membrane spanning the indentation, as in figure 8.1 and plate IX.8.3, but if the membrane is tough, as in plate IX.7.5 and figure 8.2, the poke-through will fail.

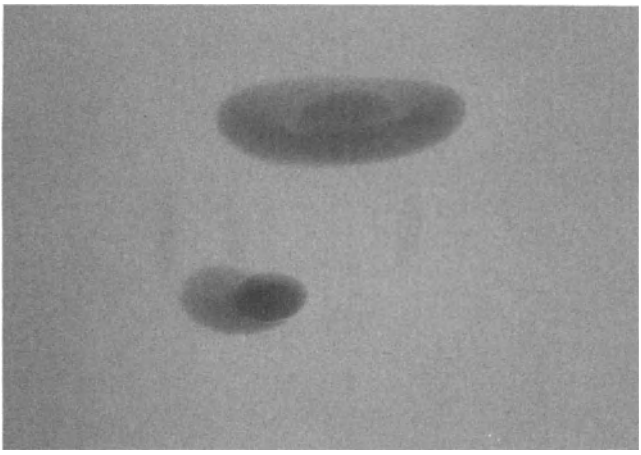

(a)

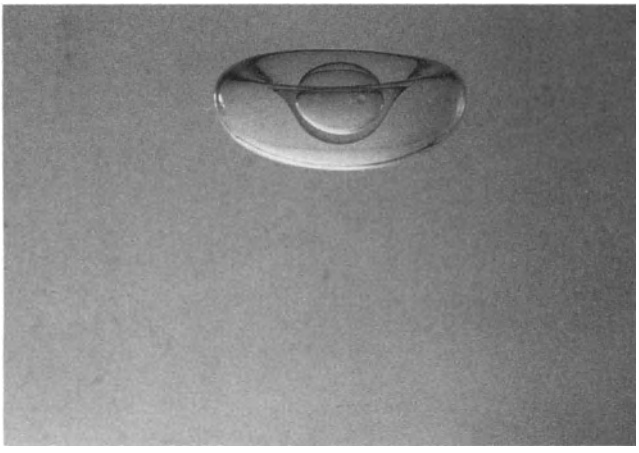

(b)

Fig. 7.3(a-b). [Baumann, Joseph, Mohr and Renardy, 1992, American Institute of Physics] Spheres nested in the wake of an indented oblate drop. (a) Glycerin falling in soy bean oil $M = 16.9$, $J = 0.45$, $S^* = 18.45$ dyn/cm. (b) 500 cs silicone oil in contaminated safflower oil.

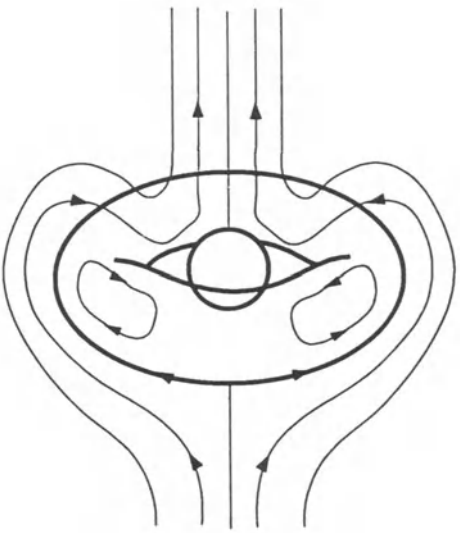

Fig. 7.4. [Baumann, Joseph, Mohr and Renardy, 1992, American Institute of Physics] A streamline pattern for figure 7.3. The flow in the wake could pull out a tail from the nested sphere if the wake were strong as in plate IX.7.5 (b), or the surface tension weak as in the case of miscible liquids.

IX.8 Formation of Rings

Stuke [1954] did experiments like those reported in this chapter. He cites the work of Northrup [1912] who used paraffin in a water bath, where interfacial tension is large. Northrup needed to inject the paraffin at high speed so that viscous forces would create a circulation of sufficient magnitude, as in the case of air injected into water. The larger the interfacial tension, the faster the intrusive speed necessary to create a ring. Stuke showed that rings would form at slower speeds when water was replaced with amyl alcohol, with a consequent lowering of interfacial tension. The slower speeds allowed these processes to be recorded in photographs which can be compared with the photographs of this chapter. Initially, there is a membrane across the hole of the ring (cf. figures 8.1-2). and then the membrane ruptures. Once formed, the ring starts to expand rapidly and the bulk of the paraffin flows into two or three bulges around the ring (cf. plates IX.8.3 (f) and IX.8.4). These heavier bulges fall faster, so that the ring bends and breaks into two or three drops (see his figure 5, figure 2b of O'Brien [1961] and our figures). If a drop were large enough, it would form another vortex ring and the

sequence repeats itself. An analogous description of the ring instability for miscible liquids at slow speed is given by Kojima *et al.* [1984] for their figure 4 and by Arecchi *et al.* [1989].

If the conditions are right, if the drop is much more viscous than the host fluid ($M >> 1$) and the ratio J/R of interfacial to viscous forces is not too large, then the spherical drop will evolve toward a vortex ring. The entries in tables 9.1 to 9.3 for drops of silicone oils in soy bean oil exemplify these effects well. The viscosity of silicone oil can be varied through careful mixing without changing their density or surface tension appreciably. It was observed that when the viscosity of the drop was lower than a certain value (about 500 centistokes here), rings did not form. In particular, when the drop was less viscous than the bath, even with very low interfacial tension, rings did not form, as in plate IX.7.6.

Inertia alone will not cause a ring to form. Indented oblate drops like those shown in figure 7.1 are the most robust of the falling drops. If conditions are such that the viscous action of the host fluid can create a permanent circulation (like that sketched in figures 7.2 (b) and 7.4) of sufficient strength, the drop will begin to look like a ring, spanned by a membrane, as in figures 7.3, 7.4, 8.1 (a) and especially 8.2 (a). A free ring will form only if the membrane breaks. The membrane may or may not break. If it breaks, it does so either by poke-through of a smaller drop caught in the wake as in figures 8.1-2, or by blow-out. Blow-out can best be understood by the failure of blow-out shown in figure 8.2 (a). Blow-out can occur only if the membrane is very weak as in miscible liquids or in low interfacial tension systems like those shown in plates IX.8.4-8.5.

Vortex rings are unstable; whether or not the membrane has broken, the ring will expand rapidly. The rapid extension is a universal characteristic of the instability. If a membrane remains and no drop rests in the wake to poke through, the membrane will stretch and either rupture or fold as in figure 8.2 (b).

Bulges develop on the ring because of capillarity, draining, or other causes; these fall faster than the rest of the ring, and fluid drains rapidly to the heavy bulges, exacerbating the instability. This instability can be considered as a manifestation of the Rayleigh-Taylor instability of the heavy fluid into the light, when the heavy fluid has the shape of a vortex ring. In our experiments, the draining almost always occurs at just two points of the ring, more or less at opposite points on the ring as in plate IX.2.2 (d), figure 2.3 (f), 8.1 (d) and plate IX.8.3 (f). This type of instability scenario can occur even for ring-like structures like the one shown in figure 8.2 (a) in which the membrane does not break and it leads to the folded ring shown in figure 8.2 (b). The heavier places fall faster and the ring bends and breaks into drops.

O'Brien [1985], in reviewing her own work and that of Stuke [1954], noted that the number of bulges which develop on the ring depends on the Reynolds number and is two for Reynolds numbers of order one or

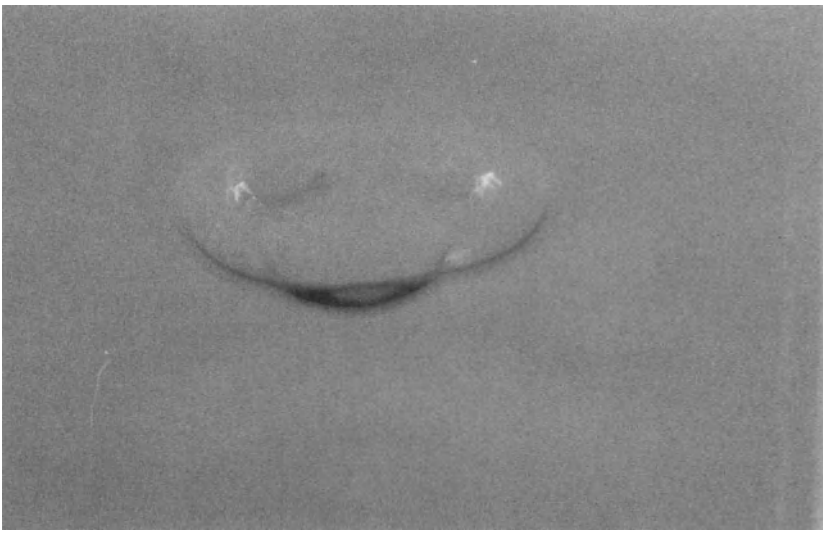

(a)

(b)

Fig. 8.1(a-d). [Baumann, Joseph, Mohr and Renardy, 1992, American Institute of Physics] Poke-through of 1000 cS silicone oil in safflower oil $M = 19.8$, $J = 0.03$, $S^* = 2.41$ dyn/cm. (a) Silicone oil spheres nested in the wake of an indented oblate drop of the same oil. (b) Poke-through leads to a vortex ring. (c) Vortex ring (Rayleigh-Taylor) instability is the rapid expansion of the ring diameter and the draining of the oil into the falling bulges. (d) Two new indented oblate drops form from the falling bulges in a replication of the dynamic sequence.

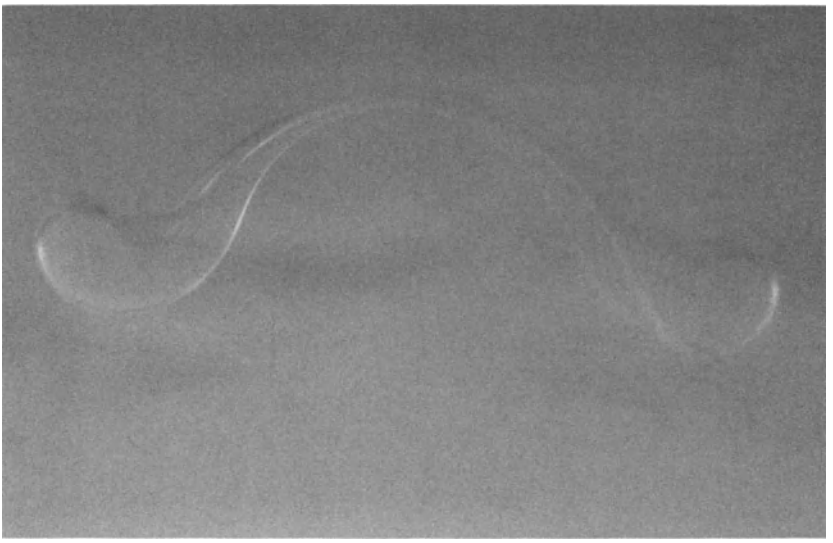

(c)

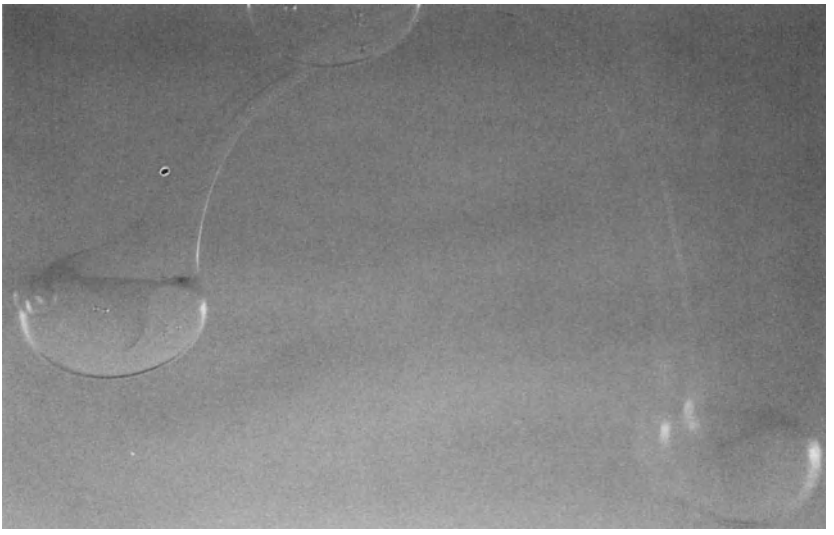

(d)

Fig. 8.1(c-d). Continued.

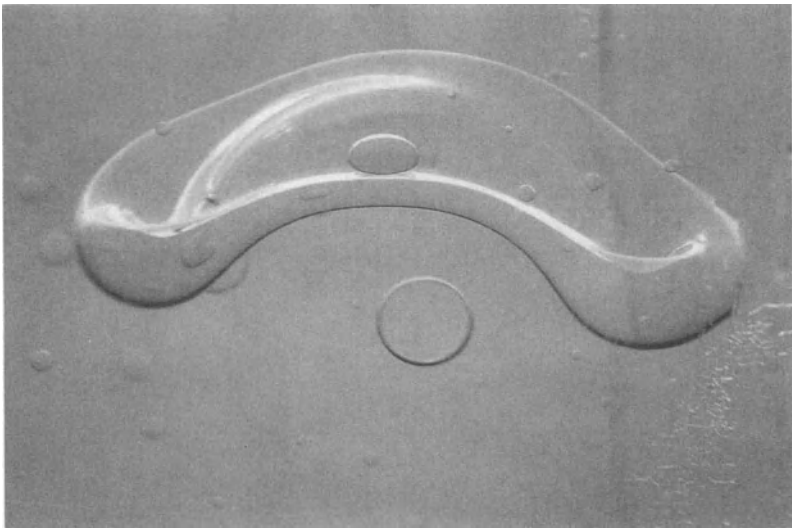

(a)

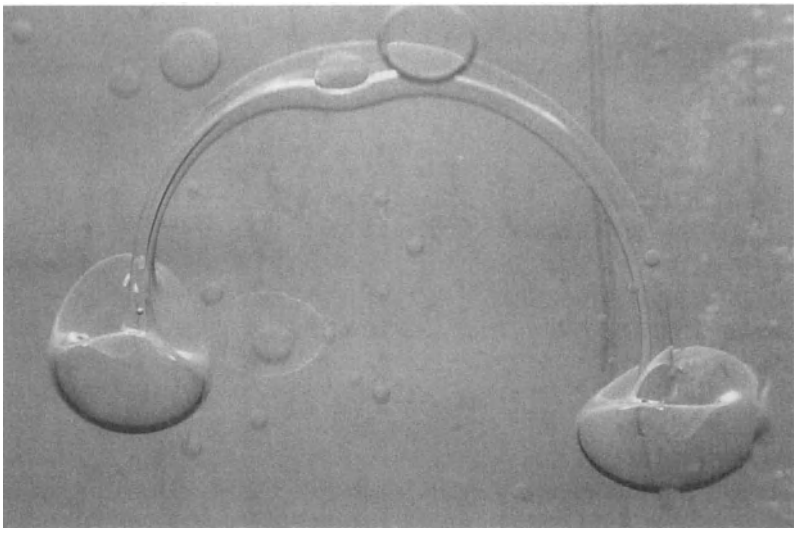

(b)

Fig. 8.2(a-b). [Baumann, Joseph, Mohr and Renardy, 1992, American Institute of Physics] 1000 cS silicone oil falling in contaminated safflower oil. (a) A vortex ring with circulation has developed but a tough membrane spans the ring. (b) The ring is unstable in the usual way (Rayleigh-Taylor instability) forming the characteristic drops (cf. figure 8.1 (d)), but the membrane breaks.

less. Basically, we observed only two bulges even at Reynolds numbers of order 100, with some very rare exceptions. Perhaps the number of bulges on the ring is related to capillary breakup and is strongly influenced by the value of interfacial tension. We saw many bulges when soap was added to water in soy bean oil (see the last entry of table 9.1). This interpretation is also suggested by the closely similar instability in miscible liquids reported by O'Brien [1961], in which case the lack of surface tension promotes the formation of many more nodules around the ring, the ring breaks into many drops, and those drops subsequently repeat the cycle and there is a vortex cascade [Thomson and Newall 1885]. Surface tension can keep subsequent drops spherical if they are small enough, and thus inhibits the cascade.

The effect of the wall on the drop and ring needs further study [Amarakoon, Hussey, Good and Grimsal 1982]. For example, when a ring approaches a wall of the apparatus, it expands considerably before touching it. Also, experiments done with a vortex tube of smaller diameter show that the walls inhibit ring formation. Observations about the way a ring behaves (in the miscible case) at a variety of boundaries is reported by Northrup [1912].

The dynamics leading to formation of vortex rings is not well understood. Data presented in the next section show that rings form from drops started from rest when the viscosity of the drop is relatively great and the interfacial forces do not dominate viscous forces.

A falling drop is relentlessly sheared by the host fluid, but only small portions of the host fluid come under the influence of the falling drop, and these only momentarily. If we move with the drop, we can think that we have a uniform flow around the drop as in figure 7.2 (b), and this picture is also suggestive of why circulations develop in the drop and not in the host fluid. The flow around the ring would, in the case where the ring fluid is very viscous, resemble that of figure 2.1 (a), where the flow is analogous to the rigid-body rotation of figure 2.1 (b) and would then be almost potential flow, with potential flow at infinity (uniform flow), and the vorticity is localized to the interface region between the fluids.

IX.9 Two-Fluid Systems That Do and Do Not Form Vortex Rings

We used formula (4.8) to compute the velocity of a falling drop (with a= $(2.39)^{1/3}$) and rising bubble (with volume 5 cc, a= $(1.19)^{1/3}$) and evaluated many of the dimensionless parameters defined in section IX.5. The parameters are listed in tables 9.1-9.3. Parameters which are not set down explicitly in these tables can be computed readily from the listed values. Table 9.1 tabulates the systems that were observed to form rings. The other two tables list the two-fluid pairs that were observed not to form rings.

We find that to form a ring, it is necessary that the drop fluid be much more viscous than the host fluid. Another criterion which appears to be necessary is that the effect of interfacial tension should be smaller than viscous effects, which may be expressed as

$$\frac{J}{R} < O(1), \tag{9.1}$$

where the notation is defined in (5.4) and (5.6). The last column of table 9.1 is comfortably in agreement with (9.1). However, the velocity U used to compute R was computed from (4.8) and the true J/R may be an order of magnitude larger than in the table. In general, however, when one inspects the tabulated data, it becomes apparent that since all of the fluids tested have low values of J/R, the factor which distinguishes a system which will form rings from a system which will not is the value of M. For the most part, the criterion for the fluids tested seems to be that M be greater than 8 or so. However, there is definitely an ambiguous range ($5 < M < 8$) within which we cannot predict whether a ring will form or not.

A very dramatic illustration of the importance of J/R and M is exhibited by data for Palmolive soap dropped in soy bean oil (a ring forms; see last entry of table 9.1) and water dropped in soy bean oil (a ring does not form). Palmolive soap is essentially water modified with a surfactant which reduces the interfacial tension enough to move J/R down to a sufficiently small value. The viscosity of Palmolive soap is greater than that of water and this alters M such that the combination of J/R and M produces a vortex ring. The evolution of the ring in this soapy solution is exceptionally rapid and the torus breaks up rapidly into small bubbles, as in the case of miscible liquids.

Table 9.2 displays systems that do not form vortex rings. The data show that a modification of the fluids will switch a system that forms a vortex ring to one that does not. An example is the glycerin and soy bean oil system. When 9 percent water is added to glycerin, the resulting diluted solution will not form a vortex ring because the viscosity ratio M has decreased and J/R has increased to the borderline level. A similar adjustment was made for golden syrup by adding water. Of course, we cannot determine in these examples which parameter is truly causing the change of the system, since in both cases, M and J/R change simultaneously. However, it is still interesting to observe the effect of altering the relevant parameters.

Table 9.1. Systems that form vortex rings. Gly denotes 100 percent glycerin; .95Gly denotes 95 percent glycerin in 5 percent water; Shell denotes Shell Research Oil; Sil denotes silicone oil with the indicated viscosity; Soy denotes soy bean oil. The difference $\Delta\rho$ denotes (density of dropped fluid) − (density of host fluid); $\Delta\nu$ denotes (viscosity of dropped fluid) − (viscosity of host fluid): this difference is negative in some of the systems in the tables.

System	$\Delta\rho$ (g/cm^3)	$\Delta\nu$ (cS)	S^* (dyn/cm)	U (cm/sec)	R_d	ρ_d/ρ	M	J_d/R_d	J/R
Gly/Soy	0.343	606	18.45	278.5	57	1.37	16.9	.008	.135
Gly /Canola	0.350	589	35.78	227.5	46	1.38	13.6	.02	.272
500cS Sil /Canola	0.056	433	2.33	37.0	10	1.06	8.0	.01	.080
Gly /Olive Oil	0.351	588	10.50	242.0	49	1.38	13.2	.005	.066
500cS Sil /Olive Oil	0.057	431	3.10	58.0	16	1.06	7.7	.01	.077
Gly /Safflower	0.345	606	15.65	291.5	59	1.38	17.6	.006	.106
500cS Sil /Safflower	0.051	450	7.44	43.6	12	1.06	10.3	.03	.309
Gly /Walnut Oil	0.340	605	39.51	285.8	58	1.37	17.6	.02	.352
500cS Sil /Walnut Oil	0.046	449	4.15	39.1	10	1.05	10.3	.02	.206
Gly /Sesame Oil	0.345	592	15.20	216.3	44	1.38	14.1	.008	.113
500cS Sil /Sesame Oil	0.051	436	3.40	34.9	9	1.06	8.2	.02	.164
500cS Sil /Soy	0.049	447	1.68	40.3	11	1.05	9.9	.008	.079
600cS Sil /Soy	0.049	547	2.68	40.1	9	1.05	11.9	.01	.119
1000cS Sil/Soy	0.049	947	2.41	39.7	5	1.06	19.8	.006	.119
10000cS Sil/Soy	0.053	9947	3.29	42.3	0.6	1.06	199.0	.0008	.159
30000cS Sil/Soy	0.053	29947	6.49	42.3	0.2	1.06	597.0	.0005	.298
Golden Syrup/Soy	0.518	20751	42.20	413.3	2.7	1.56	611.4	.0003	.183
.92Gold. Syrup/Soy	0.478	2553	28.46	382.6	19.6	1.52	74.47	.002	.149
Palmolive /Soy	0.128	185	18.10	108.0	61.0	1.14	5.10	.0006	.003

Table 9.2. Systems that do not form vortex rings

System	$\Delta\rho$ (g/cm^3)	$\Delta\nu$ (cS)	S^* (dyn/cm)	U (cm/sec)	R_d	ρ_d/ρ	M	J_d/R_d	J/R
.95 Gly /Soy	0.323	194	13.43	269.8	148	1.35	6.2	.02	.124
.91Gly /Soy	0.318	63	11.49	277.3	328	1.34	2.9	.03	.87
Water /30W Motor Oil	0.114	315	9.22	23.7	3172	1.13	0.004	38.85	.156
Water /Shell	0.105	2036	42.14	3.4	450	1.12	0.0005	1251	.625
Gly /Shell	0.370	1381	27.83	10.3	2	1.41	0.45	.34	.153
500cS Sil /Shell	0.076	1537	5.82	2.2	0.6	1.08	0.27	.53	.143
5cS Sil /Soy	0.008	-48	1.14	9.2	245	1.01	0.10	2.7	.27
100cS Sil /Soy	0.038	47	2.75	34.1	46	1.04	2.0	.08	.16
200cS Sil /Soy	0.048	147	2.16	40.9	28	1.05	4.0	.03	.12
300cS Sil /Soy	0.048	247	2.71	40.2	18	1.05	5.9	.02	.118
400cS Sil /Soy	0.048	347	2.67	39.7	13	1.05	7.9	.02	.158
Water /Soy	0.078	-52	3.39	92.3	12337	1.08	0.02	.37	.074
Water+ Alconox/Soy	0.158	-20	4.64	156.0	632	1.17	0.73	.08	.056
.60Gold. Syrup/Soy	0.342	-27.5	7.42	341.0	1788	1.37	0.659	.07	.046

Table 9.3 lists systems where bubbles of the less dense liquid were released and left to rise through the more dense liquid. In each case, an oil was released into water. No vortex rings were observed. The related case of air bubbles released into water has been shown to yield rings (see figure 7 of Walters and Davidson [1963]). The case of 12500 centistoke silicone oil was inconclusive because the silicone oil showed an affinity for the plexiglass box.

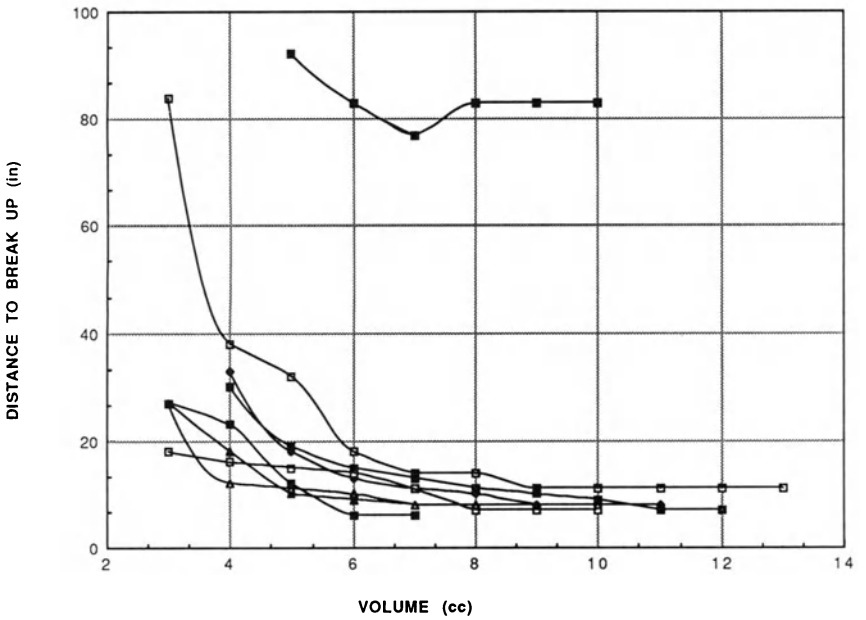

Fig. 9.1. [Baumann, Joseph, Mohr and Renardy, 1992, American Institute of Physics] Distance travelled by a falling drop before a vortex ring forms as a function of drop volume. The formation of the ring occurs when the membrane spanning the ring breaks.

Table 9.3. Systems of injected bubbles

System	S^* (dyn/cm)	ρ_d/ρ	U (cm/sec)	R_d	M	J_d/R_d	J/R
100cS Sil /Water	24.67	0.96	984	1043	96	0.03	2.88
12500cS Sil/Water	27.11	0.975	621	5.3	12188	0.0004	4.8
Soy Oil /Water	3.39	0.922	1917	3829	49	0.004	0.196
30W Motor Oil/Water	9.22	0.886			280		
Olive Oil /Water	16.42	0.914	2119	3257	63	0.012	0.72

In figure 9.1, we display the results of a study of drop size on the distance required for ring formation. This distance decreases monotonically

with volume and seems to asymptote to some small value less than 15 inches for large volumes.

IX.10 Effect of Drop Size and Surfactant

This section is based on the work by Mohr and Joseph which appears as an addendum to the paper of Baumann, Joseph, Mohr and Renardy [1992], and concerns experiments with silicone drops, and silicone drops containing the surfactant Igepal. The drops are released at the top of a four foot tall glass tube which contains soybean oil. They fall under gravity, and observations are made as they traverse the length of the tube. To control the drop size, a 1 inch diameter (60 ml) plastic syringe is used, with the end almost completely removed. Since small amounts of silicone invariably stick to the syringe and since the modified syringe volume is measured to be 0.8 ml less than with the tip intact, the plunger is consistently pulled back 1 ml beyond the desired drop size. With the plunger set, the syringe is filled with the silicone oil and the end is quickly placed into the soybean oil and the plunger is depressed. The syringe is tilted to a sharp angle and twisted to remove the clinging drop. While this method does not guarantee a great deal of accuracy for the true drop volume, it does provide for drops of very consistent volumes.

Pure Silicone Oil. Small drops (roughly those <2ml) were generally observed to remain as indented oblate spheres for the entire length of the tube. When drop sizes were increased to 2 ml, the indentation in the drop deepened, and for many drops (6 times out of 10 observations) this indentation poked all the way through until a free ring was generated. These rings would always rupture their membranes while they were on the bottom of the drop (see plate IX.10.1(a) and figure 10.2).

Drops of approximately 3 ml also form rings, but their evolution is slightly different than that of 2 ml drops in that the spanning membrane does not always break while it is on the bottom. These drops instead expand horizontally, and the membrane bulges up through the center of the surrounding annulus of fluid (see plate IX.10.1(b) and figure 10.3). The degree to which it bulges upward is strongly dependent on drop size; the larger the drop, the more extreme the expansion. For drops with volumes of 3 ml, the membrane would occasionally rupture after this expansion. However, those drops of pure silicone oil having a volume greater than 3 ml were not observed to form rings. They underwent the same evolution as the slightly smaller drops, but exhibited Rayleigh-Taylor instability before membrane rupture (see figure 8.2). The instability causes the drop to form two lobes, thus pinching off the center membrane.

Silicone Oil with 0.5% Igepal CO-530. The addition of 0.5% Igepal CO-530 to the 1000 cS silicone oil had a rather dramatic effect on the upper bound of

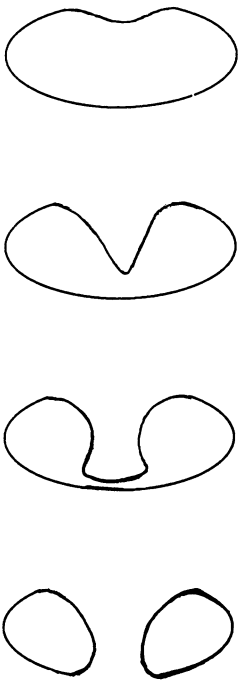

I. The drops begins to indent on top.

II. The indentation deepens. Very small drops (less than 1 ml) remain like this for the entire length of the tube.

III. The indentation reaches the bottom of the drop. Drops that are 1-2ml will sometimes remain in this configuration for the length of the tube.

IV. Membrane rupture occurs on the bottom of the drop. Those drops 2-3ml will usually exhibit this type of rupture.

Fig. 10.2. [Baumann, Joseph, Mohr and Renardy, 1992, American Institute of Physics] Drop evolution for volumes of 2-3 ml.

drop size. As mentioned above, large drops (4ml-7ml) had the tendency to become unstable, form a tough membrane and pinch off before a ring could be formed. The drops which contained Igepal proceeded in the same fashion except that the membrane usually broke; sometimes before and sometimes after the onset of instability. It was sometimes observed that a membrane would rupture during pinch-off. In other words, it appeared that the membrane rupture occurred when the total surface area of the membrane was decreasing. Without Igepal, 4ml and larger drops would invariably pinch off without membrane rupture, while with Igepal, 4 and 5 ml drops would frequently (9 and 7 times out of 10 observations respectively) form free rings (see figures 10.4(a) - (b)). Thus, large drops with Igepal more frequently experience membrane rupture than those without, and so it would appear that the membrane strength was in some sense decreased with the addition of the Igepal. The interfacial tension between the Igepal/silicone oil solution and soybean oil was found to be 1.0 dyn/cm. This is lower than the value of 2.5 dyn/cm between pure silicone oil and soybean oil.

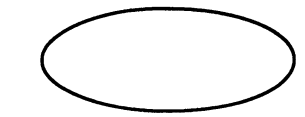

I. The drop forms an oblate sphere

II. An indentation begins to form on the top of the oblate sphere, flattening it out, and forcing more fluid towards the outer edges of the drop.

III. The indentation becomes deeper, and still more fluid is forced into the outer edges of the drop

IV. The middle of the drop is now a fairly thin membrane, with a thick annulus surrounding it.

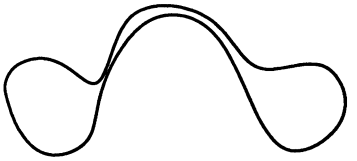

V. The membrane is stretched upward, and becomes very thin. Drops of 4 ml and more exhibit Rayleigh-Taylor instability at this point and do not proceed to phase VI.

VI. The membrane breaks, leaving only the vortex ring. This configuration is unstable, and the ring will separate into two lobes shortly after forming.

Fig. 10.3. [Baumann, Joseph, Mohr and Renardy, 1992, American Institute of Physics] Drop evolution for volumes of 3-5 ml.

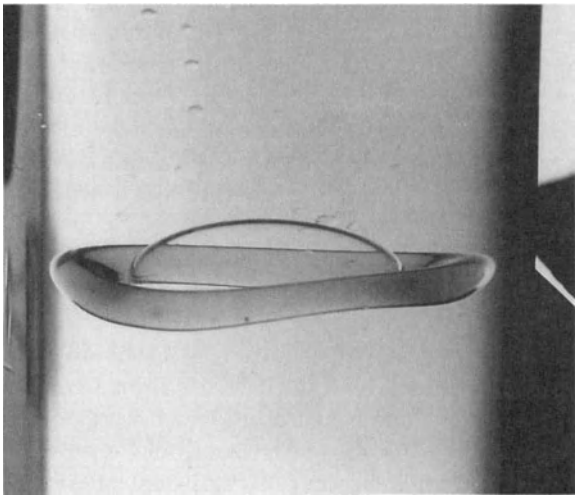

(a)

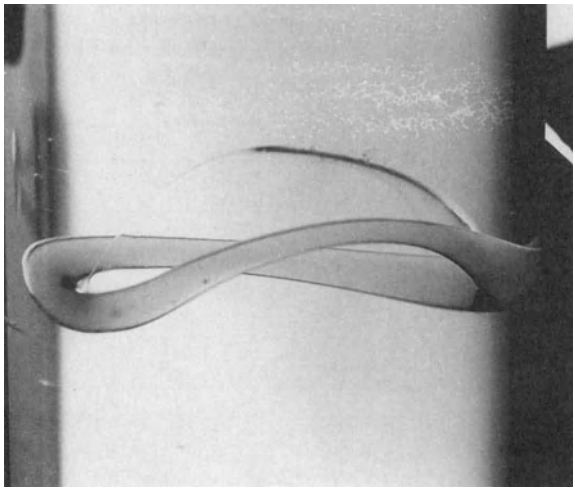

(b)

Fig. 10.4(a-b). [Baumann, Joseph, Mohr and Renardy, 1992, American Institute of Physics] (A) This 5ml drop of 1000 cS silicone containing 0.5% Igepal CO-530 has formed a membrane similar to that in plate IX.10.1(b). (b) The membrane is rupturing from the left side of the drop to the right. Rupture of membranes at this stage of development is extremely rare with pure silicone oil, but occurs frequently when Igepal is added.

The effect of Igepal on smaller drop sizes is not clear. For 2ml drops, membranes broke *less* often with the Igepal (4 out of 10 with Igepal, 6 out of 10 without). However, with 2.5ml drops membranes broke much more frequently with Igepal (10 out of 10 with, 3 out of 10 without). At 3ml, no effect was observed when Igepal was added (membranes broke 10 times in 10 trials with or without). It appears that with small drops, size is the more critical factor in determining whether a ring will form than whether or not the drop contains any Igepal.

The raw data is presented in the table below. Under each column, two numbers are given; the first is for pure 1000 cS silicone oil, the second for the same containing 0.5% Igepal. # Ruptures lists the number of times the membrane was observed to rupture, # Pinch-off lists the number of times the instability manifested itself before the membrane could rupture, and # Oblates lists the number of drops which were observed to remain as indented oblate spheres for the entire length of the tube.

The number of trials is small (10 and less) at each drop size, and it could certainly be said that more observations should be made. However, for the most part, it was found that given the drop size, we could predict whether a ring would form.

Table 10.1. Data summary. Quantities listed are: pure 1000cS silicone/1000cS silicone with 0.5% Igepal. The interfacial surface tension for the pure silicone oil in soybean oil is 2.7 dyn/cm. With 0.5% Igepal in the silicone oil, the interfacial tension is 1.0 dyn/cm.

Size(ml)	# Trials	# Ruptures	# Pinch-off	# Oblates
1.0	5/5	0/0	0/0	5/5
2.0	10/10	6/4	0/0	4/6
2.5	2/4	2/4	0/0	0/0
3.0	10/10	3/10	7/0	0/0
4.0	10/10	0/9	10/1	0/0
5.0	2/10	0/7	2/3	0/0
7.0	3/-	0/-	3/-	0/-

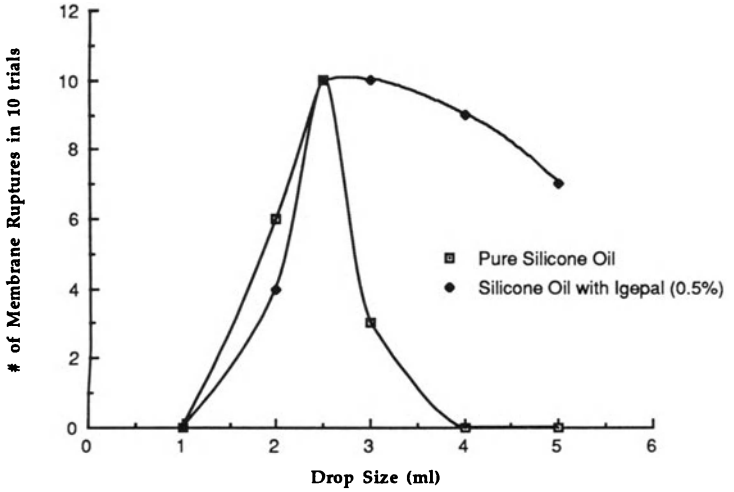

Fig. 10.5. [Baumann, Joseph, Mohr and Renardy, 1992, American Institute of Physics] Graphic data summary.

Chapter X
Fluid Dynamics of Two Miscible Liquids with Diffusion and Gradient Stresses

This chapter is based on papers by Joseph [1990b], Galdi, Joseph, Preziosi and Rionero [1991], Joseph and Hu [1991] and Hu and Joseph [1992]. The density of incompressible fluids can vary with concentration and temperature, but not with pressure. The velocity field $\mathbf{u}$ of such incompressible fluids is not in general solenoidal: $\operatorname{div} \mathbf{u} \neq 0$. We require that

the mass per unit total volume of one of the liquids in a material volume is conserved in the absence of diffusion. This yields the diffusion equation for the mass fraction ψ. Alternatively, if we obtain an equation for the volume fraction ϕ, then the left hand side of the diffusion equation differs from the usual substantial derivative of ϕ by the addition of ϕ div $\mathbf{u}$.

The possibility that stresses are induced by gradients of concentration and density in slow diffusion of incompressible miscible liquids, as in the theory of Korteweg [1901] is considered. Such stresses could be important in regions of high gradients giving rise to effects which can mimic surface tension. One could also wonder about the effect of gradients in viscosity on surface tension, when two fluids are brought into contact. However, surface tension is a quantity that remains the same whether the fluids are in motion or not, so that the effect of viscous stresses on it which are present when there is motion must be unimportant, and we do not pursue it here.

The presence of a sharp interface in the case of slow diffusion in rising bubbles and falling drops has been documented in many experiments and in the experiments reported here. The shape of such interfaces over time-scales in which diffusion is small can scarcely be distinguished from the shapes of bubbles and drops of immiscible liquids with surface tension. The usual description of interface problems for miscible liquids with classical interface conditions but with zero interfacial tension misses out on slow diffusion on the one hand and gradient stresses that mimic the effect of surface tension on the other. The usual description of diffusion with div $\mathbf{u}$ =0 is a bad approximation for some cases at certain times and places.

X.1 Motivation and Problem Statement

In figure 1.1, we present a sequence of photographs documenting the change in the shape of a water bubble (density $\rho = 1$ gm/cc) as it rises in a container filled with glycerin ($\rho = 1.2$ gm/cc). Since water and glycerin are miscible, we must admit that our perceptions trick us and that our eyes do not resolve the diffusion layer of aqueous glycerol in which the transition from pure glycerin to pure water must take place. The shape of the water bubble we see, however, is not so different from what we might expect to see in the case of a rising bubble or falling drop of one immiscible liquid in another, provided that these immiscible liquids are otherwise similar to the miscible ones in their physical properties; that is, that they have the same densities and viscosities and a small, but not zero, interfacial tension.

In figure 1.2, we show a sequence of photographs of a molasses and water mixture in glycerin. The densities are nearly matched, so that the bubble rises slowly.

In plate X.1.3, we show a sequence of photographs of a molasses drop falling in glycerin. The diffusion between this pair of fluids is very slow. Even after vigorous mixing, it takes two days for the small amount of molasses

to dissolve completely in the glycerin. It appears possible that one can find a pair of miscible liquids that mix so slowly that essentially no mixing has taken place over the time of an experiment.

Similar shapes and phenomena are observed in thermals. These are related to vortex rings and are described in chapters 6 and 7 of the book by Turner [1979]. In figure 1.4 (i), we show some photographs of a dyed thermal taken by Griffiths [1986 a]. A layer of fluid is initially at rest at a constant temperature. Subsequently, the lower boundary is set at a higher temperature, and the fluid heats up due to conduction. A boundary layer forms whose thickness increases with time; at certain critical times, some of the buoyant fluid in the boundary layer escapes upwards in blobs. For most of the time, the transfer of heat near the boundary layer is due to conduction, followed by short intervals during which the conditions are locally restored to the original uniform state by the removal of the buoyant fluid as a thermal (see figure 1.4 (ii): this shows some other possible shapes for the fluid escaping from the boundary layer). Thermals that resemble the pictures shown in figure 1.2 can be found in Griffiths [1986 b]. He considers, the idea that interfacial tension might play a role in the 22 % discrepancy between the observed rise velocity and the velocity predicted by Stokes' law. However, his observations suggested to him that the discrepancy was most likely due to the presence of the sidewalls of the apparatus.

In figure 1.5, we show photographs [Koh and Leal 1990] of an unstable spherical drop of 10000 cs Dow silicone oil in Pale 1000 oil.

A striking comparison of incipient vortex rings which arise in the free fall of liquid drops in another liquid can be formed by comparing the membrane which spans the ring in the miscible case shown in plate IX.2.2 (c) and the immiscible case shown in figure IX.8.2 (a). The existence of a membrane across the ring of one aqueous glycerol solution in another shown in plate IX.2.2(c) may be hard to explain without appeal to the notion of transient interfacial tension.

When two miscible fluids come into contact, there may initially be what looks like a sharp interface. Over time, there is diffusion across that interface due to gradients in the physical properties and there is then a transition layer from one fluid to the other; eventually, the fluids mix. The figures presented above motivate us to pose some basic questions. One question is how to model the diffusion and the force due to the gradient of composition in the transition layer.

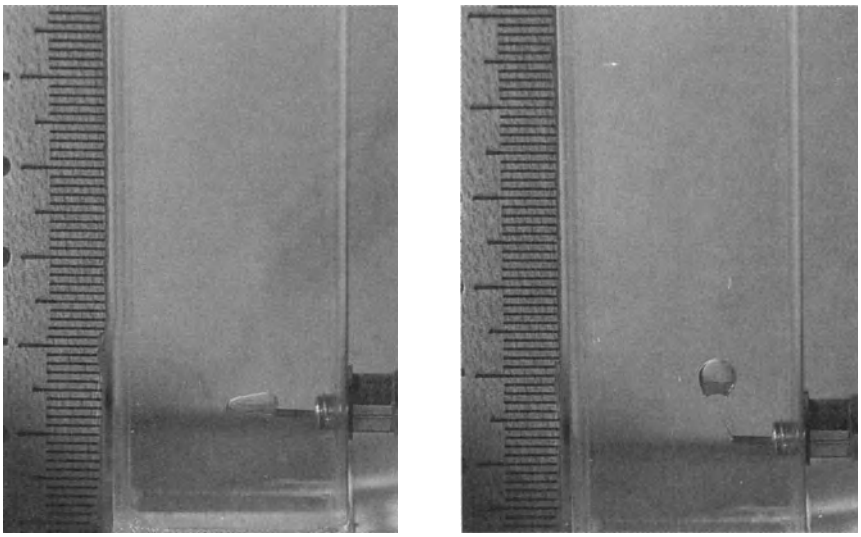

(a)-(b)

Fig. 1.1(a-f). [Joseph, 1990b, Gauthier-Villars] Water bubbles rising in a column of glycerin. The photographs (a) through (e) were taken at approximately two-second intervals with an interval of 1 to 1-$\frac{1}{2}$ seconds between (a) and (b). (f) follows (d) after 40 seconds. The density ratio ($\rho_{outer}/\ \rho_{drop}$) is 1.21 and the viscosity ratio is 69. The water bubble appears to want to pull into a sphere even and especially at the instant of injection. The spherical shape in (c) is nearly perfect. However, there is always a rearward protrusion followed by an extruded thread of water left behind as the bubble rises. A small 'capillary bubble' is visible on the water thread in (c) and (d). The sharp spherical interface at the leading edge and the protruding tail at the trailing edge are persistent. The drop shapes resemble the unstable spherical drops with nonzero interfacial tension which were computed by Koh and Leal [1989] (their figures 7 and 9), by Pozrikidis [1990] (his figure 6) and observed by Koh and Leal [1990] (see figure 1.5). The computed shapes for zero interfacial tension and no diffusion always have intrusions (which were not observed in our experiments) near the trailing edge even when a thread is ejected at the trailing edge. We have the impression that glycerin has been entrained and possibly diffused in the bubble shown in (e) and (f), as in the thermal drops studied by Griffiths [1986a].

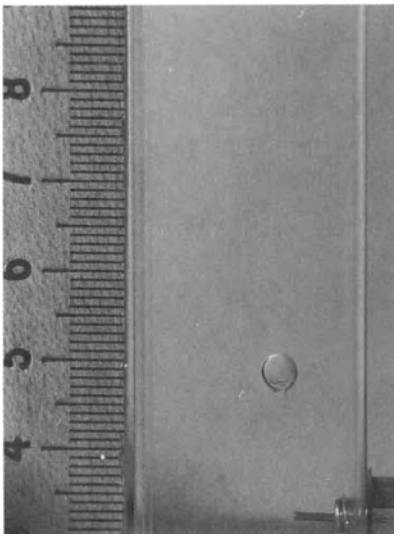

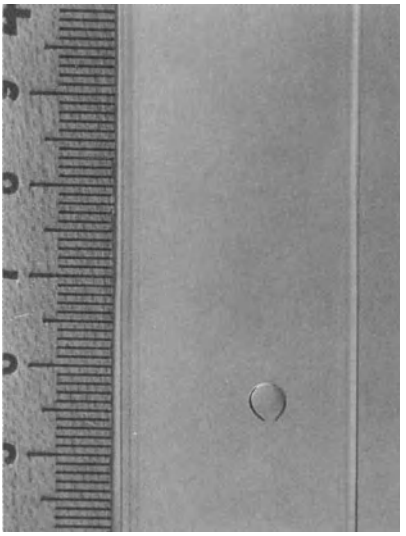

(c)-(d)

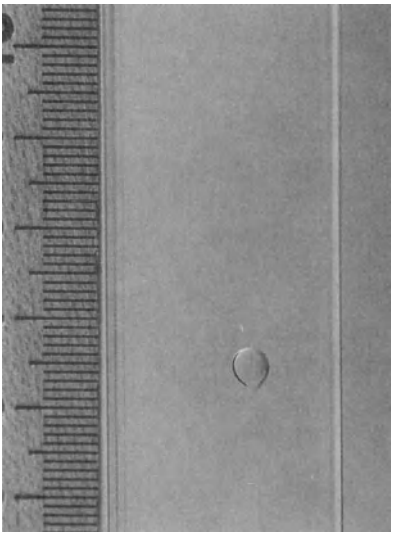

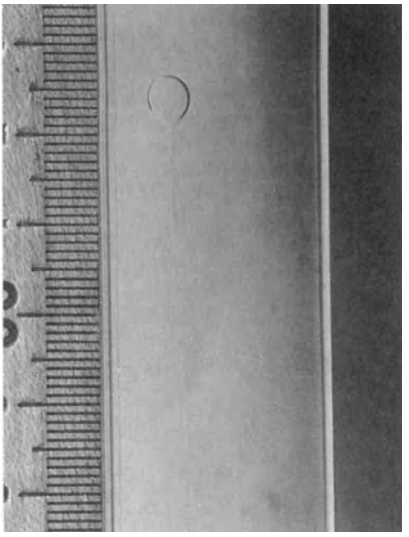

(e)-(f)

Fig. 1.1(a-f). Continued.

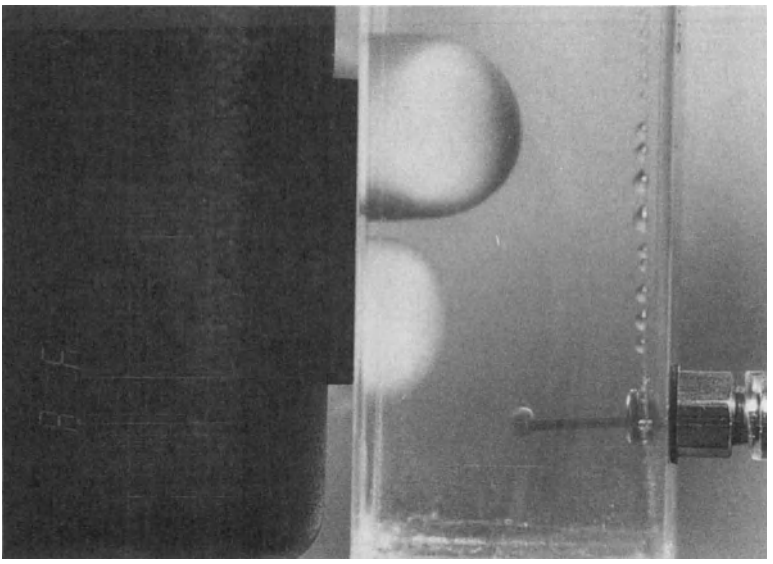

(a)

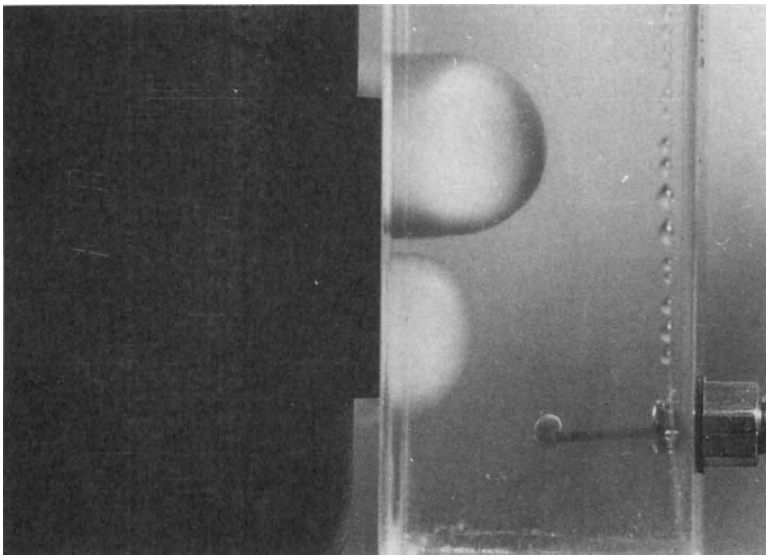

(b)

Fig. 1.2(a-f). [Joseph, 1990b, Gauthier-Villars] A mixture of molasses and water in glycerin rises slowly. The density is nearly matched. The essentially 'static' configurations in (a) through (c) possibly suggest the action of capillary-like forces. Time on the clock is in seconds: (a) 0.98, (b) 1.23, (c)1.14, (d) 1.99, (e) 9.01, (f) 15.68.

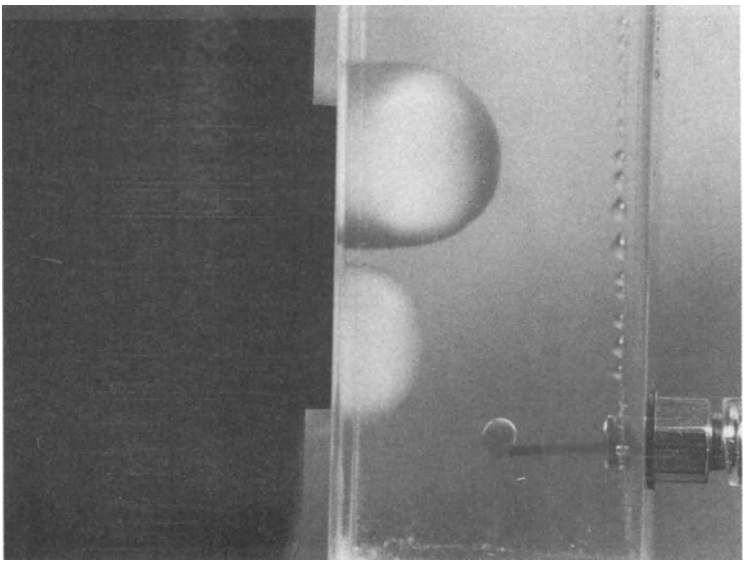

(c)

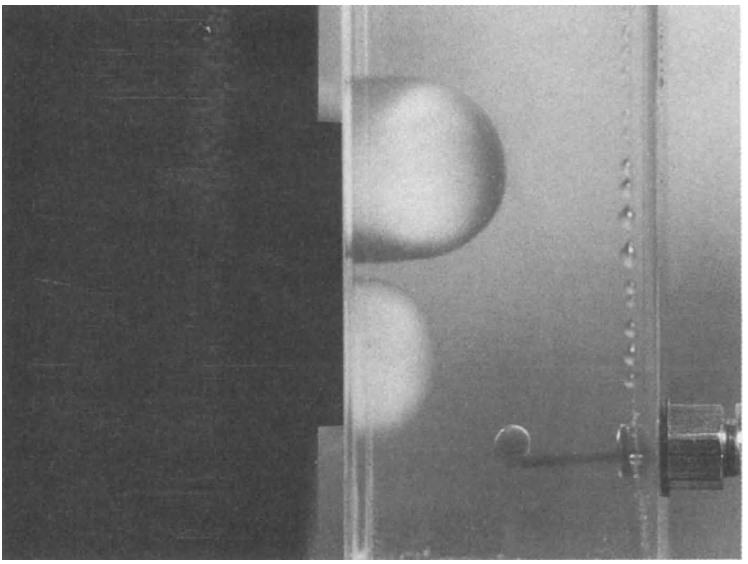

(d)

Fig. 1.2(c-d). Continued.

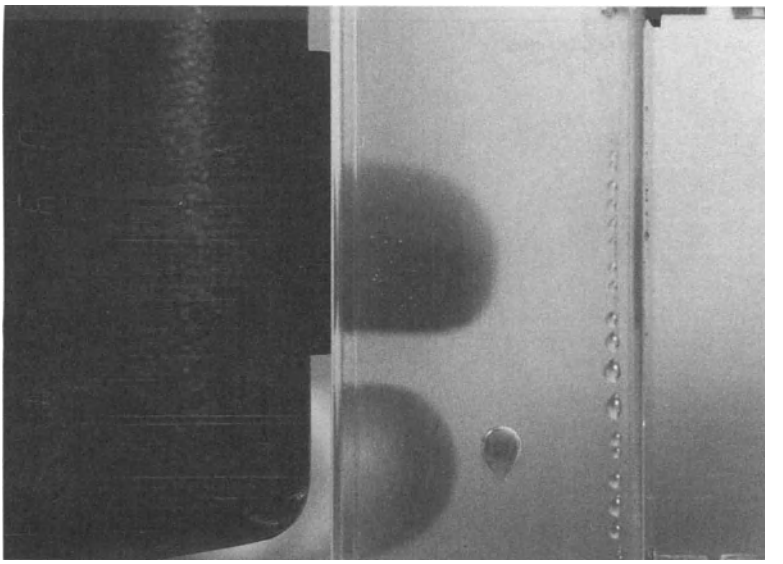

(e)

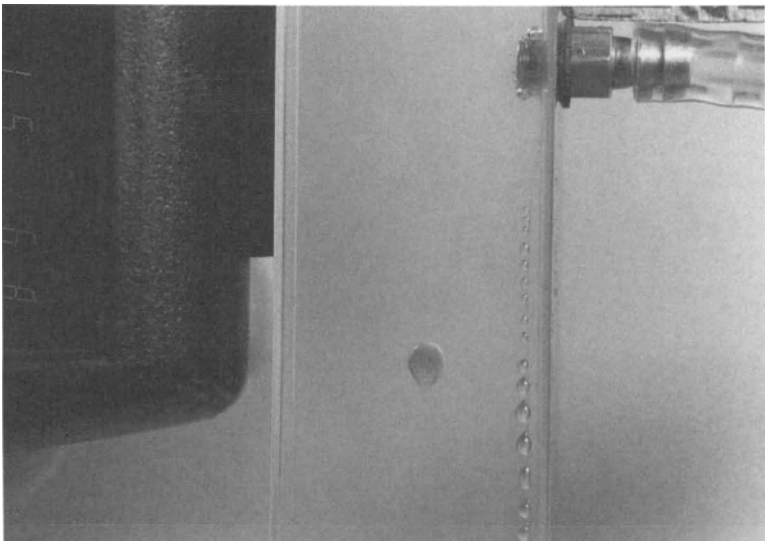

(f)

Fig. 1.2(e-f). Continued.

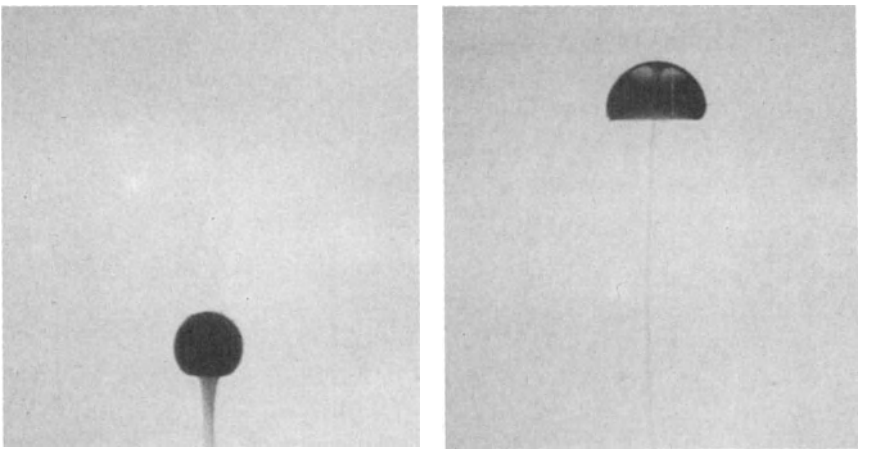

Fig. 1.4(i). [Griffiths, 1986a] A thermal of dyed liquid.

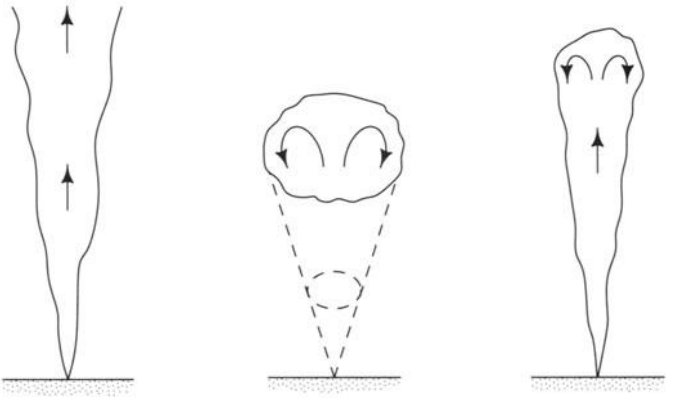

Fig. 1.4(ii). [Turner, 1979, *Buoyancy Effects in Fluid*, Cambridge University Press] Sketches of convection phenomena: (a) plume, (b) thermal, (c) starting plume. The arrows indicate the direction of mean motion.

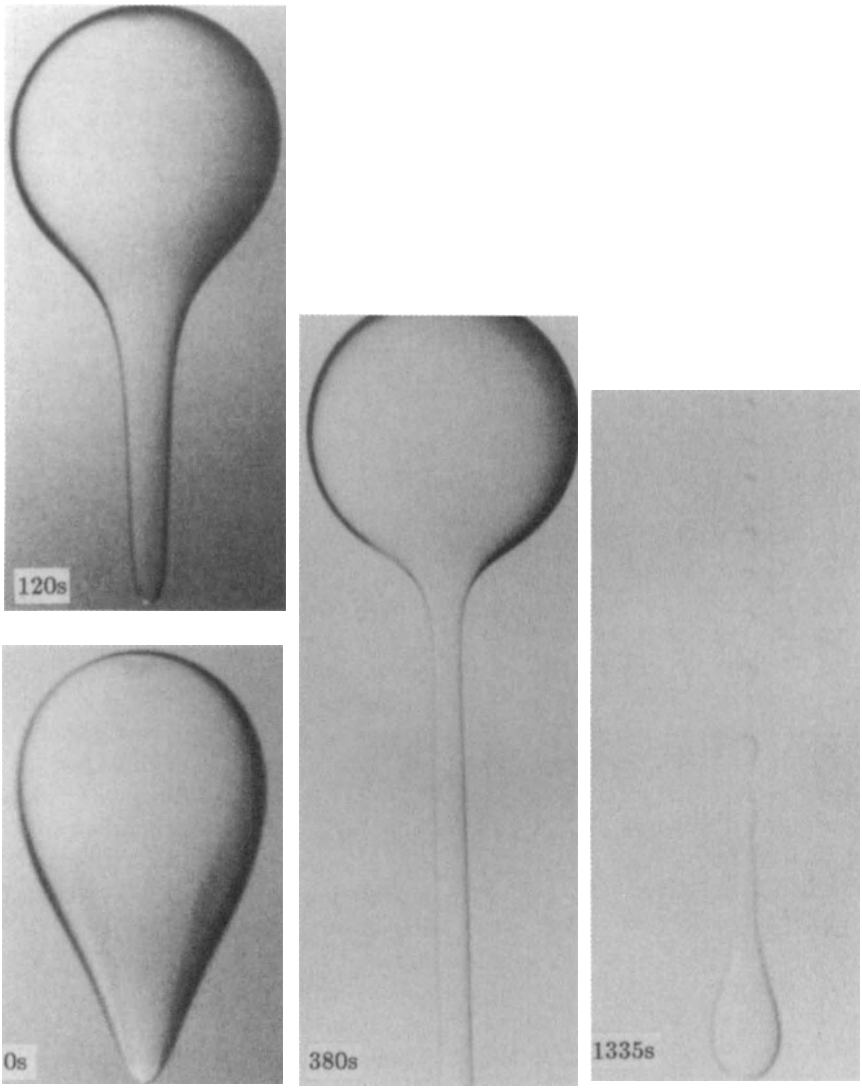

Fig. 1.5. [Koh and Leal, 1990, American Institute of Physics] Unstable spherical drop of 10000 cs Dow silicone oil ($\mu = 101$ P, $\rho = 0.972$ gm/cm^3) in Pale 1000 oil (oxidized castor oil, $\mu = 391$ P, $\rho = 1.021$).

X.2 Historical Introduction

The idea that there are capillary forces at work in a transition layer between miscible liquids goes back at least to an 1871 report of Bosscha, cited in a paper of Korteweg [1901], and reproduced here. Korteweg noted that Bosscha had published, in the proceedings of the 30th of September and the 25th of November 1871 of the Academy of Sciences of Amsterdam 1871/72, #3 and 5, some observations on the very slow motion of a solution in water, or in a less concentrated solution. The two fluids were miscible in all proportions. The most natural explanation seemed to Bosscha to be the existence of appreciable capillary forces in the layer between the two liquids. Thomson and Newall [1885], on the contrary, attribute to other causes similar phenomena that they have observed (see pages 430 and 431 of their article). Since the question seemed not to be resolved, Korteweg published, as an appendix to his paper, the French translation of some extracts of the proceedings cited above and of an unedited letter of Bosscha treating the same subject.

The following is an extract of a communication made by M. Bosscha at the Academy of Sciences of Amsterdam, on September 30th, 1871:

"A test tube, of which the bottom is stretched into a funnel with a fine opening, is partly immersed in water which fills a large cylindrical vessel. When the water in the tube reaches the same height as in the vessel, one injects a crystal of a soluble substance in the water. The liquid contained in the tube then becomes specifically heavier than the surrounding water and begins to flow in a thin thread. This liquid thread exhibits all the details of a jet of ordinary water, except that the flow is much slower so that one has no need for any artifice to observe directly all the phenomena which accompany it. Some distance from the opening, one sees the formation of bulges which more and more take the form of drops, all of them linked by very thin liquid threads. Soon these threads break and are pulled into the drops which henceforth fall freely. Because of the great resistance which they encounter in their fall the small drops thus formed flatten; at the center they shape themselves into skull caps, concave on the bottom, which terminate by breaking in their turn, in such a way that each drop is transformed into a ring which enlarges more and more and disperses slowly, as much by the motion of the liquid as by diffusion. It sometimes happens that a tight ring falls through the already enlarged ring which preceded it; in these conditions a liquid film is carried from the interior boundary of the latter large ring ac (cf. figure 2.1), which looks like a known capillary surface, but which contracts until at the end the two rings have formed only one.

"According to the observations of the author, one can do this experiment with any salt. The experiment works even when one lets flow a less concentrated solution, as long as the difference in the birifringent powers permits one to distinguish between them. If one makes use of a tube of

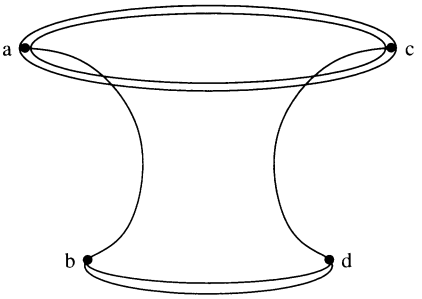

Fig. 2.1.

which the bottom is pulled into a fine point toward the interior, one can, by suitably regulating the hydrostatic pressure, make a vertical jet of the liquid from the cylindrical vessel climb in the tube; under these conditions one can also observe separation into small drops, but it is sometimes necessary to tap slightly against the glass to produce the effect.

"From a theoretical point of view it seems important to do these experiments with some liquids which combine themselves with a considerable release of heat. I have been able to verify that sulphuric acid and water, or a solution of caustic potash in dilute sulphuric acid tends thus to assume a surface as small as possible, from this it results then that capillary attractions are of an altogether different nature than chemical attraction."

The following are extracts from a letter of M. Bosscha dated 22 May, 1901:

"The phenomena which I have observed related to the slow flow of one liquid into another, however slow the flow, remains nevertheless phenomena of motion, and the states I have observed are always states of motion. It is only by way of approximation that one can think of them as states of equilibrium.

"This is why I have always tried to claim some deep scruples that capillary forces *only* produce the clearly defined forms which are taken by the flowing liquid· · ·.

"But each time that I have repeated the experiment, in other respects very simple, and that I saw the liquid thread give rise to local bulges, as in an ordinary jet of water, and resolve themselves then into small drops which finally become rings, my conviction became stronger that capillary action actually must play an important role. What strikes me especially was to see how of the two consecutive rings the higher, smaller one falls through the lower, larger one, and carries clearly in its motion a portion of the interior rim of the other, so that between the larger ac (cf. figure 2.1) and small bd a film forms a surface of revolution from it, of which a

meridional may be a catenary.[1]

"I returned to this subject later in a discussion relative to the agglutination of particles suspended in liquids. When this question became the subject of one of the sessions of the Academy, I recall that while I was occupying myself with the preceding experiments, I took note of the remarkable experiments of M. Vogelsang on globulites (microscopic drops suspended in a mixture of baum of Canada and carbon sulphide; these drops consist of a supersaturated solution of dissolved sulphur in carbon sulphide).

"M. Vogelsang has described (Arch. Néerl. (1) **5**, 166) the motion of these drops in the liquids, motions such that they approach one another until contact. An attractive action of these drops at appreciable distance cannot be attributed to molecular attraction of the drops themselves. In my opinion one is rather forced to search for a motive force in the liquid. It is thus that I thought to myself that each drop is a center of concentration of sulphur, depleting sulphur from the liquid environment, so that each drop will be surrounded by concentric layers in which the percentage of sulphur in it diminishes with increasing radius. As long as the sulphur-poor hydrospheres of neighboring drops come into contact, if there exists in reality a surface tension at the boundary of the two layers of unequal concentrations, it is necessary that the tendency of this surface of separation to become a minimum, brings about the fusion of the layers; this will be caused because some new layers of more packed drops come into contact until at the end the drops touch themselves.

"I have thought that there is a way to explain in an analogous fashion the tendency to agglutination that can be seen with small solid particles suspended in a liquid. These solid particles can more particularly concentrate around themselves certain elements of the liquid in which they are suspended."

The notion that capillary forces are responsible for the phenomena observed by Bosscha is not shared by Thomson and Newall [1885] who appear to suggest that such phenomena, which they observed independently and apparently without knowledge of Bosscha's work, are associated with instabilities of motion, and not with capillarity. It is refreshing to see the pictures which they draw to represent what they observe, at a time before the taking of photographs of these things was a common practice. Their sketched pictures are art in science, emphasizing the scientifically relevant details, suppressing the others. They wrote:

"If a tube be drawn out into a fine capillary and be filled with sulphuric acid, and held so that its capillary end is just beneath the surface of a column of water, a fine stream of acid flows down; and on it marked beadings appear. Each bead gives rise to a vortex ring, and the rings so formed behave

[1] The surface of revolution formed by a catenary is a minimal surface. Note that a catenary is the graph of a hyperbolic cosine, like the shape of a rope if you hold its ends.

in a characteristic manner (fig. 9[2]). Here there seems strong evidence of a tension between the acid and the water, but the appearances are to be explained by differences of velocity in the stream, brought about by motion in the column of water, or by vibrations communicated to the capillary tube. If the experiment be made with all care to avoid vibration, the stream falls unbroken through a column of 8 inches of water: whilst if a tap be given to the acid tube a break occurs in the stream, in consequence of a momentary stop in the flow of acid, a small bead is formed, and from it a ring. If no care is taken to avoid vibration the beads will follow one another very rapidly. It may be objected that if there existed a surface tension, it would only be when disturbances were communicated that beading would appear. But in such a case, the resolution into drops would be complete, and small spherules would be formed between the larger drops. In fact, however, the connexions between the beadings are fine filaments of acid, so that the beadings are never really separated from one another. We have, moreover, convinced ourselves of the correctness of this explanation, by allowing a stream of cold water with lycopodium powder to flow from a fine tube into a column of slightly warm water; similar cessations in flow and formations of beadings may be observed; the rings are not well formed, but this is to be expected, for the conditions are not nearly so favourable."

In fact the citation does not really tell us what might be the real cause of the capillary-like phenomena seen in their sketch. A theory in which stresses due to gradients of concentration and density are allowed, say Korteweg's theory, could conceivably give rise both to the capillary phenomena and the deviations from classical capillarity which are observed. Perhaps it is just this thought which motivated Korteweg to remark that "... the question does not seem to us to be resolved ...".

X.3 Dynamic and Instantaneous Interfacial Tension

Freundlich [1926], in his treatise on colloid and capillary chemistry, discussed methods of measuring interfacial tension between immiscible liquids and the corresponding theory. He also wrote about liquids that are miscible in some proportions but not all. He noted that

"... there is little new to be said.... We have only to remember here we are in the end always dealing with solutions. For the one liquid will always be soluble in the other to some degree, however small. Hence the *dynamic* tension of liquids, when first brought into contact, is to be distinguished from the *static* tension, when the two liquids are mutually saturated. Not only do liquids which are not miscible in all proportions have a mutual surface tension; even two completely miscible liquids, before they have united

[2] See our figure 2.2.

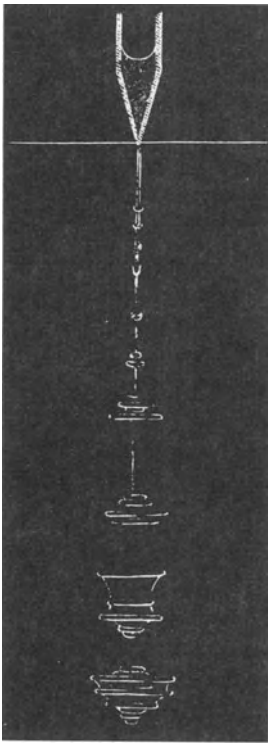

Fig. 2.2. [Figure 9 of Thomson and Newall, 1985, Royal Society of London]

to form one phase, exhibit a dynamic interfacial tension. For we get by careful overlaying of any two liquids a definite meniscus, a jet of one liquid may be generated in another, and so on. The tension decreases rapidly during the process of solution, and becomes zero as soon as the two liquids have mixed completely."

The dynamic tension is denoted by $S^*(t)$ below. Freundlich [1926] cites the measurements of the dynamic tension by Quincke [1902] of ethyl alcohol in contact with aqueous salt solutions (sulphates of zinc, copper, etc.). These two liquids are miscible in all proportions. Quincke used the method of drop weight (see, for example, §6.7 of the book by Hiemenz [1977] for a description of this method) to make his measurements. In these liquids the drop, as it emerges, does not form streaks, but keeps its shape for a while. He found values between 0.8 and 3 dyne/cm.

Smith, Van Den Ven and Mason [1981] have reported an estimate of 1 dyne/cm for the force corresponding to a 'transient interfacial tension' between a 2000 cs and a 1 cs silicone oil, measured over a period of time

and extrapolated to the time of contact. According to the authors, these are two mutually soluble liquids whose interdiffusion is sufficiently slow to enable this measurement to be made. They note that

"In principle there exists between any two separated fluid phases which have a chemical potential difference, an instantaneous interfacial tension which may or may not persist with time. We are unaware of reports in the literature of measurements of interfacial tension between two miscible liquids."

It is clear that in the case of two liquids miscible in all proportions we are not dealing with an equilibrium situation; there is no equilibrium tension. Rather, we are looking at stress effects due to differences in density and composition and possibly even temperature which influence the positions occupied by interdiffusing fluids. One could imagine that when the gradients of composition are large, as in the boundary layer between two regions of different composition suddenly put into contact, that these stresses give rise to an effect which might be called 'transient interfacial tension.'

Smith *et al.* used the Wilhelmy plate method to measure the tension as a function of time, which decreases with time because of diffusion. The Wilhelmy plate method (see, for example, §6.2 of Hiemenz [1977]) makes use of the following equation. A solid sample experiences a capillary force P due to the deformed interface

$$P = 2(l + d)\ S^* \cos\theta \tag{3.1}$$

where l is the length of the plate, d its thickness, S^* is interfacial tension and θ is the apparent contact angle. In practice, all quantities except for S^* ought to be independently measurable, and thus S^* is retrieved. However, the contact angle can be difficult to determine, as in the work of Smith *et al.* They measured the capillary force per unit length

$$F = S^* \cos\theta = P/[2(l + d)] \tag{3.2}$$

as a function of time. Their experimental result for $F(t)$ is summarized in their figure 1, reproduced below in figure 3.1. They were not able to measure $\theta(t)$ so they could not find $S^*(t)$.

Smith *et al.* present an expression for the chemical potential based on expressions for the free energy in a nonuniform system [Van der Waals 1895; Cahn and Hilliard 1954]:

$$S^* \propto \int_{-x_0}^{x_0} \left(\frac{\partial \phi}{\partial x}\right)^2 dx \tag{3.3}$$

where S^* is the interfacial tension, ϕ is the local composition and x_0 is the 'interfacial region'. The composition satisfies a diffusion equation $\phi_t =$

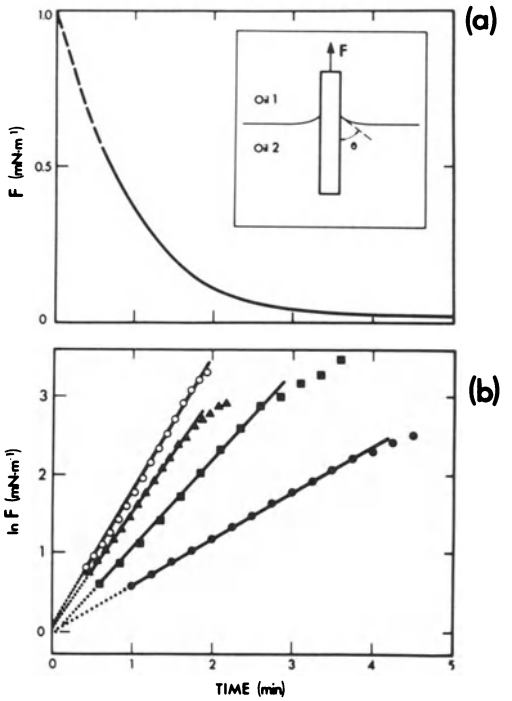

Fig. 3.1. [Smith, Van Den Ven and Mason, 1981, Academic Press, Inc.] (a) Typical decay of capillary force on a Wilhelmy plate for two mutually miscible silicone oils (schematic details of experiment are shown in the inset); (b) Logarithm of F vs time, for various experimental runs. The extrapolated force at zero time yields in all cases $F_0 = 1.0$ mN/m.

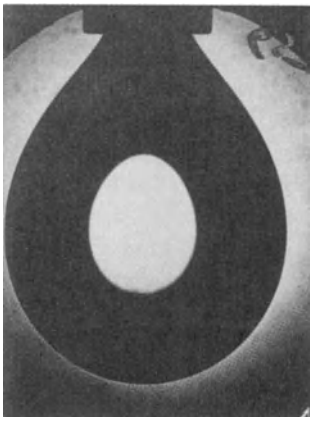

Fig. 3.3. [Joseph, 1990b, Gauthier-Villars] Profile of a Benzene-water pendant drop.

$D\phi_{xx}$ with diffusion constant D. If at $t = 0_+$, $\phi = \phi_+$ for $x > 0$ and ϕ_- for $x < 0$ and thereafter ϕ is continuous at $x = 0$, then

$$\phi(x,t) = [\phi_+ - \phi_-]f(\eta), \quad f(\eta) = \operatorname{erfc}\eta, \quad \eta = x/2\sqrt{Dt} \tag{3.4}$$

and S^* is proportional to

$$\begin{aligned}&[\phi_+ - \phi_-]^2 \int_{-x_0}^{x_0} \frac{4}{\pi} \exp(-2\eta^2) \left(\frac{\partial \eta}{\partial x}\right)^2 dx \\ &= \frac{2[\phi_+ - \phi_-]^2}{\pi\sqrt{Dt}} \int_{-\eta_0}^{\eta_0} \exp(-2\eta^2) d\eta.\end{aligned} \tag{3.5}$$

At small times the breadth of the diffusion layer scales with $\sqrt{Dt}$. Then the gradient theory (equation (3.3)) leads to a square root singularity for the dynamic tension. Figure 3.1 (b) shows that F decays exponentially and does not follow the $t^{-1/2}$ decay that would be required by $F = S^* \cos\theta$ if θ were constant. It is noteworthy that though the slopes in that figure vary between 0.6 to 1.4, the extrapolation to zero time does not vary and leads reproducibly to a force of ~1dyn/cm. They conclude that "... present experiments do indeed confirm that an instantaneous interfacial tension exists between mutually miscible liquids." Smith *et al.* remarked that the Wilhelmy technique appears to be the most sensitive and that other techniques for measuring surface tension, such as the pendant drop method, were found to be unsuitable due to the small magnitude and transient nature of the force involved. Plate X.3.2 shows pendant drops of some pairs of miscible liquids. They give rise at early times to shapes similar to, but not the same as, pendant drops of immiscible liquids; compare them with the immiscible case in figure 3.3. The experiments show a systematic difference between the miscible and immiscible pairs. Davis [1988] supplies a constant of proportionality for the expression (3.3), which he develops independently starting from the Irving-Kirkwood pressure tensor and some simplifying assumptions. He then estimates the constants in his theory to construct a table of values of S^* (γ in his notation), given here as table 3.1.

Table 3.1. Tension γ of a planar front of a miscible fluid as a function of time t of diffusive spreading of the front. In the first row, D is measured in cm^2/s.

$D =$	10^{-5}	10^{-7}	10^{-9}	10^{-5}	10^{-7}	10^{-9}
Time $t(s)$	Mixing Zone Width		$\sqrt{Dt}$(cm)	Tension	γ	(dyn/cm)
1	3.1E-3	3.1E-4	3.1E-5	6.3E-4	6.3E-3	6.3E-2
10	E-2	E-3	E-4	2.0E-4	2.0E-3	2.0E-2
10^2	3.1E-2	3.1E-2	3.1E-3	6.3E-5	6.3E-4	6.3E-3
10^3	E-1	E-2	E-4	2.0E-5	2.0E-4	2.0E-3
4×10^3	2E-1	2E-2	2E-3	1.0E-5	1.0E-4	1.0E-3

He notes that "from the entries in this table it follows that the tension of a diffusive mixing zone between miscible fluids, while small, is nevertheless not zero."

The theory used by Smith *et al.* [1981] and Davis [1988] evidently requires that one assume wrongly that the density of a mixture of incompressible fluids is constant, independent of concentration. Davis restricts his analysis to a two-component *regular solution*, in which the densities of the components 1 and 2 are $\tilde{\phi}\rho$ and $(1-\tilde{\phi})\rho$, $\tilde{\phi}$ is the mole fraction of component 1 and ρ is the total density, which he sets equal to a constant in a regular solution. We shall reinterpret Davis' work for simple mixtures by replacing the mole fraction $\tilde{\phi}$ with the mass fraction $\hat{\phi} = m_\gamma/m$ of an incompressible liquid (say, water) in a mixture (say water and glycerin) of total mass $m = m_\gamma + m_\nu$ where m_ν is the mass fraction of glycerin. Then $(m/V, m_\gamma/V_\gamma, m_\nu/V_\nu) = (\rho, \rho_\gamma, \rho_\nu)$ where V is the total material volume and ρ_γ and ρ_ν are the ordinary (constant) densities (of water and glycerin) listed in the handbooks. Moreover, if our regular solution keeps its volume after mixing, then

$$\rho(\phi) = \rho\tilde{\phi} + \rho(1-\tilde{\phi}) = \frac{m}{V}\frac{m_\gamma}{m} + \frac{m}{V}(1-\frac{m_\gamma}{m}) = \gamma + \nu = \rho_\gamma\phi + \rho_\nu(1-\phi)$$

and the regular solution of Davis is a simple mixture. Obviously, a mixture of incompressible liquids does not have a constant density, even though the density of each of its constituents is constant at a fixed temperature.

The type of calculation of dynamic tension given above, as well as the calculation to be carried out in section X.9, gives rise to a pressure difference across a spreading plane layer. This is not a good analogy to interfacial tension which is proportional to curvature and vanishes across plane layers. The calculation of forces over a spherical layer advanced in section X.10 does contain curvature terms, but the analogy is not far-reaching, even in the spherically symmetric case.

Davis [1988] expresses well the notion that gradients of composition can lead to anisotropic forces which mimic the effects of interfacial tension:

"When two miscible fluids are placed in contact they will immediately begin to mix diffusively (and convectively if their densities are such as to drive convection) across the concentration front formed at the zone of contact. Although no interface will form at the concentration front, the composition inhomogeneities can give rise to pressure anisotropies and therefore to tension at the mixing zone between the contacted fluids. Diffusive mixing will continuously broaden the mixing zone and reduce the pressure anisotropy and the associated tension. The purpose of this short paper is to examine with the aid of a molecular theory of inhomogeneous fluid the magnitude and rate of reduction of the tension by diffusive mixing of the zone of contact of miscible fluids. The results found here suggest that instabilities in miscible frontal displacement may be similar to those in ultralow

tension immiscible frontal displacement, with the added caveat that in the miscible process the tension decreases continuously in time."

More recently, it has been suggested by Barkey and Laporte [1990] that morphological instabilities observed in electrochemical deposition could have their origins in an effective surface tension between depleted and rich solutions in a mass-transfer boundary layer whose thickness is observed to be on the scale of a few tens of microns. In another recent study, Garik, Hetrick, Orr, Barkey and Ben-Jacob [1991] "...reported on the stability of the interface between two immiscible fluids of closely matching viscosities when one is driven into the other. For the case where the fluids differ only in solution concentration, we find that spontaneous cellular convective mixing can develop. We suggest that this interfacial patterning is a surface tension effect distinct from viscous fingering; the latter can occur simultaneously. ...On the basis of the above experimental results, we hypothesize that the global morphology of depositional growth, i.e., the number of branches, the stability of the branch tips, and the way it fills space (its 'dimension') is determined by the hydrodynamic stability of the interface between the depleted fluid near the growth and the bulk fluid *provided* the gradient is *sufficiently sharp* to provide an effective liquid-liquid interface. Since leading edges grow fastest, hydrodynamic modulation of the liquid-liquid interface à la Hele-Shaw would determine branch position, just as cellular mixing will. In electrodeposition the existence of a sharp gradient sustained by the growing deposit is experimentally supported."

May and Maher [1991] have extracted an effective *surface tension* between isobutylene acid and water at near-critical composition (62.1 volume % water) for change of phase from a miscible to immiscible liquid mixture. This binary liquid mixture has an upper critical temperature, $T_c = 26.31°C$, below which its two equilibrium phases act as immiscible liquids with an interfacial tension $\sigma = \sigma_0[(T_c - T)/T_c]^{1.23}$. If this system is initially at two-phase equilibrium and then has its temperature abruptly raised above T_c but is not mechanically disturbed, the interface will remain visible for many hours as diffusion can only mix the two phases slowly. May and Maher [1991] measured the autocorrelation function for light scattered from capillary waves at the interface of a two-phase equilibrium and after abruptly raising the temperature to drive the system toward one-phase equilibrium. They used a capillary wave dispersion relation to determine a decaying transient 'surface tension' with a maximum value near 0.01 dyne/cm. They note that "....This surface tension represents a dynamical integrity of the nonequilibrium interface which may affect pattern formation when the interface is driven."

X.4 Mixtures of Incompressible Miscible Liquids and Korteweg's Theory

It can be argued that the measurement of interfacial tension between miscible liquids is not a viable proposition since there is no such thing as an equilibrium interfacial tension between miscible liquids. The concepts of dynamic and instantaneous interfacial tensions, denoted by $S^*(t)$ and $S^*(0)$ respectively, are certainly more useful but they are not fundamental. What is fundamental is the study of the way in which differences of density, composition, and temperature enter into the stress tensor in a fluid mixture. The parameters we shall need to measure are ultimately to be defined by a theory giving the precise nature of general forces that give rise to capillary-like phenomena in particular situations. Korteweg's theory, discussed below, is perhaps an example of how such a theory might look. The expression (3.3) is too special to be useful in a fundamental study of an acceptable constitutive law for the layer of transition between the two fluids. Rather, we would seek a general expression involving gradients of ϕ, subject to invariance requirements (such as invariance under rotation).

X.4(a) Compressible fluids

Korteweg was motivated on the one hand by the work of Van der Waals [1895] who, in his work on fluids that have large variations of density,

" ... has shown theoretically that it is very probable that the discontinuity at the surface of a liquid and its vapor is only apparent and that there is a layer of transition, very thin to be sure, but of a thickness much larger under ordinary conditions than the radius of the sphere of action of the molecules, and which can even grow indefinitely as one approaches the critical temperature."

This comment was made in the context of the study of a fluid which consists of a liquid and its vapor, coexisting for a certain range of the temperature, and then at a critical temperature, the fluid becomes just one phase. For this problem of a liquid and its vapor, Korteweg proposed a continuum approach with a compressible fluid model with a stress $\mathbf{T}^{(1)}$ of the usual Navier-Stokes type plus a part $\mathbf{T}^{(2)}$ depending on density derivatives alone:

$$T_{ij}^{(1)} = -p\delta_{ij} + \mu\left(\frac{\partial u_i}{\partial x_j} + \frac{\partial u_j}{\partial x_i}\right) + \lambda\frac{\partial u_l}{\partial x_l}\delta_{ij} \tag{4a.1}$$

and

$$T_{ij}^{(2)} = \left(\gamma\nabla^2\rho - \alpha\nabla\rho\cdot\nabla\rho\right)\delta_{ij} - \beta\frac{\partial\rho}{\partial x_i}\frac{\partial\rho}{\partial x_j} + \delta\frac{\partial^2\rho}{\partial x_i\partial x_j} \tag{4a.2}$$

where p and the coefficients α, β, δ, γ, μ and λ are functions of the density ρ and temperature θ. Truesdell and Noll [1965] discuss this theory in section 124 of their book; we repeat some of it here and refer to them for intermediate steps.

Korteweg showed how his theory reduced to the classical theory of capillarity, in which the jump conditions at the interface between two fluids of different densities are prescribed. As an illustration, this was done for a spherical mass of fluid in equilibrium with purely radial variation of density: $\rho = \rho(r)$, where r is the distance from a fixed center. Using spherical coordinates, (4a.1) - (4a.2) yield zero shear stresses and the following normal stresses:

$$T^{<rr>} = -p - (\alpha + \beta)\rho'^2 + \gamma(\rho'' + \frac{2}{r}\rho') + \delta\rho'', \tag{4a.3}$$

$$T^{<\theta\theta>} = T^{<\phi\phi>} = -p - \alpha\rho'^2 + \gamma(\rho'' + \frac{2}{r}\rho') + \delta\frac{\rho'}{r}, \tag{4a.4}$$

where $\rho' = d\rho/dr$, $T^{<rr>} = \mathbf{e_r}.\mathbf{T}.\mathbf{e_r}$, and the stress tensor $\mathbf{T}$ is as in section I.2 (cf. equations (124.4) - (124.7) of the article by Truesdell and Noll [1965]).

Let $b(r)$ denote the radial component of the external body force. The equations of equilibrium are that the components $b^{<\theta>}$ and $b^{<\phi>}$ are zero, and the radial component of the momentum equation is

$$\frac{\partial T^{<rr>}}{\partial r} + \frac{2}{r}(T^{<rr>} - T^{<\theta\theta>}) + \rho b(r) = 0. \tag{4a.5}$$

We assume that in the region $r_1 < r < r_2$, the fluid has a layer of transition where the density varies by a lot, and that for $r < r_1$ or $r > r_2$, the density is approximately constant. Then the use of $T^{<rr>}$ and $T^{<\theta\theta>}$ in the equations of equilibrium yields the jump in $T^{<rr>}$ between the layer at $r = r_1$ and $r = r_2$:

$$T^{<rr>}\Big|_{r_1}^{r_2} = -\int_{r_1}^{r_2} \rho b(r)dr - \frac{2\delta\rho'}{r}\Big|_{r_1}^{r_2} + 2\int_{r_1}^{r_2} \frac{\beta + \frac{d\delta}{d\rho}}{r}\rho'^2 dr. \tag{4a.6}$$

We assume that $\rho' = d\rho/dr$ is approximately zero at $r = r_1$ and $r = r_2$, which are sufficiently away from the region where ρ varies rapidly, so that the second term on the right hand side vanishes. We then let $r_1 \to r_0$ and $r_2 \to r_0$ and obtain a result for a thin layer of transition. The first term on the right hand side then vanishes and if

$$(\beta + \frac{d\delta}{d\rho})\rho'^2 \to S^*\delta(r - r_0), \tag{4a.7}$$

where $\delta(r - r_0)$ is Dirac's delta function, then the last term reduces to $2S^*/r_0$ where S^* is the surface tension. Thus, the classical jump condition for the normal stress at an interface between two fluids of different densities

is retrieved. Whether the requirement (4a.7) is actually satisfied or not would have to be checked out from the equations governing the problem. For instance, this theory could not apply to the surface tension that is there between density-matched immiscible liquids because ρ' is then zero and would not satisfy (4a.7): this theory was not meant for such a problem.

There are a number of interesting papers on Korteweg-type theories for compressible fluids (see, for example, Dunn [1986]). These theories rely strongly on thermodynamic arguments for compressible fluids which evidently do not apply to the incompressible fluids under discussion here.

X.4(b) Mixtures of Incompressible Fluids

On the other hand, Korteweg suggested that his theory might apply to the processes of slow diffusion of miscible incompressible liquids such as were already described in the previously cited account of the experiments of Bosscha. In such a problem, an important variable to work with is the concentration, as well as the density, so we need to mimic and adapt his ideas to this case. He wrote:

"Let us suppose...that one must deal with two liquids miscible in all proportions, or indeed, a solution with variable concentration. In this case it cannot be a question of equilibrium, correctly speaking, before the concentration has by diffusion become equal everywhere. Moreover, in considering diffusion as a very slow process, one can deal with provisional equilibrium, where equations [3] are satisfied momentarily. In such equilibria, all possible distributions of concentration, satisfying these equations, could rigorously occur, since the distribution at a given moment depends on the initial distribution and the laws of diffusion."

Provisional equilibrium of drops and bubbles means that everything is in equilibrium except for diffusion, due to gradients in concentration, which is assumed to be a slow process compared with fluid motion. This requires at least that the density of the mixture be independent of the concentration; otherwise, buoyancy will produce motion.

We next describe some experiments done under provisional equilibrium. Several bubble injection experiments like those described in figure 1.1 were done but with two fluids of matched density. A glob of one fluid is released through a capillary tube as in figure 1.1 into a second fluid. In one case, we added just enough sugar to water to match the density of glycerin. The density-matched sugar solution has a much smaller viscosity than glycerin. When injected via the capillary tube into the glycerin, the sugar solution sometimes appears to pull into a sphere; more often after a short time it splits into two segments: one rises and one falls. These two

[3] This corresponds to our equations (4a.1) - (4a.2) with $\mathbf{u} = 0$ and ρ replaced by ϕ.

segments then take a more pronounced spherical shape. Perhaps this suggests that the spherical shape is more easily obtained by a drop in motion than by capillary forces at the surface. Next, the role of the fluids was reversed. Glycerin injected into a sugar solution did pull into a sphere but maintained the thread-like tail it had in the capillary tube. Capillary-like bulges developed on the thread before it lost its identity to diffusion.

We were never completely successful in matching the density and it may be impossible to do so. The problem is that the volume of a mixture of two constituents need not be the same as the sum of the volumes of the two constituents before mixing. For example, small changes of the total volume V_T of a mixture of glycerin and water at 20°C are observed and reported by Segur [1953] in the data shown in his figure 7.4 and table 7.12. His table is displayed here as figure 4.1 and shows the volume contraction of glycerin and water. His figure 7.4 and the 6th column of table 7.12 show that the mixture equation (4b.3) below holds to within an accuracy of about 1%. He reports a maximum change of 1.1% for a mixture of 60% glycerin by weight.

Suppose that before mixing, the volume of water is given by $V_W = m_W/\rho_W$ where m_W is the mass and similarly, for glycerin, $V_G = m_G/\rho_G$. After mixing, the density of the mixture is

$$\rho = \frac{m}{V_T} = \frac{m_W + m_G}{V_T} = \rho_W \frac{V_W}{V_T} + \rho_G \frac{V_G}{V_T}. \tag{4b.1}$$

Now if we ignore the small volume change, then

$$V_T = V_W + V_G \tag{4b.2}$$

and

$$\rho = \phi\rho_W + (1 - \phi)\rho_G \tag{4b.3}$$

where $\phi = V_W/V_T$ is the volume fraction of water. Equations (4b.2) - (4b.3) define a 'simple mixture'. The fact that simple mixtures arise only as an approximation means that the mixture of liquids with the same density will not actually retain this density after mixing because the V_T changes. The density in a diffusion layer may vary from point to point, even though the density on either side of the layer is the same.

There are other measures of composition and concentration. The mass fraction say of liquid γ in liquid ν, $\hat{\phi} = m_\gamma/m$ where $m = m_\gamma + m_\nu$, is a second measure and the mole fraction $\tilde{\phi} = n_\gamma/n$, $n = n_\gamma + n_\nu$, where n_γ is the number of moles of γ, is a third measure. The relation between these three different volume measures is nonlinear. For example,

$$\hat{\phi} = \frac{m_\gamma}{m_\gamma + m_\nu} = \frac{\rho_\gamma V_\gamma}{\rho_\gamma V_\gamma + \rho_\nu V_\nu} = \frac{\rho_\gamma \phi}{\rho_\gamma \phi + \rho_\nu (1 - \phi)}$$

and

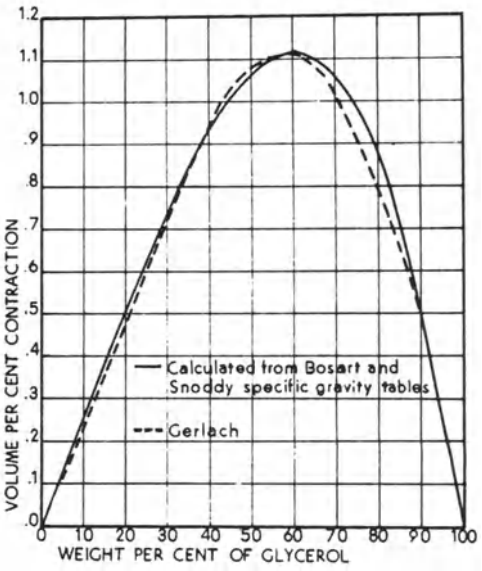

TABLE 7-12. VOLUMETRIC CONTRACTION OF GLYCEROL AND WATER WHEN MIXED AT 20°C

Calc. from sp. gr. Data of Bosart and Snoddy

Parts or % by Wt		Parts by Vol		% by Vol		Sp. Gr. 20/20°C of Soln. Bosart and Snoddy	Vol of 100 g of Soln. at 20°C	% Contraction in Vol
Glyc.	Water	Glyc.	Water	Glyc.	Water			
100	0	79.278	0.0	100.00	0	1.26362	79.278	0.000
90	10	71.350	10.018	87.69	12.31	1.23755	80.948	0.516
80	20	63.423	20.035	75.99	24.01	1.21090	82.730	0.872
75	25	59.459	25.044	70.36	29.64	1.19720	83.676	0.979
70	30	55.495	30.053	64.87	35.13	1.18355	84.641	1.059
65	35	51.531	35.062	59.51	40.49	1.16980	85.636	1.105
62	38	49.153	38.067	56.36	43.64	1.16155	86.245	1.118
60	40	47.567	40.071	54.28	45.72	1.15605	86.655	1.122
59	41	46.774	41.073	53.24	46.76	1.15325	86.865	1.118
58	42	45.981	42.074	52.22	47.78	1.15050	87.073	1.115
56	44	44.396	44.078	50.18	49.82	1.14500	87.491	1.111
54	46	42.810	46.082	48.16	51.84	1.13945	87.917	1.097
52	48	41.225	48.085	46.16	53.84	1.13395	88.344	1.082
50	50	39.639	50.089	44.18	55.82	1.12845	88.774	1.063
40	60	31.711	60.106	34.54	65.46	1.10135	90.959	0.934
30	70	23.783	70.124	25.33	74.67	1.07470	93.214	0.738
20	80	15.856	80.142	16.52	83.48	1.04880	95.516	0.502
10	90	7.929	90.160	8.08	91.92	1.02395	97.834	0.260
0	100	0.0	100.177	0.00	100.00	1.00000	100.177	0.000

Calculations: Density of water at 20°C = 0.99823.

Density of 100% glycerol at 20°C = 1.26138.

$$\text{Volume of liquid} = \text{Wt/Density} = \frac{\text{Wt} \div \text{Density of water}}{\text{Sp. gr. of liquid.}}$$

Fig. 4.1. [Segur, 1953, *Glycerol*, Reinhold Publishing Corp. Reprinted with permission of Van Nostrand-Reinhold] Volume contraction of glycerin and water.

$$\hat{\phi} = \frac{n_\gamma M_\gamma}{n_\gamma M_\gamma + n_\nu M_\nu} = \frac{M_\gamma \tilde{\phi}}{M_\gamma \tilde{\phi} + M_\nu (1 - \tilde{\phi})}$$

where M_γ and M_ν denote the masses of one mole of constituents γ and ν, respectively.

The volume fraction is the natural composition variable to introduce in the theory of simple mixtures. It defines the equation of state (4b.3) for the density of a mixture of incompressible liquids. An important consequence is that the density of such a mixture is not constant and the motion of such mixtures is not solenoidal: $\operatorname{div} \mathbf{u} \neq 0$.

X.4(c) Diffusion Equation for Mixtures of Miscible Incompressible Fluids

Now we shall derive a diffusion equation in conservation form (4c.4) by requiring that the mass per unit total volume of one of the liquids in a material volume $V(t)$ is conserved in the absence of diffusion. $\gamma = m_\gamma / V$ is the mass of γ per total volume and the mass of γ in V can change only if some γ diffuses across the boundary of V. Thus,

$$\frac{d}{dt} \int_{V(t)} \gamma dV = - \int_{\partial V} \mathbf{q}_\gamma \cdot \mathbf{n} dS \tag{4c.1}$$

where $\mathbf{q}_\gamma$ is the flux of γ.

Since $V(t)$ is a material volume, no mass crosses ∂V, in or out, and

$$\frac{d}{dt} \int_{V(t)} \rho dV = 0, \tag{4c.2}$$

where $\rho = m/V$. In the usual way, we may carry out the differentiations on the left of (4c.1) and (4c.2) using the Jacobian J of the transformation from $V(t)$ to V_0 where V_0 is independent of t and (cf. section I.2(a))

$$\frac{dJ}{dt} = J \operatorname{div} \mathbf{u} \tag{4c.3}$$

and $\mathbf{u}$ is the velocity of a material point. After writing $dV = J dV_0$, we may bring the time derivative under the integral and we have

$$\int_V \frac{d\rho}{dt} + \rho \operatorname{div} \mathbf{u} \, dV = 0$$

and

$$\int_V \frac{d\gamma}{dt} + \gamma \operatorname{div} \mathbf{u} + \operatorname{div} \mathbf{q}_\gamma \, dV = 0.$$

Thus, the integrand must vanish:

$$\frac{d\gamma}{dt} + \gamma \operatorname{div} \mathbf{u} = - \operatorname{div} \mathbf{q}_\gamma. \tag{4c.4}$$

Of course, the substantial time derivative of density $\rho(\gamma)$ given in the isothermal case by $d\rho/dt = \rho'(\gamma)d\gamma/dt$ is not zero when $d\gamma/dt = \partial\gamma/\partial t + (\mathbf{u}\cdot\nabla)\gamma \neq 0$. Hence, even when the change of ρ with temperature is suppressed,

$$\mathrm{div}\mathbf{u} = -\frac{1}{\rho}\frac{d\rho}{dt} = -\frac{1}{\rho}\rho'(\gamma)\frac{d\gamma}{dt} \neq 0. \tag{4c.5}$$

Suppose ν is the density of the other liquid per unit volume. Then because we have a simple solution, $\rho = \gamma + \nu$ and

$$\frac{d\nu}{dt} + \nu\mathrm{div}\mathbf{u} = -\mathrm{div}\mathbf{q}_\nu. \tag{4c.6}$$

The continuity equation (4c.5) may be written as

$$\frac{d\nu}{dt} + \frac{d\gamma}{dt} + (\nu+\gamma)\mathrm{div}\mathbf{u} = 0. \tag{4c.7}$$

Hence, using (4c.4-5) in (4c.7), we find that

$$\mathrm{div}(\mathbf{q}_\nu + \mathbf{q}_\gamma) = 0. \tag{4c.8}$$

The sum of the fluxes of the mass of each constituent across the boundary of any material volume V must vanish

$$\int_{\partial V} (\mathbf{q}_\nu + \mathbf{q}_\gamma)\cdot\mathbf{n}dS = 0$$

to conserve total mass. Given our interpretation of $\mathbf{q}_\gamma$ and $\mathbf{q}_\nu$ as the flux of mass relative to a varying material volume, it seems reasonable to require that at any impenetrable surface, moving or at rest,

$$\mathbf{q}_\gamma\cdot\mathbf{n} = \mathbf{q}_\nu\cdot\mathbf{n} = 0. \tag{4c.9}$$

If the volume V of a mixture of two liquids does not change on mixing, then $V = V_\gamma + V_\nu$ and the density can be expressed in terms of the volume fraction $\phi = V_\gamma/V$ of one of the constituents by the form

$$\rho(\phi) = \rho_\gamma\phi + \rho_\nu(1-\phi) \tag{4c.10}$$

where ρ_γ and ρ_ν are the densities of γ and ν, obtained from handbooks. These formulas are (4b.2-3), and mixtures satisfying these conditions are called *simple mixtures*. Since $\gamma = \rho_\gamma\phi$ and $\nu = \rho_\nu(1-\phi)$ are conserved in the absence of diffusion, it is natural to express the constitutive equation for the fluxes $\mathbf{q}_\gamma$ and $\mathbf{q}_\nu$ as a nonlinear Fick's law for each constituent in terms of the volume fraction of one of them

$$\mathbf{q}_\gamma = -D_\gamma(\phi)\nabla(\rho_\gamma\phi); \quad \mathbf{q}_\nu = -D_\nu(\phi)\nabla(\rho_\nu(1-\phi)) \tag{4c.11}$$

with different diffusion functions and assume that ρ_γ and ρ_ν are constants, as in the isothermal case. Then

$$\int_{\partial V} \mathbf{n} \cdot (\mathbf{q}_\nu + \mathbf{q}_\gamma) dS = \int_{\partial V} (D_\nu \rho_\nu - D_\gamma \rho_\gamma) \mathbf{n} \cdot \nabla \phi \, dS = 0$$

in each and every material volume V, so that either

$$div\,[(D_\nu \rho_\nu - D_\gamma \rho_\gamma) \nabla \phi] = 0$$

at each and every point in V or the ratio of diffusion functions

$$\frac{D_\nu}{D_\gamma} = \frac{\rho_\gamma}{\rho_\nu} \tag{4c.12}$$

is a constant. Equation (4c.12) also appears in conventional theories (see section 4(e)).

X.4(d) Solenoidal Fields for Simple Mixtures

We have shown in equation (4c.5) that since the density of a simple mixture of incompressible liquids changes by virtue of diffusion of the volume fraction, the velocity field cannot be solenoidal. However, we can decompose the velocity field into a solenoidal part and a non-solenoidal part, following Galdi, Joseph, Preziosi and Rionero [1991]. They eliminated $d\gamma/dt$ between (4c.4-5) and used (4b.3) to show that when $\rho_\gamma \rho_\nu / (\rho_\nu - \rho_\gamma)$ is constant (e.g., if the temperature is constant),then

$$\mathrm{div}\mathbf{W} = 0, \quad \mathbf{W} = \mathbf{u} - \frac{(\rho_\gamma - \rho_\nu)}{\rho_\gamma \rho_\nu} \mathbf{q}_\gamma. \tag{4d.1}$$

From (4c.6) we also get

$$\mathrm{div}\hat{\mathbf{W}} = 0, \quad \hat{\mathbf{W}} = \mathbf{u} - \frac{(\rho_\nu - \rho_\gamma)}{\rho_\gamma \rho_\nu} \mathbf{q}_\nu \tag{4d.2}$$

and if (4c.12) holds, then $\mathbf{W} = \hat{\mathbf{W}}$. In this case, we may introduce a stream function. For example, in plane problems, where (x, z) are the coordinates and (u, w) the velocity components, there is a function ψ which we call a stream function, such that

$$-\frac{\partial \psi}{\partial z} = \mathbf{W} \cdot \mathbf{e_x} = u - \frac{(\rho_\gamma - \rho_\nu)}{\rho_\gamma \rho_\nu} \mathbf{q}_\gamma \cdot \mathbf{e_x}, \quad \frac{\partial \psi}{\partial x} = \mathbf{W} \cdot \mathbf{e_z} = w - \frac{(\rho_\gamma - \rho_\nu)}{\rho_\gamma \rho_\nu} \mathbf{q}_\gamma \cdot \mathbf{e_z}.$$

To extract the consequences of the balance of momentum, it is desirable to frame the theory in terms of a material particle. A natural method for this is to apply balance laws to a material volume which in the continuous limit is a particle of fluid mass. The same perception is behind the use of a mass averaged velocity in mixture theories. In both cases, we defer to the statement that the laws of dynamics are framed relative to the velocity $\mathbf{u}$ of a volume of fixed mass. Hence, it is the $\mathbf{u}$ in $\mathbf{W}$ which will enter into the balance of momentum.

There is a general question about what kind of relationships between the density and composition (or temperature) would lead to a solenoidal velocity. The foregoing development may be carried out for homogeneous fluids with temperature gradients when the Boussinesq approximations are relaxed and the density ρ is related to the temperature T by the special equation

$$\rho = \rho^*(1 + \beta T)^{-1}$$

for constant ρ^* and β. Then

$$\mathbf{W} = \mathbf{u} - \beta\kappa\nabla T$$

where κ is the thermodiffusion coefficient [Pukhnachov 1991].

The relationship between the theory being developed here and mixture theories is discussed next. Mixture theories are based on an idea of interpenetrating continua in which actual material points are no longer identifiable; usually they concern solid particles suspended in a liquid and both are assumed to be present at each and every material point. An account of the ideas of mixture theory is given by Bowen [1971], with more recent developments reviewed in papers of Nunziato *et al.* [1986] and Passman *et al.* [1984]. Related ideas based on ensemble averaging can be found in Drew [1983].

For definiteness, put $\nu = g$ for glycerine and $\gamma = w$ for water (cf. figure 1.1). Evidently, glycerine and water molecules must move at different speeds; otherwise, there could be no diffusion. Mixture theories for binary mixtures usually introduce two 'average' velocities, a composite or volume-averaged velocity and a mass-averaged velocity, in addition to the velocity of each constituent. The volume-averaged velocity is solenoidal and can be identified with $\mathbf{W}$. You can generate mixture theories for binary mixtures of incompressible constituents rigorously (but not without ambiguities) by ensemble averaging, following Joseph, Lundgren, Jackson and Saville [1990]. We define an indicator function

$$H(\mathbf{x}) = \begin{cases} 0 & \text{if } \mathbf{x} \text{ is on a water molecule} \\ 1 & \text{if } \mathbf{x} \text{ is on a glycerine molecule} \end{cases}$$

and let $< >$ designate the operation of taking the average. The average is over many identical trials. We think of an experiment which is started at a certain time. At a later time, and at a certain place, we record the value of some flow variable. We repeat the experiment, wait the same time, look at the same place and record again. After many trials, we average the values by summing and dividing by the number N of trials, then we let $N \to \infty$. In this manner, we generate a function $<>(\mathbf{x}, t)$.

Now we derive some identities using ensemble averaging and the indicator function. First,

$$< H >= \epsilon(\mathbf{x}, t) = 1 - \phi(\mathbf{x}, t)$$

is the glycerin fraction and

$$< 1 - H >= 1 - < H >= \phi(\mathbf{x}, t)$$

is the water fraction. Suppose that $\mathbf{v}(\mathbf{x}, t)$ is the true velocity, the water velocity when $\mathbf{x}$ is on a water molecule, and so on. It is the actual velocity of the individual molecules and is a microscopic quantity. What appears on a macroscopic scale is an average velocity. We may define an average glycerin velocity

$$\mathbf{v_g}(\mathbf{x}, t) = \frac{< H\mathbf{v} >}{< H >} = \frac{< H\mathbf{v} >}{\epsilon} \tag{4d.3}$$

and an average water velocity

$$\mathbf{v_w}(\mathbf{x}, t) = \frac{< (1 - H)\mathbf{v} >}{< (1 - H) >} = \frac{< (1 - H)\mathbf{v} >}{\phi}. \tag{4d.4}$$

The composite velocity is

$$\mathbf{v_c}(\mathbf{x}, t) =< \mathbf{v} >=< H\mathbf{v} > + < (1 - H)\mathbf{v} >= \epsilon\mathbf{v_g} + \phi\mathbf{v_w}, \tag{4d.5}$$

and the relationship with $\mathbf{W}$ is shown in (4d.16). We may define composite averages and mass averages of any quantity f by

$$f_c =< f >= \epsilon f_g + \phi f_w$$

and

$$f_m = \frac{< \rho f >}{< \rho >} = \frac{(\rho f)_c}{\epsilon\rho_g + \phi\rho_w}$$

where ρ_g and ρ_w are the constant densities of glycerin and water, respectively. In particular, the mass-averaged velocity is

$$\mathbf{v_m} = \frac{< \rho\mathbf{v} >}{< \rho >} = \frac{\rho_g\mathbf{v_g}\epsilon + \rho_w\mathbf{v_w}\phi}{\epsilon\rho_g + \phi\rho_w}. \tag{4d.6}$$

We next note that $H(\mathbf{x}, t)$ is a material variable for materials which do not change phase, always taking the value 1 following glycerin molecules, and taking the value 0 following water molecules. That is,

$$\frac{\partial H}{\partial t} + \mathbf{v} \cdot \nabla H = 0. \tag{4d.7}$$

Using this, and div $\mathbf{v}$=0, we find

$$\begin{aligned} 0 =< \frac{\partial H}{\partial t} + \mathbf{v} \cdot \nabla H >=< \frac{\partial H}{\partial t} + \operatorname{div} H\mathbf{v} > \\ = \frac{\partial < H >}{\partial t} + \operatorname{div} < H\mathbf{v} > \\ = \frac{\partial \epsilon}{\partial t} + \operatorname{div} \epsilon\mathbf{v_g}. \end{aligned} \tag{4d.8}$$

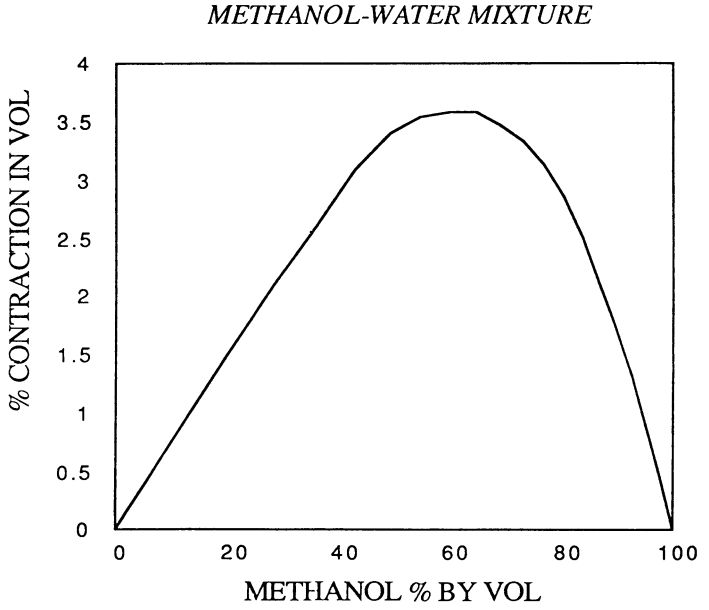

Fig. 4.2. Volume contraction of methanol and water. This figure was obtained by calculation from figure 7-8 in the book by Smith and Van Ness [1975].

In the same way, we may show that

$$\frac{\partial \phi}{\partial t} + \operatorname{div} \phi \mathbf{v_w} = 0. \tag{4d.9}$$

These are the equations of mass balance assumed by mixture theory. It follows that

$$\operatorname{div} \mathbf{v_c} = 0. \tag{4d.10}$$

The reader can prove that

$$\frac{\partial \rho}{\partial t} + \operatorname{div} (\rho_c \mathbf{v_m}) = 0. \tag{4d.11}$$

We are now in a position to draw analogies with the continuum approach (cf. Landau and Lifshitz [1959]) and the mixture theory (cf. Joseph, Lundgren, Jackson and Saville [1990]).

First we identify

$$\rho_c = \rho(\phi). \tag{4d.12}$$

This equation shows that every mixture of truly incompressible constituents is a simple mixture. Actually, incompressible liquids do not lead to simple mixtures, because of volume changes due to mixing. In glycerin-water systems, equation (4d.12) is an approximation with a maximum error of about 1% (figure 4.1). In methanol-water systems, the maximum error is 3% (figure 4.2).

Suppose that glycerin and water have been thoroughly mixed, so that the volume fractions are constants; their gradients vanish. Then there is no relative motion between glycerin and water; our mixture is a homogeneous fluid

$$\mathbf{v_g} = \mathbf{v_w} = \mathbf{v_c} = \mathbf{v_m}. \tag{4d.13}$$

In the general case, it is useful to decompose $\mathbf{v_g}$ and $\mathbf{v_w}$ into a solenoidal part $\mathbf{v_c}$ and non-solenoidal parts $\hat{\mathbf{v}}_\mathbf{g}$ and $\hat{\mathbf{v}}_\mathbf{w}$ which vanish when $\nabla\phi = 0$, and

$$\begin{aligned} \mathbf{v_g} &= \mathbf{v_c} + \hat{\mathbf{v}}_\mathbf{g}, \\ \mathbf{v_w} &= \mathbf{v_c} + \hat{\mathbf{v}}_\mathbf{w}. \end{aligned} \tag{4d.14}$$

Since $\mathbf{v_c} = \epsilon\mathbf{v_g} + \phi\mathbf{v_w}$, (4d.14) implies

$$\epsilon\hat{\mathbf{v}}_\mathbf{g} + \phi\hat{\mathbf{v}}_\mathbf{w} = 0. \tag{4d.15}$$

Noting now that both $\mathbf{W}$ and $\hat{\mathbf{W}}$ are solenoidal and using (4d.1) - (4d.2), we define

$$\mathbf{W} + \hat{\mathbf{W}} = 2\mathbf{v_c} = 2\mathbf{u} + \frac{\rho_g - \rho_w}{\rho_g\rho_w}(\mathbf{q_w} - \mathbf{q_g}). \tag{4d.16}$$

Now $\mathbf{u}$ is the mass-averaged velocity $\mathbf{v_m}$, since the material volume approach requires that we use a mass-averaged velocity (rather than the volume-averaged velocity $\mathbf{v_c}$). Thus (4d.16) may be written with $\mathbf{v_m}$ replacing $\mathbf{u}$ and using the definitions (4d.5) - (4d.6), we get

$$\epsilon\mathbf{v_g} + \phi\mathbf{v_w} = \frac{1}{\rho_c}(\epsilon\mathbf{v_g}\rho_g + \phi\mathbf{v_w}\rho_w) + \frac{\rho_g - \rho_w}{2\rho_g\rho_w}(\mathbf{q_w} - \mathbf{q_g}). \tag{4d.17}$$

Using (4d.14), we may replace $\mathbf{v_g}$ and $\mathbf{v_w}$ with $\hat{\mathbf{v}}_\mathbf{g}$ and $\hat{\mathbf{v}}_\mathbf{w}$, and after rearranging and using (4d.15), we find that

$$\frac{\rho_c - \rho_g}{\rho_c}\epsilon\hat{\mathbf{v}}_\mathbf{g} + \frac{\rho_c - \rho_w}{\rho_c}\phi\hat{\mathbf{v}}_\mathbf{w} = \frac{\rho_g - \rho_w}{2\rho_g\rho_w}(\mathbf{q_w} - \mathbf{q_g}). \tag{4d.18}$$

Noting that $\rho_c - \rho_g = (\rho_w - \rho_g)\phi$, and $\rho_c - \rho_w = (\rho_g - \rho_w)\epsilon$, we find that (4d.18) may be reduced to

$$\frac{2\rho_g\rho_w}{\rho_c}\epsilon\phi(\hat{\mathbf{v}}_\mathbf{w} - \hat{\mathbf{v}}_\mathbf{g}) = \mathbf{q_w} - \mathbf{q_g}. \tag{4d.19}$$

We use (4d.15)-(4d.19), together with the assumption for diffusion

$$\mathbf{q_w} + \mathbf{q_g} = 0, \quad \text{pointwise}, \tag{4d.20}$$

to obtain

$$\begin{aligned} \mathbf{q_w} &= \frac{\rho_g\rho_w}{\rho_c}\phi\hat{\mathbf{v}}_\mathbf{w}, \\ \mathbf{q_g} &= \frac{\rho_g\rho_w}{\rho_c}\epsilon\hat{\mathbf{v}}_\mathbf{g}. \end{aligned} \tag{4d.21}$$

Since

$$\rho_g \hat{\mathbf{v}}_\mathbf{w} = \rho_g(\mathbf{v_w} - \mathbf{v_c}) = \rho_g \mathbf{v_w} - \rho_g \phi \mathbf{v_w} - \rho_g \epsilon \mathbf{v_g}$$

$$= \rho_g \epsilon \mathbf{v_w} + \rho_w \phi \mathbf{v_w} - \rho_w \phi \mathbf{v_w} - \rho_g \epsilon \mathbf{v_g}$$

$$= \rho_c(\mathbf{v_w} - \mathbf{v_m}) = \rho_c(\mathbf{v_w} - \mathbf{u})$$

and similarly,

$$\rho_w \hat{\mathbf{v}}_\mathbf{g} = \rho_c(\mathbf{v_g} - \mathbf{u}),$$

we can express (4d.21) in terms of the mass-averaging velocity $\mathbf{u}$ and the partial densities

$$\gamma = \frac{m_w}{V} = \rho_w \phi, \qquad \nu = \frac{m_g}{V} = \rho_g \epsilon$$

as follows:

$$\mathbf{q_w} = \gamma(\mathbf{v_w} - \mathbf{u}), \qquad \mathbf{q_g} = \nu(\mathbf{v_g} - \mathbf{u}). \tag{4d.22}$$

The next step in ensemble averaging is to average the equations of motion. The usual procedure would be to write down the equations of motion for each constituent and then ensemble average. For example, Joseph, Lundgren, Jackson and Saville [1990] did ensemble averaging for solid particles in a liquid, assuming that the solid was a rigid particle and the fluid a Newtonian liquid satisfying the Navier-Stokes equations. Obviously, constitutive assumptions have been introduced. The ensemble averaging of the equations of motion then leads to many interaction terms relating to forces arising at the interface which require further modeling. This modeling is difficult and involves a lot of guesswork.

Another procedure which could be used is to guess the constitutive equation satisfied by the mass-averaged velocity. This is what is actually done using the continuum approach where it is assumed that $\mathbf{u}$ satisfies the Navier-Stokes equation. This procedure still does not close the system of equations. Further constitutive assumptions relate the fluxes to volume fractions through Fick's law and give rise to expressions for ensemble averages of the constituent velocities.

It is perhaps preferable in the case of two liquids to follow the continuum approach which is in some sense more persuasive. First of all, ensemble averages are in the best of cases a type of gedanken activity which typically is not actually carried out. In the case of two liquids, it may actually be impossible to define a boundary between the two molecules, so it is not clear when $\mathbf{x}$ is in glycerine or water. But the main reason to follow the continuum approach is perhaps a matter of belief in which the kind of persuasive modeling which leads to the Navier-Stokes equations and Fick's law is enforced. After all is said and done, it is a matter of choice, and new ideas could be tried.

X.4(e) Diffusion in Simple Mixtures

Landau and Lifshitz [1959] have considered diffusion without explicitly taking up the case of incompressible liquids. They write what might at first glance look like the usual diffusion equation (their (58.3))

$$\rho\frac{d\tilde{\phi}}{dt} = -\text{div}\mathbf{i} \tag{4e.1}$$

where

$$\tilde{\phi} = m_\gamma/m = \gamma/\rho \tag{4e.2}$$

is the mass fraction, m is the total mass and $\mathbf{i}$ is said to be the diffusion flux density, which we shall specify presently, according to our understanding.

After substituting (4e.2) into (4e.1) and using (4c.5), the left hand side of (4e.1) becomes

$$\rho\frac{d\gamma/\rho}{dt} = \frac{d\gamma}{dt} + \gamma\text{div}\,\mathbf{u}. \tag{4e.3}$$

This shows that (4e.1) is perfectly consistent with mass-conservation provided that

$$\text{div}\mathbf{i} = \text{div}\mathbf{q}_\gamma \tag{4e.4}$$

is the divergence of the flux of γ, say the flux of the solute.

Landau and Lifshitz [1959] develop a coupled thermodynamic theory for $\mathbf{i}$ and the heat flux under the condition that the concentration gradients are small (which is not the main case of interest here). When temperature and pressure gradients vanish, they find that

$$\mathbf{i} = -\alpha\text{grad}\hat{\mu} = -\alpha(\frac{\partial\hat{\mu}}{\partial\tilde{\phi}})_{p,T}\text{grad}\tilde{\phi} = -\rho D\text{grad}\tilde{\phi} \tag{4e.5}$$

where $\hat{\mu}$ is the chemical potential and D is the diffusion coefficient. For simple mixtures, $\tilde{\phi} = \gamma/\rho = \rho_\gamma\phi/\rho(\phi)$ and

$$\rho\text{grad}\tilde{\phi} = \frac{\rho_\gamma\rho_\nu}{\rho(\phi)}\text{grad}\phi. \tag{4e.6}$$

After combining (4e.3-4) with (4e.1), with ρ_γ and ρ_ν being constants, we find that

$$\frac{\partial\phi}{\partial t} + \text{div}(\phi\mathbf{u}) = \text{div}[D_\gamma(\phi)\nabla\phi] \qquad D_\gamma(\phi) = \frac{\rho_\nu D(\phi)}{\rho_\gamma\phi + \rho_\nu(1-\phi)}. \tag{4e.7}$$

Theories of diffusion in liquids lead to expressions in which D is independent of ϕ, but these expressions are not consistent with experiments (see, e.g., Segur [1953]). We have investigated what the consequences would be for mass balance and diffusion if we assume that the volumes of the incompressible constituents do not change on mixing. This assumption is expressed as (4c.10). The density of such a mixture may change by dilution

and the volume fraction is the material variable relating mass with diffusion. It follows from our theory that the velocity $\mathbf{u}$ is not solenoidal but that a linear combination $\mathbf{W}$ (or $\hat{\mathbf{W}}$) of the velocity and a species flux is solenoidal. These effects could also be obtained from equations contained in the theory of Landau and Lifshitz [1959], but these issues seem not to have been explored.

Many pairs of liquids will give rise to small volume changes upon mixing. These liquids are only approximately simple mixtures. It is probable that nearly all the interesting cases which are not already well-described by the theory of perfect incompressible mixtures could be treated as a to-be-developed perturbation of the perfect case. There are problems for which a one percent change of volume is significant. This small change, for example, will not allow a binary mixture of incompressible liquids to fill a container of fixed volume.

In many areas of applications related to mixing liquids (such as miscible displacements - cf. section X.12, binary convection, Taylor dispersion, reaction and diffusion, transport of diffusing 'passive' scalars like dyes, Marangoni convection, solidification problems) it is universally and incorrectly assumed that $\operatorname{div}\mathbf{u} = 0$. For high diffusion speeds, $\operatorname{div}\mathbf{u} = 0$ appears not to be appropriate even for short times. Presumably, the practitioners of these arts know what they are doing and recognize that they are making an approximation. In fact, though there are surely many situations in which the assumption that $\operatorname{div}\mathbf{u} = 0$ is a good one, there are others in which

$$\operatorname{div}\mathbf{u} = \frac{\rho_\gamma - \rho_\nu}{\rho_\nu \rho_\gamma}\operatorname{div}\mathbf{q}_\gamma = \frac{\rho_\nu - \rho_\gamma}{\rho_\nu}\operatorname{div}[D_\gamma(\phi)\nabla\phi] \tag{4e.8}$$

is large when $\nabla\phi$ is large, as is true when mixing liquids are placed into sudden contact. It is clear already from (4e.8) that if gradients are moderate, $\operatorname{div}\mathbf{u}$ will be small if the prefactor or the diffusion coefficient $D_\gamma(\phi)$ is small. For glycerin, ρ_ν=1.26 g/cm^3 and for water, ρ_γ=1 g/cm^3,so that the prefactor 0.26/1.26 is not negligible, but the diffusion coefficient D_γ =O(10^{-6}cm^2/sec) is. It follows then that the assumption that $\operatorname{div}\mathbf{u} = 0$ is a slow diffusion rather than a Boussinesq approximation (in which the density does not depend on temperature).

The diffusion equation (4e.7) is in a conservation form which differs from the classical equation to which it reduces when $\operatorname{div}\mathbf{u}$ =0, when the densities are matched and $D_\gamma(\phi)$ is taken as the diffusion coefficient. Another diffusion equation, based on $\mathbf{W}$ and $D(\phi)$,

$$\frac{\partial\phi}{\partial t} + (\mathbf{W}\cdot\nabla)\phi = \operatorname{div}(D\nabla\phi) \tag{4e.9}$$

follows from (4e.7) using

$$\mathbf{W} = \mathbf{u} - \zeta D_\gamma \nabla\phi \tag{4e.10}$$

and (4e.7) where $\zeta = (\rho_\nu - \rho_\gamma)/\rho_\nu$, is in a classical form. Though (4e.9) appears to be classical, it is not classical because the solenoidal velocity $\mathbf{W}$ which governs convection is not the same as the true velocity $\mathbf{u}$ of the mass particle.

X.4(f) Korteweg Stresses and the Equation of Motion

To allow for the possibility that composition gradients and density gradients can both induce stress, we may generalize Korteweg's formula (4a.2), writing

$$T_{ij}^{(2)} = \delta_1 \frac{\partial \rho}{\partial x_i}\frac{\partial \rho}{\partial x_j} + \delta_2 \frac{\partial \phi}{\partial x_i}\frac{\partial \phi}{\partial x_j} + \gamma_1 \frac{\partial^2 \rho}{\partial x_i \partial x_j} + \gamma_2 \frac{\partial^2 \phi}{\partial x_i \partial x_j} + \gamma_3\Big(\frac{\partial \rho}{\partial x_i}\frac{\partial \phi}{\partial x_j} + \frac{\partial \rho}{\partial x_j}\frac{\partial \phi}{\partial x_i}\Big). \tag{4f.1}$$

The expression (4f.1) must be invariant to a change of fluids in the binary mixture; ν for γ and $1 - \phi$ for ϕ while ρ is unchanged. This implies that (4f.1) cannot contain terms linear in derivatives of ϕ.

The notation $\mathbf{T}^{(2)}$ is used for the Korteweg stress which, together with the components described by (4f.3)-(4f.4), make up the stress tensor $\mathbf{T}$. This is an isotropic expression, invariant to a change in the sign of the axis of reference. In fact, it is the most general second order tensor composition of the first and second gradients of ρ and ϕ. We allow δ_1, δ_2, γ_1, γ_2 and γ_3 to depend on ρ, ϕ and the temperature θ, and we deal with a simple mixture (4c.10). In this case, the dependence of ρ on ϕ is displayed explicitly and the temperature-dependence is expressed through the relations $\rho_\gamma = \rho_\gamma(\theta)$ and $\rho_\nu = \rho_\nu(\theta)$. These are found in handbooks. This is an enormous simplification.

The coefficients of γ_2 and γ_3 should be invariant to a change of the fluid of reference in the binary mixture. The expression (4f.1) for the stress should not change when ρ_ν is exchanged with ρ_γ, and ϕ is exchanged with $1 - \phi$. This implies, for example, that

$$\gamma_2(\rho_\nu, \rho_\gamma, \phi) = -\gamma_2(\rho_\gamma, \rho_\nu, 1 - \phi).$$

One solution of this equation is

$$\gamma_2 = (\rho_\nu - \rho_\gamma)\gamma(\phi) \quad \text{where} \quad \gamma(\phi) = \gamma(1 - \phi).$$

It will be obvious, if it is not already, that a *pressure* which does not enter into the formula for the density must be entered as a purely mechanical variable to complete the mathematical description of our problem, so that we end up with the same number of equations as unknowns. In this case, it may be best to regard the pressure p as the mean normal stress

$$p = \frac{-1}{3}\text{trace}\mathbf{T} \tag{4f.2}$$

and to split $\mathbf{T}$ into a pressure and a deviator

$$\mathbf{T} = -p\mathbf{I} + \mathbf{T}^D \tag{4f.3}$$

where

$$T_{ij}^D = 2\mu D_{ij} - \frac{2}{3}\delta_{ij}\mu \text{div}\,\mathbf{u} + \tau_{ij} \text{ and } \underline{\tau} = \mathbf{T}^{(2)} - \frac{1}{3}\mathbf{I}\,\text{tr}\,\mathbf{T}^{(2)} \tag{4f.4}$$

are traceless: $T_{ll}^D = \tau_{ll} = 0$. In the general case $(\mathbf{u}, p, \rho, \theta, \phi)$ are unknown, and satisfy the continuity equation (4c.5), the simple mixture equation (4c.10), the diffusion equation (4e.7), the three equations of momentum

$$\rho\frac{d\mathbf{u}}{dt} = -\nabla p + \text{div}\mathbf{T}^D + \rho\mathbf{g} \tag{4f.5}$$

and an energy equation for the temperature. There are seven equations for seven unknowns. The energy equation for mixtures of incompressible miscible liquids in which the pressure is a dynamical and not a thermodynamical variable needs further study.

X.5 Motionless Solutions and Steady Solutions

Motionless solutions with $\mathbf{u}$=0 can persist only when $\text{curl}(\rho\, d\mathbf{u}/dt) = 0$. We can form an expression for this by taking the curl of (4f.5). This leads to the vorticity equations for the incompressible Korteweg equation. If, for simplicity, δ_1, δ_2, γ_1, γ_2 and γ_3 in (4f.1) are assumed to be constants, then

$$\begin{aligned}\nabla\rho \times \frac{d\mathbf{u}}{dt} + \rho\text{curl}\frac{d\mathbf{u}}{dt} - 2\text{curl div}\,(\mu\mathbf{D}[\mathbf{u}]) + \mathbf{g}\times\nabla\rho \\ + \delta_1\nabla\rho\times\nabla\left(\nabla^2\rho\right) + \delta_2\nabla\phi\times\nabla\left(\nabla^2\phi\right) \\ + \gamma_3[\nabla\rho\times\nabla(\nabla^2\phi) + \nabla\phi\times\nabla(\nabla^2\rho)] = 0.\end{aligned} \tag{5.1}$$

The constants γ_1 and γ_2 in (4f.1) which are associated with third derivatives can be absorbed by the pressure. In general motionless solutions require $\mathbf{g}\times\nabla\rho = 0$ so that $\nabla\rho$ is parallel to gravity or is zero due to density-matching.

The condition (5.1) is a necessary but not a sufficient condition for static solution. Suppose first that $d\rho/d\phi \neq 0$. Then

$$\text{div}\mathbf{u} = -\frac{1}{\rho}\frac{d\rho}{d\phi}\frac{d\phi}{dt} \tag{5.2}$$

vanishes only if ϕ is independent of t. If we imagine that density matching is possible, that $\rho(\phi) = \rho_c = \phi\rho_\gamma + (1-\phi)\rho_\nu$, with $\rho_\gamma = \rho_\nu$, then motionless solutions exist only if

$$\nabla\phi\times\nabla(\nabla^2\phi) = 0. \tag{5.3}$$

This condition holds for vertical stratification $\phi = \phi(z, t)$ and for radial stratification in spherical polar coordinates. This type of condition would be used in a Bénard problem with diffusion and no motion in a spherical geometry.

Since $\zeta D_\gamma(\phi)\nabla\phi = \nabla h(\phi)$ is a potential and $\mathbf{u} = \mathbf{W} + \nabla h(\phi)$, the mass and volume averaged velocities $\mathbf{u}$ and $\mathbf{W}$ have the same curl and a motionless solution $\mathbf{u} = 0$ does not imply a vanishing $\mathbf{W}$. In the case that $\mathbf{u} = 0$, $\mathbf{W}$ is entirely due to diffusion.

X.6 Falling Drops, Rising Bubbles and Plumes

A basic and basically unsolved problem of fluid dynamics is to determine the evolution of rising bubbles and falling drops of one miscible liquid in another. This problem is unsteady as long as diffusion operates. An important question is whether it is necessary to introduce a stress depending on gradients of concentration, temperature and density in our equations to get results which agree with experiments like those shown in the photographs of this chapter.

One method for doing such problems is to imagine that diffusion is so slow that it can be neglected. Then the problem is treated as a free interface problem, using the usual jump conditions at the interface, except that the interfacial tension is put to zero. This is the method followed by Kojima *et al.* [1984] and Pozrikidis [1990] and we discuss their comparisons with experiments later. However, if the interface were really that sharp the gradients of composition, density and temperature might be expected to induce strong capillary-like stress effects across the interface. One question is whether it is necessary to introduce such gradient stresses to explain the shape of drops, bubbles and plumes shown here and elsewhere. Another question, already framed, is how and when to take into account the effects of diffusion.

One can argue about all this using the water bubble in glycerin shown in figure 1.1 as an example. We don't know what the streamline pattern around the water bubble might be but perhaps it is like the Hadamard-Rybczynski bubble with a tail (cf. section IX.4).

As the bubble rises, its leading edge is pushed into fresh glycerin. This, together with the circulation inside the bubble which brings fresh water up to the leading edge, generates the sharpest gradients there with weaker gradients at the trailing edge. Whether or not the Korteweg terms are actually important in sustaining the spherical shape we see at the leading edge of the water bubble through the whole 48 seconds of its rise is something we would like to find out.

Kojima *et al.* [1984] presented data for falling drops of miscible liquids, see plate IX.2.2, and they carried out an analysis of the problem at vanishing Reynolds numbers. They say that:

"... Under the assumptions of zero interfacial tension and creeping flow, the theory provides a qualitative description for the initial stages of the drop evolution ... but is unable to account for the observed drop expansion during latter stages of deformation.... On the other hand, if small inertial effects are retained in the analysis, the theory predicts that a slender open fluid torus possessing an arbitrary cross-sectional geometry will expand without change of shape to first order in Reynolds number.

"Quantitative comparisons of theoretically predicted rates of expansion with experimental measurements suggest the possible existence of a small, time-dependent interfacial tension across the drop interface."

It is perhaps suggestive that the shape of miscible and immiscible vortex rings are very similar. Compare, for example, the miscible rings shown in plate IX.2.2 and figure IX.2.3 with the immiscible rings shown in figures IX.8.1 - 8.2.

The argument just given could conceivably be applied to thermal plumes; as a plume rises its leading edge pushes always into a freshly cold part of the liquid. The circulations in the plume could act to bring hot liquid to the leading edge giving rise to sharp gradients of temperature and density there. Thermals, like buoyant miscible bubbles, take on shapes which may be influenced by stresses associated with thermally induced density gradients (see figures 1.4, 6.1 and plate X.6.2).

A thermal drop was created by Kojima, Hinch and Acrivos [1984]:

" ... by using the same fluid for the drop as for the bulk medium but at a sufficiently low temperature such that the density difference was large enough for the drop to fall in the continuum under the force of gravity. Under these conditions, the effect of the interfacial tension should be negligible, since the authors are unaware of reports in the literature which suggests that a time dependent interfacial tension exists between two fluids having different temperature."

A comparison of thermal plumes and drops shows a similar structure. The plume shown in figure 6.1 has a less diffuse structure.

Thermally induced density gradients will be sharper in relatively viscous drops and plumes which are poor heat conductors and have large coefficients $d\rho/d\theta$ of thermal expansion. We do not know of any reason to reject the possible action of thermally-induced gradient stresses in some of these fluids. If there is a large temperature gradient in the system, as in the case of cold and hot liquids coming into contact, then we might model that with a Korteweg stress.

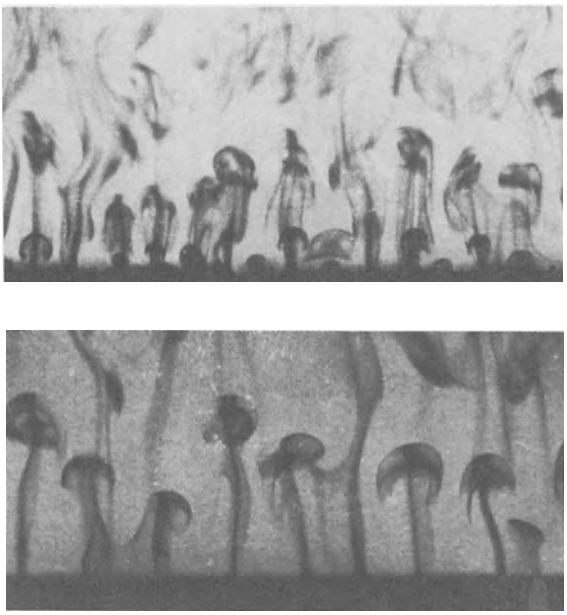

Fig. 6.1. [Sparrow, Husar and Goldstein, 1970] These are photographs of thermal plumes in water rising from a heated horizontal surface.

X.7 Isothermal Problems

The possibility that stresses are induced by gradients of concentration and density in diffusing incompressible miscible liquids, as in the theory of Korteweg [1901], can be considered. Such stresses could be important in regions of high gradients giving rise to effects which can mimic surface tension. We have already seen, in (4e.14), that it is just the same region of high gradients where the volume changes due to dilution cause the strongest departures from the classical approximation $\operatorname{div} \mathbf{u} = 0$. We are going to study the superposition of non-classical effects of volume changes such that $\operatorname{div} \mathbf{u} \neq 0$ due to diffusion and Korteweg stresses.

In the isothermal case, ρ varies with ϕ alone, and Korteweg's expression for the stress (4f.1) due to the combined effects of gradients of ϕ and $\rho(\phi)$ are

$$T_{ij}^{(2)} = \hat{\delta} \frac{\partial \phi}{\partial x_i} \frac{\partial \phi}{\partial x_j} + \hat{\gamma} \frac{\partial^2 \phi}{\partial x_i \partial x_j} \tag{7.1}$$

where

$$\hat{\delta} = \delta_1 (\frac{d\rho}{d\phi})^2 + \delta_2 + 2\gamma_3 \frac{d\rho}{d\phi} + \gamma_1 \frac{d^2\rho}{d\phi^2}$$

and

$$\hat{\gamma} = \gamma_1 \frac{d\rho}{d\phi} + \gamma_2.$$

In the case of a simple mixture (4c.10), the governing equations are

$$(\rho_\gamma - \rho_\nu)\frac{d\phi}{dt} + \rho \mathrm{div}\mathbf{u} = 0, \tag{7.2}$$

$$\frac{d\phi}{dt} + \phi \mathrm{div}\mathbf{u} = \nabla \cdot (D_\gamma \nabla \phi) \tag{7.3}$$

and (4f.5):

$$\rho \frac{d\mathbf{u}}{dt} = -\nabla p + \mathrm{div}\mathbf{T}^D + \rho \mathbf{g}, \tag{7.4}$$

where $\mathbf{T}^D$ is the stress deviator defined by (4f.4) with

$$\tau_{ij} = \hat{\delta}\frac{\partial \phi}{\partial x_i}\frac{\partial \phi}{\partial x_j} + \hat{\gamma}\frac{\partial^2 \phi}{\partial x_i \partial x_j} - \frac{1}{3}\delta_{ij}(\hat{\delta}|\nabla\phi|^2 + \hat{\gamma}\nabla^2\phi) \tag{7.5}$$

where $\hat{\delta} = (\rho_\gamma - \rho_\nu)^2\delta_1 + \delta_2 + 2\gamma_3(\rho_\gamma - \rho_\nu)$, and $\hat{\gamma} = \gamma_1(\rho_\gamma - \rho_\nu)^2 + \gamma_2$, and p is the mean normal stress.

The continuity equation (7.2) may be replaced with (4d.1):

$$\mathrm{div}\mathbf{W} = 0 \quad \text{and} \quad \mathbf{W} = \mathbf{u} - \zeta D_\gamma \nabla \phi \tag{7.6}$$

where

$$\zeta = \frac{(\rho_\nu - \rho_\gamma)}{\rho_\nu}, \tag{7.7}$$

and Fick's law (4c.11) is used. We are thinking of glycerin as ν and water as γ: then $\zeta > 0$.

Using (7.6), we may eliminate div $\mathbf{u}$ from the stress deviator (4f.4)

$$T^D_{ij} = 2\mu D_{ij} - \frac{2}{3}\delta_{ij}\zeta\mu \mathrm{div}(D_\gamma \nabla \phi) + \tau_{ij} \tag{7.8}$$

and rewrite (7.4) as

$$\rho \frac{d\mathbf{u}}{dt} = -\nabla(p + Q(\phi)) + \mathrm{div}(2\mu \mathbf{D}[\mathbf{u}] + \hat{\delta}(\nabla\phi)(\nabla\phi)^T) + \rho\mathbf{g}, \tag{7.9}$$

where

$$Q(\phi) = \frac{1}{3}\hat{\delta}|\nabla\phi|^2 + \frac{2}{3}\zeta\mu \mathrm{div}(D_\gamma \nabla\phi) - \frac{2}{3}\hat{\gamma}\nabla^2\phi. \tag{7.10}$$

In writing (7.9), we have assumed that $\hat{\gamma}$ is constant. It will simplify the calculation to also assume that $\hat{\delta}$ is a constant. Moreover, the diffusion coefficient D_γ and the classical diffusion term D given by (4e.7) satisfy the following relation:

$$D = \frac{\rho}{\rho_\nu} D_\gamma = (1 - \zeta\phi)D_\gamma. \tag{7.11}$$

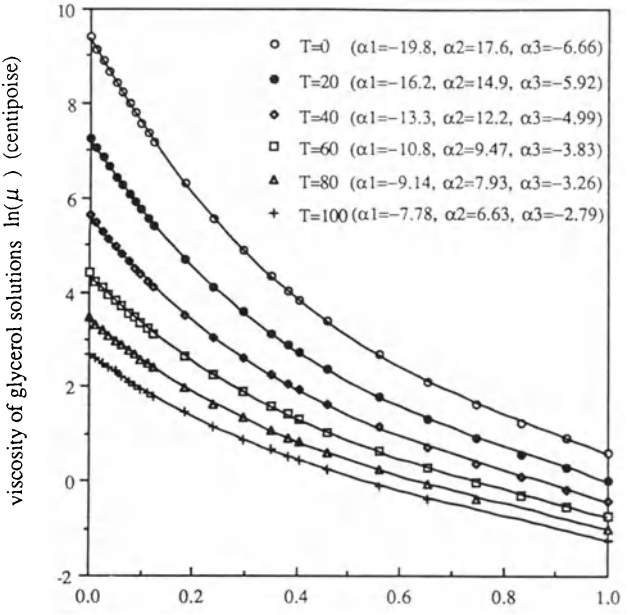

Fig. 7.1. Viscosity of glycerol solutions at temperature 0 - 100°C. The expression $\mu = \mu_G \exp(\alpha_1\phi + \alpha_2\phi^2 + \alpha_3\phi^3)$ fits the experimental data. This graph is plotted from data found in the book of Segur [1953].

We now adopt (7.3), (7.6) and (7.9) as our system of equations governing the evolution of simple mixtures of incompressible liquids. These are five equations for the components of the velocity, pressure and ϕ. In this study, we shall restrict our attention to some one-dimensional problems for which the equations decouple, but still allow for some of the basic issues to be addressed.

To keep our discussion of the basic issues concrete, we will use estimates for the material parameters for the glycerin-water system. One reference for this is the article by Segur [1953]. In figure 7.1, we have reproduced Segur's experimental data [1953] for the viscosity μ. This can be correlated well with the expression

$$\mu = \mu_G \exp(\alpha_1\phi + \alpha_2\phi^2 + \alpha_3\phi^3), \tag{7.12}$$

where the coefficients α_1, α_2 and α_3 depend on the temperature T in the way shown in the figure, and μ_G is the viscosity of pure glycerin: μ_G=14.99 poise at 20°C. The density of glycerin (G) and water (W) mixtures is given to within 1% by (4b.3) with $(\rho_\gamma, \rho_\nu) = (\rho_W, \rho_G) \sim (1, 1.26)\text{g/cm}^3$ at 20°C. Unfortunately, we do not have the global dependence of the diffusion coeffi-

cient $D_\gamma(\phi)$. Small gradient theories of diffusion are inadequate for mixing layers in which ϕ takes on all allowed values from zero to one. A representative value for $D(\phi)$, varying over the concentration ϕ, taken from Segur (p.328) is $D = 5 \times 10^{-6}\text{cm}^2/\text{s}$. We will use this representative value in our estimates.

X.8 One-Dimensional Mixing Layer Problems

We shall suppose that $\mathbf{u} = u(x,t)\mathbf{e_x}$ where x increases upward against gravity. In this case,

$$0 = \text{div}\mathbf{W} = \frac{\partial}{\partial x}(u - \zeta D_\gamma \frac{\partial \phi}{\partial x}),$$

with ζ given by (7.7). Hence,

$$u = A(t) + u_e(x,t) \tag{8.1}$$

where

$$u_e = \zeta D_\gamma \frac{\partial \phi}{\partial x} \tag{8.2}$$

is the expansion velocity which arises from mixing, and $A(t)$ is the solenoidal part of the velocity (i.e., the volume-averaged velocity). In theories in which div $\mathbf{u}$=0 is assumed, $u_e = 0$ and, of course, $u_e = 0$ when the fluids are density-matched. Using (8.1-2) we find that

$$\frac{\partial \phi}{\partial t} + A(t)\frac{\partial \phi}{\partial x} = \frac{\partial}{\partial x}\Big((1 - \zeta\phi)D_\gamma \frac{\partial \phi}{\partial x}\Big). \tag{8.3}$$

The momentum equation in one dimension is given by

$$\rho(\phi)(\frac{\partial u}{\partial t} + u\frac{\partial u}{\partial x}) = -\frac{\partial p}{\partial x} + \frac{\partial}{\partial x}\Big(\frac{4}{3}\mu\frac{\partial u}{\partial x} + \frac{2}{3}\hat{\delta}(\frac{\partial \phi}{\partial x})^2 + \frac{2}{3}\hat{\gamma}\frac{\partial^2 \phi}{\partial x^2}\Big) + \rho\mathbf{g}\cdot\mathbf{e_x} \tag{8.4}$$

where u is given in terms of $A(t)$ and ϕ by (8.1). We need p to satisfy (8.4) when, say, $u(x,t)$ and $\phi(x,t)$ are prescribed at the boundary.

The problem of diffusion is decoupled from (8.4) when $A(t) = 0$. And $A(t) = 0$ if there is a value x such that for all t, u and the diffusion flux $\partial\phi/\partial x$ are zero. This is the case at an impermeable wall across which the velocity and the flux of water must vanish. It is also true for mixing problems on unbounded domains for which u and $\partial\phi/\partial x$ vanish at $x = \pm\infty$. These problems are canonical for the development of mixing layers from initially discontinuous data which are considered below. When $A(t) = 0$,

$$u = u_e = \zeta D_\gamma \frac{\partial \phi}{\partial x} \tag{8.5}$$

and if we switch to using the classical diffusion coefficient $D(\phi)$ given by (4e.7), the diffusion equation (8.3) becomes, by (7.11),

$$\frac{\partial \phi}{\partial t} = \frac{\partial}{\partial x}(D(\phi)\frac{\partial \phi}{\partial x}). \tag{8.6}$$

In the simplest case, we assume that D is independent of ϕ: (8.6) is the classical diffusion equation. With appropriate boundary conditions (8.6) can be solved easily. Then u is given by (8.5), without any consideration from the dynamics, and the momentum equation (8.4) determines $p(x,t)$ directly. Various issues which arise in the dynamical theory of simple mixtures can be framed in terms of the one-dimensional problem as we shall see below.

X.9 Jump of the Normal Stress Across a Plane Mixing Layer

We shall now examine the problem of dynamic interfacial tension without assuming that density is constant and using the one-dimensional problem defined by (8.4-6). This is the canonical initial-value problem for mixing layers: the smoothing-out of a discontinuity in ϕ at a plane. At $t = 0$, water lies above glycerin

$$\phi = \phi_+ \quad \text{for} \quad x > 0, \quad \phi = \phi_- \quad \text{for} \quad x < 0$$

where ϕ is the water fraction. Since we are on an infinite domain,

$$\phi = \phi_+ \quad \text{for} \quad x \to \infty, \quad \phi = \phi_- \quad \text{for} \quad x \to -\infty$$

for all $t > 0$. Without loss of generality we may translate ϕ by $\Delta\phi/2$ where $\Delta\phi = \phi_+ - \phi_- > 0$ and suppose that when $t = 0$,

$$\phi = \frac{\Delta\phi}{2} \quad \text{for} \quad x > 0, \quad \phi = -\frac{\Delta\phi}{2} \quad \text{for} \quad x < 0 \tag{9.1}$$

and

$$\phi = \frac{\Delta\phi}{2} \quad \text{for} \quad x \to \infty, \quad \phi = \frac{-\Delta\phi}{2} \quad \text{for} \quad x \to -\infty \tag{9.2}$$

for all $t > 0$.

In this situation, (8.5) holds and the velocity is proportional to the volume fraction gradient $\nabla\phi$ which is infinite at $t = 0_+$ due to the step jump (9.1) in ϕ.

For simplicity, we take the diffusion coefficient D to be independent of ϕ and as an approximation for the glycerin-water mixture, D is of order 10^{-6} cm^2/sec. Then the classical diffusion equation (8.6) has a similarity solution

$$\phi = -\frac{\Delta\phi}{2} + \frac{\Delta\phi}{\sqrt{\pi}} \int_{-\infty}^{\eta} e^{-\eta^2} d\eta \tag{9.3}$$

with

$$\eta = \frac{x}{2\sqrt{Dt}}. \tag{9.4}$$

Using (9.3) we may express (8.5) as

$$u = u_e = \frac{\zeta}{2(1-\zeta\phi)}\sqrt{\frac{D}{t}}\phi'(\frac{x}{2\sqrt{Dt}}) = \frac{\zeta\Delta\phi}{2\sqrt{\pi}(1-\zeta\phi)}\sqrt{\frac{D}{t}}\exp[-(\frac{x}{2\sqrt{Dt}})^2]. \tag{9.5}$$

The variable $\phi(\eta)$ lies between $-\Delta\phi/2$ at $\eta = -\infty$ and $\Delta\phi/2$ at $\eta = \infty$. A look at the graph of (9.3) in figure 9.1 indicates that the diffusion layer can be defined from the place $-x_0$ where $\phi = -0.495\Delta\phi$ to the place x_0 where $\phi = 0.495\Delta\phi$, or by $-m < \eta < m$ with m approximately 2. The thickness of the diffusion layer is

$$\Delta x = x_0 - (-x_0) = 4m\sqrt{Dt} \tag{9.6}$$

and it tends to zero with t.

Equation (9.5) shows that the expansion velocity which enters into the dynamics can be significant at early times inside the diffusion layer. The gradient of ϕ is the machine which drives the velocity. The velocity decays as $\sqrt{D/t}$.

It is of interest to calculate the jump of the stress across the mixing layer. To find the jump in the stress, we integrate (8.4) over the diffusion layer. Outside of this layer the derivatives of ϕ vanish and

$$\int_{-x_0}^{x_0} \rho(\phi)(\frac{\partial u}{\partial t} + u\frac{\partial u}{\partial x})dx = -[\![p]\!] - g\int_{-x_0}^{x_0}\rho(\phi)dx \tag{9.7}$$

where

$$[\![p]\!] = p(x_0,t) - p(-x_0,t).$$

Equation (9.7) shows that the Korteweg stresses do not enter into the stress jump across the plane mixing layer. This is like true interfacial tension in which the curvature supports a jump in the stress. The continuity equation shows that the contribution due to inertia is always zero:

$$\int_{-x_0}^{x_0} \rho(\phi)(\frac{\partial u}{\partial t} + u\frac{\partial u}{\partial x})dx = \int_{-x_0}^{x_0}\frac{\partial \rho u}{\partial t}dx$$

$$= \zeta\rho_\nu\int_{-x_0}^{x_0}\frac{\partial}{\partial t}(D(\phi)\frac{\partial\phi}{\partial x})dx = \zeta\rho_\nu\int_{-x_0}^{x_0}\frac{\partial}{\partial x}(D(\phi)\frac{\partial\phi}{\partial t})dx = 0. \tag{9.8}$$

For the second equality above, replace u with (8.5) and D_γ with (7.11); then commute the time and x derivatives and integrate to obtain 0. (The contribution of inertia also vanishes when $D(\phi)$ depends on ϕ.) Therefore,

$$[\![p]\!] = -g\int_{-x_0}^{x_0}\rho(\phi)dx. \tag{9.9}$$

Thus, the jump in the normal stress is simply the static pressure difference across the mixing layer.

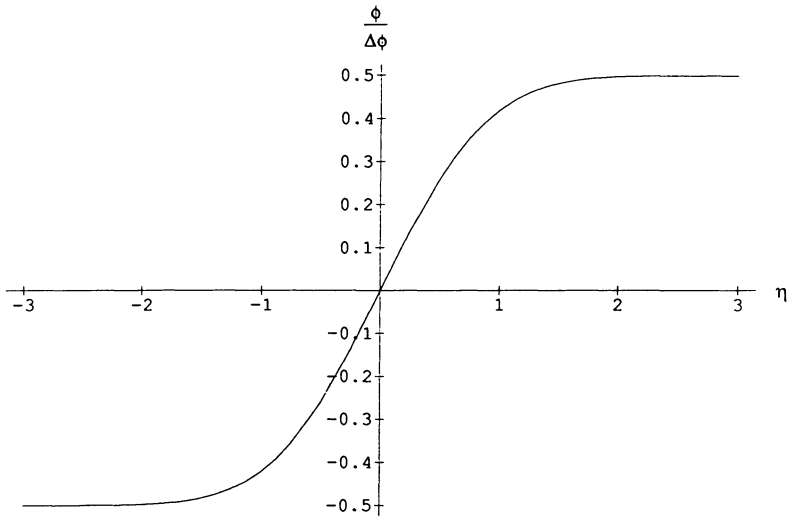

Fig. 9.1. Graph of $\frac{\phi}{\Delta\phi} = -\frac{1}{2} + \frac{1}{\sqrt{\pi}} \int_{-\infty}^{\eta} \exp(-\eta^2) d\eta$. When $\eta = 2$, $\frac{\phi}{\Delta\phi}$= 0.497661 and when η=-2, $\frac{\phi}{\Delta\phi}$ =-0.497661.

X.10 Spreading of a Spherical Diffusion Front and Korteweg Stresses

The problem of the spreading of a spherical front without gravity illustrates well how Korteweg stresses enter the normal stress balance in the case when the curvature is not zero. In fact, this kind of calculation was carried out for a vapor bubble in a liquid under equilibrium in the absence of diffusion or motion by Korteweg [1901]. A critical discussion of the Korteweg's equilibrium calculation can be found in Joseph [1990 b].

At $t = 0$, a spherical mass of radius r_0 of one liquid is inserted into an infinite reservoir of a second liquid. The two liquids are miscible in all proportions. We can imagine a sphere of glycerin in a reservoir of water. The governing equations are (7.3), (7.6) and (7.9) written for spherically symmetric solutions, for the radial component of velocity $u(r,t)$ which vanishes at $r = 0$ and $r = \infty$. Under these conditions, div $\mathbf{W}$=0 implies that

$$u(r,t) = u_e(r,t) = \zeta D_\gamma \frac{\partial \phi(r,t)}{\partial r}. \tag{10.1}$$

The diffusion equation (7.3) may then be written as

$$\frac{\partial \phi}{\partial t} = D \frac{\partial}{\partial r}\left(\frac{\partial \phi}{\partial r}\right) + \frac{2D}{r}\frac{\partial \phi}{\partial r} \tag{10.2}$$

where the water fraction $\phi(r,t) = 1$ when $r > r_0$, $t = 0$, and $\phi(r,t) = 0$ when $r < r_0, t = 0$. When the thickness of the mixing layer at $r = r_0$ is small, it is locally like a plane and the second term on the right side of (10.2) may be neglected. This reduces our problem to the one considered in section 9 centered on $r = r_0$ and it has the same self-similar solution with

$$\eta = \frac{r - r_0}{2\sqrt{Dt}}, \tag{10.3}$$

when $2\eta\sqrt{Dt} << r_0$.

The momentum equation (7.9) may be written as

$$\rho(\phi)(\frac{\partial u}{\partial t} + u\frac{\partial u}{\partial r}) = -\frac{\partial}{\partial r}[p + Q(\phi)] + 2\frac{\partial}{\partial r}(\mu\frac{\partial u}{\partial r}) + \frac{4\mu}{r}\frac{\partial u}{\partial r} - \frac{4\mu u}{r^2} + \frac{\partial}{\partial r}[\hat{\delta}(\frac{\partial \phi}{\partial r})^2] + \frac{2\hat{\delta}}{r}(\frac{\partial \phi}{\partial r})^2 \tag{10.4}$$

where $\rho(\phi)$ is given by the simple mixture formula (4c.10), and $\mu(\phi)$ by (7.12). After integrating over the mixing layer from $r_1 = r_0 - 2m\sqrt{Dt}$ to $r_2 = r_0 + 2m\sqrt{Dt}$, we find that

$$\int_{r_1}^{r_2} \rho(\phi)(\frac{\partial u}{\partial t} + u\frac{\partial u}{\partial r}) - 4\mu\frac{\partial u/r}{\partial r} - \frac{2\hat{\delta}}{r}(\frac{\partial \phi}{\partial r})^2 \, dr = [-p - Q(\phi) + 2\mu\frac{\partial u}{\partial r} + \hat{\delta}(\frac{\partial \phi}{\partial r})^2]_{r_1}^{r_2}. \tag{10.5}$$

Outside the mixing layer $(r_1(t), r_2(t))$, ϕ is essentially constant and u is essentially zero. The contribution due to the inertia on the left hand side of (10.5) is again found to be zero, as in the case of the plane layer. After writing

$$\int_{r_1}^{r_2} \mu\frac{\partial u/r}{\partial r} dr = [\mu\frac{u}{r}]_{r_1}^{r_2} - \int_{r_1}^{r_2} \mu'(\phi)\frac{u}{r}\frac{\partial \phi}{\partial r} dr \tag{10.6}$$

and setting terms outside the mixing layer equal to zero, we get

$$\int_{r_1}^{r_2} \Big(4\mu'(\phi)\frac{u}{r}\frac{\partial \phi}{\partial r} - \frac{2\hat{\delta}}{r}(\frac{\partial \phi}{\partial r})^2\Big) dr = -[\![p]\!]_{r_1}^{r_2}. \tag{10.7}$$

Now we evaluate (10.7) at very early times, when the mixing layer is very thin, with $r_2 - r_1 = 4m\sqrt{Dt}$ and $r \approx r_0$. Using the same approximations with $r \approx r_0$ in the two terms of the integral of (10.7), we find that

$$\frac{2}{r_0}\int_{r_1}^{r_2} \Big(2\mu'(\phi)u\frac{\partial \phi}{\partial r} - \hat{\delta}(\frac{\partial \phi}{\partial r})^2\Big) dr = \frac{2}{r_0}\int_{r_1}^{r_2} (\frac{2\mu'(\phi)\zeta D}{1 - \zeta\phi} - \hat{\delta})(\frac{\partial \phi}{\partial r})^2 dr$$

$$= \frac{1}{r_0}\sqrt{D/t}\int_{-m}^{m} (\frac{2\mu'(\phi)\zeta}{1 - \zeta\phi} - \frac{\hat{\delta}}{D})\phi'^2 d\eta. \tag{10.8}$$

Finally,

$$p(r_1,t) - p(r_2,t) = \frac{2T(t)}{r_0}$$

where the "transient surface tension" is given by

$$T(t) = \sqrt{D/t}\int_{-m}^{m} (\frac{\mu'(\phi)\zeta}{1-\zeta\phi} - 0.5\frac{\hat{\delta}}{D})\phi'^2 d\eta. \tag{10.9}$$

Here, $\mu' < 0$ because the solution gets more watery when ϕ is increased. For glycerin and water solutions at 20°C, we may evaluate (10.9) using values for μ' and ζ close to (7.12) as

$$T(t) = \sqrt{D/t}(164.5\frac{-\hat{\delta}}{D} - 428.7) \tag{10.10}$$

with D about $7.5\times10^{-6}\text{cm}^2/\text{sec}$, but we do not have any knowledge about the value of the Korteweg stress coefficient $\hat{\delta}$. There are two terms in the expression for the dynamic interfacial tension; one term arises from the Korteweg stress and it gives rise to a stress opposing the internal pressure as in the case of equilibrium pressure if the Korteweg coefficient $\hat{\delta}$ has a negative sign. A second term arises from the expansion velocity and is proportional to the rate of change of viscosity with volume fraction. This term has the wrong sign for interfacial tension in the case of glycerin and water solutions but has the right sign when the lighter fluid is the more viscous.

In general, $D(\phi)$ is not a constant and the error function solution (9.3) is not valid. However, even in this case, (8.6) admits a similarity solution with

$$\phi = f(\eta), \qquad \eta = \frac{x}{2\sqrt{D_0 t}}, \tag{10.11}$$

where D_0 is a representative value of $D(\phi)$ and

$$\frac{d}{d\eta}(\frac{D(f)}{D_0}\frac{df}{d\eta}) + 2\eta\frac{df}{d\eta} = 0 \tag{10.12}$$

where

$$f = \frac{\Delta\phi}{2} \text{ for } \eta = 0_+ \text{ and } f = -\frac{\Delta\phi}{2} \text{ for } \eta = 0_-$$

and

$$f = \frac{\Delta\phi}{2} \text{ as } \eta \to \infty \text{ and } f = -\frac{\Delta\phi}{2} \text{ as } \eta \to \infty.$$

Following now the derivation leading to (10.9), we find again with

$$T(t) = \sqrt{D_0/t}\int_{-\eta_1}^{\eta_2} (\frac{\mu'(\phi)\zeta}{1-\zeta\phi}\frac{D(\phi)}{D_0} - 0.5\frac{\hat{\delta}}{D_0})\phi'^2 d\eta, \tag{10.13}$$

where η_1 and η_2 mark the effective end of the diffusion layer replacing m in (10.9). In general $\phi(\eta)$ will not be antisymmetric if $D(\phi)$ is not an even function.

The computation of an effective interfacial tension given by (10.13) allows one to introduce interfacial tension into problems of slow diffusion like the drop and bubble problems discussed in section X.6. In these problems, we imagine that diffusion is confined to narrow layers outside of which $\nabla\phi$=0 and $\mathbf{u} = \mathbf{W}$. We noted that various authors like Kojima *et al.* [1984] and Pozrikidis [1990] have considered slow diffusion problems to be classical interface problems with the additional caveat that the interfacial tension vanishes. Now we can go one step further with this approach allowing $\mathbf{W} = \mathbf{u}$ outside the diffusion as in classical interface problems with no diffusion, treating the layer as an interface with a transient interfacial tension $T(t)$ given by (10.13). A higher-order theory involving matched asymptotic expansions could be considered. Of course, such approximation would be useful only in problems which start from rest at early times before the layers have greatly spread. As a general rule when $\mathbf{W} \neq 0$, it might be a better idea to abandon the idea of an interface problem and look for shapes of drops and bubbles in the level lines of the concentration field.

X.11 The Effect of Convection on Diffusion

In sections 9 and 10, we examined problems in which the velocity and stresses are induced by gradients of the volume fraction in simple mixtures. In these problems, a large concentration gradient is the engine which drives the motion, and the motion is important only at early times. In other cases, the motion is driven externally and the distribution of ϕ is driven by a balance of diffusion and convection. In all of these cases, the assumption that div $\mathbf{u}$=0 can lead to large errors. The effect of expansion on the velocity due to mixing can be studied by elementary means for the case of steady flow, in which equations (8.1) - (8.4) reduce to

$$u = A + u_e, \tag{11.1}$$

$$u_e = \frac{\zeta D}{1 - \zeta\phi}\frac{d\phi}{dx}, \tag{11.2}$$

$$A\frac{d\phi}{dx} = D\frac{d^2\phi}{dx^2}, \tag{11.3}$$

$$\rho(\phi)u\frac{du}{dx} = -\frac{d}{dx}(p + Q(\phi)) + \frac{d}{dx}[2\mu\frac{du}{dx} + \hat{\delta}(\frac{d\phi}{dx})^2] + \rho(\phi)\mathbf{g}\cdot\mathbf{e_x}. \tag{11.4}$$

From (11.3), we find that

$$\phi = C_1 + C_2\exp(Ax/D) \tag{11.5}$$

and from (11.1) - (11.2), we get

$$u_e = \frac{\zeta C_2}{1 - \zeta\phi}A\exp(Ax/D) \tag{11.6}$$

and

$$u = A[1 + \frac{\zeta C_2}{1 - \zeta\phi}\exp(Ax/D)] \tag{11.7}$$

where C_1, C_2 and A are to be determined from the boundary conditions. The variation of effective pressure $p(x)$ is determined by C_1, C_2 and A, after substituting (11.5-7) into (11.4). If, for example, we set Dirichlet conditions by prescribing $\phi(0) = \phi_0$ and $\phi(L) = \phi_L$, then

$$\phi = \phi_0 + (\phi_L - \phi_0)\frac{\exp(Ax/D) - 1}{\exp(AL/D) - 1}. \tag{11.8}$$

The distribution of ϕ between 0 and L depends on the balance between diffusion and convection. We may define a diffusion length

$$\ell = D/A, \tag{11.9}$$

or an effective diffusion parameter (the inverse Peclet number)

$$S = \frac{D}{LA} = \frac{\text{molecular diffusion}}{\text{convective diffusion}} = \frac{\text{diffusion velocity}}{\text{convective velocity}}. \tag{11.10}$$

Then the distribution of concentration (11.8) is

$$\phi = \phi_0 + (\phi_L - \phi_0)\frac{\exp(x/SL) - 1}{\exp(1/S) - 1}, \tag{11.11}$$

and the expansion velocity in (11.6) can be evaluated

$$u_e = \frac{A\zeta(\phi_L - \phi_0)\exp(x/SL)}{\exp(1/S) - 1 - \zeta[\phi_0(\exp(1/S) - 1) + (\phi_L - \phi_0)(\exp(x/SL) - 1)]}. \tag{11.12}$$

If S is very small, then $\phi = \phi_0$ for most values of x, with a narrow mixing layer of thickness of order of ℓ near $x = L$. And the expansion velocity u_e, neglected in the case when div $\mathbf{u}$ is set equal to zero, will be important inside this layer. We may estimate that

$$u_e(0) \approx 0, \quad u_e(L) \approx \frac{A\zeta(\phi_L - \phi_0)}{1 - \zeta\phi_L} \tag{11.13}$$

when S is small. The effect of the expansion velocity is confined to the narrow mixing layer and the assumption that div $\mathbf{u}$=0 is valid outside the mixing layer. (11.13) also indicates that the expansion velocity inside the mixing layer is of the same order as the constant convection velocity A if the density ratio ζ is not too small. If S is not small, and this is a realizable possibility in many situations, then the expansion velocity will not be small, and will not be confined to a boundary layer. The velocity A can be determined in the Hele-Shaw problem to be considered in the next section. In this problem we shall imagine a vertical cell $0 \leq x \leq L$ in which the liquids are mixed, with pure water at one end and pure glycerin at the

other. We may restrict our attention to free fall with atmospheric pressure at $x = 0, L$. In this case, we could imagine that the inlet concentration ϕ_0 is prescribed but that the well-mixed condition at the outlet is too restrictive, replacing a prescribed ϕ_L with a mixed condition

$$\phi + c\frac{\partial \phi}{\partial x} = 0 \quad \text{at} \quad x = L \tag{11.14}$$

for a constant c. Formulas corresponding to (11.11) and (11.13) for this case are easily derived. We shall proceed with the Dirichlet problem, leaving more general and realistic problems like (11.14) for future work.

X.12 Miscible Displacement in a Hele-Shaw Cell

In this section, we formulate a theory for the miscible displacement in a Hele-Shaw cell. An application for this is the problem of miscible displacement in oil-bearing sand. It is well known that the equations which govern the flow of a single viscous incompressible liquid between the closely spaced parallel plates defining Hele-Shaw cell are in the form of Darcy's equations with the averaged velocity proportional to the two-dimensional gradient of the piezometric pressure. From this springs an analogy between flow in a porous medium and the more easily visualized flow in a Hele-Shaw cell. This analogy has been pursued for the case of incompressible mixing liquids under the assumption of zero expansion (div $\mathbf{u}$=0) by many authors (see Homsy [1987] for a review). It was suggested already by Davis [1988] that the kind of instability leading to fingering and tip-splitting observed in the miscible displacement experiments in a Hele-Shaw cell could be associated with an ersatz surface tension due to a sharp gradient in composition. It is perhaps of even greater interest to look for instability induced by anti-surface tension forces generated by gradients of viscosity (see (10.10)) when the effects of the expansion velocity are not neglected.

It is therefore of interest to see if a reasonable Hele-Shaw theory with expansion velocity and Korteweg stresses included can be formulated to guide the interpretation of experiments. The theory given below is presumably valid under the usual assumptions resulting from small gap, which lead to low Reynolds number viscously dominated flows in which the derivatives of the velocity normal to the walls are much larger than derivatives in the plane of the motion. Obviously, this assumption cannot hold for a small diffusion layer at early times in which the velocity and the derivatives of the volume fraction are effectively infinite. So we start our discussion of the theory with the remark that it may indeed fail at early times when fresh liquids of different composition are neighbors. After this, we shall see if the lubrication approximations which are usually made [Homsy 1987] are valid.

Consider the flow in the Hele-Shaw cell of figure 12.1. The top of the cell is connected to a reservoir of glycerin and the bottom of the cell is

flush with a reservoir of water. Both reservoirs are open to the atmosphere. The flow is falling freely under gravity in a small gap of thickness b, and there is a second macroscopic dimension L, with $b/L = \epsilon << 1$. The reader should visualize this by imagining a razor-like slit protruding into a vast reservoir of freshly stirred liquid. The equations (10.2-4) can be simplified by averaging over the thin gap in this situation.

Since $\epsilon = b/L << 1$, the diffusion equation (7.3) requires that the variation of the volume concentration ϕ across the gap be small, of order ϵ^2. Moreover, since there is no flux of water across such a wall, $\partial\phi/\partial z = 0$ there. Thus, it is reasonable to assume that ϕ is independent of z. This means that the density and viscosity are also independent of z. Let the velocity $\mathbf{u} = (u_x, u_y, u_z)$ and (x, y, z) be the coordinate system shown in figure 12.1. The physics requires that $\mathbf{u} = 0$ on the walls, and we are thinking of flow driven by gravity so that $\mathbf{u}$ depends on z. When equations (7.2-3) are averaged over the gap, they become

$$\frac{\partial \rho}{\partial t} + \frac{\partial}{\partial x}(\rho u) + \frac{\partial}{\partial y}(\rho v) = 0, \tag{12.1}$$

$$\frac{\partial \phi}{\partial t} + \frac{\partial}{\partial x}(\phi u) + \frac{\partial}{\partial y}(\phi v) = \frac{\partial}{\partial x}\left(\frac{D}{1-\zeta\phi}\frac{\partial \phi}{\partial x}\right) + \frac{\partial}{\partial y}\left(\frac{D}{1-\zeta\phi}\frac{\partial \phi}{\partial y}\right), \tag{12.2}$$

where u and v are simple averages of the velocities u_x and u_y over the gap. In the momentum equation (7.9), if the Reynolds number based on the gap size is small, we can neglect the inertial terms on the left hand side of the equation. Obviously, this latter idea is erroneous at early times. A lubrication analysis yields that the pressure p is independent of z and

$$-\frac{\partial p}{\partial x} + \rho g + \frac{\partial}{\partial z}\left(\mu \frac{\partial u_x}{\partial z}\right) + \hat{\delta}\left[\frac{\partial}{\partial x}\left(\frac{\partial \phi}{\partial x}\right)^2 + \frac{\partial}{\partial y}\left(\frac{\partial \phi}{\partial x}\frac{\partial \phi}{\partial y}\right)\right] - \frac{\partial Q(\phi)}{\partial x} = 0, \tag{12.3}$$

$$-\frac{\partial p}{\partial y} + \frac{\partial}{\partial z}\left(\mu \frac{\partial u_y}{\partial z}\right) + \hat{\delta}\left[\frac{\partial}{\partial y}\left(\frac{\partial \phi}{\partial y}\right)^2 + \frac{\partial}{\partial x}\left(\frac{\partial \phi}{\partial x}\frac{\partial \phi}{\partial y}\right)\right] - \frac{\partial Q(\phi)}{\partial y} = 0. \tag{12.4}$$

These equations can be integrated twice with respect to z, leading directly to the expressions for u_x and u_y. Then the averaged velocities u and v can be obtained easily as

$$u = \frac{b^2}{12\mu}\left(-\frac{\partial p}{\partial x} + \rho g + \hat{\delta}\left[\frac{\partial}{\partial x}\left(\frac{\partial \phi}{\partial x}\right)^2 + \frac{\partial}{\partial y}\left(\frac{\partial \phi}{\partial x}\frac{\partial \phi}{\partial y}\right)\right] - \frac{\partial Q(\phi)}{\partial x}\right), \tag{12.5}$$

$$v = \frac{b^2}{12\mu}\left(-\frac{\partial p}{\partial y} + \hat{\delta}\left[\frac{\partial}{\partial y}\left(\frac{\partial \phi}{\partial y}\right)^2 + \frac{\partial}{\partial x}\left(\frac{\partial \phi}{\partial x}\frac{\partial \phi}{\partial y}\right)\right] - \frac{\partial Q(\phi)}{\partial y}\right). \tag{12.6}$$

Now we further assume that the flow is unidirectional with $v = 0$. We have (11.1) - (11.2), and

$$\frac{\partial \phi}{\partial t} + A(t)\frac{\partial \phi}{\partial x} = D\frac{\partial^2 \phi}{\partial x^2}, \tag{12.7}$$

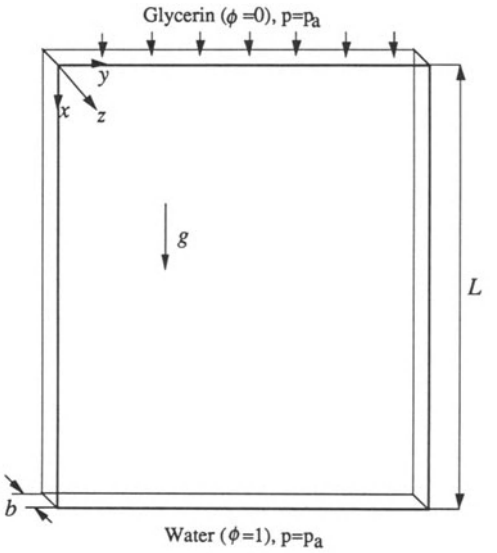

Fig. 12.1. [Hu and Joseph, 1992, Miscible displacement in a Hele-Shaw cell, ZAMP, to appear, Birkhauser-Verlag] Geometry of a Hele-Shaw cell. The top of the cell is connected to a reservoir of fluid 1 (glycerin) and the bottom of the cell is flush with a reservoir of fluid 2 (water).

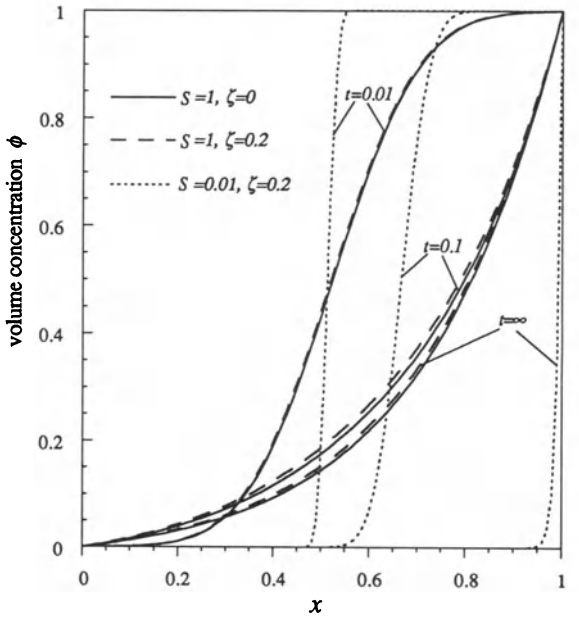

Fig. 12.2. [Hu and Joseph, 1992, Miscible displacement in a Hele-Shaw cell, ZAMP, to appear, Birkhauser-Verlag] Distribution of volume concentration ϕ at different times for three cases. (1) Solid lines, $S = 1, \zeta = 0$. (2) Long dashed lines, $S = 1, \zeta = 0.2$. (3) Short dashed lines, $S = 0.01, \zeta = 0.2$.

which is the same as the exact equations (8.1)-(8.3) for one-dimensional flow, and

$$\frac{\partial p}{\partial x} = \rho g - \frac{12\mu}{b^2}u + \hat{\delta}\frac{\partial}{\partial x}(\frac{\partial \phi}{\partial x})^2 - \frac{\partial Q(\phi)}{\partial x}. \tag{12.8}$$

The last equation differs from (8.4) because the effect of inertia which is important during the initial stage of mixing has been suppressed. We confine our attention to the evolution to the steady state, after the transients which may be poorly represented in this formulation have decayed. In this situation, $\partial\phi/\partial x$ is not too large, and we may imagine that $A(t)$ is generated from free fall in which the last two terms in (12.8) and the corresponding terms in (12.5) are negligible. A further justification for adopting (12.5) as the u-equation of momentum can be constructed for cells in which b is small and fluids for which D, $\hat{\delta}$ and $\hat{\gamma}$ are small. Inclusion of the neglected terms are expected not to change the qualitative features of the analysis to follow.

Under the aforementioned approximation, we may formulate a one-dimensional miscible displacement problem for simple mixtures of incompressible liquids in a Hele-Shaw cell as an initial-value free fall problem satisfying (4c.10), (7.12) and (12.7-8). We introduce dimensionless variables (x,t,u,U,p) related to the dimensional variables (x,t,u,A,p) by scaling $(x,t,u,U,p) = (x/L, Vt/L, u/V, A/V, p/(\rho_1 gL))$. The dimensionless equations are:

$$u = U(t) + \frac{\zeta S}{1-\zeta\phi}\frac{\partial \phi}{\partial x}, \tag{12.9}$$

$$\frac{\partial \phi}{\partial t} + U(t)\frac{\partial \phi}{\partial x} = S\frac{\partial^2 \phi}{\partial x^2}, \tag{12.10}$$

$$\frac{\partial p}{\partial x} = \rho - \mu u + \frac{\partial}{\partial x}\Big(K_1(\frac{\partial \phi}{\partial x})^2 + K_2\frac{\partial^2 \phi}{\partial x^2}\Big), \tag{12.11}$$

where

$$\rho = 1 - \zeta\phi,$$
$$\mu(\phi) = \exp(\alpha_1\phi + \alpha_2\phi^2 + \alpha_3\phi^3) \tag{12.12}$$

and

$$S = \frac{D}{LV},\ V = \frac{\rho_1 g b^2}{12\mu_1},\ \hat{\delta}_1 = \frac{\hat{\delta}}{\rho_1 gL^3},\ \hat{\delta}_2 = \frac{\hat{\gamma}}{\rho_1 gL^3},\ \mathbb{D} = \frac{Sb^2}{12L^2}, \tag{12.13}$$

$$K_1(\phi) = \frac{2}{3}\Big(\hat{\delta}_1 - \mathbb{D}\frac{\zeta^2\mu(\phi)}{(1-\zeta\phi)^2}\Big),\ K_2(\phi) = \frac{2}{3}\Big(\hat{\delta}_2 - \mathbb{D}\frac{\zeta\mu(\phi)}{1-\zeta\phi}\Big).$$

S is the effective diffusion parameter (11.10), or the inverse Peclet number. After the transients have decayed, $\partial\phi/\partial x$ is not too large, and we may imagine that $U(t)$ is generated from free fall in which the K_1 and K_2 terms in (12.11) are negligible, since the thickness of the cell b/L is small and the coefficients of the fluids D, $\hat{\delta}$ and $\hat{\gamma}$ are small. Dirichlet boundary conditions for the problem of free fall are

$$\phi(0,t) = \phi_0, \quad \phi(1,t) = \phi_L, \quad p(0,t) = p(1,t) = p_a \tag{12.14}$$

where (ϕ_0, ϕ_L) =(0,1) for glycerin displacing water, and (ϕ_0, ϕ_L)=(1,0) for water displacing glycerin. The constant p_a corresponds to atmospheric pressure. We shall assume that somehow the liquids are initially arranged so that

$$\phi = \phi_0 \text{ for } x < 1/2; \quad \text{and } \phi = \phi_L \text{ for } x > 1/2. \tag{12.15}$$

This is a common assumption for the problem of miscible displacement. $U(t)$ can be determined by integrating the pressure equation (12.11) over the cell $x = (0,1)$ and applying the pressure conditions from (12.14). Thus,

$$U(t) = \Big(\int_0^1 \rho(\phi) dx - \zeta S \int_0^1 \frac{\mu(\phi)}{1-\zeta\phi} d\phi \Big) \Big/ \int_0^1 \mu(\phi) dx. \tag{12.16}$$

Therefore, the flow in a Hele-Shaw cell is governed by the unsteady nonlinear transport equation (12.10) with $U(t)$ given by (12.16). We have an x-dependent velocity given by (12.9).

In this problem, if we use the solenoidal velocity $\mathbf{W}$ to replace the mass-averaged velocity $\mathbf{u}$ in the momentum equation, we still could have the same diffusion equation (12.10). The solenoidal theory gives rise to a uniform velocity $u = U(t)$ independent of position with

$$U(t) = \int_0^1 \rho dx \Big/ \int_0^1 \mu(\phi) dx. \tag{12.17}$$

However, the term in (12.16) which is missing in (12.17) may not be negligible. Actually, in this problem, if we compare the equations of motion for $\mathbf{u}$ and $\mathbf{W}$, they are the same when inertia is neglected except that the pressure is different. This difference alters the pressure drop across the cell and changes the velocity of free fall.

The equilibrium solution ($\partial\phi/\partial t$ =0) of (12.10) is

$$\phi = \phi_0 + (\phi_L - \phi_0) \frac{\exp(Ux/S) - 1}{\exp(U/S) - 1}$$

with $U = U(\infty)$.

The equations (12.9) and (12.16) are solved numerically. Figure 12.2 shows the distribution of the volume concentration ϕ in the cell at different times for three cases. Initially, ϕ is a step function at $x = 1/2$. As time evolves, diffusion smoothes out the front and back of the step, and convection washes the step downwards. The curves for $t = \infty$ correspond to the steady equilibrium state given in (12.18) (cf. equation (11.11)). For small S, the diffusion is confined to a narrow layer. Changing the density ratio ζ only affects the $U(t)$ in (12.16) and does not greatly influence the evolution of the diffusion profile as shown in the figure.

As in (11.1)-(11.2), the velocity in (12.9) consists of a solenoidal and an expansion part. When S is not small, as in many situations, then the

expansion velocity will not be small and will not be confined to the mixing layer. When S is small, the expansion velocity is confined to the narrow mixing layer, and it is almost zero outside this layer: thus, the assumption that div $\mathbf{u}$=0 is valid outside of the mixing layer.

X.13 Stability of Steady Miscible Displacement

Studies of the stability of miscible displacement usually focus on the stability of a moving front, as in the case (12.16), but under the assumption that div $\mathbf{u} = 0$ (see Wooding [1969], Homsy [1987], Yortsos and Zeybek [1988]). Since the moving front is unsteady, the method of normal modes does not apply unless the unsteady flow is assumed to be steady. This is called the quasi-steady approximation which tacitly assumes that we are looking at disturbances of high frequency relative to time intervals over which the basic flow appears steady. It is of interest to carry out a quasi-steady analysis of the moving front in the problem of miscible displacement based on the equations used in the previous section, for a comparison. A related problem is the stability of the steady equilibrium flow which was given in section 11 for which the quasi-steady approximation is unnecessary. We shall designate this steady flow using capital letters U, $\Phi(x)$ and $P(x)$. The velocity U is given by (12.16) as $t \to \infty$, the concentration Φ is given by (12.18) and the pressure $P(x)$ is determined by directly integrating the momentum equation (12.11). Now we linearize the Hele-Shaw equations (12.1), (12.2), (12.5) and (12.6) around the basic flow.

The perturbations are defined by

$$\phi = \Phi + \hat{\phi} \tag{13.1}$$

$$p = P + \hat{p} \tag{13.2}$$

$$\mathbf{u} = u_0\mathbf{e_x} + \hat{\mathbf{u}} = (U + \frac{\zeta S\Phi'}{1-\zeta\Phi} + \hat{u})\mathbf{e_x} + \hat{v}\mathbf{e_y} \tag{13.3}$$

$$\rho = \rho_0 + \hat{\rho}, \quad \mu = \mu_0 + \hat{\mu}, \tag{13.4}$$

$$Q = Q_0 + \hat{Q} \tag{13.5}$$

where Φ, U, P and quantities with subscript 0 satisfy the unperturbed equations and those with $\hat{}$ are the perturbations.

By (4b.3), (4e.10), (7.12) and the above equation, we obtain

$$\hat{\rho} = -\zeta\hat{\phi}, \qquad \hat{\mu} = \mu_0'(\Phi)\hat{\phi}, \tag{13.6}$$

$$\mathbf{W} = U\mathbf{e_x} + \hat{\mathbf{w}} \tag{13.7}$$

$$\hat{\mathbf{w}} = \hat{\mathbf{u}} - \frac{\zeta S}{1-\zeta\Phi}\nabla\hat{\phi} - \frac{\zeta^2 S\Phi'}{(1-\zeta\Phi)^2}\hat{\phi}\mathbf{e_x}. \tag{13.8}$$

After applying the above relations, the perturbation equations are:

$$\operatorname{div} \hat{\mathbf{w}} = 0, \tag{13.9}$$

$$\frac{\partial \hat{\phi}}{\partial t} + U\frac{\partial \hat{\phi}}{\partial x} + (\mathbf{e_x} \cdot \hat{\mathbf{w}})\Phi' = S\nabla^2\hat{\phi} \tag{13.10}$$

$$\mu_0\hat{u} + \mu_0'\hat{\phi}(U + \frac{\zeta S}{1-\zeta\Phi}\Phi')$$

$$= -\frac{\partial \hat{p}}{\partial x} - \zeta\hat{\phi} + \hat{\delta}_1\Big(\frac{\partial}{\partial x}(2\Phi'\frac{\partial \hat{\phi}}{\partial x}) + \frac{\partial}{\partial y}(\Phi'\frac{\partial \hat{\phi}}{\partial y})\Big) - \frac{\partial \hat{Q}}{\partial x} \tag{13.11}$$

$$\mu_0\hat{v} = -\frac{\partial \hat{p}}{\partial y} + \hat{\delta}_1\frac{\partial}{\partial x}(\Phi'\frac{\partial \hat{\phi}}{\partial y}) - \frac{\partial \hat{Q}}{\partial y} \tag{13.12}$$

where

$$\hat{Q} = \frac{2}{3}\hat{\delta}_1\Phi'\frac{\partial \hat{\phi}}{\partial x} - \frac{2}{3}\hat{\delta}_2\nabla^2\hat{\phi} + \frac{2}{3}\mathbb{D}\zeta\mu_0\Big(\frac{\nabla^2\hat{\phi}}{1-\zeta\Phi} + \frac{2\zeta}{(1-\zeta\Phi)^2}\Phi'\frac{\partial \hat{\phi}}{\partial x}$$

$$+\frac{\zeta\hat{\phi}\Phi''}{(1-\zeta\Phi)^2} + \frac{2\zeta^2\hat{\phi}\Phi'^2}{(1-\zeta\Phi)^3}\Big) - \frac{2}{3}\mu_0'\mathbb{D}\hat{\phi}\nabla^2\log(1-\zeta\Phi). \tag{13.13}$$

After replacing $\hat{\mathbf{u}}$ with $\hat{\mathbf{w}}$, equations (13.9) - (13.12) are four equations for two components of $\hat{\mathbf{w}}$, $\hat{\phi}$ and $\hat{p}$. We may eliminate $\hat{p}$ from (13.11) - (13.12) by cross-differentiation, taking the curl of the momentum equation and after introducing a streamfunction for $\hat{\mathbf{w}}$ via

$$\hat{\mathbf{w}} \cdot \mathbf{e_x} = -\frac{\partial \hat{\psi}}{\partial y}, \quad \hat{\mathbf{w}} \cdot \mathbf{e_y} = \frac{\partial \hat{\psi}}{\partial x} \tag{13.14}$$

we get

$$U\mu_0'\frac{\partial \hat{\phi}}{\partial y} - \mu_0\frac{\partial^2\hat{\psi}}{\partial y^2} - \frac{\partial}{\partial x}(\mu_0\frac{\partial \hat{\psi}}{\partial x}) = -\zeta\frac{\partial \hat{\phi}}{\partial y}$$

$$+\hat{\delta}_1\Big(2\frac{\partial^2}{\partial x\partial y}(\Phi'\frac{\partial \hat{\phi}}{\partial x}) + (\frac{\partial^2}{\partial y^2} - \frac{\partial^2}{\partial x^2})(\Phi'\frac{\partial \hat{\phi}}{\partial y})\Big). \tag{13.15}$$

Equations (13.10) and (13.15) are two equations for $\hat{\psi}$ and $\hat{\phi}$. We are going to solve these equations for prescribed values of ϕ at $x = 0$ and $x = 1$ which means that

$$\hat{\phi} = 0 \quad \text{at} \quad x = 0, 1. \tag{13.16}$$

Other, more general conditions like (11.14) could be treated by the same type of analysis. Two more boundary conditions arise from the condition that the pressure is prescribed at the top and bottom so that

$$\hat{p} = 0 \quad \text{at } x = 0, 1. \tag{13.17}$$

We are now ready to form the spectral problem for the stability of miscible displacement in a Hele-Shaw cell, using normal modes

$$[\hat{p}, \hat{\phi}, \hat{\psi}](x, y, t) = [p(x), \phi(x), \psi(x)]\exp(i\alpha y + ct). \tag{13.18}$$

The stability equations become

$$c\phi + U\phi' + u\Phi' = S(\phi'' - \alpha^2\phi) \tag{13.19}$$

$$U\mu_0'\phi + \mu_0 u - \frac{\mu_0 u'' + \mu_0'\Phi' u'}{\alpha^2} = -\zeta\phi$$

$$+\hat{\delta}_1\Big(2(\phi'\Phi')' - (\frac{\partial^2}{\partial x^2} + \alpha^2)(\phi\Phi')\Big) \tag{13.20}$$

where $u = -i\alpha\psi(x)$. The boundary conditions are:

$$\phi = 0 \tag{13.21}$$

and

$$\frac{\mu_0 u'}{\alpha^2} = \frac{1}{3}\hat{\delta}\Phi'\phi' + \frac{2}{3}\hat{\gamma}\phi'' - \frac{2}{3}\zeta\mathbb{D}\mu_0\Big(\frac{\phi''}{1-\zeta\Phi} + \frac{2\zeta\phi'\Phi'}{(1-\zeta\Phi)^2}\Big) \tag{13.22}$$

at $x = 0, 1$. (13.22) is the pressure condition obtained using (13.12) and (13.21).

Since the basic velocity U is a constant, it can be combined with the scaling velocity V in (12.13). This would replace V with the basic velocity $A = UV$ in the scaling, and we would have

$$c\phi + \phi' + u\Phi' = S(\phi'' - \alpha^2\phi), \tag{13.23}$$

$$\mu_0'\phi + \mu_0 u - \frac{\mu_0 u'' + \mu_0'\Phi' u'}{\alpha^2} = -G\zeta\phi$$

$$+\hat{\delta}_1\Big(\frac{d}{dx}([\phi' - \frac{\phi}{S}]\Phi') - \alpha^2\phi\Phi'\Big) \tag{13.24}$$

$$\Phi' = \frac{\phi_L - \phi_0}{S}\exp(\frac{x}{S})/\Big(\exp(\frac{1}{S}) - 1\Big), \tag{13.25}$$

where μ_0' is a derivative with respect to Φ, and ϕ', Φ' and u' are derivatives with respect to x, the boundary conditions (13.21)-(13.22) are the same with the parameters redefined as

$$S = \frac{D}{LA},\ \hat{\delta}_1 = \frac{\hat{\delta}b^2}{12A\mu_1 L^3},\ \hat{\delta}_2 = \frac{\hat{\gamma}b^2}{12A\mu_1 L^3},\ \mathbb{D} = \frac{Sb^2}{12L^2},\ G = \frac{\rho_1 g b^2}{12A\mu_1}. \tag{13.26}$$

The parameter G is the inverse of the basic dimensionless velocity $G = 1/U$ which is determined by equation (12.16) and depends solely on the distribution of ϕ. The parameters $\hat{\delta}_1$ and $\hat{\delta}_2$ are of unknown magnitude. $\mathbb{D}$ is a small parameter because D and b^2 are small; b^2 as small as we wish and D smaller than $10^{-5}\text{cm}^2/\text{sec}$.

As we have seen in this problem, the approximation of replacing $\mathbf{u}$ with the solenoidal velocity $\mathbf{W}$ results in a difference in the pressure which

alters the basic velocity of free fall. In the solenoidal theory, the stability equations would have the same form as (13.23)-(13.24) if the pressure is eliminated, but the pressure boundary condition (13.22) would be different. This difference will be small if the parameter $\mathbb{D}$ is small.

X.14 Asymptotic Analysis of Stability

The eigenvalue problem defined by (13.21)-(13.25) may be solved explicitly by expansions for long and short waves. For long waves, we write

$$\begin{aligned} \phi(x,\alpha) &= \phi_0(x) + \alpha^2\phi_1(x) + ..., \\ u(x,\alpha) &= \alpha^2 u_0(x) + \alpha^4 u_1(x) + ..., \\ c &= c_0 + \alpha^2 c_1 + ..., \text{ as } \alpha \to 0. \end{aligned} \tag{14.1}$$

These expressions are inserted into the governing equations and independent powers of α^2 are identified. At zeroth order (13.24) becomes

$$S\phi_0'' - \phi_0' - c_0\phi_0 = 0, \quad \phi_0(0) = \phi_0(1) = 0 \tag{14.2}$$

so that

$$c_0 = -(k^2\pi^2 S + \frac{1}{4S}), \quad k = \pm 1, \pm 2, ... \tag{14.3}$$

$$\phi_0 = B\exp(\frac{x}{2S})\sin(k\pi x) \tag{14.4}$$

where B is an arbitrary constant. We may find a function $u_0(x)$ which satisfies (13.21) and (13.24) at the lowest order. Hence

$$c = -(\pi^2 S + \frac{1}{4S}) + O(\alpha^2) \tag{14.5}$$

and miscible displacement is stable to long waves (however, adding in inertia leads to additional modes).

To study the stability of miscible displacement to short waves, we use the method of "frozen coefficients" [Joseph and Saut 1990; Joseph 1990a]. This method is founded on the perception that the variable coefficients of the equations are effectively constant over the short interval defining a short wave of length $2\pi/\alpha$, $\alpha \to \infty$. In this limit the highest derivatives dominate and the analysis of stability is local, at each (x, y) point, independent of boundary conditions.

To implement this method we use normal modes centered on x_0 (the interfacial region, cf. (9.6)), writing

$$[\phi(x), u(x)] = [\tilde{\phi}, \tilde{u}]\exp[i\beta(x - x_0)] \tag{14.6}$$

where $\tilde{\phi}$, $\tilde{u}$ are constants. We find that, to leading order

$$c\tilde{\phi} + \tilde{u}\Phi' = -Sk^2\tilde{\phi}, \tag{14.7}$$

$$\mu_0 k^2 \tilde{u} = -\alpha^2(G\zeta + \mu_0' + \frac{\hat{\delta}_1}{S}\Phi'')\tilde{\phi} - \alpha^2 k^2 \Phi' \hat{\delta}_1 \tilde{\phi} \tag{14.8}$$

where $k^2 = \alpha^2 + \beta^2$ and Φ', μ_0 are evaluated at x_0. Noting now that $\Phi' = \Phi/S$, we eliminate $\tilde{u}$ from (14.7) - (14.8) and find that

$$c = -Sk^2 + \frac{\hat{\delta}_1 \Phi'^2 \alpha^2}{\mu_0} + \frac{\alpha^2 \Phi'(G\zeta + \mu_0' + \frac{\hat{\delta}_1 \Phi'}{S^2})}{k^2 \mu_0} \tag{14.9}$$

where $\mu_0' = \mu'(\Phi)$ is decreasing. The diffusion term $-Sk^2$ is always stabilizing.

To bring out the main features of (14.9) we write

$$(\alpha, \beta) = k(\cos\theta, \sin\theta) \tag{14.10}$$

noting that α is a cross-stream wave number and β is a streamwise wavenumber. At the leading order,

$$c = (-S + \cos^2\theta \frac{\hat{\delta}_1 \Phi'^2}{\mu_0})k^2. \tag{14.11}$$

The second term is stabilizing when $\hat{\delta}_1 < 0$. For $\hat{\delta}_1 > 0$ and $\beta = 0$, the cross-stream disturbances will lead to instability when

$$\hat{\delta}_1 > \frac{\mu_0 S}{\Phi'^2}. \tag{14.12}$$

When (14.12) holds, miscible displacement is Hadamard unstable; ill-posed as an initial value problem with explosive instability to the shortest waves. The Korteweg coefficient $\hat{\delta}_1$ was introduced in the gradient theory to simulate surface tension: for this, we must take $\hat{\delta}_1 < 0$.

We next note that when water is displaced by glycerin, $\Phi' > 0$. The most unstable situation with $\hat{\delta}_1 \leq 0$, is when $\hat{\delta}_1 = 0$ and then

$$c = -Sk^2 + \cos^2\theta \frac{\Phi'}{\mu_0}(G\zeta + \mu_0'). \tag{14.13}$$

The only positive term is associated with gravity $G\zeta$ and it does not even operate for streamwise disturbances with $\alpha = 0$. The numerical work shows that this case is Rayleight-Taylor unstable, but not to short waves which are stabilized by diffusion.

The case of viscous fingering is associated with the problem in which water displaces glycerin for which $\Phi' < 0$. The most unstable case is for cross-stream disturbances ($\cos^2\theta = 1$). In this case, $G\zeta\Phi'$ is stabilizing. If we put $\zeta = 0$, then for fingering instability to short waves we must have $\alpha^2 \to \infty$ and

$$\frac{\mu_0'\Phi'}{\mu_0} > S\alpha^2. \tag{14.14}$$

This means that we might have instability to short waves satisfying (14.14) but the shortest waves of length $2\pi/\alpha$ with $\alpha > \sqrt{\Phi'\mu_0'/(\mu_0 S)}$ would be stable. This is a diffusion cut-off for these waves (see figure 15.7).

X.15 Growth Rates and Neutral Curves

The eigenvalue problem (13.21)- (13.24) was solved by the finite element method and checked against analytical results for long and short waves. In our computation, $(\mathbb{D}, \hat{\delta}_1, \hat{\delta}_2) = (0,0,0)$. The eigenvalues are real-valued, with zero frequency. Some representative results are shown in figures 15.1 and 15.2. Figure 15.1 shows neutral curves for glycerin displacing water. The temperature enters this problem through the normalized viscosity function $\mu(\Phi)$. The viscosity parameters $(\alpha_1, \alpha_2, \alpha_3)$ in $\mu(\Phi)$ change according to temperature as shown in figure 7.1. A strong variation of viscosity with composition (at low temperature) leads to greater instability. There is stability when diffusion is large. Therefore, within certain ranges of parameters, the miscible displacement of glycerin into water can be unstable. At higher temperatures, we find stability again. Neutral curves for a fixed temperature of 0°C and different values of G are given in figure 15.2. These show that the instability is associated with the gravity term $G\zeta$ in the stability equations: the larger the value of the driving force associated with gravity, the greater is the instability. Therefore the instability of miscible displacement of glycerin into water is basically a Rayleigh-Taylor type of instability, regularized by diffusion rather than by surface tension. The fingering of a dilute potassium permanganate solution into water shown in figure 15.3 is caused by an instability of this type.

The stabilizing effect of diffusion, of decreasing Peclet numbers $1/S$, is exhibited in figure 15.4 in a plot of the growth rate versus wave number. From the figure, it is clear that the wavelength of the most unstable disturbances decreases as the diffusion parameter S becomes smaller. When $S = 0.1$, the most unstable wave number is about 40 which gives a dimensionless wave length of 0.16. This places about six and a half waves in a length of the cell. As S becomes smaller, these waves become finer. Figure 15.5 plots the variation of the eigenfunction $\phi(x)$ and $u(x)$ across the cell, corresponding to the most unstable disturbances. The figure shows that as S decreases, the disturbances are confined within an increasingly thinner diffusion layer.

We next consider the case of water displacing glycerin. In this case, gravity is stabilizing: larger values of G give rates of decay. Diffusion is also stabilizing: larger values of S give faster rates of decay (see figure 15.6). Our numerical study suggests that water displacing glycerin is always stable. This is evident for short waves. We have found that the diffusion cut-off wave number is

$$\alpha_c = \sqrt{\frac{\mu_0' \Phi'}{\mu_0 S}} = \sqrt{|\frac{\mu_0'}{\mu_0}| \frac{1}{S^2} \exp(\frac{x}{S}) / \left(\exp(\frac{1}{S}) - 1\right)}$$

which means that the shortest waves with $\alpha > \alpha_c$ would be stable. In the above expression, μ_0'/μ_0 can not be too large: a value of 10 would give a viscosity ratio of two fluids about 2.2×10^5. The smallest α_c occurs at $x = 0$. A sample value for α_c for small $S = 0.1$ is about 0.2, which is not large enough for the short wave analysis to be valid, but supports the result that water displacing glycerin is stable. One way to think about this is that the steady equilibrium profile is not steep enough to create a fingering instability. In order to get the fingering instability, we have to do a quasi-steady analysis at an earlier time when the gradient of concentration is large, but the use of the Hele-Shaw equations at early times is problematic.

We have found that $\hat{\delta}$ must be negative to avoid Hadamard instability and ill-posedness. Miscible displacement is stable to long and short waves. Diffusion is strongly stabilizing in both cases. Within certain ranges of parameters, the miscible displacement of glycerin into water can be unstable. This instability is basically a Rayleigh-Taylor type of instability, regularized by diffusion rather than by surface tension. As the diffusion parameter S becomes smaller, the waves of disturbances become finer and are confined within an increasingly thinner diffusion layer. Water displacing glycerin is stable. This is due to the fact that the steady equilibrium profile is not steep enough to create a fingering instability.

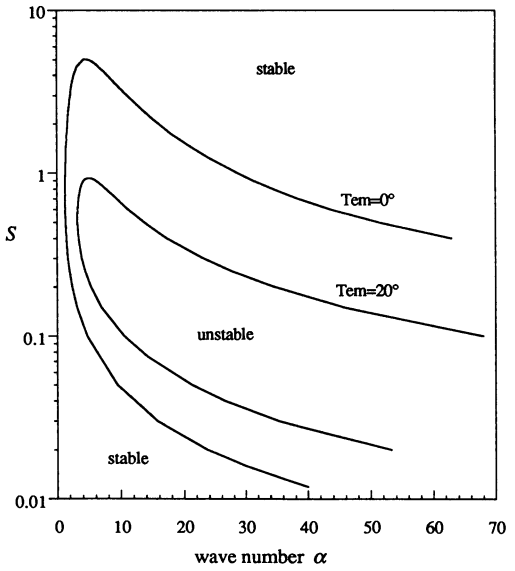

Fig. 15.1. [Hu and Joseph, 1992, Miscible displacement in a Hele-Shaw cell, ZAMP, to appear, Birkhauser-Verlag] Neutral curves for the stability of glycerin displacing water, with $G = 1$. The flow is stable for large S, when diffusion dominates. The temperature enters this problem through the function $\mu(\Phi)$ which varies more strongly with Φ at low than high temperature (see figure 7.1).

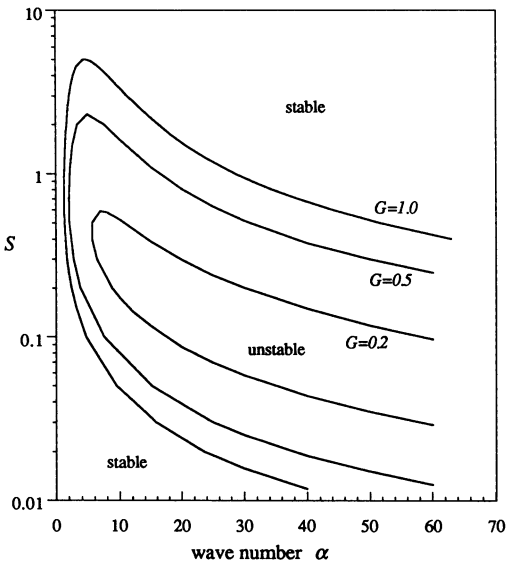

Fig. 15.2. [Hu and Joseph, 1992, Miscible displacement in a Hele-Shaw cell, ZAMP, to appear, Birkhauser-Verlag] Neutral curves for the stability of miscible displacement of heavy fluid into light. Glycerin displaces water at 0°C. The reciprocal Peclet number S is plotted against the wavenumber α for different gravity parameters G. The regions of instability grow with G.

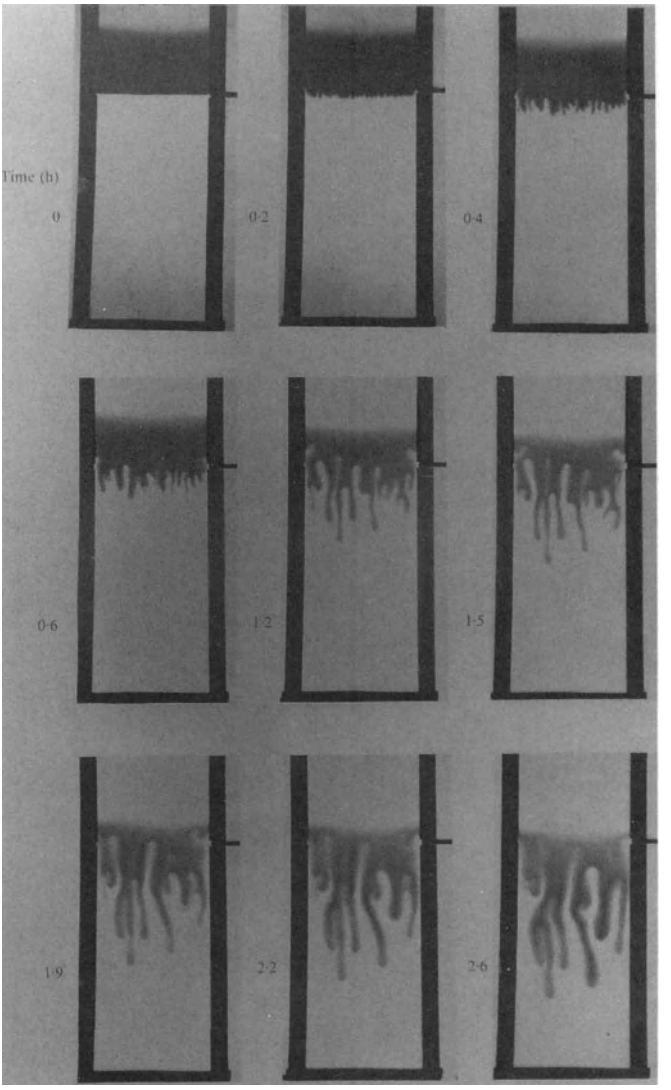

Fig. 15.3. [Wooding, 1969, Cambridge University Press] Fingering of a solution of potassium permanganate into water in a Hele-Shaw apparatus.

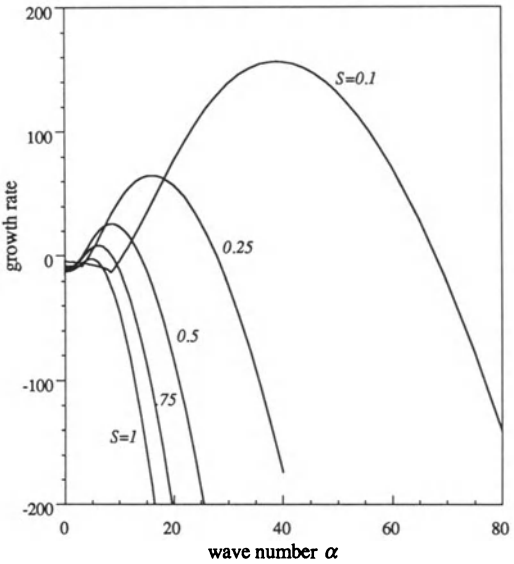

Fig. 15.4. [Hu and Joseph, 1992, Miscible displacement in a Hele-Shaw cell, ZAMP, to appear, Birkhauser-Verlag] Growth rates (Re c) for miscible displacement of heavy fluid into light (glycerin into water) at 20°C. Increasing diffusion (larger S) is stabilizing.

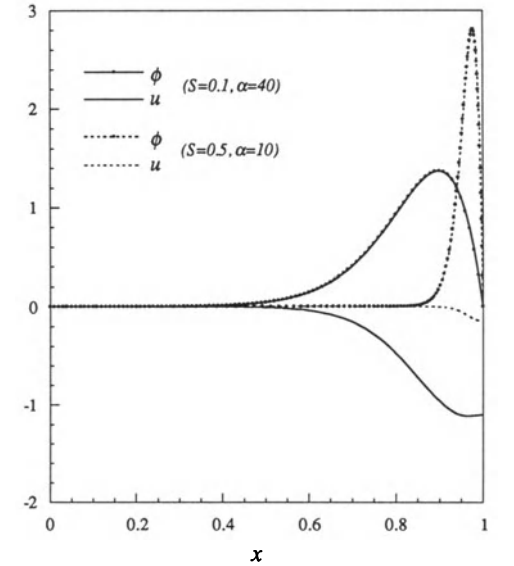

Fig. 15.5. [Hu and Joseph, 1992, Miscible displacement in a Hele-Shaw cell, ZAMP, to appear, Birkhauser-Verlag] Variation of eigenfunctions $\phi(x)$ and $u(x)$ across the cell, for miscible displacement of glycerin into water at 20°C. The solid lines are for diffusion parameter $S = 0.5$ and wavenumber $\alpha = 10$. The dashed lines are for $S = 0.1$ and α=40.

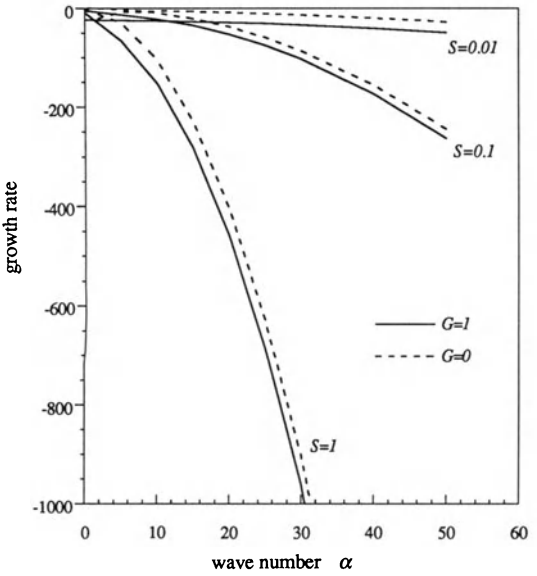

Fig. 15.6. [Hu and Joseph, 1992, Miscible displacement in a Hele-Shaw cell, ZAMP, to appear, Birkhauser-Verlag] Growth rate for water replacing glycerin with G=1 and G=0 and $\mu(\Phi)$ evaluated at 0°C. The growth rates are always negative, with faster decay for greater diffusion (larger S).

X.16 Structure of Two-Dimensional Problems

There are many problems of diffusion and mixing which can be treated in the frame of the theory of simple mixtures. Consider the problem of mixing of glycerin and water which fill a container. At the initial instant, we imagine that the bottom of the container is filled with pure glycerin and the top, up to a free surface, with pure water. As time goes on, the glycerin and water mix and eventually become a homogeneous mixture. The traditional way to treat this problem is to assume that $\mathbf{u} = 0$ and that the mixing takes place by diffusion alone. This assumption is incorrect because the density of a binary mixture changes with composition even if the two liquids are incompressible. So our mixing is not pure diffusion and a mass averaged velocity must be generated in the transient, leading to complete mixing, raising the center of mass of the mixture. To show how such problems are formulated in the frame of simple mixtures, we shall formulate this mixing problem in two dimensions, leaving the analysis for a later work.

Consider a rectangular vessel in two dimensions, closed at the bottom and on the sides but opened at the top, as in figure 16.1. We may imagine that at $t = 0$ the mixture has a known stratification in the vertical direction

$$\phi(x,y,0) = \phi_0(y) = \begin{cases} 1 & l < y \leq L \\ 0 & 0 \leq y < l \end{cases} \tag{16.1}$$

and that the solenoidal velocity vanishes

$$\mathbf{W}(x,y,0) = 0. \tag{16.2}$$

We wish to follow the evolution of mixing. The evolution may be described in terms of a streamfunction $\psi(x,y,t)$ and concentration field.

First, since div $\mathbf{W}$=0, we have a streamfunction given by

$$\mathbf{W} \cdot \mathbf{e_x} = -\frac{\partial \psi}{\partial y}, \quad \mathbf{W} \cdot \mathbf{e_y} = \frac{\partial \psi}{\partial x}. \tag{16.3}$$

The equations of motion and the boundary conditions are expressed in terms of the mass averaged velocity $\mathbf{u}$ related to $\mathbf{W}$ by

$$\mathbf{u} = \mathbf{W} + \mathbf{u_e} \tag{16.4}$$

where

$$\mathbf{u_e} = \frac{\zeta D \nabla \phi}{1 - \zeta \phi} = \nabla h(\phi) \tag{16.5}$$

and curl $\mathbf{u}$ = curl $\mathbf{W}$, div $\mathbf{u}$ = div $\mathbf{u_e}$, and

$$h(\phi) = -D \log(1 - \zeta \phi)$$

when D is a constant, independent of ϕ. The diffusion of ϕ is governed by (8.6) and the equations of motion are given by (7.9). We may eliminate $\mathbf{u}$ with $\mathbf{W}$ using (16.4). After this is done, the diffusion equation and momentum are for the coupled fields of $\mathbf{W}$ and ϕ. We may write

$$\text{div}\,(2\mu \mathbf{D}[\mathbf{u}]) = \text{div}\,(2\mu \mathbf{D}[\mathbf{w}] + 2\mu \mathbf{D}[\mathbf{u_e}])$$

$$= \text{div}\,(2\mu \mathbf{D}[\mathbf{W}]) + \mu'(\nabla \phi \cdot \nabla)\nabla h + \mu \nabla(\nabla^2 h).$$

Since

$$\text{curl div}\,(\mu \mathbf{D}[\mathbf{u_e}]) = \text{curl}\,\big(\mu'(\nabla \phi \cdot \nabla)\nabla h\big) + \mu' \nabla \phi \otimes \nabla(\nabla^2 h),$$

the part of stress associated with the expansion velocity

$$\mathbf{u_e} = \nabla h(\phi)$$

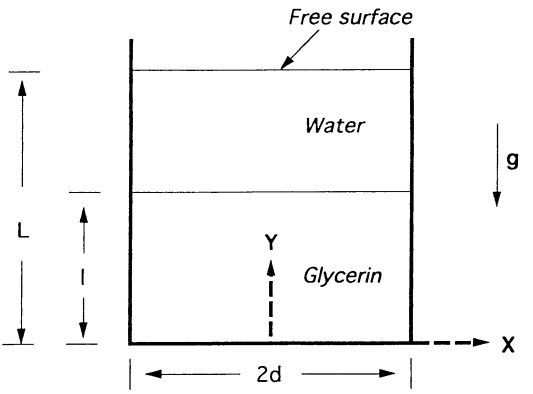

Fig. 16.1. Mixing of initially separated binary mixture of glycerin and water.

will give rise to vorticity only if $\mu' \neq 0$.

The boundary conditions for the concentration is that there is no flux of either water or glycerin across a solid boundary or a free surface. This means that

$$\mathbf{n} \cdot \nabla\phi = 0 \tag{16.6}$$

at all points of the boundary of the container in figure 16.1, even at the free surface. By using the divergence theorem, we can show that the average value of $\nabla^2\phi$ over the domain occupied by the two fluids vanishes. At a solid wall, we require that the mass-averaged velocity $\mathbf{u}$ vanish. This implies that

$$\mathbf{W} + \mathbf{u_e} = 0 \tag{16.7}$$

at solid walls, and since $\mathbf{u_e} \cdot \mathbf{n} = 0$ there,

$$\mathbf{W} \cdot \mathbf{n} = 0 \tag{16.8}$$

at a solid wall. Let $\mathbf{t}$ be any tangent vector on a solid wall. Then the tangential component of $\mathbf{W}$ is driven by the flux of ϕ:

$$\mathbf{W} \cdot \mathbf{t} = -\frac{\zeta D}{1 - \zeta\phi}\, \mathbf{t} \cdot \nabla\phi = -\mathbf{t} \cdot \nabla h(\phi) \tag{16.9}$$

at a solid wall. In our container,

$$\frac{\partial\phi}{\partial x} = \mathbf{e_x} \cdot \mathbf{W} = 0 \text{ on the side walls,} \tag{16.10}$$

$$\frac{\partial\phi}{\partial y} = \mathbf{e_y} \cdot \mathbf{W} = 0 \text{ on the bottom of the container,} \tag{16.11}$$

$$\mathbf{W}\cdot\mathbf{e_y} = -\frac{\zeta D}{1-\zeta\phi}\frac{\partial\phi}{\partial y} = -\frac{\partial h(\phi)}{\partial y} \text{ on the side wall} \tag{16.12}$$

$$\mathbf{W}\cdot\mathbf{e_x} = -\frac{\zeta D}{1-\zeta\phi}\frac{\partial\phi}{\partial x} = -\frac{\partial h(\phi)}{\partial x} \text{ on the bottom.} \tag{16.13}$$

The two components of $\mathbf{W}$ may be obtained from a streamfunction using (16.3).

The top of our container may be regarded as an ordinary free surface $F(x,y,t) = y - Y(x,t) = 0$. The kinematic equation is written

$$0 = \frac{dF}{dt} = \mathbf{W}\cdot\mathbf{e_y} + \frac{\partial h(\phi)}{\partial y} - \Big(\frac{\partial Y}{\partial t} + (\mathbf{W}\cdot\mathbf{e_x} + \frac{\partial h(\phi)}{\partial x})\frac{\partial Y}{\partial x}\Big). \tag{16.14}$$

After using (16.6), (16.14) reduces to

$$\mathbf{W}\cdot\mathbf{e_y} = \frac{\partial Y}{\partial t} + \mathbf{W}\cdot\mathbf{e_x}\frac{\partial Y}{\partial x}. \tag{16.15}$$

We next consider the stress condition at $y = Y$, supposing that the air outside is dynamically inactive. Then I.(2b.12) may be written as

$$-(p-p_a)\mathbf{n} + 2\mu\mathbf{D}[\mathbf{u}]\cdot\mathbf{n} = \frac{d\sigma}{d\phi}\nabla_{\|}\phi + 2H\sigma\mathbf{n} \tag{16.16}$$

where $\mathbf{n}$ points into air, p_a is atmospheric pressure, H is the mean curvature, and σ is surface tension. Normal and tangential equations for the stress at the free surface are given by (16.16) which may be expressed in terms of the unknown $\mathbf{W}$ using (16.4).

The equations of motion are given by (4f.5) (equation (7.9) for the isothermal case) and may be reduced to equations for $\mathbf{W}$, ϕ and p using (16.4). The equations of motion in two dimensions may be framed in terms of the streamfunction using (16.3):

$$\begin{aligned}\frac{\partial}{\partial x}(P+Q) = {}& 2\mu'\phi_x(-\psi_{xy}+h_{xx}) + \mu(-\psi_{yyy}-\psi_{xxy}+2h_{xxx}+2h_{xyy})\\ &+\mu'\psi_y(\psi_{xx}-\psi_{yy}+2h_{xy}) + \hat{\delta}(2\phi_x\phi_{xx}+\phi_{xy}\phi_y+\phi_{yy}\phi_x)\\ &-\rho(\psi_{xy}\psi_y-\psi_x\psi_{yy}-h_x\psi_{xy}-h_y\psi_{yy}-\psi_{yt}+h_{xy}\psi_x\\ &-h_{xx}\psi_y+h_{xt}+h_xh_{xx}+h_yh_{xy})-\rho g,\end{aligned} \tag{16.17}$$

$$\begin{aligned}\frac{\partial}{\partial y}(P+Q) = {}& 2\mu'\phi_y(\psi_{xy}+h_{yy}) + \mu(\psi_{xxx}+\psi_{xyy}+2h_{yyy}+2h_{xxy})\\ &+\mu'\phi_x(\psi_{xx}-\psi_{yy}+2h_{xy}) + \hat{\delta}(2\phi_y\phi_{yy}+\phi_{xx}\phi_y+\phi_{xy}\phi_x)\\ &-\rho(\psi_{xy}\psi_x-\psi_y\psi_{xx}+h_x\psi_{xx}+h_y\psi_{xy}+\psi_{xt}-h_{xy}\psi_y\\ &+h_{yy}\psi_x+h_{yt}+h_xh_{xy}+h_yh_{yy}),\end{aligned} \tag{16.18}$$

where

$$Q = \frac{1}{3}\hat{\delta}|\nabla\phi|^2 - \frac{2}{3}\hat{\gamma}\nabla^2\phi + \frac{2}{3}\mu\nabla^2 h \tag{16.19}$$

and the derivative of μ is with respect to ϕ.

The highest derivatives of ϕ in these equations are in potential form and disappear after cross-differentiation:

$$\begin{aligned}
&2(\mu''\phi_x\phi_y + \mu'\phi_{xy})(-2\psi_{xy} + h_{xx} - h_{yy}) \\
&+(\mu''\phi_y^2 + \mu'\phi_{yy} - \mu''\phi_x^2 - \mu'\phi_{xx})(\psi_{xx} - \psi_{yy} + 2h_{xy}) \\
&-2\mu'\phi_y\left(\frac{\partial}{\partial y}\nabla^2\psi - \frac{\partial}{\partial y}\nabla^2 h\right) - 2\mu'\phi_x\left(\frac{\partial}{\partial x}\nabla^2\psi + \frac{\partial}{\partial y}\nabla^2 h\right) \\
&-\mu\nabla^4\phi + \hat{\delta}\left(\phi_x\frac{\partial}{\partial y} - \phi_y\frac{\partial}{\partial x}\right)\nabla^2\phi \\
&+\zeta\rho_g\phi_y(-\psi_{yt} + h_{xt} + \mathbf{L}(-\psi_y + h_x) + g) \\
&-\zeta\rho_g\phi_x(\psi_{xt} + h_{yt} + \mathbf{L}(\psi_x + h_y)) \\
&+\rho\Big(\mathbf{L}\nabla^2\psi + \nabla^2 h\nabla^2\psi + \nabla^2\psi_t\Big) = 0
\end{aligned} \tag{16.20}$$

where ρ_g is the density for glycerin, and the differential operator $\mathbf{L}$ is defined by

$$\mathbf{L} = \mathbf{u}\cdot\nabla = (-\psi_y + h_x)\frac{\partial}{\partial x} + (\psi_x + h_y)\frac{\partial}{\partial y}.$$

Thus, we have the diffusion equation (4e.9) and the vorticity equation (16.20) to solve for two unknowns ϕ and ψ. The boundary conditions at the side wall are

$$\phi_x = 0, \quad \psi_y = 0, \text{ and } \psi_x = -\frac{\zeta D\phi_y}{1-\zeta\phi}.$$

The boundary conditions at the bottom are

$$\phi_y = 0, \ \psi_x = 0, \text{ and } \psi_y = \frac{\zeta D\phi_x}{1-\zeta\phi}.$$

The free surface conditions at $y = Y(x,t)$ are

$$\mathbf{n}\cdot\nabla\phi = 0, \quad \psi_x = \frac{\partial Y}{\partial t} - \psi_y\frac{\partial Y}{\partial x},$$

and

$$\begin{aligned}
&-(p-p_a)\mathbf{n} + 2\mu(\mathbf{D}[\mathbf{W}] + \mathbf{D}[\nabla h])\cdot\mathbf{n} \\
&\quad = \frac{d\sigma}{d\phi}\nabla_{\|}\phi + \frac{Y_{xx}\sigma}{(1+Y_x^2)^{3/2}}\mathbf{n}.
\end{aligned}$$

Various problems of mixing and even Taylor dispersion which are conventionally treated in the framework of other equations with $\operatorname{div}\mathbf{u} = 0$, could be studied using the equations developed here.

X.17 Conclusions and Discussion

1. A theory of motion and mixing of two incompressible liquids ν and γ can be developed based on the equation of state for the density of a simple mixture (4c.10). The natural variable connecting composition to density is the volume fraction ϕ say of γ with constant densities ρ_γ and ρ_ν under isothermal conditions.
2. The velocity $\mathbf{u}$ is not solenoidal because the density $\rho(\phi)$ changes due to diffusion. For simple mixtures, the vector $\mathbf{W}$ defined in (7.6) is solenoidal. The velocity $\mathbf{u}$ is then decomposed into a solenoidal part $\mathbf{u_s}$ and an expansion part $\mathbf{u_e}$ (cf (8.1-2)) where

$$\text{div } \mathbf{u_e} = \Delta = \zeta \text{div}[\frac{D}{1-\zeta\phi}\nabla\phi]$$

   is the expansion and $D(\phi)$ is a diffusion function of ϕ, a quantity of order 10^{-6} cm^2/sec in many liquids. $D(\phi)$ is assumed to be constant in standard theories of Fick's law (but it varies in experiments). The expansion velocity is driven by gradients of the volume fraction.
3. It is universally but incorrectly assumed that div $\mathbf{u}$=0 when treating problems involving the diffusion of incompressible liquids. This assumption is exact in two situations, $\zeta = 0$ and $D = 0$, and could be a good approximation for conditions close to these.
   (1) Small $|\zeta|$ means the densities are nearly matched, which is sort of like a Boussinesq approximation. There are problems, however, like that of the smoothing-out of a discontinuity at a plane or spherical front in which the expansion is infinite at the initial instant, and large for small times, no matter how small $|\zeta|$ might be.
   (2) Small D means diffusion is neglected. This kind of approximation has been applied in the literature to determine the motion of two homogeneous liquids separated by an interface across which interface conditions are applied, for instance, the continuity of the stress traction vector and velocity. This is the same formulation as in the case of immiscible liquids, except that interfacial tension is set equal to zero. It misses out on surface tension-like forces associated with the stresses induced by the expansion velocity and Korteweg stresses and, of course, it misses out on diffusion entirely.
4. The diffusion equation may be simplified by replacing $\mathbf{u}$ with $\mathbf{W}$. The volume fraction is convected by $\mathbf{W}$ rather than $\mathbf{u}$. The resulting equation is in classical form.
5. The tangential component of $\mathbf{W}$ does not vanish at a solid wall, but instead balances the flux of ϕ there.
6. The problem of dynamic interfacial tension due to effects of the expansion velocity and Korteweg stresses is analyzed by evaluating the jump of the normal stress across plane and spherical mixing layers which smooth an initial discontinuity of composition. We find no jump

across a plane layer but there is a jump proportional to the curvature across the spherical surface. The dynamic tension at the spherical interface decays as $\sqrt{D/t}$. There are two terms in the expression (10.10) for the interfacial tension; one term arises from the Korteweg stress and it gives rise to stress opposing the internal pressure as in the case of equilibrium pressure if the Korteweg coeffficient has the appropriate sign. A second term arises from the expansion velocity and is proportional to the rate of change of viscosity with volume fraction. This term has the wrong sign for interfacial tension in the case of glycerin and water solution but has the right sign when the lighter fluid is the more viscous.

7. A Hele-Shaw theory may be derived from our equations. The problem of miscible displacement in a Hele-Shaw cell is formulated and solved in a variety of cases. The stability of miscible displacement reveals a Rayleigh-Taylor type of instability with heavy fluid above and a viscous fingering instability when the displacing fluid is much less viscous. Diffusion is strongly stabilizing.

Our common perception is that the diffusion of miscible liquids is irreversible; homogeneous mixtures do not demix. Perhaps this perception is faulty and it is possible to separate homogeneous mixtures to a degree by dynamic processes. Frei and Schiffer [1947] report separating solutions of glycerin and water and of hexane and heavier paraffins using ultrasound. Other methods which can be used for separation are thermodiffusion and ultra-centrifugation. It is also of perhaps of special interest to readers of this volume to consider the separation of a homogeneous mixture by the "method of lubricated pipelines". The question is: would a homogeneous mixture, say of glycerin and water, running through a very long capillary tube, tend to segregate as it flows with more glycerin in the center than at the wall?

Appendix

Differential Geometry of Surfaces

We derive equation (2c.2) of chapter I, volume 1. Σ is a surface $F(x, y, z, t) = 0$ in three-dimensional space. Reference coordinates (u, v) locate points on Σ. The reference coordinates are independent of time; they are not unique. The position vector for points on Σ is $\boldsymbol{x}(u, v, t)$ and $\boldsymbol{x}_u = \partial \boldsymbol{x}/\partial u$, $\boldsymbol{x}_v = \partial \boldsymbol{x}/\partial v$ are base vectors tangent to Σ at (u, v) which lie along the lines v=constant and u=constant, respectively. The normal to Σ is given by

$$\boldsymbol{n} = (\boldsymbol{x}_u \wedge \boldsymbol{x}_v)/\left|\boldsymbol{x}_u \wedge \boldsymbol{x}_v\right| = \nabla F/\left|\nabla F\right|, \tag{A.1}$$

where u and v are chosen so that $\boldsymbol{x}_u \wedge \boldsymbol{x}_v$ and ∇F are in the same direction. We may use the surface Jacobian

$$\mathcal{J} \stackrel{\text{def}}{=} \boldsymbol{n} \cdot (\boldsymbol{x}_u \wedge \boldsymbol{x}_v) = \left|\boldsymbol{x}_u \wedge \boldsymbol{x}_v\right| \tag{A.2}$$

to define a set of reciprocal base vectors.

$$\begin{aligned} \mathcal{J}\, \boldsymbol{a}^u &= -\boldsymbol{n} \wedge \boldsymbol{x}_v, \\ \mathcal{J}\, \boldsymbol{a}^v &= \boldsymbol{n} \wedge \boldsymbol{x}_u, \\ \mathcal{J}\, \boldsymbol{a}^n &= \boldsymbol{x}_u \wedge \boldsymbol{x}_v, \end{aligned} \tag{A.3}$$

where $\boldsymbol{x}_u \cdot \boldsymbol{a}^u = \boldsymbol{x}_v \cdot \boldsymbol{a}^v = \boldsymbol{n} \cdot \boldsymbol{a}^n = 1$ and all other scalar products are biorthogonal. The surface Jacobian arises in the representation of surface areas in terms of reference coordinates.

$$\begin{aligned} \boldsymbol{n} d\Sigma &= (\boldsymbol{x}_u \wedge \boldsymbol{x}_v)\, du\, dv, \\ d\Sigma &= \mathcal{J}\, du\, dv. \end{aligned} \tag{A.4}$$

Now we consider the curvature of a surface. Let (u, v) be a point on Σ and ℓ is a straight line along the normal $\boldsymbol{n}$ to Σ at (u, v). Consider spheres of radius $|\rho|$, centered at points on ℓ which make a second order contact

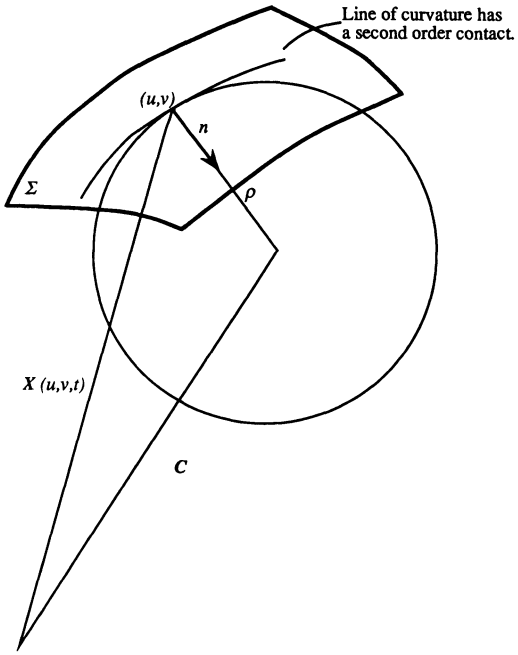

Fig. A.1. Construction for curvature and for the principal lines of curvature. $\mathbf{x}+\rho\mathbf{n}=\mathbf{c}$, $\rho>0$ in the figure, $\mathbf{x}_s+\rho\mathbf{n}_s+\rho_s\mathbf{n}=\mathbf{c}_s$ where s is arc-length on the line of curvature, $\rho_s\mathbf{n}=\mathbf{c}_s$, $\mathbf{x}_s+\rho\mathbf{n}_s=0$.

with Σ, $\rho>0$ if $\boldsymbol{n}$ is the inward normal to the sphere and $\rho<0$ if $\boldsymbol{n}$ is the outward normal to the sphere. In general there are two spheres which can make a second order contact with Σ. If we vary the size of the spheres centered on ℓ we will find that there is a large sphere and a small sphere which will, in general, make a second order contact with Σ (see figure A.1). The lines along which the spheres make a second order contact are called the principal lines of curvature and they are orthogonal. To show this, we note that if a sphere is to make a second order contact with Σ, then along this line of curvature with arc-length s, $\boldsymbol{n}_s$ must lie in the plane of $\boldsymbol{n}$ and $\boldsymbol{x}_s$:

$$\boldsymbol{n}_s\cdot(\boldsymbol{x}_s\wedge\boldsymbol{n})=\boldsymbol{n}\cdot(\boldsymbol{n}_s\wedge\boldsymbol{x}_s)=0.$$

After writing $\boldsymbol{x}_s=\boldsymbol{x}_u u_s+\boldsymbol{x}_v v_s$, etc, we find that

$$Pu_s^2+2Qu_sv_s+Ru_s^2=0, \tag{A.5}$$

where

$$
\begin{aligned}
P &= \boldsymbol{n} \cdot (\boldsymbol{n}_u \wedge \boldsymbol{x}_u)\,, \\
2Q &= \boldsymbol{n} \cdot (\boldsymbol{n}_u \wedge \boldsymbol{x}_v) + \boldsymbol{n} \cdot (\boldsymbol{n}_v \wedge \boldsymbol{x}_u)\,, \\
R &= \boldsymbol{n} \cdot (\boldsymbol{n}_v \wedge \boldsymbol{x}_v)\,.
\end{aligned} \tag{A.6}
$$

Equation (A.5) is the quadratic form for the symmetric matrix,

$$
\begin{bmatrix} R & Q \\ Q & P \end{bmatrix}, \tag{A.7}
$$

whose principal directions are orthogonal, and coincide with the principal lines of curvature.

It can be shown that, along a line of curvature, $\boldsymbol{x}_s$ and $\boldsymbol{n}_s$ are co-linear with the radius of curvature ρ as the factor of proportionality so that

$$
\kappa \boldsymbol{x}_s + \boldsymbol{n}_s = 0, \qquad \kappa = 1/\rho. \tag{A.8}
$$

From this, it follows that $\boldsymbol{n} \cdot (\kappa \mathbf{x}_v + \boldsymbol{n}_v) \wedge (\kappa \mathbf{x}_u + \boldsymbol{n}_u) u_s = 0$. Hence

$$
\mathcal{J}\,\kappa^2 + 2A\kappa + B = 0, \tag{A.9}
$$

where

$$
\begin{aligned}
2A &= \boldsymbol{n} \cdot (\boldsymbol{x}_u \wedge \boldsymbol{n}_v) + \boldsymbol{n} \cdot (\boldsymbol{n}_u \wedge \boldsymbol{x}_v)\,, \\
B &= \boldsymbol{n} \cdot (\boldsymbol{n}_u \wedge \boldsymbol{n}_v)\,.
\end{aligned}
$$

The two roots κ_1 and κ_2 of (A.9) are principal curvatures. Writing $(\kappa - \kappa_1)$ $(\kappa - \kappa_2) = 0$ we find by comparing with (A.9) that

$$
H \overset{\text{def}}{=} \frac{1}{2}(\kappa_1 + \kappa_2) = -A/\mathcal{J} \qquad \text{(mean curvature)} \tag{A.10}
$$

and

$$
\kappa_1 \kappa_2 = B/\mathcal{J} \quad \text{(Gauss curvature)}. \tag{A.11}
$$

We turn next to surface gradients. This is the usual gradient, but without the component normal to Σ; that is,

$$
\nabla_{II} = \nabla - \boldsymbol{n}(\boldsymbol{n} \cdot \nabla). \tag{A.12}
$$

This gradient is also perpendicular to level lines of scalars $\phi(u, v, t)$ defined on Σ. This latter requirement means that if $\boldsymbol{x}(u, v, t)$ is the position vector of a point on Σ, then

$$
\begin{aligned}
d\phi &= (d\boldsymbol{x} \cdot \nabla_{II})\phi = (\boldsymbol{x}_u \cdot \nabla_{II})\phi du + (\boldsymbol{x}_v \cdot \nabla_{II})\phi dv \\
&= \frac{\partial \phi}{\partial u} du + \frac{\partial \phi}{\partial v} dv.
\end{aligned} \tag{A.13}
$$

A surface gradient with the stated properties may be expressed as

$$
\nabla_{II} = \boldsymbol{a}^u \frac{\partial}{\partial u} + \boldsymbol{a}^v \frac{\partial}{\partial v}, \tag{A.14}
$$

where $\boldsymbol{a}^u$, $\boldsymbol{a}^v$ are given by (A.3). Using (A.10) we show that

$$\begin{aligned}\nabla_{II}\cdot\boldsymbol{n} &= \mathcal{J}^{-1}(-\boldsymbol{n}\wedge\boldsymbol{x}_v)\cdot\boldsymbol{n}_u + \mathcal{J}^{-1}(\boldsymbol{n}\wedge\boldsymbol{x}_u)\cdot\boldsymbol{n}_v \\ &= -2H\end{aligned} \tag{A.16}$$

and

$$\nabla_{II}\cdot\boldsymbol{n}\phi = -2H\phi. \tag{A17}$$

Moreover

$$\left.\begin{aligned}\nabla_{II}\cdot(\phi\boldsymbol{x}_u) &= \frac{1}{\mathcal{J}}\frac{\partial}{\partial u}(\mathcal{J}\phi), \\ \nabla_{II}\cdot(\phi\boldsymbol{x}_v) &= \frac{1}{\mathcal{J}}\frac{\partial}{\partial v}(\mathcal{J}\phi).\end{aligned}\right\} \tag{A.18}$$

To prove $(\text{A.18})_1$, we write

$$\begin{aligned}\nabla_{II}\cdot(\phi\boldsymbol{x}_u) &= \nabla_{II}\cdot(\mathcal{J}\phi\boldsymbol{x}_u/\mathcal{J}) \\ &= \mathcal{J}^{-1}\boldsymbol{x}_u\cdot\nabla_{II}\mathcal{J}\phi + \phi\mathcal{J}\nabla_{II}\cdot(\boldsymbol{x}_u/\mathcal{J}).\end{aligned} \tag{A.19}$$

The first term on the right of (A.19) is $\frac{1}{\mathcal{J}}\frac{\partial}{\partial u}(\mathcal{J}\phi)$. The second term vanishes:

$$\begin{aligned}\mathcal{J}\nabla_{II}\cdot(\boldsymbol{x}_u/\mathcal{J}) &= -\boldsymbol{n}\wedge\boldsymbol{x}_v\frac{\partial}{\partial u}\cdot(\boldsymbol{x}_u/\mathcal{J}) + \boldsymbol{n}\wedge\boldsymbol{x}_u\frac{\partial}{\partial v}\cdot(\boldsymbol{x}_u/\mathcal{J}) \\ = \frac{\boldsymbol{x}_u}{\mathcal{J}}\cdot\left\{\frac{\partial}{\partial u}(\boldsymbol{n}\wedge\boldsymbol{x}_v) - \frac{\partial}{\partial v}(\boldsymbol{n}\wedge\boldsymbol{x}_u)\right\} &= \frac{\boldsymbol{x}_u}{\mathcal{J}}\cdot(\boldsymbol{n}_u\wedge\boldsymbol{x}_v) = 0,\end{aligned}$$

because $\boldsymbol{n}_u$, $\boldsymbol{x}_v$, $\boldsymbol{x}_u$ are all perpendicular to $\boldsymbol{n}$.

Let $\boldsymbol{f}(\boldsymbol{x},t)$ be a vector field in three-dimensions whose components on Σ may be represented by

$$\boldsymbol{f}(\boldsymbol{x}(u,v,t),t) = f^u\boldsymbol{x}_u + f^v\boldsymbol{x}_v + f^n\boldsymbol{n}. \tag{A.20}$$

The surface divergence of this vector is

$$\begin{aligned}\nabla_{II}\cdot\boldsymbol{f} &= \nabla_{II}\cdot(f^u\boldsymbol{x}_u + f^v\boldsymbol{x}_v + f^n\boldsymbol{n}) \\ &= \mathcal{J}^{-1}\frac{\partial}{\partial u}(\mathcal{J}f^u) + \mathcal{J}^{-1}\frac{\partial}{\partial v}(\mathcal{J}f^v) - 2Hf^n.\end{aligned} \tag{A.21}$$

A surface divergence theorem may be expressed as

$$\int_\Sigma \nabla_{II}\cdot\boldsymbol{f}\,d\Sigma = \int_{\partial\Sigma}\boldsymbol{f}\cdot\hat{\boldsymbol{\tau}}\,d\ell - \int_\Sigma 2Hf^n d\Sigma, \tag{A.22}$$

where $\partial\Sigma$ is a closed curve on Σ, the boundary of Σ, and $\hat{\boldsymbol{\tau}}$ is the unit normal to $\partial\Sigma$ which lies in Σ. If $\boldsymbol{t}$ is the unit tangent vector of $\partial\Sigma$, then $\hat{\boldsymbol{\tau}} = \boldsymbol{t}\wedge\boldsymbol{n}$ is perpendicular to $\boldsymbol{t}$ and $\boldsymbol{n}$. To prove (A.22), we first write

$$\int_{\Sigma}(\nabla_{II}\cdot \boldsymbol{f}+2Hf^{n})\,d\Sigma=\int\int[\nabla_{II}\cdot(f^{u}\boldsymbol{x}_{u}+f^{v}\boldsymbol{x}_{v})]\,\mathcal{J}\,du\,dv$$
$$\int\int\left[\frac{\partial\mathcal{J}f^{u}}{\partial u}+\frac{\partial\mathcal{J}f^{v}}{\partial v}\right]du\,dv=\int_{\partial\Sigma}[\mathcal{J}f^{u}dv-\mathcal{J}f^{v}du]\,. \tag{A.23}$$

Then, to complete the proof, we note that

$$\begin{aligned}\boldsymbol{f}\cdot\hat{\boldsymbol{\tau}}d\ell&=\boldsymbol{f}\cdot(\boldsymbol{t}\wedge\boldsymbol{n})d\ell=\boldsymbol{f}\cdot(\boldsymbol{t}d\ell\wedge\boldsymbol{n})=\boldsymbol{f}\cdot(d\boldsymbol{x}\wedge\boldsymbol{n})\\&=\boldsymbol{f}\cdot(\boldsymbol{x}_{u}du+\boldsymbol{x}_{v}dv)\wedge\boldsymbol{n}=\boldsymbol{f}\cdot(\boldsymbol{x}_{u}\wedge\boldsymbol{n}\,du+\boldsymbol{x}_{v}\wedge\boldsymbol{n}dv)\\&=f^{u}\mathcal{J}\,dv-f^{v}\mathcal{J}\,du.\end{aligned} \tag{A.24}$$

Recalling next that u, v are reference coordinates which are independent of time t, we prove that

$$\frac{d\mathcal{J}}{dt}\overset{\text{def}}{=}\frac{\partial\mathcal{J}}{\partial t}(u,v,t)=\mathcal{J}\,\nabla_{II}\cdot\boldsymbol{u}_{\Sigma}, \tag{A.25}$$

where

$$\boldsymbol{u}_{\Sigma}=\frac{\partial\boldsymbol{x}}{\partial t}(u,v,t)=\frac{d\boldsymbol{x}}{dt}\overset{\text{def}}{=}\dot{\boldsymbol{x}}. \tag{A.26}$$

We recall that $\dot{\boldsymbol{n}}$ is perpendicular to $\boldsymbol{n}$ and write

$$\begin{aligned}\frac{\partial\mathcal{J}}{\partial t}&=\boldsymbol{n}\cdot(\dot{\boldsymbol{x}}_{u}\wedge\boldsymbol{x}_{v}+\boldsymbol{x}_{u}\wedge\dot{\boldsymbol{x}}_{v})\\&=\boldsymbol{n}\cdot((\boldsymbol{u}_{\Sigma})_{u}\wedge\boldsymbol{x}_{v}+\boldsymbol{x}_{u}\wedge(\boldsymbol{u}_{\Sigma})_{v})\\&=\mathcal{J}\left\{\frac{\boldsymbol{n}\wedge\boldsymbol{x}_{u}}{\mathcal{J}}\frac{\partial}{\partial v}-\frac{\boldsymbol{n}\wedge\boldsymbol{x}_{v}}{\mathcal{J}}\frac{\partial}{\partial u}\right\}\cdot\boldsymbol{u}_{\Sigma}\\&=\mathcal{J}\,\nabla_{II}\cdot\boldsymbol{u}_{\Sigma}.\end{aligned}$$

Finally, we shall use (A.25) and (A.22) to derive equation (2c.2) of chapter I, volume 1.

$$\begin{aligned}&\frac{d}{dt}\int_{\Sigma}\sigma d\Sigma=\int\int\frac{d(\sigma\mathcal{J})}{dt}du\,dv\\&=\int_{\Sigma}\left\{\frac{d\sigma}{dt}+\sigma\nabla_{II}\cdot\boldsymbol{u}_{\Sigma}\right\}d\Sigma\\&=\int_{\Sigma}\left\{\frac{d\sigma}{dt}+\nabla_{II}\cdot(\sigma\boldsymbol{u})-\boldsymbol{u}_{\Sigma}\cdot\nabla_{II}\sigma\right\}d\Sigma\\&=\int_{\Sigma}\left(\frac{d\sigma}{dt}-\boldsymbol{u}_{\Sigma}\cdot\nabla_{II}\sigma-2H\sigma\boldsymbol{u}_{\Sigma}\cdot\boldsymbol{n}\right)d\Sigma+\int_{\partial\Sigma}\sigma\hat{\boldsymbol{\tau}}\cdot\boldsymbol{u}_{\Sigma}d\ell.\end{aligned}$$

References

Numbers [(vm) n] following a reference indicate the volume m and page n on which it is referred.

Acrivos, A. and T. S. Lo, 1978, Deformation and breakup of a single slender drop in an extensional flow, J. Fluid Mech. **86**, 641. [(v1) 143]

Altobelli, S. A., R. C. Givler and E. Fukushima, 1991, Velocity and concentration measurements of suspensions by nuclear magnetic resonance imaging, J. Rheology **35** (5), 721. [(v1) 7, plate I.1.2]

Amarakoon, A. M. D., R. G. Hussey, W. J. Good, and E. G. Grimsal, 1982, Drag measurements for axisymmetric motion of a torus at low Reynolds number, Phys. Fluids **25**(9), 1495. [(v2) 313]

Anderson, P. C., C. J. Veal and V. R. Withers, 1982, Rheology of coal-oil dispersions, Powder Technol. **32**, 45. [(v1) 9]

Anturkar, N. R., T. C. Papanastasiou and J. O. Wilkes, 1990a, Linear stability analysis of multilayer plane Poiseuille flow, Phys. Fluids A **2**, 530. [(v1) 272]

Anturkar, N. R., T. C. Papanastasiou and J. O. Wilkes, 1990b, Stability of multilayer extrusion of viscoelastic liquids, AIChE J. **36**(5), 710. [(v1) 360]

Aoki, K., and C. Cercignani, 1983, Evaporation and condensation on two parallel plates at finite Reynolds numbers, Phys. Fluids **26**, 1163. [(v1) 381]

Arecchi, F. T., P. K. Buah-Bassuah, F. Francini, C. Pérez-Garcia and F. Quercioli, 1989, An experimental investigation of the break-up of a liquid drop falling in a miscible fluid, Europhys. Lett. **9**(4), 333. [(v2) 290-291, 309]

Arney, M., R. Bai, D. D. Joseph and K. Liu, 1992, Friction factor and holdup studies for lubricated pipelines, in preparation. [(v2) 7, 16, 115, 192-202]

Astarita, G. and G. Apuzzo, 1965, Motion of gas bubbles in non-Newtonian liquids, AIChE J. **11**, 815. [(v1) 144]

Atherton, R. W., and G. M. Homsy, 1976, On the derivation of evolution equations for interfacial waves, Chem. Engng. Communications **2**, 57. [(v1) 270, 324, 330; (v2) 266]

Aul, R. W., and W. L. Olbricht, 1989, Stability of a thin annular film in pressure-driven low Reynolds number flow through a capillary, preprint, School of Chem. Engng., Cornell University. [(v2) 8, 13, 50, 66-69, 83]

Babchin, A. J., A. L. Frenkel, B. G. Levich and G. I. Sivashinsky, 1983 a, Flow-induced nonlinear effects in thin liquid film stability, Ann. NY Acad. Sci. **404** 426. [(v1) 333]

Babchin, A. J., A. L. Frenkel, B. G. Levich and G. I. Sivashinsky, 1983 b, Nonlinear saturation of Rayleigh-Taylor instability in thin films, Phys. Fluids **26** (11), 3159 L. [(v1) 333]

Bai, R., K. Chen and D. D. Joseph, 1992, Lubricated pipelining: stability of core-annular flow. Part V: experiments and comparison with theory, J. Fluid Mech. [(v2) 8, 15, 16, 154-225]

Baird, M. H. I., T. Wairegi and H. J. Loo, 1977, Velocity and momentum of vortex rings in relation to formation parameters, Can. J. Chem. Eng. **55** 19. [(v2) 289]

Barkey, D. P. and P. D. Laporte, 1990, The dynamic diffusion layer in branched growth of a conductive-polymer aggregate in a 2-D electrolysis cell, J. Electrochem. Soc. **137**(5), 1655. [(v2) 343]

Barnett, S.M., A. E. Humphrey and M. Litt, 1966, Bubble motion and mass transfer in non-Newtonian fluids, AIChE J. **12**, 253. [(v1) 144]

Batchelor, G. K., 1970, *An Introduction to Fluid Dynamics*, Cambridge University Press. [(v1) 34; (v2) 155, 294]

Bhattacharji, S., 1967, Mechanics of flow differentiation in ultramafic and mafic sills, J. of Geology **75**, 101. [(v1) 5]

Baumann, N., 1989, *Vortex Rings*, Masters Thesis, U. of Minnesota. [(v2) 288-317]

Baumann, N., D. D. Joseph, P. Mohr and Y. Renardy, 1992, Vortex rings of one fluid in another in free fall, Phys. Fluids A **4**(3),567. [(v2) 288-323]

Beale, J. T., 1980, The initial value problem for the Navier-Stokes equations with a free surface, Comm. Pure Appl. Math. **34**, 359. [(v1) 183]

Beale, J. T., 1984, Large time regularity of viscous surface waves, Arch. Rational Mech. Anal. **84**, 307. [(v1) 183]

Beavers, G. S., and D. D. Joseph, 1979, Experiments on free surface phenomena, J. Non-Newtonian Fluid Mech. **5**, 323. [(v1) 15]

Beer, A., 1869, *Einleitung in die Mathematische Theorie der Elastizität und Capillarität*, Leipzig: A. Gresen Verlag. [(v1) 67]

Benguria, R. D., and M. C. Depassier, 1987, Oscillatory instabilities in the Rayleigh-Bénard problem with a free surface, Phys. Fluids **30** (6), 1678. [(v1) 171]

Benguria, R. D., and M. C. Depassier, 1989, On the linear stability theory of Bénard-Marangoni convection, Phys. Fluids A **1**(7), 1123. [(v1) 171, 173]

Benney, D. J., 1966, Long waves in liquid film, J. Math. Phys. **45** 150. [(v1) 270; (v2) 261]

Benney, D. J., and A. C. Newell, 1967, The propagation of nonlinear wave envelopes, J. Math. Phys. **46**, 133. [(v1) 324]

Bentwich, M., 1976, Two-phase axial laminar flow in a pipe with naturally curved interface, Chem. Eng. Sci. **31**, 71. [(v2) 4]

Bird, R. B., R. C. Armstrong and O. Hassager, 1977 *Dynamics of Polymeric Liquids*, volumes 1 and 2, Wiley and Sons. [(v1) 143]

Bisch, C., A. Lasek and H. Rodot, 1982, Hydrodynamic behavior of spherical semi-free liquid volumes in simulated weightlessness, J. de Mécanique théorique et appliquée **1**, 165. [(v1) 15]

Blais, P., D. J. Carlsson, T. Suprunchuk and D. M. Wiles, 1971, Bicomponent composites: preparation from incompatible polymers by corona treatment, Text. Res. J. **41**, 485. [(v1) 11]

Blennerhassett, P. J., 1980, On the generation of waves by wind, Phil. Trans. R. Soc. Lond. A **298**, 451. [(v1) 270, 271, 276, 277, 279, 287, 339, 346-350, 356-359; (v2) 51, 227, 237]

Blennerhassett, P. J., and F. T. Smith, 1987, Short-scale waves on wind-driven water ('cat's paws'), Proc. R. Soc. Lond A **410**, 1. [(v1) 270, 302, 306, 319, 351]

Bolton, B., and S. Middleman, 1980, Air entrainment in a roll coating system, Chem. Engng. Sci. **35**, 597. [(v1) 166]

Bond, R. K., 1957, Designing the gelsonite pipeline, Chem. Eng. **64**, 249. [(v1) 7]

Boomkamp, P. A. M., and R. H. M. Miesen, 1991, Nonaxisymmetric waves in core-annular flow with a small viscosity ratio, submitted to Phys. Fluids A. [(v2) 14, 94]

Bowen, R. M., 1971, *Continuum Physics*, Volume II, ed. A. C. Eringen, Academic Press. [(v2) 352]

Brand, R. H., and S. Backer, 1962, Mechanical principles of natural crimp of fiber, Text. Res. J. **32**, 39. [(v1) 11]

Bretherton, C. S., and E. A. Spiegel, 1983, Intermittency through modulational instability, Phys. Letts. **96A**, no.3, 152. [(v2) 228]

Brown, R. A. and L. E. Scriven, 1980, The shape and stability of rotating liquid drops, Phil. Trans. R. Soc. Lond. A **297**, 51. [(v1) 90]

Buckley, R. A., and R. J. Phillips, 1969, The development of bicomponent fibers, Chem. Eng. Prog. **65** (10), 41. [(v1) 11]

Buckmaster, J.D., 1972, Pointed bubbles in slow viscous flow. J. Fluid Mech. **55**, 385. [(v1) 143]

Buckmaster, J.D., 1973, The bursting of pointed drops in slow viscous flow, ASME J. Appl. Mech. **40**, 18. [(v1) 143]

Busse, F. H., 1978, A model of time-periodic mantle flow, Geophys. J. R. Astr. Soc. **52**,1. [(v1) 15, 172]

Busse, F. H., 1981, On the aspect ratio of two-layer mantle convection, Physics of the Earth and Planetary Interiors **24**, 320. [(v1) 15, 172]

Busse, F. H., 1982, Multiple solutions for convection in a two component fluid, Geophysical Research Letters **9** (5), 519. [(v1) 15, 31]

Busse, F. H., 1989, Fundamentals of thermal convection, from *Mantle Convection, Plate Tectonics and Global Dynamics*, W. R. Peltier ed., Gordon and Breach. [(v1) 15]

Busse, F. H., and G. Schubert, 1971, Convection in a fluid with two phases, J. Fluid Mech. **46**(4), 801. [(v1) 378, 399]

Busse, W. F., 1964, Two decades of high-polymer physics: a survey and forecast, Phys. Today **9**. [(v1) 376]

Buzano, E., and M. Golubitsky, 1983, Bifurcation on the hexagonal lattice and the planar Bénard problem, Phil. Trans. R. Soc. London A **308**, 617. [(v1) 176, 263]

Cahn, J. and J. Hilliard, 1954, Free energy of a nonuniform system I: interfacial free energy, J. Chem. Phys. **28**, 258. [(v2) 339]

Calderbank, P.H., 1967, Review Series No. 3 – Gas absorption from bubbles, Trans. Instn. Chem. Engrs. **45**, 209. [(v1) 144]

Calderbank, P.H., D. S. Johnson and J. Loudon, 1970, Mechanics and mass transfer of single bubbles in free rise through some Newtonian and non-Newtonian liquids, Chem. Engng. Sci. **25**, 235. [(v1) 144]

Canuto, C., M. Y. Hussaini, A. Quarteroni and T. A. Zang, 1988, *Spectral Methods in Fluid Dynamics*, Springer Verlag. [(v2) 29]

Carr, J., 1981, *Applications of Center Manifold Theory*, Springer, New York. [(v1) 176]

Carrigan, C. R., and J. C. Eichelberger, 1990, Zoning of magmas by viscosity in volcanic conduits, Nature **343**, No. 6255, 248. [(v1) 6, 15]

Castillo, J. L., and M. G. Velarde, 1982, Buoyancy-thermocapillary instability: the role of interfacial deformation in one- and two- component fluid layers heated from below or above, J. Fluid Mech. **125**, 463. [(v1) 171, 173]

Catton, I., and J. H. Lienhard V, 1984, Thermal stability of two fluid layers separated by a solid interlayer of finite thickness and thermal conductivity, J. Heat Transfer **106**, 605. [(v1) 188]

Cercignani, C., W. Fiszdon and A. Frezzotti, 1985, The paradox of the inverted temperature profiles between an evaporating and a condensing surface, Phys. Fluids **28**, 3237. [(v1) 381]

Cerisier, P., C. Jamond, J. Pantaloni and J. C. Charmet, 1984, Déformation de la surface libre en convection de Bénard-Marangoni, J. Phys. (Paris) **45**, 405. [(v1) 173]

Chandrasekhar, S., 1965, The stability of a rotating liquid drop, Proc. R. Soc. Lond. A **286**, 1. [(v1) 72]

Chandrasekhar, S., 1981 (1st ed. 1961), *Hydrodynamic and Hydromagnetic Stability*, Dover Publications Inc., New York. [(v1) 72, 115, 170, 171, 203, 209; (v2) 23, 37-38, 48, 70-73, 300]

Chang, H.-C., 1986, Traveling waves on fluid linterfaces: Normal form analysis of the Kuramoto-Sivashinsky equation, Phys. Fluids **29**, 3142. [(v1) 337]

Chapman, D. S., and P. R. Critchlow, 1967, Formation of vortex rings from falling drops, J. Fluid Mech. **29**, 177. [(v2) 289]

Charles, M. E., 1963, The pipeline flow of capsules. Part 2: theoretical analysis of the concentric flow of cylindrical forms, Can. J. Chem. Engng. April, 46. [(v2) 4, 6, 176]

Charles, M. E., G. W. Govier and G. W. Hodgson, 1961, The horizontal pipeline flow of equal density oil-water mixtures, Can. J. Chem. Eng. **39**, 17. [(v1) 3, 4, 5, 14; (v2) 2, 6, 12, 16-50, 61-65, 83, 126, 162, 164-165, 174-175, 177, 195-196, 231, 245]

Charles, M. E., and L. U. Lilleleht, 1966, Correlation of pressure gradients for the stratified laminar-turbulent pipeline flow of two immiscible liquids, Can. J. Eng. **44**, 47. [(v1) 4; (v2) 4]

Charles, M. E., and R. J. Redberger, 1962, The reduction of pressure gradients in oil pipelines by the addition of water: numerical analysis of stratified flow, Can. J. Chem. Engng. **40**, 70. [(v1) 4; (v2) 3, 4]

Chen, K., 1990, Lubricated pipelining: stability of core-annular flows, Ph. D. thesis, University of Minnesota. [(v2) 233, 241, 245]

Chen, K., 1991a, Interfacial instability due to elastic stratification in concentric coextrusion of two viscoelastic fluids, J. Non-Newtonian Fluid Mech. **40**, 155. [(v1) 360, 373]

Chen, K., 1991b, Elastic instability of the interface in Couette flow of viscoelastic liquids, J. Non-Newtonian Fluid Mech. **40**, 261. [(v1) 359, 360, 373, 375-378]

Chen, K., 1992, Shortwave instability of core-annular flow, Phys. Fluids A **4**(1), 186. [(v1) 359; (v2) 15]

Chen, K., R. Bai and D. D. Joseph, 1990, Lubricated pipelining III: stability of core-annular flow in vertical pipes, J. Fluid Mech. **214**, 251. [(v2) 16, 114-153, 196]

Chen, K., and D. D. Joseph, 1990, Application of the singular value decomposition to the numerical computation of the coefficients of amplitude equations and normal forms, Applied Num. Math. **6**, 425. [(v2) 243]

Chen, K., and D. D. Joseph, 1991a, Lubricated pipelining: stability of core-annular flows. Part IV: Ginzburg-Landau equations, J. Fluid Mech. **227**, 587. [(v2) 15, 16, 226-260]

Chen, K., and D. D. Joseph, 1991b, Long wave and lubrication theories for core-annular flow, Phys. Fluids A **3**(11), 2672 [(v2) 15, 16, 261-287]

Chen, K., and D. D. Joseph, 1992, Elastic short-wave instability in extrusion flows of viscoelastic liquids, J. Non-Newt. Fluid Mech. in press. [(v1) 359, 361, 375, 377]

Chernikin, V. I., 1956, Combined pumping of petroleum and water in pipes, Trudi. Mock. Neft in-ta **17**, 101. [(v2) 3]

Chow, S.-N., and J. K. Hale, 1982, *Methods of Bifurcation Theory*, Springer. [(v1) 176, 256, 343]

Chung, H. S., and R. Hogg, 1985, Stability criteria for fine-particle dispersions, Colloids and Surfaces **15**, 119. [(v1) 9]

Clark, A. F., and A. Shapiro, 1949, Method of pumping viscous petroleum, U. S. Patent No. 2,533,878. [(v2) 4, 5]

Clift, R., J. R. Grace and M. E. Weber, 1978, *Bubbles, drops and particles*, Academic Press. [(v2) 294, 299]

Clifton, E. G., and L. R. Handley, 1958, Method and apparatus for lubricating pipe lines, U. S. Patent No. 2,821,205. [(v2) 5]

Cohen, B. I., J. A. Krommes, W. M. Tang and M. N. Rosenbluth, 1976, Nonlinear saturation of the dissipative trapped-ion mode by mode coupling, Nuclear Fusion **16**, 971. [(v1) 271, 333-335]

Cohen, Y., and A. B. Metzner, 1985, Apparent slip flow of polymer solutions, J. Rheol. **29** (1), 67. [(v1) 375, 377]

Cotton, F. W., and H. Salwen, 1981, Linear stability of rotating Hagen-Poiseuille flow, J. Fluid Mech. **108**, 101. [(v2) 93]

Craik, A. D. D., 1966, Wind generated waves in thin liquid films, J. Fluid Mech. **26**, 369. [(v1) 338]

Craik, A. D. D., 1983, *Wave interactions and fluid flows*, Cambridge Univ. Press. [(v1) 343, 345; (v2) 241]

Dandy, D. S., and L. G. Leal, 1989, Buoyancy-driven motion of a deformable drop through a quiescent liquid at intermediate Reynolds numbers, J. Fluid Mech. **208**, 161. [(v2) 294, 304, 306]

Dauber, C. A., 1957, Pipeline coal transportation, Coal Age **62**(4),84. [(v1) 7]

Davey, A., L. M. Hocking and K. Stewartson, 1974, On the nonlinear evolution of three-dimensional disturbances in plane Poiseuille flow, J. Fluid Mech. **63**, 529. [(v1) 346-349; (v2) 244]

Davies, A.R., 1988, Reentrant corner singularities in non-Newtonian flow. Part I. Theory, J. Non-Newtonian Fluid Mech. **29**, 269. [(v1) 157]

Davis, H. T., 1988, A theory of tension at a miscible displacement front, in *Numerical Simulation and Oil Recovery*, ed. M. Wheeler, Institute for Mathematics and its Applications **2**. [(v2) 341-342, 374]

Davis, R. H., E. Herbolzheimer and A. Acrivos, 1983, Wave formation and growth during sedimentation in narrow tilted channels, Phys. Fluids **26**, 2055. [(v1) 295]

Davis, S. H., and G. M. Homsy, 1980, Energy stability theory for free-surface problems: buoyancy-thermocapillary layers, J. Fluid Mech. **98** (3), 527. [(v1) 171, 173, 178]

Dean, W.R. and P. E. Montagnon, 1949, On the steady motion of viscous liquid in a corner, Proc. Cambridge Phil. Soc. **45**, 389. [(v1) 151]

Denham, E., D. R. Wall and D. M. Whitehead, 1982, The handling and combustion characteristics of stable coal fuel oil dispersions, Proc. of 4th Int. Symp. on Coal Slurry Combustion, Orlando, Florida. [(v1) 9]

Denn, M. M., 1990, Issues in viscoelastic fluid mechanics, Annu. Rev. Fluid Mech. **23**, 13. [(v1) 375]

Deryagin, B. M., and S. M. Levi, 1964, *Film Coating Theory*, Focal Press, London and New York. [(v1) 166]

Dijkstra, H. A., and P. H. Steen, 1991, Thermocapillary stabilization of the capillary breakup of an annular film of liquid, J. Fluid Mech. **229**, 205. [(v2) 13]

Drazin, P. G., and W. H. Reid, 1982, *Hydrodynamic Stability*, Cambridge University Press, 1st paperback ed. [(v1) 24, 115, 171, 193, 203, 209, 220, 306; (v2) 98, 165]

Drew, D. A., 1983, Continuum modelling of two-phase flows, in *Theory of Dispersed Multiphase Flow*, ed. R. E. Meyer, Academic Press, 173. [(v1) 103, 352]

Drew, D. A., 1983, Mathematical modeling of two-phase flow, A. Rev. Fluid Mech. **15**, 261. [(v1) 103, 352]

Drew, D. A., 1986, Flow structure in the Poiseuille flow of a particle-fluid mixture, SIAM Workshop on Multiphase Flow, June 2-4. [(v1) 6]

Dunn, J. E., 1986, Interstitial working and a nonclassical thermodynamics, in *New Perspectives in Thermodynamics*, ed. J. Serrin, Springer Verlag. [(v2) 346]

Dussan V., E. B., 1979, On the spreading of liquids on solid surfaces: static and dynamic contact lines, *Annual Review of Fluid Mechanics*, Annual Reviews Inc., Palo Alto, **11**, 371. [(v2) 173]

Dussan V., E. B., and S. H. Davis, 1974, On the motion of a fluid-fluid interface along a solid surface, J. Fluid Mech. **65**, 71. [(v1) 105]

Engelman, M. S., 1982, FIDAP – A Fluid Dynamics Analysis Package, Adv. Eng. Software **4**, 163. [(v1) 158]

Engelman, M.S. and R. I. Sani, 1986, Finite element simulation of incompressible fluid flows with a free/moving surface. In: C. Taylor, J. A. Johnson and W. R. Smith (eds.), *Computational Techniques for Fluid Flow*, 47. Pineridge Press, Swansea. [(v1) 158]

Everage, A. E., 1973, Theory of bicomponent flow of polymer melts, I. Equilibrium Newtonian tube flow, Trans. Soc. Rheol. **17**, 629. [(v1) 10, 11, 33, 38, 42]

Falco, R. E., J. C. Klewicki and D. G. Nocera, 1990, A study of flow properties of wet solids using laser-induced photochemical anemometry. Abstract at the NSF-DOE Workshop on Flow of Particulates and Fluids, Oct. 1-3, NIST, Gaithersburg, MD. [(v1) 6]

Feeny, B.F. and F. C. Moon, 1989, Autocorrelation on symbol dynamics for a chaotic dry friction oscillation, Phys. Letters A **141**(8),9. [(v1) 115, 138, 139]

Fortes, A., D. D. Joseph, and T. S. Lundgren, 1987, Nonlinear mechanics of fluidization of beds of spherical particles, J. Fluid Mech. **177**, 467. [(v1) 127]

Frei, H., and M. Schiffer, 1947, Separation by diffusion in fields of ultrasonic waves, Phys. Rev. **71**, 555. [(v2) 395]

Frenkel, A. L., 1988, Nonlinear saturation of core-annular flow instabilities, Proc. Sixth Symposium on Energy Engineering Sciences, Argonne National Laboratory. [(v1) 333; (v2) 11, 261-271]

Frenkel, A. L., A. J. Babchin, B. G. Levich, T. Shlang and G. I. Shivashinsky, 1987, Annular flows can keep unstable films from breakup: nonlinear saturation of capillary instability, J. Colloid and Interface Sci. **115**, 225. [(v1) 333; (v2) 11, 261, 267-271]

Freundlich, H., 1926, *Colloid and Capillary Chemistry*, Mathuen and Co. Ltd. London. [(v2) 337]

Fujimura, K., 1991a, Methods of centre manifold and multiple scales in the theory of weakly nonlinear stability for fluid motions, Proc. R. Soc. Lond. A **434**, 719. [(v1) 343]

Fujimura, K., 1991b, Nonlinear equilibrium solutions for travelling waves in a free convection between vertical parallel plates, Eur. J. Mech. B/Fluids **10**(2), 25. [(v1) 171]

Funatsu, K., and M. Sato, 1984, in *Advances in Rheology*, **4**, eds. B. Mena, A. Garcia-Rejon and C. Rangel-Nafaile, UNAM, Mexico, 465. [(v1) 376]

Galdi, G. P., D. D. Joseph, L. Preziosi and S. Rionero, 1991, Mathematical problems for miscible incompressible fluids with Korteweg stresses, European J. Mech. B/Fluids **10**(3). [(v2) 324, 351]

Galdi, G. P., and B. Straughn, eds., 1988, *Energy Stability and Convection*, Research Notes in Mathematics, Longman. [(v2) 56]

Garcia-Ybarra, P. L., and M. G. Velarde, 1987, Oscillatory Marangoni-Bénard interfacial instability and capillary-gravity waves in single- and two- component liquid layers with or without Soret thermal diffusion, Phys. Fluids **30** (6), 1649. [(v1) 171]

Garik, P., J. Hetrick, B. Orr, D. Barkey and E. Ben-Jacob, 1991, Interfacial cellular mixing and a conjecture on global deposit morphology, Phys. Rev. Lett. **66**(12), 1606. [(v2) 343]

Gebhart, B., 1961, 1971, *Heat Transfer*, second edition, McGraw-Hill Book Company. [(v1) 381]

Gemmell, A. R., and N. Epstein, 1962, Numerical analysis of stratified laminar flow of two immiscible Newtonian liquids in circular pipes, Can. J. Chem. Eng. **40**, 215. [(v1) 4; (v2) 4]

Ginzburg, V. L., and L. D. Landau, 1950, Zh. Eksper. i. Teor. Fiz. **20**. [(v2) 227]

Gjevik, B., 1970, Occurrence of finite-amplitude surface waves on falling liquid films, Phys. Fluids **13**, 1918. [(v1) 336]

Glass, W., 1961, Water addition aids pumping viscous oils, Chem. Eng. Prog. **57**, 116. [(v2) 6, 8]

Goenaga, A. and B. G. Higgins, 1991, Kinematic and dynamic constraints for flow separation from free surfaces and interfaces, paper no. 111c, AIChE 1991 Annual Meeting, Los Angeles. [(v1) 150]

Golub, G. H. and C. F. Van Loan, 1983, *Matrix computations*, Johns Hopkins University Press, Baltimore. [(v2) 241]

Golubitsky, M., and I. Stewart, 1985, Hopf bifurcation in the presence of symmetry, Arch. Rat. Mech. Anal. **87**, 107. [(v1) 176, 257]

Golubitsky, M., J. W. Swift and E. Knobloch, 1984, Symmetries and pattern selection in Rayleigh-Bénard convection, Physica 10D, 249. [(v1) 175, 176, 263]

Gorodtsov, V. A., and A. I. Leonov, 1967, On a linear instability of a plane parallel Couette flow of viscoelastic fluid, J. Appl. Math. Mech. **31**, 310. [(v1) 364-366]

Gottlieb, D., and S. A. Orszag, 1983, *Numerical analysis of spectral methods: theory and applications*, CBMS-NSF Regional Conference Series in Applied Math., SIAM. [(v1) 191, 373]

Goto, T., and N. Waku, 1985, The preparation of high transition temperature superconducting Pb-Bi-Ge alloy filaments using the method of glass-coated melt spinning, J. Mat. Science **20**, 532. [(v1) 12]

Grace, J.P., 1971, Dispersion phenomena in high viscosity immiscible fluid systems and application of static mixers as dispersion devices in such systems, Engng. Found. 3rd Res. Cong. Mixing, Andover, New Hampshire. [(v1) 143]

Graham, A. L., S. A. Altobelli, E. Fukushima, L. A. Mondy and T. S. Stephens, 1991, Note: NMR imaging of shear-induced diffusion and structure in concentrated suspensions undergoing Couette flow, J. Rheol. **35** (1), 191. [(v1) 7]

Greenspan, H., 1968, *The Theory of Rotating Fluids,* Cambridge University Press. [(v1) 16]

Griffiths, R. W., 1986 a, Thermals in extremely viscous fluids, including the effects of temperature-dependent viscosity, J. Fluid Mech. **166**, 115. [(v2) 326, 328, 332]

Griffiths, R. W., 1986 b, Particle motions induced by spherical convective elements in Stokes flow, J. Fluid Mech. **166**, 139. [(v2) 326]

Grimshaw, R., and A. P. Hooper, 1991, The non-existence of a certain class of travelling wave solutions of the Kuramoto-Sivashinsky equation, Physica D **50**(2), 231. [(v1) 337]

Guckenheimer, J., and P. Holmes, 1983, *Nonlinear Oscillations, Dynamical Systems, and Bifurcation of Vector Fields*, Springer, New York. [(v1) 176]

Guillopé, C., D. Joseph, K. Nguyen and F. Rosso, 1987, Nonlinear stability of rotating flow of two fluids, Journal de Mécanique théorique et appliquée **6** (5), 619. [(v1) 45, 56, 114, 117]

Gumerman, R. J., and G. M. Homsy, 1974, Convective instabilities in concurrent two-phase flow: Part I. Linear stability, AIChE J. **20**, 981; Part II. Global stability, AIChE J. **20**, 1161; Part III. Experiments, AIChE J. **20**, 1167. [(v1) 173, 196, 276, 278]

Han, C. D., 1973, A study of bicomponent coextrusion of molten polymers, J. Appl Polym. Sci. **17**, 1289. [(v1) 11]

Han, C. D., 1975, A study of coextrusion in a circular die, J. Appl. Polym. Sci. **19**, 1875. [(v1) 11]

Hansen, E. B., 1987, Stokes flow down a wall into an infinite pool, J. Fluid Mech. **178**, 243. [(v1) 164]

Happel, J., and H. Brenner, 1983, *Low Reynolds number hydrodynamics*, Martinus Nijhoff Publishers, Boston. [(v2) 155, 294]

Hassager, O., 1985, The motion of viscoelastic fluids around spheres and bubbles. In: A. S. Lodge, M. Renardy and J. A. Nohel (eds.), *Viscoelasticity and Rheology*, Academic Press, Orlando, 1. [(v1) 144]

Hasson, D., U. Mann and A. Nir, 1970, Annular flow of two immiscible liquids, I: Mechanisms, Canadian J. Chem. Eng. **48**, 514. [(v2) 8, 174]

Hasson, D., and A. Nir, 1970, Annular flow of two immiscible liquids, II: Analysis of core-liquid ascent, Canadian J. Chem. Eng. **48**, 521. [(v2) 8]

Hatzikiriankos, S. G., and J. M. Dealy, 1991, Wall slip of molten high density polyethylene. I. sliding plate rheometer studies, J. Rheol. **35** (4), 497. [(v1) 377]

Herbert, T., 1980, Nonlinear stability of parallel flows by higher order amplitude expansions, AIAA J. **18**, 243. [(v2) 240]

Hermanrud, B., 1981, The compound jet: a new method to generate fluid jets for ink jet printing, Report 1/1981, Dept. of Electrical Measurements, Lund Institute of Technology. [(v1) 11]

Hertz, C. H., and B. Hermanrud, 1983, A liquid compound jet, J. Fluid Mech. **131**, 271. [(v1) 11, 12]

Hesla, T. I., F. R. Pranckh and L. Preziosi, 1986, Squire's theorem for two stratified fluids, Phys. Fluids **29**, 2808. [(v1) 276, 277]

Heywood, N. I., 1986, A review of techniques for reducing energy consumption in slurry pipelining, Hydrotransport 10, Tenth International Conference on the Hydraulic Transport of Solids in Pipes, Innsbruck, Austria, Oct. 29-31, 319. [(v1) 8]

Hickox, C. E., 1971, Instability due to viscosity and density stratification in axisymmetric pipe flow, Phys. Fluids **14**, 251. [(v1) 269; (v2) 12, 13, 31, 50, 65, 132]

Hicks, E. M., J. F. Ryan, R. B. Taylor and R. L. Tichenor, 1960, Reversible crimp in an acrylic fiber, Textile Res. J. **30**, 675. [(v1) 11]

Hicks, E. M., E. A. Tippets, J. V. Hewett and R. H. Brand, 1967, *Man-made fibers*, Vol. 1, H. Mark, S. M. Atlas, and E. Cernia, Eds., Wiley (Interscience), New York. [(v1) 11]

Hiemenz, P. C., 1977, *Principles of Colloid and Surface Chemistry*, Marcel Dekker, Inc., New York. [(v2) 338-339]

Hinch, E. J., 1984, A note on the mechanism of the instability at the interface between two shearing fluids, J. Fluid Mech. **144**, 463. [(v1) 297]

Hinch, E.J. and A. Acrivos, 1979, Steady long slender droplets in two-dimensional straining motion, J. Fluid Mech. **91**, 401. [(v1) 143]

Hocking, L. M., and K. Stewartson, 1972, On the nonlinear response of a marginally unstable plane parallel flow to a two-dimensional disturbance, Proc. R. Soc. Lond. A. **326**, 289. [(v2) 240]

Hoffman, R. L., 1975, A study of the advancing interface. I. Interface shape in liquid-gas systems, J. Colloid Interface Sci. **50**, 228. [(v1) 166]

Holmes, P., 1986, Spatial structure of time - periodic solutions of the Ginzburg - Landau equation, Physica **23**D, 84. [(v2) 240-241]

Homsy, G., 1974, *Lectures in Applied Mathematics*, ed. A. C. Newell, Am. Math. Soc., volume 15, 191. [(v1) 270, 324]

Homsy, G., 1987, Viscous fingering in porous media, Ann. Rev. Fluid Mech. **19**, 271. [(v2) 374, 379]

Hooper, A. P., 1985, Long-wave instability at the interface between two viscous fluids: Thin layer effects, Phys. Fluids **28**, 1613. (Erratum, **28**, 3182) [(v1) 269, 270, 279, 290-296]

Hooper, A. P., 1988, A note on the energy stability equation for Couette flow of two superposed viscous fluids, *Energy Stability and Convection*, eds. G. P. Galdi and B. Straughn, Research Notes in Mathematics, Longman. [(v1) 271; (v2) 56]

Hooper, A. P., and W. G. C. Boyd, 1983, Shear flow instability at the interface between two viscous fluids, J. Fluid Mech. **128**, 507. [(v1) 199, 269, 270, 271, 290, 294, 296-302, 305-306, 320, 349; (v2) 34-35, 56, 106]

Hooper, A. P., and W. G. C. Boyd, 1987, Shear flow instability due to a wall and a viscosity discontinuity at the interface, J. Fluid Mech. **179**, 201. [(v1) 270, 303, 305-319; (v2) 36, 56, 80, 83, 106]

Hooper, A. P., and R. Grimshaw, 1985, Nonlinear instability at the interface between two viscous fluids, Phys. Fluids **28**, 3. [(v1) 270, 287, 324-338; (v2) 262-264]

Hooper, A. P., and R. Grimshaw, 1988, Traveling wave solutions of the Kuramoto-Sivashinsky equation, Wave Motion **10**, 405. [(v1) 337]

Hu, H., and D. D. Joseph, 1989 a, Lubricated pipelining: stability of core-annular flow. Part 2, J. Fluid Mech. **205**, 359. [(v1) 396; (v2) 13, 16, 50-84]

Hu, H., and D. D. Joseph, 1989 b, Stability of core-annular flow in a rotating pipe, Phys. Fluids A **1** (10), 1677. [(v2) 13, 16, 93-94]

Hu, H., and D. D. Joseph, 1992, Miscible displacement in a Hele-Shaw cell, Army High Performance Computing Research Center, University of Minnesota, Preprint 92-007. [(v2) 324]

Hu, H., T. Lundgren and D. D. Joseph, 1990, Stability of core-annular flow with a small viscosity ratio, Phys. Fluids A **2** (11), 1945. [(v2) 14, 16, 94-113]

Huang, A., and D. D. Joseph, 1992a, Instability of the equilibrium of a liquid below its vapor between horizontal heated plates, J. Fluid Mech., to appear. [(v1) 378-399]

Huang, A., and D. D. Joseph, 1992b, Stability of liquid-vapor flow down an inclined channel with phase change, Army High Performance Computing Research Center, University of Minnesota, Preprint 91-98. [(v1) 378-399]

Hurle, D. T. J., and E. Jakeman, 1971, Soret-driven thermosolutal convection, J. Fluid Mech. **47**, 667. [(v1) 171]

Hwang, C. C., and C.-I. Weng, 1987, Finite-amplitude stability analysis of liquid films down a vertical wall with and without interfacial phase change, Int. J. Multiphase Flow **13** (6), 803. [(v1) 378]

Iooss, G., and D. D. Joseph, 1990, *Elementary Stability and Bifurcation Theory*, second edition, Springer-Verlag New York, Inc. [(v1) 60, 61, 204, 241, 256, 343]

Isaacs, J. D., and J. B. Speed, 1904, Method of piping fluids, U. S. Patent No. 759,374. [(v2) 3]

ISF-85, 1985, *Proceedings of the International Symposium on Fiber Science and Technology*, The Society of Fiber Science and Technology, Hakone, Japan, Elsevier Applied Science Publishers. [(v1) 12]

Ishii, M., 1975, *Thermo-Fluid Dynamic Theory of Two-Phase Flow*, Eyrolles. [(v1) 381]

Jeong, J. T., and H. K. Moffatt, 1992, Free surface cusps associated with flow at low Reynolds number, submitted to J. Fluid Mech. [(v1) 140, 141, 143, 153, 154, 162, 168]

Jones, R. S., and O. D. J. Thomas, 1989, The coextrusion of two incompressible elastico-viscous fluids through a rectangular channel, J. Appl. Math. and Phys. (ZAMP) **40**, 425. [(v1) 11]

Joseph, D. D., 1973, Domain perturbations: the higher order theory of infinitesimal water waves, Arch. Rat. Mech. Anal. **51**, 295. [(v1) 184]

Joseph, D. D., 1976, *Stability of fluid motions* , I and II, Springer-Verlag New York, Inc. [(v1) 23, 24, 51, 115, 171, 203, 209, 272; (v2) 93]

Joseph, D. D., 1987, Two fluids heated from below, *Energy Stability and Convection*, eds. G. P. Galdi and B. Straughn, Research Notes in Mathematics, Longman. [(v1) 178; (v2) 57]

Joseph, D. D., 1988, videocassette on coal-oil dispersions. [(v1) 9]

Joseph, D. D., 1990 a, *Fluid Dynamics of Viscoelastic Liquids*, Springer-Verlag New York, Inc. [(v1) 15, 18, 25, 184, 361; (v2) 382]

Joseph, D. D., 1990 b, Fluid dynamics of two miscible liquids with diffusion and gradient stresses, Eur. J. Mech. B/Fluids **9** (6), 565. [(v2) 324-365, 369]

Joseph, D. D., 1990 c, Separation in flowing fluids, Nature **348**, 487. [(v1) 6]

Joseph, D. D., 1992, Understanding cusped interfaces, J. Non-Newt. Fluid Mech., to appear. [(v1) 152, 153]

Joseph, D. D., M. Arney, G. Gillberg, H. Hu, D. Huttman, C. Verdier and H. Vinagre, 1992, A spinning drop extensiotensiometer, J. Rheology. [(v1) 83]

Joseph, D. D., M. Arney and G. Ma, 1992, Upper and lower bounds for interfacial tension using spinning drop devices, J. Colloid and Interface Science **148**(1), 291. [(v1) 81]

Joseph, D. D., and G. S. Beavers, 1977, Free surface problems in rheological fluid mechanics, Rheol. Acta **16**, 169. [(v1) 15]

Joseph, D. D., G. S. Beavers, A. Cers, C. Dewald, A. Hoger and P. T. Than, 1984, Climbing constants for various liquids, J. Rheol. **28** (4), 325. [(v1) 15]

Joseph, D. D., and S. Carmi, 1969, Stability of Poiseuille flow in pipes, annuli and channels, Q. Appl. Math. **XXVI**(4), 576. [(v2) 93]

Joseph, D. D., and H. Hu, 1991, Interfacial tension between miscible liquids, Army High Performance Computing Research Center, University of Minnesota, preprint 91-58; Non-solenoidal effects and Korteweg stresses in simple mixtures of incompressible liquids, preprint 91-03. [(v2) 324-378]

Joseph, D. D., T. S. Lundgren, R. Jackson and D. A. Saville, 1990, Ensemble averaged and mixture theory equations for incompressible fluid-particle suspensions, Int. J. Multiphase Flow **16** (1), 35. [(v2) 352, 354, 356]

Joseph, D. D., J. Nelson, M. Renardy and Y. Renardy, 1991, Two-dimensional cusped interfaces, J. Fluid Mech. **223**, 383. [(v1) 140, 145, 152]

Joseph, D. D., K. Nguyen and G. S. Beavers, 1984, Nonuniqueness and stability of the configuration of flow of immiscible fluids with different viscosities, J. Fluid Mech. **141**, 319. [(v1) 3, 27, 29, 31, 34, 45, 95, 101, 111; (v2) 187]

Joseph, D. D., K. Nguyen and G. S. Beavers, 1986, Rollers, Phys. Fluids **29**, 2771. [(v1) 45]

Joseph, D. D., and L. Preziosi, 1987, Stability of rigid motions and coating films in bicomponent flows of immiscible liquids, J. Fluid Mech. **185**, 323. [(v1) 45, 48, 52, 69, 71, 77, 114]

Joseph, D. D., M. Renardy and Y. Renardy, 1984, Instability of the flow of immiscible liquids with different viscosities in a pipe, J. Fluid Mech. **141**, 309; 1983, Mathematics Research Center Technical Summary Report 2503, University of Wisconsin. [(v1) 40, 42; (v2) 13, 16, 18, 29, 30, 59, 130]

Joseph, D. D., M. Renardy, Y. Renardy and K. Nguyen, 1985, Stability of rigid motions and rollers in bicomponent flows of immiscible

liquids, J. Fluid Mech. **153**, 151. [(v1) 45, 52, 63, 65, 95]

Joseph, D. D., and D. H. Sattinger, 1972, Bifurcating time periodic solutions and their stability, Arch. Rat. Mech. Anal. **45**, 79. [(v2) 240]

Joseph, D. D., and J.-C. Saut, 1990, Short-wave instabilities and ill-posed initial-value problems, Theoretical and Computational Fluid Dynamics **1**, 191. [(v1) 297; (v2) 13, 382]

Joseph, D. D., P. Singh and K. Chen, 1990, Couette flows, rollers, emulsions, tall Taylor cells, phase separation and inversion, and a chaotic bubble in Taylor-Couette flow of two immiscible liquids, in *Nonlinear Evolution of Spatio-temporal Structures in Dissipative Continuous Systems*, ed. F. H. Busse and L. Kramer, Plenum Press, New York. [(v1) 114]

Kao, T. W., 1965 a, Stability of two-layer viscous stratified flow down an inclined plane, Phys. Fluids **8**, 812. [(v1) 272]

Kao, T. W., 1965 b, Role of the interface in the stability of stratified flow down an inclined plane, Phys. Fluids **8** (12), 2190. [(v1) 272]

Kao, T. W., 1968, Role of viscosity stratification in the stability of two-layer flow down an incline, J. Fluid Mech. **33**, 561. [(v1) 272]

Kao, T. W., and C. Park, 1972, Experimental investigations of the stability of channel flows. Part 2. Two-layered co-current flow in a rectangular channel, J. Fluid Mech. **52**, 401. [(v1) 4, 287; (v2) 4]

Karnis, A., H. L. Goldsmith and S. G. Mason, 1966, The kinetics of flowing dispersions: I. Concentrated suspensions of rigid particles, J. Colloid and Interf. Sci. **22**, 531. [(v1) 6]

Kawahara, T., 1983, Formation of saturated solutions in a nonlinear dispersive system with instability and dissipation, Phys. Rev. Lett. **51**, 381. [(v1) 334-336]

Kelly, R. E., D. A. Goussis, S. P. Lin and F. K. Hsu, 1989, The mechanism for surface wave instability in film flow down an inclined plane, Phys. Fluids A **1**, 819. [(v1) 271]

Kennedy, R. J., 1966, Towards an analysis of plug flow through a pipe, Can. J. Chem. Eng., December 1, 354. [(v1) 7]

Kevorkian, J. and J. D. Cole, 1980, *Perturbation Methods in Applied Mathematics*, Springer, Berlin. [(v2) 99]

Khan, A. A. and C. D. Han, 1976, On the interface deformation in the stratified two-phase flow of viscoelastic fluids, Trans. Soc. Rheol. **20**:4, 595. [(v1) 11]

Khan, A. A. and C. D. Han, 1977, A study on the interfacial instability in the stratified flow of two viscoelastic fluids through a rectangular duct, Trans. Soc. Rheol. **21**, 101. [(v1) 359]

Knappe, W., and E. Krumbock, 1984, in *Advances in Rheology*, eds. B. Mena, A. Garcia-Rejon and C. Rangel-Nafaile, UNAM, Mexico, **4**, 417. [(v1) 376]

Knobloch, E., 1980, Convection in binary fluids, Phys. Fluids **23** (9), 1918. [(v1) 172]

Koh, C. J., and L. G. Leal, 1990, An experimental investigation on the stability of viscous drops translating through a quiescent fluid, Phys. Fluids A **2**(12), 2103. [(v2) 295, 326, 328, 333]

Kohn, R. V., and R. Lipton, 1986, The effective viscosity of a mixture of two Stokes fluids, in *Advances in Multiphase Flow and Related Problems*, ed. G. Papanicolaou, SIAM, 123. [(v1) 42]

Kojima, M., E. J. Hinch and A. Acrivos, 1984, The formation and expansion of a toroidal drop moving in a viscous fluid, Phys. Fluids **27** (1), 19. [(v2) 290, 292, 309, 361-362, 372]

Korteweg, D., 1901, Sur la forme que prennent les equations du mouvement des fluids si l'on tient compte des forces capillaires causees par des variations de densite, Arch. Neerl. Sciences Exactes et Naturelles, Series II **6**, 1. [(v2) 325, 334-337, 363, 369]

Krantz, W. B., and S. L. Goren, 1970, Industrial Engineering Chem. Fundamentals **9**, 107. [(v1) 324]

Krishna, M. V. G., and S. P. Lin, 1977, Nonlinear stability of a viscous film with respect to three-dimensional side-band disturbances, Phys. Fluids **20** (7), 1039. [(v1) 324]

Kuramoto, Y., and T. T. Tsuzuki, 1976, Persistent propagation of concentration waves in dissipative media far from thermal equilibrium, Prog. Theor. Phys. **55**, 356. [(v1) 333]

Lamb, H., 1932, *Hydrodynamics*, Cambridge University Press. [(v1) 142]

Landau, L. D., and E. M. Lifshitz, 1959, *Fluid Mechanics*, Pergamon Press. [(v2) 354, 357-358]

LaQuey, R. E., S. M. Mahajan, P. H. Rutherford and W. M. Tang, 1975, Nonlinear saturation of trapped-ion mode, Phys. Rev. Lett. **34**, 391. [(v1) 270, 333]

Leach, R. W., 1957, Pipeline designed for viscous crude, The Pipeline Engineer, November. [(v2) 5]

Leal, L.G., J. Skoog and A. Acrivos, 1971, On the motion of gas bubbles in a viscoelastic liquid, Can. J. Chem. Engng. **49**, 569. [(v1) 144]

Lebovitz, N. R., 1982, Perturbation expansions on perturbed domains, SIAM Review **24**, 381. [(v1) 184]

Lee, G. W. T., P. Lucas and A. Tyler, 1983, Onset of Rayleigh-Bénard convection in binary liquid mixtures of ^{3}He in ^{4}He, J. Fluid Mech. **135**, 235. [(v1) 171]

Lee, B. L., and J. L. White, 1974, An experimental study of rheological properties of polymer melts in laminar shear flow and of interface deformation and its mechanisms in two-phase stratified flow, Trans. Soc, Rheol. **18:3**, 467. [(v1) 11]

Leighton, D., and A. Acrivos, 1986, Viscous resuspension, Chem. Eng. Sci. **41**, 1377. [(v1) 7]

Leslie, F., 1985, Measurements of rotating bubble shapes in a low-gravity environment, J. Fluid Mech. **161**, 269. [(v1) 76]

Li, C.-H., 1969 a, Stability of two superposed elasticoviscous liquids in plane Couette flow, Phys. Fluids **12**, 531. [(v1) 269, 360]

Li, C.-H., 1969 b, Instability of three-layer viscous stratified flow, Phys. Fluids **12**, 2473. [(v1) 272, 279]

Li, C.-H., 1970, Role of elasticity on the stability of stratified flow of viscoelastic fluids, Phys. Fluids **13**, 1701. [(v1) 269, 272, 359]

Lin, S. P., 1969, Finite amplitude stability of a parallel flow with a free surface, J. Fluid Mech. **36**, 113. [(v1) 324, 336]

Lin, S. P., 1983 a, Effects of surface solidification on the stability of multilayered liquid films, J. Fluids Engng. **105**, 119. [(v1) 272]

Lin, S. P., 1983 b, Film waves, in *Waves on Fluid Interfaces*, R. E. Meyer ed., Academic Press Inc. [(v1) 272]

Lin, S. P., and E. A. Ibrahim, 1990, Instability of a viscous liquid jet surrounded by a viscous gas in a vertical pipe, J. Fluid Mech. **218**, 641. [(v2) 13]

Lin, S. P., and M. V. G. Krishna, 1977, Stability of a liquid film with respect to initially finite three-dimensional disturbances, Phys. Fluids **20** (12), 2005. [(v1) 324]

Lin, S. P., and C. Y. Wang, 1983, Modeling wavy film flows, in *Encyclopedia of Fluid Mechanics*, chapter 28. [(v1) 272]

Lions, J. L., and E. Magenes, 1972, *Non-Homogeneous Boundary Value Problems and Applications*, Springer-Verlag. [(v1) 58]

Lister, J. R., 1987, Long-wavelength instability of a line plume, J. Fluid Mech. **175**, 413. [(v2) 15]

Loewenherz, D. S., and C. J. Lawrence, 1989, The effect of viscosity stratification on the stability of a free surface flow at low Reynolds number, Phys. Fluids A **1**(10), 1686. [(v1) 16, 272]

Looman, M. D., 1916, Method of conveying oil, U. S. Patent No. 1,192,438. [(v2) 3]

Lundgren, T. S., and N. N. Mansour, 1990, Vortex ring bubbles, J. Fluid Mech. **224**, 177. [(v2) 290]

Lurie K., A. V. Cherkaev and A. V. Fedorov, 1982, Regularization of optimal design problems for bars and plates, J. Opt. Theor. Appl. **37**, 499. [(v1) 42]

Mackrodt, P. A., 1976, Stability of Hagen-Poiseuille flow with a superimposed rigid rotation, J. Fluid Mech. **73**, 153. [(v2) 93]

MacLean, D. L., 1973, A theoretical analysis of bicomponent flow and the problem of interface shape, Trans. Soc. Rheol. **17:3**, 385. [(v1) 11, 33, 38]

Macosko, C. W., M. A. Ocansey and H. H. Winter, 1982, Steady planar extension with lubricated dies, J. Non-Newtonian Fluid Mech. **11**, 301. [(v1) 13]

Manfré, G., G. Servi and C. Ruffino, 1974, Copper microwires spun from the melt, J. Mat. Sci. **9**, 74. [(v1) 12]

Manneville, P., 1981, Statistical properties of chaotic solutions of a one-dimensional model for phase turbulence, Phys. Lett. **84A**, 129. [(v1) 333]

May, S. E. and J. V. Maher, 1991, Capillary wave relaxation for a meniscus between miscible liquids, submitted to Phys. Rev. Lett. [(v2) 343]

Merkle, C. L., and S. Deutsch, 1990, Drag reduction in liquid boundary layers by gas injection, in *Viscous Drag Reduction in Boundary Layers*, ed. D. M. Bushnell and J. M. Hefner **123**, Progress in Astronautics and Aeronautics, published by AIAA, 351. [(v1) 5]

Mhatre, M.V. and R. C. Kintner, 1959, Fall of liquid drops through pseudoplastic liquids, Ind. Engng. Chem. **51**, 865. [(v1) 144]

Michael, H.D., 1958, The separation of a viscous liquid at a straight edge, Mathematika **5**, 82. [(v1) 151]

Miesen, R., G. Beijnon, P. E. M. Duijvestijn, R. V. A. Oliemans and T. Verheggen, 1991, Interfacial waves in core-annular flow, J. Fluid Mech. to appear. [(v2) 14, 94]

Miles, J. W., 1960, The hydrodynamic stability of a thin film, J. Fluid Mech. **8**, 593. [(v1) 338]

Miller, M. C., 1990, Elimination of viscous liquid-fill flight instability by means of lower viscosity, immiscible liquid additives, Proceedings of the 1990 U.S. Army Chemical Research, Development and Engineering Center Scientific Conference on Chemical Defense Research (preprint). [(v1) 16]

Minagawa, N., and J. L. White, 1975, Coextrusion of unfilled and TiO_2-filled polyethylene: influence of viscosity and die cross-section on interface shape, Poly. Eng. and Sci. **15**, 825. [(v1) 11]

Moffatt, H. K., 1977, Behavior of a viscous film on the outer surface of a rotating cylinder, J. de Mécanique **16** (5), 651. [(v1) 31, 48, 49, 66, 85, 86, 87, 88, 92, 110]

Moller, K., and G. G. Duffy, 1978, An equation for predicting transition-regime pipe friction loss, Tappi **61** (1), 63. [(v1) 8]

Moon, H. T., 1982, Transition to chaos in the Ginzburg-Landau equation, Ph. D. thesis, University of Southern California. [(v2) 240]

Moon, H. T., P. Huerre and L. G. Redekopp, 1983, Transition to chaos in the Ginzburg-Landau equation, Physica **7D**, 135. [(v2) 228]

Moynihan, R. H., D. G. Baird and R. R. Ramanathan, 1990, Additional observations on the surface melt fracture behavior of linear low-density polyethylene, J. Non-Newtonian Fluid Mech. **36**, 256. [(v1) 375-376]

Nagata, W., and J. W. Thomas, 1986, Bifurcation in doubly-diffusive systems, Parts I and II, SIAM J. Math. Anal. **17**, 91; Part III, ibid, 289. [(v1) 171, 176, 243]

Nakoryakov, V. Ye., and S. V. Alekseyenko, 1981, Waves on a film flowing down an incline, Fluid Mech. **10** (3), 18. [(v1) 270, 324]

Nataf, H. C., S. Moreno and Ph. Cardin, 1988, What is responsible for thermal coupling in layered convection?, J. Phys. France **49**, 1707. [(v1) 175]

Nelson, J., P. Mohr and D. D. Joseph, 1992, Nonlinear stability of two fluids in a combined Couette-Poiseuille flow, in preparation. [(v1) 320]

Newell, A. C., 1974, Envelope equations, in Lectures in Applied Math. **15**, ed. A. C. Newell, 157. [(v2) 235, 240]

Newell, A. C., 1985, *Solitons in mathematics and physics*, CBMS-NSF Regional Conference Series in Applied Mathematics, SIAM publication. [(v2) 241]

Newell, A. C., T. Passot and M. Souli, 1989, The phase diffusion and mean drift equations for convection at finite Rayleigh numbers in large containers I. private communication. [(v2) 243]

Newell, A. C., and J. A. Whitehead, 1969, Finite bandwidth, finite amplitude convection, J. Fluid Mech. **38**, 279. [(v2) 227]

Norman, B., K. Moller, R. Ek and G. G. Duffy, 1977, Hydrodynamics of papermaking fibers in water suspension, paper presented to the Sixth Fundamental Research Symposium, B. P., B. M. A., Oxford, England, September. [(v1) 8]

Northrup, E., 1912, A photographic study of vortex rings in liquids, Nature **88**, 463. [(v2) 308, 313]

Nunziato, J., S. Passman, C. Givler, D. MacTigue and J. Brady, 1986, Continuum theories for suspensions. In *Advancements in Aerodynamics, Fluid Mechanics and Hydraulics* (Proc. ASCE Special Conf., Minneapolis, Minn.) Ed. R. Arndt, A. Stefan, C. Farrell and S. N. Peterson, 465. [(v2) 352]

O'Brien, V., 1961, Why raindrops break up – vortex instability, J. of Meteorology **18**, 549. [(v2) 290, 292, 308, 313]

O'Brien, V., 1985, On spheroidal gravity-driven vortices, personal communication. [(v2) 309]

Oliemans, R. V. A., 1986, *The Lubricating Film Model for Core-Annular Flow*, Delft University Press. [(v1) 5, 338; (v2) 1, 195-196, 200]

Oliemans, R. V. A., and G. Ooms, 1986, Core-annular flow of oil and water through a pipeline, *Multiphase Science and Technology*, Vol.2, eds. G. F. Hewitt, J. M. Delhaye and N. Zuber, Hemisphere Publishing Corporation. [(v1) 4, 5; (v2) 1, 19]

Oliemans, R. V. A., G. Ooms, H. L. Wu and A. Duÿvestin, 1985, Core-annular oil/water flow: the turbulent-lubricating model and measurements in a 2 in. pipe loop, presented at the Society of Petroleum Engineers 1985 Middle East Oil Technical Conference and Exhibition, held in Bahrain, March 11 - 14, 1985. [(v2) 7, 10]

Onishi, Y., 1984, 14th International Symposium on Rarefied Gas Dynamics, Tsukuba, Japan. [(v1) 381]

Ooms, G., 1971, Fluid-mechanical studies of core-annular flow, Ph. D. Thesis, Delft University of Technology. [(v2) 12]

Ooms, G., A. Segal, S. Y. Cheung and R. V. A. Oliemans, 1985, Propagation of long waves of finite amplitude at the interface of two viscous fluids, Int. J. Multiphase Flow, 481. [(v1) 5, 271, 338; (v2) 11]

Ooms, G., A. Segal, A. J. Van der Wees, R. Meerhoff and R. V. A. Oliemans, 1984, A theoretical model for core-annular flow of a very viscous oil core and a water annulus through a horizontal pipe, Int. J. Multiphase Flow **10**, 41. [(v1) 338; (v2) 10]

Orszag, S. A., 1971, Accurate solutions of the Orr-Sommerfeld stability equation, J. Fluid Mech. **50**, 689. [(v1) 191, 303, 342, 350; (v2) 28]

Orszag, S. A., and L. C. Kells, 1980, Transition to turbulence in plane Poiseuille and Couette flow, J. Fluid Mech. **96**, 159. [(v2) 28]

Pao, Y. P., 1971, Application of kinetic theory to the problem of evaporation and condensation, Phys. Fluids **14**, 306. [(v1) 381]

Papageorgiou, D. T., C. Maldarelli and D. S. Rumschitzki, 1990, Nonlinear interfacial stability of core annular film flows, Phys. Fluids A **2**, 340. [(v2) 11, 98, 261, 268-271]

Papageorgiou, D. T., and Y. S. Smyrlis, 1991, The route to chaos for the Kuramoto-Sivashinsky equation, Theoret. Comput. Fluid Dynamics **3**, 15. [(v1) 337]

Palmquist, K. E., and S. F. Kistler, 1992, Formation of cusped interface by liquid film plunging into a pool. [(v1) 140, 141, 153, 157, 162, 169]

Passman, S., J. W. Nunziato and E. K. Walsh, 1984, A theory for multiphase mixtures. In *Rational Thermodynamics.* Ed. C. Truesdell, Springer Verlag, New York, 286. [(v2) 352]

Pearlstein, A. J., 1985, On the two-dimensionality of the critical disturbances for stratified viscous plane parallel shear flows, Phys. Fluids **28**, 751. [(v1) 276]

Pearlstein, A. J., 1987, American Physical Society Division of Fluid Dynamics Annual Meeting, Paper HC6; Bull. Am. Phys. Soc. **32**, 2087. [(v1) 276]

Pedley, T. J., 1968, The toroidal bubble, J. Fluid Mech. **32**, 97. [(v2) 290]

Pedley, T. J., 1969, On the instability of viscous flow in a rapidly rotating pipe, J. Fluid Mech. **35**, 97. [(v2) 93]

Pekeris, C. L., and B. Shkoller, 1967, Stability of plane Poiseuille flow to periodic disturbances of finite amplitude in the vicinity of the neutral curve, J. Fluid Mech. **29**, 31. [(v1) 346]

Pellew, A. and R. V. Southwell, 1940, On maintained convective motion in a fluid heated from below, Proc. Roy. Soc. A **176**, 312. [(v1) 171]

Pérez-Garcia, C., J. Pantaloni, R. Occelli and P. Cerisier, 1985, Linear analysis of surface deflection in Bénard-Marangoni instability, J. Phys. (Paris) **46**, 2047. [(v1) 173]

Petrie, C. J. S., and M. M. Denn, 1976, Instabilities in polymer processing, AIChE J. **22**, 209. [(v1) 375]

Philippoff, W., 1937, The viscosity characteristics of rubber solutions, Rubber Chem. Tech. **10**, 76. [(v1) 144]

Pipkin, A., and R. Tanner, 1972, A survey of theory and experiment in viscometric flows of viscoelastic liquids, Mech. Today **1**, 262. [(v1) 15]

Plateau, J. A. F., 1863, Experimental and theoretical researches on the figures of equilibrium of a rotating liquid mass withdrawn from the action of gravity, Annual Report of the Board of Regents of the Smithsonian Institution, Washington, DC, 270. [(v1) 67, 90]

Plateau, J. A. F., 1873, *Statique Expérimentale et Théorique des Liquides*, Gauthier-Villars. [(v1) 27]

Plesset, M. S., and S. A. Zwick, 1954, The growth of vapor bubbles in superheated liquids, J. Applied Phys. **25**(4), 493. [(v1) 381]

Porteous, K. C., and M. M. Denn, 1972, Linear stability of plane Poiseuille flow of viscoelastic liquids, Trans. Soc. Rheol. **16**, 295. [(v1) 361]

Power, H., and M. Villegas, 1990, Viscous-inviscid model for the linear stability of core-annular flow, ZAMP **41**, 1. [(v2) 13]

Pozrikidis, C., 1990, The instability of a moving viscous drop, J. Fluid Mech., **210**, 1. [(v2) 295, 328, 361, 372]

Preziosi, L., 1986, Ph. D. thesis, University of Minnesota. [(v1) 71]

Preziosi, L., K. Chen and D. D. Joseph, 1989, Lubricated pipelining: stability of core-annular flow, J. Fluid Mech. **201**, 323. [(v2) 13, 16-49, 59]

Preziosi, L., and D. D. Joseph, 1988, The run-off condition for coating and rimming flows, J. Fluid Mech. **187**, 99. [(v1) 76, 85, 90, 92]

Preziosi, L., and F. Rosso, 1991, Interfacial stability in a two-layer shearing flow between sliding pipes, Eur. J. Mech., B Fluids **10** (3), 269. [(v2) 14]

Princen, H. M., I. Y. Z. Zia and S. G. Mason, 1967, Measurements of interfacial tension from the shape of a rotating liquid drop, J. Colloid Interface Sci. **23**, 99. [(v1) 78]

Pukhnachov, V. V., 1991, Mathematical model of natural convection under low gravity, University of Minnesota Institute for Mathematics and Its Applications Preprint 796. [(v2) 352]

Pumir, A., P. Manneville and Y. Pomeau, 1983, On solitary waves running down an inclined plane, J. Fluid Mech. **135**, 27. [(v1) 333]

Quincke, G., 1902, Die Oberfächenspannung an der Grenze von Alkohol mit wässerigen Salzlösungen, Ann. Phys. **9**, 1. [(v2) 338]

Raitum, U. E., 1978, The extension of extremal problems connected with a linear elliptic equation, Sov. Math. Dokl. **19**, 1342. [(v1) 42]

Raitum, U. E., 1979, On optimal control problems for linear elliptic equations, Sov. Math. Dokl. **20**, 129. [(v1) 42]

Rallison, J.M. and A. Acrivos, 1978, A numerical study of the deformation and burst of a viscous drop in an extensional flow, J. Fluid Mech. **89**, 191. [(v1) 143]

Ramamurthy, A. V., 1986, Wall slip in viscous fluids and influence of materials of construction, J. Rheol. **30** (2), 337. [(v1) 377]

Ranger, K. B., and A. M. J. Davis, 1979, Steady pressure driven two-phase stratified laminar flow through a pipe, Can. J. Chem. Eng. **57**, 688. [(v2) 4]

Rasenat, S., 1987, Konvektion in zwei Geschichteten Flüssigkeiten, Diplomarbeit, University of Bayreuth. [(v1) 175]

Rayleigh, Lord, 1879, On the instability of jets, Proc. Roy. London Math. Soc., **10**, 4. [(v2) 38, 48]

Rayleigh, Lord, 1914, The equilibrium of revolving liquid under capillary force, Phil Mag. **28**, 161. [(v1) 72]

Rayleigh, Lord, 1916, On convection currents in a horizontal layer of fluid, when the higher temperature is on the under side, Phil. Mag. (6) **32**, 529. [(v1) 171]

Reid, W. H., and D. L. Harris, 1958, Some further results on the Bénard problem, Phys. Fluids **1**, 102. [(v1) 171, 192, 194]

Renardy, M., and D. D. Joseph, 1986, Hopf bifurcation in two-component flows, SIAM J. Math. Anal. **17**, 894. [(v1) 183, 245; (v2) 19, 51]

Renardy, M., and Y. Renardy, 1986, Linear stability of plane Couette flow of an upper convected Maxwell fluid, J. Non-Newtonian Fluid Mech. **22**, 23. [(v1) 363, 364]

Renardy, M., and Y. Renardy, 1988, Bifurcating solutions in a two-layer Bénard problem, Physica D **32**, 227. [(v1) 201-202, 236-267, 269]

Renardy, M., and Y. Renardy, 1992, Pattern selection in the Bénard problem for a viscoelastic fluid, Zeitschrift für Angewandte Mathematik und Physik **43**(1), 154. [(v1) 171]

Renardy, Y., 1985, Instability at the interface between two shearing fluids in a channel, Phys. Fluids **28**, 3441. [(v1) 270, 304, 320; (v2) 80]

Renardy, Y., 1986, Interfacial stability in a two-layer Bénard problem, Phys. Fluids **29**, 356. [(v1) 222-235]

Renardy, Y., 1987 a, The thin-layer effect and interfacial stability in a two-layer Couette flow with similar liquids, Phys. Fluids **30**, 1627. [(v1) 304]

Renardy, Y., 1987 b, Viscosity and density stratification in vertical plane Poiseuille flow, Phys. Fluids **30**, 1638. [(v2) 14, 15, 115-116, 130, 138, 145, 167, 171]

Renardy, Y., 1988 a, Instabilities in steady flows of two fluids, Rocky Mount. J. Math. **18**, Spring, 455. [(v1) 174]

Renardy, Y., 1988 b, Stability of the interface in two-layer Couette flow of upper convected Maxwell liquids, J. Non-Newt. Fluid Mech. **28**, 99. [(v1) 271, 359-375]

Renardy, Y., 1989, Weakly nonlinear behavior of periodic disturbances in two-layer Couette-Poiseuille flow, Phys. Fluids A **1**, 1666. [(v1) 270, 271, 338-359; (v2) 51]

Renardy, Y., and D. D. Joseph, 1985 a, Two-fluid Couette flow between concentric cylinders, J. Fluid Mech. **150**,381. [(v1) 31, 114, 117, 118, 269, 270, 296, 303; (v2) 36]

Renardy, Y., and D. D. Joseph, 1985 b, Oscillatory instability in a two-fluid Bénard problem, Phys. Fluids **28**, 788. [(v1) 173, 174, 269, 296]

Renardy, Y., and M. Renardy, 1985, Perturbation analysis of steady and oscillatory onset in a Bénard problem with two similar liquids, Phys. Fluids **28**,2699. [(v1) 203-235, 269]

Reynolds, W. C., and M. C. Potter, 1967, Finite-amplitude instability of parallel shear flows, J. Fluid Mech. **27**, 465. [(v1) 346-347]

Richardson, S., 1968, Two-dimensional bubbles in slow viscous flows, J. Fluid Mech. **33**, 475. [(v1) 141, 142, 144]

Richter, F. M., and C. E. Johnson, 1974, Stability of a chemically layered mantle, J. Geophys. Res. **79**, 1635. [(v1) 15]

Roberts, M., J. W. Swift and D. H. Wagner, 1986, The Hopf bifurcation on a hexagonal lattice, *Multiparameter Bifurcation Theory*, AMS Series: Contemporary Mathematics, eds. M. Golubitsky and J. M. Guckenheimer, Vol. 56, 283. [(v1) 176, 177, 239, 242, 243]

Robinson, I., 1976, An algorithm for automatic integration using the adaptive Gaussian technique, Aust. Comput. J. **8**, 106. [(v2) 107]

Romanov, V. A., 1973, Stability of plane parallel Couette flow, Func. Anal. and Its Applic. **7**, 137. [(v1) 277]

Rosenthal, D. K., 1962, The shape and stability of a bubble at the axis of a rotating liquid, J. Fluid Mech. **12**, 358. [(v1) 72, 78]

Ross, D. K., 1968, The shape and energy of a revolving liquid mass held together by surface tension, Austral. J. Phys. **21**, 823. [(v1) 72]

Rothman, D. H., and J. M. Keller, 1988, Immiscible cellular-automaton fluids, J. Statistical Physics **52** (3/4), 1119. [(v1) 6]

Rowell, R. L., S. R. Vasconcellos, R. J. Sala and R. S. Farinato, 1981, Surfactant effectiveness on coal-oil mixture stability measured with a sedimentation column device, Ind. Eng. Chem. Process Res. Dev., **20**, 283. [(v1) 9]

Ruelle, D., 1973, Bifurcations in the presence of a symmetry group, Arch. Rat. Mech. Anal. **51**, 136. [(v1) 174, 178]

Rumscheidt, F.D. and S. G. Mason, 1961, Particle motion in sheared suspensions. XII. Deformation and burst of fluid drops in shear and hyperbolic flow, J. Colloid Sci. **16**, 238. [(v1) 143]

Russell, T. W. F., and M. E. Charles, 1959, The effect of the less viscous liquid in the laminar flow of two immiscible liquids, Can. J. Chem. Eng. **39**, 18. [(v1) 4, 6, 33; (v2) 4, 6, 187]

Russell, T. W. F., G. W. Hodgson and G. W. Govier, 1959, Horizontal pipeline flow of mixtures of oil and water, Can. J. Chem. Eng. **37**, 9. [(v1) 3, 4; (v2) 4, 6, 196]

Russo, M. J. and P. H. Steen, 1986, Instability of rotund capillary bridges to general disturbances, experiment and theory, J. Colloid Interface Sci. **113**, 154. [(v1) 90]

Russo, M. J., and P. H. Steen, 1989, Shear stabilization of the capillary breakup of a cylindrical interface, Phys. Fluids A **1**(12), 1926. [(v2) 13]

Saffman, P., and G. I. Taylor, 1958, The penetration of a fluid into a porous medium or a Hele-Shaw cell containing a more viscous liquid, Proc. Roy. Soc., **A245**, 312. [(v1) 2]

Salwen, H., F. W. Cotton and C. E. Grosch, 1980, Linear stability of Poiseuille flow in a circular pipe, J. Fluid Mech. **98**, 273. [(v2) 30]

Salwen, H. and C. E. Grosch, 1972, The stability of Poiseuille flow in a pipe of circular cross-section, J. Fluid Mech. **54**, 93. [(v2) 30]

Saric, W. S., and B. W. Marshall, 1971, An experimental investigation of the stability of a thin liquid layer adjacent to a supersonic stream, A. I. A. A. J. **9**, 1546. [(v1) 338]

Schechter, R. S., M. G. Velarde and J. K. Platten, 1974, The two component Bénard problem, Adv. Chem. Phys. **26**, 265. [(v1) 171]

Schlichting, H., 1960, *Boundary Layer Theory*, Pergamon Press, New York. [(v2) 192]

Schrage, R., 1953, *A Theoretical Study of Interphase Mass Transfer*, Columbia University Press. [(v1) 381]

Schreiber, H. P., and S. H. Storey, 1965, Molecular fractionation in capillary flow of polymer fluids, Polymer Letters **3**, 723. [(v1) 376]

Schreiber, H. P., S. H. Storey and E. B. Bagley, 1966, Molecular fractionation in the flow of polymeric fluids, Transactions of the Soc. of Rheol. **10**:1, 275. [(v1) 376]

Schrenk, W. J., and T. Alfrey, 1978, Coextruded multilayer polymer films and sheets, in *Polymer Blends*, vol. 2, D. R. Paul and N. Seymour, eds., Academic Press, New York, 129. [(v1) 11]

Schubert, G., and J. Strauss, 1980, Gravitational stability of water over steam in vapor-dominated geothermal systems, J. Geophys. Res. **85**, 6505. [(v1) 378, 399]

Schulten, A., D. G. M. Anderson and R. G. Gordon, 1979, An algorithm for the evaluation of the complex Airy function, J. Comp. Phys. **31**, 60. [(v2) 107]

Scriven, L. E., and C. V. Sternling, 1964, On cellular convection driven by surface tension gradients: effects of mean surface tension and surface viscosity, J. Fluid Mech. **19**, 321. [(v1) 171]

Segel, L. A., 1969, Distant side-walls cause slow amplitude modulation of cellular convection, J. Fluid Mech. **38**, 203. [(v2) 227]

Segré, G., and A. Silberberg, 1962, Behavior of macroscopic rigid spheres in Poiseuille flow. Part 1: Determination of local concentration by statistical analysis of particle passages through crossed light beams, J. Fluid Mech. **14**, 115. Part 2: Experimental results and interpretation, J. Fluid Mech. **14**, 136. [(v1) 6]

Segur, J. B., 1953, Physical properties of glycerol and its solutions, in *Glycerol*, eds. C. S. Miner and N. N. Dalton, Reinhold Publishing Corp. [(v2) 347-348, 357, 365-366]

Sen, P. K., and D. Venkateswarlu, 1983, On the stability of plane Poiseuille flow to finite-amplitude disturbances, considering the higher-order Landau coefficients, J. Fluid Mech. **133**, 179. [(v2) 240]

Shankar, P. N., and M. D. Deshpande, 1990, On the temperature distribution in liquid-vapor phase change between plane liquid surfaces, Phys. Fluids A **2**(6), 1030. [(v1) 381]

Shertok, J. T., 1976, Velocity profiles in core-annular flow using a laser-Doppler velocimeter, Ph.D. thesis, Princeton University. [(v2) 8]

Sherwood, J.D., 1981, Spindle shaped drops in a viscous extensional flow, Math. Proc. Cambridge Phil. Soc. **90**, 529. [(v1) 143]

Shirtcliffe, T. G. L., 1969, An experimental investigation of thermosolutal convection at marginal stability, J. Fluid Mech. **35** (4), 677. [(v1) 172]

Shirtcliffe, T. G. L., 1973, Transport and profile measurements of the diffusive interface in double diffusive convection with similar diffusivities, J. Fluid Mech. **57**, 27. [(v1) 171]

Shlang, T., G. I. Sivashinsky, A. J. Babchin and A. L. Frenkel, 1985, Irregular wavy flow due to viscous stratification, Le Journal de Physique **46**, 863. [(v1) 270, 324]

Shlang, T., and G. I. Sivashinsky, 1982, Irregular flow of a liquid film down a vertical column, J. Physique **43**, 459. [(v1) 324]

Sijbrand, J., 1981, *Studies in Non-Linear Stability and Bifurcation Theory*, Ph. D. thesis, Rijksuniversiteit, Utrecht. [(v1) 176]

Simons, G. A., and R. S. Larson, 1974, Formation of vortex rings in a stratified atmosphere, Phys. Fluids **17**, 8. [(v2) 289]

Sinclair, A. R., 1970, Rheology of viscous fracturing fluids, J. Petroleum Technology, June, 711. [(v2) 196, 200]

Singh, P. and D. D. Joseph, 1989, Autoregressive methods for chaos on binary sequences for the Lorenz attractor, Phys. Letters A **135**, 247. [(v1) 133, 135, 138, 139]

Singh, P., P. Mohr and D. D. Joseph, 1992, Application of binary sequences to problems of chaos, Video Journal of Engineering Research, to appear. [(v1) 133]

Sisson, W. A., and F. F. Morehead, 1953, The skin effect in crimped rayon, Text. Res. J. **23**, 152. [(v1) 11]

Sivashinsky, G. I., 1977, Nonlinear analysis of hydrodynamic instability in laminar flames – I. Derivation of basic equations, Acta Astronaut. **4**, 1177. [(v1) 333]

Sivashinsky, G. I., 1983, Instabilities, pattern formation, and turbulence in planes, Ann. Rev. Fluid Mech. **15**, 179. [(v1) 271, 333, 334]

Sivashinsky, G. I., and D. M. Michelson, 1980, On irregular wavy flow of a liquid film down a vertical plane, Prog. Theor. Phys. **63**, 2112. [(v1) 324]

De Smedt, C., and S. Nam, 1987, The processing benefits of fluoroelastomer application in LLDPE, Plastics and Rubber Process. Appl. **8**, 11. [(v1) 376]

Smith, J. M., and H. C. Van Ness, 1975, *Introduction to Chemical Engineering Thermodynamics*, 3rd ed., McGraw-Hill. [(v2) 354]

Smith, M. K., 1989, The axisymmetric long-wave instability of a concentric two-phase pipe flow, Phys. Fluids A **1**, 494. [(v1) 269, 271; (v2) 15]

Smith, M. K., 1990 a, The mechanism for the long-wave instability in thin liquid films, J. Fluid Mech. **217**, 469. [(v1) 271]

Smith, M. K., 1990 b, The long-wave instability in heated or cooled inclined liquid layers, J. Fluid Mech. **219**, 337. [(v1) 271]

Smith, M. K., and S. H. Davis, 1982, The instability of sheared liquid layers, J. Fluid Mech. **121**, 187. [(v1) 338]

Smith, M. K., and S. H. Davis, 1983, Instabilities of dynamic thermocapillary liquid layers, Part 2. Surface-wave instabilities, J. Fluid Mech. **132**, 145. [(v1) 171]

Smith, P. G., M. Van Den Ven and S. G. Mason, 1981, The transient interfacial tension between two miscible fluids, J. Colloid Interface Sci. **80**(1), 302. [(v2) 338-342]

Smyrlis, Y. S., and D. T. Papageorgiou, 1991, Predicting chaos for infinite dimensional dynamical systems: the Kuramoto-Sivashinsky equation, a case study, Proc. Natl. Acad. Sci. USA Applied Mathematics **88**. [(v1) 337]

Sone, Y., and Y. Onishi, 1978, Kinetic theory of evaporation and condensation - hydrodynamic equation and slip boundary condition, J. Phys. Soc. Jpn. **44**, 1981; **45** 1054. [(v1) 381]

Sotin, C., and E. M. Parmentier, 1989, On the stability of a fluid layer containing a univariant phase transition: application to planetary interiors, Phys. Earth and Planetary Interiors **55**, 10. [(v1) 378, 398]

Southern, J. H., and R. L Ballman, 1973, Stratified bicomponent flow of polymer melts in a tube, Appl. Polymer Symp. **20**, 175. [(v1) 10, 11, 33, 38]

Sparrow E. M., R. B. Husar and R. J. Goldstein, 1970, Observations and other characteristics of thermals, J. Fluid Mech. **41**, 793. [(v2) 363]

Spindler, B., 1982, Linear stability of liquid film with interfacial phase change, Int. J. Heat Mass Transfer **25**, 161. [(v1) 379]

Squire, H. B., 1933, On the stability of three-dimensional disturbances of viscous flow between parallel walls, Proc. Roy. Soc. A **142**, 621. [(v1) 276, 278]

Stein, M. H., 1978, Concentric annular oil-water flow, Ph. D. Thesis, Purdue University. [(v2) 7]

Sternling, C. V., and L. E. Scriven, 1959, Interfacial turbulence: hydrodynamic instability and the Marangoni effect, AIChE J. **5**(4), 514. [(v1) 173]

Stewartson, K., and J. T. Stuart, 1971, A nonlinear instability theory for wave system in plane Poiseuille flow, J. Fluid Mech. **48**, 529. [(v1) 356; (v2) 227, 235]

Stockman, H. W., C. T. Stockman and C. R. Carrigan, 1990, Modelling viscous segregation in immiscible fluids using lattice-gas automata, Nature **348**, 523. [(v1) 6]

Stuart, J. T., and R. DiPrima, 1978, The Eckhaus and Benjamin-Feir resonance mechanisms, Proc. Roy. Soc. Lond. A **362**, 27. [(v2) 240]

Stuke, B., 1954, Zur Bildung von Wirbelringen, Zeitschrift für Physik **137**, 376. [(v2) 308-309]

Sturges, L., and D. D. Joseph, 1980, A normal stress amplifier for the second normal stress difference, J. Non-Newtonian Fluid Mech. **6**, 325. [(v1) 15]

Tartar, L., 1975, Problèmes de contrôle des coefficients dans des équations aux dérivées partielles, Lecture Notes in Economics and Mathematical Systems, Springer **107**, 420. [(v1) 42]

Taylor, G.I., 1931, Effect of variation in density on the stability of superposed streams of fluid, Proc. R. Soc. Lond. A **132**, 499. [(v1) 279]

Taylor, G.I., 1934, The formation of emulsions in definable fields of flow, Proc. Roy. Soc. London A **146**, 501. [(v1) 143]

Taylor, G.I., 1964, Conical free surfaces and fluid interfaces, *Proc. 11th Int. Congr. Appl. Mech.*, Munich. [(v1) 143]

Taylor, T. D., and A. Acrivos, 1964, On the deformation and drag of a falling viscous drop at low Reynolds number, J. Fluid Mech. **18** 466. [(v2) 295]

Temam, R., 1979, *Navier-Stokes Equations*, North-Holland. [(v1) 42, 205]

Than, P. T., L. Preziosi, D. D. Joseph and M. Arney, 1988, Measurement of interfacial tension between immiscible liquids with the spinning rod tensiometer, J. Colloid and Interface Sci. **124**(2), 552. [(v1) 79]

Than, P. T., F. Rosso and D. D. Joseph, 1987, Instability of Poiseuille flow of two immiscible liquids with different viscosities in a channel, Int. J. Eng. Sci. **25**, 189. [(v1) 269; (v2) 15]

Thomson, J. J., and H. F. Newall, 1885, On the formation of vortex rings by drops falling into liquids, and some allied phenomena, Proc. Roy. Soc. Lond. **39**, 417. [(v2) 289, 292, 313, 334, 336, 338]

Tipman, E. and G. W. Hodgson, 1956, Sedimentation in emulsions of water in petroleum, J. Petroleum Tech., September, 91. [(v2) 155]

Tlapa, G., and B. Bernstein, 1970, Stability of a relaxation-type viscoelastic fluid with slight elasticity, Phys. Fluids **13**, 565. [(v1) 363]

Topper, J., and T. Kawahara, 1978, Approximate equations for long nonlinear waves on a viscous fluid, J. Phys. Soc. Japan **44**, 663. [(v1) 270]

Tordella, J. P., 1958, An instability in the flow of molten polymers, Rheol. Acta **1**, 216. [(v1) 375]

Truesdell, C. and W. Noll, 1965, *The Non-Linear Field Theories of Mechanics*, Handbuch der Physik, ed. S. Flügge, **3**, Springer-Verlag. [(v2) 345]

Tryggvason, G., and S. O. Unverdi, 1990, Computations of three - dimensional Rayleigh-Taylor instability, Phys. Fluids A **2**(5), 656. [(v1) 272]

Tryggvason, G., and S. O. Unverdi, 1991, Full numerical simulations of multifluid flows, Phys. Fluids A **3**(5), 1455. [(v1) 272; (v2) 294]

Turner, J. S., 1979, *Buoyancy Effects in Fluids*, Cambridge University Press, Great Britain. [(v1) 172; (v2) 289, 326, 332]

Valenzuela, G. R., 1976, The growth of gravity-capillary waves in a coupled shear flow, J. Fluid Mech. **76** (2), 229. [(v1) 270]

Van der Waals, M., 1895, Théorie thermodynamique de la capillarité dans l'hypothèse d'une variation de densité, Arch. Neerl. Sci. Ex. Nat. **28**, 121. [(v2) 339, 344]

Van Dyke, M., 1975, *Perturbation Methods in Fluid Mechanics*, The Parabolic Press, Stanford, California. [(v2) 99, 289]

Van Dyke, M., 1982, *An Album of Fluid Motion*, The Parabolic Press. [(v1) 171]

Veal, C. J., D. R. Wall and A. J. Groszek, 1979, Stable coal/fuel-oil dispersions, Proc. 2nd Int. Symp. on Coal-Oil Mixture Combustion, Danvers, Massachusetts. [(v1) 9]

Wahal, S., and A. Bose, 1988, Rayleigh-Benard and interfacial instabilities in two immiscible liquid layers, Phys. Fluids **31**, 3502. [(v1) 173]

Walmsley, M. R., and G. G. Duffy, 1987, Hydraulic transport of solid particles and capsulized materials in pipelines with friction losses lower than water, J. of Pipelines **6**, 33. [(v1) 8]

Walters, J. K., and J. F. Davidson, 1963, The initial motion of a gas bubble formed in an inviscid liquid, Part 2. The three-dimensional bubble and the toroidal bubble, J. Fluid Mech. **17**, 321. [(v2) 290, 316]

Walters, K., 1984, Some modern developments in non-Newtonian fluid mechanics, *Advances in Rheology*, Proc. IX Intl. Congress on Rheology, Mexico, ed. B. Mena, A. Garcia-Rejon, C. Rangel-Nafaile, 31. [(v1) 13]

Walters, K., 1985, Overview of macroscopic viscoelastic flow, *Viscoelasticity and Rheology*, ed. A. S. Lodge, M. Renardy and J. A. Nohel, Acad. Press. [(v1) 13]

Wang, C. K., J. J. Seaborg and S. P. Lin, 1978, Instability of multi-layered liquid films, Phys. Fluids **21**, 1669. [(v1) 269, 272]

Wang, T. G., R. Tagg, L. Cammack and A. Croonquist, 1981, Non-axisymmetric shapes of a rotating drop in an immiscible system, in *Proc. 2nd Int. Colloq. on Drops and Bubbles* (ed. D. H. LeCroisette), pp. 203 - 213, NASA-JPL. [(v1) 90]

Warshay, M.E., E. Bogusz, M. Johnson, and R. C. Kintner, 1959, Ultimate velocity of drops in stationary liquid media, Can. J. Chem. Engng. **37**, 29. [(v1) 144]

Waters, N. D., 1983, The stability of two stratified "power-law" liquids in Couette flow, J. Non-Newtonian Fluid Mech. **12**, 85. [(v1) 269, 359, 360]

Waters, N. D., and A. M. Keeley, 1987, The stability of two stratified Non-Newtonian liquids in Couette flow, **24**, 161. [(v1) 269, 359, 360]

Wedemeyer, E. H., 1964, The unsteady flow within a spinning cylinder, J. Fluid Mech. **20**, 383. [(v1) 16]

Weinstein, S. J., and M. R. Kurz, 1991, Long-wavelength instabilities in three-layer flow down an incline, Phys. Fluids A **3**(11), 2680. [(v1) 272, 279]

White, J. L., and B.-L. Lee, 1975, Theory of interface distortion in stratified two-phase flow, Trans. Soc. Rheol. **19**, 457. [(v1) 11]

Whitham, G. B., 1974, *Linear and Nonlinear Waves*, John Wiley and Sons, New York. [(v1) 332, 333]

Wilkinson, J. H., 1977, Some recent advances in numerical linear algebra, in *The state of the art in numerical analysis*, ed. D. Jacobs, Academic Press. [(v2) 242]

Williams, M. B., and S. H. Davis, 1982, Nonlinear theory of film rupture, J. Colloid Interface Sci. **90**, 220. [(v2) 264-267]

Williams, P. R. and R. W. Williams, 1985, On the planar extensional viscosity of mobile liquids, J. Non-Newtonian Fluid Mech. **19**, 53. [(v1) 13, 14]

Wollkind, D. J., and J. I. D. Alexander, 1982, Kelvin-Helmholtz instability in a layered Newtonian fluid model of the geological phenomenon of rock folding, SIAM J. Appl. Math. **42** (6), 1276. [(v1) 16]

Wooding, R. A., 1969, Growth of fingers at an unstable diffusing interface in a porous medium or Hele Shaw cell, J. Fluid Mech. **39**, 477. [(v2) 379, 387]

Xu, J.-J., and S. H. Davis, 1985, Instability of capillary jets with thermocapillarity, J. Fluid Mech. **161**, 1. [(v2) 13]

Yakubovich, V. A., and V. M. Starzhinskii, 1975, *Linear Differential Equations with Periodic Coefficients 1*, Halsted, Jerusalem. [(v1) 204, 220]

Yiantsios, S. G., 1988, Ph.D. thesis, University of California, Davis. [(v1) 302]

Yiantsios, S. G., and B. G. Higgins, 1988, Linear stability of plane Poiseuille flow of two superposed fluids, Phys. Fluids. **31**, 3225. (Erratum, Phys. Fluids A **1**, 897) [(v1) 269, 270, 276, 278, 279, 287, 296, 300, 302, 350]

Yiantsios, S. G., and B. G. Higgins, 1989, Rayleigh-Taylor instability in thin viscous films, Phys. Fluids A **1** (9), 1484. [(v1) 272]

Yih, C.-S., 1960, Instability of a rotating liquid film with a free surface, Proc. R. Soc. Lond. A **258**, 63. [(v1) 66]

Yih, C.-S., 1963, Stability of liquid flow down an inclined plane, Phys. Fluids **6**, 321. [(v1) 378]

Yih, C.-S., 1967, Instability due to viscosity stratification, J. Fluid Mech. **26**,337. [(v1) 173, 193, 196, 268, 269, 279-287, 320, 329, 331, 338, 339, 350, 360; (v2) 31, 132]

Yih, C.-S., 1986, Instability resulting from stratification in thermal conductivity, Phys. Fluids **29**, 1769. [(v1) 174]

Yortsos, Y. C., and M. Zeybek, 1988, Dispersion driven instability in miscible displacement in porous media, Phys. Fluids **31**(12), 3511. [(v2) 379]

Yu, H. S., and C. D. Han, 1973, Stratified two-phase flow of molten polymers, J. Appl. Polym. Sci. **17**, 1203. [(v1) 11]

Yu, H. S., and E. M. Sparrow, 1967, Stratified laminar flow in ducts of arbitrary shape, AICHE J. **13**(1),10. [(v2) 3]

Yu, H. S., and E. M. Sparrow, 1969, Experiments on two-component stratified flow in a horizontal duct, Trans. ASME C:J. Heat Transfer, **91**, 51. [(v1) 5, 339]

Zana, E. and L. G. Leal, 1978, The dynamics and dissolution of gas bubbles in a viscoelastic fluid, Int. J. Multiphase Flow **4**, 237. [(v1) 144]

Zeren, R. W., and W. C. Reynolds, 1972, Thermal instabilities in two-fluid horizontal layers, J. Fluid Mech. **53**, 305. [(v1) 173, 192]

Zondek, B., and L. H. Thomas, 1953, Stability of a limiting case of plane Couette flow, Phys. Rev. (2) **90**, 738. [(v1) 294]

Index

The index entry "(vm) n" refers to "volume m, page n".